

INSTITUTE OF THEORETICAL PHYSICS ,WARSAW UNIVERSITY ,WARSAW  
INSTITUTE OF NUCLEAR RESEARCH ,WARSAW

INIS-mf-9489

PROCEEDINGS  
OF THE IV WARSAW SYMPOSIUM  
ON ELEMENTARY PARTICLE PHYSICS

KAZIMIERZ , POLAND , 24 - 31 MAY 1981

WARSZAWA 1981

INSTITUTE OF THEORETICAL PHYSICS, WARSAW UNIVERSITY, WARSAW

INSTITUTE OF NUCLEAR RESEARCH, WARSAW

PROCEEDINGS  
OF THE IV WARSAW SYMPOSIUM  
ON ELEMENTARY PARTICLE PHYSICS  
KAZIMIERZ, POLAND, 24-31 MAY 1981

Edited by Z. AJDUK and K. DROBA

WARSZAWA 1981

Orga

G. B

L. LU

S. POK

R. SOS

A. WRÓ

f r o

INSTIT

INSTI

INSTI

This i

1. Pro

S

2. Pro

St

3. Pr

Pa

jo

# Organizing Committee

G. BIAŁKOWSKI

L. ŁUKASZUK

S. POKORSKI

R. SOSNOWSKI

A. WRÓBLEWSKI

Z. AJDUK

K. DOROBA

G. WILK

from

INSTITUTE OF THEORETICAL PHYSICS, WARSAW UNIVERSITY, WARSAW

INSTITUTE OF EXPERIMENTAL PHYSICS, WARSAW UNIVERSITY, WARSAW

INSTITUTE OF NUCLEAR PHYSICS, WARSAW

This is the fourth volume in the series of Proceedings:

1. Proceedings of the I International Symposium on Hadron Structure and Multiparticle Production, Kazimierz, 1977;
2. Proceedings of the II International Symposium on Hadron Structure and Multiparticle Production, Kazimierz, 1979;
3. Proceedings of the III Warsaw Symposium on Elementary Particle Physics, Jodłowy Dwór, 1980 /appeared in the journal "Nukleonika" 26/1981//.

# LIST OF PARTICIPANTS

|                    |          |                        |                |                   |
|--------------------|----------|------------------------|----------------|-------------------|
| 1. M. Adamus       | Warsaw   | 25. M. Górski          | Warsaw         | 49. K. Iang       |
| 2. Z. Ajduk        | Warsaw   | 26. M. Gourdin         | Paris          | 50. E. Lendva     |
| 3. J. Alitti       | Saclay   | 27. F. Gutbrod         | Hamburg        | 51. M. Leopold    |
| 4. F. Barreiro     | Siegen   | 28. B. Grządkowski     | Warsaw         | 52. W. Lohman     |
| 5. J. Bartelski    | Warsaw   | 29. J. Gwiżdż          | Warsaw         | 53. L. Łukasz     |
| 6. A. Bartnik      | Warsaw   | 30. T. Hansl-Kozanecki | Aachen/CERN    | 54. P. Malinowski |
| 7. L. Becker       | Zeuthen  | 31. R. Haymaker        | Cracow         | 55. L. Mankiewicz |
| 8. W. Beusch       | CERN     | 32. T. Hofmohl         | Warsaw         | 56. P. Minkowski  |
| 9. A. Białas       | Cracow   | 33. B. Humpert         | CERN           | 57. L. Mlodin     |
| 10. H. Białkowska  | Warsaw   | 34. C. Itzykson        | Saclay         | 58. F. Müller     |
| 11. G. Burgun      | Saclay   | 35. A. Jacholowska     | Warsaw         | 59. K. Muś        |
| 12. B. Combridge   | Didcot   | 36. A. Jacholowski     | Warsaw         | 60. W. Nahm       |
| 13. N.S. Craigie   | Trieste  | 37. J. Kalinowski      | Warsaw         | 61. R. Nowak      |
| 14. R. Crewther    | Berne    | 38. J. Kempa           | Łódź           | 62. M. Otwinowski |
| 15. A. Czechowski  | Warsaw   | 39. T. Kiss-Toth       | Wuppertal      | 63. S. Otwinowski |
| 16. K. Doroba      | Warsaw   | 40. E. Kluge           | Heidelberg     | 64. L. Palla      |
| 17. Z. Dziembowski | Warsaw   | 41. K. Konishi         | Pisa           | 65. F. Palombi    |
| 18. F. Eisele      | Dortmund | 42. W. Kozanecki       | Riverside/CERN | 66. A. Para       |
| 19. E. Engels      | Saclay   | 43. M. Krawczyk        | Warsaw         | 67. R. Peccei     |
| 20. A. Filipkowski | Warsaw   | 44. P. Krawczyk        | Warsaw         | 68. A. Piotrowski |
| 21. V. Flaminio    | Pisa     | 45. J. Kripfganz       | Leipzig        | 69. S. Pokorski   |
| 22. W. Geist       | CERN     | 46. E. Krys            | Łódź           | 70. J. Ranft      |
| 23. J. Glazer      | Warsaw   | 47. K. Kurek           | Warsaw         | 71. M. Roman      |
| 24. B. Gładysz     | Cracow   | 48. J. Lach            | Batavia        | 72. E. Rondio     |
|                    |          |                        |                | 73. Z. Ryzak      |



|                   |           |                    |               |
|-------------------|-----------|--------------------|---------------|
| 49. K. Lang       | Warsaw    | 74. P. Scharbach   | Didcot        |
| 50. E. Lendvai    | Budapest  | 75. K. Schilling   | Wuppertal     |
| 51. M. Leopold    | Warsaw    | 76. G. Senjanovic  | Brookhaven    |
| 52. W. Lohmann    | Zeuthen   | 77. P. Sikivie     | CERN          |
| 53. L. Lukaszuk   | Warsaw    | 78. R. Sosnowski   | Warsaw        |
| 54. P. Malinowski | Białystok | 79. M. Staszek     | Warsaw        |
| 55. L. Mankiewicz | Warsaw    | 80. P. Steffen     | Hamburg       |
| 56. P. Minkowski  | Berne     | 81. J. Stepaniak   | Warsaw        |
| 57. L. Mlodinov   | Munich    | 82. J. Strauss     | Vienna/CERN   |
| 58. F. Muller     | CERN      | 83. M. Szczekowski | Warsaw        |
| 59. K. Muś        | Gdańsk    | 84. M. Szeptycka   | Warsaw        |
| 60. W. Nahm       | CERN      | 85. A. Szymacha    | Warsaw        |
| 61. R. Nowak      | Warsaw    | 86. L. Tarasiuk    | Warsaw        |
| 62. M. Otwinowska | Warsaw    | 87. S. Tatur       | Warsaw        |
| 63. S. Otwinowski | Warsaw    | 88. T. Taylor      | Warsaw        |
| 64. L. Palla      | Budapest  | 89. S. Tkaczyk     | Warsaw        |
| 65. F. Palombo    | Milan     | 90. A. Turski      | Warsaw        |
| 66. A. Para       | Warsaw    | 91. T. Tymieniecka | Warsaw        |
| 67. R. Peccei     | Munich    | 92. G. Wilk        | Warsaw        |
| 68. A. Piotrowska | Łódź      | 93. S. Wojcicki    | Stanford/CERN |
| 69. S. Pokorski   | Warsaw    | 94. J. Wosiek      | Cracow        |
| 70. J. Ranft      | Leipzig   | 95. J. Wotschack   | CERN          |
| 71. M. Romaniuk   | Warsaw    | 96. A. Wróblewski  | Warsaw        |
| 72. E. Rondio     | Warsaw    | 97. B. Wyśłouch    | Warsaw        |
| 73. Z. Ryzak      | Warsaw    | 98. J. Szwed       | Cracow        |

## C O N T E N T S \*

SESSION IHIGH  $p_T$  HADRONIC COLLISIONS

Chairman: E. KLUGE

|             |  |    |
|-------------|--|----|
| W. GEIST    | - Aspects of experimental high transverse momentum physics                                     | 9  |
| G. BURGUN   | - Experimental review of some predictions of the Drell-Yan model in hadroproduction of dimuons | 45 |
| J. SZWED    | - Hyperon polarization in inclusive and exclusive processes                                    | 69 |
| M. GORSKI   | - High energy photoproduction experiment   | —  |
| S. WOJCICKI | - Prompt single muon production by protons on iron   | 75 |

SESSION IILEPTON INTERACTIONS

Chairman: F. MULLER

|              |  |     |
|--------------|--|-----|
| F. EISELE    | - What can we learn from structure functions measured in neutrino interactions?              | 81  |
| J. WOTSCHACK | - Neutrino oscillations - present and future experiments                                     | 103 |
| V. FLAMINIO  | - Neutron and proton structure functions from inelastic antineutrino scattering in deuterium | 125 |
| F. EISELE    | - Charm production by neutrinos  | --- |

SESSION III $e^+e^-$  PHYSICS

Chairman: J. IACH

|             |   |     |
|-------------|---|-----|
| F. BARREIRO | - Jets in $e^+e^-$ annihilation and QCD | 489 |
|-------------|---|-----|

\*We list here the names of the speakers only. A complete list of the authors is given in the text of the talk.

|               |  |     |
|---------------|--|-----|
| P. STEFFEN    | - Weak interactions; gluon jet fragmentation                     | --- |
| F. GUTBROD    | - Inclusive baryon production and fragmentation models           | --- |
| J. RANFT      | - Spin effects in $e^+e^-$ annihilation                          | 135 |
| M. OTWINOWSKA | - Jets in hadron-hadron, $e^+e^-$ , neutrino-proton interactions | --- |

#### SESSION IV

##### $\bar{p}p$ PHYSICS AND OTHER TOPICS

Chairman: E. ENGELS

|                    |   |
|--------------------|---|
| W. KOZANECKI       | - An overview of the $\bar{p}p$ collider project at CERN--- |
| ✓ J. STRAUSS       | - Physics at the $\bar{p}p$ collider 427                    |
| T. HANSI-KOZANECKI | - Cosmic ray physics and $\bar{p}p$ collider experiment --- |
| J. LACH            | - Hyperons beam ---   |
| F. GUTBROD         | - Selected topics from $\gamma\gamma$ physics ---           |

#### SESSION V

##### LOW $p_T$ HADRONIC COLLISIONS

Chairman: W. BEUSCH

|                 |   |     |
|-----------------|---|-----|
| F. MULLER       | - Hadroproduction of charmed particles  | 141 |
| A. BIAŁAS       | - Heavy ion collisions at high energies   | --- |
| R. SOSNOWSKI    | - Hadroproduction of beauty?  | --- |
| F. PALOMBO      | - A new $O^+S$ meson and new results on the $1^+S$ state in the $3\pi$ system coherently produced on nuclei; $5\pi$ coherent production on nuclei | 187 |
| ✓ S. OTWIKOWSKI | - Two particle correlations in pion-nucleus interactions at 40 GeV/c  | 197 |
| H. BIAŁKOWSKA   | - Pion production in collisions of relativistic ions  | 207 |

SESSION VISTATUS OF QUANTUM CHROMODYNAMICS

Chairman: F. GUTBROD

|               |   |     |
|---------------|---|-----|
| J. KALINOWSKI | - Perturbative QCD beyond „classical“ problems  | 407 |
| N.S. CRAIGIE  | - Spin physics at short distances as a means<br>of studying QCD                           | 213 |
| B. HUMPERT    | - Diagrammatic mass factorization   | 261 |
| B. COMBRIDGE  | - QCD-sensitive differences between $\bar{p}$ - and p-<br>-beams in large $p_T$ reactions | --- |

SESSION VIINON-PERTURBATIVE METHODS IN GAUGE THEORY

Chairman: K. SCHILLING

|              |  |     |
|--------------|--|-----|
| C. ITZYKSON  | - Lattice gauge theory   | 263 |
| R. CREWSTER  | - Gluon condensate and the master field                                  | --- |
| W. NAHM      | - Gribov copies and instantons   | 275 |
| L. MLODINOV  | - Large N expansions work  | 283 |
| J. KRIPFGANZ | - Gluon condensate from lattice calculations:<br>SU(3) pure gauge theory | 299 |

SESSION VIIIDYNAMICAL SYMMETRY BREAKING

Chairman: P. MINKOWSKI

|              |  |     |
|--------------|--|-----|
| P. SIKIVIE   | - Electroweak gauge theories without scalars                       | --- |
| K. SCHILLING | - Bounds from finite sizes lattice<br>expectation values           | --- |
| K. KONISHI   | - Pattern of chiral symmetry breaking in<br>quantum chromodynamics | 327 |
| S. TATUR     | - Chiral symmetry and bag model                                    | 341 |

SESSION IX

P CP AND MOD

Chairman: J.

|               |     |
|---------------|-----|
| G. SENJANOVIC | 407 |
| R.D. PECCEI   | 213 |
| G. SENJANOVIC | 261 |

E. ENGELS

SESSION X

SPONTANEOUS S

Chairman: M.

|               |     |
|---------------|-----|
| P. MINKOWSKI  | 263 |
| R.D. PECCEI   | --- |
| A. CZECHOWSKI | 275 |
| L. PALLA      | 283 |

299

SESSION IXP, CP AND MODELS OF WEAK INTERACTIONS. GRAND UNIFICATION

Chairman: J. RANFT

|               |   |     |
|---------------|---|-----|
| G. SENJANOVIĆ | - Symmetry breaking at high temperature                                     | 307 |
| R.D. PECCEI   | - Patterns of CP violation  | 347 |
| G. SENJANOVIĆ | - An oasis in the desert: weakly broken parity<br>in grand unified theories | 363 |
| E. ENGELS     | - Review of proton lifetime experiments                                     | 383 |

SESSION XSPONTANEOUS SYMMETRY BREAKING AND OTHER TOPICS

Chairman: M. GOURDIN

|               |   |     |
|---------------|---|-----|
| P. MINKOWSKI  | - Spontaneous parameters and associated mass<br>scales    | --- |
| R.D. PECCEI   | - Spontaneous lepton number non-conservation              | --- |
| A. CZECHOWSKI | - Higgs fields in M.A.C.                                  | 403 |
| L. PALLA      | - Generating multimonopoles by Bäcklund<br>transformation | --- |

ASPECTS OF EXPERIMENTAL HIGH TRANSVERSE MOMENTUM PHYSICS

W.M. Geist<sup>(\*)</sup>

Institut für Hochenergiephysik der Universität Heidelberg, Fed. Rep. Germany

ABSTRACT

New results from experiments looking for large transverse momentum processes in hadron interactions are discussed. Multiparticle final states associated with a single high  $p_T$  particle show clear jet structure. Properties of these jets and inclusive single particle spectra indicate that, in addition to valence quarks, gluons contribute substantially to high  $p_T$  phenomena. Evidence for multijet production is briefly presented. Data from calorimeter experiments, which aim at a detection of the total jet energy, do not show jet structure.

(author)

(\*) Now at CERN, Geneva, Switzerland.

1. INTRODUCTION

The  
phenomena  
purely  
assumed

(a) The  
from  
describ  
re.  
(b) Two  
includi  
only

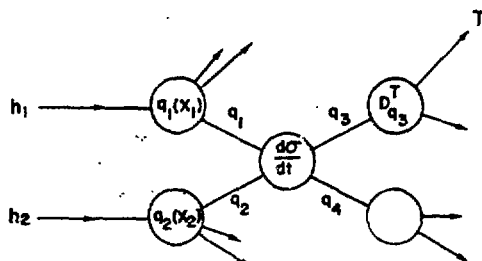
(c) The  
be  
jet  
the  
mo

(d) Mo  
th  
pe  
st

Tr  
process  
plane

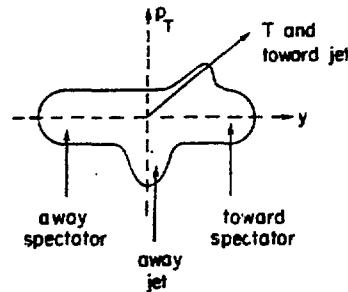
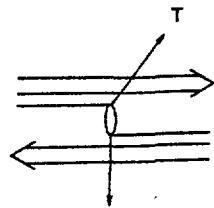
# 1. INTRODUCTION

The goal of experiments dealing with high transverse momentum phenomena is to probe the parton structure of hadrons by measurements of purely hadronic final states. The relevant underlying processes are assumed to be factorizable into four steps:



- (a) The two incoming hadrons  $h$  are beams of free partons  $q$  carrying fractions  $x$  of the hadron momenta. The structure function  $q(x)$  describes the distribution in  $x$ .
- (b) Two partons, one from each hadron, undergo point-like (i.e. small impact parameter, hence large transverse momentum) scattering.
- (c) The two partons emerging from the collision at large angles to the beam and opposite in azimuth carry colour and therefore fragment into jets of hadrons roughly preserving the parton direction. According to the fragmentation function  $D_q^T(z)$  a fraction  $z$  of the parton's momentum is transferred to a single hadron  $T$ .
- (d) Most of the constituents of the incoming hadrons do not participate in the interaction (spectator partons). They hadronize into two jets of particles approximately collinear with the direction of the initial state hadrons.

The diagram below shows a short-hand notation used here for these processes and the expected coplanar 4-jet event structure in the scattering plane (transverse momentum ( $p_T$ ) - rapidity ( $y$ ) plane).



A first order QCD prediction based upon these ideas for the Lorentz invariant inclusive cross section for the production of particles T at high transverse momentum reads as follows [1]:

$$E \frac{d\sigma}{dp}(T) \sim \sum_i \int q_1(x_1, Q^2) q_2(x_2, Q^2) dx_1 dx_2 \frac{d\sigma}{dt_i} \frac{1}{z} D_q^T(z, Q^2) \\ = J(q_1, q_2, \frac{d\sigma}{dt}, D_q^T).$$

The scale-breaking structure functions  $q(x, Q^2)$  ( $Q^2 = \beta p_T^2$ ,  $\beta = 1 \dots 4$ ) as well as the fragmentation functions  $D_q^T(z, Q^2)$  are derived from deep inelastic lepton scattering experiments [2]; the differential cross sections  $d\sigma/dt_i$  for the various QCD subprocesses contain the strong coupling constant  $\alpha_s(Q^2)$  and  $t$  is the four-momentum transfer at the parton level. As an example contributions of various subprocesses to high  $p_T$   $\pi^0$  production are shown in fig. 1 [3]. Agreement of theory and data is reasonably good for  $p_T \gtrsim 5$  GeV/c. Note the gluon contributions for  $p_T \lesssim 5$  GeV/c. Experimentally one finds for the range of very large  $p_T$ :  $E \frac{d\sigma}{dp} \sim p_T^{-3}$ , whereas  $E \frac{d\sigma}{dp} \sim p_T^{-2}$  for  $p_T \approx 3$  GeV/c. There is no unique theoretical solution of the problem at  $p_T \lesssim 5$  GeV/c as yet. The most important subprocesses are sketched below (— : quarks,  $\sim$  : gluons).



Other sum  
experimental

One real  
on equal foot  
crucial ingre

The aim  
one tries to  
to a determin  
self-coupling

In the fa  
experiments i  
inclusive spec  
and away side  
jets (sect. 6  
In the latter  
briefly discus  
collected in s

The inter  
physics. The  
from more deta  
many aspects a

## 2. CALORIMETER EXPERIMENTS

Measuring  
particle produ  
events where t  
momentum (e.g.  
compared to th  
total jet (i.e.



Other subprocesses are not considered here because of lacking experimental evidence.

One realizes the unique situation that gluons appear in the Born terms on equal footing with quarks; especially the triple gluon vertex is a crucial ingredient of QCD as a non-abelian gauge theory.

The aim of high  $p_T$  experiments can now be rephrased by saying that one tries to disentangle the QCD subprocesses and to eventually contribute to a determination of gluon properties and to a proof for the gluon self-coupling.

In the following a search for jet structure with calorimeter experiments is discussed (sect. 2). A presentation of new measurements of inclusive spectra and particle ratios (sect. 3), of toward jets (sect. 4) and away side jets (sect. 5) as well as of the forward/backward spectator jets (sect. 6) will show evidence for the various subprocesses expected. In the latter section also the question of parton transverse momenta is briefly discussed. First indications for multijet ( $> 5$ ) production are collected in sect. 7.

The intention is to convey an intuitive understanding of high  $p_T$  physics. The interpretations given are simplified and await confirmation from more detailed experimental and theoretical analyses. More details on many aspects are collected in several recent reviews [4].

## 2. CALORIMETER EXPERIMENTS

Measuring the differential cross section  $J(q_1, q_2, \frac{d\sigma}{dt}, D_q^T)$  for single particle production at high  $p_T$  means recording only that fraction of jet events where the triggering particle T carries most of the quark-jet's momentum (e.g.  $z = 0.6$  [5]). This cross section is expected to be small compared to the cross section  $J(q_1, q_2, \frac{d\sigma}{dt}, \delta(1-z))$  for observing the total jet (i.e. parton) momentum:

$$\frac{J(q_1, q_2, \frac{d\sigma}{dt}, \delta(1-z))}{J(q_1, q_2, \frac{d\sigma}{dt}, D_q^T(z))} \gg 1 \quad [6]$$

This is called "trigger bias".

Calorimeter experiments try to overcome this trigger bias by detecting the total energy of hadrons emitted into a solid angle of typically 1 or 2 sterad. As will be seen later (sect. 4) most of the jet energy is only contained well within the calorimeter, if the jet points toward its centre. Because of this problem of jet containment the interpretation of the first calorimeter experiments [7] is not unambiguous. Here only the latest results of the BKLMM Collaboration [8] are presented. The experiment was performed with  $\pi^-$  and p beams of 300 GeV/c hitting a hydrogen target. The target was surrounded by a streamer chamber to measure charged multiplicities and to reconstruct tracks. The special feature of the experiment was the use of a segmented combined hadron/photon calorimeter covering the full azimuth ( $\Delta\phi = 2\pi$ ) for  $|\eta| \leq 0.75$ .

The idea of extending the azimuthal coverage to  $2\pi$  was to minimize possible containment problems; since, however, the rapidity range covered is small, only those jet events are recorded in which both high  $p_T$  jets are produced at the same polar angle of  $\sim 90^\circ$  (sect. 5). This is why present experiments of this type detect only a small number of all jet events produced (calorimeter bias).

Fig. 2 shows preliminary results for the non-invariant cross sections integrated over  $\eta$  and  $\Delta\phi$  as functions of the transverse momentum  $p_T$  deposited in a "single calorimeter arm" ( $\Delta\phi = \pi/2$ ), in a "double arm" (two trigger arms of  $\Delta\phi = 2\pi$ ,  $180^\circ$  apart in  $\phi$ ) and in the full calorimeter ( $\Delta\phi = 2\pi$ ). The data are not corrected as yet for acceptance and energy resolution.

The single arm data are compatible with earlier results from other experiments [7]. For  $p_T = 2$  (6) GeV/c the single arm cross section is about 10(2000) times larger than the inclusive particle yield ( $\sigma(\text{single particle}) = 3\sigma(\pi^0) + 2\sigma(K^+ + K^-) + 2\sigma(p) + 2\sigma(\bar{p})$ , [9]). A ratio much larger than one is usually explained by the trigger bias.

given  
genera  
sectio  
and a  
other  
(1 +  
much  
equiva  
used i  
in the  
from  
the di  
predic  
hand  
inelat  
incor  
analy  
[10]  
to w  
-ang  
high  
detec  
Event  
/s =  
cross  
three  
fig.  
than  
for c.  
into

calor  
a  
(\*)  
fro  
: sec  
d (e  
atio

The cross section obtained from the two arm data is even larger at given  $\Sigma p_T$ ! This is expected from production of two high  $p_T$  jets and, more generally, from momentum conservation. If  $\sigma_1(\Sigma p_T = \Sigma_1)$  is the cross section for producing a multiparticle system (or jet) with  $\Sigma p_T$  in one arm and a fraction  $r$  of  $\Sigma_1$  is compensated by a multiparticle system in the other arm, a cross section  $\sigma_2(\Sigma p_T = \Sigma_1 + r\Sigma_1) = \sigma_1(\Sigma_1)$  for depositing  $(1+r)\Sigma_1 > \Sigma_1$  in two arms must be found. Finally the 2 $\pi$  trigger yields a much larger cross section than the two arm trigger at given  $\Sigma p_T$ . This is equivalent to the experimental finding (not shown) that the two arms, when used for triggering, do not contain a large fraction of the energy detected in the full calorimeter. This is in contrast to what one expects naively from production of two high  $p_T$  jets. The interesting fact is now that the discrepancy between the data and the 4 jet QCD Monte-Carlo predictions<sup>(\*)</sup> increases with larger azimuthal coverage. On the other hand the data can be explained to a large extent as fluctuations of normal inelastic events. These events were simulated by a cluster model incorporating energy-momentum conservation and KNO-scaling. A preliminary analysis shows also that about 1/3 of the measured energy is due to  $\pi^0$  [10] like in normal inelastic interactions.

The CCDHW Collaboration tried to reproduce these results using the SFM detector with its nearly 4 $\pi$  detection capability for charged tracks. Events with at least one reconstructable track were recorded at  $\sqrt{s} = 63$  GeV; this sample of events corresponds to  $\sim 95\%$  of the inelastic cross section. Vertex tracks with  $|y| < .75$  were used to simulate the three calorimeter triggers. The resulting cross sections are shown in fig. 3 [11] exhibiting slightly stronger transverse momentum dependencies than the calorimeter results. The solid line is obtained when correcting for charged particle losses and assuming that 1/3 of the energy emitted into the solid angle covered is due to undetectable  $\pi^0$ .

A preliminary planarity analysis of the energy deposited in the calorimeter (not shown, [8]) gives no evidence for jet structure in agreement with the cluster model.

---

(\*) It should be pointed out that a good simulation of spectator jets is not trivial.

Finally the average charged event multiplicity as measured with the streamer chamber for  $\pi^+p$  interactions is displayed in fig 4 as function of  $\Sigma p_T$  for  $2\pi$  trigger data. Again one finds that the data (reaching  $n_{ch} \sim 25 = 3\langle n_{ch} \rangle$  for  $\Sigma p_T > 8$  GeV/c at  $\sqrt{s} = 24$  GeV) can be reproduced by the cluster model. The QCD model of constituent scattering predicts much smaller charged multiplicities independent of  $\Sigma p_T$  above 2 GeV/c. This is easily explained on the basis of 4-jet structure:

$$\langle n_{ch}(\sqrt{s}, \Sigma p_T) \rangle = \underbrace{\langle n_{ch}(\sqrt{s} - 2E_{jet}) \rangle}_{2 \text{ spectator jets}} + \underbrace{\langle n_{ch}(2E_{jet}) \rangle}_{2 \text{ high } p_T \text{ jets}}.$$

Inserting multiplicities measured in  $e^+e^-$  interactions [12] and keeping in mind that  $2E_{jet} = \Sigma p_T$  for real jet events detected in the calorimeter one roughly verifies the QCD prediction of fig. 4.

Since the QCD prediction is not borne out by the calorimeter data it is worthwhile noting that in a single particle experiment such a trend is indeed observed. Fig. 5 shows the preliminary, uncorrected charged event multiplicities as function of the transverse momentum of a single particle emitted at a polar angle  $\theta = 52^\circ$  in pp collisions at  $\sqrt{s} = 63$  GeV [11]. The losses of about two charged particles per event were checked to be independent of  $p_T$ . The relatively small values of  $\langle n_{ch} \rangle$  and its independence of  $p_T$  actually support the simple 4-jet picture of hard scattering processes; here of course the trigger jet consists of about two particles only, such that  $\langle n_{ch}(2E_{jet}) \rangle = 1/2 \langle n_{ch}(2E_{jet}) \rangle + 2$  and  $E_{jet} = \Sigma p_T(\text{trigger})$ ,  $.6 < a < .9$ , [5].

This section can be summarized by stating that there is no evidence that present calorimeter experiments, which trigger on multiparticle systems, yield a substantial number of events with genuine jet structure. The data are dominated by normal inelastic events with rather high multiplicities. However, "absence of evidence is not evidence for absence" [13]. To demonstrate the truth of this saying, a typical 4-jet event as reconstructed in the SFM by the CDDHW Collaboration is shown in fig. 6 together with a schematic top view of the wire planes.

The eve  
P<sub>T</sub> jet phys  
balance of  
central par  
relative ene  
cross secti

### 3. INCLUSIVE SP

Measur  
the ISR [14]  
then exper  
at 90°. New  
 $\theta = 50^\circ - 54^\circ$   
(fig. 7). I  
magnitude f  
 $\pi^0$  spectrum  
show a flatt

Some or  
forward angl

(a) A measu  
transve  
subproc  
 $\theta = 90^\circ$   
trend wa

(b) High p<sub>T</sub>  
collidi  
of part  
transver

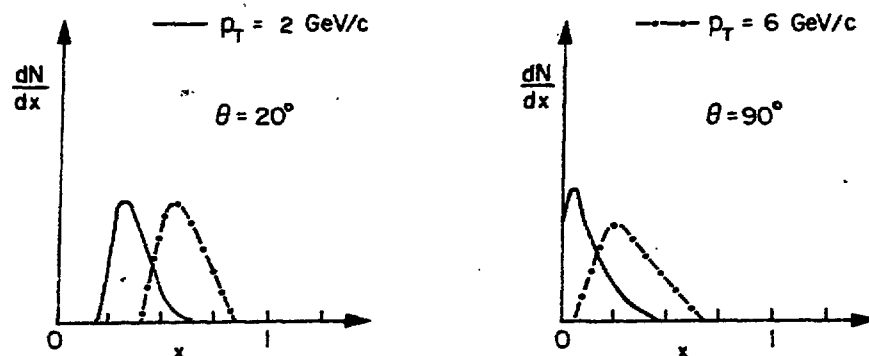
The eventual contribution of future calorimeter experiments to high  $p_T$  jet physics, even at ISR or collider energies, depends on a delicate balance of jet opening angle, solid angle of the calorimeter, production of central particles uncorrelated with two high  $p_T$  jets and the unknown relative energy dependence of high  $p_T$  jet production and of topological cross sections (e.g. for  $n_{ch} = 3\langle n_{ch} \rangle$ ).

### 3. INCLUSIVE SPECTRA AND PARTICLE RATIOS

Measurements of inclusive high  $p_T$   $\pi^0$  spectra at  $\theta = 90^\circ$  performed at the ISR [14] provided first evidence for hard scattering mechanisms. Since then experimental efforts were mainly concentrated on spectra of particles at  $90^\circ$ . New preliminary results for Cerenkov identified pion production at  $\theta = 50^\circ$ - $54^\circ$  were obtained by the CCDHW Collaboration [11] with the SFM (fig. 7). The cross sections were measured over about 7 orders of magnitude from  $p_T = 3$  GeV/c up to  $\approx 11.5$  GeV/c. For comparison a  $\pi^0$  spectrum from the CCOR Collaboration [15] is also given. All spectra show a flattening toward larger transverse momenta.

Some of the reasons to perform a high  $p_T$  experiment by triggering at forward angles are:

- (a) A measurement of the  $\theta$ -dependence of particle production at high transverse momentum puts constraints on models describing hard subprocesses: fig. 7 shows e.g. that the ratio  $\sigma(pp \rightarrow \pi^0 X, \theta = 90^\circ) / \sigma(pp \rightarrow \pi^\pm, \theta = 52^\circ)$  gets larger with increasing  $p_T$ . Such a trend was already found earlier [16].
- (b) High  $p_T$  experiments try to probe the valence quark structure of the colliding hadrons. The diagram below [17] shows the distribution in  $x$  of partons contributing to the production of pions with fixed transverse momenta:



It is clear that at  $\theta = 90^\circ$  only for  $p_T \gtrsim 6$  GeV/c mesons are due to partons from the valence region ( $x \gtrsim .3$ ). On the other hand at a trigger angle of  $20^\circ$  mainly valence partons are involved in the hard process even for  $p_T = 2$  GeV/c. This indicates that probing the valence quark region requires either very high transverse momenta at  $\theta = 90^\circ$  (however,  $d\sigma/dp_T$  ( $p_T = 6$  GeV/c) =  $d\sigma/dp_T$  ( $p_T = 2$  GeV/c)  $\times 10^{-4}$  at  $\theta = 90^\circ$  and  $\sqrt{s} = 63$  GeV) or smaller polar angles for the lower  $p_T$  range (here,  $d\sigma/dp_T$  ( $\theta = 20^\circ$ ) =  $d\sigma/dp_T$  ( $90^\circ$ )  $\times 0.5$  at  $p_T = 2$  GeV/c and  $\sqrt{s} = 63$  GeV!). Choosing the latter configuration offers larger cross sections at lower transverse momenta to study a given  $x$  range of constituents.

In fig. 8 preliminary results [11] show a rise with increasing transverse momentum of the relative  $\pi^+$  and  $\pi^-$  cross sections (" $\pi^+/\pi^-$ -ratio"). The cross sections were measured at slightly different polar angles, therefore these data need some further small upward corrections. Since single particle triggers carry most of the original (valence) parton momentum ( $z \gtrsim .6$ ) and e.g.  $D_u^+(z) \gg D_d^+(z)$  for  $z > .6$  [1], a naive prediction for the  $\pi^+/\pi^-$  ratio is

$$\frac{\pi^+(ud)}{\pi^-(du)} = \frac{J(\bar{u}(x), q(x), \frac{d\sigma}{dt}, D_u^+)}{J(\bar{d}(x), q(x), \frac{d\sigma}{dt}, D_d^+)} \gtrsim 2$$

using  $p_T$   
since  
close  
than  
is t  
prod

Now  
to t  
trans  
it a  
qua  
over  
of p  
90  
ass  
e (h  
eV!  
over  
negativ

From  
( $\pi^-$ /  
to d  
( $\pi^-$ /  
the  
for

fra  
do n  
mome  
valu  
[20]

(\*)

using  $D_u^+(z) = D_d^-(z)$ . This ratio is also expected to rise with  $p_T$ , since  $u(x)/d(x) \sim (1-x)^{-1}$  [18] rises with  $x$  and since  $p_T$  and  $\langle x \rangle$  are closely related (diagram p.17). The experimental ratio is, however, smaller than 2 for  $p_T \lesssim 8$  GeV/c not in agreement with the simple ansatz. A way out is to assume a substantial contribution of gluons (see also fig. 1) to pion production at lower  $p_T$ :

$$\frac{\pi^+}{\pi^-} = \frac{J(g(x), q(x), \frac{d\sigma}{dt}, D_g^+) + J(u(x), q(x), \frac{d\sigma}{dt}, D_u^+)}{J(g(x), q(x), \frac{d\sigma}{dt}, D_g^-) + J(d(x), q(x), \frac{d\sigma}{dt}, D_d^-)}$$

Now the ratio turns out to be much smaller than 2 at intermediate  $p_T$  due to the additional gluon terms<sup>(\*)</sup>. It increases at larger values of the transverse momentum due to the dominance of the  $u^-$  and  $d^-$  quark terms, i.e. it approaches the values predicted by the previous relation.

Fig. 9 shows the fraction of  $\pi^-$  among negative secondaries as function of  $p_T$ . Since  $\bar{p}$ -production is negligible in this kinematic range [19] and assuming that all  $K^- (= s\bar{u})$  are due to gluon fragmentation, one has

$$\frac{\pi^-}{\text{negatives}} = \frac{\pi^-}{\pi^- + K^-} = \frac{[J(g(x), q(x), \frac{d\sigma}{dt}, D_g^-) + J(d(x), q(x), \frac{d\sigma}{dt}, D_d^-)]}{[J(g(x), q(x), \frac{d\sigma}{dt}, D_g^-) + J(d(x), q(x), \frac{d\sigma}{dt}, D_d^-) + J(g(x), q(x), \frac{d\sigma}{dt}, D_g^{K^-})]}$$

From a dominance of gluon terms and from  $D_g^{K^-}(z) = 1/2 D_g^-(z)$  [3] one expects  $(\pi^-/\text{negatives}) < 1$  at  $p_T \lesssim 4$  GeV/c, whereas the  $d^-$  quark terms are supposed to dominate at higher values of  $p_T$  yielding an asymptotic value of  $(\pi^-/\text{negatives}) = 1$ . This is in good agreement with the data.

The argument that e.g. a  $\pi^+$  at large  $p_T$  is predominantly due to a fragmenting  $u^-$  quark holds, of course, only if vector mesons like  $\rho$ ,  $\omega$  ... do not contribute significantly to pion production at large transverse momenta via the chain  $u^- \rightarrow \rho \rightarrow \pi^+$ . Even if one finds relatively large values for the relative  $\pi$  and vector meson cross sections, e.g.  $\omega^0/\pi^0 = 0.8$  [20] at  $p_T \gtrsim 5$  GeV/c, only about 3-5% of the particles at a given value

(\*) Sea (anti)-quarks would also give a ratio of about 1; their contribution should be small, since they contribute only little to the structure function for  $x \gtrsim 0.3$  [2].

$p_T = 6$  GeV/c

$\theta = 90^\circ$

ons are due to  
d at a trigger  
rd process even  
quark region

however,

$90^\circ$  and

e (here,  $d\sigma/dp_T$   
eV!). Choosing  
lower transverse

ncreasing

.s

ily different  
upward

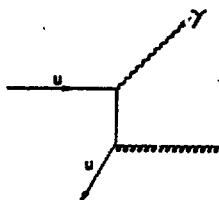
the original

for  $z > .6$

of transverse momentum are due to vector meson decay. This is a reflection of sort of a trigger bias: only in rare very asymmetric vector-meson decays most of the resonance momentum is transferred to a single particle.

Apart from that, resonance production at high  $p_T$  is interesting in itself since it may lead to a determination of fragmentation functions of quarks and gluons into resonances. Good data on this subject are rather scarce so far.

An important prediction of QCD is the existence of single photon production at high  $p_T$  mainly due to the process  $ug \rightarrow \gamma u$ :



A precise measurement of the cross section would bear on a detailed knowledge of the gluon structure function. Unfortunately the experiments are difficult due to the abundance of background from  $\pi^0$ ,  $\eta$  and  $\eta'$  decays.

Some measurements of  $\gamma/\pi^0$  as obtained by the A<sup>2</sup>BC Collaboration [21] are displayed in fig. 10; these ratios are larger than the CCOR findings [22]. From the equation

$$\frac{\gamma}{\pi^0} = \frac{J(g(x), u(x), \frac{d\sigma}{dt}(\gamma), \delta(1-z))}{J(q(x), q(x), \frac{d\sigma}{dt}(\pi^0), D_q^{\pi^0}(z))}$$

one concludes that the small value of  $\gamma/\pi^0$  at small  $p_T$  is a reflection of the ratio  $\alpha_{QED}/\alpha_s (\frac{d\sigma}{dt}(\gamma) \sim \alpha_{QED}\alpha_s$  and  $\frac{d\sigma}{dt}(\pi^0) \sim \alpha_s^2$ ). The increase with  $p_T$  of  $\gamma/\pi^0$  indicates that the  $\pi^0$  is due to parton fragmentation ( $D_q^{\pi^0}(z)$ ) whereas the photon carries all the energy ( $\delta(1-z)$ ) transferred at the upper vertex in the above diagram. In other words: the increase with  $p_T$  of  $\gamma/\pi^0$  is a measure of the trigger bias (sect. 2).

The diag  
accompanied c  
away jets sho  
First exper

#### 4. TOWARD JETS

Additio  
trigger parti  
shows the no  
emitted into  
 $\pi^+$  and  $K^-$  tri  
features of t

(a) There is  
taken as

(b) The dis  
expected  
due to t  
with an  
fragment

(c) The rati  
(excludi  
expected

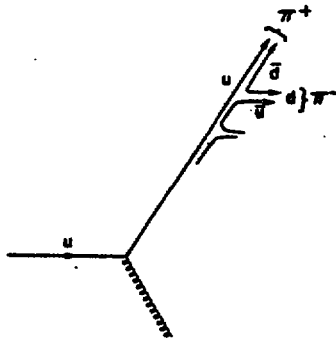


The diagram above implies, that single photons are not frequently accompanied close in phase space by other particles and that most of the away jets should be due to u-quarks ( $\gamma$  couple to electric charges). First experimental results are compatible with this picture [23].

#### 4. TOWARD JETS

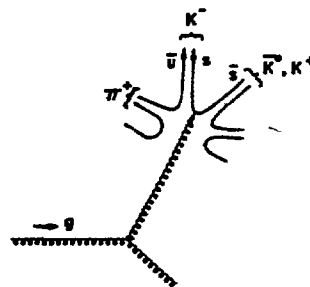
Additional particles alongside the trigger (toward jet) and the trigger particle are supposed to originate from the same parton. Fig. 11 shows the normalized rapidity distributions for particles with  $p_T > 1$  GeV/c emitted into an azimuthal wedge of  $\pm 25^\circ$  around the direction ( $\phi = 0$ ) of  $\pi^+$  and  $K^-$  triggers with  $p_T > 4$  GeV/c and  $p_T > 6$  GeV/c [11]. The main features of these data, obtained by the CCDHW Collaboration, are the following:

- (a) There is a strong enhancement above the inclusive yield. This is taken as a proof for jet structure.
- (b) The distributions are centred at the trigger rapidity. This is expected, if the trigger momentum is nearly identical to the jet axis due to the trigger bias. The width of the distribution is consistent with an average transverse momentum of  $\sim 400$  to  $500$  MeV/c of the jet fragments relative to the jet axis.
- (c) The ratio of negative to positive charges carried by the jet fragments (excluding the trigger particle) is about 1.6 for  $\pi^+$  triggers, as expected qualitatively from u-quark fragmentation:



It is easier to produce a particle with negative (opposite) charge than with positive (equal) charge close in phase space to the positive trigger particle. It was already mentioned that vector mesons decays can be neglected, therefore they cannot be made responsible for this charge asymmetry.

In fig. 11(b) the charge ratio for  $K^-$  triggers is equal to 3, larger than the corresponding ratio for  $\pi^+$  triggers. This means that the sum of the charges of the  $K^-$  and the second fastest particle in the jet is more often neutral than for  $\pi^+$  triggers, suggesting that  $K^-$  are fragments of neutral parton, i.e. gluons. A pictorial representation of this explanation is given below:



The diagram also suggests that  $K^0$  should frequently be produced in the toward jet. Actually, preliminary results based upon reconstructed  $K_S^0$  [11] show that the yield of  $K_S^0$  correlated with  $K^-$  triggers is about a factor 2 higher than the corresponding value for triggering  $\pi^-$ . This is certainly very indicative of gluons dominating high  $p_T$   $K^-$  production.

Most of the previous high  $p_T$  experiments gave evidence for toward jets [4]. The recent experiment performed by the CERN Collaboration allows now for the first time to analyze in detail the quantum number (charge, strangeness and baryon number) content and phase space structure of toward jets for different triggering particles ( $\pi^\pm$ ,  $K^\pm$ ) at very high transverse momenta. Gluon effects have already shown up. It should be possible to determine quantitatively the relative contributions of various partons from the valence region to jet production. Also an experimental evaluation of the trigger bias, predicted to be  $p_T$  dependent [5], seems to become feasible.

5. AWA: charge  
itive  
jet s can  
bea s char  
( $\phi$  =  
and  
mom to 3,  
obt at the  
 $\theta$  = jet i  
 $P_T$  > ragen  
mome this

(a)

(b)

(c)

uced in  
structe  
is abou  
rg  $\pi^-$ .  
- produ

for to  
laborat  
tum num  
ace st:  
at very  
It shou  
ions of  
experim

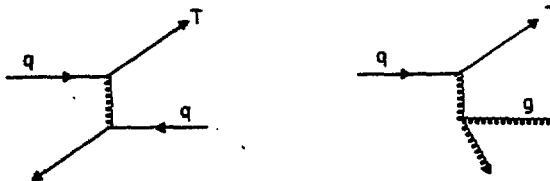
aver  
the

t [5],

5. AWAY JETS

In the hard-scattering picture a second jet of parton fragments (away jet) should emerge from the parton-parton collision at large angles to the beam axis and at opposite azimuth ( $\phi = 180^\circ$ ) to the trigger particle ( $\phi = 0^\circ$ ). Away jets have been found in most of the previous experiments and it has been shown that the effects seen are not just a consequence of momentum conservation [4]. One example of recent results on away jets obtained by the CCDHW Collaboration is given in fig. 12 for  $\pi^+$  triggers at  $\theta = 50^\circ$ . It shows the normalized rapidity distributions of secondaries with  $p_T > 1 \text{ GeV}/c$  at  $\phi = 180^\circ \pm 25^\circ$  for two values of the  $\pi^+$  transverse momentum. The dominant characteristics of the data are:

- (a) A strong excess of particles above the inclusive yield. This is considered as a proof for jet structure.
- (b) The distribution is wider (FWHM  $> 2.0$  unit of rapidity) than that for the toward jets. This can be explained by a  $\theta$  dependence for away jet production such that the observed distribution is a superposition of narrow structures similar to those given in fig. 11. It should be mentioned here that so far calorimeter experiments were only sensitive to away jet fragments with  $|y| < 1$ .
- (c) For  $\pi^+$  triggers with transverse momenta above  $6 \text{ GeV}/c$  the ratio of charges carried by away jet fragments is different for the two rapidity hemispheres:  $y < 0$ : positive charge/negative charge = 1.35;  $y > 0$ : positive charge/negative charge = 1.0. This trend can be understood from the diagram below:



It illustrates that the quark-quark rest system coincides on the average with the proton-proton centre of mass system; therefore one finds the trigger particle and the away jet predominantly in opposite rapidity

hemispheres ("back-to-back"). In case of gluon-quark scattering the gluon-quark rest system moves along the quark line of flight. Triggering on a valence quark fragment (here  $\pi^+$ ) one should find the away jet (due to a gluon) mainly in the rapidity hemisphere of the trigger particle (back-to-antiback). This holds if the gluon structure function has a stronger  $x$  dependence than the quark structure functions [1]. In this case one expects for the back-to-back configuration more positive than negative charges in the away jet, since there are more valence  $u$ -quarks than valence  $d$ -quarks in a proton. For the back-to-antiback situation there is an equal amount of both charges from gluon fragmentation<sup>(\*)</sup>.

These subprocesses ( $qg \rightarrow qg$ ,  $qq \rightarrow qq$ ) cannot easily be disentangled when triggering on particles at  $\theta = 90^\circ$  because of the polar angle symmetry of all away jets.

Further support of the above picture comes from fig. 13 which shows distributions of  $x_E = (\vec{p}_T(\text{away jet fragm.}) \cdot \vec{p}_T(\text{trigger})) / |\vec{p}_T(\text{trigger})|$ , i.e. the fraction of the trigger's transverse momentum compensated by an away jet fragment. Asymptotically, for  $\vec{p}_T(\text{trigger}) = \vec{p}_T(\text{toward jet}) = \vec{p}_T(\text{away jet})$ ,  $x_E$  is equivalent to  $z$  (sect. 1) thus  $x_E$  distributions are closely related to fragmentation functions  $D_q^h(z)$ . In fig. 13 the  $x_E$  distribution for particles with  $y > 0$  and  $\phi = 180^\circ \pm 25^\circ$  (back-to-antiback) in events with  $\pi^+$  triggers with  $p_T > 4$  GeV/c is steeper than the corresponding distribution for  $y < 0$ , as expected from gluon fragmentation<sup>(\*\*)</sup> and quark fragmentation, respectively.

If both quarks and gluons fragment via different processes ( $D_g^h(z) \neq D_q^h(z)$ ) into away jets with relative contributions which depend on the transverse momentum of the triggering particle, it is difficult to understand the experimental indications for  $x_E$ -scaling [4], i.e. the independence of  $d\sigma/dx_E$ , summed over both rapidity hemispheres, of the transverse momentum of the trigger and of  $\sqrt{s}$ .

(\*) This is also true for sea (anti)-quarks.

(\*\*) This is not expected from sea (anti)-quarks!

Further jets are expected to have properties of away jet separation) means of a lines is in

## 6. SPECTATOR JET

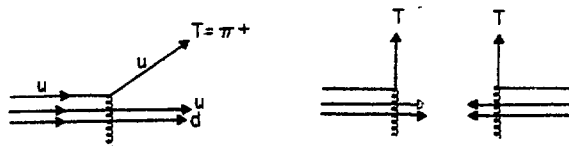
The spectra of the constituents e.g. a high scattered valence fragments are triggering correlation

Among the undetected not many  $\Delta^{++}$  fragments produced [17,24]. Correlation summarized by  $y > 3.0$ . These correlations

Further analyses of quantum number content and event structure of away jets are expected to add valuable information, especially on gluon properties. In the GCDHW experiment it is possible to identify a fraction of away jet particles by either a time-of-flight method ( $\pi/K/p$  separation) or by reconstruction of decays of short lived particles or by means of a liquid argon calorimeter ( $\pi^0$  detection). Work along these lines is in progress.

## 6. SPECTATOR JETS

The spectator jets (see diagram on p.11) are due to hadronization of the constituents not affected by the hard parton-parton interaction. If, e.g. a high  $p_T \pi^+$  is detected in pp collisions and which is a fragment of a scattered valence u-quark, a ud system remains "untouched". The ud fragments are emitted into the rapidity hemisphere of the high  $p_T \pi^+$ , when triggering off  $90^\circ$ . The diagram below shows that there is no net correlation between a trigger particle at  $90^\circ$  and the spectator systems:



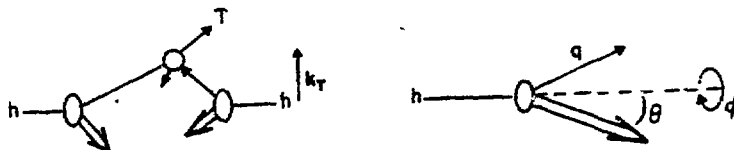
Among the ud fragments the same number of  $\pi^+$  and  $\pi^-$  should be found, but not many  $\Delta^{++}$  (= uuu). A  $\pi^-$  trigger signals that a remaining uu system fragments producing mainly  $\pi^+$ , little  $\pi^-$  and a substantial number of  $\Delta^{++}$  [17,24]. The experimental results obtained so far [24,25] can be summarized by stating compatibility with the simple picture outline above. Correlation studies of this type require a forward spectrometer covering  $y > 3.0$ . This is why up to now only a few experiments were able to measure these correlations.

Measurements of spectator fragments are not only useful to gain a more complete picture of QCD subprocesses, they also yield insight into di-quark fragmentation processes, like

$$ud + \pi^+, \pi^-, K^+, K^-, \rho, \Lambda \text{ or } uu + \pi^+, K^+, \rho, \Lambda^{++} \dots$$

More work in this field is necessary, also with different beam particles, as well as a comparison with target fragmentation in deep inelastic lepton scattering and with spectator fragmentation in Drell-Yan processes [26]. One difficulty has to be mentioned here: The total diquark energy  $\sqrt{s}_{qq}$  and its fractional momentum  $x_{qq}$  has to be known in order to determine the diquark fragmentation function  $D_{qq}^h(x_{qq})$ . Since even for a fixed value of the transverse momentum of the trigger particle the fractional momenta  $x$  of both active partons are not uniquely defined (diagram p.17),  $x_{qq}$  is not known exactly for a given event, either. Thus the extraction of diquark fragmentation functions require detailed Monte-Carlo calculations.

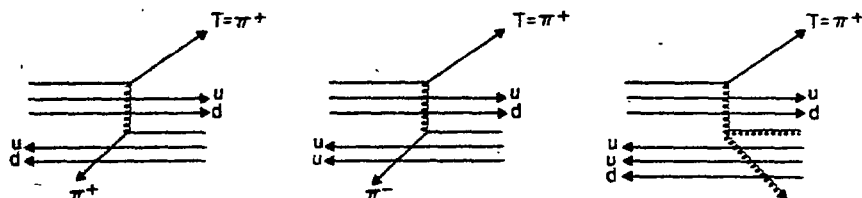
A different type of spectator studies deals with the transverse motion of partons (see also sect. 7) which is due to their binding inside the proton and to gluon bremsstrahlung. Triggering on a single particle at high transverse momentum means selecting preferentially those configurations in which the transverse momenta  $k_T$  of the active partons point toward the trigger:



Hence the spectator jets recoil causing asymmetries in both the polar angle and azimuthal distributions of jet fragments. A study of this effect by the CCHK Collaboration [27] gave evidence for the first time for rather large values of  $k_T$ . It was also shown that large parton transverse momenta can make experimental and theoretical inclusive spectra (fig. 1) agree for  $p_T \lesssim 4 \text{ GeV}/c$  [27].

The most recent measurements of asymmetric distributions from spectator fragments (protons of  $x > 0.4$ ) are shown in fig. 14 for trigger pions at  $\theta = 30^\circ$  with transverse momenta up to 5 GeV/c produced in pp collisions at  $\sqrt{s} = 63$  GeV [28]. The increase of the asymmetries observed at larger transverse momenta of the triggering particles is expected from stronger gluon radiation of more energetic partons. Equivalent results were reported in ref. [29].

One extension of jet studies is obvious: double high  $p_T$  experiments as given in the diagram below:



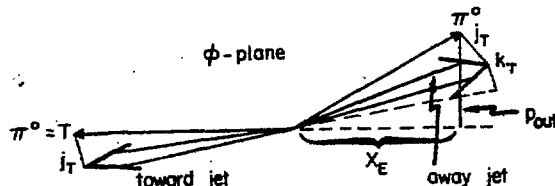
By varying the identity of the two high transverse momentum particles and their relative configuration (back-to-back or back-to-antiback) the contribution of various parton-parton subprocesses can be enhanced. To fully exploit this method a simultaneous analysis of all 4 jets is desirable.

## 7. MULTIJETS?

Leaving the safer ground of 4-jet physics one might now venture into the question of multijet ( $\geq 5$ ) production in high  $p_T$  reactions. Theoretical estimates suggest [30] that these processes may occur more frequently than 3-jet production in  $e^+e^-$  annihilations.

The first experimental indication for these processes is due to the CS Collaboration [31]. Fig. 15 shows the spectrum of particles produced at  $\phi = 90^\circ \pm 15^\circ$  in association with triggering  $\nu^0$  at  $\phi = 0^\circ$  and  $p_T > 5$  GeV/c normalized to the inclusive spectrum. The inclusive spectrum is not proportional to  $e^{-6p_T}$  which is taken as evidence for hard processes. Since two spectra exhibit the same shape, also the spectrum at  $\phi = 90^\circ$

Fig. 16 shows the average value of the transverse momentum component  $P_{out}$  perpendicular to the scattering plane as function of  $x_E$  for opposite side  $\pi^0$  in events with a triggering  $\pi^0$  at large transverse momentum. The experiment was performed by the A<sup>2</sup>BC Collaboration. The relevant quantities are defined in the diagram:



The magnitude of  $p_{out}$  reflects effects of parton transverse momenta  $k_T$  which cause an acoplanarity of the two high  $p_T$  jets and of the transverse momenta  $j_T$  of jet fragments relative to the jet axis:

$$\langle p_{\text{out}}^2 \rangle = \langle j_T^2 \rangle + x_F^2 (\langle k_T^2 \rangle + \langle j_T^2 \rangle)$$

The sudden increase of  $\langle k_T \rangle$  from  $\sim 1.0$  GeV/c (dashed lines) to  $\langle k_T \rangle \sim 1.7$  GeV/c for the largest values of the transverse momentum of the triggering  $\pi^0$  could be evidence for an apparent broadening of the away jet due to emission of a gluon jet along the away jet.

The most recent hint for multijet production comes from a cluster analysis [32] of CCOR data;  $\pi^0$  with  $p_T > 6$  GeV/c were used for triggering. It is claimed that about 30% of all events contain a third jet with  $\langle n_{ch} \rangle \sim 3$ , total transverse momentum of  $\sim 2.2$  GeV/c and which are confined by the the detector acceptance to  $|\eta| \lesssim .7$ . They mainly populate the  $\phi$  hemisphere of the away jet and can only be distinguished from the away jet if they are separated by  $\gtrsim 0.7$  rad. The field of multijet searches in high  $p_T$  reactions is still in its infancy. It seems to be worthwhile to pursue it with more effort, making use of detectors which cover large solid angles. It is also important to have a precise momentum determination for the few particles which are responsible for the effects mentioned above.

## 8. SUMMARY AND C

It was an experimental out ide

Results  
from toward a  
are consiste  
quarks, to ha

More det  
content of 4-  
should yield  
near future.  
three-gluon v

Quantum  
energy-moment  
number effec-  
covering lar

More ex  
particles at  
information.

It was d  
so-called tri  
eventually st

The tri  
experiments.  
(jet)-to-bac  
energies whe  
much larger [



## 8. SUMMARY AND CONCLUSIONS

It was tried to give a simple but comprehensive review of recent experimental activities in the field of high transverse momentum phenomena.

Results on ratios of single particle cross sections, on charge ratios from toward and away jets and on the momentum distribution in away jets are consistent with a strong contribution of gluons, in addition to valence quarks, to hard processes.

More detailed analyses of momentum structure and quantum number content of 4-jet events, especially from double high  $p_T$  experiments, should yield rich information on parton-parton subprocesses in the very near future. One hopes to find direct experimental evidence for the three-gluon vertex and to determine gluon properties.

Quantum number correlations have the advantage of not being subject to energy-momentum conservation. A fairly complete investigation of quantum number effects require substantial particle identification and detectors covering large solid angles.

More experimental effort should be devoted to triggering on single particles at forward angles; symmetrical configurations contain less information.

It was demonstrated that in single particle high  $p_T$  experiments the so-called trigger bias helps to "tag" special QCD subprocesses and to eventually study diquark fragmentation.

The trigger bias is to some extent avoided by calorimeter experiments. Present experiments of this type suffer from serious signal (jet)-to-background problems. One way out may be offered by higher energies where the jet yield at very large transverse momentum should be much larger [33].

The success in the field of high  $p_T$  physics of future calorimeter experiments depends on the unknown relative energy dependence of jet cross section, jet opening angle and of topological cross sections for very large charged multiplicities ( $n_{ch} \gtrsim 3\langle n_{ch} \rangle$ ).

But already at ISR energies a number of interesting new questions in addition to those discussed above deserve further consideration. To list just a few subjects: multijet production, high  $p_T$  (anti)-baryon production, nuclear effects at large transverse momentum.

So, after nearly 10 years of high  $p_T$  physics at the ISR, there remains a rich field for further and more ambitious experimentation.

#### Acknowledgements

This was an opportunity to present part of the recent results of the CCDHW Collaboration. I thank my colleagues for their contributions and particularly Dr. H.G. Fischer, Dr. K. Pretzl, Dr. P. Seyboth and Prof. R. Sosnowski for discussions. I am grateful for the hospitality of our Polish colleagues and friends.

#### REFERE

[1] E

[2] S

[3] J

[4] (

(

(

(

[5] S

[6] M

[7] .

[8]

[9] .

[10]

[11]

[12]

[13]

[14]

[15]

[16]

[17]

[18]

[19]

[20]

[21]

[22]

[23]

[24]

[25]

[26]

[27]

[28]

[29]

[30]

[31]

[32]

## REFERENCES

- [1] E. Reya, Phys. Rep. 69 (1981) 197.
- [2] See e.g. H.J. Lubatti, CERN/EP 81-64.
- [3] J.F. Owens, E. Reya and M. Glück, Phys. Rev. D18 (1978) 1501.
- [4] (a) M. Jacob, Proceedings of the Int. Conf. on High Energy Phys., Geneva, 1979, p. 473;  
 (b) R. Stroynowski, Proceedings of Summer Institute on Particle Physics, SLAC-224, p. 93.  
 (c) L. Di Lella, CERN/EP 79-145.  
 (d) P. Darriulat, CERN/EP 80-16.
- [5] S.D. Ellis and M.B. Kislenger, Phys. Rev. D9 (1974) 2027.
- [6] M. Jacob and P.V. Landshoff, Nucl. Phys. B113 (1976) 395.
- [7] W. Selove, Proceedings of the Moriond Meeting, Les Arcs (1979).
- [8] Bari-Krakow-Liverpool-MPI Munich-Nijmegen Collaboration, presented by K.P. Pretzl at the XVI Rencontre de Moriond, 1981.
- [9] H.J. Frisch, Proceedings of the Summer Institute on Particle Physics, SLAC-224, p. 461.
- [10] K.P. Pretzl and P. Seyboth, private communication.
- [11] CERN-Collège de France-Dortmund-Heidelberg-Warsaw Collaboration, preliminary results.
- [12] See e.g. P. Duinker, DESY 81-012.
- [13] Unknown author, due to A. Wróblewski
- [14] British-Scandinavian Collaboration, B. Alper et al., Phys. Lett. 44B (1973) 521;  
 Saclay-Strasbourg Collaboration, M. Banner et al., Phys. Lett. 44B (1973) 537;  
 CERN-Columbia-Rockefeller Collaboration, F.W. Büsser et al., Phys. Lett. 46B (1973) 471.
- [15] CERN-Columbia-Oxford-Rockefeller Collaboration, A.L.S. Angelis et al., Phys. Lett. 79B (1978) 505.
- [16] Stony-Brook-Pisa Collaboration, D. Lloyd Owen et al., Phys. Rev. Lett. 45 (1980) 89.
- [17] H.G. Fischer, Talk at the Third Warsaw Symposium, Jodłowy Dwór, Poland, 1980, CERN/EP 80-6, published in Nukleonika 26 1981 .

## REFERENCES (Cont'd)

- [18] Aachen-Bonn-CERN-Munich-Oxford Collaboration, P. Allen et al., Phys. Lett. 103B (1981) 71.
- [19] British-Scandinavian Collaboration, B. Alper et al., Nucl. Phys. B100 (1975) 237.
- [20] Athens-Brookhaven-CERN Collaboration, M. Diakonou et al., Phys. Lett. 89B (1980) 432.
- [21] Athens-Brookhaven-CERN Collaboration, M. Diakonou et al., CERN/EP 80-2.
- [22] CERN-Columbia-Oxford-Rockefeller Collaboration, A.L.S. Angelis et al., Phys. Lett. 98B (1981) 115.
- [23] Athens-Brookhaven-CERN-Copenhagen-Lund-Rutherford-Tel Aviv Collaboration, M. Diakonou et al., CERN/EP 80-3 and [22].
- [24] CERN-Collège de France-Heidelberg-Karlsruhe Collaboration, Nucl. Phys. B156 (1979) 309.
- [25] Aachen-CERN-Harvard-Munich Univ.-Northwestern-Riverside Collaboration, D. Hanna et al., Phys. Rev. Lett. 46 (1981) 398.
- [26] B. Pietrzyk, Properties of Hadrons Associated with Lepton-Pair Production, presented at the Moriond Workshop on Lepton-Pair Production, Les Arcs, France, January 1981.
- [27] CERN-Collège de France-Heidelberg-Karlsruhe Collaboration, M. Della Negra et al., Nucl. Phys. B127 (1977) 1.
- [28] Aachen-CERN-Harvard-Munich Univ.-Northwestern-Riverside Collaboration, D. Hanna et al., submitted to the XXth International Conference on High Energy Physics, Madison, U.S.A. July 1980.
- [29] Caltech-Los Angeles-Fermilab-Chicago-Indiana Collaboration, C. Bromberg et al., CALT-68-761.
- [30] T. Gottschalk, E. Monsay and D. Sivers, Phys. Rev. D21 (1980) 1799.
- [31] Athens-Brookhaven-CERN-Syracuse Collaboration, C. Kourkouvelis et al., Phys. Rev. Lett. 45 (1981) 966.
- [32] CERN-Saclay Collaboration, A.G. Clark et al., Nucl. Phys. B160 (1979) 397.
- [33] J.S. Wallace-Hadrill, Ph.D. Thesis, Corpus Christi College, 1981.
- [34] R. Horgan, quoted by M. Jacob [4(a)].

## FIGURE CAPTION.

- Fig. 1 Invar  
calc  
the B10
- Fig. 2 Non-i  
as ob  
trans P 80  
calor  
predi t al
- Fig. 3 Prel  
|y| <  
funct Phy  
the v atio  
line  
ass
- Fig. 4 Total  
the f
- Fig. 5 Uncor  
trans atio  
e on
- Fig. 6 A 4-j  
scatt 99.  
the w t
- Fig. 7 Invar  
angle 1979  
Colla
- Fig. 8 Prel  
funct
- Fig. 9 Fract  
θ = 54

## FIGURE CAPTIONS

- Bl00
- Lett.
- P 80-2.
- et al.,
- Phys.
- ation,
- ation,  
e on
- 99.
- t
- 1979)
- Fig. 1 Invariant  $\pi^0$  cross section as function of  $p_T$ ; a theoretical calculation of various QCD subprocesses is given in addition to the experimental data (see [3]).
- Fig. 2 Non-invariant cross sections integrated over  $|y| \lesssim .75$  and  $\Delta\phi$  as obtained by the BKLMM Collaboration as function of the total transverse momentum  $\Sigma p_T$  deposited in the sectors of the calorimeter used for 3 different triggering modes. Model predictions are also given.
- Fig. 3 Preliminary non-invariant cross sections integrated over  $|y| < .75$  and  $\Delta\phi$  for the production of charged particles as function of their total transverse momentum  $\Sigma p_T$  contained in the various  $\phi$ -regions indicated. For  $\Delta\phi = 2\pi$  the solid line includes corrections for charged particle losses and for an assumed 33% contribution of neutrals to the energy produced.
- Fig. 4 Total charged event multiplicity as function of  $\Sigma p_T$  deposited in the full calorimeter and model predictions.
- Fig. 5 Uncorrected charged event multiplicities as function of the transverse momentum of a single particle emitted at  $\theta \sim (52 \pm 2)^\circ$ .
- Fig. 6 A 4-jet event as reconstructed in the SFM and projected onto the scattering plane. It is superimposed on a schematic top view of the wire chambers; the single particle trigger is labelled T.
- Fig. 7 Invariant  $\pi^+$  and  $\pi^-$  cross sections as function of  $p_T$  for polar angles  $\theta = 52^\circ$ .  $\pi^0$  cross sections at  $\theta = 90^\circ$  from the CCOR Collaboration are also given.
- Fig. 8 Preliminary  $\pi^+/\pi^-$  ratio measured by the CCDHW Collaboration as function of  $p_T$  for  $\theta = 52^\circ$  and  $\sqrt{s} = 63$  GeV/c.
- Fig. 9 Fraction of  $\pi^-$  among negative secondaries as function of  $p_T$  for  $\theta = 54^\circ$  and  $\sqrt{s} = 63$  GeV/c.

## FIGURE CAPTIONS (Cont'd)

- Fig. 10  $\gamma/\pi^0$  ratio as function of  $p_T$  as measured by the A<sup>2</sup>BC Collaboration at three ISR energies.
- Fig. 11 Preliminary, normalized rapidity distributions for secondaries with  $p_T > 1$  GeV/c emitted into a  $\phi$  wedge of  $\pm 25^\circ$  around the trigger direction for triggering  $\pi^+$  (11(a)) and  $K^-$  (11(b)) with transverse momenta above 4 GeV/c and 6 GeV/c. The rapidity of the trigger particle is indicated; dashed lines correspond to inclusive distributions. Charge ratios are also given.
- Fig. 12 Preliminary, normalized rapidity distributions for secondaries with  $p_T > 1$  GeV/c in a  $\phi$  wedge of  $\pm 25^\circ$  around  $180^\circ$  for triggering  $\pi^+$  at  $\phi = 0^\circ$  and with transverse momenta above 4 GeV/c and 6 GeV/c. The rapidity of the triggering  $\pi^+$  is indicated; dotted lines correspond to inclusive distributions. Charge ratios are also given.
- Fig. 13 Preliminary distributions of the quantity  $x_E$  defined in the text obtained from secondaries with  $y < 0$  and  $y > 0$  in events with  $\pi^+$  triggers at  $y > 0$  and with  $p_T > 4$  GeV/c.
- Fig. 14 Distributions in azimuth  $\Delta\phi$  relative to the azimuth of the trigger from secondaries associated with triggering  $\pi^+$  at  $\theta = 30^\circ$  and  $\sqrt{s} = 63$  GeV. (a)  $p_T(\pi^+) < 0.5$  GeV/c; (b)  $p_T(\pi^+) > 1$  GeV/c; (c)  $p_T(\pi^+) > 2$  GeV/c.
- Fig. 15 Cross section for particles produced at  $90^\circ$  in events triggered by a  $\pi^0$  with  $p_T > 6$  GeV/c at  $\phi = 0$  ( $\sqrt{s} = 63$  GeV) normalized to the inclusive cross section as function of  $p_T$ .
- Fig. 16 Average transverse momentum component perpendicular to the scattering plane versus  $x_E$  for  $\pi^0$  associated with triggering  $\pi^0$  at  $\sqrt{s} = 63$  GeV/c for various transverse momenta of the triggering  $\pi^0$ . Dashed and dotted lines correspond to model predictions based upon two Gaussian widths assumed for the  $k_T$  distribution:  $\langle k_T \rangle = \sqrt{\pi/2} \sigma$ .

 $E d^3\sigma/dp^3 \text{ (cm}^2 \text{ c}^3/\text{GeV}^2\text{)}$

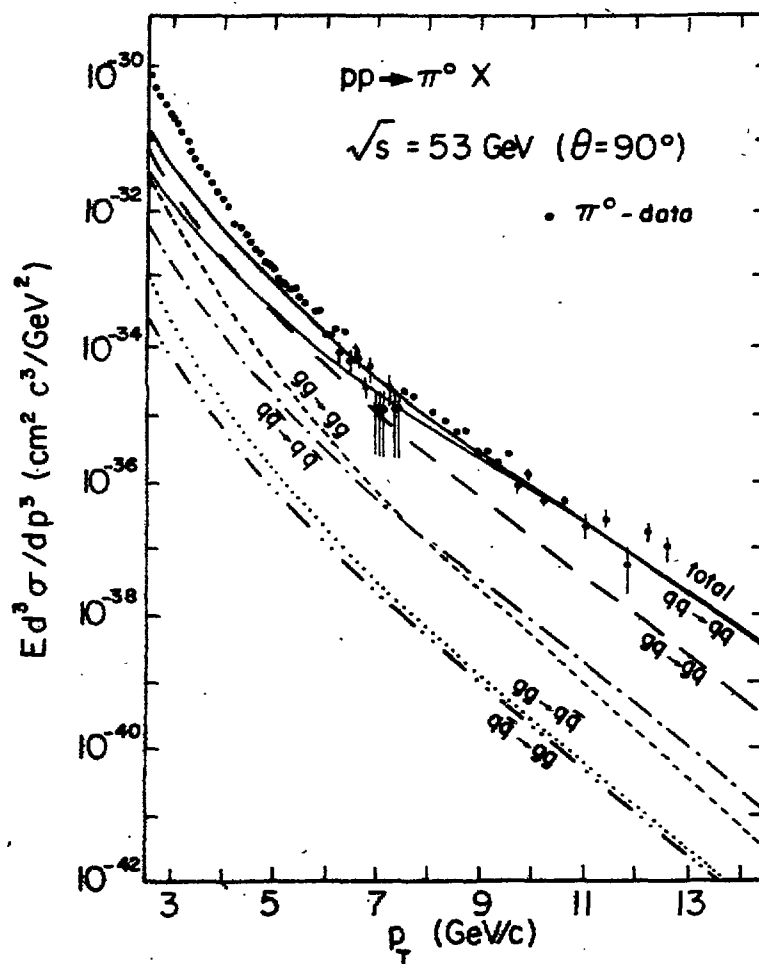


Fig. 1

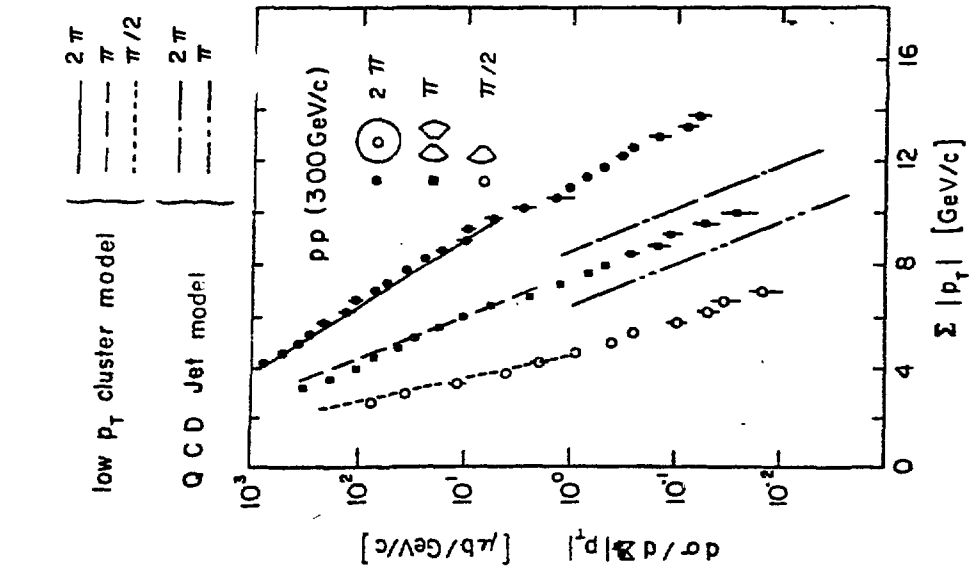


Fig. 2

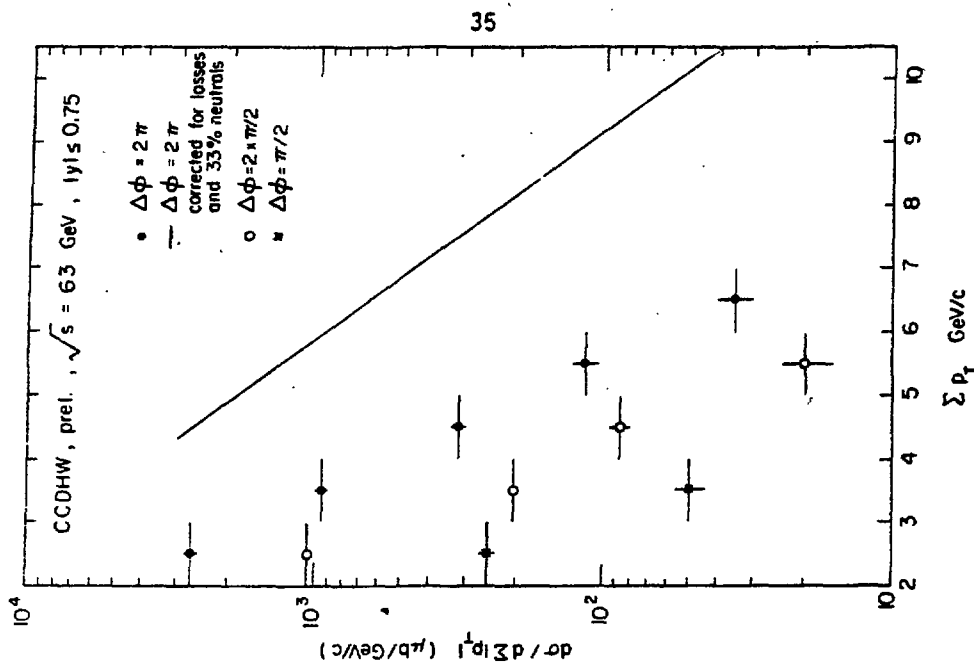


Fig. 3

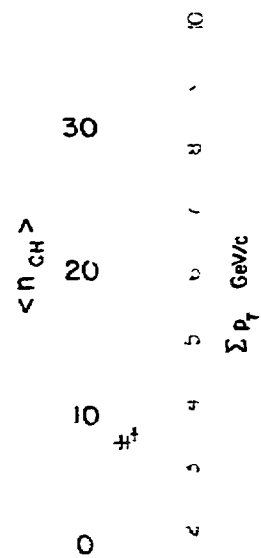
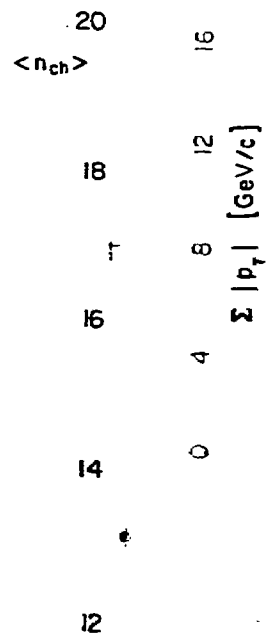




Fig. 3

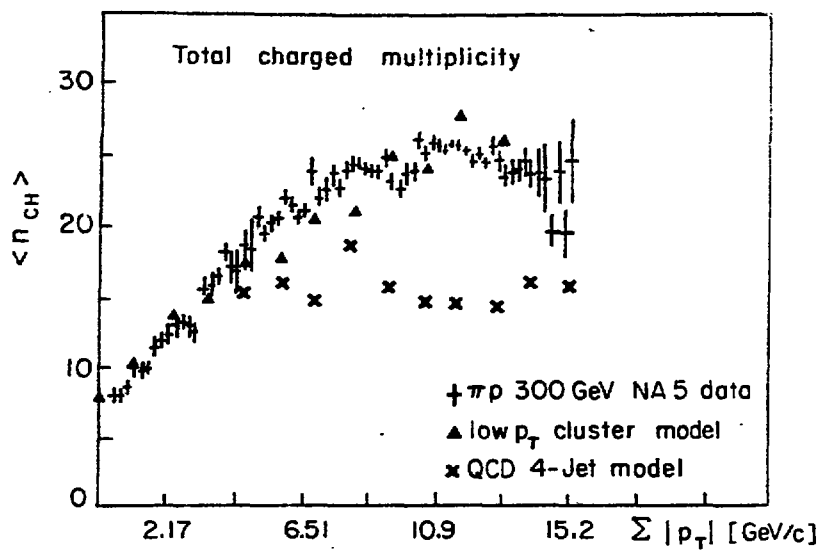


Fig. 4

Fig. 2

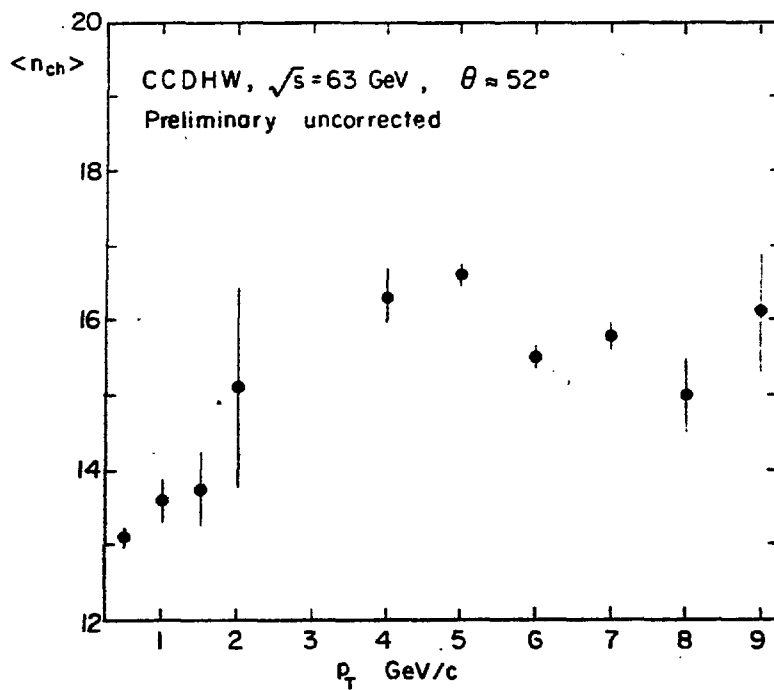


Fig. 5

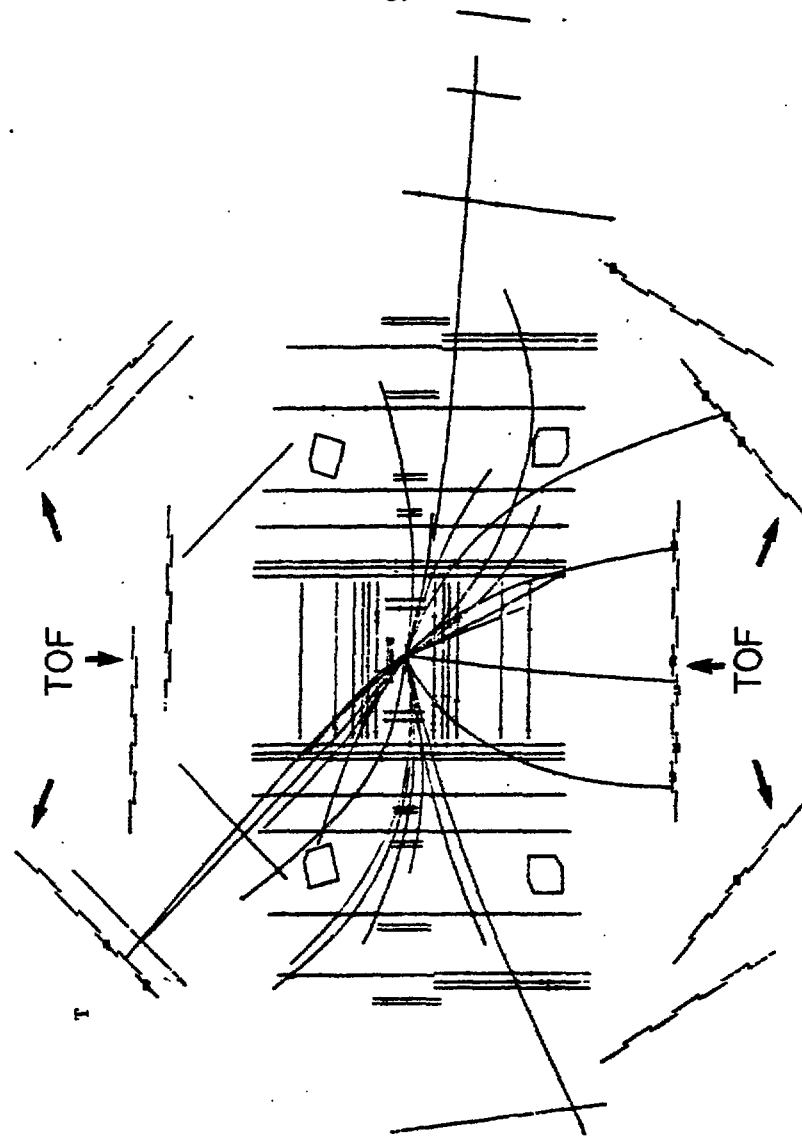


Fig. 6

$$E \frac{d^3\sigma}{dp^3} \text{ (cm}^2 \text{ c}^3 \text{ / GeV}^2 \text{)}$$

$10^{-1}$     $10^{-1}$     $10^{-1}$     $10^{-2}$     $10^{-3}$     $10^{-3}$     $10^{-4}$     $10^{-5}$

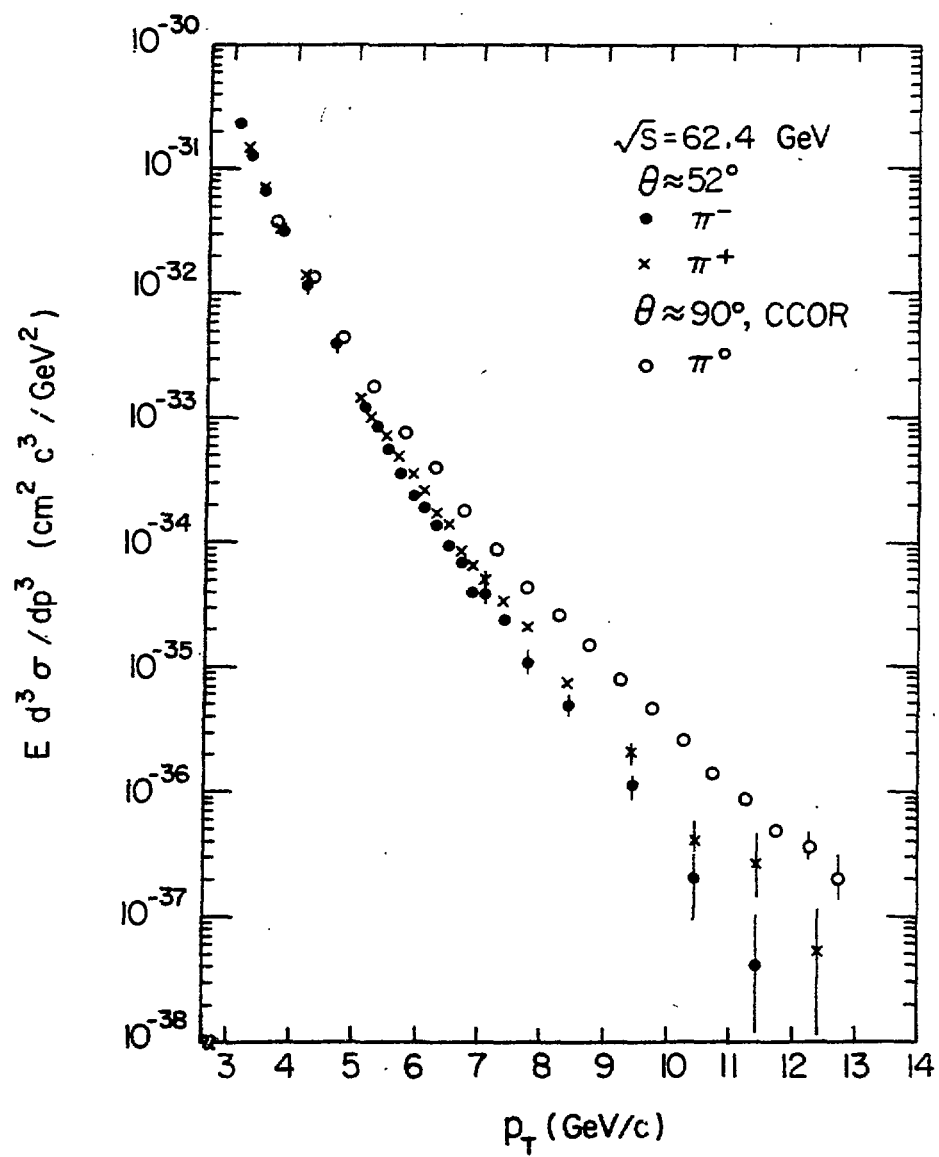


Fig. 7

Fig. 6

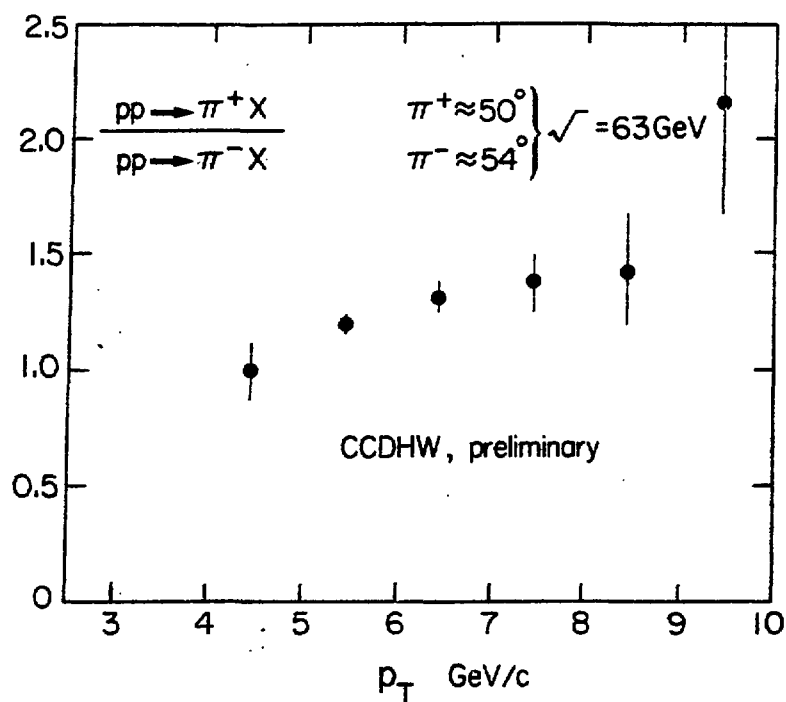


Fig. 8

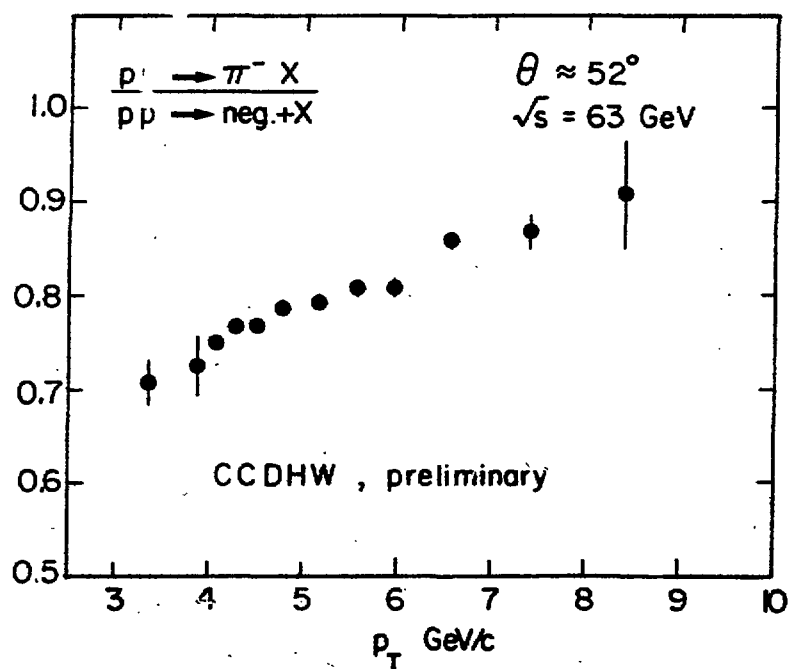


Fig. 9

Corrected Ratio  $\gamma/\pi^0$ 

0.7  
0.6  
0.5  
0.4  
0.3  
0.2  
0.1  
0  
0.7  
0.6  
0.5  
0.4  
0.3  
0.2  
0.1  
0  
0  
2

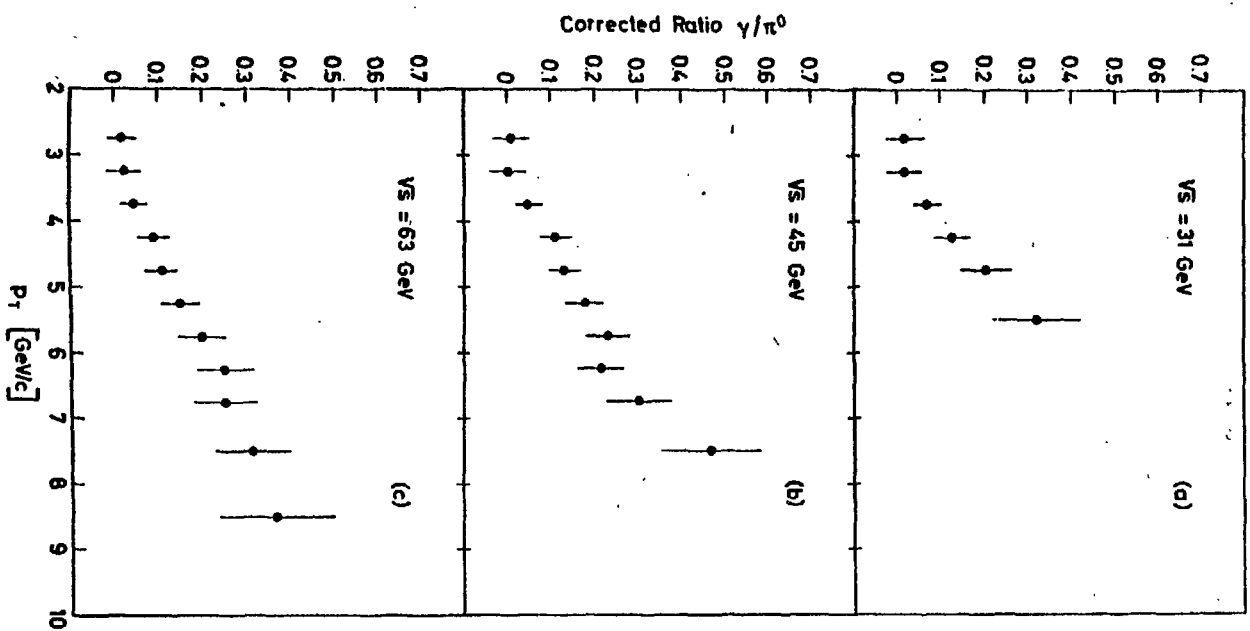


Fig. 10

Toward jets CCDHW, prel.,  $\sqrt{s}=63$  GeV,  $\theta \approx 50^\circ$

$p_T$  (trigger):

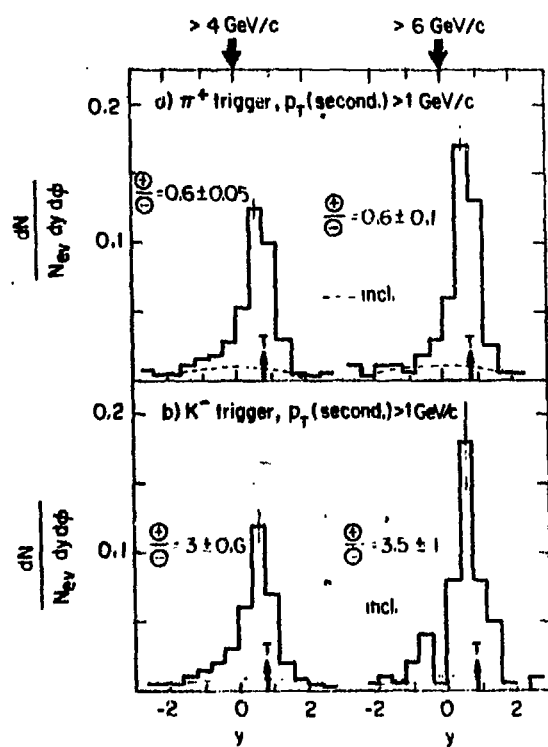


Fig. 11

Away jets: CCDHW, prel.,  $\sqrt{s}=63$  GeV,  $\theta \approx 50^\circ$

$p_T$  (trigger):

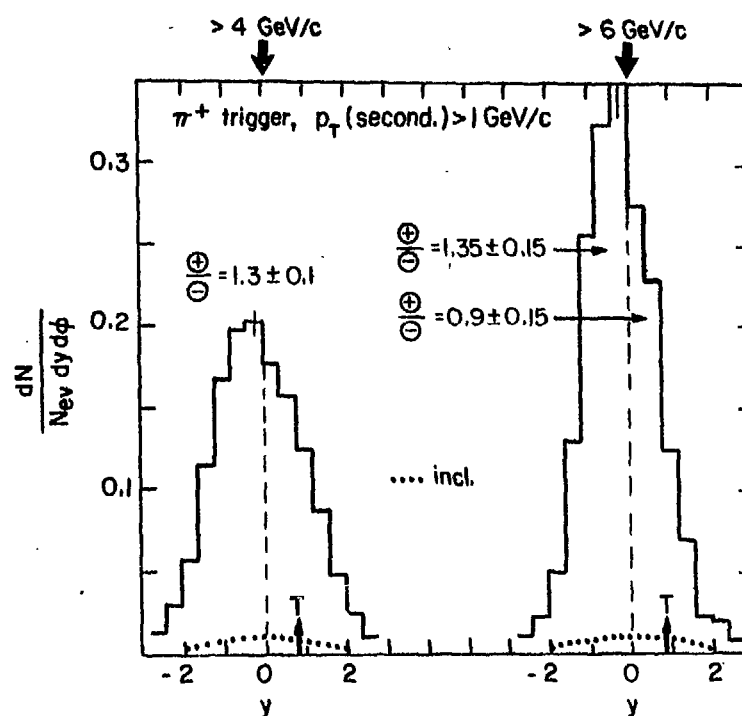
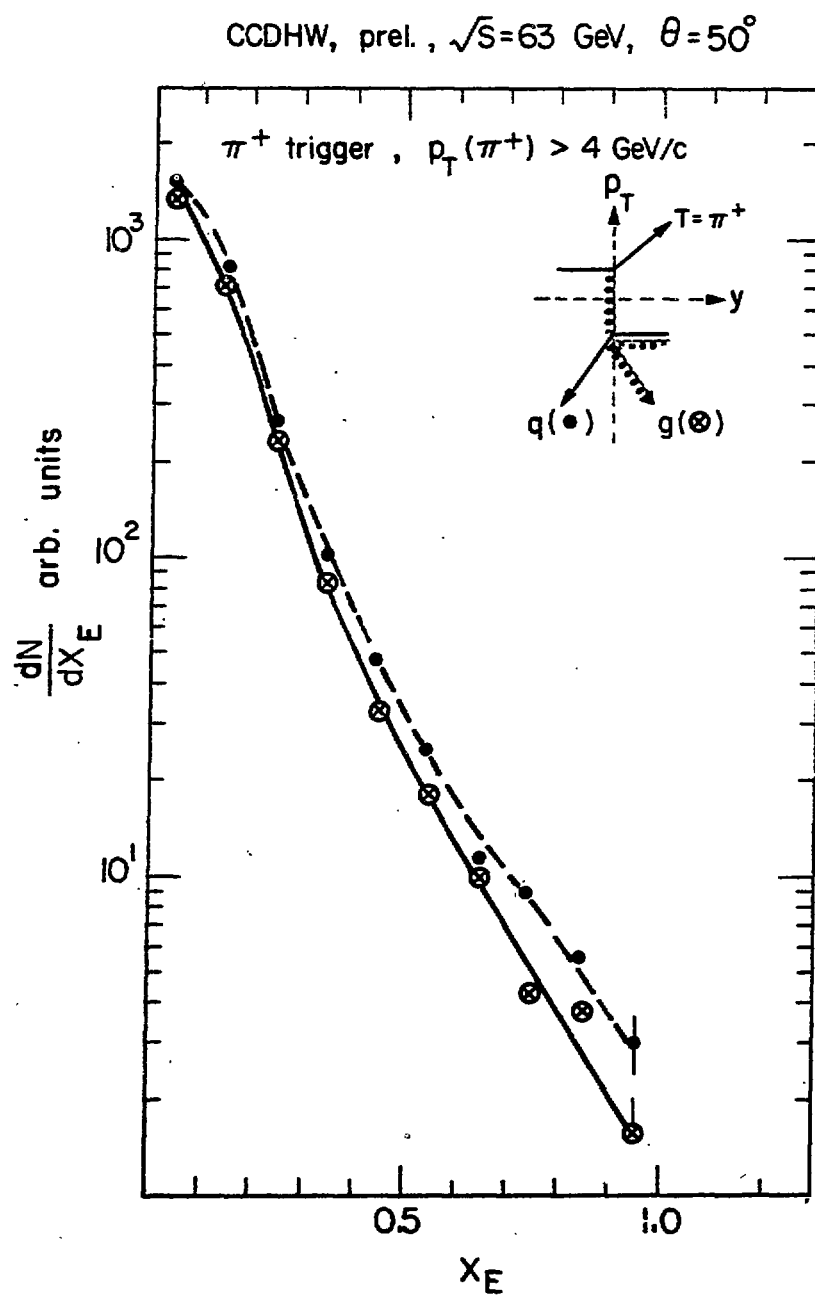


Fig. 12

Fig. 12

Fig. 11



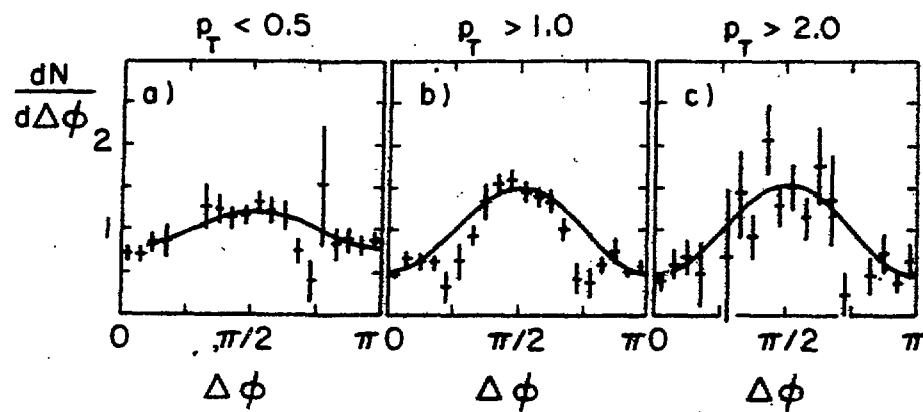


Fig. 14

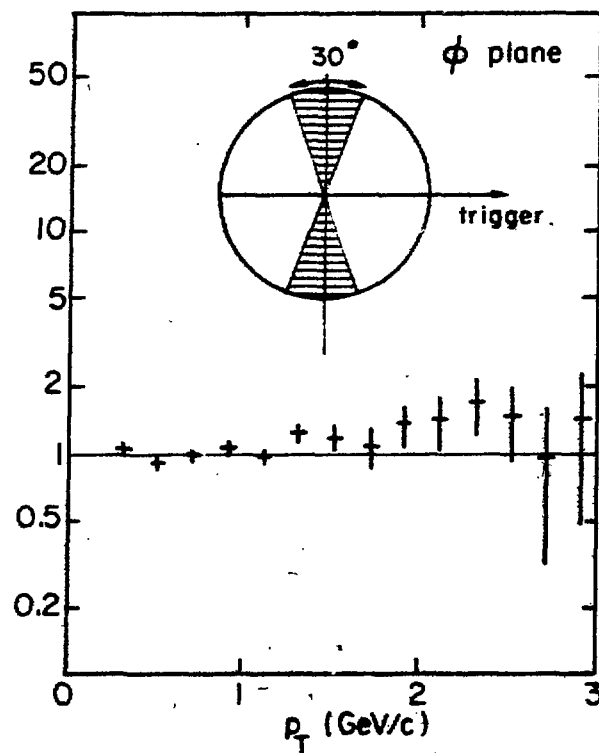


Fig. 15



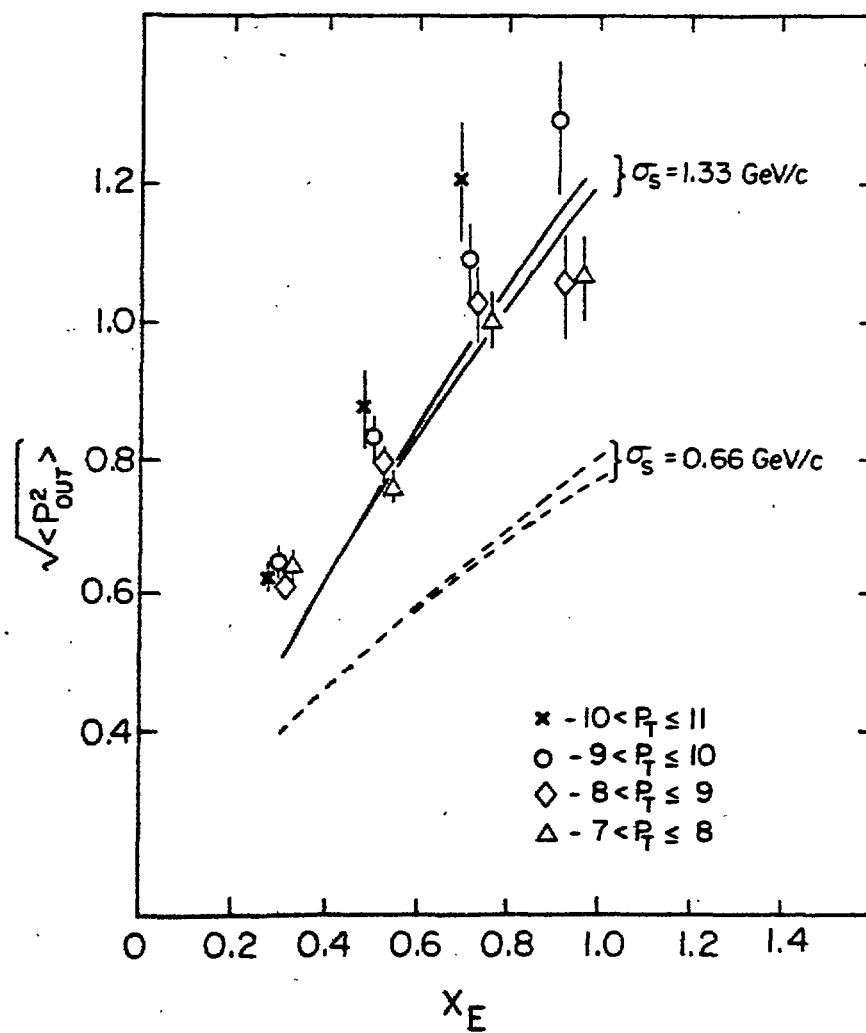


Fig. 16

# EXPERIMENTAL REVIEW OF SOME PREDICTIONS OF THE DRELL YAN MODEL IN HADROPRODUCTION OF DIMUONS

reported by G. BURGUN

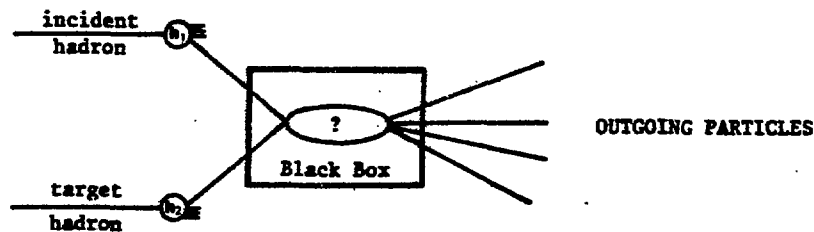
Département de Physique des Particules Élémentaires  
 CEN-Saclay, 91191 Gif sur Yvette Cedex, France

## I - INTRODUCTION

During the past 10 years, the analysis of dimuons produced in collisions between incident hadrons and nuclear targets have shed much light on the knowledge of fundamental constituents of particles and on the mechanisms involved in their interactions.

Several excellent recent papers have reported on the situation of hadroproduction of dileptons [ref. 1].

The first kind of experiments (the so called deep inelastic scattering D.I.S. of leptons experiments) have reached part of this goal in probing nuclear matter with incident point-like particles ( $e, \mu, \nu$ ). This type of probe enables us to obtain a precise idea about the constitution of nucleons. Unfortunately this kind of method cannot be used for unstable particles. In that case, the most natural and unique way is to look at hadron-hadron collisions.



to coll  
 problem

T. Yan  
 dion-ha

The con

-  $q_i$   
 t

- de used

At this d muc

calcula he m

lisions

$q_i \bar{q}_t$  situat

valence

that q

astic

probin

probi

fortu

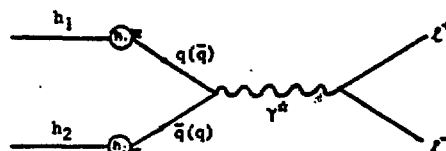
case

where :

G PA

One can hope that the study of the outgoing particles will allow us to collect information on the structure of incident and/or target particles. The problem then is to know what happens in the black box.

In 1970, in the frame work of the quark-parton model, S. Drell and T. Yan [2] have proposed a model which describes the mechanism occurring in hadron-hadron collisions. The graph corresponding to this model is :



The contents of the black box are :

- $q_i - \bar{q}_t$  (or  $\bar{q}_i - q_t$ ) annihilation into a virtual photon (i for incident, t for target) ;
- decay of the photon into two leptons of opposite charge.

At this stage, the interaction is purely electromagnetic. This graph allows to calculate the inclusive cross section of lepton pair production in hadron collisions. Besides the cross section is directly proportional to the number of  $q_i \bar{q}_t$  ( $\bar{q}_i q_t$ ) couples which can annihilate. Thus valence-valence, sea-sea and valence-sea terms will contribute to the cross section. It should be noticed that  $q$  and  $\bar{q}$  have to be of the same flavour.

The differential cross-section is then given by the following formula :

$$\frac{d^2\sigma}{dx_1 dx_2} = \frac{4\pi\alpha^2}{3x_1 x_2 s} \cdot \frac{1}{3} \cdot \sum_i \frac{Q_i^2}{x_1 x_2} \left[ f_i^q(x_1) \cdot g_i^{\bar{q}}(x_2) + f_i^{\bar{q}}(x_1) \cdot g_i^q(x_2) \right] \quad (1)$$

where :  $\frac{4\pi\alpha^2}{3x_1 x_2 s}$  is the point-like electromagnetic annihilation cross-section at an equivalent energy of  $M_{\mu\mu}^2$  ;

- $\frac{1}{3}$  is the colour factor ;
- $Q_i$  is the quark electric charge ( $\frac{1}{3}$  or  $\frac{2}{3}$ ) ;
- $x_1$  and  $x_2$  are the fraction of momentum taken by the quarks, respectively, in hadron  $h_1$  or hadron  $h_2$  ;
- $\frac{f_i(x)}{x}$  is the probability for a quark to carry the fraction  $x$  of the available energy  $\sqrt{s}/2$  ;
- the summation runs over all quark flavours (in practice only u, d, s).

G PARTICLES

At this point, some comments on the Drell-Yan formula can be made :

a/ Notice that  $f$  and  $g$  are called the structure functions respectively of the incident hadron  $h_1$  and the target nucleon  $h_2$ . One of the important reason to study hadroproduction of dileptons is that the structure functions used in the Drell-Yan formula are the same as those determined in D.I.S. of  $e$ ,  $\mu$  and  $\nu$  experiments. This fact allows a good cross-check of the same functions which are obtained by two different methods. In that case, the space-like  $Q^2$  variable in D.I.S. corresponds to the time-like  $M_{\mu\mu}^2$ .

b/ Another interesting aspect which can be derived from the Drell-Yan formula if the following : if  $f$  and  $g$  are known, then due to the fact that no free parameters exist in the formula, we are able to compute an absolute value for the cross-section. On the other hand, if the cross-section is experimentally measured and if  $g$  (structure function of the nucleon of the target) is known (from D.I.S. experiment for example), the Drell-Yan formula enables us to determine the structure function of unstable incident hadrons such as pions or kaons.

c/ In the Drell-Yan model, the transverse momentum of lepton pairs is due only to the transverse momentum of the quarks which annihilate. Therefore, the dilepton transverse momentum is expected to be small and independent of the overall center of masse energy.

d) For different reactions, the relative yield of dileptons produced depends on the quark content of interacting particles.

These brief qualitative comments on the Drell-Yan formula lead us to the predictions of the model.

## II - PREDICTIONS OF THE D-Y MODEL

### 1. Nuclear effects

Due to the nature of the collisions (hard scattering), the quark-antiquark annihilations are point-like interactions which is consistent with the fact that quarks are dimensionless objects. Therefore no shadow effects of nucleons in the target should occur as is the case in coherent processes. For hard scattering processes of point like constituents, a linear dependence with the number of partons is expected, i.e. if the cross section is parametrised as  $A^\alpha$  (where  $A$  is the atomic number of the target)  $\alpha = 1$  is predicted by the Drell-Yan model.

### 2. Scaling beh

The

with :  $X = x$

$H(x_1$

This relation

where  $C$  is a di-  
structure func-  
dent of  $s$  and

### 3. Beam de end

The

$q - \bar{q}$  annihilar  
(valence and se  
composed of pro  
be expected to  
than for proton  
The Drell-Yan f  
yield of dilept

### 4. An ular dist

In c  
which was creat  
polarisation is  
the dilepton re

## 2. Scaling behaviour

The Drell-Yan formula should be written as :

$$\frac{d^2\sigma}{dM dX} = \frac{8\pi\alpha^2}{3M^3} \frac{1}{3} \sum_i \frac{q_i^2}{x_1 + x_2} H(x_1, x_2) \quad (2)$$

$$\text{with : } X = x_1 - x_2 \quad M^2 = x_1 x_2 s$$

$H(x_1, x_2)$  = product of beam x target structure functions.

This relation can be rewritten as :

$$M^3 \frac{d^2\sigma}{dM dX} = C F(x_1, x_2) = C F\left(\frac{M^2}{s}, X\right) \quad (3)$$

where  $C$  is a dimensionless factor and  $F$  is called the scaling function. If the structure functions do not depend on the  $M^2$  scale,  $F$  is expected to be independent of  $s$  and to be only a function of the scaling variable  $\sqrt{T} = M/\sqrt{s}$ .

## 3. Beam dependence

The Drell-Yan cross section is directly related to the number of  $q - \bar{q}$  annihilations which could occur between projectile and target quarks (valence and sea) having the same flavour. Due to the fact that targets are composed of protons ( $u u d$ ) and neutrons ( $d d u$ ), the yield of dimuons will be expected to be higher with incident particles containing valence  $\bar{u}$  or  $\bar{d}$  than for protons, especially at high masses where valence quarks dominate. The Drell-Yan formula allows us to make some predictions on the relative yield of dileptons produced with various beam particles.

## 4. Angular distribution

In our case, dimuons are produced after the decay of a virtual photon which was created by the annihilation of two quarks of spin  $1/2$ . A transverse polarisation is then expected for the muons and their angular distribution in the dilepton rest frame should be :

$$\frac{dN}{d \cos \theta} \propto 1 + \cos^2 \theta$$

where  $\theta$  is the polar angle of emission of a muon with respect to the  $q\bar{q}$  line of flight. The determination of this direction is complicated by the fact that the dimuon and hence the original  $q\bar{q}$  system has a transverse momentum. In order to approach this polarization axis, the lines of flight of the pion and of the proton are used.

### 5. Absolute cross-section

Since no free parameter is needed in the general expression (1) for the cross-section, then if the structure functions of incident and target particles are known, the Drell-Yan cross-section can be exactly computed. Proton-proton and antiproton-proton collisions are well suited for testing this prediction.

To conclude this chapter, it is now clear that the study of hadroproduction of dileptons is a mine of information concerning the behaviour of fundamental constituents in collisions and it is thus the only way to determine the structure functions of unstable particles.

## III - DIFFICULTIES WITH THE DRELL-YAN MODEL

### 1. Introduction of gluon effects

The Drell-Yan model seems to be relevant for describing hadrons collisions, but unfortunately nature is much more complicated ! As soon as high statistics of dilepton data became available, two main problems arose :

- i) The dimuon transverse momentum was found to be larger than expected : clearly in that case, the angular distributions should be affected !
- ii) The experimental dimuon cross section was found to be much larger than that computed in the Drell-Yan frame work.

The problem arising with these experimental results is to find the origin of the discrepancy between experiment and the simple Drell-Yan model. A solution is clearly that gluons do exist in nature and the Drell-Yan process is the lowest order diagram of the general QCD theory which itself is the leading candidate for the theory of strong interactions [3]. Due to the fact that gluons are present in the particles, their emission or absorption are responsible for new graphs which resemble QED diagrams used for calculating radiative corrections.

These 1

$q\bar{q}$  line  
fact t  
. In o  
and of

on (1)  
target  
d. Prot  
this pr

of hadr  
viour o  
o deter

2. Some

verse  
is much  
a dynami  
The hypo  
 $k_T$  of co  
( $k_T$  is e

adrons  
on as h  
e :

which sh  
the foll

ed : cl  
than t

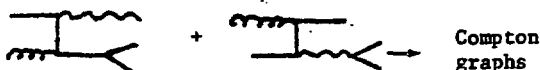
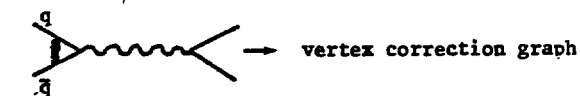
where :

find t  
in model  
an proc  
s the l

calculati  
terms in  
ment in t  
in  $\alpha_s$  cal

that g  
nsible  
ive corr

These lowest order diagrams are :



These graphs allow transverse momentum to be given to the dileptons.

## 2. Some qualitative comments on dilepton transverse momentum

The quark-parton model can be easily extended by assigning a transverse momentum to the quarks. But the experimental results show that  $P_T^{\mu\mu}$  is much larger than expected and increases dramatically with  $s$ . In that case, a dynamical explanation is then required and can be provided by QCD theory. The hypothesis is that  $P_T^{\mu\mu}$  is the sum of the "primordial" transverse momentum  $k_T$  of constituents inside the hadrons and of terms arising from gluon effects ( $k_T$  is expected to be of the order of 300-400 MeV).

In the QCD frame work [ref. 4] the annihilation and Compton graphs which should allow the calculation of the  $P_T^{\mu\mu}$  distribution at large  $P_T$ , give the following prediction for the average value of  $P_T$  :

$$\langle P_T \rangle = C + \alpha_s(M^2) \cdot f(\tau) \cdot \sqrt{s}$$

where : •  $C$  is a constant, independent of the incident energy of the hadrons which should be equal to the intrinsic transverse momentum.

•  $f(\tau)$  is a function of  $\tau$ , positive but not monotonic, which has a maximum around  $\sqrt{\tau} \approx 0.3 - 0.4$  and falls to 0 at  $\tau = 0$  and  $\tau = 1$  [5].

A more general study has led Dokshitzer et al. [6] to perturbative calculations in the "leading logarithm approximation" taking into account all terms in  $\log(P_T^2/M^2)$ . The result of their work has been to find better agreement in the shape of the  $P_T^{\mu\mu}$  distribution with data, than with the simple order in  $\alpha_s$  calculations.

The presence of dileptons produced with large transverse momentum has some effects on the angular distribution [7].

To conclude this chapter, we can summarize that which QCD theory brings to the understanding of the dimuon data :

- It allows for large dilepton transverse momentum.
- It explains the change expected in the angular distribution.
- It predicts a different value of the cross section than that of the naive Drell-Yan model (See chap. V.5).
- In addition, if higher-order graphs are included, scaling violation will be generated (as observed in DIS of lepton experiments) due to gluon emission.

The consequence of these predictions is to replace the "naive" Drell-Yan model which was proposed in the framework of the parton-quark model, by the so-called "educated" Drell-Yan model developed within the QCD framework.

#### IV - SOME EXPERIMENTAL COMMENTS ON HADROPRODUCTION OF DIMUONS

##### 1. Main experimental features

In a hadroproduction of dimuons experiment, we need only the inclusive detection in the final state of two muons of opposite charge. We have to make sure that the 2 muons are not decay products of  $\pi$  or K mesons. In addition, the leptons have to be produced "promptly" (i.e. within  $\leq 10^{13}$  sec.) in the primary interaction. Due to the low cross-section of dilepton production, the use of high intensity and high energy beams is strongly advised. But, in that case, high multiplicity of secondary particles is expected. A good way to get rid of this problem is then to perform a dump experiment in which secondary hadrons are largely killed. But this experimental condition leads to a poor resolution that can be achieved, due to the multiple scattering of particles in the dump that crucially affects the measurement of the momenta and angles of the muons. Clearly a compromise has to be found between all these parameters in order to get the best experimental conditions possible. Finally the acceptance of the apparatus should be as large as possible, especially for the study of the angular distribution.

##### 2. Kinematical

From the dimuon mass are derived :

where :  $\bullet P_L$  i  
mass  
 $\bullet x_1$

From the set of

Note that in

##### 3. Kinematical

Thr

i)

Thi

blematic beca  
petitive [ref.  
Drell-Yan even  
mental resolut

ii)

Th

large amount of

iii)

Thi

mass dependenc  
are statistica



## 2. Kinematical variables

From the measurements of the momentum of the muons, one can compute the dimuon mass  $M_{\mu\mu}$ . The total energy  $\sqrt{s}$  is known and the following relations are derived :

$$\begin{aligned} M_{\mu\mu}^2 &= x_1 x_2 s \\ x_{\mu\mu} &= \frac{2 P_L}{\sqrt{s}} = x_1 - x_2 \end{aligned} \quad (3)$$

where : •  $P_L$  is the longitudinal momentum of the dimuon in the total center of mass energy system.

•  $x_1$  and  $x_2$  are defined in chapter I (see relation (1)).

From the set of equations (3), one can calculate :

$$x_1 = \frac{1}{2} \left( x_{\mu\mu} + \sqrt{x_{\mu\mu}^2 + 4 M_{\mu\mu}^2 / s} \right)$$

Note that in the naive Drell-Yan model the  $P_T$  of the dimuons is neglected.

## 3. Kinematical mass range

Three regions in mass are useful for testing the Drell-Yan model.

i)  $\rho, \omega, \phi < M_{\mu\mu} < \Psi, \Psi'$

This region between the  $\rho, \omega, \phi$  resonances and the  $\Psi$  family is problematic because other possible mechanisms than the Drell-Yan process are competitive [ref. 1]. In addition there are some difficulties in separating the Drell-Yan events from the surrounding bumps due essentially to the poor experimental resolution.

ii)  $\Psi, \Psi' < M_{\mu\mu} < T$  family

These region is well suited for testing the Drell-Yan model and a large amount of data is now available.

iii)  $T$  family  $< M_{\mu\mu} < \text{new bump ?}$

This third region would be very interesting in order to test the mass dependence of the structure functions but the data currently available are statistically very limited.

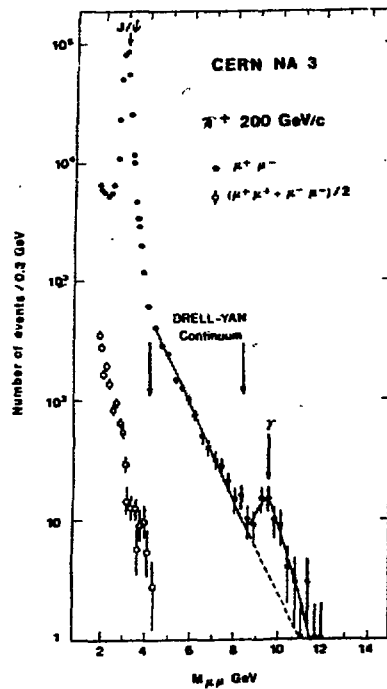


Fig. 1

The figure 1 shows the mass spectrum of the NA3 collaboration [8]. Between the  $J/\psi$  and  $T$  resonances, for masses from 4 GeV to 8.5 GeV, the large number of dimuons events for several kinds of incident hadrons ( $\pi^+$ ,  $K^+$ ,  $p$  and  $\bar{p}$ ) at several energies allows a good analysis of the Drell-Yan model. In order to test the Drell-Yan process many other experiments have brought data which have been reported in the table 1. This table also gives the characteristic features of each experiment.

Table 1

| Collaboration | Incident particle | $P_{inc}$                               | Target             | $\pi^0$ acceptance | $M_{\mu\mu}$ range | N. Evts.   | Typical features of experiment.                            | Ref. |
|---------------|-------------------|---|--------------------|--------------------|--------------------|--|--|------|
| I S R         | ASCS ( $e^+e^-$ ) | $\sqrt{s} = 28, 31, 32, 33, 35, 37, 40$ | p                  | -0.2-0.2           | 4-18               | 1000   | Transition radiation detector and liquid argon calorimeter | [9]  |
|               | CHIMP             | $\sqrt{s} = 62$                         | p                  | -0.1-0.5           | 5-25               | 2500   | Iron toroids spectrometer                                  | [10] |
| CERN          | CFS               | 200-300                                 | Be, Cu, Pt         | -0.1-0.1           | 5-20               | 180000   | Two arm spectrometer                                       | [11] |
|               | CIP               | 225                                     | C, Cu, W           | 0-1                | 4-8.5              | $\pi^-$ 2700<br>$\pi^+$ 400  | Chicago Cyclotron magnet                                   | [12] |
|               | INTW              | 400                                     | Fe                 | -0.2-1             | 4.5-18             | $> 10^5$   | Spectrometer   | [13] |
|               | SISI              | 150                                     | Be                 | -0.2-0.8           | 3.9-8              | 1300   | Coliath spectrometer                                       | [14] |
| CERN          | Q                 | 60                                      | W                  |                    | 2.0-2.7            | several $10^3$   | Omega spectrometer   | [15] |
|               | NA3               | 150, 200, 280, 400                      | Fe, W <sub>2</sub> | -0.3-1             | 4-14               | $\pi^-$ 50000<br>$\pi^+$ 2200<br>$\mu^-$ 1000<br>$\mu^+$ 370<br>$p$ 1300<br>( $> 50000p$ ) | Lenard spectrometer  | [16] |
|               | NA10              | 280                                     | C, W, Cu           |                    | 4-14               | $\sim 2000$  | Spectrometer   | [17] |
|               | NA10              | 280                                     | C, W, Cu           |                    | 4-14               | $\sim 2000$  | Spectrometer   | [17] |

ASCS : Athens, Brookhaven, CERN, Syracuse.

CHIMP : CERN, Harvard, Frascati, MIT, Naples, Pisa.

CFS : Columbia, Fermilab, Stony Brook.

CIP : Chicago, Illinois, Princeton.

INTW : Michigan, Northwestern, Tulane, Washington.

SISI : Saclay, Imperial College, Southampton, Indiana.

Q : Birmingham, CERN, Ecole Polytechnique.

NA3 : Saclay, CERN, Collège de France, Ecole Polytechnique, LAL Group.

NA10 : Zurich, Ecole Polytechnique, Strasbourg.

V-EXPERI

1. Nuc

usuall  
tation  
tion  
in ord  
cross  
marize

compar  
deviat  
absolu  
inter  
Indee  
MUON  
and

and M

## V - EXPERIMENTAL RESULTS

## 1. Nuclear dependence

Due to the low cross section of dimuon production, experimentalists usually use heavy nuclear targets instead of hydrogen even though the interpretation of data is much simpler with a hydrogen target. The measured cross section "per nucleus" must then be converted into the cross section "per nucleon" in order to be able to compare results on different high density targets. The cross section is parametrised as  $A^\alpha$  where  $A$  is the atomic number. Table 2 summarizes the results of  $\alpha$  for several experiments.

- Table 2 -

| Experiment | Targets            | Beam (GeV)            | Result                      | Ref     |
|------------|--------------------|-----------------------|-----------------------------|---------|
| CFS        | Pt, Be             | proton<br>200-300-400 | $1.007 \pm 0.018 \pm 0.028$ | [11]    |
| CIP        | Cu, C, W           | $\pi^-$ 225           | $1.12 \pm 0.05$             | [12]    |
| NA3        | Pt, H <sub>2</sub> | $\pi^-$ 200           | $1.02 \pm 0.03$             | [18-19] |
|            |                    | $\pi^+$ 200           | $0.95 \pm 0.04$             |         |
|            |                    | $(\pi^- - \pi^+)$ 200 | $1.03 \pm 0.05$             |         |
|            |                    | $\pi^-$ 150           | $1.00 \pm 0.02$             |         |
|            |                    | $\pi^-$ 280           | $1.00 \pm 0.02$             |         |
| NA10       | C, W, Cu           | $\pi^-$ 280           | $0.97 \pm 0.02 \pm 0.02$    | [17]    |

With the exception of the CIP result for  $\alpha$ , all the results are compatible with  $\alpha = 1$  as expected by the Drell-Yan model. The 2.5 standard deviation from 1 observed in the CIP result is directly connected to the absolute normalisation factor  $K$  as discussed elsewhere [20]. Notice the interesting result of the NA3 experiment concerning the  $(\pi^- - \pi^+)$  data. Indeed, in that case, the possible contribution of hadronic processes to muon pair production disappears in the difference as it is the same for  $\pi^+$  and  $\pi^-$ .

Figures 2 and 3 show that no dependence of  $\alpha$  is observed with  $p_T^{\mu\mu}$  and  $M_{\mu\mu}$  for incident protons at 400 GeV.

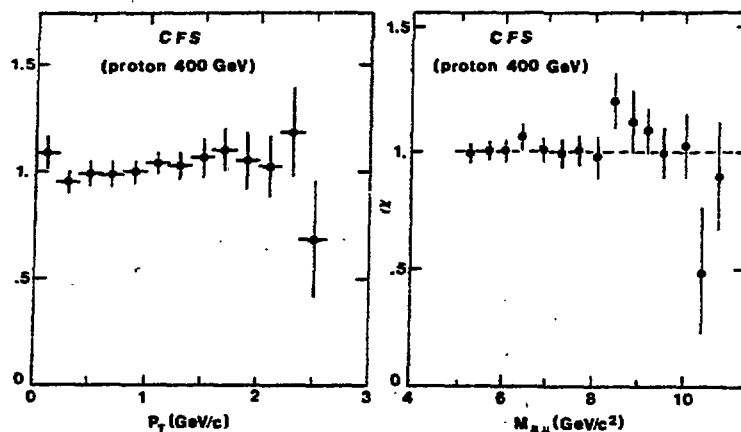


Fig. 2

Fig. 3

For incident  $\pi$ 's, no obvious  $P_T^{\mu\mu}$  and  $x_F$  dependences have been observed in the CIP experiment or in the NA10 experiment for  $P_T^{\mu\mu}$ . The NA3 analysis of pion data [19] at 150, 200 and 280 GeV on hydrogen and platinum targets used simultaneously shows that the ratio of the cross section is in good agreement with the Drell-Yan prediction within a 10 % error which is mainly due to systematics. Variation of this ratio with the dimuon mass,  $x_1$  and  $x_2$  is also in good agreement and no variation with the transverse momentum is observed as shown in figure 4.

$$R = \frac{A \sigma(\pi^- H_2 \rightarrow \mu^+ \mu^-)}{\sigma(\pi^- Pt \rightarrow \mu^+ \mu^-)}$$

( $\pi^-$  at 150 GeV)

— Drell-Yan model prediction

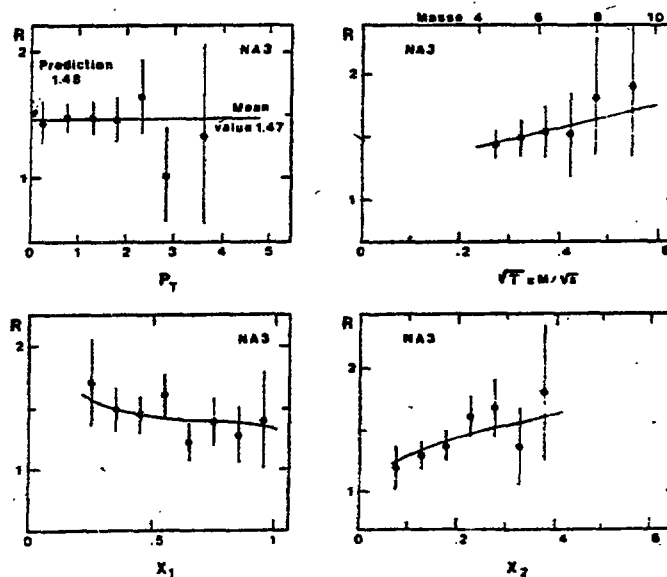
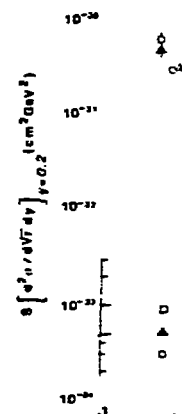


Fig. 4

## 2. Scali

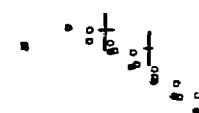
be a fun

400 GeV)  
electron  
the pres  
the expe



the  
data  
3ne-  
he  
S. Va-  
ment  
e 4.

$\frac{d^2 \sigma}{dx_1 dx_2} (\pi^- H_2 \rightarrow \mu^+ \mu^-)$



40 GeV (NA3)  
200 GeV  
280 GeV (NA3)  
380 GeV

82 83

## 2. Scaling

If scaling invariance is assumed (see chap. II.2)  $M^3 \frac{d^2\sigma}{dM dX}$  should be a function only of  $\tau = \frac{M^2}{s}$  ( $\tau$  is called the scaling variable).

Figure 5 shows the data of the CFS collaboration (protons at 200-300-400 GeV). In figure 6, a comparison between the proton data at 400 GeV and di-electron data at the ISR is presented. In the range of  $\sqrt{\tau}$  (between 0.1 and 0.5) the present data on protons are consistent with the scaling prediction to within the experimental accuracy of the measurements.

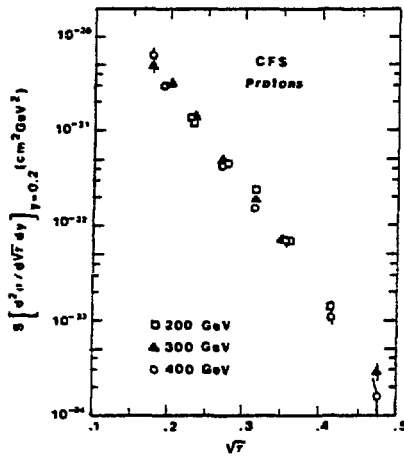


Fig. 5

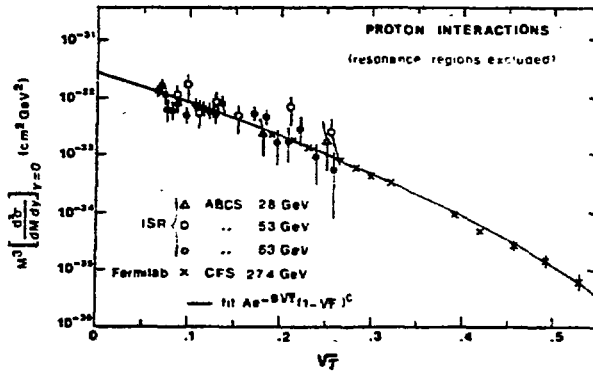


Fig. 6

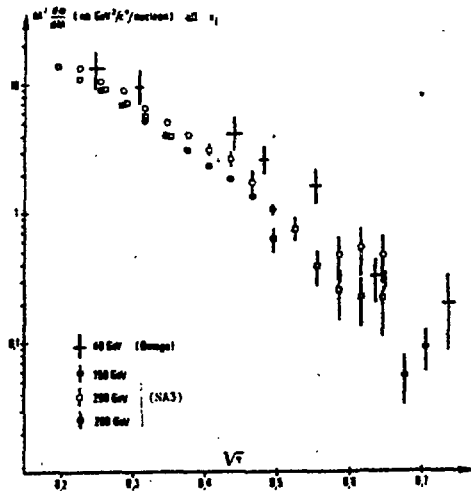


Fig. 7

A comparison between the  $\pi^-$  data of the NA3 experiment and the  $\Omega$  results [15] are presented in fig. 7. Although the  $\Omega$  data seem to show a small systematic deviation relative to the NA3 data, this is not a clear manifestation of  $Q^2$  dependence of the structure function as observed in D.I.S. of leptons. Indeed, we have to be very careful in our conclusions because the scaling violation should be of the order of magnitude of the systematical errors. However, the experimental problems such as normalisation between different

experiments and the small span in the center of mass energy of presently available data, are crucial considerations before one can draw any conclusions. The most conservative approach is to state that within present experimental accuracy (at the level of 20 %), the data support the scaling invariance prediction as expected by the naive Drell-Yan model.

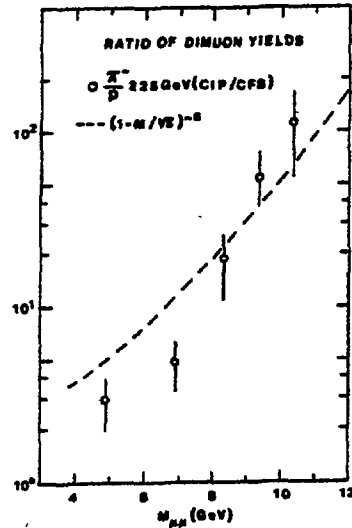


Fig. 8

### 3. Beam dependence

The Drell-Yan formula (1) shows that the differential cross section is directly proportional to all possible  $q\bar{q}$  arrangements between projectile and targets constituents of the same flavour. The yield of dileptons produced should be different because the quark contents of the incident hadrons are different.

Figure 8 shows the ratio of dimuons produced by  $\pi^-$ 's and p's at 225 GeV. This ratio is in rather good agreement with a prediction [ref. 1a] given by a naive quark counting rule and represented by the dashed line.

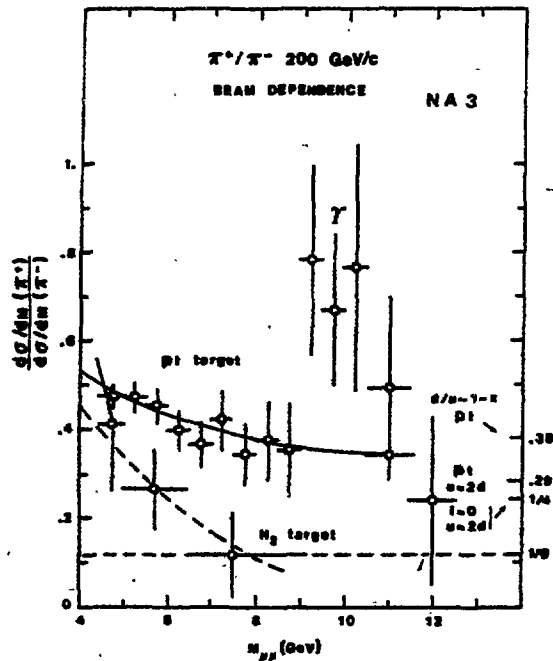


Fig. 9

The  $\pi^+/\pi^-$  ratio is shown in figure 9 provided by the NA3 collaboration. This ratio decreases with  $M_{\mu\mu}$  to limits given by several models [8] for both platinum and hydrogen targets. The T region clearly shows a different behaviour which confirms that its production is not due only to quark fusion processes. The Drell-Yan prediction is represented respectively by the solid line for the platinum target and the dashed line for the hydrogen target.

sently  
as. Th  
accur  
tion a

ws th  
actly  
ements  
ts of  
oduce  
tents

dimuon  
This r  
The err  
results  
model.

4. An ui

of 2 qua  
distribu

where  $\theta$   
of the

$\vec{L}$  be der

Because  
and we p

ws th  
actly  
ements  
ts of  
oduce  
tents

dimuon  
This r  
The err  
results  
model.

io is  
d by t  
ratio

limits  
3] for

gen ta  
y show

which  
uction

rk fusi  
l-Yan

respec  
or the

dashed  
rget.

sently available  
ns. The most  
accuracy (at  
tion as expected

Because of the several different incident particles available to NA3,  
this experiment has measured some ratios of dimuon yields summarized in the table 3  
for  $M_{\mu\mu}$  masses between 4.1 and 8.5 GeV on a platinum target at 200 GeV :

- Table 3 -

| Ratio           | Valence quark contents             | Naive prediction | Experimental result |
|-----------------|------------------------------------|------------------|---------------------|
| $K^-/\pi^-$     | $\frac{\bar{u}s}{\bar{u}d}$        | 1                | $0.98 \pm 0.1$      |
| $\bar{p}/\pi^-$ | $\frac{\bar{u}u\bar{d}}{\bar{u}d}$ | $\sim 1$         | $1.07 \pm 0.2$      |
| $\pi^+/\pi^-$   | $\frac{u\bar{d}}{\bar{u}d}$        | 0.4 - 0.5        | $0.51 \pm 0.01$     |
| $K^+/\pi^-$     | $\frac{u\bar{s}}{\bar{u}d}$        | small            | $0.23 \pm 0.02$     |
| $p/\pi^-$       | $\frac{uud}{\bar{u}d}$             | small            | $0.23 \pm 0.02$     |

ws that the  
ectly propor-  
ements between  
ts of the same  
duced should  
tents of the

dimuons pro-  
This ratio is  
ediction  
ounting rule

The errors quoted are mainly due to relative luminosity estimates. The experimental results are in fairly good agreement with the naive predictions of the Drell-Yan model.

#### 4. Angular distribution

Due to the fact that the virtual photon is produced in an annihilation of 2 quarks of spin  $\frac{1}{2}$ , the  $\gamma^*$  should be transversely polarized and the  $\mu$  angular distribution can be written as follows :

$$\frac{dN}{d\cos\theta} \propto 1 + \lambda \cos^2\theta \quad \text{with } \lambda = 1 \text{ expected by the Drell-Yan model}$$

where  $\theta$  is the angle between one  $\mu$  and the  $q\bar{q}$  line of flight ( $\vec{L}$ ) in the c.m.s. of the dimuon.

This definition is the source of an experimental problem : how can  $\vec{L}$  be determined ?

- if  $P_T^{\mu\mu}$  is 0, then  $\vec{L}$  coincides with the beam axis
- if  $P_T^{\mu\mu}$  is not 0, then  $\vec{L}$  becomes more complicated.

Because experimentally  $P_T^{\mu\mu}$  is not equal to zero, one must choose an  $\vec{L}$  direction and we present 3 possibilities (see figure 10).

io is shown  
d by the NA3  
ratio de-  
limits given  
8] for both  
gen targets.  
y shows a  
which con-  
uction is  
rk fusion  
l-Yan predic-  
respectively  
or the plati-  
dashed line  
rget.

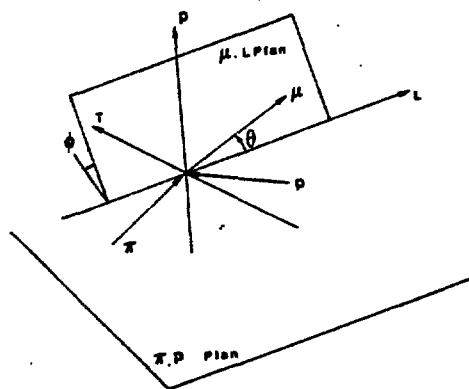


Fig. 10

#### a) Experimental measurement of $\lambda$

Figures 11 and 12 show the experimental data for incident  $\pi$ 's and protons from NA3 and CHFMP experiments respectively, presented in the C-S frame. The data are in good agreement with  $\lambda = 1$  within the experimental accuracy.

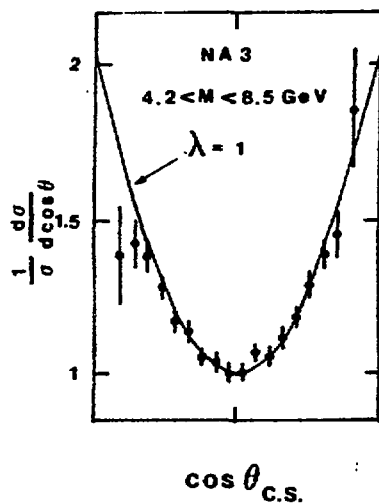


Fig. 11

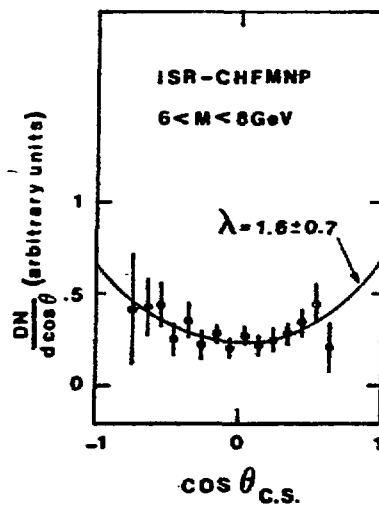


Fig. 12

In the case of  $\pi p$  collisions :

i)  $\vec{L} = \vec{\pi}$  : we are in the t-channel frame also called Gottfried-Jackson (G-J) frame.

In that case,  $P_T^{\mu\mu}$  is given by the target nucleon.

ii)  $\vec{L} = \vec{p}$  : this is the u-channel frame and  $P_T^{\mu\mu}$  is given by the  $\pi$ .

iii)  $\vec{L}$  is the external bissectrice between  $\vec{\pi}$  and  $\vec{p}$  directions (Collins-Soper frame (C-S)). This is an intermediate situation where  $P_T^{\mu\mu}$  is given by the proton and the pion.

#### b) More accurate

The g el

kson

$W(\theta, \phi)$

where the W's are

Sever el

i) One pion ex

$\pi$   $\pi$

ii) A second mo  
which the  $P_T$  of  
annihilation gra

iii) C. Lam and  
momentum of the  
C-S and G-J fr

In s  
tions :

The NA3 expe  
angular distribu

$W(\theta,$

where A is relat  
B, C have been  
 $P_T/M$  dependence



b) More accurate analysis of the angular distribution

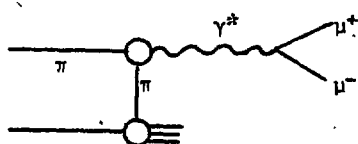
The general form of the angular distribution can be written :

$$W(\theta, \phi) = W_T(1 + \cos^2\theta) + W_L \sin^2\theta + W_\Delta \sin 2\theta \cos\phi + W_{\Delta\Delta} \sin 2\theta \cos 2\phi$$

where the W's are functions of  $M_{\mu\mu}$ ,  $x_F^{\mu\mu}$  and  $P_T^{\mu\mu}$ .

Several models have been proposed. We will only mention 3 of them :

i) One pion exchange (OPE) model of K.V.L. Sarma [21]. The diagram is the following :



This graph gives rise to a  $\sin^2\theta$  term in the angular distribution. Qualitatively, a polarization dependence with  $x_1$  is predicted : at small  $x_1$  only transverse polarization is present as expected by the Drell-Yan model, while there appears a partial longitudinal polarization at  $x_1$  close to 1.

ii) A second model of gluon emission was proposed by J. Collins [ref. 22] in which the  $P_T$  of the dimuon was provided by 1st order QCD corrections of the annihilation graphs (see chap. III.1).

iii) C. Lam and Wu Ki Tung [ref. 23] assumed that  $P_T^{\mu\mu}$  was due to the primordial momentum of the quarks and predicted  $\phi$  terms for the angular distribution in the C-S and G-J frames.

In summary, all these type of calculations give the following predictions :

- a longitudinal term of order  $P_T^2/M^2$
- a  $\sin\theta \cos\phi$  term of order  $P_T/M$
- a  $\sin^2\theta \cos 2\phi$  term of order  $\frac{1}{2} P_T^2/M^2$

The NA3 experiment has analysed its data in the following way [ref. 19]. The angular distribution is written as :

$$W(\theta, \phi) = (1 + \cos^2\theta) + A \sin^2\theta + B \sin 2\theta \cos\phi + C \sin^2\theta \cos 2\phi$$

where A is related to the previous  $\lambda$  parameter by :  $A = \frac{1-\lambda}{\lambda+1}$ . The parameters A, B, C have been determined in the 3 different frames and we have studied their  $P_T/M$  dependence (for  $0.4 < x_1 < 0.8$  and  $4.5 < M_{\mu\mu} < 8.5$  GeV).

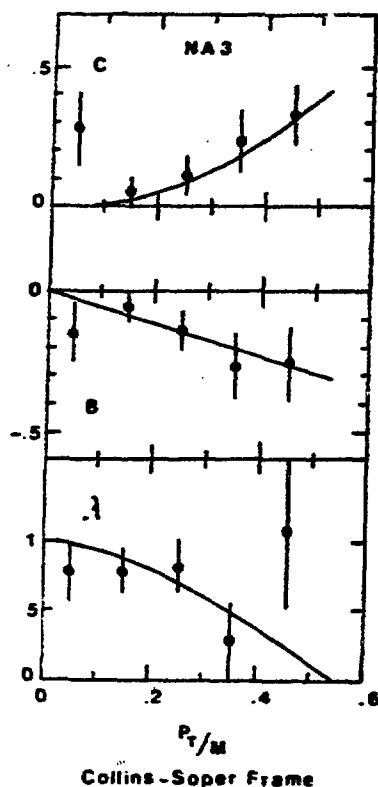


Fig. 13

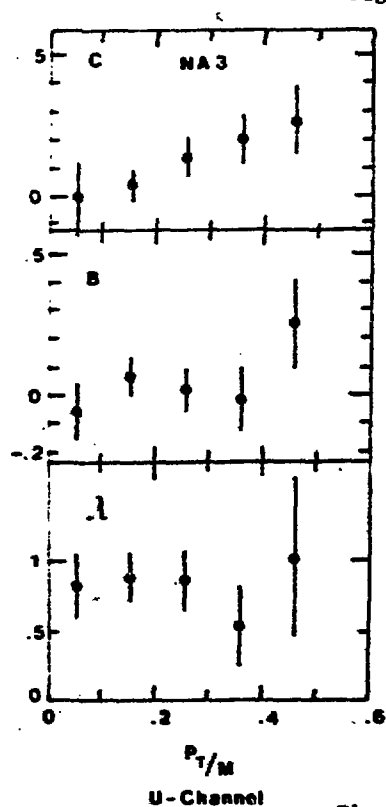


Fig. 14

## \* C-S frame

- $\lambda \sim 0.8$
- $B \sim (-0.6 \pm 0.2) P_T/M$
- $C \sim (1.5 \pm 0.5) P_T^2/M^2$

Figure 13 shows the  $P_T/M$  dependence of  $\lambda$ ,  $B$  and  $C$ . Curves are sketched using a linear (for  $B$ ) and quadratic (for  $C$ ) dependence of  $P_T/M$ .

## \* G-J frame

- $B \sim (-1.4 \pm 0.2) P_T/M$
- $C \sim (2 \pm 0.5) P_T^2/M^2$

Either in the C-S or G-J frames the relative magnitudes of the  $B$  and  $C$  terms may simply result from the choice of the reference frame.

## \* u-channel

Figure 14 shows the results of  $B$ ,  $C$ ,  $\lambda$  in the u-channel frame.

- $B \sim 0$
- $C \sim (1 \pm 0.5) P_T^2/M^2$

If one makes the assumption that the true physical angular distribution is  $1 + \cos^2 \theta$  with the line of flight of quarks as the  $\vec{L}$  axis, then the mean axis of quarks should be the u-channel frame where  $B$  and  $C$  are small. Moreover, no  $x_1$  dependence of  $\lambda$ ,  $B$  and  $C$  is observed in the u-channel frame.

c) Higher

duction with

 $\pi$  $p$ 

The correction

 $d\sigma =$ where  $\theta <$   
quark.

2

 $\lambda$ 

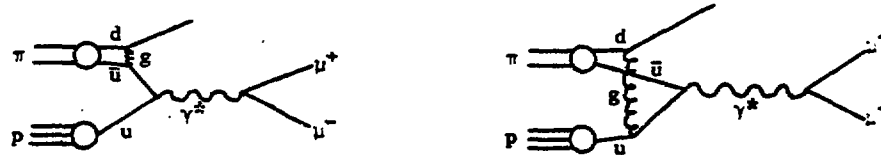
0

-1

0

c) Higher twist model of Berger and Brodsky

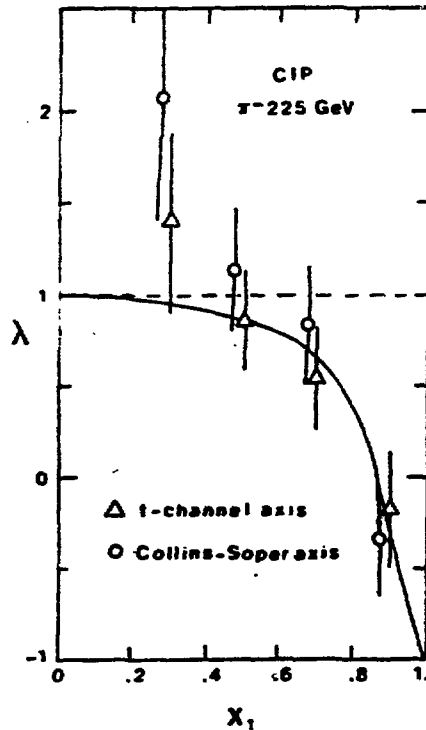
This model [ref. 24] is a specific model for the case of dimuon production with incident pions at large  $x_1$  ( $x_1 \geq 0.7$ ). The graphs are :



The corresponding cross section is then :

$$d\sigma = (1-x_1)^2 (1+\cos^2\theta) + \frac{4}{9} \frac{\langle k_T^2 \rangle}{M^2} \sin^2\theta + \frac{2}{3} \frac{\langle k_T \rangle}{M} (1-x_1) \sin 2\theta \cos\theta$$

where :  $\langle k_T^2 \rangle$  is the average of the square of the transverse momentum of the quark.



The main ideas of this model are :

- i) it works only for  $x_1$  greater than 0.7 ;
- ii) the first term shows a structure function of the  $\pi$  which behaves as  $(1-x_1)^2$  and a transverse polarization is expected ;
- iii) the second term predicts a longitudinal polarization with the presence of a scale breaking term (due to the  $1/M^2$  factor) ;
- iv) the third term shows the existence of an interference term.

In order to test this model, a good acceptance for  $x_1$  close to 1 is needed. The figure 15 shows the result of the CIP experiment for  $\pi^-$  at 225 GeV at Fermilab. The data are in good agreement with the Berger and Brodsky model which corresponds to the solid line in the figure.

Fig. 15

### 5. Absolute cross section

The Drell-Yan formula (1) allows us to compute the cross section for dimuon production if the hadron structure functions are known. In proton-proton or antiproton-proton collisions, the check of the model is possible as, in that case, the nucleon structure functions have been determined in DIS of leptons.

#### a) Proton-nucleon (uud) x (uud - ddu)

In that case, no valence-valence terms are present. Only valence-sea, sea-valence and sea-sea terms contribute in the calculation of the cross section. If sea quark distributions are not well-known, the calculated cross section could be wrong !

#### b) Antiproton-nucleon ( $\bar{u}ud$ ) x (uud - ddu)

Now, valence-valence terms are dominant, but the other terms still do exist.

#### c) ( $\bar{p}$ - nucleon) - (p - nucleon)

This is the best way to test the Drell-Yan prediction as, in that case, only valence-valence terms remain.

However, it is very hard to obtain high intensity  $\bar{p}$  beams.

From a sample of 275  $\bar{p}$  events at 150 GeV, the NA3 collaboration has measured the ( $\bar{p}$  - p) cross section and has compared the experimental result with the prediction of the Drell-Yan model. The disagreement observed gave rise to the now well-known K factor :

$$\left[ \frac{d^2\sigma}{dx_1 dx_2} \right]_{\text{exp}} = K \left[ \frac{d^2\sigma}{dx_1 dx_2} \right]_{\text{D-Y}}$$

Many other experiments have now measured the K factor in several experimental conditions. Table 4 summarizes the results :

|          |                       |           |
|----------|-----------------------|-----------|
|          |                       | tion for  |
|          |                       | -proton   |
|          |                       | in that   |
|          |                       | tons.     |
| Exp      | Be                    |           |
| NA3      | ( $\bar{p}$ -p<br>150 |           |
| NA3      | $\pi^+$<br>200        | nce-sea   |
| NA3      | $\pi^-$<br>200        | ; section |
| NA3      | $\pi^-$<br>200        | ion cou   |
| NA3      | ( $\pi^-$ - $\tau$    |           |
|          |                       | still     |
| NA3      | p<br>200              |           |
| NA3      | $\bar{p}$<br>150      |           |
| $\Omega$ | $\pi^-$<br>40         | that      |
| $\Omega$ | $\pi^+$<br>40         |           |
| $\Omega$ | ( $\pi^-$<br>40       |           |
| SISI     | $\pi^-$<br>150        | on has    |
| CFS      | p<br>200-4            | ult with  |
| MNTW     | p                     | se to     |

In conclusion,  
matic due to ab

tal

- Table 4 -

| Exp      | Beam                          | K               | Comments   |
|----------|-------------------------------|-----------------|--|
| NA3      | ( $\bar{p}$ -p) Pt<br>150 GeV | $2.3 \pm 0.4$   | • Poor knowledge of the sea distribution cannot explain K as only valence-valence terms are present.   |
| NA3      | $\pi^+$ Pt<br>200 GeV         | $2.4 \pm 0.4$   |  |
| NA3      | $\pi^-$ Pt<br>200 GeV         | $2.2 \pm 0.3$   | • Nuclear dependence is excluded to explain K factor.  |
| NA3      | $\pi^-$ He<br>200 GeV         | $2.4 \pm 0.4$   |  |
| NA3      | ( $\pi^- - \pi^+$ ) Pt        | $2.2 \pm 0.4$   | • This result excludes explaining K as due to contamination events like $\pi$ decays ; indeed such events cancel in the difference as they act in the same way for $\pi^+$ and $\pi^-$ . |
| NA3      | p Pt<br>200 GeV               | $2.2 \pm 0.4$   |  |
| NA3      | $\bar{p}$ Pt<br>150 GeV       | $2.3 \pm 0.4$   |  |
| $\Omega$ | $\pi^-$ W<br>40 GeV           | $2.45 \pm 0.42$ |  |
| $\Omega$ | $\pi^+$ W<br>40 GeV           | $2.52 \pm 0.49$ |  |
| $\Omega$ | ( $\pi^- - \pi^+$ )<br>40 GeV | $2.22 \pm 0.41$ |  |
| SISI     | $\pi^-$ C<br>150 GeV          | $2.8 \pm 0.6$   |  |
| CFS      | p W<br>200-400 GeV            | $\sim 1.5$      |  |
| MNTW     | p Fe                          | $1.6 \pm 0.3$   |  |

In conclusion, K is of the order of 2 - 2.5. The errors quoted are mainly systematic due to absolute normalisation problems.

### Origin of the K factor ?

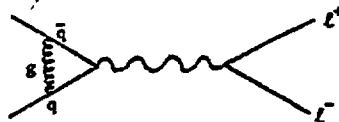
Calculations performed in the QCD framework by many theorists have led to the following conclusions :

- Scaling violation in DIS of leptons is a direct consequence of QCD effects. In the leading log approximation, these same QCD effects should be responsible for scaling violations in the structure function derived in the framework of the Drell-Yan model.
- Calculations in 1st order of QCD (25) have shown that the non leading log terms (NLL) give a large correction to the Drell-Yan cross section :

$$\sigma_{DY,QCD, \text{first order}} = K \sigma_{DY}$$

K is quasi constant and equal to 1.8 and is about the same for incident  $\pi$ 's or p's.

The most important contribution to this K factor corresponds to the vertex corrections shown in the graph :



- In addition Parisi has conjectured [ref. 26] that all higher order terms of this kind can be exponentiated.

The agreement between the experimental K factor and the theoretical calculation to 1st order of QCD seems satisfactory. But this might not be the end of the story as higher order terms have still not been calculated and some crucial questions remain open : does the K factor depend of  $M_{\mu\mu}$ ,  $P_T^{\mu\mu}$  or/and  $x_{\mu\mu}$  ?

### VI - CONCLUSIONS

In order to summarize the actual situation concerning the Drell-Yan model, some assertions of T.M. Yan given at the last 1981 Morions Workshop on Lepton Pair Production at Les Arcs, are appropriate :

$$\text{PARTON MODEL} = (\text{QCD})^0$$

$$\text{and } \text{REAL WORLD} = \text{PARTON MODEL} + \text{QCD CORRECTIONS}$$

The comparison between the experimental data on hadroproduction of dimuons and the "naive" Drell-Yan model are presented in table 5. In addition, the predictions of the "educated" Drell-Yan model are also shown.

- Table 5 -

| Topics                 | "Naive" Drell-Yan model | "Educated" Drell-Yan model  |
|------------------------|-------------------------|---|
| A dependence           | O.K.                    | O.K.  |
| Beam dependence        | O.K.                    | O.K.  |
| Scaling                | O.K. But ...            | • Violation is predicted but higher dilepton masses and more accurate experiments are needed.                               |
| Angular distribution   | O.K. But ...            | • Problem with high $P_T$ still not resolved<br>• Shape of the distribution not clear at $x_1$ close to 1.                  |
| Absolute cross section | No !                    | • Theoretical calculation of K factor seems satisfactory but is it accidental ? The question is still open (higher orders). |

A clear success of the Drell-Yan model is that it allows us to calculate the structure functions of unstable hadrons.

The experimental situation for the future is the following :

- NA3 will give results on the K dependence with their proton data at 400 GeV on platinum targets (more than 50 000 events) in a few months.
- NA10 and MNTW are performing high statistic experiments, respectively, with  $\pi^+$ ,  $\pi^-$  and protons. The data should soon be available.
- The new CIP collaboration has proposed a specific experiment for a better understanding of the angular distribution at  $x_1$  close to 1.
- Finally, at the Fermilab tevatron a new experiment (CFS extended collaboration) at high masses has been announced.

In conclusion, the study of hadroproduction of dileptons has already yielded many interesting results about the knowledge of fundamental constituents of particles and the future experiments will shed more light on the problems which are still not clearly resolved.

#### ACKNOWLEDGMENTS

I want to thank Professors A. Wreblewski and R. Sosnowski for their kind hospitality during the Conference.

## REFERENCES

- [1] See for example :
- a) G. Mathiae, CERN-EP/80-183 (9 Oct. 1980)  
To be published in the Rivista del Nuovo Cimento ;
  - b) R. Stroynowski, SLAC-PUB-2650 (Nov. 1980)  
To be published in Physics Reports ;
  - c) L. Lyons, Oxford University, Ref. 80/80 ;
  - d) J. Boucrot, XVIth International School of Elementary Particle Physics,  
Kupari-Dubrovnik (Oct. 2,3,4, 1980) LAL/80-40 (Dec. 1980) ;
  - e) J. Lefrançois, International Conference on High Energy Physics, Madison,  
Wisc. USA 17-23 July 1980 (LAL80/30, Sept. 1980).
- [2] S.D. Drell and T.M. Yan, Phys. Rev. Letters 25 (1970) 316.
- [3] H.D. Politzer, Phys. Reports 14C (1974) 129 ;  
A.J. Buras, Rev. Mod. Phys. 52 (1980) 199.
- [4] G. Altarelli et al., Phys. Letters 76B (1978) 351 and 356 ;  
H. Fritzsch and P. Minkowski, Phys. Letters 73B (1978) 80 ;  
K. Kajantie and R. Raitio, Nuclear Phys. B139 (1978) 72 ;  
G. Altarelli, Proc. EPS Conf. on High-Energy Physics, Geneva, 1979  
(CERN, Geneva, 1980), p. 727.
- [5] E.L. Berger, SLAC-PUB-2314 (1979).
- [6] Yu.L. Dokshitzer et al., Phys. Letters 78B (1978) 290 and 79B (1978) 269.
- [7] K. Kajantie et al., Phys. Letters 74B (1978) 384 ;  
J. Cleymans and M. Kuroda, Phys. Letters 80B (1979) 385 ;  
J.C. Collins, Phys. Rev. Letters 42 (1979) 291.
- [8] J. Badier et al., Contributions to the EPS International Conference on  
High Energy Physics, Geneva 1979, CERN Reports EP 79-67 and EP 79-68 ;  
J. Badier et al., Phys. Letters 89B (1979) 145 and contributions to the  
XXth International Conference on High Energy Physics, Madison 1980 ;  
CERN/EP 80-147 EP 80-148 and EP 80-150.
- [9] J.H. Cobb et al., Nuclear Instr. Met. 140 (1977) 413 and 158 (1979) 93 ;  
C. Kourkouvelis et al., Phys. Letters 91B (1980) 475.
- [10] D. Antreasyan et al., Proc. EPS Conf. on High-Energy Physics, Geneva, 1979  
(CERN, Geneva, 1980), p. 779 and Phys. Rev. Letters 45 (1980) 93.
- [11] S.W. Herb  
W.R. Innes  
L.M. Lederer  
(Physical  
A.S. Ito
- [12] K.J. Anderson
- [13] Contributions  
Janv. 25-
- [14] M.A. Abolmajeed
- [15] M.J. Cordery  
EP/80-152
- [16] J. Badier  
J. Badier  
Instr. Met.
- [17] K. Freudenreich
- [18] J. Badier
- [19] O. Callot
- [20] J. Badier
- [21] K.V.L. Sarin
- [22] J.C. Collins
- [23] C.S. Lam
- [24] E.L. Berger  
E.L. Berger
- [25] J. Kubar  
G. Altarelli  
J. Abad  
B. Humper  
293 and 83  
K. Harada
- [26] G. Parisi



- [11] S.W. Herb et al., Phys. Rev. Letters 39 (1977) 252 ;  
 W.R. Innes et al., Phys. Rev. Letters 39 (1977) 1240 ;  
 L.M. Lederman, Proc. 19th Int. Conf. on High-Energy Physics, Tokyo, 1978  
 (Physical Society of Japan, Tokyo, 1979), p. 706 ;  
 A.S. Ito et al., Fermilab-Pub-80/19-Exp (to be published in Phys. Rev.).
- [12] K.J. Anderson et al., Phys. Rev. Letters 36 (1976) 237.
- [13] Contribution to the Moriond Workshop on Lepton Pair Production - Les Arcs -  
 Janv. 25-31, 1981, To be published.
- [14] M.A. Abolins et al., Phys. Letters 82B (1979) 145.
- [15] M.J. Corden et al., Phys. Letters 76B (1978) 226 and CERN Preprint CERN  
 EP/80-152 (1980).
- [16] J. Badier et al., Phys. Letters 86B (1979) 98 ;  
 J. Badier et al., Preprint CERN EP/80-36 (1980), to be published in Nuclear  
 Instr. Met.
- [17] K. Freudenreich, Private communication.
- [18] J. Badier et al., To be published in Phys. Letters.
- [19] O. Callot, Thèse d'Etat, Université Paris-Sud, LAL 81/05.
- [20] J. Badier et al., Phys. Letters 89B (1979) 145.
- [21] K.V.L. Sarma, Tata Institute TIFR/TH/80-15.
- [22] J.C. Collins, Phys. Rev. Letters 42 (1979) 291.
- [23] C.S. Lam and W.K. Tung, Phys. Letters 80B (1979) 228.
- [24] E.L. Berger and S.J. Brodsky, Phys. Rev. Letters 42 (1979) 940 ;  
 E.L. Berger, Z. Physik C4 (1980) 289.
- [25] J. Kubar-André and F.E. Paige, Phys. Rev. D19 (1979) 221 ;  
 G. Altarelli, R.K. Ellis and G. Martinelli, Nuclear Phys. B157 (1979) 461 ;  
 J. Abad and B. Humpert, Phys. Letters 80B (1979) 286 ;  
 B. Humpert and W.L. Van Neerven, Phys. Letters 84B (1979) 327, 85B (1979)  
 293 and 89B (1979) 69 ;  
 K. Harada, T. Kaneko and N. Sakai, Nuclear Phys. B155 (1979) 169.
- [26] G. Parisi, Phys. Letters 90B (1980) 295.

# HYPERON POLARIZATION IN INCLUSIVE AND EXCLUSIVE PROCESSES

J. Szwed

Institute for Computer Science, Jagellonian University, Cracow, Poland

## Abstract

Hyperon polarization in inclusive and exclusive processes is explained by multiple scattering of the strange quark. Energy, Feynmann x and transverse momentum dependence is discussed, relations between polarizations of different hyperons in various processes is given. The charmed and bottom baryons are predicted to be analogically polarized.

I would like to report in the idea which explains qualitatively why the hyperons are polarized when produced in high energy processes at non zero transverse momentum. The subject causes some excitement since the measurements [1] of the  $\Lambda$  polarization which is essentially independent of energy and decreases from zero with increasing transverse momentum (Fig. 1). Similarly behaves the polarization of  $\Xi$ , the  $\Sigma$  gets polarized in the opposite direction. The axis with respect to which the polarization is measured points in the direction perpendicular to the scattering plane and is defined by

$$\hat{y} = \frac{\vec{p}_p \times \vec{p}_H}{|\vec{p}_p \times \vec{p}_H|}$$

where  $\vec{p}_p$  and  $\vec{p}_H$  are the c.m. momenta of the incoming proton and the hyperon, respectively. Similar measurements showed no sign of polarization for the protons and  $\bar{\Lambda}$ . To summarize the experimental facts one can say that there exists quite a complete set of information. At the same time we have no convincing explanation of this phenomenon. The data were a surprise - many people did not

expect  
transve

Let

Here th

of ud

is enti

rization

Loc

diquark

which a

come fr

by gluo

c.m. sy

the ud-

Loc

automat

transve

$p_{\perp}$  • Cu

by mult

bute to

rather

suming

g is th

and  $I^2$ ,

Polariz

theory

ACCESS

Cracow

processe

energ

sed,

rious

ected

valit

rgy

es se

rization

from

behav

osite

is a

ring

ton a

o sig

exper

set

atic

id na

expect important spin effects at high energies, the more at higher transverse momentum where a real, hard amplitude dominates.

Let me start to present the model with the  $\Lambda$  polarization. Here the situation is the clearest. The  $\Lambda$  wave function consists of  $ud$  diquark in spin zero state so the spin projection of the  $\Lambda$  is entirely given by that of the  $s$ -quark and consequently their polarizations are equal:  $\mathcal{P}(\Lambda) = \mathcal{P}(s)$ .

Looking into the proton hemisphere one already has an  $ud|_{s=0}$  diquark originating from the proton. The source of the  $s$ -quarks which are needed to recombine into the  $\Lambda$  are twofold: they either come from the proton sea or are produced in the interaction region by gluons in the subprocess  $g \rightarrow s\bar{s}$ . In both cases its energy in the c.m. system is low. The  $\Lambda$  energy is essentially given by that of the  $ud$ -diquark.

Looking for the  $\Lambda$ 's with a given transverse momentum  $p_{\perp}$  one automatically chooses states in which the  $s$ -quark has considerable transverse momentum  $k_{\perp}$  pointing in most cases in the direction of  $p_{\perp}$ . Our main assumption is that the  $s$ -quark gets its required  $k_{\perp}$  by multiple scattering off quarks and gluons. Many diagrams contribute to this process and there is no clear summing technique due to rather low momentum transfers. We approximate the procedure by assuming the scattering off external gluonic field

$$\phi^a(\vec{q}) = \frac{4\pi g I^a}{\vec{q}^2},$$

$g$  is the quark-gluon coupling constant,  $\vec{q}$  - the momentum transfer and  $I^a$ ,  $a = 1, \dots, 8$  is the vector representing the external field. Polarization appears already in the second order of perturbation theory and reads then [2]

$$\mathcal{P} = \frac{C g^2 m |\vec{k}|}{2\pi E^2} \frac{\sin^3 \theta/2 \ln \sin \theta/2}{(1 - \frac{k^2}{E^2} \sin^2 \theta/2) \cos \theta/2} \cdot \hat{s} \quad (1)$$

where  $m$ ,  $k$ ,  $E$  and  $\theta$  are the mass, momentum, energy and scattering angle of the quark. The unit vector  $\hat{v} = \frac{\vec{k}_i \times \vec{k}_f}{\sin \theta}$  points in the direction perpendicular to the scattering plane. The colour factor  $C = \frac{1}{2}(d^{abc}I^a I^b I^c)/(I^a)^2$ . For positive  $C$  the expression multiplying  $\hat{v}$  is negative, thus the polarization is opposite to  $\hat{v}$  (Fig. 2). Another way of calculating  $\mathcal{P}(q)$  is to solve the Dirac equation in external field. The exact answer [3] looks then qualitatively the same as in Fig. 2. Many required features follow immediately. Increasing  $k_{\perp}$  means increasing  $\theta$  between  $0^\circ$  and  $90^\circ$  - one sees that the polarization increases then in magnitude with  $p_{\perp}$ . The polarization increases with the quark mass. We thus expect stronger polarization of baryons containing charmed and bottom quarks (e.g.  $\Lambda_c$ ) if the  $c$ - or  $b$ -quark sea is not much different from the  $s$ -quark sea. This is also the reason why we do not expect the protons to be polarized.

Because  $x_{\Lambda}$  comes predominately from the  $x_{ud}$  there is no strong  $x_{\Lambda}$  dependence of polarization. This statement concerns however directly produced  $\Lambda$ 's, the total sample which contains  $\Lambda$ 's being resonance decay products may show some increase of  $\mathcal{P}(\Lambda)$  with  $x_{\Lambda}$ .

Once the mechanism of the quark polarization is fixed many relations among polarizations of different hyperons are given by their spin-flavour wave functions. So one expects e.g.  $\mathcal{P}(\Xi) = -1/3 \mathcal{P}(\Lambda)$  a relation which holds experimentally [4] but without the factor  $1/3$ . This can again be attributed to the resonance decays which predominately "pollute" the  $\Lambda$  sample.

It is crucial that the  $s$ -quark is relatively slow, otherwise the polarization would be negligible. This is the reason why  $\bar{\Lambda}$  is not polarized in proton induced reactions, for its finite  $x_{\bar{\Lambda}}$  one needs

finite  $x_{\bar{s}}$ . I  
in the  $\pi$

Our idea  
Strong  $\Lambda$   
production w  
teresting ef

In both case  
sphere. In t  
small angle  
proton - one  
production.  
angle to fo  
to the scat  
in  $\mathcal{P}(\Lambda)$ ,  
at  $\hat{v} \sim \vec{k}_i$   
process (2a)

one expects  
but of oppos  
To summ  
qualitativel  
be interest

It is wo  
the known m  
tion require  
I would  
discussions.

tor  
ing  
2).  
in  
the  
n-  
at  
iza-  
ari-  
c)  
sea.  
pola-  
 $x_{\Lambda}$   
ectly  
onanc  
re-  
their  
 $\mathcal{P}(\Lambda)$   
tor  
pre-  
se the  
not  
needs

finite  $x_g$ . It can be however polarized in the  $\pi$  induced reactions in the  $\pi$  hemisphere.

Our idea can be easily implemented in exclusive processes. Strong  $\Lambda$  and  $\Sigma$  polarizations analogical to these in inclusive production was observed in  $pp \rightarrow \Lambda \bar{\Lambda}$  and  $pp \rightarrow \Sigma \bar{\Sigma}$  [5]. An interesting effect appears when comparing two processes

$$K^- p \rightarrow K \bar{K} \Lambda + \text{pions} \quad (2a)$$

$$\bar{K} p \rightarrow \Lambda + \text{pions} \quad (2b)$$

In both cases one looks at the  $\Lambda$  polarization in the proton hemisphere. In the first process the kaon scatters predominately by a small angle so the  $\Lambda$  gets the s-quark in the usual way from the proton - one expects thus no difference as comparing to inclusive production. In the second case however the s-quark turns by a large angle to form the  $\Lambda$  in the proton hemisphere ( $p_{\perp} = 0$  corresponds to the scattering by  $180^\circ$ ). Increasing  $p_{\perp}$  means again an increase in  $\mathcal{P}(\Lambda)$ , but the question is with respect to which axis. Looking at  $\vec{V} \sim \vec{k}_1 \times \vec{k}_f$  one sees that it changes sign when going from the process (2a) to (2b) because  $k_1$  changes its direction. Consequently one expects in both processes analogical behaviour of polarization but of opposite sign. This is in fact what is seen experimentally [6].

To summarize, we have shown how a single idea is able to account qualitatively for all known facts of hyperon polarization. It would be interesting to check the predictions which were made in this talk.

It is worth noting that this idea can be easily implemented in the known models of low and intermediate  $p_{\perp}$ . A quantitative description requires only the knowledge of the quark structure functions.

I would like to thank M. Krawczyk, W. Ochs and L. Stodolsky for discussions.

## References

- [1] G. Bunce et al.: Phys. Rev. Lett. 36 (1976) 1113,  
 S. Erhan et al.: Phys. Lett. 82B (1979) 301,  
 M.L. Facinni-Turluer et al.: Z. Phys. C1 (1979) 19,  
 F. Lomanno et al.: Phys. Rev. Lett. 43 (1979) 1905,  
 K. Rayadhuri et al.: Phys. Lett. 90B (1980) 313,  
 K. Heller et al.: Phys. Lett. 68B (1977) 480,  
 K. Heller et al.: Phys. Rev. Lett. 41 (1978) 607.
- [2] A.W. McKinley and H. Feshbach: Phys. Rev. 74 (1948) 1759,  
 R.H. Dalitz: Proc. Roy. Soc. (London) A206 (1951) 509.
- [3] N.F. Mott and H.S.N. Masey: Theory of Atomic Collisions,  
 III ed., Oxford.
- [4] R. Polvado: Talk at HEPPBPT Conference (1978).
- [5] H.W. Atherton et al.: Nucl. Phys. B69 (1974) 1.
- [6] Amsterdam-CERN-Nijmegen-Oxford Coll.: Report CERN/EP/Phys.  
 80-167,  
 S. Al-Harran et al.: preprint CERN/EP 80-167.

## Figure captions

- Fig. 1. Polarization as a function of the transverse momentum  
 $p_{\perp}$  (from Ref. [1]).
- Fig. 2. Polarization of the quark in external gluonic field  
 (arbitrary normalization).
- Fig. 3.  $\Lambda$  polarization in the process  $K^- p \rightarrow KKA + \text{pions}$   
 (circles) and  $K^- p \rightarrow A + \text{pions}$  (squares) at 4.2 GeV/c  
 (from Ref. [6]).

19,  
05,

18) 1759,  
) 509.  
lisions,

V/EP/Phys.

momentum

field

pions  
4.2 GeV/c

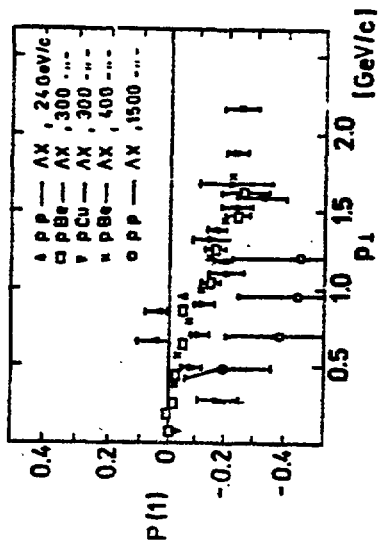


Fig.1

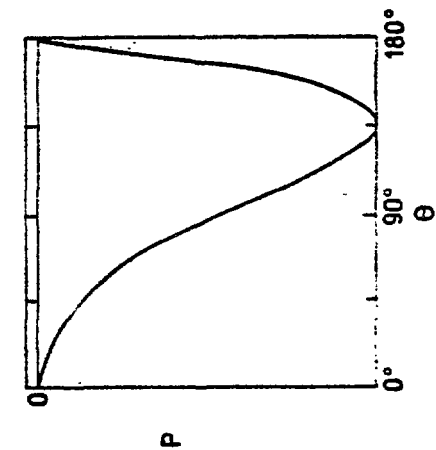


Fig.2

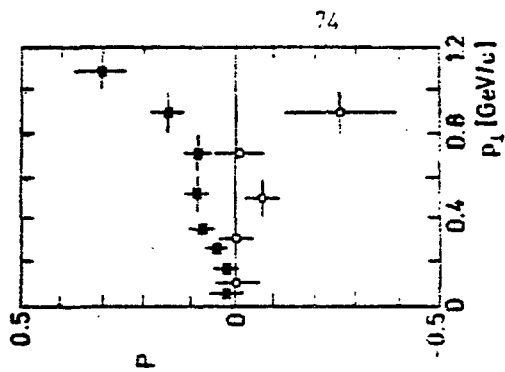


Fig.3

PROMPT SINGLE MUON PRODUCTION BY PROTONS ON IRON

A. Bodek,<sup>1</sup> R. Breedon, R.N. Coleman, W. Marsh, S. Olsen, and J.L. Ritchie  
University of Rochester, Rochester, New York 14627

B.C. Barish, R.L. Messner, M.H. Shaevitz,<sup>2</sup> and E.J. Siskind<sup>3</sup>  
California Institute of Technology, Pasadena, California 91125

F.S. Merritt  
University of Chicago, Chicago, Illinois 60637

H.E. Fisk, P.A. Rapidis, and Y. Fukushima  
Fermilab, Batavia, Illinois 60510

G. Donaldson and S.G. Wojcicki  
Stanford University, Stanford, California 94305

presented by S. G. Wojcicki

ABSTRACT

A new experiment has been performed at Fermilab to measure the hadronic production of prompt single muons. A preliminary analysis of a sample of the data indicates approximately equal production of prompt single  $\mu^+$ 's and  $\mu^-$ 's in 350 GeV p-Fe interactions. The observed momentum distributions of prompt single  $\mu^+$ 's and  $\mu^-$ 's can satisfactorily be fit by the hypothesis of central production of D mesons with a cross section of  $16 \pm 4 \mu\text{b/nucleon}$ .

1. Alfred P. Sloan Foundation Fellow
2. Present address: Columbia University, New York, NY 10027
3. Present address: Brookhaven National Laboratory, Upton, NY 11973

We have  
of prompt s  
both 350 G  
instrumente  
nique was e  
nating from  
Prompt dimu  
tifier.

Data w  
required on  
This corres  
sphere, all  
cross secti  
the semi-le  
figuration  
20 GeV.

Result  
GeV trigger  
Results fro  
tributions  
dominated by  
induced and  
The de  
momentum of  
variable de  
trometer.

The ta  
lation coun  
independent  
varied. Of  
the density  
at three di  
most compac  
steel.

Ritchie

3  
1125

had-  
a  
mpt  
momentu  
fit  
ion of

1973



We have performed an experiment at Fermilab to measure the production of prompt single muons in hadronic interactions. Data were taken with both 350 GeV protons and 280 GeV  $\pi^-$ 's incident on an iron "beam dump" instrumented with scintillation counters. The density extrapolation technique was employed to separate prompt muons from non-prompt muons originating from decays of long-lived particles such as  $\pi$ 's,  $K$ 's, and hyperons. Prompt dimuons were identified with a very large acceptance muon identifier.

Data were taken in two different triggering configurations. One required only that the produced muon have momentum greater than 8 GeV. This corresponds, for the 350 GeV proton data, to most of the forward hemisphere, allowing a fairly model-independent determination of the charm cross section, if prompt single muons are interpreted as the products of the semi-leptonic decays of charmed hadrons. The other triggering configuration was more restrictive. It required a minimum muon momentum of 20 GeV.

Results are reported here only for the proton data taken with the 20 GeV trigger. (We have analyzed about one-half of this data sample.) Results from the full data set will i) extend the prompt single muon distributions to lower  $p$ , ii) reduce the size of the errors, which are dominated by statistics, and iii) allow a comparison between proton induced and pion induced charm production.

The detector<sup>1)</sup> consisted of a beamline spectrometer to measure the momentum of each incoming hadron, a target-calorimeter which served as a variable density "beam dump", a muon identifier and an iron toroid spectrometer. See Figure 1.

The target-calorimeter consisted of 49 steel plates with a scintillation counter on the downstream face of each. The plates were mounted independently on rails so that the spacing between the plates could be varied. Of the 2.4 meters of steel comprising the target-calorimeter, the density of the upstream most 1.7 meters was varied. Data were taken at three different effective densities,  $\rho$ , in the ratio 1:2/3:1/2. The most compact density of the target-calorimeter was about 3/4 that of steel.

Ritchie

3

1125

had-  
f a  
mpt  
momentum  
fit by  
ion of

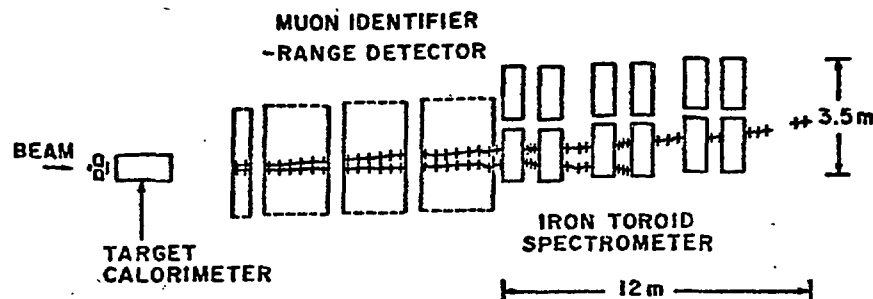


Figure 1. Plan view of the apparatus.

The muon identifier consisted of 42 3mx3m scintillation counters and 21 3mx3m spark chambers sandwiched periodically throughout 4.5 meters of steel. This device allowed identification of muons down to 5 GeV/c in momentum.

The toroid spectrometer, composed of 24 magnetized iron disks of radius 3.6 meters and interspersed with scintillation counters and spark chambers, allowed a determination of muon sign and momentum (with resolution of about 12%). It should be noted that the toroid spectrometer was placed "off-axis" (i.e., displaced laterally from beam center by one-half radius) to avoid a hole in the acceptance for low  $p_T$  muons.

Each event was required to pass selection criteria which consisted of a beamline PWC requirement of one and only one incoming hadron with momentum within 2% of beam momentum, a hadronic interaction in the upstream 25cm of the calorimeter, a requirement that muons originate in the target-calorimeter (to remove triggers from halo muons in time with hadrons) and a requirement that the triggering muon traverse the entire toroid system.

Events passing these selection criteria were placed in one of four categories: (i) a single triggering  $\mu^+$ , (ii) a single triggering  $\mu^-$ , (iii) dimuon with a triggering  $\mu^+$ , and (iv) dimuon with a triggering  $\mu^-$  (note that an event with two muons of opposite sign both of which trigger will fall into both iii and iv). Figure 2 shows the trigger rates of these types of events versus density. The intercepts at  $1/\rho = 0$  of the lines drawn through the single  $\mu^+$  and  $\mu^-$  rates are the prompt single  $\mu^+$  and  $\mu^-$  signals, respectively. The difference in the slopes of these two lines is a result of more  $\pi^+$ 's than  $\pi^-$ 's being produced in proton interactions.

There was  
metric di  
identifi  
calculat  
dimuon e  
are show  
producti  
muon rat  
proton a.  
A  
in this  
place in  
interact  
calorime  
earlier  
this bac  
The  
with two  
pendent)

ters and  
ters of  
/c in  
s of  
d spark  
resolu-  
ter was  
one-half  
sisted  
with  
e  
nate in  
e with  
entire  
lines  
and  $\mu^-$   
lines i  
ions.

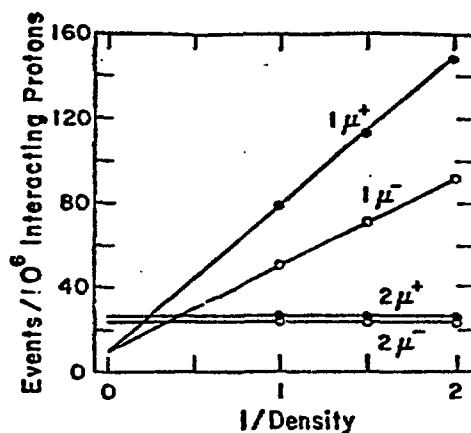


Figure 2. Event rates versus 1/density.

There was a contamination in the single muon sample from highly asymmetric dimuon events because muons of momentum less than 5 GeV were not identified. This background was subtracted with the aid of a Monte Carlo calculation which was normalized to the observed number of identified dimuon events. The resulting prompt single muon distributions versus  $p$  are shown in Figure 3a and 3b. The data indicate equal rates for the production of  $\mu^+$  and  $\mu^-$  events. The efficiency corrected prompt single muon rates for  $p > 20$  GeV/c are  $(12.2 \pm 3.8) \times 10^{-6}$   $\mu^+$ 's per interacting proton and  $(10.1 \pm 2.6) \times 10^{-6}$   $\mu^-$ 's per interacting proton.

A possible source of additional background has not been subtracted in this preliminary analysis. Decays from non-prompt sources which take place in the unexpanded region of the target-calorimeter (recall that 10 interaction lengths are expanded), or in the drift space following the calorimeter, would result in a false prompt single muon signal. In an earlier experiment<sup>2)</sup> with a significantly smaller target-calorimeter, this background was calculated to be small.

The prompt single muon distributions in Figure 3 have been compared with two models of  $D\bar{D}$  production. In model A, D's were produced independently according to

$$E \frac{d^3\sigma}{d^3p} = (1-x)^{\alpha} e^{-\beta p_T}$$

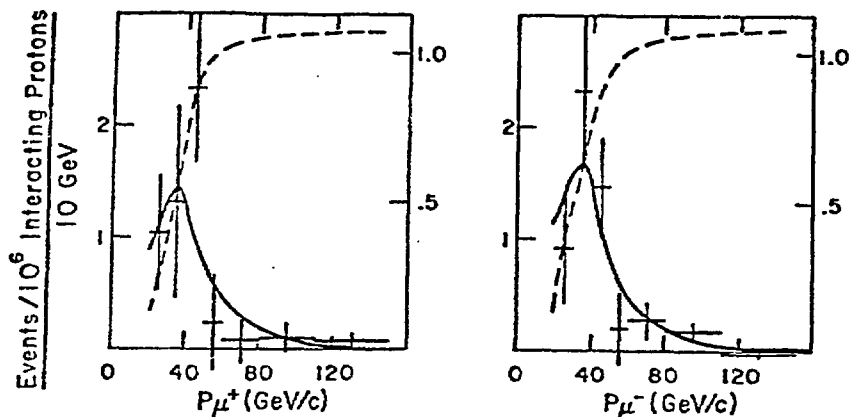


Figure 3. Prompt single muon rates versus momentum for  $\mu^+$  (a) and  $\mu^-$  (b). The rates are not corrected for trigger efficiency. The dashed line is the efficiency. It can be greater 1.0 because it includes resolution smearing effects. The solid line is from the best fit DD production model A (see text).

In model B,  $c\bar{c}$  pairs were produced with a mass  $m$  according to

$$E \frac{d^3\sigma}{d^3p} = \frac{1}{n^3} (1-x)^\alpha e^{-2p_T/c} e^{-\gamma m/\sqrt{s}}$$

and the composite  $c\bar{c}$  systems decayed into  $D\bar{D}$  pairs. For both models, we have assumed that the semi-leptonic decay modes of the  $D$  are  $D \rightarrow K\mu\nu$  (60%) and  $D \rightarrow K^*\mu\nu$  (40%). Both of these models adequately fit the data. The best fit with model A was achieved with  $\alpha = 4.7 \pm 1.0$  and  $\beta = 2.5$  ( $\beta$  was kept fixed). The best fit with model B was achieved with  $\alpha = 2 \pm 1.2$ ,  $\beta = 2.5$ , and  $\gamma = 15$  ( $\beta$  and  $\gamma$  were kept fixed).

It is instructive to plot the rate for producing single muons with momentum  $p$  greater than  $p_{\min}$ . This plot, Figure 4, was obtained by correcting the data in Figure 3 for efficiency and adding the  $\mu^+$  and  $\mu^-$  rates. The corresponding curves calculated from models A and B, discussed above, are similar (the curve for model A is shown in Figure 4). The intercept of these curves at  $p_{\min}=0$  is simply the total prompt single muon rate. For model A this rate is  $(1.9 \pm 0.4) \times 10^{-4}$  and from model B it is  $(1.8 \pm 0.6) \times 10^{-4}$ . If we assume an 8% average branching ratio and linear  $A$ -dependence, these rates correspond to total charm production cross sections of  $16 \pm 4 \mu\text{b/nucleon}$  and  $15 \pm 5 \mu\text{b/nucleon}$ , respectively. Here the errors are only statistical, and mainly come from the uncertainty in  $\alpha$ .

Also sh  
production r  
When our ne  
tial improve  
In conc  
prompt  $\mu^+$ 's  
firm results  
 $\nu_\mu$  and  $\bar{\nu}_\mu$  ra  
a central  $D\bar{D}$   
The data do  
sections of

Figure 4. To

#### REFERENCES

1. Parts of Caltech-
2. K.H. F...
3. J.L. Ric with
4. K. Klein Physics Pondron cor-
5. G. Sago discussed

Also shown in Figure 4 is a measurement of the total prompt muon production rate above 8 GeV from an early test run of this experiment<sup>3)</sup>. When our new low momentum data is analyzed, it will provide a substantial improvement in this region.

In conclusion the data indicate approximately equal production of prompt  $\mu^+$ 's and  $\mu^-$ 's in 350 GeV p-Fe interactions. The data do not confirm results<sup>4)</sup> from beam dump experiments which indicate unequal prompt  $\nu_\mu$  and  $\bar{\nu}_\mu$  rates. The momentum distribution are adequately described by a central  $D\bar{D}$  production model with a cross section of  $16 \pm 4 \mu\text{b/nucleon}$ . The data does not indicate a large diffractive charm production cross sections of the magnitude reported<sup>5)</sup> by ISR experiments ( $\sqrt{s} = 60 \text{ GeV}$ ).

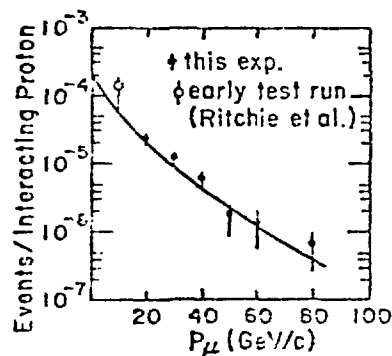


Figure 4. Total prompt single  $\mu$  rates ( $\mu^+ + \mu^-$ ) with  $p$  greater than  $p_{\min}$ .

#### REFERENCES

1. Parts of the detector have been used in neutrino experiments by the Caltech-Fermilab-Rochester-Rockefeller group.
2. K.W. Brown, Ph.D. thesis, Caltech, 1980.
3. J.L. Ritchie, et al., Phys. Rev. Lett. **44** 230 (1980).
4. K. Kleinknecht, Proceedings of the XXth International High Energy Physics Conference, Madison, June 1980, p. 237, L. Durand and L.G. Pondrom editors.
5. G. Sagot ibid p. 193, also S. Wojcicki ibid p. 1430.

WHAT CAN WE LEARN FROM STRUCTURE FUNCTIONS MEASURED  
IN NEUTRINO INTERACTIONS

F. Eisele

Abteilung Physik, Universität Dortmund, Fed. Rep. Germany

Summary

The new measurements of structure functions by the CDHS-collaboration are substantially improved compared to published results. It is discussed how much we can learn from these data about QCD and the gluon distribution by the analysis of moments and of the full  $x$ -dependence. It is shown that these new data combined with SLAC ed-data are able to separate QCD-effects from higher twist and other possible non perturbative effects within "reasonable" assumptions. The presence of non perturbative contributions is required at large  $x$  ( $x \gtrsim .5$ ) and low  $Q^2$  only. Their shape and magnitude agree well with popular models of diquark contributions. The analysis results in a value of  $\overline{\alpha}_{MS} = .2 \pm .1$ . (auth)

I The experimental data

I.1 The measurement of total cross-sections: experimental problem or hint for new physics ?

The determination of structure functions relies on a decent knowledge of neutrino and antineutrino fluxes, i.e. total cross-sections. A summary of old and new measurements is given in table I.

Table I [1]:  $\sigma_t/E_\nu \cdot 10^{38} \text{ cm}^2/\text{GeV}$

| Experiment     | $E_\nu$ | $\bar{\nu}$     | $\nu$           | $\bar{\nu}/\nu$ |
|----------------|---------|-----------------|-----------------|-----------------|
| GGM 73         | 2-10    | .28 $\pm$ .02   | .74 $\pm$ .05   | .38 $\pm$ .02   |
| CTFR 77        | 45-205  | .29 $\pm$ .015  | .61 $\pm$ .03   | .48 $\pm$ .02   |
| CDHS 78        | 30-200  | .30 $\pm$ .02   | .62 $\pm$ .03   | .48 $\pm$ .02   |
| GGM 79         | 3       |                 | .69 $\pm$ .05   |                 |
|                | 9       |                 | .61 $\pm$ .06   |                 |
| BEBC 77        |         | .29 $\pm$ .03   | .63 $\pm$ .05   |                 |
| CFRR (79)      | 60-260  |                 | .70 $\pm$ .038  |                 |
| CFRR (80)      | 40-225  | .376 $\pm$ .019 | .719 $\pm$ .036 | .523 $\pm$ .03  |
| CHARM (80)     | 20-200  | .301 $\pm$ .018 | .604 $\pm$ .032 | .498 $\pm$ .019 |
| BEBC (prel.)   | 20-200  | .299 $\pm$ .016 | .634 $\pm$ .029 | .472 $\pm$ .019 |
| GGM (SPS) (80) | 10-150  | .29 $\pm$ .04   | .61 $\pm$ .08   | .475 $\pm$ .09  |

We have the worrying and frustrating fact, that the CFRR-experiment, which has invested a lot of time and effort into these measurements finds values which are incompatible with all other experiments within the statistical and known systematic errors. Do neutrinos disappear in Fermilab:  $\nu_\mu \leftrightarrow \nu_\tau$ ? This is indeed a remote possibility since the CFRR-experiment has a significant different value of  $L/E_\nu$  from all other experiments. An explanation in terms of neutrino oscillations is however not very likely as will be explained in detail by J.Wotschak in his talk[2].

Thus we have to live with the fact that the experimental basis of our structure function measurements may not be as sound as it should be. It should be noted however that the  $\bar{\nu}/\nu$  ratio (which can be checked by the physical requirement of charge symmetry) is not affected by this problem. This is fortunate since any absolute simultaneous flux error for neutrinos and antineutrinos affects the structure functions only as an absolute scale error but does not change their shape.

I.2 Str

It is  
tribut  
on isos

F2<sup>W</sup>

xF3<sup>W</sup>

$\bar{\nu}$   
q (x)

The mea  
QCD fit  
small a  
SLAC [3  
ion de  
differe  
errors

Fig. 1:

## 1.2 Structure Functions

It is by now well known that neutrino experiments are able to measure the distributions of valence and sea quarks separately. Three structure functions on isoscalar targets have been measured by the CDHS collaboration:

$$F_2^{\nu N}(x, Q^2) = x(u+d+s+c+\bar{u}+\bar{d}+\bar{s}+\bar{c}) \propto \frac{d\sigma^{\nu N}}{dx} + \frac{d\sigma^{\bar{\nu} N}}{dx}$$

$$xF_3^{\nu N}(x, Q^2) = q_{\text{valence}}(x, Q^2) \propto \frac{d\sigma^{\nu N}}{dx} - \frac{d\sigma^{\bar{\nu} N}}{dx}$$

$$\bar{q}^{\nu}(x, Q^2) = x(\bar{u}+\bar{d}+2\bar{s}) \propto \frac{d\sigma^{\bar{\nu} N}}{dx} \text{ at high } y$$

The measurements of  $F_2$  are shown in figure 1 together with the result of a QCD fit.  $F_2$  is well measured and shows substantial scaling violations both at small and large values of  $x$ . This measurement agrees well with e-d-data from SLAC [3] and with the preliminary results of the EMC-collaboration [4] from muon-ion deep inelastic scattering. To my best knowledge there is no significant difference between these data sets within the known statistical and systematic errors.

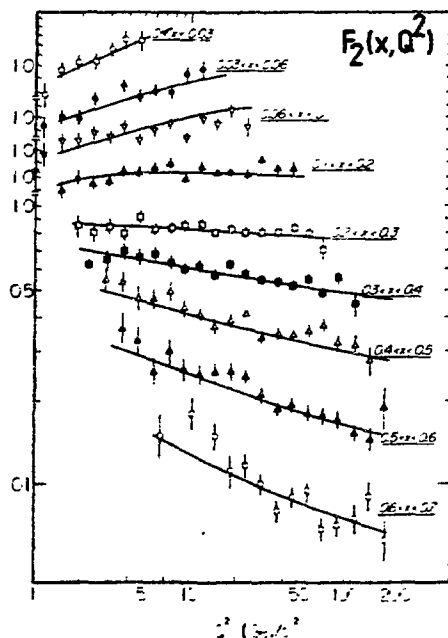


Fig.1:  $F_2^{\nu N}(x, Q^2)$  as measured by the CDHS collaboration

A value of  $R = \sigma_L/\sigma_T = .1$  was assumed. The solid lines are the results of the leading order QCD-fit described in sect. III.1.

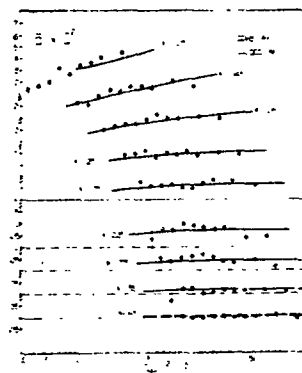


Fig.2:  $\bar{q}^{\nu}(x, Q^2)$  as measured by the CDHS collaboration

The valence distribution  $xF_3$  is rather badly known in the sea region where it contributes independent information. This situation will be substantially improved in the near future when a new analysis based on high statistics wide band beam data will be finished. At present, however, the measurement of  $xF_3$  plays a minor role in the analysis of structure functions.

Important new information is contributed by the new measurement of the antiquark distribution in the nucleon which is based on  $\sim 150000$  events  $\bar{\nu}_\mu + N \rightarrow \mu^+ + X$  from wide band beam and  $\sim 25000$  events from narrow band beam exposures. The extraction of  $\bar{q}(x, Q^2)$  is illustrated in figure 3, where the differential cross section  $d\sigma^{\bar{\nu}N}/dx$  is displayed for two energy bins and several bins in  $y$ . The cross sections of quarks is subtracted by using the neutrino cross-section multiplied by  $(1-y)^2$ .

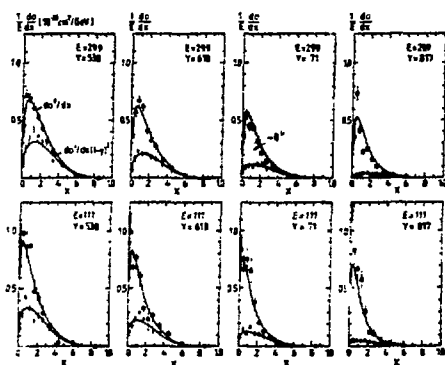


Fig.3:  $d\sigma^{\bar{\nu}N}/dx$  for 2 energy bins and several bins in  $y$ . Also shown is  $d\sigma^{\bar{\nu}N}/dx \cdot (1-y)^2$  which measures the cross section for the scattering off quarks

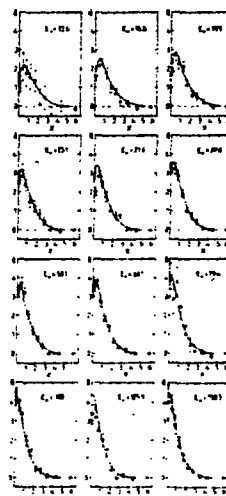


Fig.4:  $\bar{q}(x, E_h)$   
(A value of  $R=.1$  was assumed.)

The measured antiquark distribution (assuming a value  $R = \sigma_L/\sigma_T = .1$ ) is shown in fig.2 versus  $Q^2$  and in figure 4 for fixed  $\nu = E_h$ -bins. Evidently the antiquark distribution rises substantially with  $Q^2$ . The most important fact however is, that there are no antiquarks above  $x = .45$ . This poses a severe limitation on the width of the gluon distribution as we will see later.

To be more precise, it should be stated that there are no light antiquarks with charge  $1/3$  ( $\bar{s}, \bar{d}$ ) above  $x = .45$ . Unfortunately no bound can be given on the presence of  $c\bar{c}$  and  $b\bar{b}$  quarks at large  $x$  since antineutrinos cannot scatter off a  $\bar{c}$  or  $\bar{b}$ -quark.

The determination of  $F_2$  and  $\bar{q}$  is affected by uncertainties in the value of  $R = \sigma_L/\sigma_T$  and in the effect of charm-threshold. How much these uncertainties affect the analysis of structure functions will be discussed in section III.

## II. Analysis

It has been verified that the function  $1/(x^2 F_2(x, Q^2))$  of moments for

- simple prediction
- second order
- are available
- target mass
- QCD ingredients

In the following we are restricted to a  $Q^2$ -range, pro

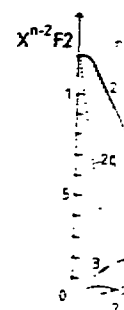


Fig.5a: Structure weight arrows value

Figure 5a shows of  $x$  for  $Q^2 =$  are very strong of  $F_2$  are used of sea quarks, second moment of the moments Thus if we want  $F_2$  we are rest ment of  $\langle x \rangle_{\text{glu}}$  moments. This



## II. Analysis of moments

It has been very popular (and still is) to interpret the  $Q^2$ -evolution of structure functions by using their (Nachtmann) moments at fixed  $Q^2$ :  $\langle F_i(Q^2) \rangle_n = \int_0^1 x^n F_i(x, Q^2) dx$ . It is certainly true that we have a lot of arguments in favour of moments from a theoretical point of view:

- simple predictions for their  $Q^2$ -evolution
- second order corrections for non-singlet and singlet structure functions are available
- target mass corrections are straight forward
- QCD ingredients can be tested separately

In the following I want to demonstrate that a meaningful use of moments is restricted to a small number of nonsinglet moments ( $n = 3, 4, 5, 6$ ) in a limited  $Q^2$ -range, provided that correlations are correctly included in the analysis.

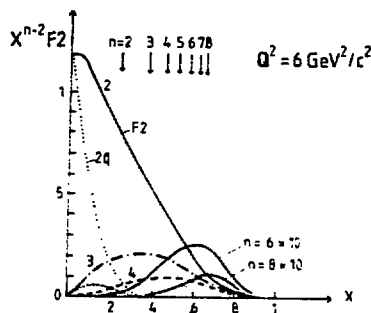


Fig.5a: Structure functions  $F_2$  and  $2\bar{q}$  weighted by powers of  $x$ . The arrows on top give the average value of  $x$  for the indicated moments.

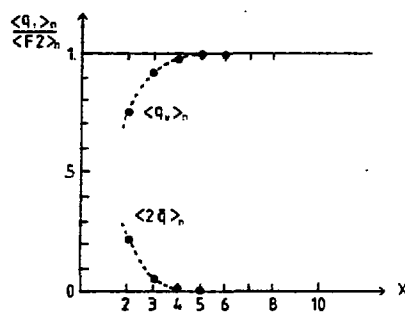


Fig.5b: Ratio of moments of  $xF_3$  and  $2\bar{q}$  relative to  $F_2$  as a function of  $n$ .

Figure 5a shows the measured structure functions  $F_2$  and  $2\bar{q}$  weighted by powers of  $x$  for  $Q^2 = 6 \text{ GeV}^2/c^2$ . Two facts are easily to be seen: i) different moments are very strongly correlated especially at large  $n$ , i.e. the same measurements of  $F_2$  are used over and over again to calculate moments. ii) The contribution of sea quarks, which distinguish  $xF_3$  and  $F_2$ , is measurable for the third and second moment only. This is further illustrated in figure 5b where the magnitude of the moments for  $xF_3$  and  $2\bar{q}$  are shown relative to the moments for  $F_2$ .

Thus if we want to learn about the gluon distribution from a moment analysis of  $F_2$  we are restricted to the second and third gluon moments which give a measurement of  $\langle x \rangle_{\text{glue}}$  only provided we are able to measure the  $Q^2$ -dependence of these moments. This however is not possible as can be seen from figures 6a and b.

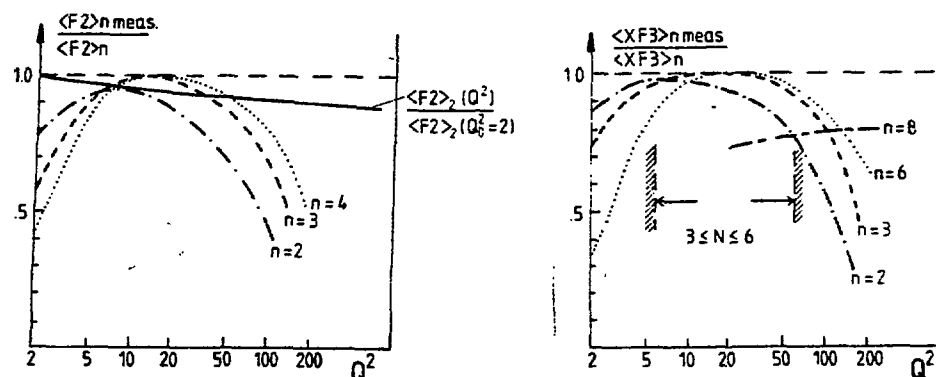


Fig.6: Fraction of the moment which is measurable as a function of  $Q^2$ . The requirements are:  $E_\nu < 280$  GeV,  $x < .7$  for  $Q^2 > 20$  GeV $^2/c^2$  and  $W^2 > 2$  GeV $^2$ . The prediction for the structure functions outside the measured range is based on a QCD extrapolation.

They show what fraction of the moment of  $x F_3$  and  $F_2$  is actually measured as a function of  $Q^2$ . At small  $Q^2$ -values the loss is due to the requirement  $W^2 > 2$  GeV $^2$  which is not really necessary if one does not want to test QCD. (Some people are courageous enough to find even QCD-tests meaningful in this region.) At high  $Q^2$  and low moments of  $F_2$ , however, there is no way to replace missing data since all experiments miss the low  $x$  region due to the kinematical limit, imposed by the maximal energy of the incoming lepton. Thus the  $Q^2$ -evolution of the second and third moment of  $F_2$  is strictly unmeasurable in any reasonable relation to their expected change with  $Q^2$  (indicated in figure 6a). The point is further illustrated in figure 7 where the expected  $Q^2$ -evolution of  $F_2$  and  $\bar{q}$  is shown together with the visible fraction of these structure functions.

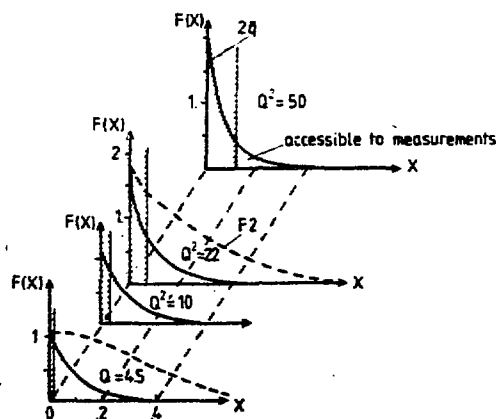


Figure 7:  
 $Q^2$ -evolution of  $\bar{q}$  and  $F_2$  as predicted by the QCD-evolution. Only a small fraction of  $\bar{q}$  is measurable at large  $Q^2$  due to the requirement  $E_\nu < 220$  GeV.

Any info:  
this is

I have  
which as  
their r  
"measur  
[A rece  
in the  
What ca.  
A new a  
the new  
"slope

of and  
measure  
tion [5  
termine  
result

and

The err  
The inc  
and t  
proved  
becomes  
That is  
the sin  
x-depen

$Q^2$ . The  
2 GeV $^2$ .  
range i

sured a  
nt  $W^2 > 2$   
me peop.  
) At hi  
ata sing  
, impose  
the se  
relation  
is furth  
is show

$F_2$  as p  
ution. Q  
measur  
require

Any information about the gluon moments relies on the change of  $\bar{q}$  with  $Q^2$  and this is measurable by no experiment at present accelerator energies.

I have put some emphasis into these questions since we are flooded by publications which analyse moments of structure functions. You should be very sceptical about their results if no correlations are included and especially if they are able to "measure" the  $Q^2$ -evolution of moments which are just not accessible to experiments. [A recent example is able to "measure" the gluon moments  $n = 2, 3, \dots, 10$  !! in the  $Q^2$ -range  $2 < Q^2 < 50 \text{ GeV}^2/c^2$ .]

#### What can we reasonably learn from moments ?

A new analysis of non-singlet moments has been performed by A. Para from CDHS using the new CDHS data together with the SLAC e-d data. Figure 8 shows the well known "slope plot" for the Nachtmann moments  $\bar{N}_3$  and  $\bar{N}_5$ . The slope is given by the ratio

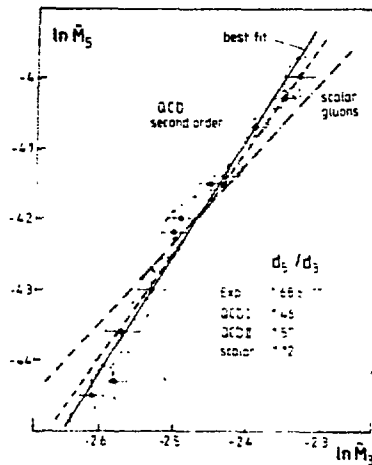


Figure 8:  
"slope plot" for the Nachtmann moments  $\bar{N}_3$  and  $\bar{N}_5$  including correlations. Indicated as straight lines are the predictions of QCD scalar gluons and the result of the best straight line fit.

of anomalous dimensions which depend on the vector nature of the gluons. The measured slope  $d_5/d_3 = 1.68 \pm .11$  agrees well with the second order QCD prediction [5] and excludes scalar gluons. In a second step the value of  $\Lambda$  can be determined. A combined fit to  $\bar{N}_3$ ,  $\bar{N}_4$  and  $\bar{N}_5$  including all correlations gives the result

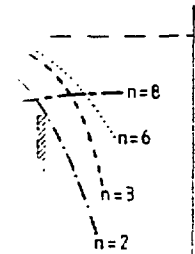
$$\Lambda_{L.O.} = .3 \pm .1 \quad \text{for leading order}$$

$$\text{and } \Lambda_{\overline{MS}} = .25 \pm .08 \quad \text{for a second order fit.}$$

The error includes an estimate of systematic uncertainties.

The inclusion of correlations is essential for this analysis. Both the value of  $\Lambda$  and the error differ substantially if they are disregarded. In addition it proved impossible to include more (higher) moments because the correlation matrix becomes singular [6].

That is about all we dare to do with moments. Any further analysis especially for the singlet structure functions should be based on the analysis of the full  $x$ -dependence.



$Q^2$ . The  
2  $\text{GeV}^2$ . The  
range is

measured as a  
function of  $W^2 > 2 \text{ GeV}^2$   
some people are  
) At high  $Q^2$   
data since  
, imposed by  
the second  
relation to  
is further  
is shown to-

F2 as pre-  
diction. Only a  
measurable  
requirement

### III. Analysis of x-dependence

The QCD-evolution of structure functions is obtained from the numerical integration of the Altarelli-Parisi equations which are given and graphically illustrated in figure 9. The method was introduced by Abbot and Barnett [7] and allows to make first and second order fits, to include target mass corrections and higher twist contributions.

The main advantage, however, is that it makes full use of the available data without strong dependence on unmeasured kinematical regions. In the following I will discuss a simultaneous fit to  $F_2$ ,  $\bar{q}$  and the gluon distribution. This leads to a system of coupled differential equations:

$$\begin{aligned}\frac{dF_2(x_i)}{dQ^2} &= F_i(F_{2x_1}, \dots, F_{2x_n}, G_{x_1}, \dots, G_{x_n}, Q^2) \\ \frac{d\bar{q}_{x_i}}{dQ^2} &= Q_i(\bar{q}_{x_1}, \dots, \bar{q}_{x_n}, G_{x_1}, \dots, G_{x_n}, Q^2) \quad i = 1, 14 \\ \frac{dG_{x_i}}{dQ^2} &= G_i(F_{2x_1}, \dots, F_{2x_n}, G_{x_1}, \dots, G_{x_n}, Q^2)\end{aligned}$$

There is one D.E for each measured value of x. In total there are 3-14=42 coupled differential equations.

In addition we have to fix the starting values at  $Q^2 = Q_0^2$  and the free parameter  $\Lambda$ . This is done by using simple parametrizations:

$$\begin{aligned}F_2(x, Q_0^2) &= a_2(1-x)^{p_2}(1+c_2x) \\ \bar{q}(x, Q_0^2) &= a_q(1-x)^{p_q} \\ G(x, Q_0^2) &= a_g(1-x)^{p_g}(1+c_gx)\end{aligned}$$

where the parameters are determined by a least squares fit to the data.

For the gluon distribution it is usual to enforce the energy momentum sum rule:  $\langle G \rangle_2 = 1 - \langle F_2 \rangle_2$ . In this case  $a_g = a_g(a_2, p_2, c_2, p_g, c_g)$  is determined.

#### III.1 The gluon distribution

Gluons carry about 55 % of the nucleon momentum. Information on the shape of their momentum distribution may be obtained from:

##### i) deep inelastic scattering

The gluon distribution enters indirectly via the slope of the sea distribution at small x which according to QCD is mainly due to gluon pair production. This can be seen from figures 9a b where the QCD contributions due to gluon pair production and gluon bremsstrahlung are given separately for the structure functions  $F_2$  and  $\bar{q}$ . The slopes of  $\bar{q}$  are entirely dominated by the gluon pair production and thus measure directly the gluon distribution weighted by the probability to generate a  $q\bar{q}$ -pair i.e. the convolution  $P_{q\bar{q}} \otimes G(x)$ . Wherever this convolution is positive we will measure an antiquark content of the nucleon (or it will evolve at somewhat higher  $Q^2$ ). Thus the function  $P_{q\bar{q}} \otimes G(x)$  has to be zero for  $x \gtrsim .45$  where no antiquarks are found. The  $Q^2$ -evolution of  $F_2$  measures the combined effect of pair production and bremsstrahlung and both are equally important in the intermediate x-range where the slopes are wellmeasured. It is evident from figure 9a that both contributions are very strongly correlated for  $F_2$ .

The gluon pair production gives also a strong dynamic contribution to the longitudinal structure function  $F_L$  at small x as will be shown later. The measurement of  $F_L$  is however by no means good enough at present to learn something about the gluon distribution.

$$a) \frac{dF_2(x)}{d \ln Q^2}$$

$$* [P_{q\bar{q}}(x)]$$

$$+ 2N_F$$

$$b) \frac{d\bar{q}(x, Q^2)}{d \ln Q^2}$$

$$* [P_{q\bar{q}}(x)]$$

$$+ N_F$$

$$c) \frac{dxF_3(x)}{d \ln Q^2}$$

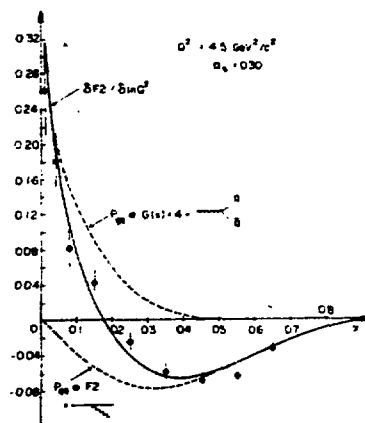
$$* [P_{q\bar{q}}(x)]$$

Fig.9:

egra-  
strated  
to  
gher

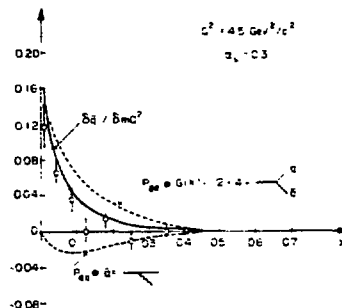
a  
ng I  
eads

$$a) \frac{dF_2(x, Q^2)}{d \ln Q^2} = \frac{\alpha_s}{2\pi} \int_x^1 \frac{x dy}{y^2} * \\ * \left[ P_{qg}\left(\frac{x}{y}\right) F_2(y, Q^2) \right. \\ \left. + 2N_F P_{qq}\left(\frac{x}{y}\right) G(y, Q^2) \right]$$



coupled  
meter A.

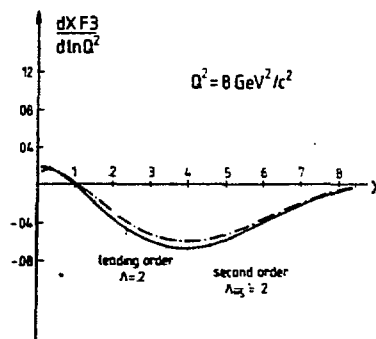
$$b) \frac{d\bar{q}(x, Q^2)}{d \ln Q^2} = \frac{\alpha_s}{2\pi} \int_x^1 \frac{x dy}{y^2} * \\ * \left[ P_{qg}\left(\frac{x}{y}\right) \bar{q}(y, Q^2) \right. \\ \left. + N_F P_{qq}\left(\frac{x}{y}\right) G(y, Q^2) \right]$$



ule:

f their

$$c) \frac{dxF_3(x, Q^2)}{d \ln Q^2} = \frac{\alpha_s}{2\pi} \int_x^1 \frac{x dy}{y^2} * \\ * \left[ P_{qg}\left(\frac{x}{y}\right) xF_3(y, Q^2) \right]$$

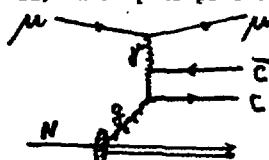


bution  
his can  
duc-  
ons F2  
and  
gene-  
is  
olve  
.45  
effect  
inter-  
a that

ongi-  
ement  
the

Fig.9: QCD-slopes for  $F_2$ ,  $\bar{q}$  and  $xF_3$  for fixed values of  $Q^2$ . The contributions of gluon bremsstrahlung and gluon pair production are given separately. The data points are obtained from linear fits in  $\ln \ln Q^2$  to the CDHS structure functions.

## ii) charm pair production in muon experiments



"gluon fusion model"

The production of  $c\bar{c}$  pairs in muon production is reasonably well described by the gluon fusion model. The cross section in this model is given by

$$\sigma(\gamma N \rightarrow c\bar{c} X) = \frac{x_2}{x_1} \int dx G(x) \sigma(\gamma g \rightarrow c\bar{c})$$

which involves the gluon distribution  $G(x)$ .

## iii) Hadron-hadron collisions

Large contributions from quark-gluon and gluon-gluon scattering are expected in hard collisions i.e. high  $p_T$  reactions, single photon and lepton pair production. For the analysis of these processes it is very important to know the gluon distribution a priori in order to learn something about the gluon-quark interaction and the triple gluon vertex.

## Results

Leading order fits to  $F_2$  and  $\bar{q}$  including target mass corrections have been performed to determine  $\Lambda$  and the gluon distribution. To reduce possible contributions due to higher twist the region of large  $x$  and low  $Q^2$  was excluded by the requirement  $W^2 = Q^2(1-x)/x > 11 \text{ GeV}^2$ . A very satisfactory fit was obtained with the following parameters:

$$\Lambda_{L.O.} = .18 \pm .02$$

$$\langle F_2 \rangle_2 = .45$$

$$\langle \bar{q} \rangle_2 = .055$$

$$\langle G \rangle_2 = 1. - \langle F_2 \rangle_2$$

$$\langle x \rangle_{F_2} = .25$$

$$\langle x \rangle_{\bar{q}} = .095$$

$$\langle x \rangle_{\text{glue}} = .16 \pm .02$$

$$Q_0^2 = 5 \text{ GeV}^2/c^2$$

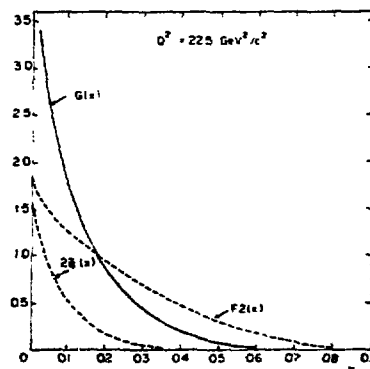
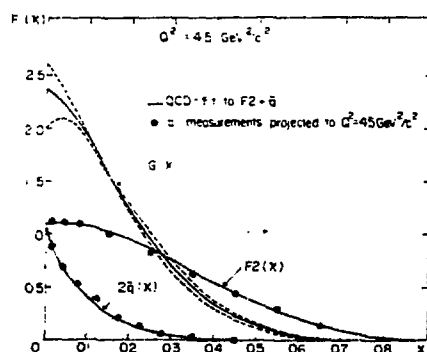


Fig.10: Shape of structure functions  $F_2$ ,  $\bar{q}$  and  $G(x)$  for two values of  $Q^2$  obtained from a leading order QCD fit to  $F_2$  and  $\bar{q}$ . The error bars give the full statistical power of the data at all values of  $Q^2$ . (The shape of  $G(x)$  is measured at one value of  $Q_0^2$  only, but can be calculated for every other value of  $Q^2$  using the evolution equations.)

The fit given i linear : equival indicat do not tions i

oproduct gluon model

c) ation

The sha to  $Q^2 = G(x) \sim$  parameter  $Q^2 = 2$  Everbod depende

ng are con pa to kn gluon-

This fi shape o 2.63. (1 this fu There : only we fact th correla a gluon

ave be le con by the ned wi

In a se free pa tation which d

## Depende

The pre violati mainly non-QCD i) unce Both ef functio tainty  $F_2$  has

$F_2$  is o section

$$\frac{d\sigma}{dx}$$

The st is obta This re Alterna strange by the estimat evoluti

s of  $Q^2$  give th nape of : every

The fit is compared to  $F_2$  and  $\bar{q}$  in figures 1 and 2. The resulting slopes are given in figures 9a b and compared to data points which have been obtained from linear fits in  $\ln \ln Q^2$  for each  $x$ -bin. It should be noted that such a fit is not equivalent to the QCD evolution (especially not for  $\bar{q}$ ). Therefore these data points indicate the statistical significance of the observed scaling violations but they do not have to fall on the QCD curves. The shape of the resulting structure functions is shown in figure 10 a and b for 2 values of  $Q^2$ .

The shape of the gluon distribution changes dramatically going from  $Q^2 = 4.5 \text{ GeV}^2/c^2$  to  $Q^2 = 22.5 \text{ GeV}^2/c^2$  and cannot be described by a simple parametrization  $G(x) \sim (1-x)^P(Q^2)$  over the whole  $Q^2$ -range. As an example, if one enforces such a parametrization at  $Q^2 = 20 \text{ GeV}^2/c^2$  the gluon distribution becomes negative below  $Q^2 = 2 \text{ GeV}^2/c^2$  at small  $x$ .

Everybody who wants to use the gluon distribution has to include this strong  $Q^2$ -dependence to get meaningful results.

This fit enforced the energy momentum sum rule and allowed some freedom in the shape of the gluon distribution by the parametrization  $G(x) = a_g(1-x)^P g(1+C_g \cdot x) = 2.63 \cdot (1-x)^{5.3} (1+3.5x)$  at  $Q^2 = 5 \text{ GeV}^2/c^2$ . Clearly there is a prejudice in choosing this functional form and other shapes of the gluon distribution are possible. There is however one important fit result: the width of the gluon distribution is only weakly correlated with  $\Lambda$  and therefore well determined. This is due to the fact that  $\bar{q}$  has to be zero above  $x = .45$ . A fit to  $F_2$  alone gives a very strong correlation between  $\Lambda$  and  $\langle x \rangle_{\text{glue}}$ . Values of  $\Lambda = .4$  are possible together with a gluon distribution which extends to very large values of  $x$ .

In a second step we can also test the energy momentum sum rule by leaving  $a_g$  as a free parameter. The result is  $\langle G \rangle_2 = .55 \pm .11$  in good agreement with the expectation  $1 - \langle F_2 \rangle = .55$ . Thus there is little room for constituents in the proton which do not carry colour.

#### Dependence on systematic uncertainties

The present analysis depends entirely on the assumption that the measured scaling violations are QCD effects only. The determination of the gluon distribution is mainly affected by uncertainties in the slopes at small  $x$ . We know at least two non-QCD effects which give rise to scaling violations in this region: i) uncertainties in  $\sigma_L/\sigma_T$ , ii) threshold effects due to heavy quark production. Both effects have rather severe consequences for the slope of  $\bar{q}$ . The structure function  $F_2$  on the other hand is only weakly affected by the experimental uncertainty in  $\sigma_L/\sigma_T$ . To see the effect of heavy quark production the structure function,  $F_2$  has been extracted making different assumptions about strange and charmed sea.

$F_2$  is obtained from the sum of neutrino and antineutrino differential cross sections:

$$\frac{d\sigma}{dx} \frac{vN}{\bar{v}N} = x(u+d+\bar{u}+\bar{d})(1+(1-y)^2) + 4x\bar{s}(x) + 4x\bar{c}(x)(1-y)^2$$

The standard set of structure functions which was used in the previous analysis is obtained by the assumption  $2(S-C)/(u+d) = .2$  i.e. assuming no threshold effect. This results in the structure function  $F_2 = x(u+d+s+c+\bar{u}+\bar{d}+\bar{s}+\bar{c})$  with  $N_f=4$  flavours. Alternatively we have tried different assumptions about the contributions from strange and charmed sea. Since the charmed sea contribution is strongly suppressed by the  $(1-y)^2$ -factor it may be better to subtract it's contribution. This was estimated by setting  $c(x) \equiv 0$  für  $Q^2 = 1 \text{ GeV}^2/c^2$  and then calculating it's  $Q^2$ -evolution. The correction in any case is rather small. The strange sea contributes

mainly to single charm production and is thus suppressed by threshold effects. To estimate this effect we used the slow rescaling model in two different versions: i) effective charm mass  $m_c = 1.5$  GeV and  $2s/(\bar{u}+\bar{d}) = .5$ , ii)  $m_c = 1.85$  GeV,  $2s/(\bar{u}+\bar{d}) = 1$ . This procedure leads to a structure function  $\bar{F}_2 = x(u+d+s+\bar{u}+\bar{d}+\bar{s})$  with only  $N_f=3$  flavours!

The effect on the slopes of  $\bar{F}_2$  is shown in figure 11 together with the result of a leading order fit to  $\bar{F}_2$  with  $N_f=3$ . The structure function  $\bar{q}$  was used for  $x > .3$  only. Thus the large uncertainty in the slopes of  $\bar{q}$  does no longer enter but the requirement that there are no antiquarks at large  $x$  is still kept.

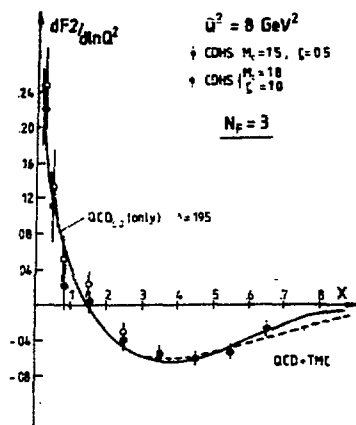


Fig.11: Slopes of  $\bar{F}_2 = x(u+d+s+\bar{u}+\bar{d}+\bar{s})$  for two different assumptions on slow rescaling and the magnitude of the strange sea

The results are rather encouraging. The value of  $\Lambda$  remains unchanged and the shape and magnitude of the gluon distribution is only moderately affected as can be seen in figure 12. The width of the gluon distribution at  $Q_0^2 = 5 \text{ GeV}^2/c^2$  is in the range  $.13 < \langle x \rangle_{\text{glue}} < .17$ .

#### Summary

The  $Q^2$ -evolution of  $\bar{F}_2$  and  $\bar{q}$  are well described by leading order QCD with  $\Lambda=.2$ . The slopes of  $\bar{F}_2$  at small  $x$  are only moderately affected by known uncertainties in  $\sigma_L/\sigma_T$  and charmed threshold effects.

The measurement of  $\bar{q}$  contributes the very important constraint that there are no light antiquarks at  $x \gtrsim .45$ . This fact decouples the determination of  $\Lambda$  and the width of the gluon distribution. The shape of the gluon distribution is reasonably well determined and the momentum carried by gluons is in agreement with the energy momentum sum rule.

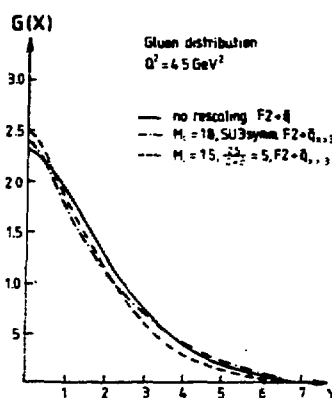


Fig.12: Shape of gluon distribution for three different assumptions about strange and charmed sea

#### IV Higher twist

Higher twist nucleon constituents evolve like  $1/Q^2$  a diquark system

s. rations:

$\bar{q}+\bar{s}$

it or nter

What is known a

i) They should hadron mass. duction. The

ii) The  $Q^2$ -dependence  $F(x, Q^2)_{H.T.}$

What is not known

We do not know contributions. This distribution is calculated perturbative distribution determined experimentally

#### IV.1 Strategie (leading)

In the past theoretical violations. Monte Carlo kinematic region perturbative calculation all or most of be very small.

There are two

i) Try to distinguish approach if requires theoretical

ii) Start in region in the sea singlet structure involve the gluon

Fix the value higher twist

For both strategies regime" i.e. a electroweak production to the CDHS at the range  $2 < Q^2 < 10 \text{ GeV}^2$

ions sea

$1/Q^2$

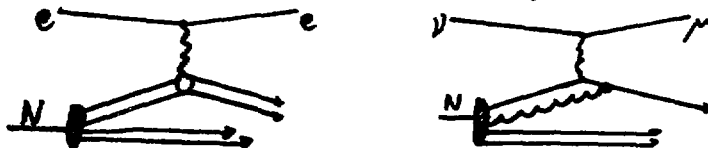
0.2. The in

re no the sonably energy



#### IV Higher twist contributions to scaling violations: How large is the $\Lambda_{\overline{MS}}$ ?

Higher twist contributions arise from scattering processes where two or more nucleon constituents act simultaneously. Examples of twist-4 contributions which evolve like  $1/Q^2$  are given below. The diagram on the left is the scattering off a diquark system which has been discussed widely in the literature [8].



What is known about higher twist contributions?

- i) They should contribute dominantly at high  $x$  and low  $Q^2$  i.e. low invariant hadron mass. Well known examples are quasielastic scattering and resonance production. The relevant variable is  $1/W^2 = x/((1-x)Q^2)$ .
- ii) The  $Q^2$ -dependence should be dominated by inverse powers of  $Q^2$ :  

$$F(x, Q^2)_{H.T.} \sim a(x)/Q^2 + b(x)/Q^4 + c(x)/Q^6 + \dots$$

What is not known?

We do not know the shape, magnitude and even the sign of the individual contributions. This is evident for the above example of diquark scattering: the momentum distribution (structure function) of a diquark system in the nucleon cannot be calculated perturbatively for the same reason that we cannot calculate the momentum distributions of single quarks. All nucleon structure functions have to be determined experimentally.

#### IV.1 Strategies to separate higher twist contributions from perturbative (leading log) QCD contributions

In the past there have been two extreme approaches to explain the observed scaling violations. Most people were glad that QCD was able to do the whole job even in kinematic regions where it was not expected to work. Others insisted what non perturbative effects, especially higher twist contributions, are able to explain all or most of the observed scaling violations with the consequence that  $\Lambda$  might be very small.

There are two strategies to separate higher twist and QCD contributions:

- i) Try to distinguish  $1/\ln Q^2$  variations from  $1/Q^2$ ,  $1/Q^4$ .... This is the natural approach if the analysis is restricted to nonsinglet structure functions. It requires the maximal available range in  $Q^2$  and  $x$ .
- ii) Start in regions where higher twist contributions are most likely small i.e. in the sea region and for higher  $W^2$ . This naturally leads to the analysis of singlet structure functions which have been avoided so far because they involve the gluon distribution.

Fix the value of  $\Lambda$  and extrapolate to the low  $W^2$  region to determine additional higher twist contributions.

For both strategies it is essential to have accurate data in the "higher twist regime" i.e. at large  $x$  and low  $Q^2$ . The best data set in this region comes from electroproduction experiments at SLAC. We therefore use e-d data [3] in addition to the CDHS structure functions. These data are displayed in figure 13. They cover the range  $2 < W^2 \lesssim 12 \text{ GeV}^2$  with an average value of  $Q^2 = 8 \text{ GeV}^2/c^2$ .

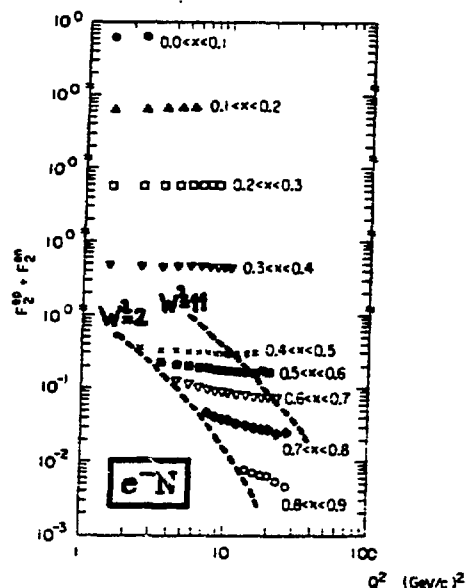


Figure 13:

F2 structure function derived from inelastic electron nucleon data at SLAC.

#### IV.2 Fits to the nonsinglet structure function

These fits are based on the CDHS measurements of  $x F_3$  and in addition on  $2x F_1$  for  $x > .4$  (Statistically the information is mostly due to  $2x F_1$ ). They include target mass corrections [9] and a correction for the propagator effect with  $m_W = 80 \text{ GeV}$ .

##### i) Pure QCD fits:

We require  $W^2 > 11 \text{ GeV}^2$  (which corresponds to  $x/(Q^2(1-x)) < .1$ ) and  $Q^2 > 2 \text{ GeV}^2/c^2$ . Leading and second order fits give the following results:

$$\Lambda_{L.O.} = .19 \pm .08 \quad \chi^2/DF = 156/107$$

$$\Lambda_{\overline{MS}} = .21 \pm .08 \quad \chi^2/DF = 155/107$$

The two fits are equally good and differ very little from each other. This underlines the well known fact that second order corrections are small in the  $\overline{MS}$ -scheme. The slopes of  $x F_3$  for leading and second order are shown in fig.9c for the same value of  $\Lambda = .2$  and  $Q^2 = 8 \text{ GeV}^2/c^2$ . Including estimates of various systematic errors, the value of  $\Lambda_{\overline{MS}}$  has to be in the range

$$.09 < \Lambda_{\overline{MS}} < .3$$

assuming that higher twist contributions are negligible in this kinematic region.

##### ii) Fits including twist-4 contributions:

To increase the sensitivity we now include all data points with  $Q^2 > 2 \text{ GeV}^2/c^2$  and use in addition the SLAC e-d data. The structure functions are parametrized in the following way:  $F(x, Q^2) = F^{QCD}(x, Q^2)(1 + (\mu - f(x))/Q^2)$  where  $\mu$  is the unknown scale parameter of twist-4 contributions. For their shape  $f(x)$  various functions were assumed.

The res

I) le

II) sec

III) sec

The main

equally

$\Lambda \approx .2$

assumed

tic chan

IV.3 Ana

a)  $Q^2$ -ev

The use

$F_2$  and

twist co

instead

followin

(1)  $d<$

$d^2$

(2)  $d<$

$d^2$

Here we

Experi

$F_2$ ,  $q$

a

value in

and

Using  $N_F$

If we no

drops ou

are pres

It is na

and we o

$d<F_2>$

$d \ln Q$

kinema

which c

moment o

A preli

the foll

$d<F_2>$

$d \ln Q$

$d<\bar{q}>$

$d \ln Q$

deriv  
cleon

n. on 2  
they in  
act wit

and  
result

ther. 1  
small  
own in  
res o

kinema

$Q^2 > 2$   
re para  
u is  
 $f(x)$

The results of three representative fits are given below:

derived from  
clean data

| Fit                                       | Parameters                                   | $\chi^2/DF$ |
|---|--|-------------|
| I) leading order, $f(x) = \frac{x}{1-x}$  | $\Lambda_{L.O.} = .4 \pm .03$ $\mu = -.07$   | 182/145     |
| II) second order, $f(x) = \frac{x}{1-x}$  | $\Lambda_{MS} = .24$ $\mu = .74^{+.4}_{-.3}$ | 177/145     |
| III) second order, $F(x) = \frac{1}{1-x}$ | $\Lambda_{MS} = .43$ $\mu = -.15$            | 178/145     |

The main conclusion is that  $\Lambda$  and  $\mu$  are very strongly correlated. There are two equally probable solutions with either  $\Lambda \approx .4$  and no twist-4 contribution or  $\Lambda \approx .2$  and a large twist-4 contribution. The result depends strongly on the assumed shape of the twist-4 contribution and is very sensitive to small systematic changes. To summarize, this sort of analysis is not conclusive.

#### IV.3 Analysis of singlet structure functions: $F_2$ and $\bar{q}$

##### a) $Q^2$ -evolution of second moments

The use of second moments has been proposed by Glück and Reya one year ago [11] for  $F_2$  and  $xF_3$ . Their method gives the unique possibility to learn something on higher twist contributions without any assumption on their  $Q^2$  or  $x$ -behaviour. We will instead use  $\langle F_2 \rangle_2$  and  $\langle \bar{q} \rangle_2$  for which the Altarelli-Parisi equation gives the following  $Q^2$ -evolution:

$$(1) \quad \frac{d\langle F_2 \rangle_2}{d\ln Q^2} = \frac{3_s(Q^2)}{12\pi} \left[ -\frac{32}{3} \langle F_2 \rangle_2 + 2N_F \langle G \rangle_2 \right] + \frac{d\langle F_2 \rangle_{H.T.}}{d\ln Q^2}$$

$$(2) \quad \frac{d\langle \bar{q} \rangle_2}{d\ln Q^2} = \frac{3_s(Q^2)}{12\pi} \left[ -\frac{32}{3} \langle \bar{q} \rangle_2 + N_F \langle G \rangle_2 \right] + \frac{d\langle \bar{q} \rangle_{H.T.}}{d\ln Q^2}$$

Here we have added possible higher twist contributions on the right hand side. Experimentally we can measure the slopes on the L.H.S. and the second moments of  $F_2$ ,  $\bar{q}$  and the gluons making use of the energy momentum sum rule. Thus we know the value in square brackets for both equations.

Using  $N_F = 4$  flavours we find a value of  $-.77$  for  $F_2$  and  $+1.5$  for  $\bar{q}$  at  $Q^2 = 8 \text{ GeV}^2/c^2$ . If we now add equations (1) and (2) in the ratio  $1:.53$  the QCD term  $3_s(Q^2)$  drops out i.e.  $d\langle F_2 \rangle_2/d\ln Q^2 + .53 d\langle \bar{q} \rangle_2/d\ln Q^2$  has to be zero if only QCD-terms are present.

It is natural to neglect higher twist contributions to  $\langle \bar{q} \rangle_2$  with respect to  $\langle F_2 \rangle_2$  and we obtain the following relation

$$\frac{d\langle F_2 \rangle_{H.T.}}{d\ln Q^2} = \frac{d}{d\ln Q^2} \left[ \frac{T_4}{Q^2} + \frac{T_6}{Q^4} + \frac{T_8}{Q^6} + \dots \right] = \frac{T_4}{Q^2} + 2\frac{T_6}{Q^4} + 3\frac{T_8}{Q^6} + \dots$$

$$= \left[ \frac{d\langle F_2 \rangle_2}{d\ln Q^2} + .53 \frac{d\langle \bar{q} \rangle_2}{d\ln Q^2} \right]$$

which can be used to derive a limit on higher twist contributions to the second moment of  $F_2$ .

A preliminary estimate of the slopes of  $\langle \bar{q} \rangle_2$  and  $\langle F_2 \rangle_2$  from the CDHS data leads to the following values:

$$\left. \begin{aligned} \frac{d\langle F_2 \rangle_2}{d\ln Q^2} &= -.009 \pm .005 \\ \frac{d\langle \bar{q} \rangle_2}{d\ln Q^2} &\approx +.01 \pm .01 \end{aligned} \right\} \quad Q^2 = 8 \text{ GeV}^2/c^2$$

on  $2xF_1$   
they include  
ect with

and  
results:

ther. This  
small in the  
own in fig.9c  
tes of various

kinematic

$Q^2 > 2 \text{ GeV}^2/c^2$   
re parametrized  
 $\mu$  is the un-  
e  $f(x)$  various

The errors include (conservative) estimates of the uncertainties due to charm threshold and  $R = \sigma_L/\sigma_T$ . They can hopefully be improved in the near future.

We get the following result:

$$\frac{d\langle F2 \rangle_{H.T.}}{d\ln Q^2} = \left( \frac{T_4}{Q^2} + 2\frac{T_6}{Q^4} + 3\frac{T_8}{Q^6} + \dots \right) = .004 \pm .015$$

which says that the total contribution of higher twist terms is rather small. If we use the twist-4 model of the previous analysis

$$T_4 = \int_0^1 dx \left( \frac{x}{1-x} \right) F2 dx$$

we obtain the result  $\mu = .09 \pm .35$ .

Though the data is not very accurate at present it gives us an indication that higher twist contributions to the second moment are most likely small. Thus their contribution may be small altogether or they are large only at large  $x$  or there are several large contributions with opposite sign which cancel each other.

#### b) Use of full $x$ -dependence of $F2$ and $\bar{q}$

In a first step we repeat the leading order fits to  $F2$  and  $\bar{q}$  which were used to determine the gluon distribution. To reduce possible higher twist contributions we require  $W^2 > 20 \text{ GeV}^2$ . Figure 14a shows the resulting slopes for  $F2$  extrapolated to  $Q^2 = 8 \text{ GeV}^2/c^2$  where we finally want to look for additional higher twist contributions.

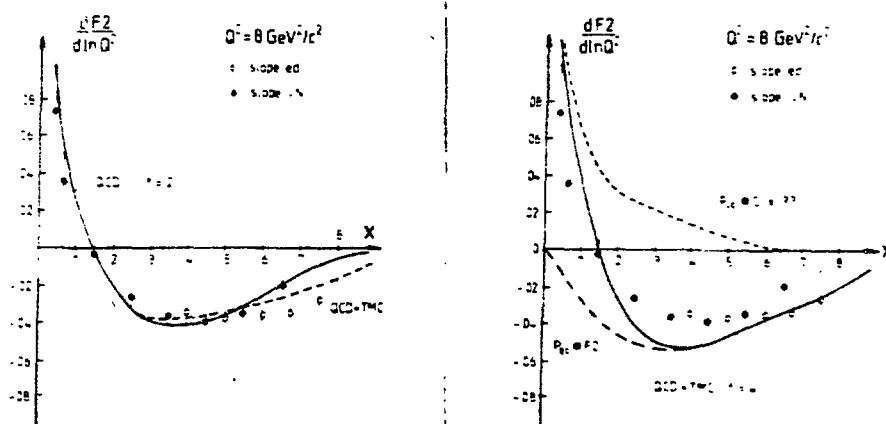


Fig.14: Slopes for CDHS and SLAC data at  $Q^2 = 8 \text{ GeV}^2/c^2$

The data points are obtained from linear fits to  $\ln \ln Q^2$  to the total available  $Q^2$ -range. The slopes for the SLAC data are multiplied by the QPM-prediction 9/5.

a) The indicated lines give the separate contributions of QCD and target mass corrections.

b) Slopes for  $\Lambda = .4$ . Also indicated is the function  $P_{qq} = G(x)$  which would be necessary to give the measured slopes for a value of  $\Lambda = .4$ .

The result is  
taneously th  
The data po  
total availa  
corrections  
describe th  
 $x = .65$  corr  
are expected

In a second  
(including +  
of  $8 \text{ GeV}^2/c^2$   
Thus we need  
target mass  
Why is it n  
Such a poss  
answer is g

The gluon b  
large and i  
they would  
on top. Thi  
at large  $x$   
figure 14 b  
mediate and  
we could no  
come back  
highly arti  
SLAC e-d da

We can then  
much smaller  
chance to  
threshold!)  
corrections  
to the non-  
second orde  
very unlike  
conclusions  
The only al  
which mimic

#### Shape of hi

We need con  
addition to  
possible to  
might have:  
i) target  
ii) additic  
might b  
iii) scaling  
iv) ....

Let us howe  
 $\sim 1/Q^2$  or  
tude of the

The resulting value of  $\Lambda$  is  $\Lambda_{L.O.} = .20 \pm .02$  which describes very well simultaneously the shrinkage at large  $x$  and  $Q^2$  and the rise of the sea at small  $x$ . The data points in figure 14 are obtained from linear fits in  $\ln Q^2$  to the total available  $Q^2$ -range. The QCD contribution and the effect of target mass corrections are given separately. Obviously QCD plus target mass corrections describe the CDHS data very well. (It should be noted that the data point at  $x = .65$  corresponds to an average  $Q^2$  of  $\approx 80 \text{ GeV}^2/c^2$  where target mass corrections are expected to be negligible).

In a second step we can now compare the slope of the extrapolated QCD-fit (including target mass corrections) with the e-d data which has an average  $Q^2$  of  $8 \text{ GeV}^2/c^2$ . Obviously their measured slopes are significantly larger for  $x > .5$ . Thus we need additional contributions other than leading order QCD and standard target mass corrections.

Why is it not possible to increase the value of  $\Lambda$  in order to explain the data? Such a possibility existed for the nonsinglet data for a value of  $\Lambda = .4$ . The answer is given in figure 14 b:

The gluon bremsstrahlung for  $\Lambda = .4$  gives very large negative contributions for large and intermediate values of  $x$ . In order to obtain the measured slopes of  $F_2$  they would have to be compensated by a very broad gluon contribution as indicated on top. This however is incompatible with the data since there are no antiquarks at large  $x$ . The best fit to the data for a fixed value of  $\Lambda = .4$  is also shown in figure 14 b. It passes through the SLAC points but misses very badly in the intermediate and small  $x$  region and gives an unacceptable value of  $\chi^2$ . Strictly speaking we could now start to add negative higher twist contributions below  $x = .5$  to come back to the measured slopes. Such an option can never be excluded but is highly artificial. A pure QCD fit (plus target mass corrections) to CDHS and SLAC e-d data gives a very bad fit ( $\Delta\chi^2 = +50$ ) with a value of  $\Lambda_{L.O.} = .24$ .

We can therefore conclude that  $\Lambda_{L.O.}$  cannot be large and also that it cannot be much smaller since it has to explain the rise of the sea at small  $x$ . The only chance to make  $\Lambda$  much smaller is to invent still another mechanism (not charm threshold!) to explain the rise of the low  $x$  data. What about second order corrections? At large  $x$ , where we need additional contributions,  $F_2$  is identical to the non-singlet structure function. The difference in slope for leading and second order QCD is very small as has been shown in figure 9c. It is therefore very unlikely that the inclusion of second order corrections would change the main conclusions: we do see perturbative QCD effects with a value of  $\Lambda_{QCD}$  around .2. The only alternative is to construct very complicated higher twist contributions which mimic QCD.

#### Shape of higher twist contributions

We need contributions to scaling violations in the large  $x$  low  $Q^2$  region in addition to QCD and standard target mass corrections. There is a long list of possible contributions and it is rather hopeless to separate all of them. We might have:

- i) target mass corrections which are not included in our treatment
- ii) additional leading log contributions near the kinematic boundary  $x \rightarrow 1$  which might be absorbed by a change of argument in the running coupling constant [12]
- iii) scaling violations due to Fermi motion effects
- iv) ....

Let us however assume that the main effect is due to higher twist contributions  $\sim 1/Q^2$  or  $1/Q^4$ . Then we can use the SLAC e-d data to determine the shape and magnitude of these contributions. A separate fit is done for each  $x$ -bin to the

expression  $F(x, Q^2) = F_{\text{QCD}}(x, Q^2) + F^{\text{H.T.}}(x, Q^2)$  where  $F^{\text{H.T.}}(x, Q^2) = \mu_4(x)/Q^2$  or  $F^{\text{H.T.}}(x, Q^2) = \mu_6(x)/Q^4$  is assumed. The normalization factor between e-d and neutrino data is determined independently for each x-bin in order to get rid of possible shape differences between the two data sets. Figure 15 shows the e-d data for three large x bins together with QCD, target mass and twist-4 contributions. Whereas QCD plus target mass corrections alone cannot describe the data (for  $\Lambda = .2$ ) the inclusion of additional higher twist terms gives a perfect fit.

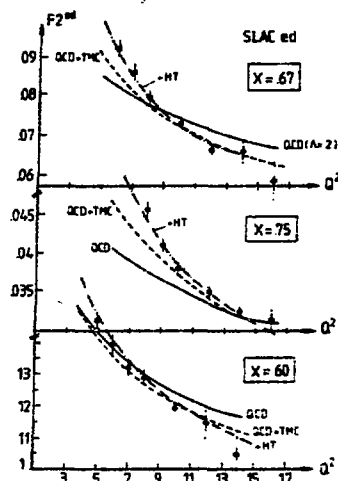


Fig.15: SLAC e-d data for three bins in x versus  $Q^2$ . The contributions of QCD ( $\Lambda=.2$ ) target mass corrections and higher twist are given separately.

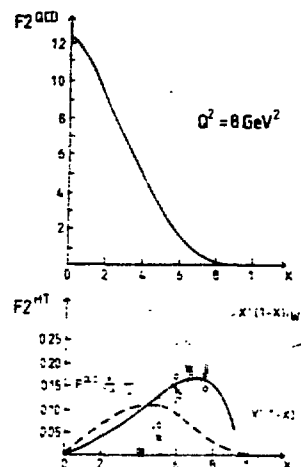


Fig.16: QCD and higher twist contributions to the structure function  $F_2$  at  $Q^2 = 8 \text{ GeV}^2/c^2$ . ( $\frac{1}{3}$ ) twist-4 contribution ( $\frac{2}{3}$ ) 2-twist-6 contribution

Twist-4 and twist-6 contributions give equally good fits. The resulting shape of the higher twist contributions is shown in figure 16 for  $Q^2 = 8 \text{ GeV}^2/c^2$ . It is peaked around  $x = 2/3$  and is restricted to  $x \gtrsim .5$ . It should be noted that this is the higher twist contribution to e-d scattering. The CDHS-data alone are not precise enough in this kinematic region to establish higher twist contributions though they also favour their presence. The shape of the higher twist contributions agrees reasonably well with the expected shape for diquark scattering  $F^{\text{H.T.}}(x, Q^2) \sim x^2(1-x)/Q^2$  [8] but is incompatible with the shape which is normally assumed in nonsinglet analysis:  $F^{\text{H.T.}} = F_{\text{QCD}} \cdot x/((1-x)Q^2) \cdot \mu$ . If such a parametrization is enforced, higher twist contribution comes out very small and the fit is unacceptable.

In a i  
QCD and  
 $Q^2 > 1$   
 $F(x, Q^2)$

The val  
restric

To sum  
The CD  
 $\Lambda \approx .2$   
tions  
presen  
about  
mass a

In con  
serve  
rather  
has no

c) Eff

The ob  
they m  
cluded  
of Sch  
They a  
tion t  
ling v  
of diq

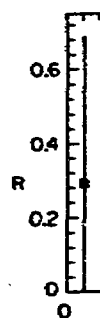


Fig.17

$(x)/Q^2$   
 e-e  
 r to get  
 15 shows  
 nd twist-4  
 describe  
 gives a

In a final step we can look if these results still hold if we allow simultaneously QCD and higher twist contributions in a fit to all CDHS and SLAC data with  $Q^2 > 1 \text{ GeV}^2/c^2$ . As an example we give the results for a fit  $F(x, Q^2) = F^{\text{QCD}} \cdot (1 + \mu \cdot x^\alpha / (1-x) \cdot 1/Q^2)$  where  $\Lambda$ ,  $\alpha$  and  $\mu$  are free parameters:

$$\begin{aligned}\Lambda_{\text{L.O.}} &= .195 \pm .02 \text{ GeV} \\ \mu &= 1.5 \pm .2 \text{ GeV}^2 & \chi^2/\text{DF} &= 210/206 \\ \alpha &= 3.7 \pm .3\end{aligned}$$

The value of  $\Lambda$  remains unchanged and the higher twist contribution is again restricted to the high  $x$  region.

To summarize:

The CDHS data on  $F_2$  and  $\bar{q}$  at high  $W^2$  and in the sea region require a value of  $\Lambda \sim .2$ . This value of  $\Lambda$  is however not sufficient to explain the scaling violations of the SLAC e-d data at large  $x$ . A possible (and natural) solution is the presence of higher twist contributions  $\sim 1/Q^2$  or  $1/Q^4$  at large  $x$ . They explain about 1/3 of the observed scaling violations, the rest is due to QCD and target mass effects.

In contrast to previous analyses [13] it is no longer possible to explain the observed scaling violations by QCD or higher twist terms only. This is due to the rather precise data at high  $Q^2$  and especially the observed rise of the sea which has not been included previously.

### c) Effect of diquark contributions

The observed shape of the "higher twist" contributions is very suggestive that they may be due to diquark scattering though other possibilities cannot be excluded at present. The effect of diquark scattering has been discussed in a paper of Schmidt and Blankenbecher and recently by Donnachie and Landshoff [8]. They argue that the presence of diquarks contributions gives a natural explanation to the observed Callan-Gross violation at large  $x$  and to the fact that scaling violations are larger for e-d than for e-n scattering. Thus the presence of diquark contributions may be even desirable.

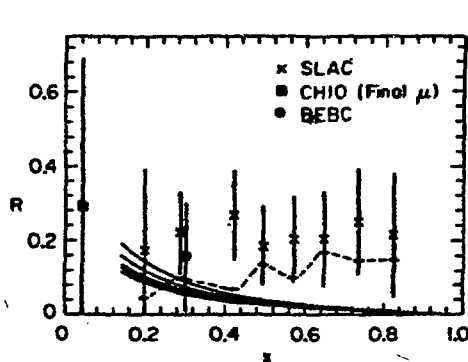


Fig.17:  $R = \sigma_L/\sigma_T$  as measured in electron deep inelastic scattering at SLAC. The dotted line gives the expected kinematic contribution.

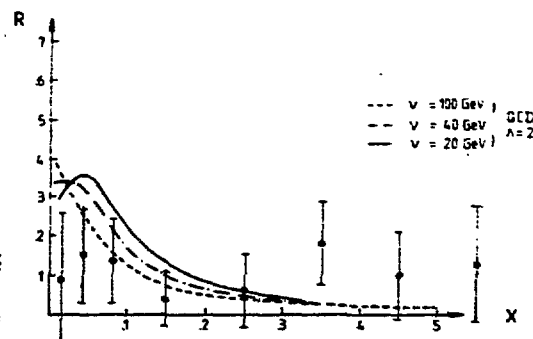


Fig.18:  $R = \sigma_L/\sigma_T$  measured by CDHS. The lines are QCD predictions for different values of  $\nu$  using  $\Lambda = .2$  and the new gluon distribution

wist contri-  
 structure func-  
 $\text{GeV}^2/c^2$ .  
 ibution  
 ribution

ing shape of  
 $/c^2$ . It is  
 d that this  
 one are not  
 ntributions  
 t contribu-  
 ttering

n is nor-  
 If such a  
 small and

### Callan-Gross violation

The SLAC data on  $R = \sigma_L/\sigma_T$  are shown in figure 17 versus  $x$ . The data indicate that  $R$  is nonzero at large  $x$  in contrast to the QCD expectations. The presence of diquark contributions gives a natural explanation since they are effective integer spin constituents for which the Callan-Gross relation does not hold. This has been thoroughly discussed by Abbott et al. [14].

The CDHS experiment gives an independent measurement of  $R$  at an average  $Q^2 \approx 20 \text{ GeV}^2/c^2$  and  $\langle v \rangle \approx 100 \text{ GeV}$ . The measurement agrees within rather large errors with the QCD prediction which depends essentially on the shape of the gluon distribution. This can be seen in figure 19 where the contributions to the longitudinal structure function from gluon pair production and gluon bremsstrahlung are given separately.

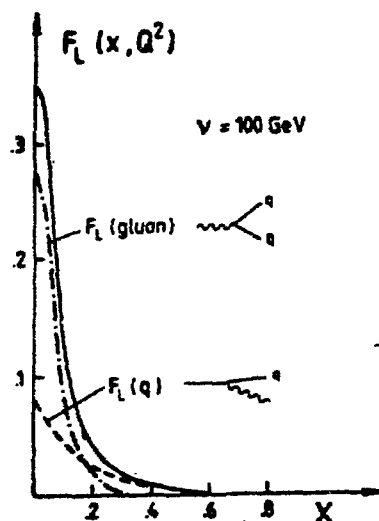


Figure 19:  
QCD prediction for the longitudinal structure function  $F_L(x, Q^2)$ . The contributions due to gluon pair production and gluon bremsstrahlung are given separately.

The present experimental knowledge is very unsatisfactory. Nevertheless it supports the notion that we have a large QCD contribution and additional diquark contributions in the SLAC large  $x$  regime.

$$u(x) = 2d(x)?$$

Diquark scattering gives larger contributions to  $e-p$  than to  $e-n$  scattering. If they were substantial it might be even possible to restore the naive QPM-prediction  $u(x) = 2d(x)$  for single quark densities [8]. A recent measurement of  $F_2^{vp}/F_2^{ep}$  based on  $vp$ -scattering by the ABCMO collaboration [15] is shown in figure 20. If no diquarks were present this measurement is equal to  $u(x)/d(x)$  and the ratio deviates strongly from 2 towards large  $x$ . Also shown is the prediction of the diquark model of Donnachie and Landshoff [8]. The model is not able to explain fully the difference between  $u(x)$  and  $2d(x)$ .

If one adds up the present knowledge the conclusion is that diquark contribution might play an important role to explain the difference in the scaling violations between  $e-n$  and  $e-p$  which are not covered by QCD. They are however too small to restore the relation  $u(x) = 2d(x)$ .

A final conclusion whether or not we see diquark contributions is probably possible in the near future. A list of possible experiments and specific "diquark"-predictions is given in reference [14].

### V Conclusions

The shape of well measured described by the sea region perturbative large  $x$  ( $x \approx$  experiment, the observed

The fact that the shape of

The value of and with a pr

### Aknowledgement

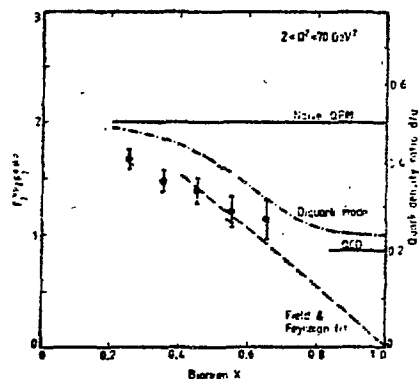
I am grateful higher twist

The results and are to b



Figure 20:

$F_2^{VP}/F_2^{EP}$  based on 3400  $\nu p$ -events in BEBC measured by the ABCMO collaboration [14] and SLAC e-p measurements. Predictions of the naive QPM model and a diquark model are also given.



### V Conclusions

The shape of  $F_2$ ,  $xF_3$  and the antiquark distribution for isoscalar target is now well measured in a large  $Q^2$  range. The observed scaling violations are well described by QCD effects with a value of  $\Lambda_{\overline{MS}} \approx .2$  both at large  $x$  and  $Q^2$  and in the sea region. They find no other simple explanation. The presence of additional non perturbative contributions is required to explain the slopes of the e-d data at large  $x$  ( $x \gtrsim .5$ ) and low  $Q^2$ . A natural explanation, which is even favoured by experiment, is the presence of diquark scattering which explains about 1/3 of the observed scaling violations in the SLAC e-d data.

The fact that we see perturbative QCD effects allows us finally to determine also the shape of the gluon distribution which is now reasonably well measured.

The value of  $\Lambda_{\overline{MS}}$  agrees with new results from deep inelastic muon scattering and with a preliminary analysis of the Gargamelle SPS-collaboration.

### Acknowledgement

I am grateful to M. Glück and E. Reya for valuable discussions on the question of higher twist contributions.

The results (except those of section IV.3) were obtained by the CDHS-collaboration and are to be published soon.

# References

- [1] H.Wahl: Nucleon structure functions in neutrino deep inelastic scattering, XVI Rencontre de Moriond, Les Arcs 81
- [2] J.Wotschack: Neutrino oscillations, talk at the IV Symposium on Elementary Particle Physics, Kazimierz, May 1981, Proceedings p.103.
- [3] A.Bodek et al., Phys.Rev. D 20, 1471 (1979)  
A.Bodek, SLAC-PUB-2248 (1979)
- [4] EMC-collaboration: R.Rith, contribution to the Frühjahrstagung der Deutschen Physikalischen Gesellschaft, Hamburg 1981
- [5] The prediction for the ratio of anomalous dimensions is only weakly dependent on the renormalization scheme.
- [6] A.Para, private communication
- [7] L.F.Abbott and R.M.Barnett, Ann.Phys. (N.Y.) 125, 276 (1980)  
We use a modified version of Barnett's program.
- [8] I.A.Schmidt and R.Blankenbecher, Phys.Rev. D 16, 1318 (1977)  
A.Donnachie and P.V.Landshoff, DAMTP 80/6, Univ.of Cambridge
- [9] Barbieri et al., Nucl.Phys. B 117, 50 (1976)
- [10] F.Eisele et al., to be published.  
The CDHS collaboration has no responsibility for this part of the analysis nor for any conclusion drawn from it.
- [11] M.Gluck and E.Reya, Univ.of Dortmund preprint DO-TH-80/7 (1980)
- [12] D.Amati et al., Nucl.Phys. B 173, 429 (1980)  
S.I.Brodsky and G.P.Lepage, SLAC-PUB-2447 (1979)
- [13] L.F.Abbott and R.M.Barnett, Ann.Phys. 125, 276 (1980)  
L.F.Abbott et al., Phys.Rev. D 22, 582 (1980)
- [14] L.F.Abbott et al., PL 88 B, 157 (1979)
- [15] P.Allen et al., ABCMO collaboration, to be published in Physics Letters



NEUTRINO OSCILLATIONS  
- PRESENT AND FUTURE EXPERIMENTS -

Jörg Wotschack  
CERN, Geneva, Switzerland

1. INTRODUCTION

There are good reasons to search for neutrino oscillations:

- Gauge theories favour small lepton number violations<sup>1)</sup>.
- Some grand unified theories<sup>2)</sup> expect neutrino mixing with neutrino masses of  $10^{-5} \text{ eV} < m_\nu < 1 \text{ eV}$ .
- Big bang theories suggest a high neutrino density in the universe and even a very small neutrino mass would lead to enormous gravitational forces inside and between galaxies<sup>3)</sup>.
- The Moscow tritium  $\beta$ -decay experiment reports an electron neutrino mass of  $14 \text{ eV} < m_{\nu_e} < 46 \text{ eV}$ <sup>4)</sup>.

The idea of neutrinos being massive and oscillating between different neutrino flavours was born some 20 years ago<sup>5)</sup>, however, at that time, with very little chance to be experimentally verified. Today's improved neutrino facilities and experimental techniques allow detection of neutrino oscillations due to neutrino mass differences smaller than 1 eV.

A series of experimental searches have been performed during the last few years. "Evidence for neutrino instability" has been claimed by one reactor experiment<sup>6)</sup>, while a second reactor experiment<sup>7)</sup> fails to find evidence for neutrino oscillations. Bubble chamber and emulsion experiments at FNAL and CERN<sup>8-14)</sup> looking for  $\nu_e$  and  $\nu_\tau$  in  $\nu_\mu$ -beams gave negative results and also an oscillation search at Los Alamos<sup>15)</sup> saw no indication of neutrino oscillations in the range of mass differences ( $\Delta m^2$ ) accessible to these experiments. Then there are the Cl<sup>37</sup> solar neutrino experiment<sup>16)</sup>, the deep mine cosmic ray measurements<sup>17,18)</sup>, the CERN beam dump experiments<sup>19-21)</sup>, and a new high-energy total cross section measurement at FNAL<sup>22)</sup> all of which give results which could be interpreted as evidence for neutrino oscillations.

2. THE GENERAL CONCEPT OF NEUTRINO OSCILLATIONS

Neutrino oscillations may arise if the weak interaction eigenstates  $\nu_e, \nu_\mu, \nu_\tau, \dots$  which couple to  $e, \mu, \tau, \dots$  are linear combinations of neutrino mass eigenstates  $\nu_1, \nu_2, \nu_3, \dots$  with masses  $m_1, m_2, m_3$ :

The neu  
angles if th  
of the compo  
time or dist

Dependi  
the weak int  
different ne

The pro  
after a dist

where  $\alpha$  is t  
 $\Delta m^2 = |m_1^2 - m_2^2|$   
masses in eV  
maximum is

The sen  
determined b  
neutrino sou

Of course, s  
experiments  
Figure 1 sho  
neutrinos fr

†) This form  
that only  
for pract  
good enou

$$\nu_e = a_1 \nu_1 + a_2 \nu_2 + a_3 \nu_3 + \dots$$

$$\nu_\mu = b_1 \nu_1 + b_2 \nu_2 + b_3 \nu_3 + \dots$$

$$\nu_\tau = c_1 \nu_1 + c_2 \nu_2 + c_3 \nu_3 + \dots$$

The neutrino mass eigenstates  $\nu_1, \nu_2, \dots$  develop with different phase angles if their masses  $m_1, m_2, \dots$  are different. This leads to a change of the composition of the weak interaction's eigenstates as a function of time or distance.

Depending on the type of mass eigenstates (Majorana or Dirac masses) the weak interaction's eigenstates will oscillate between  $\nu \leftrightarrow \bar{\nu}$  and/or different neutrino flavours<sup>23)</sup>.

The probability that a neutrino  $\nu_a$  has oscillated into a neutrino  $\nu_b$  after a distance of flight  $L[m]$  is essentially given by

$$P(\nu_a \rightarrow \nu_b) = \sin^2 2\alpha \cdot \sin^2(1.27 \cdot \Delta m^2 \cdot \frac{L}{E_\nu})^\dagger$$

where  $\alpha$  is the mixing angle determining the oscillation amplitude,  $\Delta m^2 = |m_i^2 - m_j^2|$  is the difference of the squares of the two neutrino masses in  $\text{eV}^2$ ,  $E_\nu$  is the neutrino energy in MeV. The first oscillation maximum is obtained if  $\Delta m^2 \cdot \frac{L}{E_\nu} \approx 1.2$ .

The sensitivity of an experiment to  $\Delta m^2$  is then in first order determined by the neutrino energy  $E_\nu [\text{MeV}]$  and the distance  $L[m]$  between neutrino source and detector to be

$$\Delta m^2 \gtrsim \frac{E}{L}.$$

Of course, smaller limits for  $\Delta m^2$  for fixed  $E_\nu$  and  $L$  may be achieved if experiments are sensitive to effects due to less than maximal oscillation. Figure 1 shows the range of  $\Delta m^2$  which is accessible to experiments with neutrinos from various neutrino sources.

<sup>†</sup>) This formula is very much simplified and only true under the assumption that only two mass eigenstates contribute to the oscillation. However, for practical purposes of illustrating present experiments it is probably good enough. More complete formulae can be found in Ref. 24.

Neutrino oscillations can be detected either by observing a decrease of the primary neutrino flux (method A) or by observing the appearance of neutrinos not present at the source (method B).

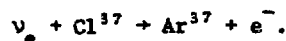
Method A, the disappearance approach, has the advantage of being independent of the oscillation products and their properties. Its disadvantage is the difficulty of measuring the neutrino flux to a sufficiently high precision to establish a small decrease of the primary neutrino flux.

Method B overcomes the latter problem provided that the flux of the oscillation products at the source is very much smaller than that of the primary beam.

### 3. EXPERIMENTAL RESULTS

#### 3.1 The solar neutrino puzzle

Davis et al.<sup>16)</sup> have been measuring the flux of solar neutrinos for more than ten years via  $\nu_e$  capture by  $\text{Cl}^{37}$ :



Their latest results<sup>36)</sup> are:

$$R = \frac{\text{observed rate}}{\text{expected rate}} = \frac{2.1 \pm 0.3}{7.8 \pm 1.5}.$$

The observed rate is only about 30% of what is expected from current solar fusion models. One possible explanation could be the oscillation of  $\nu_e$  into other neutrino flavours not being captured by the  $\text{Cl}^{37}$ .

Solar neutrinos ( $L \approx 10^{11} \text{ m}$ ,  $E_\nu \approx 1 \text{ MeV}$ ) are unique in the sense that they may explore mass differences  $\Delta m^2$  as small as  $10^{-11} \text{ eV}^2$ . Unfortunately the experiment is sensitive only to a tail of the solar  $\nu_e$  spectrum due to the threshold energy of  $\sim 0.8 \text{ MeV}$  for the  $\nu_e$  capture by  $\text{Cl}^{37}$  while the bulk of the solar neutrinos has energies below  $0.4 \text{ MeV}$ .

As pointed out by Schatzmann et al.<sup>25)</sup> the calculated  $\nu_e$  flux changes drastically if turbulences inside the sun are taken into account giving agreement with the observed  $\nu_e$  flux.

Even if it cannot be excluded that the measured solar  $\nu_e$  flux is suppressed by neutrino oscillations, it does not seem to be justified to conclude their existence being completely dependent on the calculated  $\nu_e$  flux.

A similar experiment using Gallium instead of  $\text{Cl}^{37}$  as captor is being considered by the same group. The threshold energy of this process is only

$\sim 0.2$   
solar

ences  
lation  
this i  
dimens  
oscill

3.2 C

deep  
horiz  
rock

based  
about

on cos  
make

future  
(neutr  
would  
as sm

3.3

thick  
in the  
 $10^{-11}$   
BEC<sup>18</sup>  
Mosco  
All tr

$\sim 0.2$  MeV and would permit a measurement of a much larger part of the solar neutrino spectrum.

Solar neutrinos cover by far the widest range in neutrino mass differences (see Fig. 1). However, to become independent of neutrino flux calculations measurements at different distances from the sun are necessary. Since this is not possible for earth based experiments given the large distance and dimensions of the sun, solar neutrinos are probably not very well suited for oscillation studies.

### 3.2 Cosmic ray experiments

Data are available from the Kolar-Goldfield<sup>17)</sup> and the Johannesburg<sup>18)</sup> deep mine experiments ( $\sim 3000$  m underground). Both experiments measure the horizontal  $\mu$ -flux which is almost to 100% induced by  $\nu_\mu$  interacting in the rock around the detectors.

The Johannesburg experiment finds

$$R = \frac{\text{observed rate}}{\text{expected rate}} = 0.62 \pm 0.17$$

based on less than 100 events over many years. The Kolar experiment finds about half of the expected events however based on 16 events only.

Again an interpretation in terms of neutrino oscillations depends on cosmic neutrino flux calculations with uncertainties of  $> 30\%$  which make these measurements inconclusive.

There is hope that cosmic neutrinos can be detected directly in future underground proton decay experiments. A comparison of upward (neutrinos having traversed the whole earth) to downward neutrino flux would be an important contribution and could detect mass differences  $\Delta m^2$  as small as  $10^{-3} - 10^{-4} \text{ eV}^2$ .

### 3.3 The CERN beam dump experiments

In the CERN beam dump experiments 400 GeV protons are dumped into a thick Cu-target. The flux of prompt neutrinos produced either directly in the p-Cu interactions or via the decay of short lived particles ( $\tau < 10^{-11}$  sec) has been measured by three experiments in the bubble chamber BEBC<sup>19)</sup> and the electronic detectors of the CERN-Hamburg-Amsterdam-Rome-Moscow (CHARM)<sup>20)</sup> and CERN-Dortmund-Heidelberg-Saclay (CDHS)<sup>21)</sup> collaborations. All three experiments observe an excess of prompt  $\nu_\mu$  over  $\nu_e$  induced events

$$R = \frac{\nu_e + \bar{\nu}_e}{\nu_\mu + \bar{\nu}_\mu} = \begin{array}{ll} 0.59 \pm 0.35 & \text{ABCLOS/BEBC} \\ 0.48 \pm 0.12 \pm 0.10 & \text{CHARM} \\ 0.64 \pm 0.08 \pm 0.15 & \text{CDHS (averaged)} \end{array}$$

If the bulk of the prompt neutrinos is due to production and decay of charmed particles (as commonly believed) the same number of electron and muon neutrinos should be observed.

While oscillations between  $\nu_\mu$  and  $\nu_e$  would not change the  $\nu_e/\nu_\mu$  ratio, oscillations between  $\nu_e$  and  $\nu_\tau$  could in principle explain a value  $R < 1$ . Charged current  $\nu_\tau$  interactions

$$\begin{array}{lcl} \nu_\tau + N \rightarrow \tau + X \\ \quad \quad \quad \downarrow \\ \quad \quad \quad \begin{array}{ll} e & 17\% \\ \mu & 17\% \\ \text{hadrons} & 66\% \end{array} \end{array}$$

lead in more than 60% to a purely hadronic final state and in less than 20% to an electron.

The bubble chamber identifies electrons while the counter experiments cannot distinguish between electron and hadronic final states.

If the observed rate of  $\nu_e/\nu_\mu$  was indeed due to  $\nu_e + \nu_\tau$  oscillations then bubble chamber and counter experiments should find different ratios which seems not to be the case.

The reason for the observed  $\nu_e - \nu_\mu$  asymmetry has yet to be understood, an explanation in terms of neutrino oscillation seems, however, unlikely.

An improved beam dump experiment scheduled for Spring 1982 should clarify the situation.

### 3.4 High energy total cross section

In two measurements of the total charged current neutrino cross section in 1979 and 1980 the CFRR experiment at FNAL<sup>22)</sup> has found cross section slopes to be 15-20% higher than older measurements performed by the same group at FNAL and BEBC, CDHS, and CHARM at CERN<sup>26)</sup>, see Table I.

|                 |        |
|-----------------|--------|
| FERMILAB 1977   | of     |
| FERMILAB 1979   | on and |
| FERMILAB 1980   | ratio  |
| CDHS/CHARM/BEBC | < 1.   |

In the experiment of neutrino sources the question was oscillations? and the oscillation cross section of the cross section experiments going to half

Figure 2 shows ratios measured by the ratios compatible with be 15-20% is clearly understood,

### 3.5 Reactor experiments

Reactor experiments products. The experiment placed 5-20 m events/day with

#### 3.5.1 The cross section

The only experiment so far, is a detector at Savannah River



TABLE 1

|                 | L (m) | $E_\nu$ (GeV) | $\sigma^\nu/E$  | $\sigma^{\bar{\nu}}/E$ |
|-----------------|-------|---------------|-----------------|------------------------|
| FERMILAB 1977   | 600   | 45 - 225      | $0.61 \pm 0.03$ | $0.39 \pm 0.015$       |
| FERMILAB 1979   | 1100  | 50 - 260      | $0.70 \pm 0.05$ |                        |
| FERMILAB 1980   | 1100  | 40 - 225      | $0.72 \pm 0.04$ | $0.37 \pm 0.02$        |
| CDHS/CHARM/BEBC | 600   | 30 - 200      | $0.62 \pm 0.05$ | $0.30 \pm 0.02$        |

In the experiments with the higher cross sections the distance detector-neutrino source was roughly doubled compared to the other experiments. The question was raised<sup>22)</sup>: Is the enhanced cross section due to neutrino oscillations? If this was the case the  $\Delta m^2$  would be of the order of  $200 \text{ eV}^2$  and the oscillation effect should be clearly visible as a variation of the cross section over the covered energy range. Furthermore the 15-20% increase of the cross section by doubling the distance L should be reproducible by going to half the energy at a fixed distance.

Figure 2 shows the cross section slope as a function of energy as measured by the CFRR and the CDHS experiment<sup>27)</sup>. Both data sets are compatible with being flat. In the CDHS data a variation of the order of 15-20% is clearly excluded between 50 and 280 GeV.

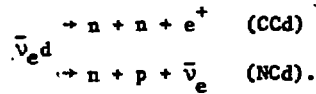
### 3.5 Reactor experiments

Reactor experiments measure the  $\bar{\nu}_e$  flux from  $\beta$ -decaying fission products. The neutrino energy is typically 2-10 MeV and detectors are placed 5-20 m from the reactor core. Typical event rates are 20-100 events/day with a signal/background ratio  $\geq 1$ .

#### 3.5.1 The Savannah River Reactor experiment

The only experiment which has claimed evidence for neutrino instability, so far, is a deuteron experiment performed by a UC Irvine group at the Savannah River power reactor<sup>6)</sup>.

The group measured the neutral and charged current reactions of  $\bar{\nu}_e$  on deuterium at a distance of 11.2 m from the reactor core.



The ratio of these cross sections which is very little dependent on the actual neutrino flux has been found to be only about 40% of the expected ratio (see Table II).

TABLE II

| Distance from core, m | Reaction | $\nu$ detection threshold MeV | Ratio, $R = \bar{\sigma}(\text{expt})/\bar{\sigma}(\text{theor.})$ |                 |                                  |
|-----------------------|----------|-------------------------------|--|-----------------|----------------------------------|
|                       |          |                               | Avignone spectrum  | Davis spectrum  | Meas. $\nu_e$ spectrum (prelim.) |
| 11.2                  | CCd/NCd  | 4.0/2.2                       | $0.43 \pm 0.17$  | $0.45 \pm 0.17$ | $0.53 \pm 0.20$                  |
| 11.2                  | NCd      | 2.2                           | $0.84 \pm 0.13$  | $1.09 \pm 0.16$ | $1.20 \pm 0.20$                  |
| 11.2                  | CCd      | 4.0                           | $0.36 \pm 0.13$  | $0.49 \pm 0.16$ | $0.64 \pm 0.24$                  |
| 11.2                  | CCp      | 4.0                           | $0.76 \pm 0.08$  | $0.99 \pm 0.10$ |                                  |
| 11.2                  | CCp      | 6.0                           | $0.46 \pm 0.05$  | $0.66 \pm 0.07$ |                                  |
| 6                     | CCp      | 1.8                           | $0.70 \pm 0.10$  | $0.91 \pm 0.13$ |                                  |
| 6                     | CCp      | 4.0                           | $0.83 \pm 0.12$  | $1.05 \pm 0.16$ |                                  |

Neutrino oscillations of the type  $\bar{\nu}_e \rightarrow \text{anything}$  could explain a value of  $R < 1$ . If  $\bar{\nu}_e$  would oscillate into  $\bar{\nu}_\mu$  or  $\bar{\nu}_\tau$  the charged current rate should be suppressed ( $\mu$  or  $\tau$  cannot be produced) while the neutral current rate is not affected.

How  
oscillat  
using es  
- If the  
ratio  
(CCd i  
oscill  
- The ch  
at 6 m  
rates  
- In the  
final  
those

3.5

A  
 $\bar{\nu}_e p \rightarrow e$   
(ILL) re  
spectrum

The  
of the r  
Davis et  
gives a

The  
oscillat  
shown in  
from the

3.6 Bub

Acc  
(from K-  
to look

actions of  $\bar{\nu}_e$

However, an interpretation of this result as evidence for neutrino oscillations has been criticized by A. Dar<sup>28)</sup> and Feynman and Vogel<sup>29)</sup> using essentially the following arguments:

- If the actually measured reactor spectrum at 11.2 m is used, the ratio of measured and expected charged current deuteron cross section (CCd in Table II) is still below unity, which cannot be explained by oscillations.
- The charged current data on H<sub>2</sub> (CCp) measured by the same experiment at 6 m and 11.2 m agree very well, if there were oscillations these rates should differ.
- In the calculation of the expected NC and CC cross sections neutron final state interactions have been omitted by the UCI group. Including those leads to agreement with the measured ratio.

### 3.5.2 The Grenoble reactor experiment

A Caltech-Grenoble-Munich group<sup>7)</sup> has measured the reaction  $\bar{\nu}_e p \rightarrow e^+ n$  at 8.7 m distance from the core of the Institut Laue-Langevin (ILL) research reactor at Grenoble. Figure 3 shows the measured neutrino spectrum.

The data are in very good agreement with the measured neutrino flux of the reactor from  $e^-$  measurements and with a calculation of the flux by Davis et al.<sup>37)</sup> while a flux calculation of Avignone and Greenwood<sup>38)</sup> gives a systematically  $\sim 30\%$  higher flux.

The Caltech-Grenoble-Munich group sees no evidence for neutrino oscillations and sets limits for the combination of  $\Delta m^2$  and  $\sin^2 2\alpha$  as shown in Fig. 4. Also indicated is the allowed region of  $\sin^2 2\alpha$  and  $\Delta m^2$  from the UCI experiment, clearly incompatible with the Grenoble result.

### 3.6 Bubble chamber and emulsion experiments at accelerators

Accelerators produce almost pure  $\nu_\mu$  beams with small  $\nu_e$  admixtures (from K-decay) of the order  $10^{-2}$ - $10^{-3}$ . They are ideal neutrino sources to look for the oscillation channels  $\nu_\mu \rightarrow \nu_e$ ,  $\nu_\tau$  or  $\nu_e \rightarrow \nu_\tau$  by direct

observation of the oscillation products via the charged current reactions

$$\nu_e N \rightarrow e^- + X$$

$$\nu_\tau N \rightarrow \tau^- + X$$

Table III gives a compilation of bubble chamber and emulsion experiments performed at FNAL and CERN.

TABLE III

| Experiment                                | Oscillation  | # events     | L[m]        | $E_\nu$ [GeV] | $\Delta m^2$ [eV <sup>2</sup> ] |
|---|--|--------------|-------------|---------------|---------------------------------|
| GGM/PS <sup>9)</sup>                      | $\nu_\mu \rightarrow \nu_e$  | 200          | $\sim 100$  | $\sim 3$      | $< 1.4$                         |
|   | $\bar{\nu}_\mu \rightarrow \bar{\nu}_e$  | 60           |             |               | $< 2$                           |
| GGM/SPS <sup>8)</sup>                     | $\nu_\mu \rightarrow \nu_e$<br>$\nu_\mu \rightarrow \nu_\tau$  | 4/540        | $\sim 1000$ | $\sim 25$     | $< 2$<br>$< 4$                  |
| BBC <sup>10)</sup>                        | $\nu_\mu \rightarrow \nu_e$<br>$\nu_\mu \rightarrow \nu_\tau$<br>$\bar{\nu}_\mu \rightarrow \bar{\nu}_e$ | $110 \pm 13$ | 900         | $\sim 53$     | $< 10$<br>$< 1.7$<br>$< 6$      |
| BBC <sup>13)</sup>                        | $\nu_\mu \rightarrow \nu_\tau$   | 73/70        | 550         | $\sim 80$     | $< 55$                          |
| FNAL <sup>11)</sup><br>Col.-BNL<br>15' BC | $\nu_\mu \rightarrow \nu_e$<br>$\nu_\mu \rightarrow \nu_\tau$<br>$\bar{\nu}_\mu \rightarrow \bar{\nu}_e$ |              | 1600        | $\sim 40$     | $< 0.6$<br>$< 3$<br>$< 17$      |
| FNAL <sup>12)</sup><br>Mich.-II<br>15' BC | $\bar{\nu}_\mu \rightarrow \bar{\nu}_e$<br>$\bar{\nu}_\mu \rightarrow \bar{\nu}_\tau$                    |              | 1600        | $\sim 40$     | $< 1.7$<br>$< 6.3$              |
| FNAL <sup>14)</sup><br>ES31<br>Emulsion   | $\nu_\mu \rightarrow \nu_\tau$   | 0/600        | 800         | $\sim 30$     | $< 3.5$                         |

The rat  
NBB), and the  
expected  $\nu_e$

A Japan-  
did not find

From the  
can be concl

### 3.7 Oscillati

The only  
detectors at  $\pi$   
Los Alamos e  
A 600  $\mu$ A beam  
Secondary  $\pi^+$  a  
This results i  
rest and  $\nu_e$  an  
factor  $\sim 1000$ .

A 6 t H<sub>2</sub>O  
stop serves as

The exper-  
appearance of  $\bar{\nu}$

No signs of osc

ctions

The rates of  $e^\pm$  events observed in GGM (PS and SPS), BEPC (WBB and NBB), and the 15' bubble chamber at FNAL agree in all cases with the expected  $\nu_e$  flux.

iments

A Japan-Korea-Canada-FNAL emulsion experiment looking for  $\tau$ -production did not find a single  $\tau$  among  $\sim 600$  charged current interactions.

From these negative results upper limits for  $\Delta m^2$  for maximal mixing can be concluded:

$$\begin{aligned}\nu_\mu \rightarrow \nu_e & \quad \Delta m^2 < 0.6 \text{ eV}^2 \\ \nu_\mu \rightarrow \nu_\tau & \quad \Delta m^2 < 3.5 \text{ eV}^2 \\ \nu_e \rightarrow \nu_\tau & \quad \Delta m^2 < 17. \text{ eV}^2.\end{aligned}$$

### 3.7 Oscillation searches at accelerators with electronic detectors

The only dedicated neutrino oscillation experiment with electronic detectors at accelerators which has produced results so far is a Yale-Los Alamos experiment at the Los Alamos Meson Physics Facility (LAMPF)<sup>15</sup>. A 600  $\mu\text{A}$  beam of 750 MeV protons is dumped into a beam stop (see Fig. 5a). Secondary  $\pi^+$  are stopped and decay while  $\pi^-$  are absorbed immediately. This results in a nearly equal flux of monochromatic  $\nu_\mu$  from  $\pi^+$  decay at rest and  $\nu_e$  and  $\bar{\nu}_\mu$  from  $\mu^+$  decay with a  $\bar{\nu}_e$  flux being suppressed by a factor  $\sim 1000$ . The average neutrino energy is about 35 MeV (see Fig. 5b).

A 6 t  $\text{H}_2\text{O}$  ( $\text{D}_2\text{O}$ ) Čerenkov counter at 9 m distance from the beam stop serves as detector (see Fig. 5a).

The experiment looked for both the disappearance of  $\nu_e$  and the appearance of  $\bar{\nu}_e$  studying the reactions

$$\begin{aligned}\bar{\nu}_e p & \rightarrow e^+ n \quad \text{in the } \text{H}_2\text{O} \text{ Čerenkov} \quad \text{and} \\ \nu_e d & \rightarrow p e^- p \quad \text{in the } \text{D}_2\text{O} \text{ Čerenkov}.\end{aligned}$$

No signs of oscillations have been found. The results

$$R = \frac{\bar{\nu}_e}{\nu_e} < 0.09 \quad \text{and}$$

$$R = \frac{\nu_e}{\mu^+} = 1.09^{+0.37}_{-0.41}$$

lead to upper limits on  $\Delta m^2$  for maximal mixing of

$$\bar{\nu}_\mu + \bar{\nu}_e : \Delta m^2 < 0.9 \text{ eV}^2$$

$$\nu_e + \text{anything} : \Delta m^2 < 2.5 \text{ eV}^2.$$

### 3.8 Conclusion on the present experiments

There is at present no convincing experimental evidence for neutrino oscillations. The 2-3 standard deviation effect as reported by the UCL reactor deuteron experiment has not been confirmed by the Grenoble reactor experiment and may have explanations related to neutral final state interactions being different for the measured neutral and charged current reactions.

Negative results from a number of bubble chamber, emulsion, and counter experiments set upper limits in terms of neutrino mass differences and mixing angles as shown in Fig. 6. The most sensitive limit is set by the ILL reactor experiment for the oscillation  $\bar{\nu}_e + \text{anything}$  which however depends on calculated reactor neutrino flux. Best limits in accelerator experiments have been obtained for the channel  $\nu_\mu + \nu_e$  and  $\bar{\nu}_\mu + \bar{\nu}_e$  by the Columbia-BNL 15' bubble chamber experiment at FNAL and by the LAMPF experiment.

## 4. FUTURE OSCILLATION EXPERIMENTS

A number of experiments dedicated to neutrino oscillation search are either under construction or proposed at Brookhaven, CERN, Los Alamos and at nuclear reactors.

One of the important new features - if not for the experiments now under construction but for those now being proposed - is the measurement of the neutrino flux at two or more positions. Studying only event ratios makes them independent of the precise knowledge of the absolute neutrino flux which has limited most of the present day experiments.

### 4.1 Reactor experiments

Both the UC Irvine and the Caltech-Grenoble-Munich groups will continue their measurements and plan to take data at different distances from the reactor core. In addition a group from Georgia Tech-University of South

Caroli:  
detect  
flux  
May, 1  
dista

4.2

facil  
the

E225:

E609:

under  
the n

Carolina is setting up an experiment. The Grenoble group has moved its detector to the Bugly power reactor (near Lyon) providing a higher neutrino flux than the ILL reactor. Installation was planned to be completed by May, 1981. It is foreseen to measure the  $\bar{\nu}_e$  spectrum at 13.5 and 18 m distance from the core with a rate of  $\sim 20\,000$  events/month<sup>30</sup>).

#### 4.2 The Los Alamos oscillation programme<sup>31)</sup>

##### 4.2.1 Experiments under preparation

Two experiments are under preparation at the Los Alamos beam stop facility (see Chapter 3.7). Both experiments search for oscillations of the type  $\bar{\nu}_\mu \rightarrow \bar{\nu}_e$  and are scheduled to start data taking in the autumn of 1981.

E225: An UC Irvine-Los Alamos collaboration will place a detector consisting of 9 t of liquid scintillator interspersed with 4 t of flash chambers at a distance of 9 m from the beam stop. It will search for  $\bar{\nu}_e$  interacting in the detector via the inverse  $\beta$ -decay reaction.

$$\bar{\nu}_e p \rightarrow e^+ n.$$

The expected event rate is about 100/day. With a running time of  $\sim 100$  days they should be sensitive to a neutrino mass difference  $\Delta m^2 \geq 0.3 \text{ eV}^2$ .

E609: A Los Alamos group has constructed a detector containing 4.5 t of Gadolinium loaded liquid scintillator.  $\bar{\nu}_e$  from oscillations  $\bar{\nu}_\mu \rightarrow \bar{\nu}_e$  will be detected via the reaction  $\bar{\nu}_e p \rightarrow e^+ n$  by measuring both the positron and the neutron with a background  $< 1$  event/30 days. The neutron is captured with high probability ( $\sim 80\%$ ) after some tens of  $\mu\text{sec}$ 's leading to two 4 MeV  $\gamma$ -rays. The detector will be installed at 30 m from the beam stop and will be sensitive to  $\Delta m^2 \geq 0.1 \text{ eV}^2$ .

##### 4.2.2 Proposed experiments

In addition to the experiments E225 and E609 there are three proposals under discussion at Los Alamos. All three experiments propose to measure the neutrino flux at varying distances from the neutrino source.

E559: A Rice-Houston-Los Alamos collaboration proposes to place two 15 t detectors consisting of liquid scintillator interspersed with drift chambers at 50 m and 75 m distances from the beam stop. The same inverse  $\beta$ -decay reaction as in E609 and E225 is used to search for oscillations  $\bar{\nu}_\mu \rightarrow \bar{\nu}_e$ . Both  $e^+$  and  $n$  will be detected via fast coincidence between backward  $e^+$  and forward neutron. Backgrounds are estimated to smaller than 1 event/10 days. The experiment will be sensitive to  $\Delta m^2 \geq 0.06 \text{ eV}^2$ .

E645: An Ohio State-ANL group wants to construct two detectors formed of  $\text{H}_2\text{O}$  ( $\text{D}_2\text{O}$ ) Cerenkov modules and drift chambers. A small 5 t detector in a fixed position close to the beam stop serves as neutrino flux monitor. A 15 t detector will be installed to be movable between 20 and 60 m. Using  $\text{H}_2\text{O}$   $\bar{\nu}_\mu$  modules transitions  $\bar{\nu}_\mu \rightarrow \bar{\nu}_e$  can be searched for by looking for reactions  $\bar{\nu}_e p \rightarrow e^+ n$ . For this oscillation channel the experiment will be sensitive to  $\Delta m^2 \geq 0.05 \text{ eV}^2$ .

With a  $\text{D}_2\text{O}$  filling of the modules the experiment is sensitive to oscillations of the type  $\nu_e \rightarrow \text{anything}$  by measuring the  $\nu_e$  flux via the reaction  $\nu_e D \rightarrow p e^-$ . Here a sensitivity  $\Delta m^2 \geq 0.3 \text{ eV}^2$  can be achieved.

E638: A Los Alamos-Maryland collaboration has proposed to build a new low energy muon neutrino facility which could serve oscillation experiments. A 100  $\mu\text{A}$  proton beam produces 150-200 MeV  $\nu_\mu$ 's from in-flight pion decay with very small  $\nu_e$  contamination. The novel feature is a movable beam transport and target - muon shield arrangement which allows changing the distance between neutrino source and detector from 50 m to 300 m.

The group wants to measure the charged current reactions

$$\nu_\mu N \rightarrow \mu^- X \text{ and } \nu_e N \rightarrow e^- X$$

using a large modular 50 t detector made of liquid scintillator and drift chambers. Measurements at different distances from the target allows them to look for the disappearance of  $\nu_\mu \rightarrow \text{anything}$  with a sensitivity  $\Delta m^2 \geq 0.2 \text{ eV}^2$  and for the appearance of  $\nu_e$ . For the latter process which could be due to oscillations  $\nu_\mu \rightarrow \nu_e$  a sensitivity of  $\Delta m^2 \geq 0.025 \text{ eV}^2$  can be achieved.

#### 4.3 The Brookhaven Experiment

At the Brookhaven experiment, a muon beam of energy  $\sim 200 \text{ MeV}$  is used to produce neutrinos.

For low energy neutrinos, the experiment is sensitive to form an allowed electronic decay induced event rate of two events per  $0.25 \text{ eV}^2$  for  $\Delta m^2 \geq 0.05 \text{ eV}^2$ .

In the Brookhaven experiment, two detectors are used. The detector modules will be used for part of the experiment.  $\nu_\mu \rightarrow \nu_e$  comparison of charged current reactions. The experiment is sensitive to  $\Delta m^2 \geq 0.05 \text{ eV}^2$ .

Two experiments are being performed: one for the disappearance of  $\nu_\mu$  and one for the appearance of  $\nu_e$ .

at different distances from the target.

One experiment is using a 1000 t  $\text{H}_2\text{O}$  detector and 1000 m of shielding. The other is using a line of several detectors and 1000 m of shielding. The sensitivity would be of the order of  $\Delta m^2 \geq 0.05 \text{ eV}^2$ .

#### 4.4 The CERN Experiment

Four oscillation experiments are being performed: a new neutrino experiment, a muon experiment, a tau experiment, and a neutrino experiment.



#### 4.3 The Brookhaven oscillation programme<sup>36)</sup>

At the Brookhaven National Laboratory a variety of neutrino oscillation experiments are being discussed including a proposal to use a muon storage ring as the source of neutrinos with an energy of  $\sim 200$  MeV.

For low energy oscillation studies (P764) 1.5 GeV protons are used to form an almost pure  $\nu_\mu$  beam with neutrino energies of 150-200 MeV. An electronic detector at  $\sim 100$  m distance from the target will look for  $\nu_e$  induced events via the charged current reaction  $\nu_e N + e^- X$ . With an event rate of two events/day and a total of 100 events mass differences  $\Delta m^2 \geq 0.25 \text{ eV}^2$  for the oscillation channel  $\nu_\mu \rightarrow \nu_e$  can be explored.

In the 28 GeV AGS wide band beam ( $\langle E_\nu \rangle \sim 1.5$  GeV) an experiment with two detectors at 130 m and 1000 m from the target is proposed. At 130 m the detector E734 consisting of 170 t of liquid scintillators/drift-tube modules will be used. At the 1000 m position a new detector of 50 or 200 t or part of E734 could be used. The experiment would look for oscillations  $\nu_\mu \rightarrow \nu_e$  comparing the  $\nu_e$  and  $\nu_\mu$  flux ratios at the two distances. The charged current reaction  $\nu_\mu N + \mu^- X$  and  $\nu_e N + e^- X$  are used as signature. The experiment aims at a sensitivity of  $\Delta m^2 = 0.05 \text{ eV}^2$ .

Two experiments are proposed in a new  $K_L^0$  beam line providing a very much enhanced  $\nu_e$  flux with  $\langle E_\nu \rangle = 3$  GeV. Both experiments want to look for the disappearance of  $\nu_\mu$  and/or  $\nu_e$  measuring the charged current rates

$$\nu_\mu N + \mu^- X \text{ and } \nu_e N + e^- X$$

at different distances from the target.

One experiment wants to use the detector E734 at  $\sim 100$  m and install a 1000 t  $\text{H}_2\text{O}$  Čerenkov counter at 1000 m. The second proposal is to build a line of seven  $\text{H}_2\text{O}$  Čerenkov counters (180 t each) placed at 90, 250, 500, and 1000 m from the target (Fig. 7). The sensitivity of both experiments would be of the order of  $\Delta m^2 = 0.5-1 \text{ eV}^2$ .

#### 4.4 The CERN oscillation programme

Four oscillations experiments have been proposed at CERN. Three in a new neutrino beam at the PS and one in the SPS wide band beam line.

#### 4.4.1 The PS experiments

A low energy neutrino beam,  $\langle E_\nu \rangle \approx 1$  GeV, pointing towards the existing neutrino detectors (BEBC, CDHS, CHARM) will be constructed (see Fig. 8a). The distance between target and detectors is approximately 900 m. The experiments could take data in the autumn of 1982 or early 1983.

BEBC: A Padova-Pisa-Athens-Wisconsin collaboration<sup>32)</sup> has proposed to search for electron neutrinos in a horn focussed (19 GeV proton)  $\nu_\mu$  beam. The  $\nu_e$  contamination of such a beam is calculated to be  $< 2 \times 10^{-3}$ . In about one month of data taking at full PS intensity the experiment could set limits on the mass differences for the oscillation channel  $\nu_\mu \rightarrow \nu_e$  of  $\Delta m^2 < 0.1$  eV<sup>2</sup>. In addition a limit for the oscillation  $\nu_\mu \rightarrow \nu_\tau$  of  $\Delta m^2 < 0.7$  eV<sup>2</sup> could be achieved by studying the rate of neutral over charged current reactions.

CDHS: The CERN-Dortmund-Heidelberg-Saclay collaboration<sup>33)</sup> has proposed to look for the disappearance of  $\nu_\mu$ 's by measuring the rate of  $\nu_\mu$  events at 150 m and 900 m. 18 GeV protons will be used to form a bare target neutrino beam without any magnetic elements and thus easy to calculate. Fe-scintillator modules (350 t) identical to the ones at 900 m will be placed at 150 m from the target to measure the  $\nu_\mu$  flux (Fig. 8b). The detector at 900 m (1200 t) will look simultaneously for deviations from the extrapolated ( $\sim \frac{1}{L^2}$ ) spectrum. Quasielastic events  $\nu n \rightarrow \mu^- p$  which form  $\sim 90\%$  of the total cross section, serve as a signature. Their rate will be measured as a function of muon length in iron and is thus independent of calibration biases. In one month of data taking  $\sim 4000$  events in the far position are expected. The experiment aims to see deviations of the order of 10% and is sensitive to  $\Delta m^2 \geq 0.25$  eV<sup>2</sup> for  $\nu_\mu \rightarrow$  anything.

CHARM: The experiment proposed by the CERN-Hamburg-Amsterdam-Rome-Moscow<sup>34)</sup> collaboration follows to a large extent the CDHS proposal. Two detectors of marble-scintillator-proportional tube assemblies at 150 m and 900 m of 40 t and 135 t respectively, are used. In addition to the disappearance of  $\nu_\mu$  the experiment hopes to be sensitive to  $\nu_e$  appearance by electron detection.

#### 4.4.2 The SPS experiment

In the proposal of the Annecy-CERN-Imperial College-Oxford collaboration<sup>35)</sup> neutrino energy and path of flight are scaled by a factor of  $\sim 15$  compared to the PS experiments. It is intended to use the normal CERN SPS wide band beam with an average energy  $\langle E_\nu \rangle = 20-40$  GeV. Two detectors of 0.32 t and 100 t will be placed at 1000 m and 17 km from the target, the latter being situated in the Jura mountains (see Fig. 9).

A detector of 3 mm Fe plates interleaved with flash tubes and a muon absorber (Fe and driftchambers) is proposed. The experiment intends to look for the disappearance of  $\nu_\mu$ 's ( $\Delta m^2 \geq 0.15$  eV<sup>2</sup>) and aims at the same time to identify electron neutrino induced events ( $\Delta m^2 \geq 0.06$  eV<sup>2</sup>). The beam time needed to reach these limits is of the order of one year of SPS operation.

#### 5. ~~CONCLUSIONS~~

### SUMMARY

Neutrino oscillations have still not been discovered. Several experiments have searched for oscillations and explored the range of neutrino mass differences to values as small as  $1-10^{-1}$  eV<sup>2</sup> without finding any convincing evidence for neutrino instability.

Future experiments at accelerators will be able to improve the existing upper limits on mass differences for the different oscillation channels by roughly one order of magnitude. If neutrino oscillations have not been discovered by that time only deep mine experiments (proton decay?) might have a chance to extend the observable  $\Delta m^2$  range to  $10^{-3}-10^{-4}$  eV<sup>2</sup> by studying cosmic neutrinos having traversed the earth. Neutrino mass differences smaller than this are probably not accessible using present day methods.

the  
ected  
roximately  
early

sed to  
)  $\nu_\mu$  beam.  
)<sup>-3</sup>. In  
ent could  
 $\nu_\mu \rightarrow \nu_e$   
 $\nu_\tau$  of  
over

proposed  
 $\nu_\mu$  events  
target  
iculate.  
will be placed  
detector at  
extrapolated  
% of the total  
ed as a function  
ases.  
e expected.  
s sensitive

me-Moscow<sup>34)</sup>  
detectors of  
00 m of  
pppearance of  
electron

## REFERENCES

- 1) See e.g. R. Barbieri, CERN TH 2850 (1980).
- 2) R. Barbieri, J. Ellis and M.K. Gaillard, LAPP TH 10/CERN TH 2787 (1979).
- 3) see e.g. G. Steigmann, Ann. Rev. Nucl. Part. Sci. 29 (1979) 313.
- 4) V.A. Lubimov et al., Phys. Lett. 94B (1980) 266.
- 5) B. Pontecorvo, Sov. Phys. JETP 6 (1958) 429; 7 (1958) 172; 26 (1968) 984.
- 6) F. Reines et al., Phys. Rev. Lett. 45 (1980) 1307.
- 7) F. Boehm et al., Phys. Lett. 97B (1980) 310.
- 8) J. Blietschau et al., Nucl. Phys. B133 (1978) 205.
- 9) N. Armenise et al., preprint CERN-EP/80-226 (1980).
- 10) O. Erriquez et al., Phys. Lett. 102B (1981) 73.
- 11) A.M. Cnops et al., Phys. Rev. Lett. 40 (1978) 144.
- 12) FNAL-Michigan-IHEP-ITEP collaboration, B.P. Roe in Ref. 36.
- 13) H. Deden et al., Phys. Lett. 98B (1981) 310.
- 14) T. Kondo, FERMILAB-Conf.-80/92-EXP.
- 15) P. Nemethy et al., Phys. Rev. Lett. 44 (1980) 522; Phys. Rev. D23 (1981) 262.
- 16) R. Davis et al., Phys. Rev. Lett. 20 (1968) 1205; see also:  
B.T. Cleveland, R. Davis, J.K. Rowley in Ref. 36.
- 17) Kolar gold field experiment, M.R. Kriskaswamy et al., Proc. Roy. Soc.  
London A323 (1971) 489.
- 18) Johannesburg mine experiment, M.F. Goud et al., Phys. Rev. D18 (1978)  
2239.
- 19) see Ref. 21.
- 20) M. Jonker et al., Phys. Lett. 96B (1980) 435.
- 21) F. Dydak, Rapporteurs talk, International Conf. on Neutrino Physics  
and Astrophysics, Erice, Italy, 23-27 June, 1980.
- 22) T. Kondo, talk given at the 16th Rencontre de Moriond, Les Arcs, 1981.  
B.C. Barish et al., Phys. Rev. Lett. 39 (1977) 1595.
- 23) L. Maiani, preprint CERN TH 2846.
- 24) V. Barger et al., DOE-ER/00881-151 (1980).
- 25) E. Schat
- 26) BEBC: P.  
CDHS: J.  
CHARM: M
- 27) H. Wahl,
- 28) A. Dar, T
- 29) R.P. Fey
- 30) J.F. Cava
- 31) R.L. Bu  
Jan. 19
- 32) Padova-Pa  
and CE.
- 33) CERN-Dor
- 34) CHARM co
- 35) Annecy-CE  
propos
- 36) Proceedi  
Labora
- 37) B.R. Davi
- 38) F.T. Avig

- at  
P.C.  
J.C.  
M  
9).
- l,  
, T  
ey 84.  
ava  
u  
19  
-P1  
CEP  
ort  
col  
-CE  
os  
di  
ra  
avi 81) 262.  
vig
- 25) E. Schatzmann and A. Maeder, Seminar at CERN, 25 September, 1980.
  - 26) BEBC: P.C. Bosetti et al., Phys. Lett. 70B (1977) 273.  
CDHS: J.G.H. de Groot et al., Z. Physik C1 (1979) 143.  
CHARM: M. Jonker et al., Phys. Lett. 99B (1981) 265.
  - 27) H. Wahl, talk given at the 16th Rencontre de Moriond, Les Arcs, 1981.
  - 28) A. Dar, TECHNION-PH 80-40 (1980).
  - 29) R.P. Feynman and P. Vogel, Comments on "Evidence for neutrino instability".
  - 30) J.F. Cavaignac, private communication.
  - 31) R.L. Burman, talk presented at the Neutrino Oscillation Workshop, BNL, Jan. 1981, LA-UR-81-1010.
  - 32) Padova-Pisa-Athens-Wisconsin collaboration, proposal CERN/SPSC/80-57/P146 and CERN/PSCC/80-130/P33; PSCC/80-132/P33 Add. 1.
  - 33) CERN-Dortmund-Heidelberg-Saclay collaboration, proposal CERN/PSCC/80-106/P30.
  - 34) CHARM collaboration, proposal CERN/PSCC/81-8/P37.
  - 35) Annecy-CERN-Imperial College-Oxford collaboration, proposal CERN/SPSC/81-14/P158; 81-53/P158 Add. 1.
  - 36) Proceedings of the Neutrino Oscillation Workshop, Brookhaven National Laboratory, January 30-31, 1981, BNL 51380.
  - 37) B.R. Davis et al., Phys. Rev. C19 (1979) 2259.
  - 38) F.T. Avignone and Z.D. Greenwood, Phys. Rev. C22 (1980) 594.

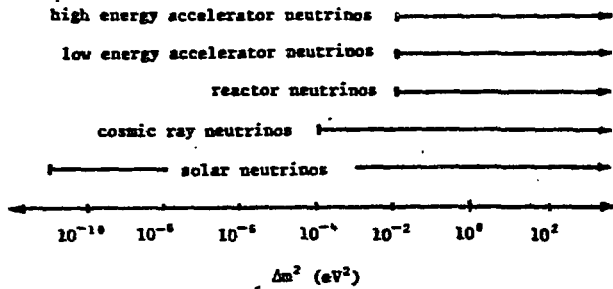


FIG.1 The range of neutrino mass differences  $\Delta m^2$  which may be explored by experiments using neutrinos from the indicated sources. The lower limits are given by the distance source-detector and the neutrino energy.

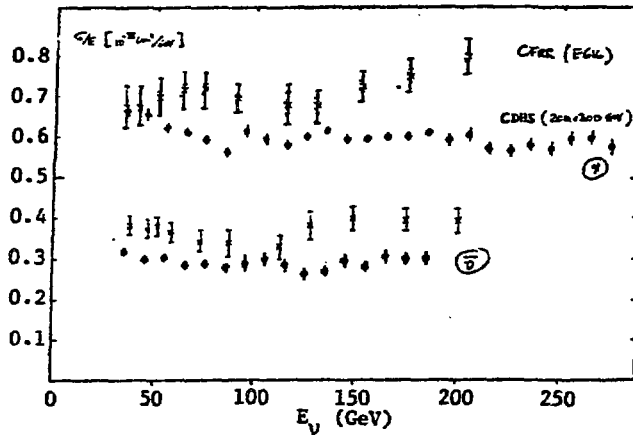


FIG.2 The total cross section slope in units  $10^{-38} \text{ cm}^2/\text{GeV}/\text{nucleon}$  as a function of the neutrino energy. Shown are the 1980 measurement of the CFRR experiment<sup>12)</sup> and the results of the CDHS experiment<sup>27)</sup> at CERN.

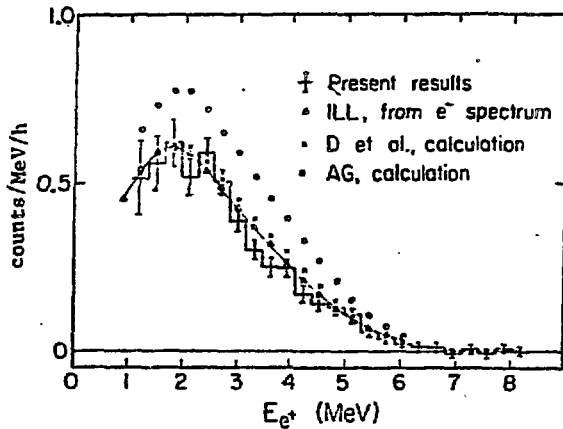


FIG.3 The positron energy spectrum as measured by the ILL group. Also indicated are the expected  $e^+$ -spectrum based on the measured  $e^-$ -spectrum and the calculated spectra of Davis et al. and Avignone and Greenwood.

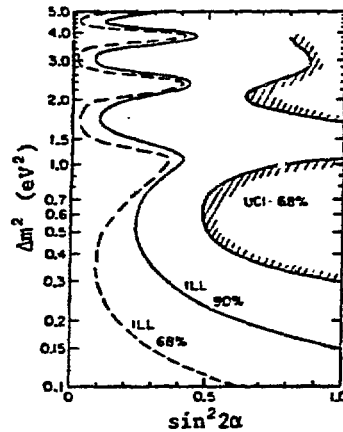
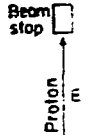


FIG.4 The limits on oscillation amplitude  $\sin^2 2\alpha$  and mass difference  $\Delta m^2$ . The ILL result excludes the region above the curve labelled ILL. The UCI experiment excludes the region outside the shaded boundaries.

a)



b)

NEUTRINO SPECTRA

of neut  
rich may  
ing neut  
res. Th  
the d  
d the n

cross se  
cm²/GeV  
he neut  
measure  
and the  
r<sup>27)</sup> at C

b)  
or

Preliminary  
Liner

2° PCP Pos 5  
Structure for

UCI-68%

90%

68%

sin²2α

on oscilla  
d mass dif  
excludes  
ve labell  
excludes t  
aded bound

a) of neutrino mass which may be explored using neutrinos from reactors. The lower limit is the distance between the neutrino emission

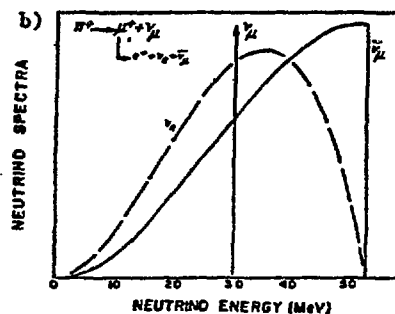
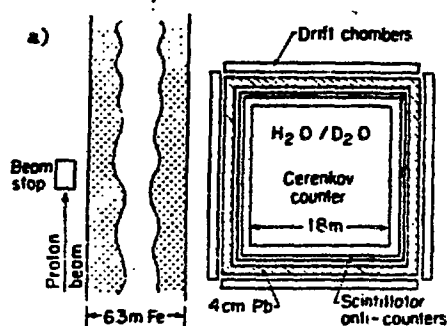


FIG.5 a) Experimental set-up of the LAMPF oscillation experiment and b) neutrino spectrum from the decay of stopping  $\pi^+$  and  $\mu^+$ .

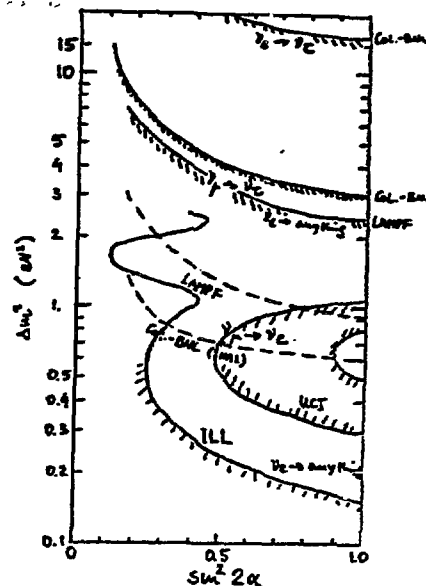


FIG.6 Summary of the presently achieved best limits on  $\sin^2 2\alpha$  and  $\Delta m^2$  for various oscillation processes. Data are from Col-BNL, LAMPF, and reactor experiments.

SCHEMATIC LAYOUT OF THE  $\nu_e$  BEAM MODULE LOCATIONS ALONG BEAM LINE

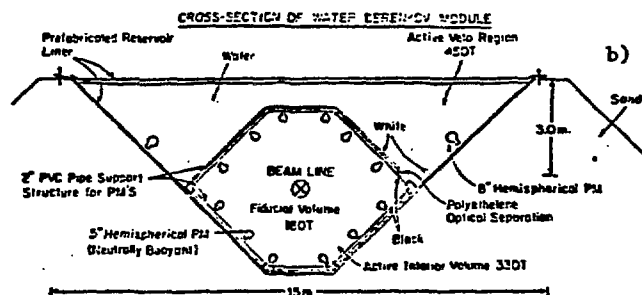
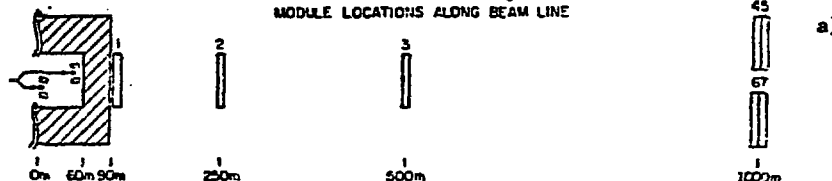


FIG.7 Layout of the proposed BNL  $H_2O$  Cerenkov experiment a) target and module layout along the beam line and b) cross section through one water Cerenkov module.

b) cross section  $10^{-38} \text{ cm}^2/\text{GeV/nucleon}$  of the neutrino energy. measurement of the and the results of  $\tau^{12}$  at CERN.

UCI-88%

90%

$\sin^2 2\alpha$

on oscillation and mass difference  $\Delta m^2$  excludes the  $\nu_e$  labelled ILL. excludes the  $\nu_\mu$  labelled boundaries.

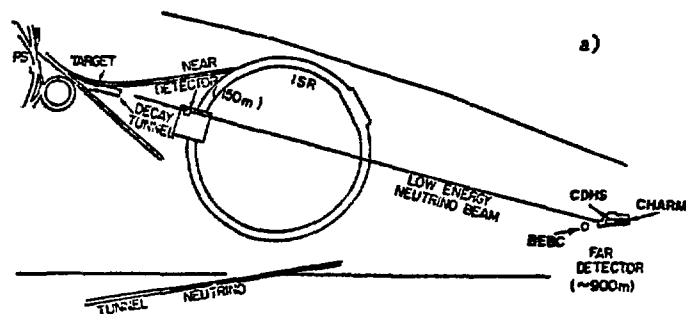
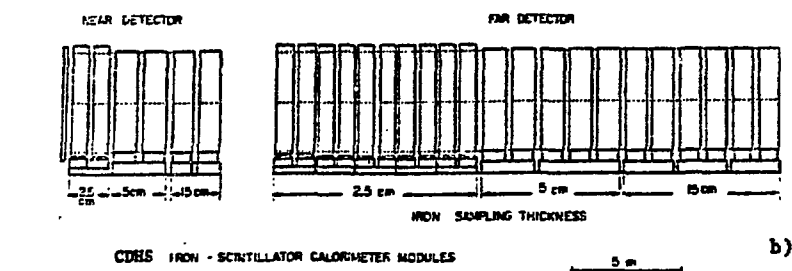


FIG.8 Layout of the proposed CERN PS oscillation facility a) target station and existing neutrino detectors BEBC, CDHS, CHARM, in the CDHS and CHARM proposals additional detectors will be placed at the position labelled "NEAR DETECTOR". b) layout of the near and far detectors for the CDHS experiment.

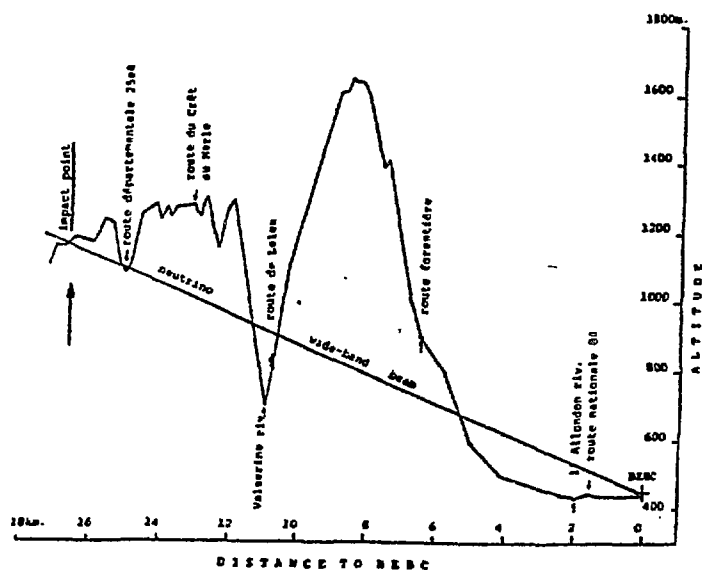


FIG.9 Direction of the CERN SPS wide-band beam crossing the Jura mountains. The proposed detector position at 17 km is indicated as "impact point".





NEUTRON AND PROTON STRUCTURE FUNCTIONS FROM INELASTIC ANTINEUTRINO  
SCATTERING IN DEUTERIUM

Amsterdam - Bologna - Padova - Pisa - Saclay - Torino

Collaboration

Presented by V. Flaminio

It is clear from what we heard at this Conference, that most experimental investigations now being carried out, deal with the quark-parton substructure of hadrons and with the related QCD theory.

In turn, many investigations require, for a proper interpretation of the results, a knowledge of the properties and  $x$  - distributions of quarks having a definite flavour:  $x_u(x)$ ,  $x_d(x)$ ,  $x_s(x)$ , .....

A typical, but by no means only example, is the Drell-Yan production of lepton-pairs in hadronic interactions, where a knowledge of structure functions extracted from deep-inelastic lepton scattering has been successfully used to predict the yield of dimuons as a function of the scaling variable  $M^2/S$ , once QCD corrections are incorporated.

Detailed information on the  $x$ -distributions of partons with a definite flavour can best be obtained by neutrino/antineutrino scattering on neutrons and protons, which can be performed using a deuterium target.

We have carried out such an experiment at the CERN-SPS, using the Big European Bubble Chamber filled with deuterium, exposed to wide-band neutrino/antineutrino beams. A double plane of large pwc<sup>s</sup> (EMI) surrounding the downstream part of the chamber was used for the identification of  $\mu^\pm$ . The results I will present here are based on the analysis of approximately 60% of the antineutrino exposure, corresponding to about 12000 events. Preliminary results from this experiment have already been given<sup>(2)</sup>.

The neutrino energy was computed for each event starting from the measured momenta of all detected particles, using the method suggested by Heilmann<sup>(2)</sup>.

5630 events turned out to be charged-current (cc) antineutrino events, and 1372 were identified as charged-current neutrino events (these are always present as a background in the antineutrino beam). The remaining events were classified as neutral-current candidates.

Charge NEUT

ction:  
a low  
ining

Corre-  
dure.

A cor v - To  
terium

On the  
GeV on

Correc  
EMI a

most  
ne qu  
tory.

The d  
x = q<sup>2</sup>  
as fo

van pr  
edge o  
atteri

a<sup>2</sup>  
a fu

a<sup>2</sup>  
with a  
scat  
deute

using  
sed to

For 1  
cross  
sed on

A mea  
under  
this

mind  
cordi  
(1-x)

Farre  
to pr

The d  
nts (

Fig.  
Feynm

NEUTRINO

Charged current events were moreover classified as neutron (n) interactions if they had an even number of prongs or on odd number, including a low energy proton (spectator) in the backward direction. All the remaining events were classified as proton(p) interactions.

Corrections were applied for events lost or misclassified by this procedure.

A correction of (12.2. )% was also applied for rescattering in the deuterium nucleus.

On the data presented here a cut at 4 GeV/c on muon momentum and at 10 GeV on the reconstructed neutrino energy was applied.

Corrections were applied for the effect of the cut on  $P_{\mu}$ , for the finite EMI acceptance, for smearing coming from uncertainties on the neutrino energy, and for radiative corrections.

Details of these corrections will be given in a forthcoming paper<sup>(3)</sup>.

The double-differential cross section in the usual scaling variables  $x = q^2/2Mv$  and  $y = v/E_{\nu}$ , can be written, assuming the quark-parton model, as follows:

$$\frac{\partial^2 \bar{\sigma}^{\nu p}}{\partial x \partial y} = \frac{G^2 m E_{\nu}}{\pi} 2x \left[ u(x) (1-y)^2 + (\bar{d}(x) + \bar{s}(x)) \right] \quad (1a)$$

$$\frac{\partial^2 \bar{\sigma}^{\bar{\nu} p}}{\partial x \partial y} = \frac{G^2 m E_{\nu}}{\pi} 2x \left[ d(x) (1-y)^2 + (\bar{u}(x) + \bar{s}(x)) \right] \quad (1b)$$

Integrating these over y and taking the ratio of the two, one obtains:

$$\frac{d\bar{\sigma}^{\nu p}/dx}{d\bar{\sigma}^{\bar{\nu} p}/dx} = \frac{(1/3) u(x) + \bar{d}(x) + \bar{s}(x)}{(1/3) d(x) + \bar{u}(x) + \bar{s}(x)}$$

For large x, when the sea terms become negligible, the ratio of the two cross sections becomes therefore equal to the ratio  $u^v(x)/d^v(x)$ .

A measurement of this ratio as a function of x is therefore useful to understand the relative behaviour of valence u and d quarks. A simple minded quark parton model would in fact predict  $u(x) = d(x)$ , while according to Field and Feynman<sup>(4)</sup> the ratio d/u should go to zero like (1-x) for  $x \rightarrow 1$ .

Farrar and Jackson have used QCD arguments augmented by SU(6) symmetry, to predict  $d/u \rightarrow 0.2$  for  $x \rightarrow 1$ .

The dependences of  $\bar{R}$  on x, y and  $E_{\nu}$  are presented in fig. 1.

Fig. 1a shows the ratio as a function of x, compared with the Field and Feynman model.

It seems that our data at  $x \sim 0.7$  lie higher than the Field and Feynman prediction, although the errors are still too large to draw any final conclusion. The data are clearly also in agreement with the prediction of ref<sup>5</sup>.

A fit of the ratio to an expression of the form  $A+B(1-x)^n$  gives  $A=0.15 \pm 0.05$ . This favours the prediction of ref<sup>(5)</sup>, although the presence of systematic errors may modify this result.

Fig. (1c) compares the ratio, under the cuts  $W^2 > 4 \text{ GeV}^2$ ,  $Q^2 > 2 \text{ GeV}^2$ , with the prediction of the model of Buras and Gaemers<sup>(6)</sup>. The agreement is not very good.

The main qualitative conclusion one can draw from our data at  $x > 0.2$ , is that the  $x$  distribution  $xu_p(x)$  in the proton is broader than  $xu_n(x)$  in the neutron.

The same effect has already been observed in a neutrino experiment<sup>(7)</sup>, as well as in our own neutrino data<sup>(1)</sup>.

The values of the ratios of cross sections, integrated over the kinematical variables is given, for the indicated cuts, in table I, where a comparison is also made with the Field-Feynman and the Buras-Gaemers models. There is in general agreement with the Field-Feynman predictions.

We have also extracted the distributions of valence and sea quarks from our  $y$ -distributions, fitting them to expressions 1a, 1b.

In doing this we have assumed an antineutrino nucleon total cc cross section  $\sigma = 0.30 \times 10^{-38} E_\nu$  ( $\text{cm}^2/\text{nucleon}$ ), and a ratio  $\sigma_{\nu n}^-/\sigma_{\nu p}^- = 0.51$  as measured in this experiment.

The fit to the  $y$  distribution, integrated over  $x$ , yields for the integrals of quark distribution functions and of structure functions the values given in table 2.

The values of  $\bar{D}+\bar{S}$  and  $\bar{U}+\bar{S}$  indicate that the fraction of momentum carried by  $\bar{d}$ -quarks in the proton is larger than the fraction carried by  $\bar{u}$ -quarks. This is in agreement with the preliminary results of a  $\nu_{\mu}$ -deuterium experiment<sup>(7)</sup>. Our result for  $\bar{D}+\bar{S}$  is in agreement with the value found in a  $\nu_{\mu}$  experiment in hydrogen ( $0.033-0.012$ )<sup>(8)</sup>. The total fraction of antiquarks  $(\bar{U}+\bar{D}+2\bar{S})/(\bar{U}+\bar{D}+\bar{U}+\bar{D}+2\bar{S})=0.125 \pm 0.015$  corroborates the results of high statistics experiments on isoscalar targets and in particular the value  $0.12 \pm 0.02$  obtained from a fit to  $\nu_{\mu}y$ -distributions at similar  $\langle Q^2 \rangle$ <sup>(9)</sup>.

To study the detailed  $x$ -dependence of these distributions, the fits to the  $y$ -distributions were performed for several  $x$  intervals. The  $y$  range was restricted from a lower limit of 0.1 to an upper limit of 0.6 to 0.8, depending on  $x$ . The overall  $\chi^2$  per degree of freedom was 75/78 for the neutron data and 113/86 for the proton data. The results obtained are shown in Fig. 2.

The results are in agreement with those of a  $\nu_{\mu}p$  experiment<sup>(8)</sup>. The Field of Feynman predictions<sup>(4)</sup> (dashed lines in Fig.2) agree with the data points for  $xu(x)$ , while they compare less satisfactorily with the points for  $xd(x)$ .

In order to compare proton, we have (shown by the solid two slopes, at the Field - Feynman per  $xu(x)$  distribution to check this conclusion of a difference between in an experiment

#### References and

- (1) Allasia et al. 20<sup>th</sup> Int.
- (2) H.G. Heilmann unpublished work on a baryon makes a significant difference 0-c or 3-c
- (3) D.Allasia et al. current experiments (1981)
- (4) R.Field and J.Feynman
- (5) G.R.Farrar et al.
- (6) A.J.Buras et al.
- (7) J.Hanlon et al.
- (8) Fernandez et al.
- (9) S.M. Heath et al.
- (10) A.S. Ito et al.

In order to compare the shapes of the sea distribution for neutron and proton, we have fitted them to an expression of the form  $A(1-x)^{\alpha}$ . The fits (shown by the solid lines in figs. 2c, 2d) show a difference between the two slopes, at the level of 1.5 standard deviations, in agreement with the Field - Feynman predictions (shown by the dashed lines in fig. 2) of a steeper  $\bar{x}u(x)$  distribution compared to  $\bar{x}d(x)$ . Systematics is being studied to check this results, but systematic effects are unlikely to change the conclusion of a difference between the two slopes. We note that a similar difference between the slopes of  $\bar{x}u(x)$  and  $\bar{x}d(x)$  has recently been observed in an experiment on hadronic production of muon pairs<sup>(10)</sup>.

#### References and footnotes

- (1) Allasia et al., high energy antineutrino interactions in deuterium. 20<sup>th</sup> Int. Conf. on High Energy Physics, Madison, Wisconsin, (1980)
- (2) H.G. Heilmann, University of Bonn Int. Rep. n WA21 - int - 1 (1978), unpublished. This method for determining  $E_{\bar{\nu}}$  neglects the presence of a baryon in the final state. In the kinematical region where this makes a significant difference ( $q^2 < 1 \text{ (GeV/c)}^2$  and  $\nu < 2.2 \text{ GeV}$ ) a 0-c or 3-c fit was applied to obtain the antineutrino energy.
- (3) D.Allasia et al., (Measurement of the ratio of  $\bar{\nu}_{\mu} n$  to  $\bar{\nu}_{\mu} p$  charged-current cross sections at high energies). Submitted to Physics Letters (1981)
- (4) R.Field and R.P. Feynman, Phys. Rev. D15 (1977) 2590
- (5) G.R.Farrar et al, Phys. Letters 69B (1977) 112
- (6) A.J.Buras and K.J.F. Gaemers. Nuclear Phys. B132 (1978) 249
- (7) J.Hanlon et.al., Phys. Rev. Letters 45 (1980), 1817
- (8) Fernandez et al., Phys. Rev. Letters, 43 (1979) 1975
- (9) S.M. Heagy et al., Phys. Rev. D23 (1981) 1045
- (10) A.S. Ito et al., Phys. Rev. D23 (1981) 604

a) Antineutrino

| Cuts   | $\bar{R}$                |      |      |
|--|--------------------------|------|------|
|  | this experiment          | FF   | BG   |
| NO   | $0.51 \pm 0.01 \pm 0.03$ | -    | -    |
| $W^2 > 4 \text{ GeV}^2$                            | $0.55 \pm 0.02 \pm 0.04$ | 0.58 | -    |
| $W^2 > 4 \text{ GeV}^2$<br>$Q^2 > 2 \text{ GeV}^2$ | $0.49 \pm 0.02 \pm 0.03$ | 0.51 | 0.59 |

b) Neutrino

| Cuts   | R                        |      |      |
|--|--------------------------|------|------|
|  | this experiment          | FF   | BG   |
| NO   | $2.22 \pm 0.12 \pm 0.25$ | -    | -    |
| $W^2 > 4 \text{ GeV}^2$                            | $2.17 \pm 0.13 \pm 0.25$ | 1.90 | -    |
| $W^2 > 4 \text{ GeV}^2$<br>$Q^2 > 2 \text{ GeV}^2$ | $2.38 \pm 0.15 \pm 0.25$ | 2.03 | 1.87 |

- TABLE 1 -

Cross section ratios  $\bar{R} = \frac{\sigma(\bar{\nu}n)}{\sigma(\bar{\nu}p)}$  and  $R = \frac{\sigma(\nu n)}{\sigma(\nu p)}$  for cc interactions.

The values in the table are for  $E(\bar{\nu}) > 10 \text{ GeV}$ , and for the indicated kinematical cuts.

For  $\bar{R}$  and R the value  $f = 0.12 \pm 0.03$  was used and both the statistical (first) and systematic errors are given. The predictions computed according to the FF<sup>(4)</sup> and BG<sup>(6)</sup> model are also quoted.

Table 2 - Values of the integrals of the quark distribution functions and of the structure functions. The values were obtained by fitting the data over the range  $0.1 < y < 0.8$ . The errors are statistical only. Systematic uncertainties have been estimated to be smaller than the sta-

BG  
-  
-  
1.87  
or cc i  
and for  
and both  
even.  
and BG (6)

BG  
 0.59  
 1.87  
 BG  
 or cc intera  
 id for the  
 id both the  
 ren.  
 d BG (6)  
 model

Table 2 - Values of the integrals of the quark distribution functions and of the structure functions. The values were obtained by fitting the data over the range  $0.1 < y < 0.8$ . The errors are statistical only. Systematic uncertainties have been estimated to be smaller than the statistical ones.

|  |  |
|--|--|
| $U = \int_0^1 x u(x) dx = 0.285^{+0.012}$          | $\bar{D} + \bar{S} = \int_0^1 x (\bar{d}(x) + \bar{s}(x)) dx = 0.034^{+0.004}$ |
| $D = \int_0^1 x d(x) dx = 0.129^{+0.010}$          | $\bar{U} + \bar{S} = \int_0^1 x (\bar{u}(x) + \bar{s}(x)) dx = 0.021^{+0.003}$ |
| $\int_0^1 F_2^{\bar{\nu}p}(x) dx = 0.638^{+0.019}$ | $\int_0^1 x F_3^{\bar{\nu}p}(x) dx = 0.502^{+0.029}$                           |
| $\int_0^1 F_2^{\bar{\nu}n}(x) dx = 0.300^{+0.015}$ | $\int_0^1 x F_3^{\bar{\nu}n}(x) dx = 0.216^{+0.024}$                           |

Figure captions

Fig.1) The ratio  $\bar{R} = \sigma(\bar{\nu}n)/\sigma(\bar{\nu}p)$  as a function of  $x$  (fig.1a. and 1b ),  $y$  (fig.1c) and  $E_{\bar{\nu}}$  (fig.1d). The kinematical regions selected for each plot are indicated. The curves are the predictions of the Field and Feynman parametrisation <sup>(4)</sup> (fig.1a,1c,1d ) and of the Buras and Gaemers <sup>(6)</sup> model (fig.1b).

Fig.2)  $x$  dependence of the quark structure functions : (a)  $xu(x)$ , (b)  $xd(x)$  (c)  $x(\bar{d}(x)+\bar{s}(x))$  and (d)  $x(\bar{u}(x)+\bar{s}(x))$ .

The dashed lines represent the Field - Feynman predictions <sup>(4)</sup>. The solid lines are the results of fitting the sea - quark distribution functions to the formula  $A(1-x)^{\alpha}$

1.

$$\frac{d\sigma_{\bar{\nu}n}}{dx} / \frac{d\sigma_{\bar{\nu}p}}{dx} .5$$

, y  
plot  
an  
odel

xd(x)

0  
0

solid li  
s to

1.

$$\frac{d\sigma_{\bar{\nu}n}}{dx} / \frac{d\sigma_{\bar{\nu}p}}{dx} .5$$

0  
0



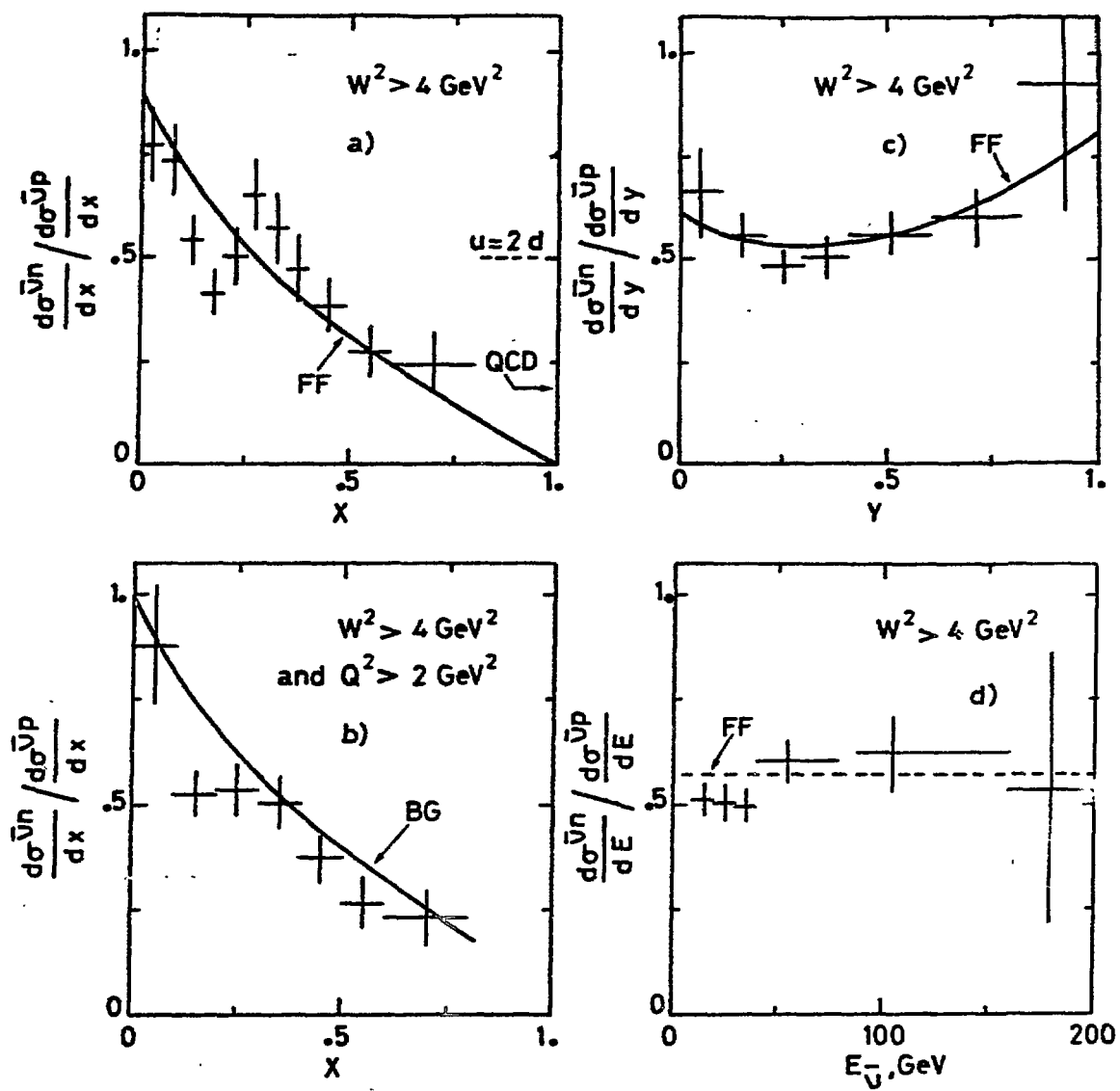


Fig.1

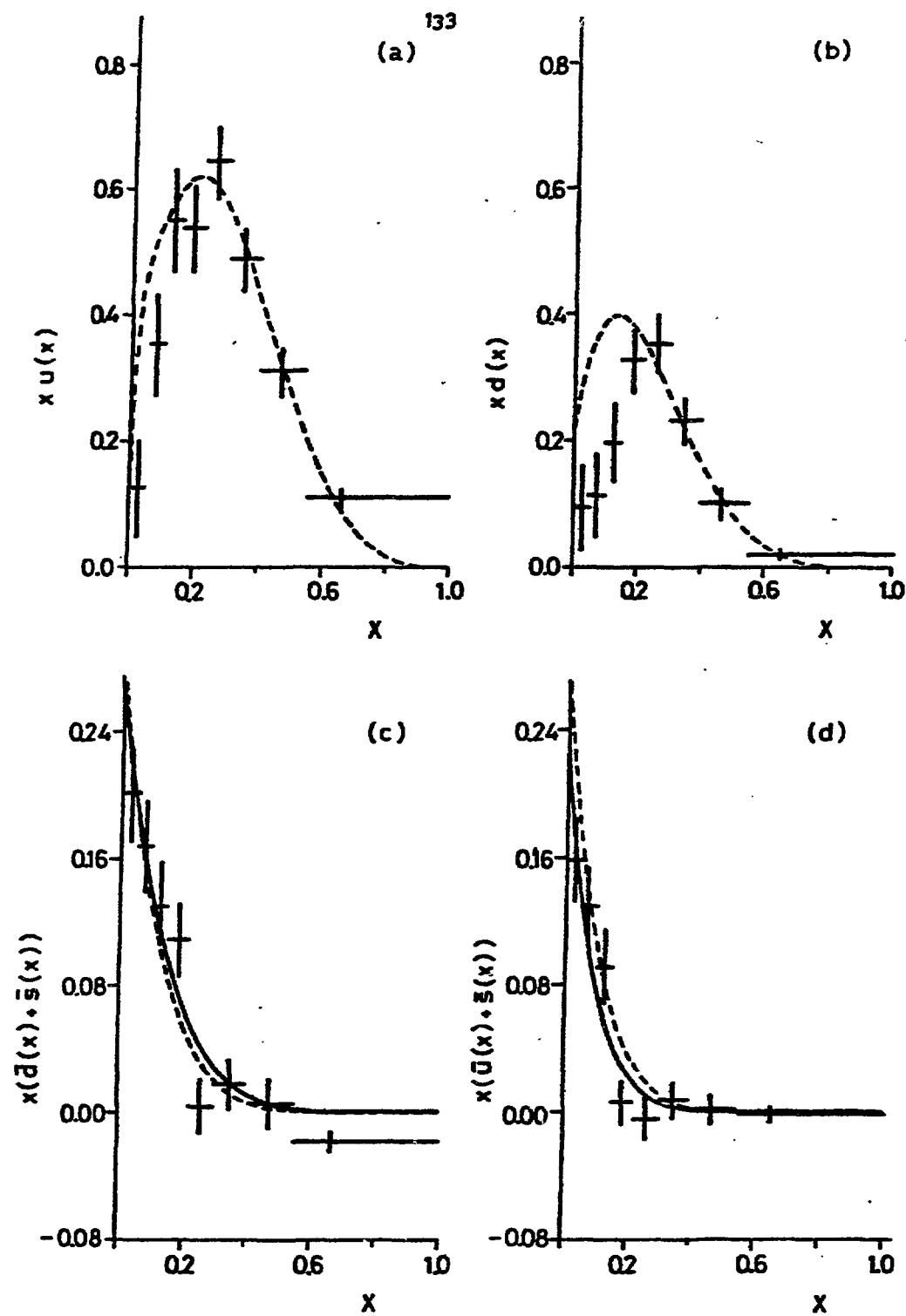


Fig. 2



SPIN EFFECTS IN  $e^+e^-$  ANNIHILATION

J. Ranft, Sektion Physik, Karl-Marx-Universität,  
Leipzig, DDR

1. Summary of spineffects in  $e^+e^-$  annihilation

Longitudinal polarization of electrons and positrons in future  $e^+e^-$  storage rings is rather difficult to be obtained. A recent discussion of this question was recently given for the future CERN-LEP storage rings /1/. In contrast to this, it should be straightforward, to obtain a linearly polarized electron beam in a linear  $e^+e^-$  collider like the SLAC Single Pass Collider /2/ or the VLEPP project /3/ at Novosibirsk. Polarized Electrons have been accelerated in the past in the SLAC Linear Accelerator.

Quite a few experiments with polarized  $e^+e^-$  collisions have been proposed in the past. The most interesting proposals include:

- The observation of gauge theory cancellations in  $e^+e^- \rightarrow W^+W^-$ , discussed by Gaemers and Gounaris /4/.
- The precise measurement of neutral current couplings on top of the  $Z^0$  peak, discussed by Prescott /5/.
- Flavor separation by means of transverse beam polarization /6/.

In the past, the azimuthal asymmetry of two jet events with transversely polarized beams was measured at SPEAR and provided evidence, that these jets could be associated with spin 1/2 quarks /7/.

~~We will discuss here~~ cross sections and spin asymmetries for large  $p_T$  jet production from two photon processes in  $e^+e^-$  collisions with definite helicities ~~/8/~~. ~~We will discuss elsewhere /9/~~ the production of polarized hadrons in polarized and unpolarized single photon  $e^+e^-$  annihilation processes. *not discussed*

## 2. Spin asym

two pho

Recentl

jet producti  
nism is acce

QCD pre  
scattering c  
sed /11,12/

spin asymmet  
ding to larg  
these tests

are produced  
Jet pro  
studied by B  
dictions for

with definit  
We use  
production.

are the foll

i) The dis  
tons, q  
ty. We  
leading  
where b  
electro

ii) The cro  
with de  
tions f  
scatter  
the cro  
ys  
are

d  
c

d  
d

## 2. Spin asymmetries in large $p_{\perp}$ jet production in two photon processes

Recently first measurements have shown, that hadron jet production in  $e^+e^-$  collisions via the two photon mechanism is accessible experimentally /10/.

QCD predicts sizeable spin asymmetries for the hard scattering of quarks and gluons. In the past it was proposed /11,12/ to measure as a test for QCD the corresponding spin asymmetries in polarized hadron-hadron collisions leading to large  $p_{\perp}$  jet production. Here we point out, that these tests are more unambiguous if the large  $p_{\perp}$  hadron jets are produced via two photon processes.

Jet production in unpolarized  $2\gamma$  processes were first studied by Brodsky et al /13/. Here we estimate the QCD predictions for jet production asymmetries for primary  $e^+$  and  $e^-$  with definite helicities.

We use the basic hard scattering model for large  $p_{\perp}$  jet production. The essential ingredients for the calculation are the following.

- i) The distribution functions of polarized partons (photons, quarks, gluons) in electrons of definite helicity. We use the distributions obtained in a modified leading log approximation by Kripfganz and Schiller /14/ where both occurring scale parameters ( $\Lambda_{\text{QCD}}$  and the electron mass) are included.
- ii) The cross sections for the scattering of constituents with definite helicities. The corresponding cross sections for quark-quark, quark-gluon and gluon-gluon scattering were given in /11,12/. Additionally we use the cross sections for  $\gamma\gamma \rightarrow q\bar{q}$ ,  $e\gamma \rightarrow e\gamma$ ,  $\gamma q \rightarrow gq$  and  $\gamma g \rightarrow q\bar{q}$ . For the latter process the cross sections are

$$\frac{d\sigma^{++}}{dt}(\gamma g \rightarrow q\bar{q}) = 0 ;$$

$$\frac{d\sigma^{+-}}{dt}(\gamma g \rightarrow q\bar{q}) = e_q^2 \frac{\pi \alpha_s}{s^2} \cdot 2 \left( \frac{t}{u} + \frac{u}{t} \right) .$$

Experimentally, the jet structure of hadronic events can be disentangled. Therefore we consider separately the following jet topologies

- (i) Two jets at large  $p_{\perp}$ , no forward/backward jet, hard scattering processes:  $\gamma\gamma \rightarrow q\bar{q}$ ,  $\gamma\gamma \rightarrow gg$ .
- (ii) One jet at large  $p_{\perp}$ , one forward or backward jet, hard scattering process:  $e\gamma \rightarrow e\gamma$ .
- (iii) Two large  $p_{\perp}$  jets, one forward or backward jet, hard scattering processes:  $\gamma q \rightarrow gq$ ,  $\gamma g \rightarrow q\bar{q}$ .
- (iv) Two large  $p_{\perp}$  jets, two forward/backward jets, hard scattering processes:  $qq \rightarrow qq$ ,  $qg \rightarrow qg$ ,  $gg \rightarrow gg$ .

In Fig. 1 we plot at  $\sqrt{s} = 30$  GeV all contributions to the large  $p_{\perp}$  two jet distribution  $d^3\sigma / d\tau, dY, dx_{\perp}$  for the two jet rapidity  $Y = 0$  and for  $x_{\perp} = 0.95$  ( $x_{\perp}$  is for vanishing transverse momentum of the two jet system defined as  $x_{\perp} = 2 p_{\perp}(\text{single jet}) / \sqrt{s}$ ) as function of  $\tau = M^2/s$ .  $M$  is the two jet invariant mass. The clearly developed differences between the production cross sections for equally and oppositely polarized electrons result in sizeable spin asymmetries

$$A = \frac{\sigma^{++} - \sigma^{+-}}{\sigma^{++} + \sigma^{+-}}$$

which are given in Fig. 2. The dominating 2 jet process (i) ( $\gamma\gamma \rightarrow q\bar{q}$ ) leads to a big negative asymmetry whereas all other jet topologies give positive asymmetries  $A$ . The asymmetries  $A$  plotted as functions of the variables  $x_{\perp}$  and  $Y$  are rather featureless and flat, we do not show them here.

We stress again, most of the asymmetries shown are characteristic for QCD and not easily obtained in different models. Measuring these asymmetries in two photon processes has furthermore the advantage, that no information from experiment is needed for the calculation. The parton distributions in pointlike objects like photons or electrons are calculable. Therefore this measurement of QCD predicted spin asymmetries would have a great advantage against the corresponding measurements using collisions of polarized hadrons.

Acknow:

I

with E

Refere

/1/

/2/

/3/

/4/

/5/

/6/

/7/

/8/

/9/

/10/

/11/

/12/

/13/

/14/

events  
ly the

jet,  
—  $gg$  .  
d jet,

jet,  
—  $q\bar{q}$  .  
s,  
 $qg$  ,  $gg \rightarrow gg$ .  
butions  
,  $dx_1$   
( $x_1$  is  
stem de-  
f  $\tau = L^2/s$ .  
ped diffe-  
ually and  
pin asymmet-

cess (i)  
as all  
ne asymmet-  
y are  
re.  
are ana-  
erent mo-  
cesses  
from expe-  
tributions  
calculable.  
ymmetries  
ing measure-

### Acknowledgements

I acknowledge the collaboration and many discussions  
with H.J. Möhring, G. Ranft and A. Schiller.

### References

- /1/ B.W. Montague, CERN-Report, CERN 81-02 (1981).  
A.W. Chao, SLAC-Pub 2600 (1980).
- /2/ SLAC Linear Collider Conceptual design report,  
SLAC-Report, SLAC-229 (1980).
- /3/ V.E. Balakin, G.I. Budker, A.M. Skrinsky, Novosibirsk  
preprint I.Jad. Fys.-101 (1978).
- /4/ K.J.F. Gaemers and G.J. Gounaris, Z.Phys.C. 1,(1979), 259.
- /5/ C.Y. Prescott, presented at the 1980 Internat. Symp. on  
High Energy Physics with polarized beams and polarized  
targets, Lausanne, 25.9.-1.10.1980; see also SLAC-Pub-  
2649 (1980).
- /6/ H.A. Olsen, P. Osland and I. Overbo, Nordita preprint  
80/4 (1980).
- /7/ R.F. Schwitters et. al., Phys. Rev.Lett. 35 (1975), 1320.
- /8/ H.J. Möhring, J. Ranft and A. Schiller, Leipzig preprint  
KNU-HEP 80-13 (1980), to be published in Phys. Lett. B.
- /9/ G. Ranft, J. Ranft, to be published.
- /10/ see for instance Proc. of the Internat. Workshop on  $\gamma\gamma$   
collisions, (ed. G. Cocharde and P. Kessler), Springer  
Verlag, Berlin, (1980).
- /11/ J. Ranft and G. Ranft, Phys.Lett. 37 B, 309, (1978).
- /12/ J. Babcock, E. Monsay, D. Sivers, Phys. Rev. Lett. 40,  
1161 (1978).
- /13/ S.J. Brodsky et. al., Phys. Rev. D 19, 1418, (1978).
- /14/ J. Kripfganz and A. Schiller, Leipzig preprint  
KNU-HEP 80-14 (1980), and to be published.

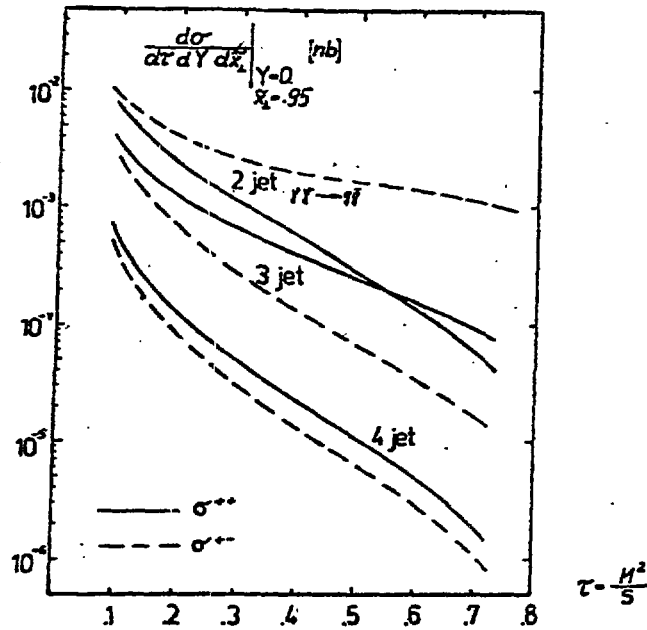


Fig. 1 Two jet cross sections for different jet topologies in collisions of  $e^+e^-$  with equal and opposite helicities as function of  $\tau = M^2/s$  at  $x_1 = 2 p_1/M = 0.95$  and two jet rapidity  $Y = 0$ .

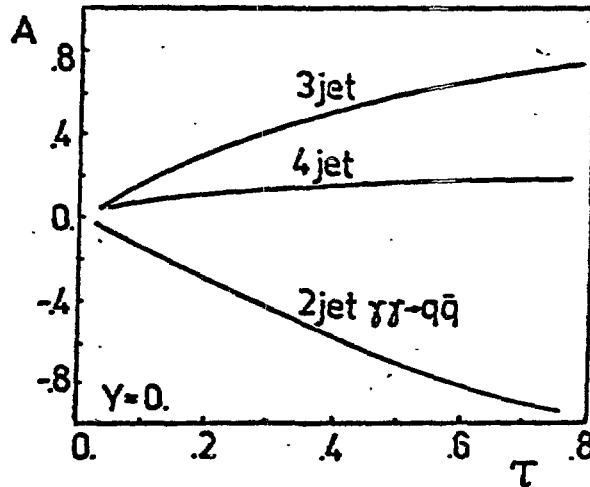


Fig. 2 Spin asymmetries  $A$  for various jet topologies in two jet production as function of  $\tau = M^2/s$ .





HADROPRODUCTION OF CHARMED PARTICLES

Francis Muller  
CERN, Geneva, Switzerland

Up to 1979, hadroproduction of charmed particles had but been hinted at by observations of single leptons [1] or lepton pairs [2] presumably originating from the decay of one or two charmed particles. Since then, evidence has accumulated from different sources, the main ones being beam-dump experiments detecting prompt neutrinos or muons, and spectrometer experiments observing mass peaks in hadronic decay channels. Total charm cross section values of the order of 30 nb at SPS energies and several hundred microbarns at the ISR are found. Standard QCD-models [3] did not foresee such a large value for the cross section at SPS energy; a fortiori, the enormous ISR cross sections are even more of a problem [4]. In this review, experimental results since 1979 will be presented and discussed, and some attempts of theoretical interpretation will be mentioned.

1. GENERAL COMMENTS ON HADROPRODUCTION EXPERIMENTS

Hadronic reactions leading to production of charmed particles are of the general type  $h_1 h_2 \rightarrow C_1 \bar{C}_2 X$ . The projectile  $h_1$  is generally a proton, in some cases a pion, and the target  $h_2$  may be a heavy nucleus A (beam-dump) or a proton (ISR).  $C_1$  is a charmed particle (charm quantum number  $c = +1$ ), i.e. a meson  $D^0$ ,  $D^+$  or a baryon  $\Lambda_c$ ,  $\bar{C}_2$  a particle with  $c = -1$  ( $\bar{D}$  or  $\bar{\Lambda}_c$ ). The observed  $C_1$  and  $C_2$ -particles may originate from excited states, such as  $D^{*+} \rightarrow D\pi$ , or higher mass charmed particles, such as  $\Sigma_c \rightarrow \Lambda_c \pi$ .

T.  
charac

(a) P  
(b)

(c)  
b  
E  
abunda  
branch  
for in  
exper  
combin  
state  
quant  
only b  
In ca  
measur  
three

requir  
either  
lepton  
visibl  
b  
sectio  
of a s  
- The  
cha  
misl  
kno  
sinc  
is a

been  
presum  
Since  
es bein  
nd spec  
Total  
nd seve  
s [3] d  
gy; a f  
]. In  
o discu  
ionned.  
ricle  
ly a pr  
A (be  
number  
i ( $\bar{D}$  or  
states,

The production of charmed particles is detected via some characteristic feature of their decays. The following have been used:

- (a) Prompt lepton ( $e$ ,  $\mu$  or  $\nu$ ) emission:  $C \rightarrow \bar{l}\nu K$  ( $\Delta c = \Delta Q$ ), and c.c.
- (b) mass peaks in Cabibbo favoured ( $\Delta c = \Delta S$ ) hadronic final states:

$$D^+ \rightarrow K^- \pi^+, \quad D^+ \rightarrow K^- \pi^+ \pi^+, \quad A_c^+ \rightarrow K^- p \pi^+ \quad (\text{and c.c.})$$

- (c) small distance  $d$  between the interaction and decay vertices, which can be observed by detectors with high resolution in space ( $< 100 \text{ } \mu\text{b}$ ).

Each of these methods suffers from high background due to the more abundant non-charm reactions, the signal itself being reduced by the small branching ratios for individual decay channels (table 1) [5]. In case (a), for instance, a large fraction of muons or neutrinos detected in beam-dump experiments originate from  $\pi$  or  $K$  decays. In case (b), there is a high combinatorial background due to the large number of particles in the final state (in addition, final states such as  $K^- \pi^+$  or  $K^- p \pi^+$  have the same quantum number as strange resonances, and can be ascertained as charmed only by the sharpness of the mass-peak, implying a good mass-resolution). In case (c), single decays (especially when the final particles are not measured) can be due to strange particle decays, and only the decays into three charged particles are relatively safe.

This situation can be improved - at the expense of yield - by requiring a positive signature from each of the produced charmed particles, either two unlike-charge leptons [2], or a mass-peak associated with leptons of the right charge (i.e.,  $D^+ \rightarrow K^- \pi^+ \pi^+$  with an  $e^-$  or  $\mu^-$ ) or two visible short-distance decays.

Besides these experimental difficulties, the extraction of cross sections from the observed leptons, peaks or decays, is subject to problems of a systematic nature:

- The leptonic branching ratios may well be different for the various charmed particles so that using the world average, 0.08 [5], may be misleading. Also some hadronic branching ratios are still very poorly known, in particular those of the  $A_c$ . Finally, with method (c), since decays can be observed only in a certain interval of length, there is a non-negligible, lifetime-dependent weight factor on each event.

- In all cases where a heavy target is used, the hadron-nucleon results have to be inferred from the hadron-nucleus measurements. Usually, it is assumed that  $\sigma(A) = A\sigma(p)$ ; an  $A^{2/3}$  law would lead to  $\sigma(p)$ 's higher by a factor of 4 for the iron or copper targets used in beam-dump experiments.
- Last but not least, most experiments are sensitive only in a certain range of kinematic variables. Going back from the data collected in that region to the total cross section is obviously, and very often highly, model-dependent. Ideally, for each production model, one should compare the predicted  $x$  and  $p_T$  distributions of the charmed particles with the observed distributions. The statistics are often too scanty to allow a distinction to be made between models on that basis (this method was used with success in the case of charm production in a muon-beam [6], thanks to the high statistics - 20000 muons from charm decay).

Experimental results will now be presented, grouped according to the method used.

## 2. PROMPT LEPTON EXPERIMENTS

### 2.1 Neutrino beam dump experiments

The CERN beam-dump experiments were performed with the layout sketched in fig. 1 (for a detailed description, see ref. [7]). An intense 400 GeV/c proton beam impinges on a variable density copper target, in which the primary protons interact and the secondary hadrons are absorbed after a few interaction lengths, while penetrating particles can escape. In the CERN experiments the neutrino-sensitive detectors are located more than 800 m away downstream with an acceptance of less than 1.8 mrad around the forward direction ( $p_T < .18$  GeV for a 100 GeV neutrino). These detectors are:

- A big bubble chamber (BEBC), filled with a heavy Ne-H<sub>2</sub> mixture.
- The CDHS iron-plate detector, of large fiducial mass ( $\sim 500$  t).
- The fine-grain marble CHARM detector.

$\nu_\mu$ 's (or  $\bar{\nu}_\mu$ 's) are observed by the characteristic charged current (CC) events, yielding a  $\mu^-$  (or  $\mu^+$ ) - similarly for  $\nu_e$ 's when electrons are directly observable. The number of  $\nu_e + \bar{\nu}_e$  events can also be obtained as the number of no  $\mu$  events, minus the contribution of neutral current events (calculated from the  $1\mu$ -events). Two methods are used for

obtaining the  $\nu$  it is different target observed number  $\pi$  or K-decay.  $F \mu^+$  events for the extrapolation), both methods for spectra obtained found in ref. [7]

- The three  $\nu_e/\nu_\mu$  ratio neutrinos of [7(c)] this
- The  $\bar{\nu}_\mu - \nu_\mu$  from CHARM but agree with the CERN unity for production.

Cross section GeV/c central products an electron branch  $18 \pm 6$  nb (CHARM  $\bar{\nu}_e/\nu_e = 1$ . CDHS from  $\nu_e + \bar{\nu}_e$  by fits of the cent fig. 4. Since  $t$  to  $E_\nu^3$ , a product rising at high  $E$  been evaluated (excess of  $\nu_\mu$  over

- The beam-d
- The set-up CIT-Stanford Col interactions in

obtaining the number of prompt neutrinos: extrapolating the yields at two different target densities to infinite density, or subtracting from the observed number at high density the calculated number due to neutrinos from  $\pi$  or K-decay. Fig. 2 illustrates the extrapolation method for the  $\mu^-$  and  $\mu^+$  events for the 3 experiments (the straight line is the CDHS extrapolation), while fig. 3 gives the (not very well agreeing) results of both methods for the CDHS  $\mu^-$  and  $\mu^+$  events; fig. 4 gives the  $(\nu_e + \bar{\nu}_e)$  spectra obtained by CHARM and CDHS. Detailed numerical results can be found in ref. [7] and [8]. Here we shall just outline the main features:

- (a) The three experiments agree on the  $(\nu_e + \bar{\nu}_e)$  yield, but give  $\nu_e/\nu_\mu$  ratios of the order of 0.6, whereas one expects unity if all neutrinos originate from charm decay [according to the BEBC group [7(c)] this anomaly cannot be due to  $\nu$ -oscillations].
- (b) The  $\bar{\nu}_\mu - \nu_\mu$  ratio from the CDHS data appears to be smaller than that from CHARM and BEBC (fig. 2), which are statistically less precise, but agree with unity, as well as the BEBC result for  $\bar{\nu}_e/\nu_e$ , and also the CFRS result for  $\mu^-/\mu^+$  (see below). This ratio is expected to be unity for  $D\bar{D}$  pair production, but may be different for  $A_c \bar{D}$  associated production.

Cross sections for  $D\bar{D}$  production have been calculated assuming a central production law  $E d^3\sigma/dp^3 \sim (1-x)^n e^{-2p_T}$ , a linear A dependence and an electron branching ratio of 8%. CHARM and BEBC obtain [9]:  $\sigma(pp \rightarrow D\bar{D}x) = 18 \pm 6 \text{ } \mu\text{b}$  (CHARM),  $17 \pm 4 \text{ } \mu\text{b}$  (BEBC), using the  $\nu_e + \bar{\nu}_e$  prompt yield, with  $\bar{\nu}_e/\nu_e = 1$ . CDHS finds [9]  $\sigma \sim 10 \text{ } \mu\text{b}$ , using the  $\bar{\nu}_e$  yield only (calculated from  $\nu_e + \bar{\nu}_e$  by assuming that  $\nu_e/\bar{\nu}_e = \nu_\mu/\bar{\nu}_\mu = 2.3$ ). The goodness of the fits of the central production model with the data can be appreciated from fig. 4. Since the acceptance to neutrinos from charm decay is proportional to  $E_\nu^3$ , a production law such as  $d\sigma/dx = c^x$  would lead to an energy spectrum rising at high E values. The possible admixture of such a process has not been evaluated (note that some  $A_c \bar{D}$  associated production could explain the excess of  $\nu_\mu$  over  $\bar{\nu}_\mu$  found by CDHS).

## 2.2 The beam-dump muon experiment at FNAL

The set-up shown in fig. 5 uses the neutrino detector of the CIT-Stanford Collaboration. In the new CFRS experiment [10] muons from interactions in an expandable iron target (which is also used as a

calorimeter) are detected in a toroidal muon spectrometer. The yield of prompt muons is obtained by the extrapolation method, illustrated in fig. 6; from that number one subtracts the number of apparently single muons, which actually come from a  $\mu^+\mu^-$  pair in which one  $\mu$  was not detected, and also the calculated number of decays between the target and the detector. The resulting  $\mu^-/\mu^+$  ratio is found to be  $1.3 \pm .3$ , in agreement with that expected from  $pp \rightarrow D\bar{D}X$  production ( $\sim .9$ ), and in disagreement with the  $\bar{\nu}_\mu/\nu_\mu$  value ( $< 1$ ) found by CDHS.

The acceptance region covers practically the whole available phase space for the muons from charm decay. The observed  $p_\mu$  distribution is very similar to the BEBC  $E_\mu$  distribution (fig. 7). A central production model, where the D and  $\bar{D}$  are independently produced according to  $Ed^3\sigma/dp^3 \sim (1-x)^\beta e^{-\alpha p_T}$  ( $1 < \alpha < 3$ ,  $2 < \beta < 6$ ) fits well the data. With a linear A dependence and a value of 8% for the  $D \rightarrow \mu$  branching ratio, a value of  $22 \pm 9 \mu\text{b}$  is obtained for  $\sigma(pp \rightarrow D\bar{D}X)$ . Diffractive production of  $\Lambda_c^0 \bar{D}$ , with flat x distributions, would badly fit the data; a preliminary value of  $\sim 25\%$  can be put as an upper limit to the contribution of this process (as reported by S. Wojcicki at this Symposium).

### 2.3 Some other results from single lepton experiments

Beam dump experiments with 28 GeV/c protons at BNL [11] did not yield positive results. A beam-dump experiment with 70 GeV/c protons at Serpukhov published [12] a  $D\bar{D}$  cross section of  $(5 \pm 4)\mu\text{b}$ , which gives  $(7.5 \pm 6)\mu\text{b}$  [13] when corrected by using the same parameters as in the other beam dump experiments. A 70 GeV/c  $\pi^-$  experiment [14] was made in BEBC equipped with a hydrogen track sensitive target inside a Ne-He mixture; from the five observed single electrons (calculated background  $0.7 \pm 0.2$ ), the calculated cross section for  $\pi^- p \rightarrow D\bar{D}X$  is  $(24 \pm 14)\mu\text{b}$ , with  $BR(D \rightarrow e) = .08$  and a central production model similar to that used in beam dump experiments (the result is very little sensitive to the parameters of the model). Older results are summarized in ref. [13].

### 3. SEARCHES FOR MASS PEAKS

The first positive results came from three spectrometer experiments at the ISR, which gave evidence for large D [15] and  $\Lambda_c$  [16-18] production

cross  
 $K^- p \pi^+$   
more  
this  
the o  
two e  
after

The yield  
strated in  
ently sing  
was not  
the target  
 $3 \pm .3$ , in  
9), and in

3.1 available ph  
distribution  
production  
(a)  $Ed^3\sigma/dp^3$   
With a

angul  
the 1  
LSM e  
Beam  
it; i  
more  
react

ing ratio,  
ive product  
a; a preli  
ution of t

( $x_1 \gtrsim$   
 $\Lambda_c^0 D(n^-)$   
thres

11] did not  
rotons at  
which give

the K  
(2262  
charme  
former  
calcu  
of  $\Lambda_c$   
range  
= 240

4] was made  
e a Ne-He  
ted backgr  
( $24 \pm 14$ )  
er to that  
ive to the  
ref. [13]

limit  
event  
limits

ter experin  
18) product

(\*) 1

cross sections, as well as proved the existence of the  $\Lambda_c$  via its  $K^- p \pi^+$  decay-mode [16,18]. Since then, these results have been confirmed by more recent experiments [19-21] with essentially the same spectrometers, this time triggered by an electron, thus ascertaining the charmed nature of the observed mass peaks. Also D production has been directly observed in two experiments at FNAL [22,23] - for the first time below ISR energies, after many unsuccessful searches [13].

### 3.1 The first series of ISR experiments (forward triggers)

These were made at  $\sqrt{s} = 52$  GeV, except the LSM experiment ( $\sqrt{s} = 63$  GeV).

#### (a) The Lamp Shade Magnet (LSM) ACHMNR experiment

The LSM (Lamp Shade Magnet) detector (fig. 8) covers the  $14-40^\circ$  angular range around Beam 1 of the ISR; a septum magnet spectrometer covers the  $1-6^\circ$  forward region and provides K and p identification. In this first LSM experiment [16] a small high field septum magnet spectrometer along Beam 2 allowed the apparatus to be triggered whenever a particle crossed it; in addition the trigger required the presence of a total of  $n \geq 6$  or more particles in the beam 1 detectors. The purpose was to select reactions of the type  $p_2 + p_1 \rightarrow p_2' + X$  where  $p_2'$  is a high-momentum proton ( $x_2 \gtrsim .5$ ) and X a high-mass protonic state, which eventually decays into  $\Lambda_c^0 D(\pi^+ \pi^-)$ 's. It was found that the condition  $n \geq 6$  corresponds to a quasi threshold  $M_X \sim 10$  GeV.

Retaining those events with a  $K^-$  and a proton identified, one obtained the  $K^- p \pi^+$  mass spectrum of fig. 9(a). The sharpness of the peak at  $(2262 \pm 10) \text{ MeV}$  [24] and its absence in  $K^- p \pi^-$  allowed to identify it with a charmed baryon, presumably the  $\Lambda_c$  in view of the agreement of the mass with former neutrino results [25]<sup>(\*)</sup>. The production cross section has been calculated in the diffractive region ( $10 < M_X < 28$  GeV) by referring the number of  $\Lambda_c$  events to the total number of events in the same region. In the range of observation ( $.5 < x(\Lambda) < .8$ ) one thus finds [26]  $\Delta\sigma/\Delta x = 240 \pm 120 \text{ } \mu\text{b}$ , using  $\text{BR}(\Lambda_c \rightarrow K^- p \pi^+) = .022$ . This is probably an upper limit, since the multiplicity condition enhances the proportion of  $\Lambda_c$  events [24]. No signal was found for  $D^\pm \rightarrow K^\mp \pi^\pm \pi^\pm$  or  $(\bar{D})^\pm \rightarrow K^\pm \pi^\mp$ ; upper limits [26], calculated as for the  $\Lambda_c$ , are given in table 2.

(\*) The presently favoured value,  $m = 2285 \pm 6 \text{ MeV}$ , was measured later [5].

(b) The UCLA-Saclay experiment

This experiment [17] used the same forward septum magnet as the preceding one (however the measurement precision was not quite as good). With an inclusive trigger requiring only the presence of charged particles in the spectrometer, marked structures are observed at  $m = 2280$  MeV in the  $\Lambda(3\pi^+)$  system and at  $m = 2290$  MeV in the  $K^-p\pi^+$  system. The sum of the  $\Lambda(3\pi^+)$  and  $K^-p\pi^+$  mass-distributions (fig. 9(b)) shows a significant peak at  $m = 2280 \pm 7$  MeV ( $\pm 8$  MeV systematic); the mass resolution ( $\sigma = 25$  MeV) is consistent with the width, making it likely to be due to the  $\Lambda_c$ , but not completely ruling out, in the eyes of the authors, the possibility of it being a  $\Sigma$  resonance. The cross section in the range  $.75 < |x| < .9$ , as calculated from the  $K^-p\pi^+$  channel ( $B = 0.022$ ), is  $\Delta\sigma/\Delta x = 700 \pm 90$   $\mu\text{b}$ .

(c) The Split Field Magnet (SFM) CCHK experiment

In the CCHK experiment the Split Field Magnet (SFM) spectrometer (fig. 10), a detector of essentially  $4\pi$  angular coverage, was triggered on a negative particle at  $\sim 8^\circ$ , with  $p_T > .5$  GeV/c, recognized as a possible  $K^-$  by a threshold Cerenkov counter. In contrast with the two preceding experiments, the other particles were not identified and all possible  $K^- \pi^+ \pi^+$  or  $K^- p \pi^+$  combinations were retained in the searches for  $D^+$  [15] or  $\Lambda_c$  [18] mass peaks. In both cases, similar criteria were used in order to diminish the combinatorial background and to favour forward production (by requiring the presence of a "leading" opposite system), and the  $K^- \pi^+$  mass was required to lie in the  $K^*$  region.  $K^- \pi^+ \pi^+$  (fig. 11(a)) and  $K^- p \pi^+$  (fig. 9(c)) mass distributions thus obtained show significant peaks around the  $D$  and  $\Lambda_c$  masses, while the corresponding non-charmed mass distributions are smooth (fig. 11(b)). The proportion of  $\bar{K}^*$  inside  $K^- \pi^+$  is found to be  $0.3 \pm 0.2$  for the  $D^+$  and  $0.4 \pm 0.2$  for the  $\Lambda_c$ ; these experimental values (higher than those found at SLAC, table 1) are used in the cross section calculations which are performed using several production models. The updated results [20] are given in tables 2 and 3. The big value of the  $D\bar{D}$  cross section in the hypothesis of central production was recognized [15] as an indication for the necessity of some other mechanism. The cross sections obtained with flat  $x$  or  $y$  production laws are smaller and agree rather well with the LSM results.

## 3.2 The second

Three ISR  
the two other o  
mass peaks asso  
are first descr

(a) The LSM ( $\Lambda$   
 $\text{CO}_2$ -Cerenk  
in conjunction  
two consecutive  
the range  $25^\circ <$   
additional char

( $K^+p\pi^-$ ) mass di  
in fig. 12(a) (  
 $m = 2260 \pm 10$  h  
with the same  
in fig. 12(b)  
(fig. 12) obta  
trigger show n  
peaks represent  
 $\Lambda_c(\bar{\Lambda}_c)$  producti

(b) The SFM (  
em), and  
11(a))

In the upg  
counters at  $90^\circ$   
readings of a  
and kept single  
were identified  
combinations w  
in the CCHK ex  
was required (  
associated wit  
around  $m = 227$   
no peaks. New  
(fig. 15), and



### 3.2 The second series of ISR experiments (central electron trigger)

Three ISR experiments (at  $\sqrt{s} = 63$  GeV), one using the LSM detector, the two other ones the improved SFM spectrometer, recently reported charmed mass peaks associated with the right sign  $e^\pm$ -trigger. These experiments are first described, a common presentation of their results follows.

#### (a) The LSM (ACHMN) experiment [19]

$\text{CO}_2$ -Cerenkov counters between the coils of the LSM (fig. 8) were used, in conjunction with lead-liquid scintillator shower counters downstream and two consecutive  $dE/dx$  counters upstream, to define an electron trigger in the range  $25^\circ < \theta < 35^\circ$  and  $p_T > .4$  GeV/c. The trigger also included two additional charged particles in the LSM detector, and a  $p$  (or  $\bar{p}$ ) identified in the forward spectrometer was required in the analysis. The  $K^- p^+$  ( $K^+ \bar{p}^-$ ) mass distributions associated with electrons (positrons) are shown in fig. 12(a) (12(b)). In fig. 12(a), a sharp  $3\sigma$  peak is seen at  $m = 2260 \pm 10$  MeV, the same mass-value as the one previously measured [24] with the same instrument. Similarly a less significant peak ( $\sim 2\sigma$ ) is seen in fig. 12(b) at a compatible mass. The  $K^- \bar{p}^+$  ( $K^+ p^-$ ) mass distributions (fig. 12) obtained either with the wrong sign electron or with a pion trigger show no signal at the  $\Lambda_c$ -mass. It is concluded that the observed peaks represent - at their respective level of significance - evidence for  $\Lambda_c(\bar{\Lambda}_c)$  production. No  $D^\pm \rightarrow K^\mp \pi^\pm \pi^\pm$  peak is observed.

#### (b) The SFM (ACCDHW) experiment [20]

In the upgraded SFM detector (fig. 13), two consecutive Cerenkov counters at  $90^\circ$  allowed an electron trigger. The analysis used the  $dE/dx$  readings of a MWPC near the thin vacuum chamber to reject electron pairs, and kept single electron candidates with  $p_T > .4$  GeV/c. Other particles were identified by time of flight counters, up to 1-2 GeV/c. All possible combinations were used, subject to selection criteria similar to those used in the CCHK experiment [15,18], in particular an opposite leading system was required (but not the presence of a  $K^*$ ). The  $K^- p^+$  mass distribution associated with  $e^-$ 's is shown in fig. 14. A clear ( $\sim 4\sigma$ ) peak is seen around  $m = 2270$  MeV whereas the spectrum obtained with  $e^+$ 's (insert) shows no peaks. New preliminary results are the observation of a  $D^0 \rightarrow K^- \pi^+$  bump (fig. 15), and of a possible [27(b)]  $\bar{\Lambda}_c \rightarrow K^+ \bar{p}$  signal with  $e^+$ 's (not shown).

(c) The SFM (BCF) experiment [21]

The set-up and trigger were the same as in the ACCDHW experiment (fig. 13), but the purity of the electron trigger was enhanced by the requirement of an energy deposit greater than 0.5 GeV in electromagnetic shower counters. For the  $\Lambda_c^- + K^- p \pi^+$  search the highest  $x$  ( $x > .3$ ) positive particle was assumed to be a proton, and the two other particles had to have  $y > 1$ . Like in the ACCDHW analysis, an opposite leading system was required. The  $K^- p \pi^+$  mass distribution associated with  $e^-$ 's (fig. 16(a)) shows a clear peak at  $m = 2.33$  GeV, 45 MeV above the SLAC  $\Lambda_c^-$  mass, the shift being attributed to local systematic effects, no peak is seen in association with  $e^+$ 's (fig. 16(b)). Similarly to ACCDHW [18], the BCF group observes the presence of  $K^{*0}$  and  $\Delta^{++}$  in the  $K^- p \pi^+$  system, in compatible proportions:  $(0.28 \pm 0.16$  and  $0.40 \pm 0.17)$ , again higher than those reported by SLAC (Table 1).

The same data show preliminary evidence [27(a)] for production of  $D^+ + K^- \pi^+ \pi^+$  and  $D^0 + K^- \pi^+ \pi^+$  in conjunction with the  $e^-$  triggers. For the  $D^+$  search, the  $K^-$  is required to be positively identified (hence  $p_K < 1.5$  GeV/c), the  $\pi^+$ 's are any non-p or K particles with  $|x| < 0.3$ , and the  $K\pi\pi$  system has to have  $p_T \geq 0.7$  GeV/c. The ensuing distribution has a  $39 \pm 11$  events signal at the D mass with  $e^-$ 's (fig. 17(a)), no signal with  $e^+$ 's. For the  $D^0$  search, the same  $p_T$  cut was used, and the presence of an associated identified  $K^+$  was the only other positive requirement; a  $D^0$  signal was then seen (fig. 17(b)) in the  $K^- \pi^+$  mass-spectrum obtained with an  $e^-$  trigger.

(d) Cross sections and production characteristics

In the experiments described above, the reactions are assumed to be (\*)

$$pp \rightarrow DDX, D + K^- \pi^+ \pi^+ \text{ (BR} = 0.026) \text{ or } K^- \pi^+ \pi^+ \text{ (BR} = 0.045), \bar{D} + e^- \quad (1)$$

$$pp \rightarrow \Lambda_c^- DDX, \Lambda_c^- + K^- p \pi^+ \text{ (BR} = 0.022), \bar{D} + e^- \dots \text{ (BR} = 0.08) \quad (2)$$

(\*) All  $\Lambda_c^-$ 's observed are supposed to come from  $\Lambda_c^- \bar{D}$ . There is some indication [19, 27(b)] for  $\Lambda_c^-$  production, hence a fraction of the  $\Lambda_c^-$ 's should come from  $\Lambda_c^- \Lambda_c^-$ . Assuming  $B(\Lambda_c^- + e^+ \dots) = 0.1$ , the cross section for  $\Lambda_c^-$  has been evaluated in ref. [19] to be about 1/2 of that of  $\Lambda^0$ , a ratio similar to that of  $\Lambda^0$  with respect to  $\Lambda^+$  [28].

The  
which ea

eriment  
by the  
romagnetic  
.3)  
r particles  
eading  
ith  $e^-$ 's  
the SLAC  $\Lambda_c^-$   
no peak is  
HW [18],  
system, in  
higher than

In a  
flat  $x$  ( $\Lambda$   
function  
tables 2  
experime  
electron,  
with  $x$ ;

models f  
The valid  
observed  
attempt  
rather f  
(fig. 10  
20); in

From  
experime.  
previous  
is illus

for the  
obtained  
of about  
ratios (  
( $\Lambda_c^- \bar{D}, D^+$   
of that

This cer  
qualitat  
wide  $x$  d

uction of  
For the  
nce  
< 0.3,  
istribution  
(...), no signal  
he presence  
quirement; a  $D^0$   
btained with

sumed to be (\*)  
(...),  $\bar{D} + e^-$  (1)  
= 0.08) (2)

some  
on of the  $\Lambda_c^-$ 's  
re cross  
ut 1/2 of that  
[28].

(\*) Cor  
hav

The three groups have tried essentially the same production models, in which each of the two charmed particles independently follows either<sup>(\*)</sup>:

$$\frac{d\sigma}{dx dp_T^2} \sim f(x) \quad (\text{flat } x \text{ law}) \quad (a)$$

$$Ed^3\sigma/dp^3 \sim f(x) \quad (\text{flat } y \text{ law}) \quad (b)$$

$$Ed^3\sigma/dp^3 \sim (1 - |x|)^2 f(x) \quad (\text{central production}) \quad (c)$$

In addition, for reaction (2), a mixed model (a'), with central  $\bar{D}$  and flat  $x$  ( $\Lambda_c$ ) has been used. The results are not very sensitive to the function  $f(x)$ , taken as  $e^{-2p_T}$  (SFM) or  $e^{-4p_T^2}$  (LSM), but, as seen in tables 2 and 3, depend very strongly on the  $x$  dependence. For all three experiments, central production gives the best acceptance for the trigger electron, while in general the acceptance for hadronic decays increases with  $x$ ; the smallest cross sections are obtained with the flat  $y$  or central models for  $D\bar{D}$  production and with the mixed model (a') for  $\Lambda_c \bar{D}$  production. The validity of these models could in principle be checked by comparing the observed  $x$  and  $p_T$  distributions with the ones predicted by the model, as attempted [19] by the LSM group (fig. 18). The BCF group find [27(a)] a rather flat  $x$  distribution for the  $\Lambda_c$ , very similar to that of the  $\Lambda^0$  (fig. 19), and favour either a  $(1 - x)^2$  or a flat  $y$  law for the  $D$  (fig. 20); in both cases they observe  $e^{-bp_T}$  distributions, with  $b = 2.5 \text{ GeV}^{-1}$ .

From tables 2 and 3, it is seen that the results of the three experiments are in rather good agreement (they are also comparable to the previous results of the LSM and SFM groups, using different triggers); this is illustrated in figs 21 and 22, which use models (b) for the  $D$  and (a') for the  $\Lambda_c$ . With these models, total cross sections of  $200 \div 400 \text{ nb}$  are obtained for each of the  $\Lambda_c$ ,  $D^+$  and  $D^0$ , hence a total charm cross section of about  $1 \text{ mb}$ . One should note that these cross sections lead to  $\langle e/\pi \rangle$  ratios (for  $p_T > 0.4 \text{ GeV}/c$ ) of the order of  $3 \cdot 10^{-4}$  for each process ( $\Lambda_c \bar{D}$ ,  $D^+ \bar{D}$ ,  $D^0 \bar{D}$ , with  $\bar{D} \rightarrow e^-$ ) whereas the only directly measured value [1] of that ratio in the same conditions (at  $\sqrt{s} = 52 \text{ GeV}$ ) is about  $2.5 \cdot 10^{-4}$ . This certainly sheds some doubt about the quantitative results but the qualitative features - large cross sections and, at least for the  $\Lambda_c$ , wide  $x$  distribution - seem well-established.

(\*) Correlated models, in which for instance a  $\Lambda_c \bar{D}$  system is produced, have been also tried, with comparable results (see for example [19]).

### 3.3 Fixed target spectrometer experiments

Two experiments recently observed D production at FNAL.

In the first one [22] the reaction used was  $\pi^-$  (217 GeV/c) + p + p + D +  $\bar{D}$  + ...; D +  $\mu^+$ ,  $\bar{D}$  + hadrons (and C.C.). The set-up is shown in fig. 23; recoil protons from an H<sup>2</sup> target were detected at angles  $\theta = 60-75^\circ$  by wire chambers and TOF counters, the forward particles were analyzed by the Chicago Cyclotron Magnet spectrometer, kaons were identified by Čerenkov counters and muons by a 2.2 m steel absorber. Fig. 24 shows the observed  $D^\pm \rightarrow K^\mp \pi^\pm \pi^\pm$  signals and their x distribution, compared to that expected from a flat-x production law. A diffractive model of production, strongly suggested by these data, of an  $X^- - D^+ \pi^-$  system, yields  $\sigma(pp \rightarrow pX^-) = (7 - 10) \pm 4 \mu\text{b}$ , using  $\text{BR}(D^\pm \rightarrow \mu^\pm \dots) = 0.23$  (table 1). The non-observation of  $D^0$  production can be explained by the smaller  $D^0 \rightarrow \mu$  branching ratio (Table 1).

The other FNAL experiment [23], shown in fig. 25, aimed at detecting  $D^*$  production by 200 GeV/c  $\pi^-$ 's using the property that, in the  $D^{*+} \rightarrow D^0 \pi^+$  decay, the  $\pi^+$  is practically at rest in the  $D^*$  c.m. In the lab,  $\pi^+$ 's emitted at  $90^\circ$  c.m. are slow forward pions, detected by a spectrometer near the Be target; fast kaons and pions from the  $D^0$  decay are identified and measured by a double arm-spectrometer.  $D^*$  events are recognized as a bump around 6 MeV (fig. 26(a)) in the Q value spectrum of the decay  $K\pi\pi \rightarrow D^0\pi$ ; conversely the  $K\pi$  mass spectrum for events with the nominal Q value exhibits a D signal (fig. 26(b)). The observed  $D^{*+}$  and  $\bar{D}^{*+}$  yields are compatible, yielding a model-independent  $D^*$  cross section  $d\sigma/dy = 1.6 \pm 0.5$  ( $\pm 0.7$  system.)  $\mu\text{b}$  at  $y = 0$  ( $\text{BR}(D^* \rightarrow \pi D) = 0.64 \pm 0.11$  is used). A central production model leads to  $\sigma(D^*) = 4.2 \pm 1.4 \mu\text{b}$ .

### 4. VISUAL EXPERIMENTS

Detectors of short decays operated at SPS energies in hadron beams have measured the total charm cross sections at those energies. In general, the decaying particles are not identified; the decay is assumed to be charmed on the basis of the decay length.

From the observation of two events, each one displaying charm-pair production, an experiment at FNAL using an emulsion chamber [29] (emulsion layers sandwiched between tungsten plates to convert  $\gamma$ -rays and electrons) found, with 400 GeV/c protons, a cross section  $\sigma(pp \rightarrow c\bar{c} \dots) =$

$40 \pm 30 \mu\text{b}$ ,  $E(d^2\sigma)/dp^2 \sim$   
 $(\alpha = 3-6, \beta =$   
 resolution ( $\sim$   
 $\pi^-$  beam; 12 e  
 calculated at  
 the efficiency  
 $E(d^2\sigma)/dp^2 \sim$   
 lifetime. T  
 production ra  
 to account fo  
 three-prong d  
 $\sigma(D) \sim 35 \mu\text{b}$   
 compared with  
 a 350 GeV/c p  
 $\sigma = 160 \pm 40$   
 experiment.  
 experiments  
 experiments,

### 5. CONCLUSIONS

Fig. 27 d  
 (for the ISR e  
 $\sigma(D^0)$  as deriv

For compa  
 plain curve co  
 creation by gi  
 found [6] to  
 quark mass has  
 section at SPS  
 ISR energies,  
 $\sigma(\text{charm})$  deduc  
 and badly kno  
 cross section  
 be increased t  
 proportional t  
 the results fr

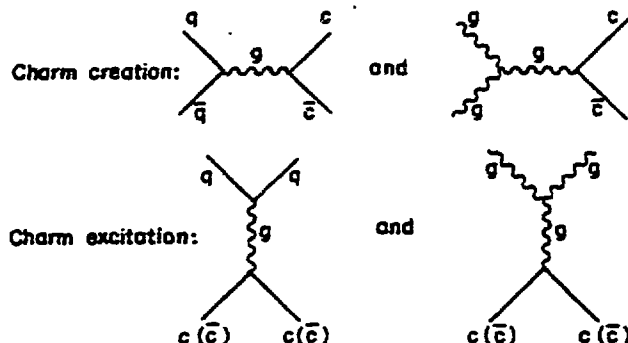
$40 \pm 30 \text{ } \mu\text{b}$ , for lifetimes of a few units of  $10^{-13} \text{ s}$ ;  $\sigma(\text{pA}) = A\sigma(\text{pp})$  and  $E(d^3\sigma)/dp^3 \sim (1-x)^\alpha \exp(-\beta p_T)$  laws were used to obtain this result ( $\alpha = 3-6$ ,  $\beta = 2-4$ ). At CERN, a small (20 cm diameter) fast-cycling, high-resolution ( $\sim 40 \text{ } \mu$ ) hydrogen chamber [30] (LEBC) was exposed to a 340 GeV/c  $\pi^-$  beam; 12 events showing two associated decays were observed above the calculated strange-particle background. Since momenta are not measured, the efficiency for observing a decay, calculated with the standard  $E(d^3\sigma)/dp^3 \sim (1-x)^\beta \exp(-2p_T)$  law, is an almost linear function of lifetime. The cross section reported by the authors is  $\sigma \sim 40 \text{ } \mu\text{b}$  for equal production rates of particles with lifetimes  $\tau = 10^{-13} \text{ s}$  and  $\tau = 10^{-12} \text{ s}$ , to account for  $D^0$  and  $D^+$  production (table 1). Also, from eight observed three-prong decays consistent with  $D^+ \rightarrow K^+ \pi^+ \pi^-$ , a cross section  $\sigma(D) \sim 35 \text{ } \mu\text{b}$  is inferred for a lifetime  $\tau = 10^{-12} \text{ s}$ . These results can be compared with results from a high-pressure streamer chamber [31] which, in a 350 GeV/c p beam at FNAL, reported  $\sigma = 20-50 \text{ } \mu\text{b}$ . A preliminary result of  $\sigma = 160 \pm 40 \text{ } \mu\text{b}$  with 400 GeV/c protons was reported [32] by an emulsion experiment. In summary and with the exception of this last result, these experiments find total cross sections in rough agreement with beam dump experiments, performed at similar energies.

## 5. CONCLUSIONS

Fig. 27 displays the measured total charm cross sections versus energy (for the ISR experiments, the total  $\sigma$  is obtained by adding  $\sigma(\Lambda_c)$ ,  $\sigma(D^+)$ ,  $\sigma(D^0)$  as derived from the models giving the smallest cross sections).

For comparison, some theoretical predictions are plotted. The higher plain curve corresponds to the Carlson-Suaya model [33] of charm-anticharm creation by gluon-gluon fusion. This model, with  $m_c = 1.5 \text{ GeV}$ , has been found [6] to agree with charm muoproduction. In ref. [33], the charmed-quark mass has been chosen to be 1.15 GeV in order to give a  $30 \text{ } \mu\text{b}$  cross section at SPS energy. An  $\sim 100 \text{ } \mu\text{b}$  cross section is then predicted at ISR energies, to be compared with an experimental value of  $\sim 1 \text{ mb}$  for  $\sigma(\text{charm})$  deduced from the ISR results. Even with systematic uncertainties and badly known branching ratios, it seems difficult to lower the total ISR cross section to that  $100 \text{ } \mu\text{b}$  value. The beam dump cross sections could be increased to about  $100 \text{ } \mu\text{b}$  if the cross section  $\sigma(A)$  were proportional to  $A^{2/3}$  rather than  $A$ , but this would be in conflict with the results from detectors of short decays.

Using the Buras-Gaemers [34] quark and gluon distribution functions, Combridge [35] has calculated the various lowest-order QCD diagrams for charm production, such as



He found that at SPS and ISR energies, charm excitation (not considered in ref. [33]) dominates over charm creation; the calculated total charm cross sections are plotted in fig. 27 (lower plain curve). They are below those calculated by Carlson but exhibit a much faster rise with energy. Actually the absolute values of the cross section depend critically on the quark mass. The Combridge curve was calculated with the a priori choice  $m_c = 1.87$  GeV, whereas  $m_c = 1.3$  GeV would lead to values of  $\sigma(\text{charm})$  of about 30  $\mu\text{b}$  at SPS energies and about 1000  $\mu\text{b}$  at the ISR (dotted curve). The agreement with experiment may be fortuitous, but could indicate that the data are not necessarily in conflict with QCD.

The high cross sections and the extended  $x$  distributions observed at the ISR (and also now at FNAL [22]) could be explained by other formerly suggested mechanisms, such as diffractive production [36] or gluoproduction [37]. Recently the presence in the proton of an  $\sim 1\%$  intrinsic charm component has been proposed [38]. Due to its mass, the charmed quark would carry a good fraction of the momentum (fig. 28), resulting in wide  $x$ -distributions for the produced  $\Lambda$ 's and  $D$ 's (fig. 29). With this model, the rather copious production of same sign muon pairs by neutrinos [39] might be explained by the reaction  $\nu + \bar{c} \rightarrow b + \mu^-$ ,  $b + \mu^- \rightarrow \dots$

To charm diagrams  
interpre latest r

The M.G. Alb and R. S

ot consid  
otal char  
are below  
energy. A  
on the qu  
choice  
 $\sigma(\text{charm})$   
3 (dotted  
out could  
h QCD.

Othe.  
With  
 $\overline{D}^+$   
- The  
an e  
and  
d $\sigma$ /  
in a  
sect:

To conclude, more precise data on production (and decay properties) of charmed particles are needed, to help toward a well-founded theoretical interpretation of the salient features of charm production indicated by the latest results, i.e. sizeable cross sections over a wide  $x$  range.

The author wishes to thank S. Wojcicki for useful discussions, M.G. Albrow, L. Cifarelli and W. Geist for communication of recent results, and R. Sosnowski and A. Wróblewski for their friendly hospitality.

Note added in proof

New results were reported at the Lisbon Conference (July 9-15), some of which are summarized here:

- The BCF (p.149) group obtains (A. Contin)<sup>(\*)</sup>, under the assumption of a central production law for D and  $\bar{D}$ ,  $Ed^3\sigma/dp^3 \sim (1 - |x|)^3 e^{-2p_T}$ :

$$\left. \begin{aligned} \sigma(pp \rightarrow \bar{D}D^0 X) &= 575 \text{ } \mu\text{b} (\pm 50\%) \\ \sigma(pp \rightarrow \bar{D}D^+ X) &= 305 \text{ } \mu\text{b} \end{aligned} \right\} (\sqrt{s} = 62 \text{ GeV}, e^- \text{ trigger})$$

Other models (p.150) lead to cross sections more than twice bigger.

With an  $e^+$  trigger, they have also some evidence (A. Zichichi)<sup>(\*)</sup> for  $\bar{D}^+ \rightarrow K^+ \pi^- \pi^-$  and  $A_c^+ \rightarrow p K^+ \pi^-$ .

- The ACCMOR Collaboration, using a large aperture forward spectrometer and an electron trigger, finds (R. Klanner)<sup>(\*)</sup> in  $\pi^-$ -Be interactions at 175 and 200 GeV/c, production of  $D^0 \rightarrow K^+ \pi^-$ , mostly via  $B^{*+} \rightarrow D^0 \pi^+$ . With  $d^3\sigma/dp^3$  assumed to be  $\sim e^{-2.5p_T^2} (1 - |x|)^3$  for each D or  $\bar{D}$  ( $x$  distribution in agreement with experimental data), they obtain for the  $\pi^- p$  cross sections (linear A dependence assumed):

$$\begin{aligned} \sigma(D^{*+} X) + \sigma(D^{*-} X) &= 9.5 \pm 4 \text{ } \mu\text{b} \\ \sigma(D\bar{D}X) &= 14 \pm 5 \text{ } \mu\text{b} \end{aligned}$$

(\*) Names between brackets are those of authors of presentations to the EPS International Conference on High Energy Physics, Lisbon, July 1981.

With the same apparatus and trigger in a 150 GeV/c proton beam, they observe a 4.5  $\sigma$  peak in  $A_c \rightarrow pK^- \pi^+$  at  $m = 2260 \pm 8$  MeV, part of which originates from  $\Sigma^{++} \rightarrow A_c \pi^+$ , with  $m(\Sigma^{++}) = 2440$  MeV. Using production laws in  $(1-x)^n e^{-2.25 P_T^2}$  for the  $A_c$  ( $n = 1$ ) and the associated  $\bar{D}$  ( $n = 4.5$ ), they obtain:

$$\sigma(pp \rightarrow A_c \bar{D} X) = 75 \pm 50 \text{ nb.}$$

- The LEBC Collaboration, using LEBC (see p.152) associated with a forward spectrometer, in a 360 GeV/c  $\pi^-$  beam, obtains (S. Reucroft)<sup>(\*)</sup> from 6 fully reconstructed  $D^{\pm} \rightarrow K^{\mp} \pi^{\pm} \pi^{\pm}$  ( $n\pi^0$ ) decays, using  $\tau(D^{\pm}) = 10^{-12}$  s<sup>(\*\*)</sup>

$$\sigma(\pi^- p \rightarrow D^{\pm} X) = 8 \pm 4 \text{ nb} \quad (x > 0).$$

The D production distribution is compatible with  $d\sigma/dx \sim (1-x)^n$ , with  $n = 3.5 \pm 1$ , and gives  $\langle p_T \rangle = 750$  MeV/c. In charm pair production, a correlation in rapidity is observed between the two mesons:  $\langle \Delta y \rangle = 0.4$ . Two associated  $\bar{D}$  events, but no  $A_c$ , were observed.

These new results are in general agreement - at their respective c.m. energy - with those reviewed in this report. At the Lisbon Conference, there was a general tendency to accept the high ISR cross section values (with some restrictions concerning the  $e/\pi$  ratio - see p.150) and some new theoretical interpretations were presented (A. Donnachie, B. Margolis)<sup>(\*)</sup>.

(\*) Names between brackets are those of authors of presentations to the EPS International Conference on High Energy Physics, Lisbon, July 1981.

(\*\*) The LEBC group measures in units of  $10^{-12}$  s  $\tau(D^{\pm}) = 9.3 \pm 1.5$  and  $\tau(D^0) = 3.0 \pm 1.5$ . Similar results were obtained by the emulsion experiment E531 (G. Prentice)<sup>(\*)</sup> at FNAL and a photoproduction experiment at SLAC (S. Reucroft)<sup>(\*)</sup>. Both LEBC and E531 observe a tail of long-lived  $D^0$  events, suggesting the possibility of two life-times.

## REFERENCES

- [1] M. Barone
- [2] N. Chiri
- [3] See for i. F. Halzen
- [4] R.J.N. Phillips Energy (hereaf
- [5] For more c J. Wiss, preprint
- [6] A. Clark, R. Mount, referen
- [7] (a) K. Ki dump ex (b) F. N 400 GeV (c) P.O. in
- [8] S. Wojcik HEP 80
- [9] F. Dydak, April 19
- [10] J. Ritchie See also K HEP-80,
- [11] J. Lo Secc
- [12] A.E. Asrat
- [13] W. Geist,
- [14] R. Barlou
- [15] D. Drijard
- [16] K.L. Gibon to the July 1981.
- [17] W. Lockman

, they  
ich  
tion laws  
5), they  
forward  
rom 6  
s<sup>(\*\*)</sup>  
with  
on, a  
= 0.4.  
ive c.m.  
ence,  
values  
some  
to the  
July 1981.  
and  
sion  
n  
ive a  
so



REFERENCES

- [1] M. Barone et al., Nucl. Phys. B132 (1978) 29 and refs therein.
- [2] N. Chilingarov et al., Phys. Lett. 83B (1979) 136.
- [3] See for instance A.M. Georgi et al., HUTP 78/A008 (1978);  
F. Halzen and S. Matsuda, Phys. Rev. D17 (1978) 1344.
- [4] R.J.N. Phillips in "Phenomenology of New Particle Production", High  
Energy Physics 80 (L. Durant and L.G. Pondrom ed.), p. 1470  
(hereafter referred to as HEP-80).
- [5] For more complete tables, see the review papers of G. Goldhaber and  
J. Wiss, LBL-10632 preprint (1980) and G.H. Trilling, LBL-12283  
preprint (1981).
- [6] A. Clark, Open and hidden charm muoproduction, in HEP-80, p. 412;  
R. Mount, Multimuo production in 280 GeV  $\mu^\pm$  interactions, same  
reference, p. 205.
- [7] (a) K. Kleinknecht, Measurement of Prompt Neutrino fluxes in a beam  
dump experiment, in HEP-80, p. 237;  
(b) F. Niebergall, Experimental Study of prompt neutrino production in  
400 GeV proton-nucleus collisions, same ref. p. 242.  
(c) P.O. Hulth, Study of Prompt neutrino production in proton-Cu  
interactions, same ref. p. 247.
- [8] S. Wojcicki, New Flavour production in  $\gamma$ ,  $\mu$ ,  $\nu$  and hadrons beams,  
HEP 80 p. 1430.
- [9] F. Dydak, report at the ISR discussion meeting, series 2, number 4,  
April 1981 (M.G. Albrow, M. Jacob, ed.) p. 62.
- [10] J. Ritchie et al., Phys. Rev. Lett. 44 (1980) 230;  
See also K.W.B. Merritt, Hadronic production of prompt single muons,  
HEP-80, p. 257, and ref. [8] for older results with the same set-up.
- [11] J. Lo Secco, 28 GeV/c beam dump experiments, HEP 80, p. 252.
- [12] A.E. Asratyan et al., Phys. Lett. 79B (1978) 497.
- [13] W. Geist, CERN/EP 79-78 (1979).
- [14] R. Barloutaud et al., Nucl. Phys. B172 (1980) 25.
- [15] D. Drijard et al., Phys. Lett. 81B (1979) 250.
- [16] K.L. Giboni et al., Phys. Lett. 85B (1979) 437.
- [17] W. Lockman et al., Phys. Lett. 85B (1979) 443.

## REFERENCES (Cont'd)

- [18] D. Drijard et al., Phys. Lett. 85B (1979) 452.
- [19] J. Irion et al., Phys. Lett. 99B (1981) 495.
- [20] G. Sajot, Production of charm in the SFM at the ISR, in HEP-80, p. 192, and private communication by W. Geist.
- [21] M. Basile et al., CERN/EP 80-214 to be published in Nuovo Cimento.
- [22] L.J. Koester, Diffractive hadronic production of D mesons, HEP-80, p. 190.
- [23] V.L. Fitch et al., Measurement of  $D^*$  production in  $\pi^-N$  interactions at 200 GeV/c, preprint C00-3072-124.
- [24] K.L. Giboni, Thesis, Aachen University (1979).
- [25] E.G. Cazzoli et al., Phys. Rev. Lett. 34 (1975) 1125;  
C. Baltay et al., Phys. Rev. Lett. 42 (1979) 1721.
- [26] J. Eickmeyer et al., Cross sections for diffractive charm production, contributed paper given at the Int. Conf. on High Energy Phys., Madison (1980), and HEP-80, p. 193.
- [27] (a) P. Giusti, Report at the ISR discussion meeting (M.G. Albrow and M. Jacob, ed.), Series 2, number 4, (April 1981) p. 17;  
(b) A. Putzer, same ref. p. 5.
- [28] S. Efran et al., Phys. Lett. 85B (1979) 447.
- [29] H. Fuchi et al., Phys. Lett. 85B (1979) 135.
- [30] W. Allison et al., Phys. Lett. 93B (1980) 509.
- [31] J. Sandweiss et al., Fermilab/Pub 80/16 (1980).
- [32] P.K. Malhotra, Charm production by protons in emulsions, EHP-80, p. 361.
- [33] C.E. Carlson and R. Suaya, Phys. Lett. 81B (1979) 329.
- [34] A.J. Buras and K.J.F. Gaemers, Nucl. Phys. B132 (1978) 248.
- [35] B.L. Combridge, Nucl. Phys. B151 (1979) 426.
- [36] G. Gustafson and C. Peterson, Phys. Lett. 67B (1977) 81.
- [37] H. Fritzsch and K.H. Streng, Phys. Lett. 78B (1978) 447.
- [38] S.J. Brodsky et al., Phys. Lett. 93B (1980) 451, and SLAC 2660 (1981).
- [39] A. Benvenuti et al., Phys. Rev. Lett. 41 (1979) 725;  
M. Shaevitz, Recent results from the CFRR Neutrino Experiment at Fermilab, HEP-80, p. 741.

EP-80, p. 1

Cimento.

, HEP-80, p

teractions

Ma

production  
Phys.,

.. Albrow a

D<sup>0</sup>D<sup>+</sup>A<sub>c</sub>

EHP-80, p-

S.

2660 (1981)

ment at

D, p. 192,

ento.

p-80, p. 190.

ctions

TABLE 1

Relevant properties of charmed particles (from ref. [5])  
 Masses, branching ratios and fractions are averages from results of two experiments  
 at SPEAR. The numbers for  $\tau$  and  $B$  ( $d + e^+ \dots$ ) of the D-mesons are from four  
 different experiments (2 at SPEAR for  $B_e$ , 2 in emulsions for  $\tau$ );  
 they should verify the relation  $\tau^+/\tau^- = B_e^+/B_e^-$

|       | M(MeV)           | $\tau(10^{-12} \text{ s})$                     | $B_e (\%)$                   | Main<br>hadronic<br>channels           | Branching<br>ratio<br>(%)    | Resonance<br>content                                   |
|-------|------------------|--|------------------------------|--|------------------------------|--|
| $D^0$ | $1863.7 \pm 0.4$ | $1.0^{+0.3}_{-0.27}$<br>$0.53^{+0.27}_{-0.25}$ | $< 5$<br>$5.5 \pm 3.7$       | $K^- \pi^+$<br>$\bar{K}^0 \pi^+ \pi^-$ | $2.6 \pm .4$<br>$3.9 \pm .9$ | $70\% K^*$   |
| $D^+$ | $1868.4 \pm 0.4$ | $10.3^{+10.5}_{-4.0}$<br>$2.5^{+2.2}_{-1.1}$   | $24 \pm 4$<br>$16.8 \pm 6.4$ | $\bar{K}^0 \pi^+$<br>$K^- \pi^+ \pi^+$ | $1.8 \pm .5$<br>$4.7 \pm .8$ | $\bar{K}^{*0} < 39\%$                                  |
| $A_c$ | $2285 \pm 6$     | $1.36^{+0.4}_{-0.6}$                           |                              | $K^- p \pi^+$                          | $2.2 \pm 1.0$                | $K^{*-0}: (12 \pm 7)\%$<br>$\Delta^{++}: (17 \pm 7)\%$ |

D, p. 361.

(1981).

at

TABLE 2

ISR cross sections for  $pp \rightarrow D\bar{D}X$  ( $D^+ \rightarrow K^- \pi^+ \pi^+$  or  $D^0 \rightarrow K^- \pi^+$ )

Numbers (in  $\mu\text{b}$ ) are calculated with the branching ratios of table 1 and  $\text{BR}(D \rightarrow e) = 0.08$ . The numbers for refs [19] and [26] are 95% upper-limits and, for ref. [26],  $d\sigma/dx$  values. The numbers for ref. [27(a)] are preliminary estimates.

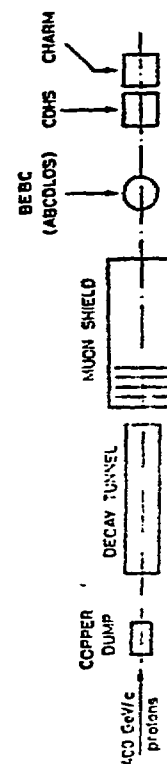
|              | Ref.  | Trigger        | Part.      | Assumed D and $\bar{D}$ production law |                    |                    | x-range         |
|--------------|-------|----------------|------------|--|--------------------|--------------------|-----------------|
|              |       |                |            | Central                                | $d\sigma/dy = c^T$ | $d\sigma/dx = e^T$ |                 |
| SFM (CCHK)   | [15]  | Forward $K^-$  | $D^+$      | 1100 ( $\pm 60\%$ )                    | 390                | 210                | $.2 <  x  < .8$ |
| LSM          | [26]  | Diffractive    | $D^+$      | (< 300)                                |                    |                    | $.2 < x < .45$  |
|              |       |                | $D^0$      | (< 160)                                |                    |                    | $.2 < x < .65$  |
| SFM (ACCDHW) | [20]  | $90^\circ e^-$ | $D^0$      | 245 ( $\pm 60\%$ )                     | 395                | 890                | $0 <  x  < 0.3$ |
| LSM          | [19]  | $30^\circ e^-$ | $D^+$      | < 530 ( $\pm 30\%$ )                   | < 340              | < 280              | $.14 < x < .9$  |
| SFM (BCF)    | [27a] | $90^\circ e^-$ | $D^+, D^0$ | $\sim 500$                             | $\sim 1000$        |                    | $0 <  x  < .4$  |

TABLE 3

ISR cross sections for  $pp \rightarrow A_c \bar{D}X$  ( $A_c \rightarrow K^- p \pi^+$ )

Numbers (in  $\mu\text{b}$ ) are calculated as in table 2. The numbers for ref. [16] and [17] are  $d\sigma/dx$  values.

|                 | Ref. | Trigger        | Assumed $A_c$ production law     |               |        | x-range         |
|-----------------|------|----------------|----------------------------------|---------------|--------|-----------------|
|                 |      |                | $da/dx = \text{const.}$          | $da/dy = c^T$ |        |                 |
| SFM<br>(CCHK)   | [18] | Forward $K^-$  | 300 ( $\pm 40\%$ )               |               | 610    | $.4 <  x  < .8$ |
| LSM             | [16] | Diffractive    | (240 $\pm$ 120)                  |               |        | $.5 < x < .8$   |
| UCLA-SAC        | [17] | Inclusive      | (700 $\pm$ 90)                   |               |        | $.75 < x < .9$  |
| SFM<br>(ACCDHW) | [20] | $90^\circ e^-$ | 290 ( $\pm 60\%$ )               | 1460          | 430    | $0 <  x  < .3$  |
| LSM             | [19] | $30^\circ e^-$ | 840 ( $\pm 50\%$ )               | 1220          | 1650   | $.14 < x < .94$ |
| SFM (BCF)       | [21] | $90^\circ e^-$ | 184 ( $\pm 40\%$ )               | 1125          | 750    | $.3 <  x  < 1$  |
|                 |      |                | Central                          | Flat x        | Flat y |                 |
|                 |      |                | Assumed $\bar{D}$ production law |               |        |                 |



s.

ge

&lt; .8

&lt; .45

&lt; .65

&lt; 0.3

&lt; .9

&lt; .4

.8

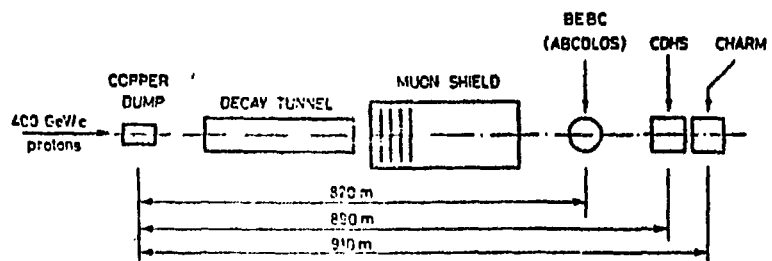
.

.9

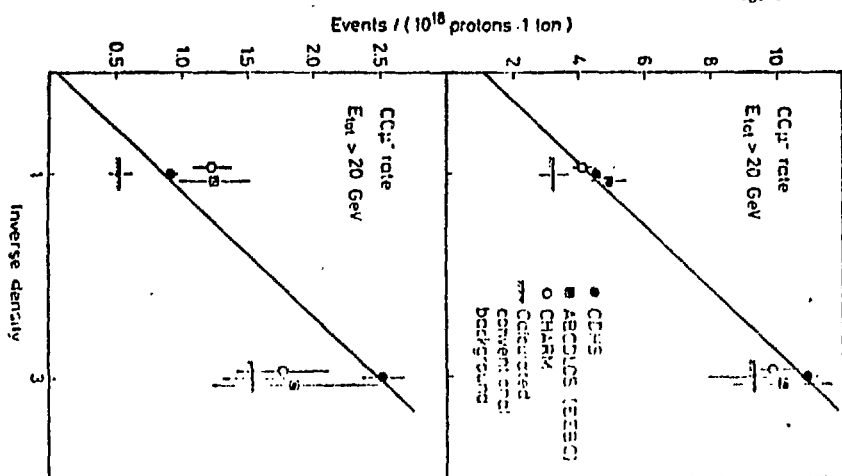
.3

.94

1



Schematic layout of the 1979 CERN beam dump experiments



The extrapolation method for prompt neutrinos

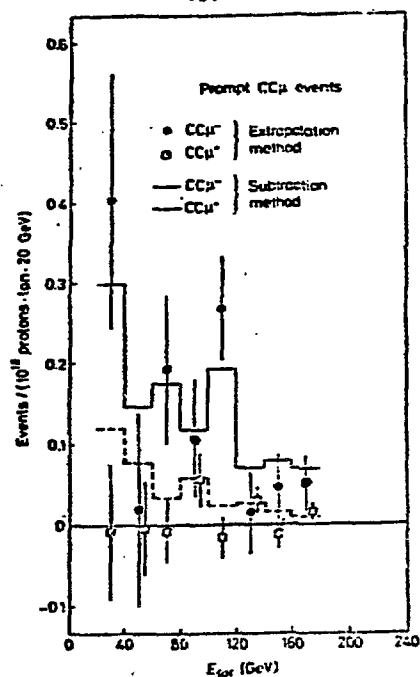


Fig. 3

Comparison of the results of the extrapolation and subtraction methods  
(CCNS data)

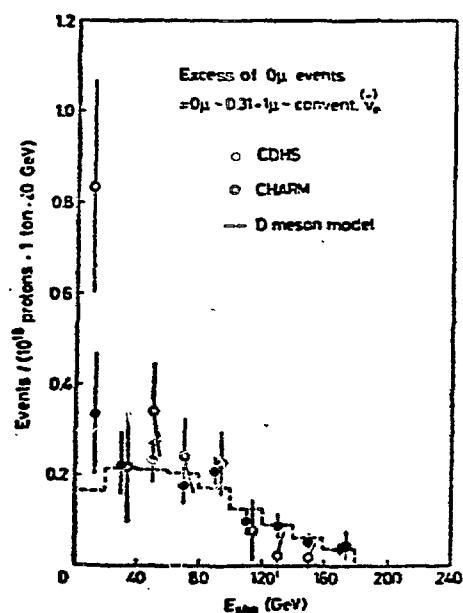
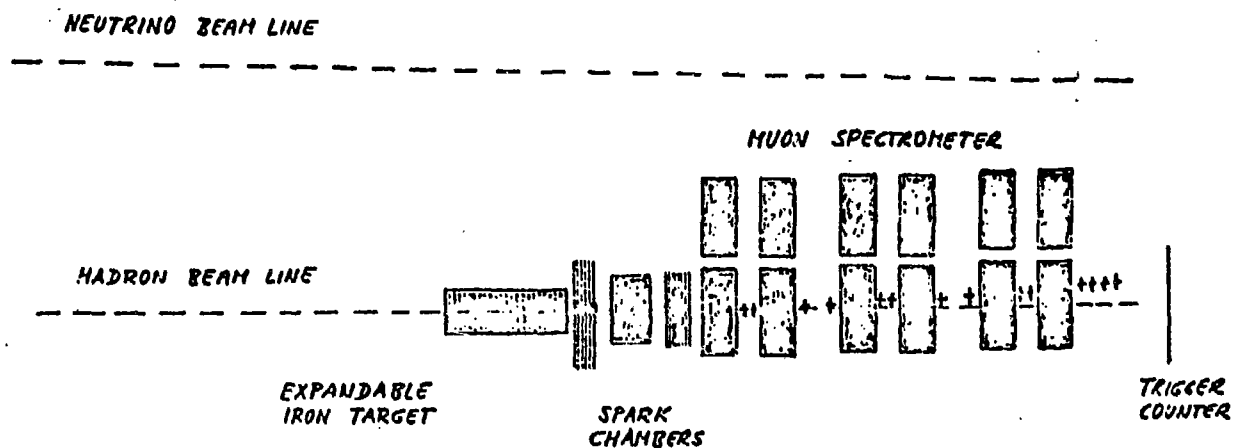


Fig. 4

Energy distribution of prompt ( $\nu_e + \bar{\nu}_e$ )



162

Fig. 5

The CFRS muon beam dump experimental set-up

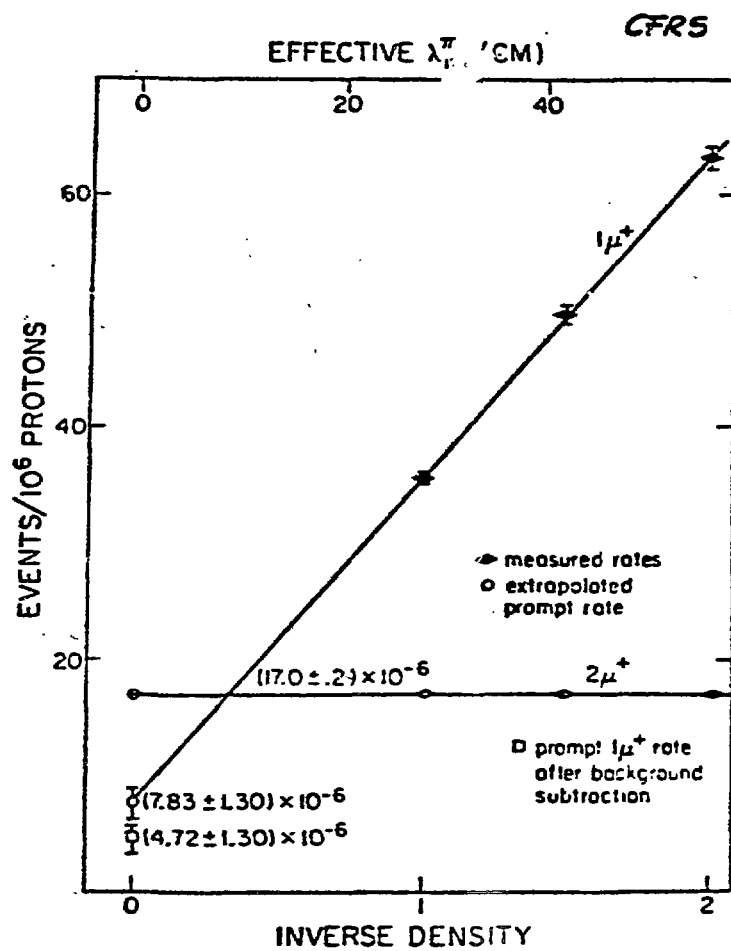


Fig. 6

The extrapolation method for prompt muons

PROMPT LEPTONS/PROTON  $\mu$ ster

10

10

1  
2

Energy s



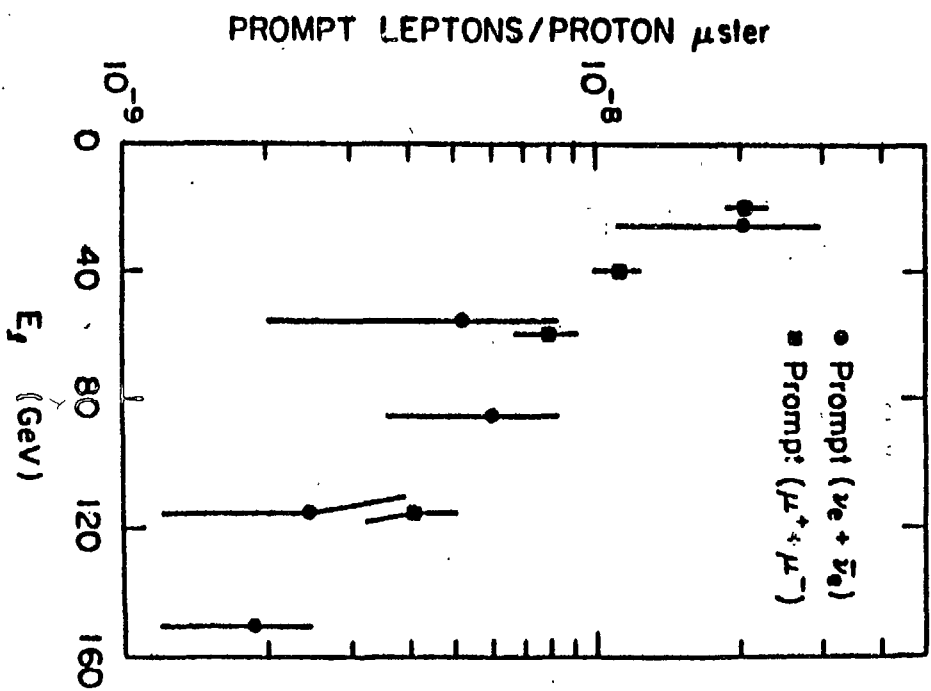
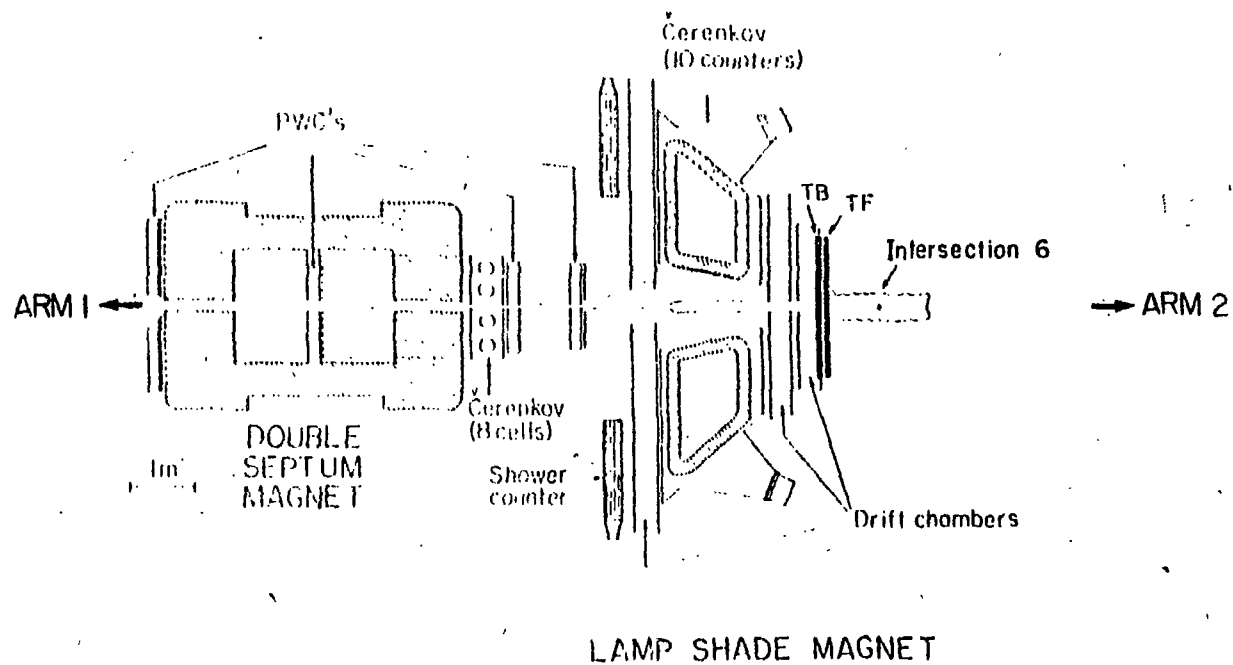


Fig. 7

Energy spectra of prompt neutrinos (BEBIC) and muons (CFRS)



165

Fig. 8

The Lamp Shade Magnet detector

Fig. 8

The Lamp Shade Magnet detector

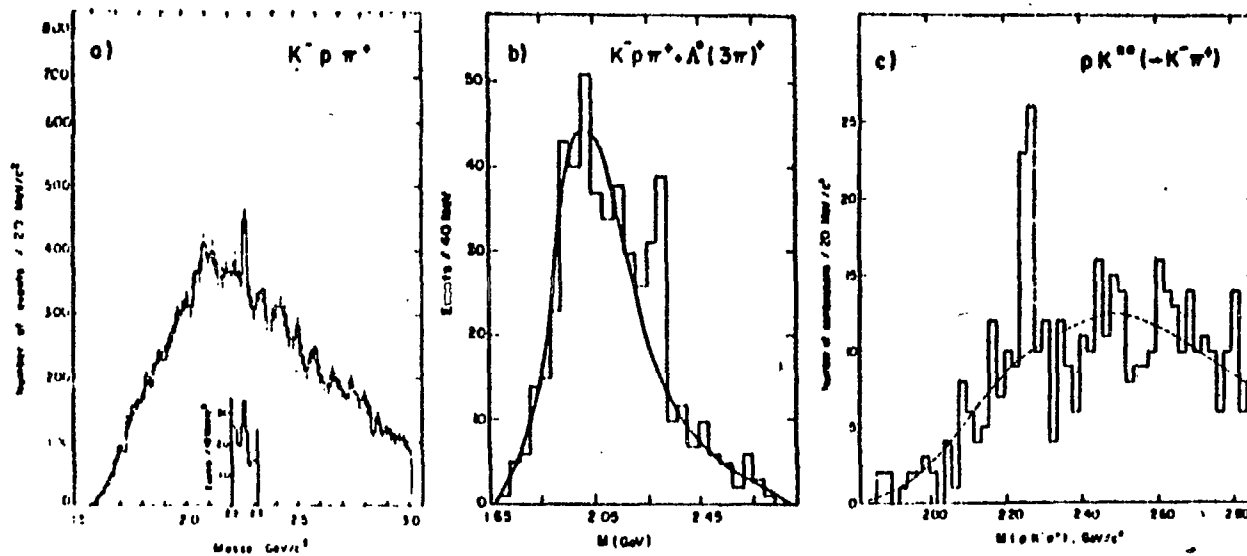
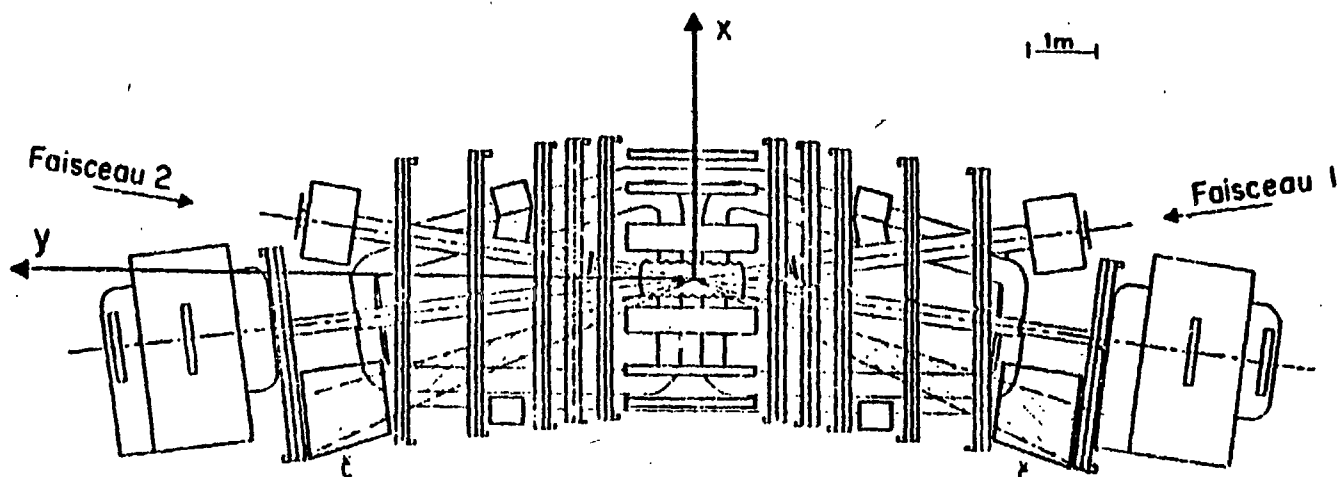


Fig. 9

The first  $\Lambda_c$  peaks obtained (a) by the LSM, (b) by UCLA-Saclay (c) by the SFM (CCHK)



167

Fig. 10

The Split Field Magnet detector in its original configuration

Fig. 10

The Split Field Magnet detector in its original configuration

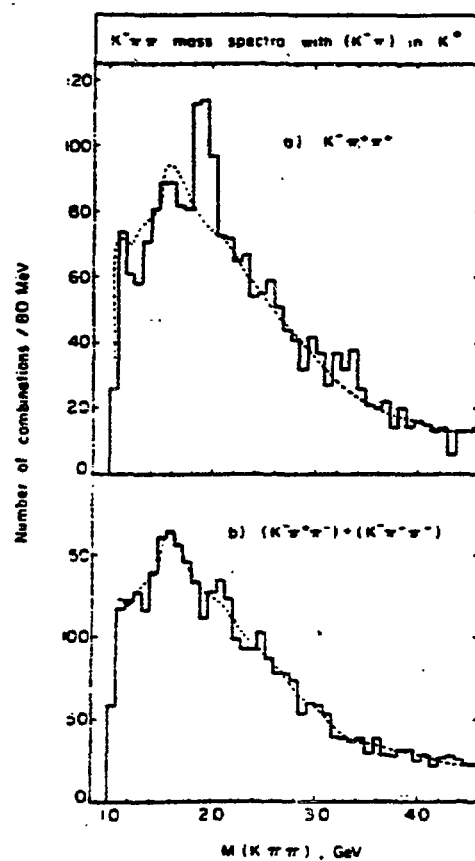


Fig. 11

The  $D \rightarrow K^- \pi^+ \pi^+$  signal obtained by CCHK with the SFM

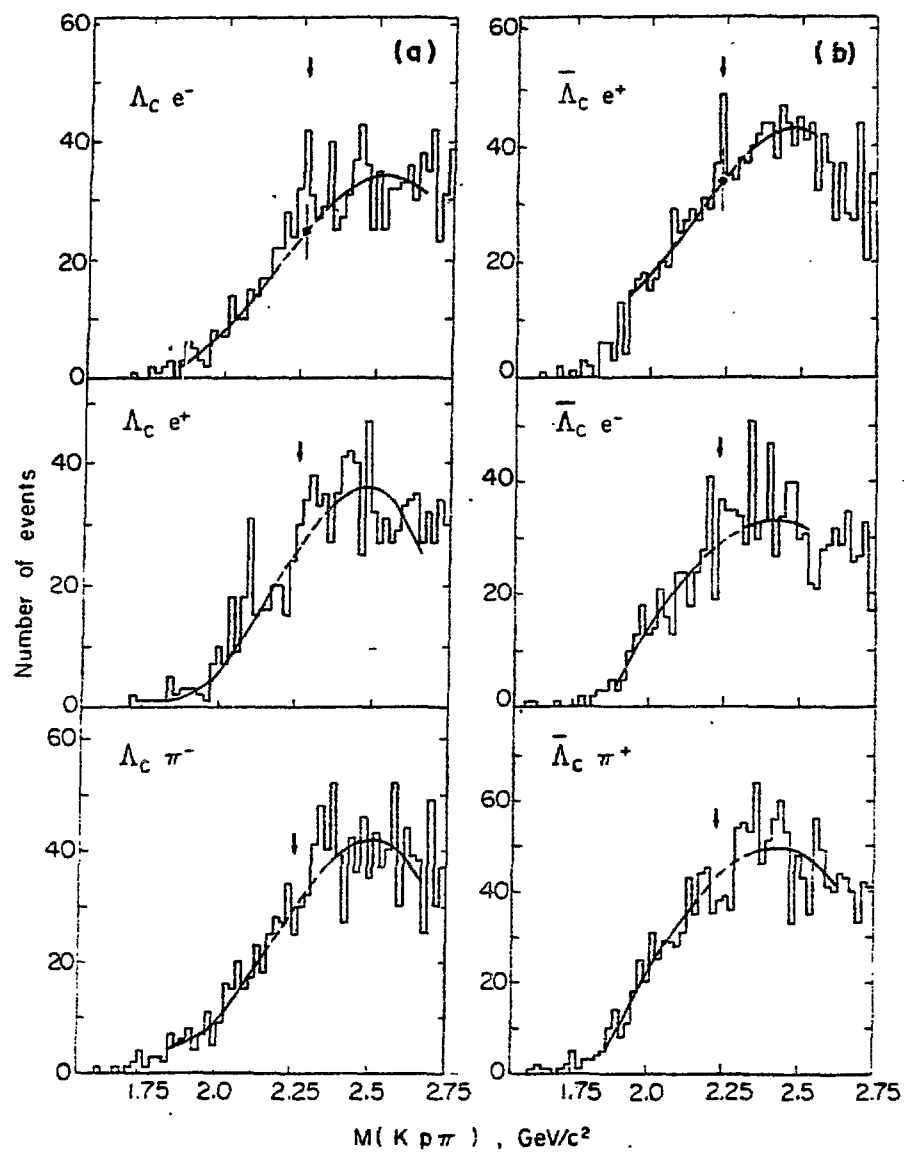
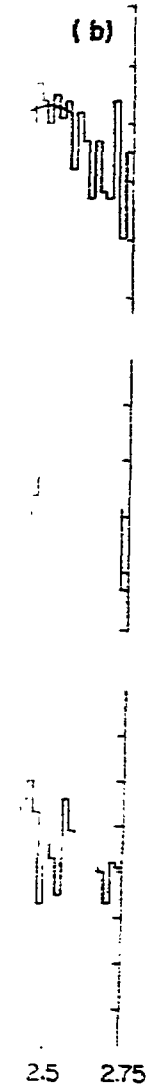


Fig. 12

The  $\Lambda_c$  ( $\bar{\Lambda}_c$ ) signals obtained at the LSM with an  $e^-$  ( $e^+$ ) trigger



gger

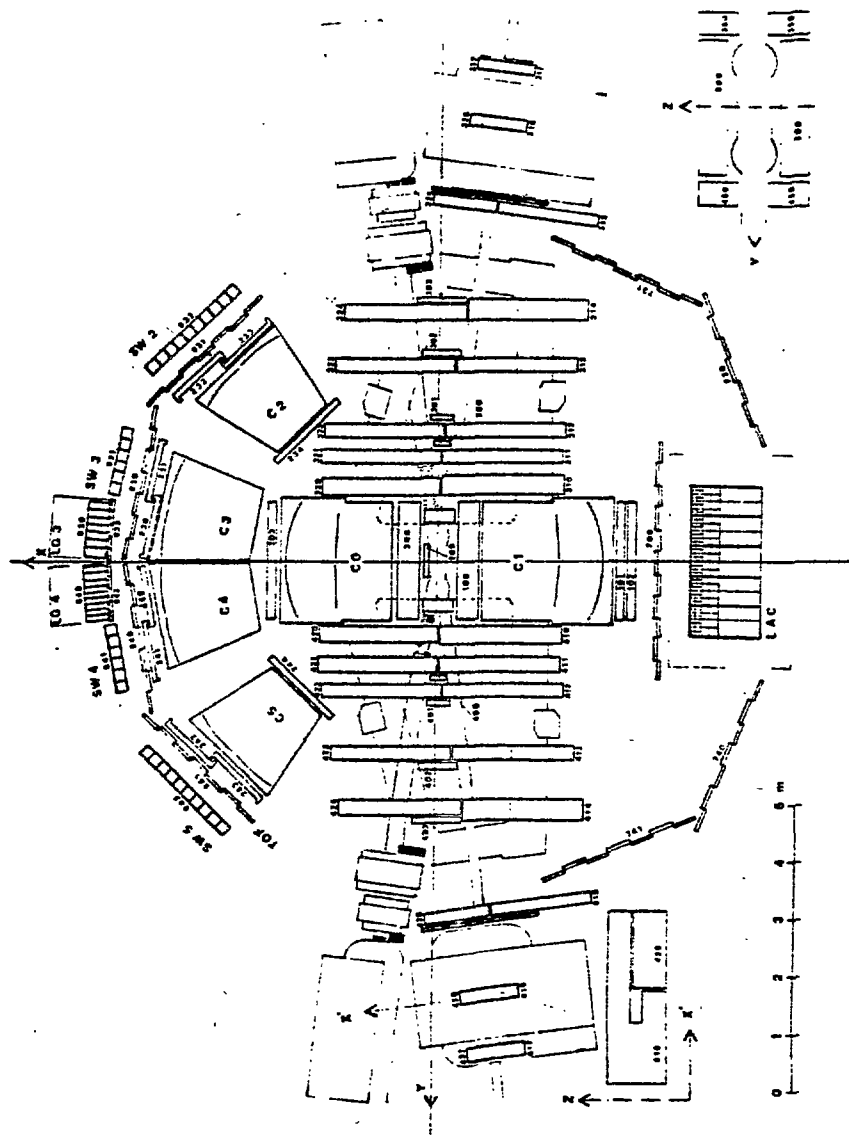


Fig. 13

The upgraded SFM detector

2.75

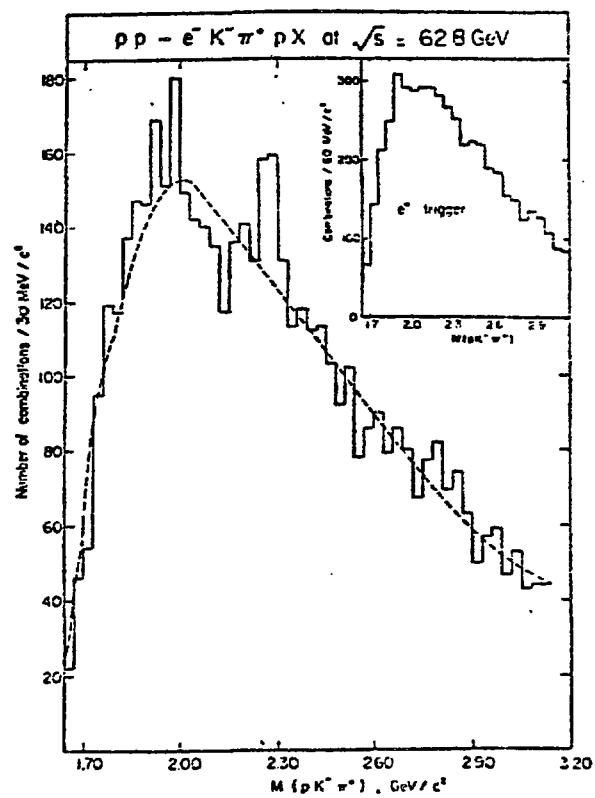


Fig. 14

The  $\Lambda_c$  signal obtained by ACCHDW at the SFM with an  $e^-$  trigger

Number of events / 0.10 GeV

150 1. Trigger

The  $D_0$



172  
ACCDHW

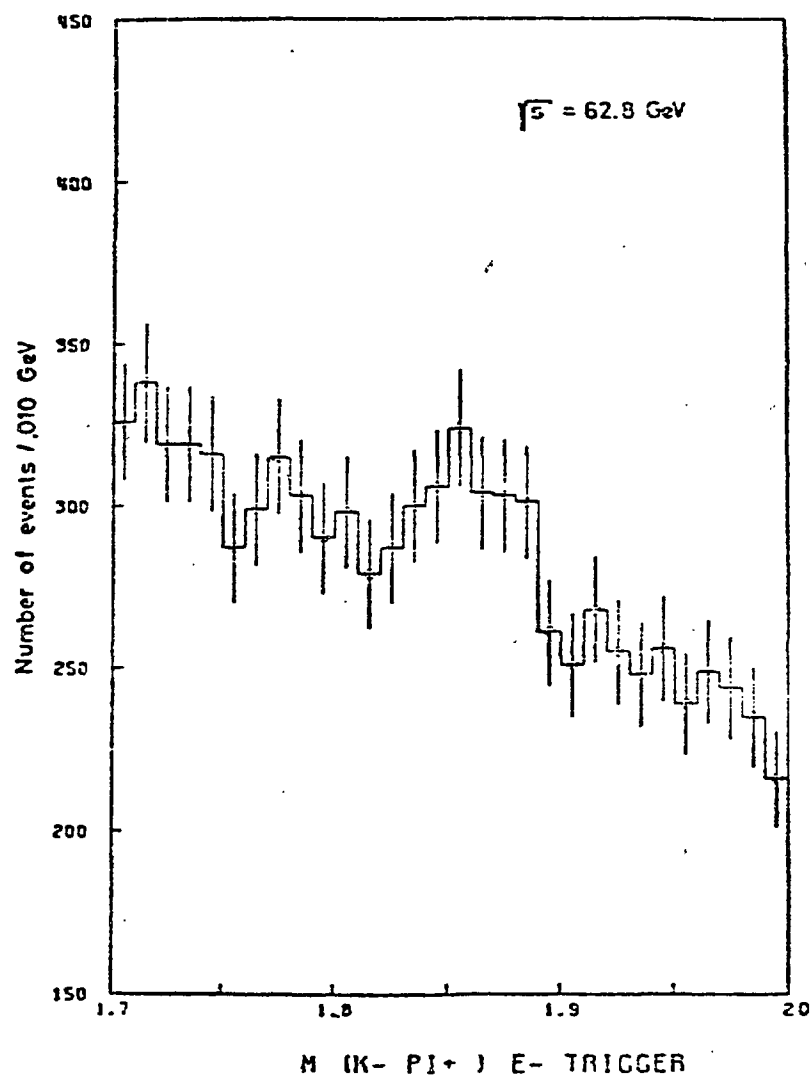


Fig. 15

The  $D_s$  signal obtained by ACCDHW at the SFM with an  $e^-$  trigger

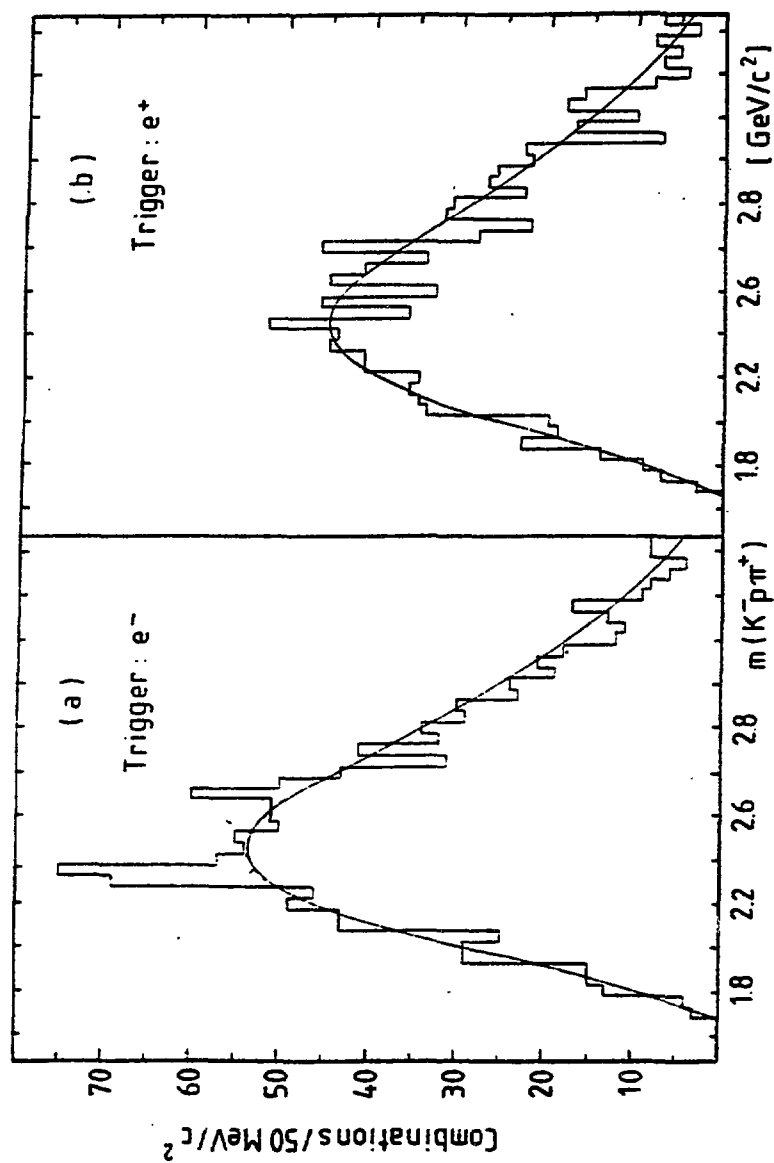


Fig. 16

The  $\Lambda_c$  signal obtained by BCF at the SFM with an e<sup>-</sup> trigger

18 2.2 2.6 2.8 2.2 2.6 2.8 2.8 [GeV/c<sup>2</sup>]

Fig. 16

The  $\Lambda_c$  signal obtained by BCF at the SFM with an e<sup>+</sup> trigger

The  $\Lambda_c$  signal obtained by BCF at the SFM with an  $e^-$  trigger

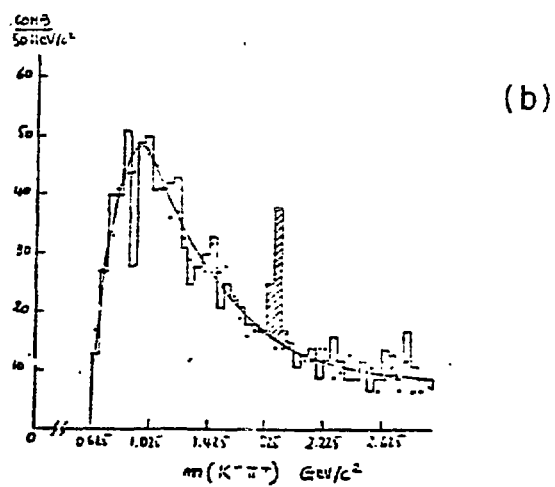
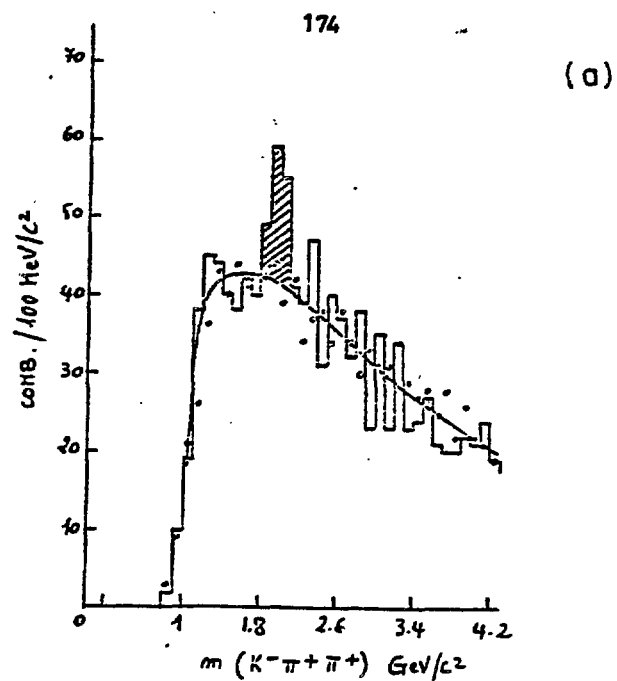


Fig. 17

The  $D^+$  and  $D^0$  signals obtained by BCF at the SFM with an  $e^-$  trigger

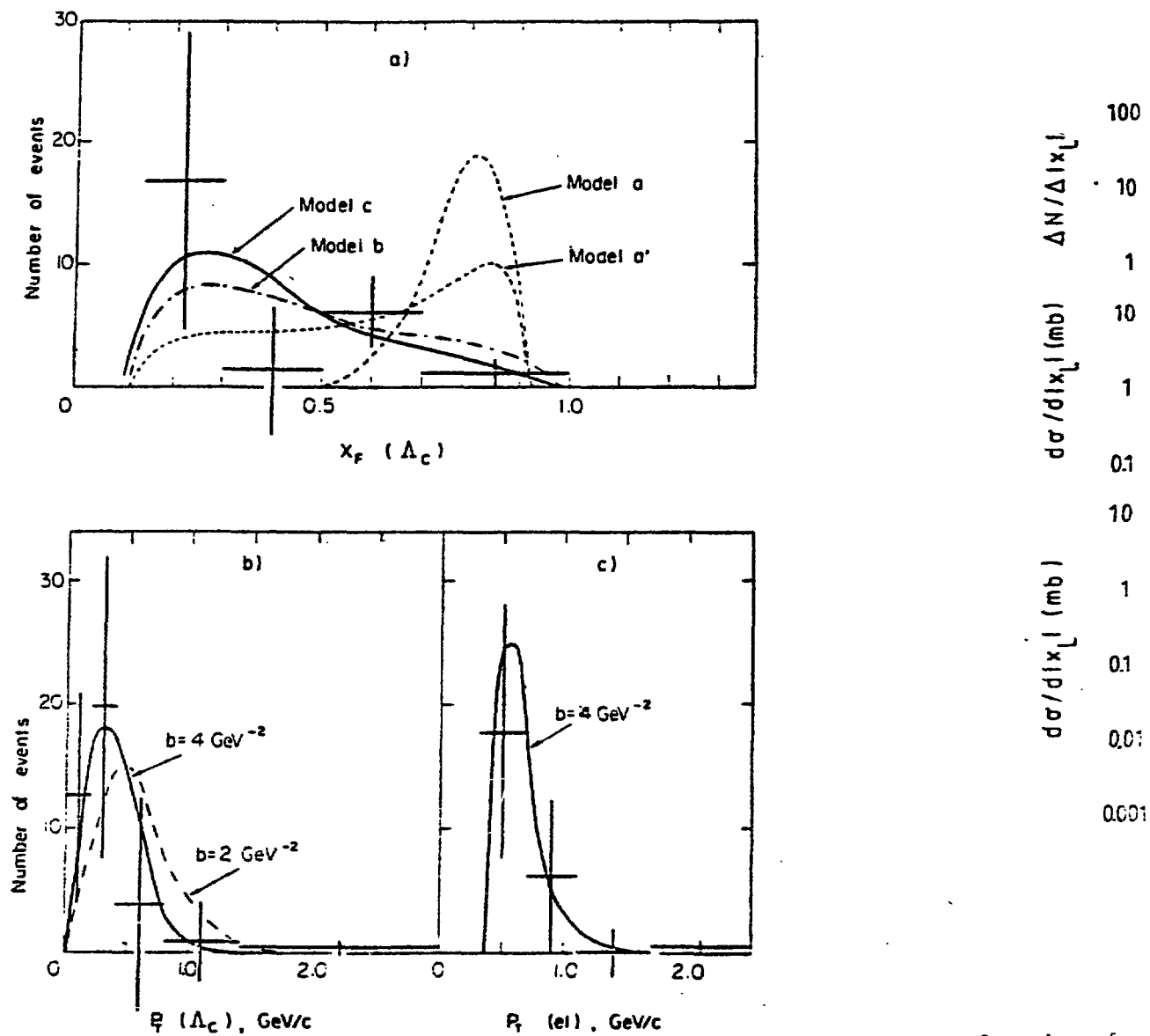


Fig. 18

Comparison of  $\Lambda_c$  and electron distributions observed at the LSM with those predicted by models

Comparison of  $x$

H with

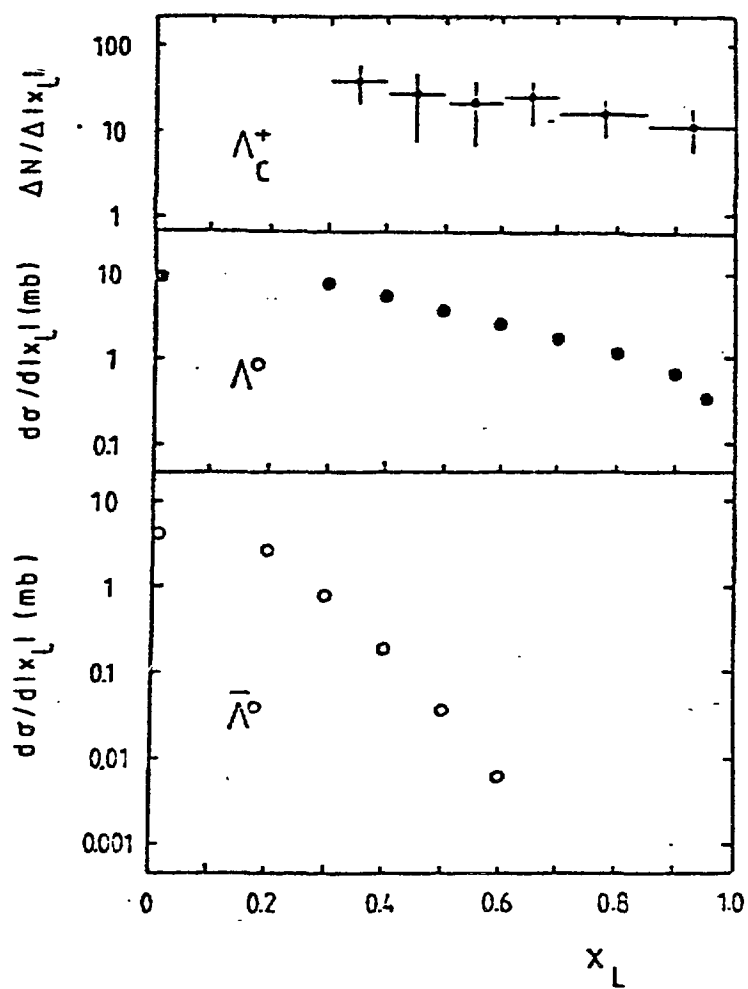


Fig. 19

Comparison of  $x$  distributions of  $\Lambda_c$  (from BCF),  $\Lambda$ , and  $\bar{\Lambda}$ , (from ref. [28])

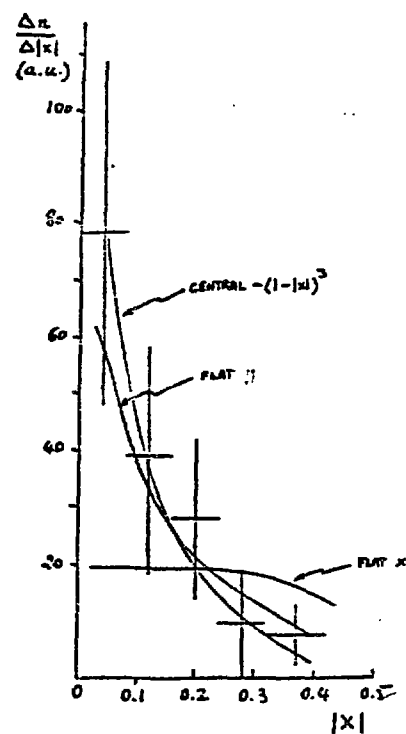


Fig. 20

Comparison of the  $\pi(D^0)$  distribution observed by BCF with that predicted by various models

$d\sigma/dx$  ( $\mu b$ )

1000

100

at predicted

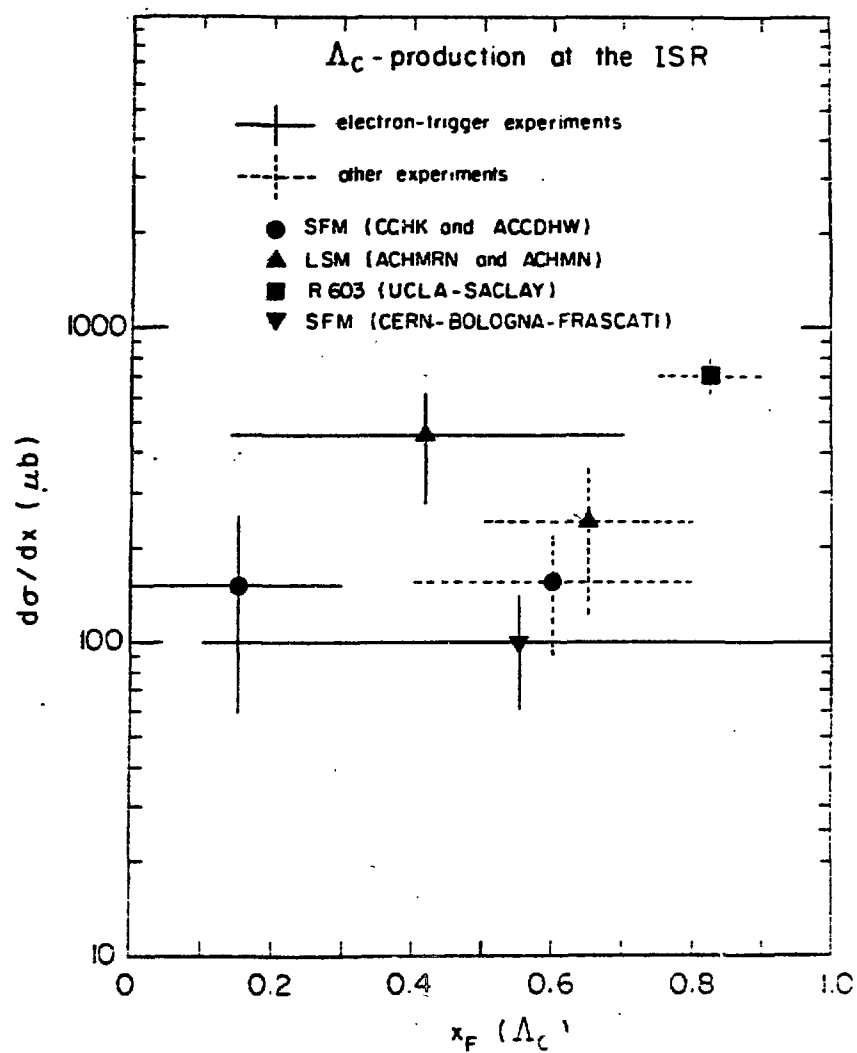


Fig. 21

$d\sigma/dx$  values obtained for  $\Lambda_c$  production at the ISR, using model a' for the electron trigger experiments

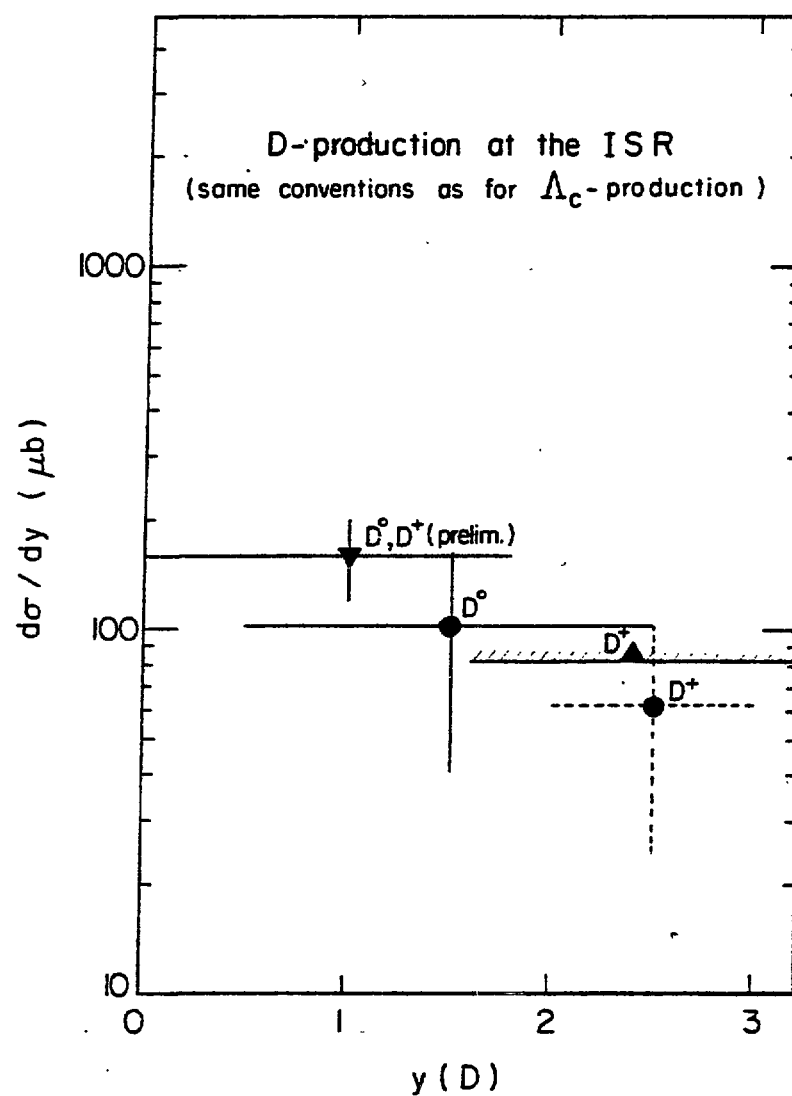
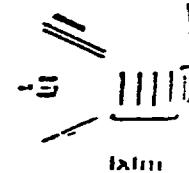


Fig. 22

$d\sigma/dy$  values obtained for D-production at the ISR,  
assuming a flat  $y$  production law



The Ch1



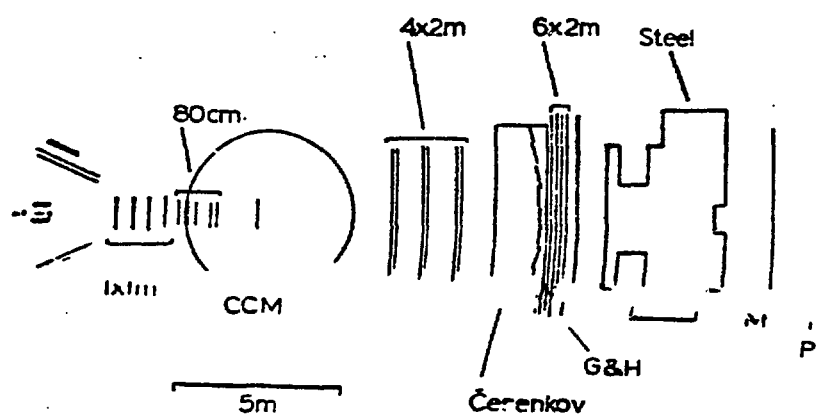


Fig. 23

The Chicago Cyclotron experiment for DD diffractive production

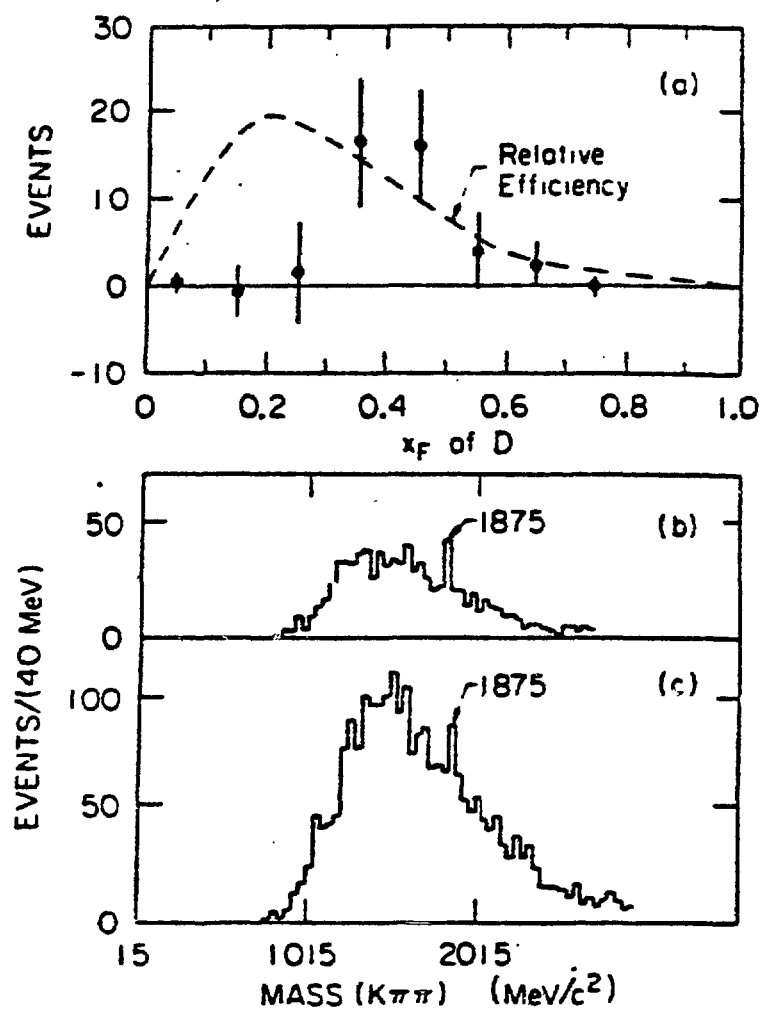


Fig. 24

The  $D^+$ (b) and  $\bar{D}^+$ (c) signals obtained in the Chicago Cyclotron experiment and their  $x$  distribution (a) compared to the one expected from a flat  $x$  (D) production law

rn experiment  
ected

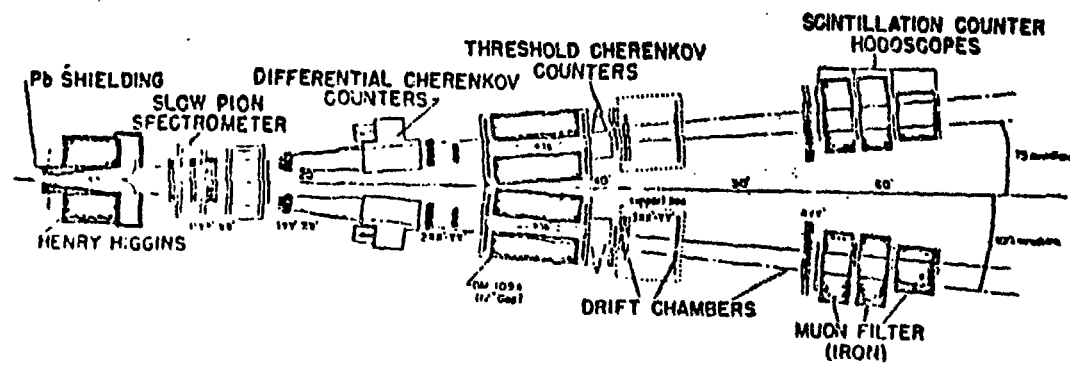


Fig. 25

The experimental set-up used for  $D^* \rightarrow D\pi$  detection

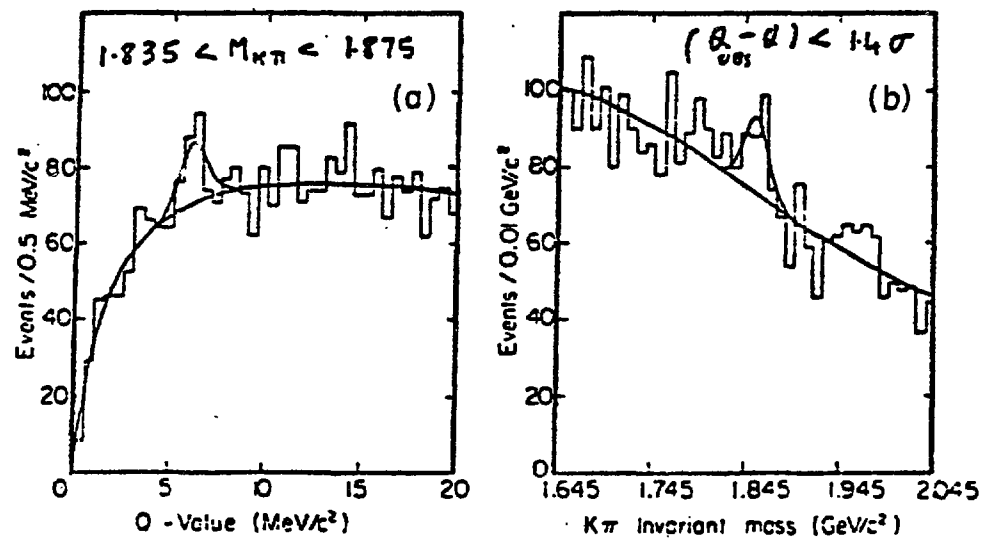
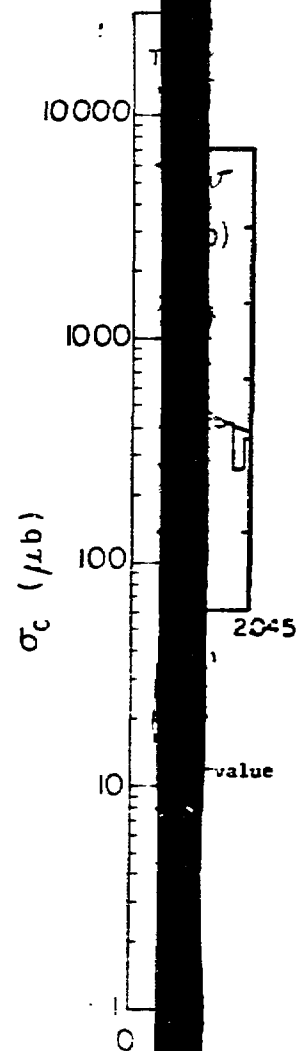


Fig. 26

Spectra of Q-values in  $K\pi\pi \rightarrow D\pi$  decay and of  $K^{\pm}\pi^{\mp}$  masses for the right Q-value



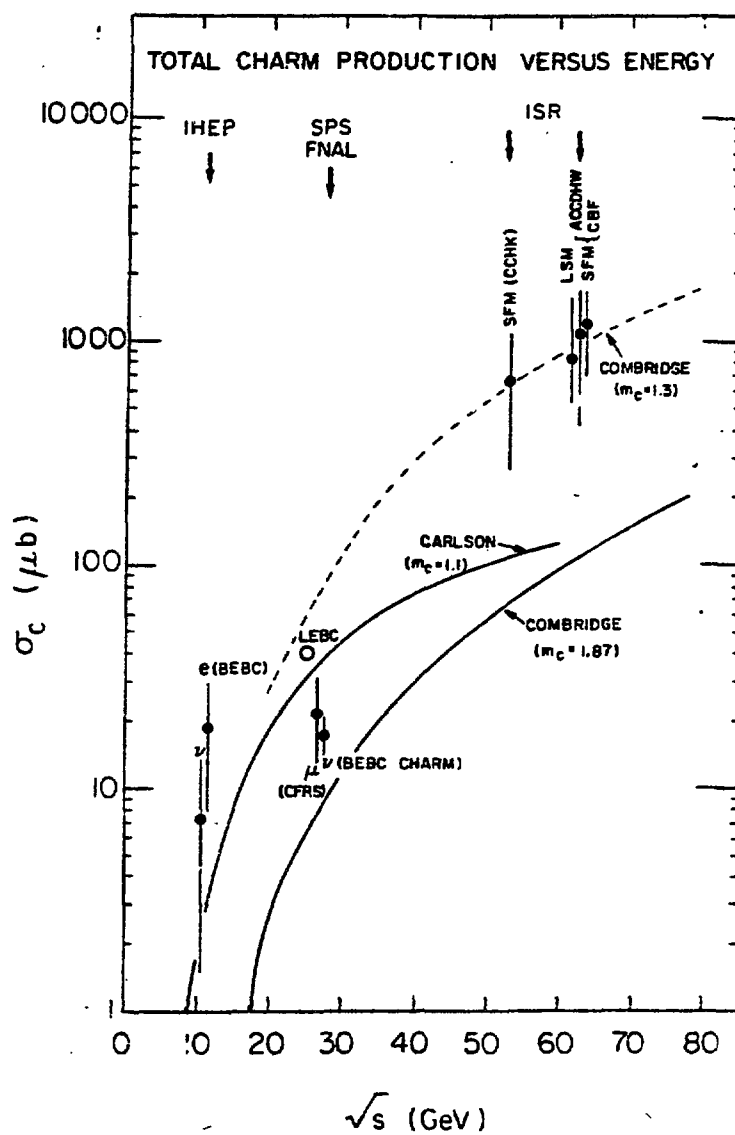


Fig. 27

Total charm cross sections versus c.m. energy

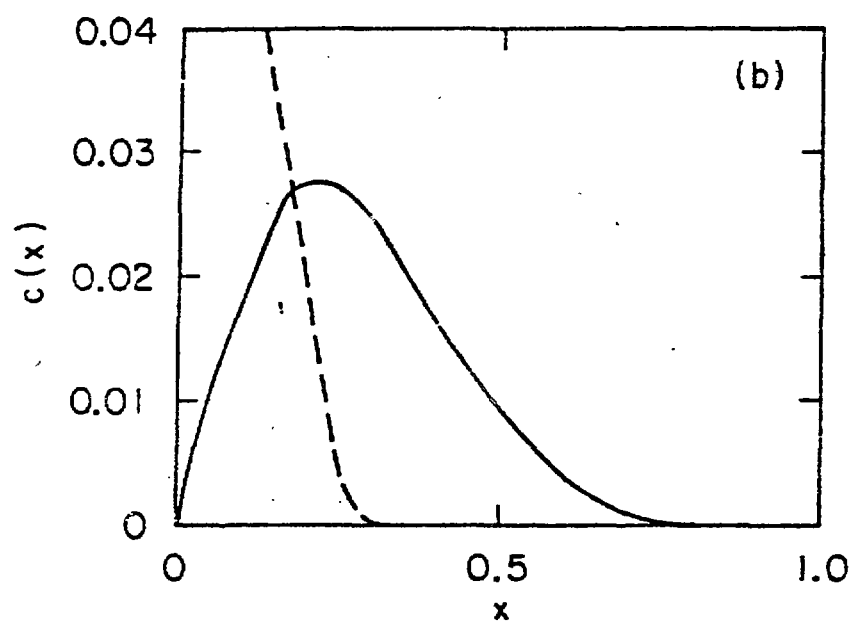
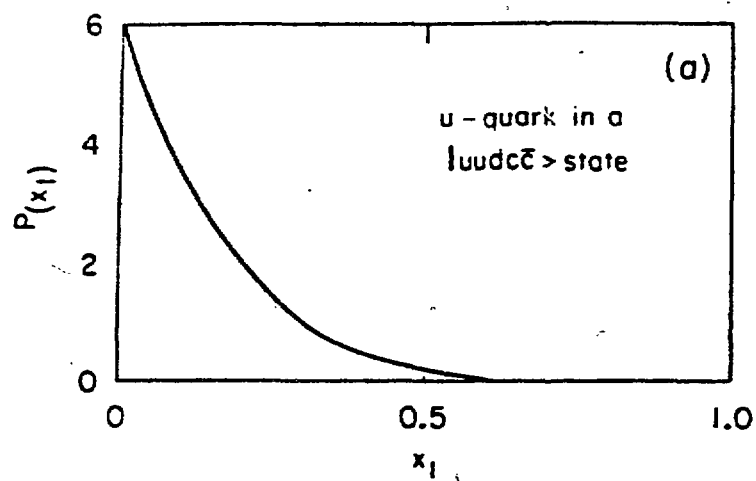
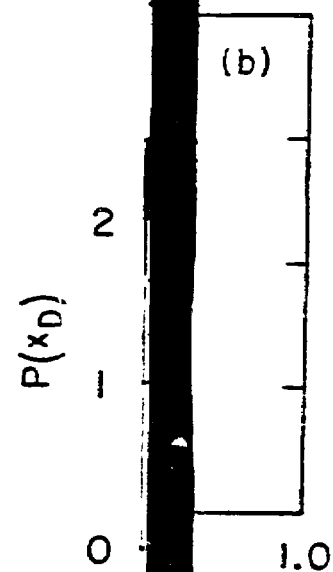
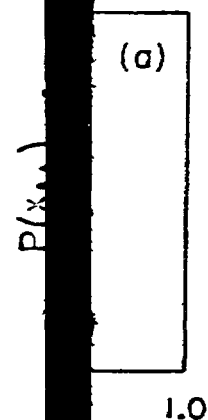


Fig. 28

$x$  distributions of light quarks (a) and charmed quarks (b) in an intrinsic charm state (plain) or in a QCD-sea (dotted).



quarks (b) in a (dotted).

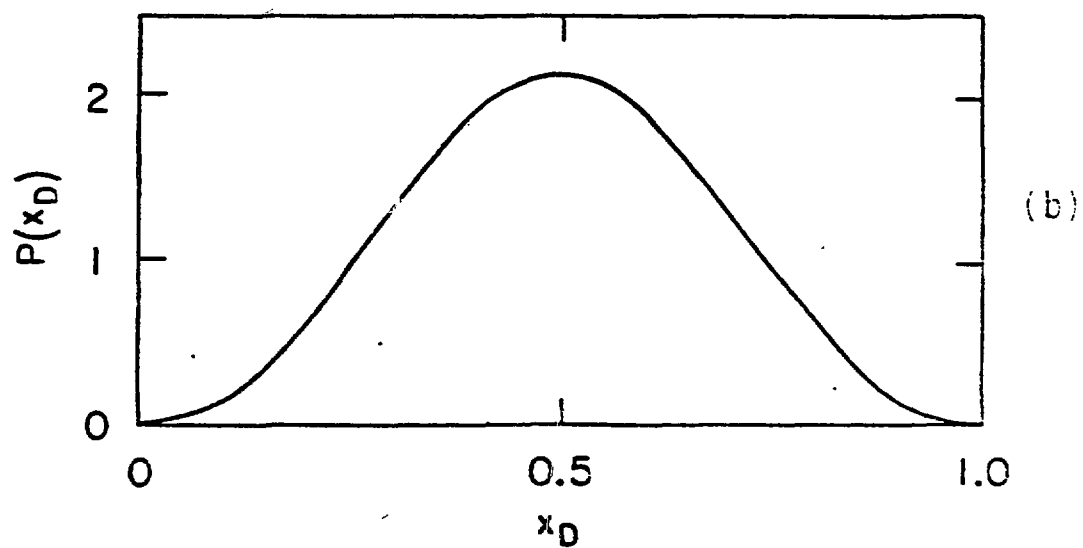
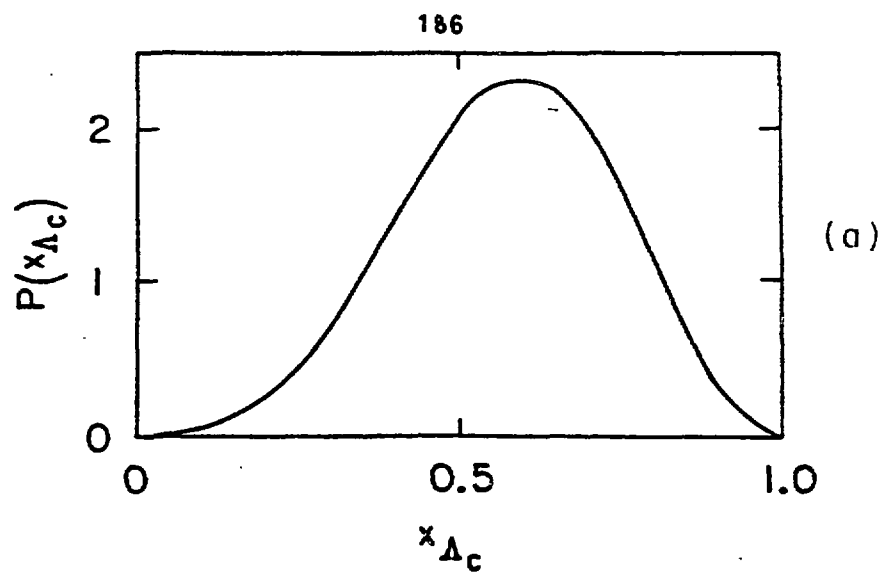


Fig. 29

x distributions of  $\Delta_c$  (a) and D (b) produced from an intrinsic charm state

I) A NEW  $O^-S$  MESON AND NEW RESULTS ON THE  $1^+S$  STATE IN THE  
3H SYSTEM COHERENTLY PRODUCED ON NUCLEI

II) 5H COHERENT PRODUCTION ON NUCLEI

G. Bellini , M. di Corato , P.L. Frabetti , Yu I. Ivanshin ,  
L.K. Litkin , D. Menasce , S. Otwinowski , F. Palombo , J. Pernegr ,  
A. Sala , S. Sala , S.I. Sychkov , A.A. Tjapkin , I.M. Vassilevski ,  
G. Vegni , V.V. Visniakov , O.A. Zaimidoroga

Dubna - Milano Collaboration

Presented by F. Palombo

I - The  
been produ  
place insi  
with the nu  
A sys  
5x channel

with A = E  
GeV at the  
events.

Detail

The

mass range  
example in  
region ).  
vents with  
sections 1  
measured b

The

PWA ( Part  
coherent s  
 $O^-S$ ,  $O^-P$ ;  
negligible  
ferences f  
ction of M

Firs

the sample  
shapes and  
 $O^-S$  amplit

The

lues :  $M_3$ ,  
riation is



I - The behaviour of the hadronic matter immediately after it has been produced can be studied in principle if the production takes place inside the nucleus. The new-born hadronic system can interact with the nucleons before it reaches asymptotic conditions.

A systematic study of the hadronic states going into  $3\pi$  and  $5\pi$  channels has been carried out by our collaboration. The channel :

$$\pi^- A \rightarrow \pi^- \pi^- \pi^+ A \quad (1)$$

with  $A = \text{Be, C, Al, Si, Ti, Cu, Ag, Ta, Pb}$ , has been studied at 40 GeV at the Serpukhov PS accelerator, with a statistics of  $\sim 120,000$  events.

Details of the experimental set-up can be found in ref. 1.

The coherence mechanism is strongly present in the data in the full mass range, as shown by the  $t' = |t - t_{\min}|$  distributions (see as an example in fig 1 the  $t'$  distributions of the  $3\pi$  system in the low mass region). Coherent samples are defined for every target selecting the events with  $t'$  smaller than the first diffractive minimum. Total cross sections for the coherent production in the full  $t'$  range were also measured by subtracting the incoherent background.

The data of the channel (1) were analyzed using the program PWA (Partial Wave Analysis)<sup>(2)</sup>. The set of important waves in the coherent sample consists of eight contributions :  $1^+S, 1^+P, 1^+D$  ;  $0^-S, 0^-P$  ;  $2^-S, 2^-P, 2^+D$ . The spin flip amplitudes have been found negligible. The behaviour of the contributions and of the phase differences for the more important waves has been investigated as a function of  $M_{3\pi}$ ,  $t'$  and of the atomic weight ( $A$ ) of the nuclear target.

First of all we have performed the  $3\pi$  mass dependent PWA in the sample of the events of all targets together (fig. 2). The mass shapes and the phase variations show not only for  $1^+S$ , but also for  $0^-S$  amplitudes, a resonance behaviour in the  $A_1$  region.

The parameters of the  $0^-S$  resonance have the following values :  $M_{3\pi} = 1.20 \pm 0.03 \text{ GeV}$  and  $\Gamma = 0.330 \pm 0.040 \text{ GeV}$  ; its phase variation is  $\sim 80^\circ$  (fig. 2).



i) the nucleus is a powerful mean in selecting and enhancing resonances, as  $1^+S$  and  $0^-S$ ;

ii) the characteristics of the  $0^-S$  resonances do not change with the nuclear target, while the  $1^+S$  moves and it is more pronounced as larger as the nuclear atomic weight;

We do not have a clear explanation of the  $1^+S$  dependence on the nuclear target. We can only mention some mechanisms which could be responsible for this behaviour:

i) the coherent mechanism selects and enhances the production at very small  $t'$ .

ii) the nucleus can absorb in different way the different states or contribution and the absorption effects increase with the atomic weight; in such a frame the nuclear absorption could clean some states cutting the contribution of mechanisms, which normally interfere in negative way with the resonant states.

iii) an intermediate or transition state after the hadron-hadron collision but before fixed final states have been reached, probably exists; during this transition time the new-born hadronic matter could interact with the nucleons and its characteristics can be changed, as it is found for  $1^+S$ .

A more detailed analysis of the nuclear effects on the contribution of the different waves can be carried out using a specific model. To this purpose the K lbjerg-Margolis-Glauber model has been used, even if in its approach the interaction is assumed to be instantaneous and point-like. As well known, the nuclear absorption is measured by the parameter  $\sigma_2$ , which in the frame of this model is interpreted as the collision cross-section between the state under investigation and the bound nucleons.

The best fit value obtained for  $\sigma_2$  is of the order of 15 mb, with small fluctuations for the different mass regions.  $\sigma_2$  has been evaluated also for the different partial waves.  $0^-$  and  $1^+$  give for  $\sigma_2$

the following ranges: 2I - 30 and II - 16 mb, respectively, which reflect the different contributions of these waves in the coherent region as shown in figs. 6a and 6b.

## II. $5\pi$ coherent production on nuclei.

A sample of  $\sim 15,000$  events of the channel

$$\pi^- A \rightarrow \pi^- \pi^- \pi^- \pi^+ \pi^+ A$$

on the same nine targets has been analyzed. The geometrical acceptance of the apparatus as a function of  $t'$  and  $M_{5\pi}$  was estimated, using Monte Carlo calculations. It is almost independent of  $t'$  (at least for  $t' \leq .5 \text{ (Gev/c)}^2$ ) and decreases smoothly from 75% to 55% when  $M_{5\pi}$  ranges from 1.8 to 3.  $\text{Gev/c}^2$ .

The inefficiency of the reconstruction programs was calculated, recovering the lost events by means of an interactive graphic systems<sup>(6)</sup>. This inefficiency is  $\sim 25\%$ , almost independent of  $t'$  and  $M_{5\pi}$  values.

Fig. 8 shows the five-pion mass distribution, not corrected for acceptance and with  $t'$  cut at  $t' = .5 \text{ (Gev/c)}^2$ . The differential cross section  $\frac{d\sigma}{dt'}$  versus  $t'$  and versus  $A$  and the total cross section  $\sigma_c$  versus  $A$ , have been fitted using the K lbig-Margolis formula. The procedure used was the same as in ref. I. The full line drawn in fig. 9 is the result of the fit on the total coherent cross section. The parameter  $\sigma_c(5\pi)$  is always definitely smaller than 10 mb and tends to decrease with increasing  $M_{5\pi}$ .

## REFERENCES

- 1) G. Bell, y, which  
product coher  
Submitted
- 2) G. Asco
- 3) For exam
- 4) C. Daum  
and 94 GeV
- 5) J. Fern
- 6) D. Mena

al ac-  
estim  
dent o  
from  
ulated  
raphic  
of  $t'$   
ted fo  
ential  
cross  
argolis  
full  
coher  
smaller

## REFERENCES

G. Bellini et al., which  
products coherent

Submitted

G. Ascoli

For exam

C. Daum

94 GeV

J. Perneger

D. Menasce

al ac-  
estima-  
dent of  
from

ulated,  
graphic  
of t'

ted for  
ential  
cross  
rgolis  
full  
coherent  
maller

## REFERENCES

- 1) G. Bellini et al., The  $(3\pi)$ -nucleon collision in coherent production on nuclei at 40 GeV/c; preprint CERN-EP/81-40(1981). Submitted to Nuclear Physics.
- 2) G. Ascoli et al., Phys. Lett. 25 (1970) 962
- 3) For example: D.P. Stanley and D. Robson; Phys. Rev. 21 (1980) 3180
- 4) C. Daum et al., Diffractive production of  $3\pi$  states at 63 and 94 GeV. CERN-EP/80-219 (1980)
- 5) J. Perneger et al., Nucl. Phys. B134 (1978) 436
- 6) D. Menasce, F. Palombo, S. Sala; Comp. Phys. Commun. 22(1981) 317

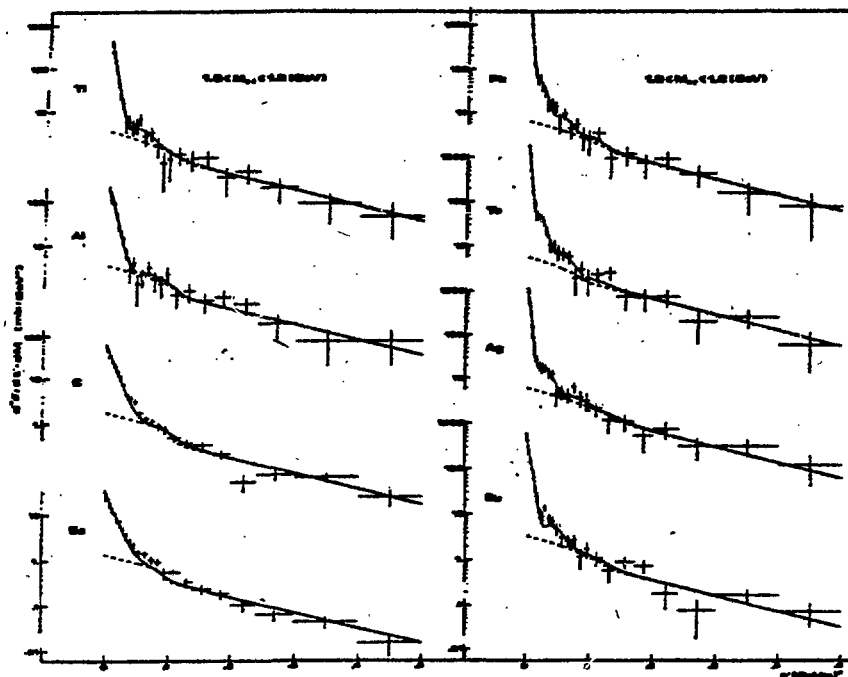


Fig. 1

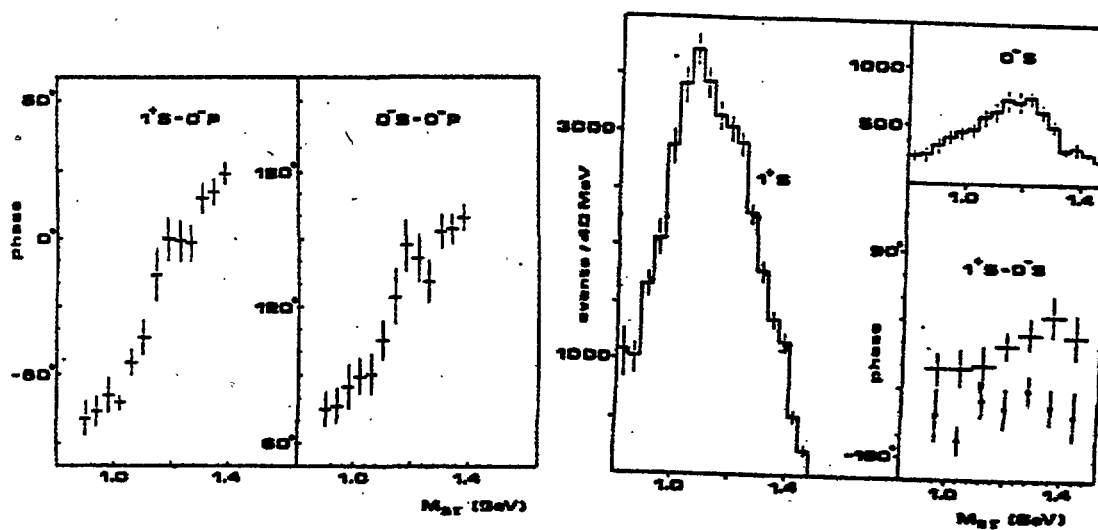


Fig. 2

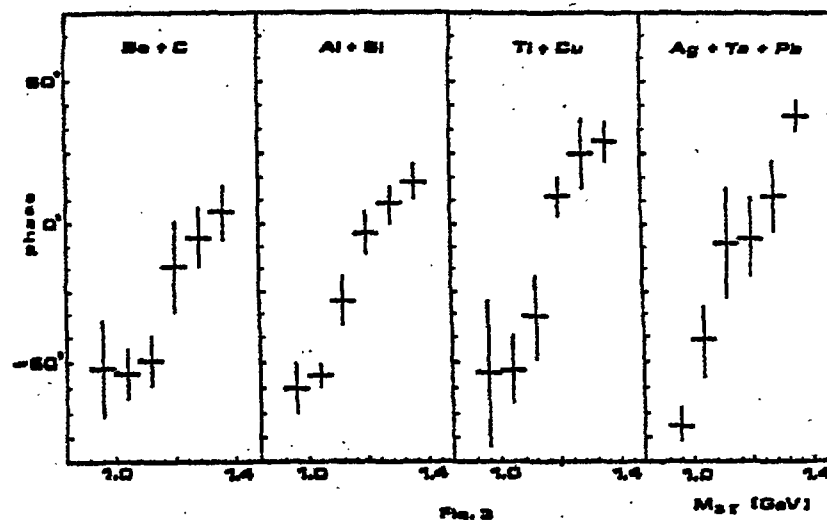


Fig. 3

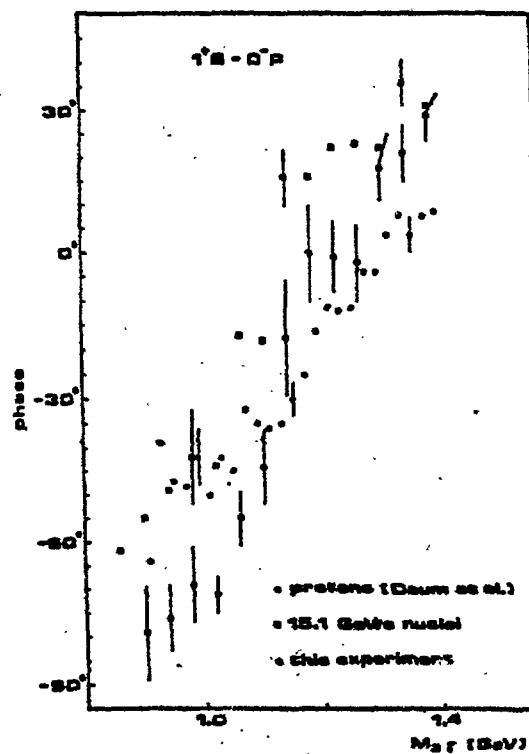


Fig. 4

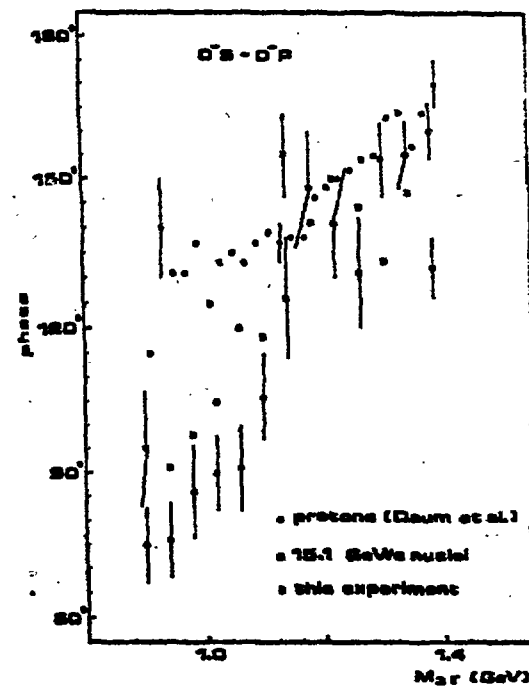


Fig. 5

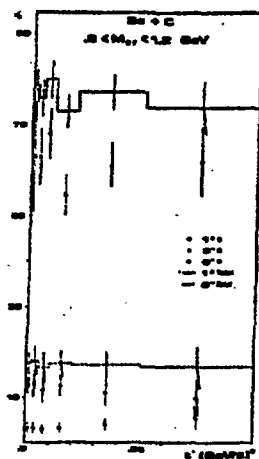


Fig. 6a

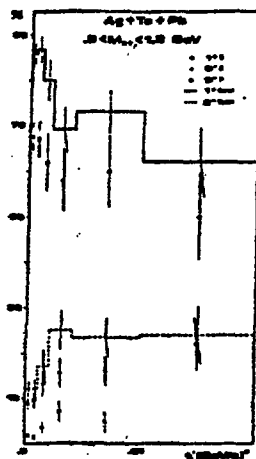


Fig. 6b

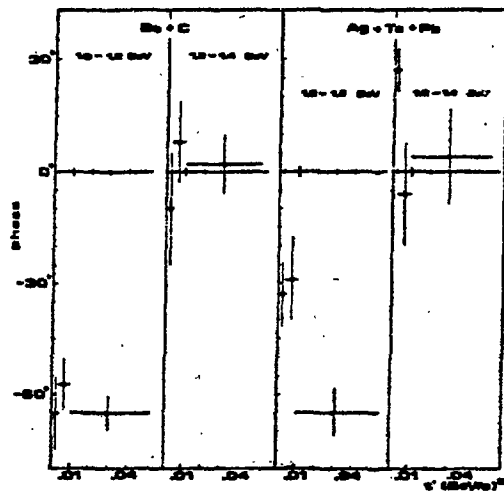
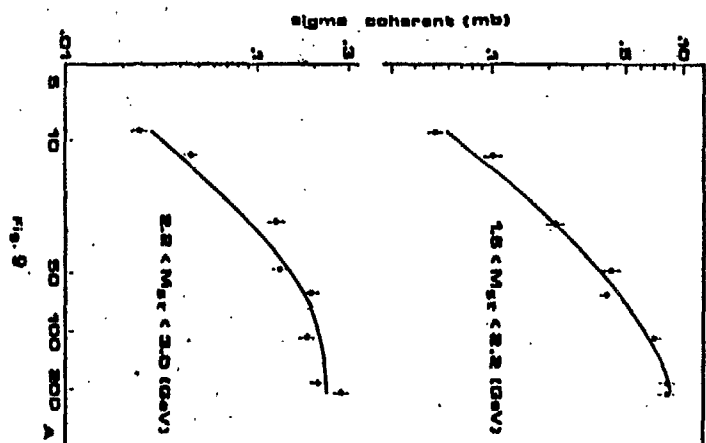
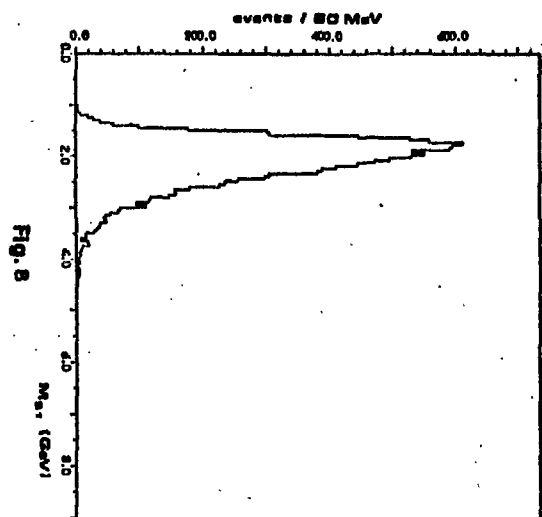
 $\frac{d^2N}{dp_T^2 dp_{\perp}^2}$ 

Fig. 7





TWO PARTICLE CORRELATIONS IN PION-NUCLEUS INTERACTIONS AT 40 GeV/c

A.T. Abrosimov<sup>1)</sup>, G. Bellini<sup>2)</sup>, M. di Corato<sup>2)</sup>, P.L. Frabetti<sup>3)</sup>,  
L.K. Litkin<sup>4)</sup>, V.P. Lobanova<sup>1)</sup>, V.I. Nikanorov<sup>4)</sup>, S. Otwinowski<sup>5)</sup>,  
F. Palombo<sup>2)</sup> and K.P. Vishnievskaja<sup>1)</sup>

- 1) Moscow State University, Moscow, USSR.
- 2) Istituto di Fisica dell'Università and INFN, Milano, Italy.
- 3) Istituto di Fisica dell'Università and INFN, Bologna, Italy.
- 4) Joint Institute for Nuclear Research, Dubna, USSR.
- 5) Institute for Nuclear Research, Warsaw, Poland.

Presented by S. Otwinowski

Abstract

Multiplicity distributions and two-particle correlation functions are presented for shower particles with pseudorapidity  $\eta > 1$  produced in  $\pi^-$  interactions on C, Al, Cu, Pb targets at incident pion momentum 40 GeV/c. Results are compared with the  $\pi^-p$  data. No noticeable differences were found between the nuclear and elementary distributions of the correlation function. The data are compared with the predictions of the additive quark model and the quasieikonal model.

(author)

Recent  
observed  
nuclei 14  
correlati  
results o  
the data  
Data o  
emulsion  
They res  
nuclei ex  
The d  
chamber  
40 GeV/c  
and data  
with the  
the data  
85% (for  
produced  
with  $\beta <$   
In the  
multipli  
Events o  
on nucle  
is about  
The v  
nuclear  
in Table  
are incl

Recently a big experimental and theoretical effort was observed in studying the mechanism of hadron interactions on nuclei [1]. However only few results were reported on two-particle correlations for pure nuclear targets. The papers [2-4] reported results on the light nuclei (C, Al), in the experiment [5] the data were taken on Cr and W nuclei.

Data on two-particle correlations obtained with nuclear emulsion as a target are more numerous but difficult to interpret. They result from a superposition of contributions from different nuclei and this may generate additional correlations [6,7].

The data presented in this paper were taken with the spark chamber spectrometer, MHS, with C, Al, Cu, Pb targets exposed to 40 GeV/c beam of  $\pi^-$  at the IHEP accelerator. Experimental set-up and data analysis were presented elsewhere [8]. Charged particles with the pseudorapidity  $\eta = -\ln(\tg \frac{\theta_{lab}}{2}) > 1$  were detected. Using the data [9] we estimated that the region  $\eta > 1$  contains from 85% (for carbon) to 75% (for lead) of all charged secondaries produced in  $\pi^-$  interaction with nucleus at 40 GeV/c (protons with  $\beta < 0.7$  excluded).

In the present analysis are included events with charged multiplicities 0 and 1, omitted in our previous publication [8]. Events of elastic scattering and of coherent dissociation on nuclei were removed. The total number of analysed interactions is about 500 for each nucleus.

The values of the average charged multiplicities for different nuclear targets in several pseudorapidity intervals are presented in Table 1. The  $\pi^-p$  data at 40 GeV/c [10] in the same  $\eta$  intervals are included for comparison.

The contribution of slow protons with the velocities  $0.3 < \beta < 0.7$  was estimated in a separate exposure of our spectrometer with a low magnetic field [8]. The values of the average charged multiplicities without the slow protons are also given in Table 1. The errors include the statistical errors and the uncertainties in the slow proton subtraction.

The main features of the multiplicity data, discussed in the previous paper [8], remain unchanged after the addition of events with topology 0 and 1. The multiplicity increases with the target mass for low pseudorapidities  $\eta < 3$ ; at higher values of  $\eta$  the variation flattens off and in the very forward cone ( $\eta > 4$ ) the multiplicity tends to be smaller on nuclei than on hydrogen.

The charged multiplicity distributions were analysed using the KNO scaling variables [11],  $\langle N \rangle \frac{\sigma_N}{\sigma_{inel}}$  and  $z = \frac{N}{\langle N \rangle}$ , where  $\sigma_N$  is the cross section for topology N,  $\sigma_{inel}$  is the total inelastic cross section excluding the coherent component and  $\langle N \rangle$  is the average charged multiplicity. The KNO scaling is known to be satisfied by the hadron-hadron data at various energies. With our data we are testing the scaling hypothesis for different nuclear targets at a fixed energy of the incident pion.

The scaled multiplicity distributions in  $\pi^-$ -nucleus and  $\pi^-p$  interactions at 40 GeV/c [10] are plotted in Fig. 1. In this analysis the multiplicity refer to the region  $\eta > 1$  and do not include slow protons. The multiplicity distribution for  $\pi^-p$  interactions was calculated for particles selected in the same

way as in that the K targets. with slow scaling.

We have function of

$$R_2(\eta_1,$$

where  $\frac{d\sigma}{d\eta}$  inclusive biases as less then influence of  $R_2(\eta_1,$  nuclei. The for other

We do distributions with published The formulae for targets as

An appropriate  $R_2(0, \gamma)$  for experiment

The  $R_2$  300 GeV/c

way as in the case of our data. The data shown in Fig. 1 indicate that the KNO scaling is well satisfied for different nuclear targets. The multiplicity distributions (not shown) for events with slow protons included are also consistent with the KNO scaling.

We have studied two-particle pseudorapidity correlation function defined as

$$R_2(\eta_1, \eta_2) = \frac{\sigma_{\text{inel}} \left( \frac{d^2\sigma}{d\eta_1 d\eta_2} - \frac{d\sigma}{d\eta_1} \frac{d\sigma}{d\eta_2} \right)}{\frac{d\sigma}{d\eta_1} \frac{d\sigma}{d\eta_2}}$$

where  $\frac{d\sigma}{d\eta}$  and  $\frac{d^2\sigma}{d\eta_1 d\eta_2}$  are the single-particle and two-particle inclusive distributions. They were corrected for the experimental biases as described in [8]; the mean correction per track was less than 10%. Slow protons were subtracted statistically. Their influence is significant for  $\eta < 2.5$ . Fig. 2 shows the variation of  $R_2(\eta_1, \eta_2)$  with  $\eta_2$  for several bins of  $\eta_1$  for C, Al, Cu and Pb nuclei. The error bars are shown for carbon only. They are similar for other nuclei.

We do not observe significant differences between  $R_2(\eta_1, \eta_2)$  distributions for C, Al, Cu and Pb nuclei. To compare these distributions with the  $R_2(\eta_1, \eta_2)$  plot for  $\pi^-p$  interactions at 40 GeV/c published in ref. [2], we used the formula  $\eta = y^{\text{lab}} - 0.25$ . The formula was found empirically by comparing  $\frac{d\sigma}{d\eta}$  and  $\frac{d\sigma}{dy^{\text{lab}}}$  distributions for  $\pi^-p$  events [10]. The correlation functions for nuclear targets agree with the  $\pi^-p$  data shown by the histogram in Fig. 2.

An approximate equality between correlation functions  $R_2(0, y)$  for proton and aluminium targets was reported in the experiment of Ref. [4] using  $\pi^-$  and  $p$  beams at 200 GeV/c.

The  $R_2(\eta_1, \eta_2)$  distributions measured in the interactions of 300 GeV/c protons with Cr and W nuclei [5] are also in

agreement with our data (notice, however, that our statistic is about ten times bigger for each nucleus).

In Table 2 we compare our data in the central region with predictions of the additive quark model - AQM [13,14] and the quasieikonal model - QEM [15,16]. Both models use the formula [17]:

$$R_2^A(y_1, y_2) = \frac{\langle v^2 \rangle - \langle v \rangle^2}{\langle v \rangle^2} + \frac{R_2^N(y_1, y_2)}{\langle v \rangle},$$

which relates the correlation functions for nucleus (A) and nucleon (N) with the "number of interactions" in the nucleus,  $v$ . Here  $y_1$  and  $y_2$  are the C.M. rapidities. The AQM and QEM models differ in predicting  $\langle v^2 \rangle$  and  $\langle v \rangle$  as a function of the atomic number. We calculated the AQM and QEM predictions in the central region using  $\langle v^2 \rangle$  and  $\langle v \rangle$  values presented in [17] and taking the experimental value of  $R_2^N(0,0)$  for  $\pi^-p$  interactions at 40 GeV/c [3]. The experimental values of  $R_2^A(0,0)$  given in Table 2 are calculated by taking the mean value of  $R_2(\eta_1, \eta_2)$  over the region  $2.2 < \eta_1, \eta_2 < 2.5$ . Within error bars both models are consistent with our data, the AQM model seems to provide a slightly better agreement.

### Conclusions

Multiplicity distributions of charged particles produced with pseudo-rapidity  $\eta > 1$  by 40 GeV/c  $\pi^-$ 's on various targets from proton to lead, are consistent with the KNO scaling.

We do not observe noticeable differences in the correlation distributions for C, Al, Cu and Pb nuclei measured in the pseudorapidity range  $\eta > 1$ . There is a good agreement between our data and the results for  $R_2$  function obtained for 40 GeV/c  $\pi^-p$  interactions.<sup>(2)</sup> The results agree within errors with the predictions of the additive quark model<sup>(13,14,17)</sup> and the quasieikonal model<sup>(15,16,17)</sup> however the quark model is preferred.

The authors thank to the propane bubble chamber Collaboration<sup>(10)</sup> for making accessible their 40 GeV/c  $\pi^-p$  data. They are also grateful to Drs. M. Bardašin-Otwinowska, M. Szeptycka and G. Wilk for helpful discussions.

### Referer

#### 1. For

a) 1

b) 1

1

c) 1

M

d) 1

M

#### 2. N. A

#### 3. S. B

#### 4. C. B

#### 5. M. Y.

#### 6. A. B

Pavi

#### 7. B. W

#### 8. A. T.

#### 9. M. A.

#### 10. ABB

K. P.

#### 11. Z. F

#### 12. A. V

#### 13. A. F

389

#### 14. V. V.

Phys

#### 15. Yu. M.

#### 16. A. C

#### 17. E. M.

2780

## References

1. For experimental reviews see, eg:
  - a) W. Busza, Acta Phys. Pol. B8, (1977), 333.
  - b) T. Ferbel, Proc. 19th Int. Conf. on High-energy Physics, Tokyo, 1978, p. 465.
  - c) W. Busza, Proc. 2nd Int. Symp. on Hadron Structure and Multiparticle Production, Kazimierz, 1979, p. 145.
  - d) H. Miettinen, Proc. 21th Int. Conf. on High-energy Physics, Madison, 1980.
2. N. Angelov et al., Journ. of Nucl. Phys. 22, (1975), 122.
3. S. Backovic et al., JINR preprint P1-12777, Dubna 1979.
4. C. Bromberg et al., Nucl. Phys. B171, (1980), 38.
5. M.Y. Lee et al., Phys. Rev. D19 (1979), 55.
6. A. Bialas, Proc. 4th Int. Symp. on Multiparticle Hydrodynamics, Pavia, 1973, p. 93.
7. B. Wosiek, Acta Phys. Pol. B8 (1977), 493.
8. A.T. Abrosimov et al., Nucl. Phys. B158 (1979), 11.
9. M.A. Faessler et al., Nucl. Phys. B157 (1979), 1.
10. ABBWDCMSTTUC Propane Bubble Chamber Collaboration  
K.P. Vishnevskaja, private communication.
11. Z. Koba, H.b. Nielsen and P. Olesen, Nucl. Phys. B40 (1972) 633.
12. A. Wróblewski, Acta Phys. Pol. B4 (1973) 857.
13. A. Bialas, M. Bleszynski and W. Czyż, Acta Phys. Pol. B8 (1977) 389.
14. V.V. Anisovich, Yu.M. Shabelsky and V.M. Shekhter, Nucl. Phys. B133 (1978) 477.
15. Yu.M. Shabelski, Journ. of Nucl. Phys. 26, (1977), 1084.
16. A. Capella and A. Krzywicki, Phys. Rev. D18 (1978) 3357.
17. E.M. Levin, G.M. Ryskin and N.N. Nikolaev preprint CERN TH. 2780 (1979).

TABLE 1. Average multiplicity of charged secondaries.

/upper numbers: all particles included, lower numbers: slow protons ( $0.3 < \beta < 0.7$ ) excluded/

| target $\eta$   | 1.0 - 2.0                          | 2.0 - 3.0                          | 3.0 - 4.0                          | 4.0 - 6.28                         | 1.0 - 6.28                         |
|-----------------|------------------------------------|------------------------------------|------------------------------------|------------------------------------|------------------------------------|
| p <sup>a)</sup> | $1.18 \pm 0.01$<br>$1.12 \pm 0.01$ | $1.48 \pm 0.01$<br>$1.46 \pm 0.01$ | $1.25 \pm 0.01$<br>$1.25 \pm 0.01$ | $0.77 \pm 0.01$<br>$0.77 \pm 0.01$ | $4.68 \pm 0.02$<br>$4.60 \pm 0.02$ |
| C               | $1.65 \pm 0.05$<br>$1.52 \pm 0.12$ | $1.93 \pm 0.06$<br>$1.89 \pm 0.06$ | $1.40 \pm 0.05$<br>$1.39 \pm 0.05$ | $0.66 \pm 0.06$<br>$0.66 \pm 0.06$ | $5.63 \pm 0.12$<br>$5.46 \pm 0.16$ |
| Al              | $1.98 \pm 0.06$<br>$1.69 \pm 0.11$ | $2.27 \pm 0.06$<br>$2.19 \pm 0.07$ | $1.65 \pm 0.05$<br>$1.64 \pm 0.05$ | $0.63 \pm 0.06$<br>$0.63 \pm 0.06$ | $6.52 \pm 0.12$<br>$6.15 \pm 0.15$ |
| Cu              | $2.48 \pm 0.08$<br>$2.06 \pm 0.12$ | $2.42 \pm 0.08$<br>$2.32 \pm 0.08$ | $1.57 \pm 0.06$<br>$1.55 \pm 0.06$ | $0.70 \pm 0.06$<br>$0.70 \pm 0.06$ | $7.18 \pm 0.14$<br>$6.63 \pm 0.17$ |
| Pb              | $3.01 \pm 0.08$<br>$2.34 \pm 0.17$ | $2.55 \pm 0.08$<br>$2.39 \pm 0.09$ | $1.47 \pm 0.06$<br>$1.45 \pm 0.06$ | $0.63 \pm 0.06$<br>$0.63 \pm 0.06$ | $7.66 \pm 0.14$<br>$6.81 \pm 0.21$ |

<sup>a)</sup> Data from  $\pi^-p$  interaction at 40 GeV/c. [10]

TABLE 2. 1

 $\pi$ 

TARGET

h,p

C

Al

Cu

Pb

7) Normal

Fi

Fig. 1 -

Fig. 2 -



TABLE 2. Two particle correlation function  $R_2(0,0)$  for  $\pi^-$  interaction on various targets at 40 GeV/c.

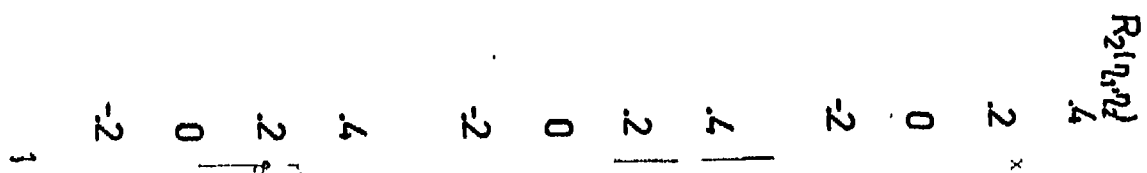
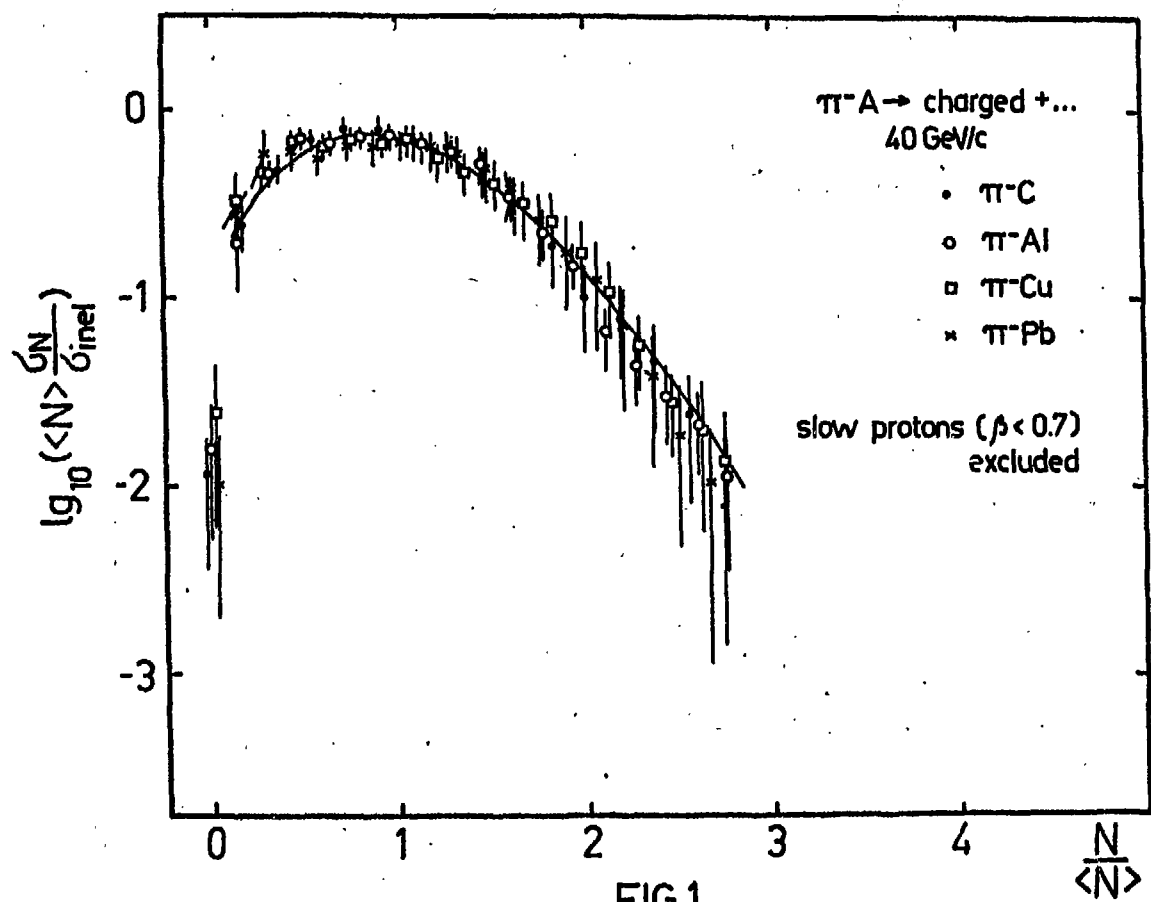
| TARGET | TARGET | data                | AGM                | QEM                |
|--------|--------|---------------------|--------------------|--------------------|
| n,p    | n,p    | $0.44 \pm 0.03$ [3] | 0.44 <sup>*)</sup> | 0.44 <sup>*)</sup> |
| C      | C      | $0.41 \pm 0.15$     | 0.46               | 0.56               |
| Al     | Al     | $0.45 \pm 0.14$     | 0.47               | 0.57               |
| Cu     | Cu     | $0.30 \pm 0.14$     | 0.45               | 0.58               |
| Pb     | Pb     | $0.36 \pm 0.15$     | 0.39               | 0.57               |

<sup>\*)</sup> Normalization point

#### Figure captions

Fig. 1 - Multiplicity distributions for  $\pi^-A$  and  $\pi^-p$  (solid line) interactions in the KNO variables.

Fig. 2 - Two particle correlation function  $R_2(n_1, n_2)$  at several fixed  $n_1$  intervals for  $\pi^-A$  and  $\pi^-p$  interactions at 40 GeV/c. The error bars are shown for carbon only. They are similar for other nuclei.



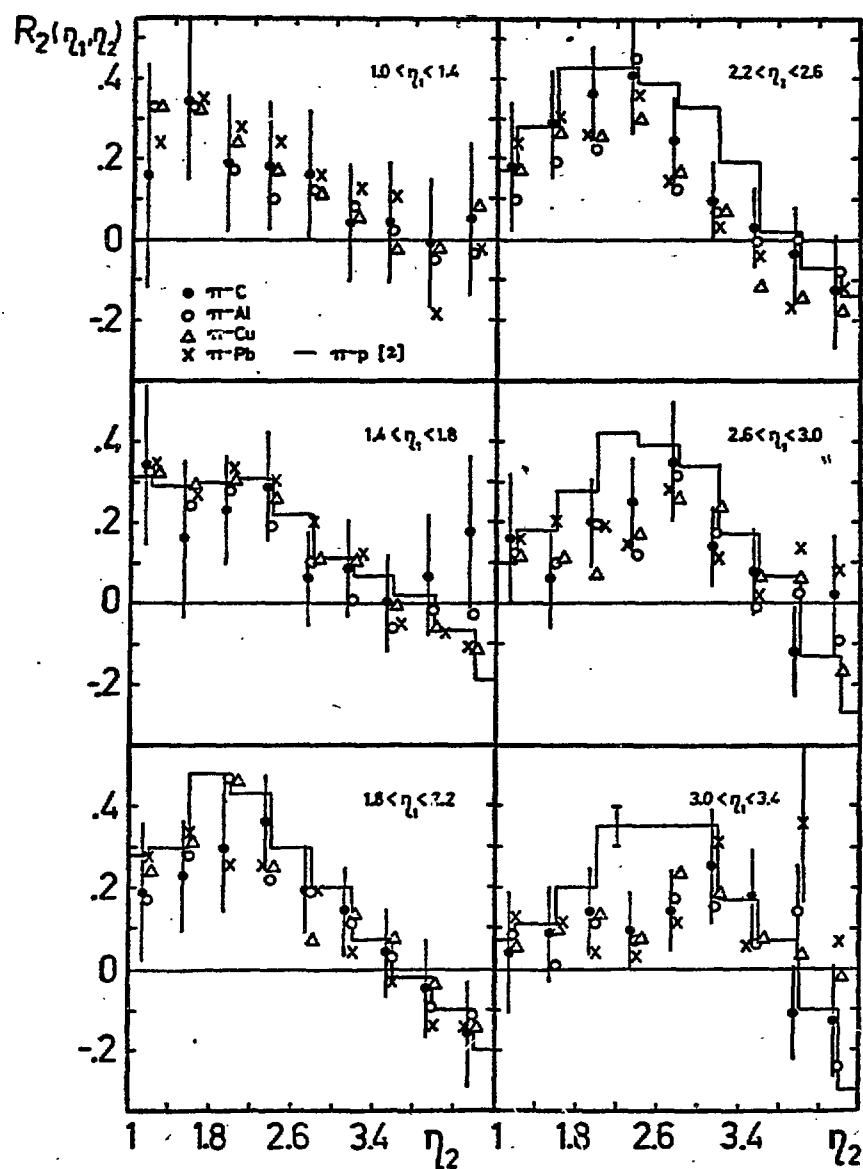
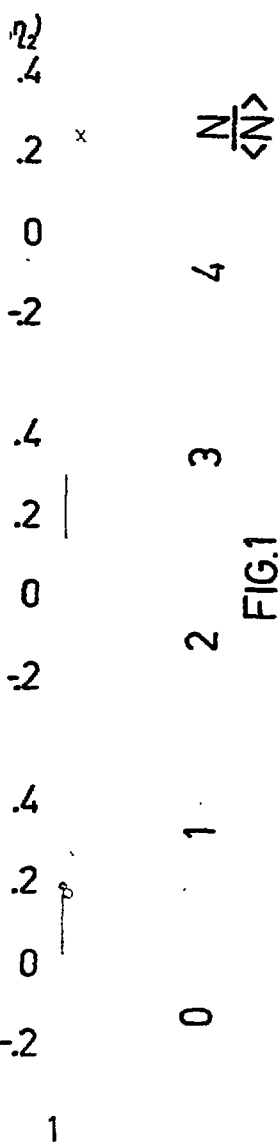


FIG.2.

PION PRODUCTION IN COLLISIONS OF RELATIVISTIC IONS

Helena Białkowska  
Institute of Nuclear Research, Warsaw, Poland

Professor Białas has told why it may be exciting to study nucleus - nucleus collisions at high energy, therefore I feel justified to say a few words about some experimental data. The results I will show come from an extensive study of pion production in the collisions of relativistic ions of d,  $\alpha$  and  $^{12}\text{C}$  with heavy target Ta mounted inside the propane bubble chamber, performed in Dubna, at the energy per nucleon of 4.2 GeV/c. In the same laboratory other experiments study the interactions of relativistic ions, in particular in the streamer chamber with various metallic targets. Some of the results are already published [1], [2]; I will discuss some new data on the following subjects: 1/ rapidity distributions of pions 2/ shape of the multiplicity distributions of pions for various classes of collisions

1. With a  $4\pi$  geometry and good momentum measurements we can compare the rapidity spectra of  $\pi^-$  for various nuclear beams incident on the same nuclear target. Fig.1 shows the ratio of the rapidity spectrum of  $\pi^-$ , /normalized to the full average  $\pi^-$  multiplicity/ in the collisions of  $\alpha$  and  $^{12}\text{C}$  with Ta to the spectrum of  $\pi^-$  from dTa collisions. In this way we compare the production of  $\pi^-$  by various beams to the production by the average (p + n) nucleon. Fig.2 shows the same ratio for the so called "central" events, that is, events where no fast forward beam fragment has been observed.

Two observations can be made. First, there is no preferential region in rapidity for the production of pions - the ratios are flat, within the errors, as a function of rapidity. Second, for the "central" C-Ta collisions, the  $\pi^-$  multiplicity is about 6 times that for dTa, or, in other words, in a central collision, carbon acts approximately as six deuterons.

One may be tempted to compare the observed ratios of  $\frac{dn}{dy}$  with

the predicted  
the following  
very low en

cent

$0 < y$

Mode

3.0

1.9

1.6

2. The mul  
classes of  
nucleons,  
projectile  
of the pro  
spectators  
slow / $p \leq 2$   
the number  
measure of  
This certa  
The estima

Fig.3 show  
for  $\alpha$  Ta a  
proportion  
Fig.4 show  
as a funct

the predictions of Bialas quark model [3]. As can be seen from the following table, the predictions are not far from such relatively low energy data.

| central rapidity region<br>$0 < y < 1.2$ |               | beam fragmentation region<br>$y > 1.2$ |               |
|--|---------------|--|---------------|
| Model                                    | Exp           | Model                                  | Exp           |
| 3.0                                      | $3.6 \pm 0.2$ | 3.4                                    | $4.1 \pm 0.3$ |
| 1.9                                      | $2.1 \pm 0.1$ | 2.1                                    | $2.4 \pm 0.2$ |
| 1.6                                      | $1.7 \pm 0.1$ | 1.7                                    | $1.7 \pm 0.2$ |

2. The multiplicity distributions of pions may differ for different classes of collisions, depending on the number of participating nucleons,  $V$ . The number of charged participant nucleons from the projectile can be evaluated as the difference between total charge of the projectile and the observed number of charged projectile spectators,  $V_p = Z_p - n_{sp}$ . Our detector does not register very slow  $/p \lesssim 250$  MeV/c/ protons-target spectators. Therefore we use the number of knock-out protons  $/250 \text{ MeV/c} \lesssim p \lesssim 800 \text{ MeV/c}/$  as a measure of the number of participant protons from the target,  $V_T$ . This certainly is only an approximate estimation.

The estimate of the number of participant protons is thus evaluated as

$$"V" = V_p + V_T$$

Fig.3 shows the dependence of the average  $\pi^-$  multiplicity on " $V$ " for  $\alpha$ Ta and CTa collisions. For the CTa data there is a clear proportionality between  $\langle n_- \rangle$  and  $V$ .

Fig.4 shows the dispersion  $D_-$  of the  $\pi^-$  multiplicity distribution as a function of  $\langle n_- \rangle$ , for fixed number of participants  $V$ . Here  $D_-$

is not a linear function of  $\langle n_- \rangle$  as is the case for hadron - hadron collisions.

The  $\pi^-$  distributions for fixed  $\sqrt{s}$ , or, physically speaking, for each selected narrow range of the number of nucleons participating in the collision, which may correspond to a narrow range of impact parameter, are not far, but wider than the Poisson distribution.

### References

1. E.O.Abdrahmanov et al., Z.Physik C5,1,/1980/
2. H.H.Agakishiev et al., Preprint INR 1904 /VI /PH/A, Warsaw,1981
3. A.Bialas, Preprint Fermilab - Conf - 79/35 THY, May 1979.

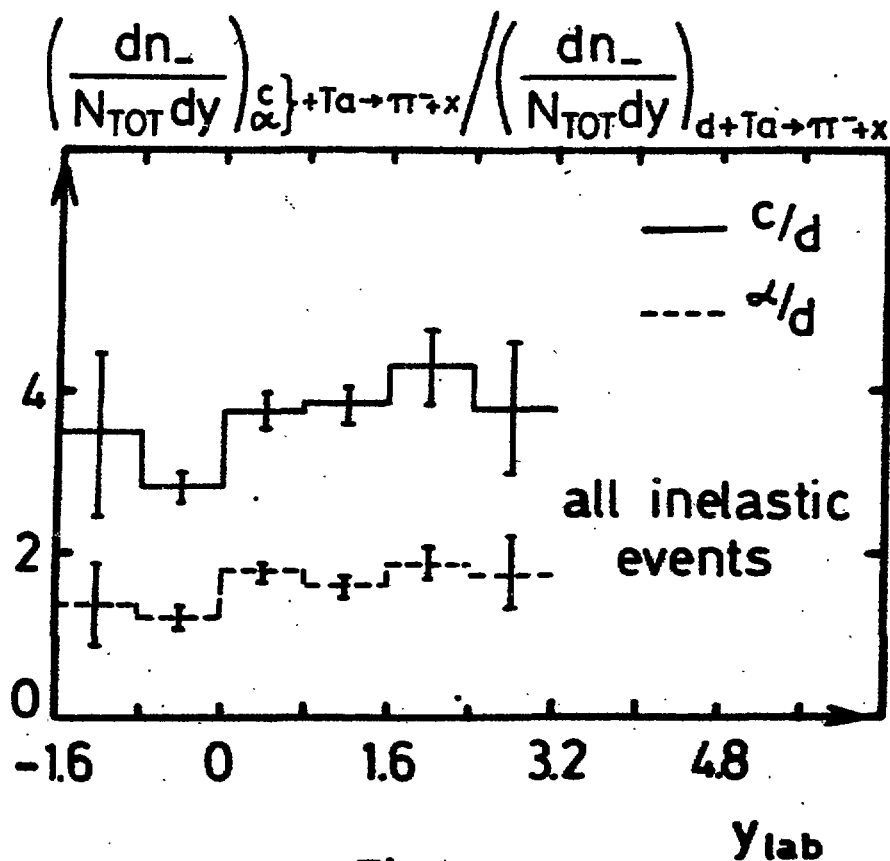


Fig. 1

hadron -

aking, for  
articipating  
e of impact  
tribution.

$$\left( \frac{dn_-}{N_{TOT} dy} \right)_{c}^{+Ta \rightarrow \pi + x} / \left( \frac{dn_-}{N_{TOT} dy} \right)_{d+Ta \rightarrow \pi + x}$$

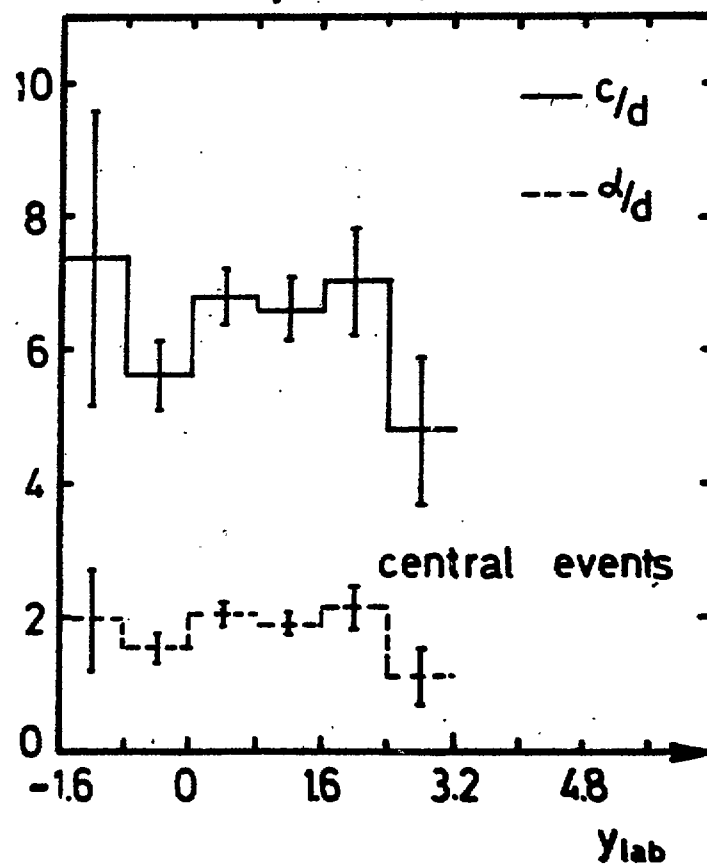
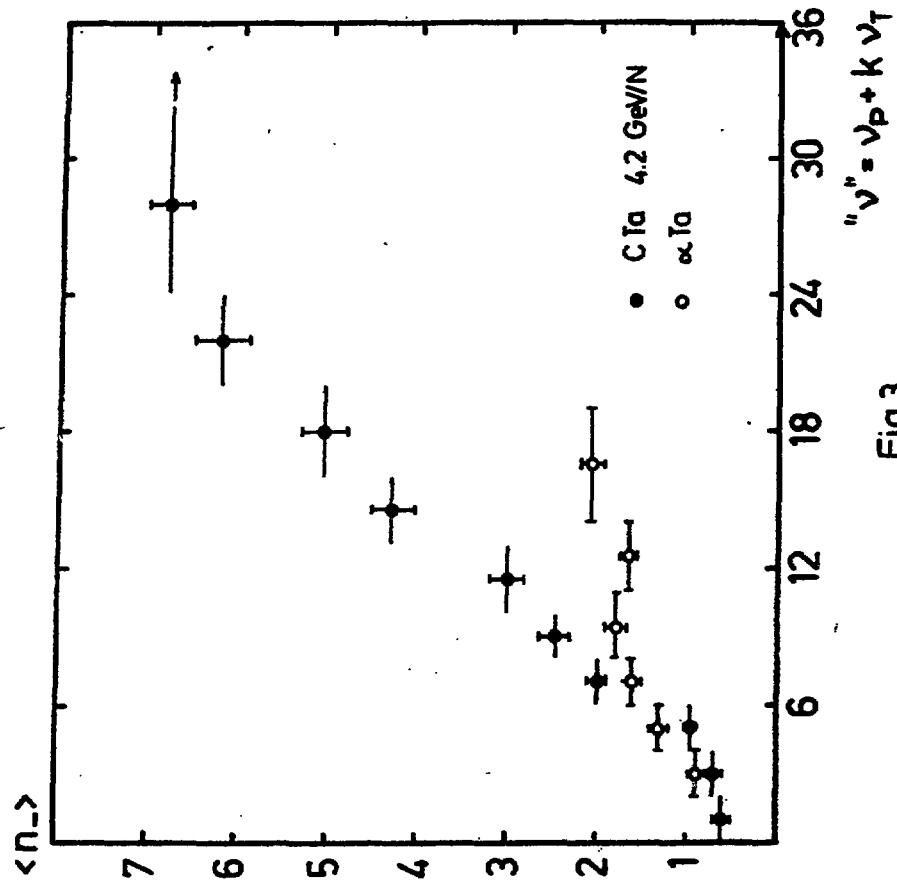


Fig. 2





$$v'' = v_p + k v_T$$

Fig.3

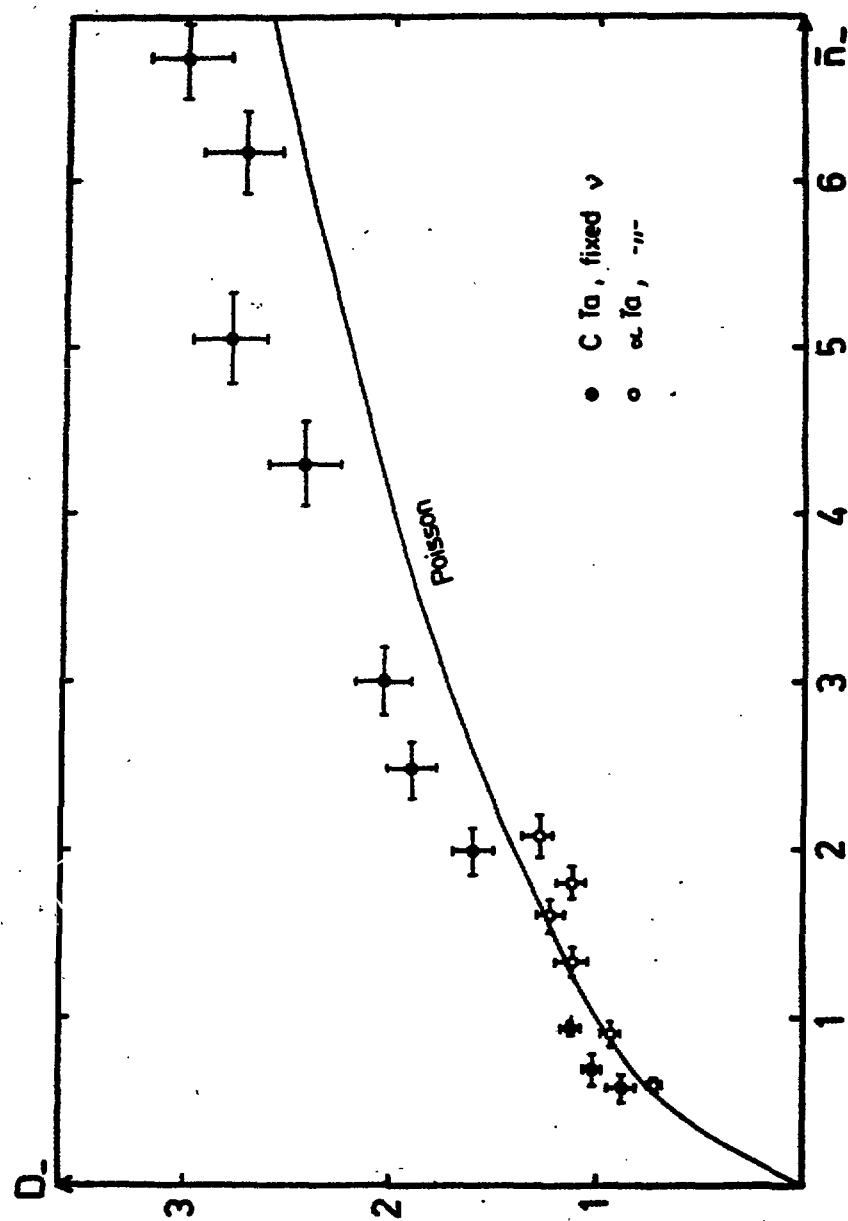


Fig.4

SCOPE OF T

1. Int
2. Ext
3. Le
- 3.1

SPIN PHYSICS AT SHORT DISTANCES AS A MEANS OF STUDYING QCD

M.S. Craigie

International Centre for Theoretical Physics, Trieste, Italy

and

Istituto Nazionale di Fisica Nucleare, Sezione di Trieste, Italy

ABSTRACT

We review how experiments with polarized beams and/or targets can be used to test QCD perturbation theory and to throw some light on the role of next to leading logarithmic orders and power corrections. All the processes we will consider, are the so-called hard processes involving a single short distance scale and are characterized by the remarkable factorization property of parton densities.

(author)

4. Th

References:  
references

1. F.  
(t
2. J.  
K.
3. J.
4. F.  
6
5. N.
6. K.

E OF T

SCOPE OF TALK

- Int 1. Introductory background on factorization of parton probabilities in QCD.
- Ext 2. Extension to polarized hadrons and asymmetries.
- Le 3. Leading order QCD predictions for the processes:
- 3.1. 3.1. Deep-inelastic lepton-proton processes
- $$\bar{e} \vec{P} + e' + X$$
- $$\nu \vec{P} + \mu + X$$
- 3.2. 3.2.  $e \vec{P} + \vec{B} + X$  ( $B = A, Z, A_c \dots$ )
- 3.3. 3.3. Massive lepton pair production
- $$\bar{A} \vec{B} + \mu^+ \mu^- + X$$
- $$\bar{A} B + \mu^+ \mu^- + X$$
- 3.4. 3.4. Hadron production at large transverse momentum
- $$\bar{A} \vec{B} + C + X \quad (C = \pi, K, \text{jet } \dots)$$
- $$\vec{P} \vec{P} + \vec{A} + X$$
- $$P \vec{P} + \vec{A} + X$$
3. 3.5. Prompt photon production at large  $P_T$
- $$\vec{P} \vec{P} + \gamma + X$$
- $$\vec{P} \vec{P} + \gamma + X$$
- $$P \vec{P} + \gamma + X$$
- can  
e role  
pro-  
single  
ation property
- Th 4. The effects of non leading logarithm and power orders in QCD.

ferences:  
ferences

References: The talk will be based on the following material. (Other references to be found therein).

- F. 1. F. Baldrichini, N.S. Craigie, V. Roberto and M. Socolovsky, ICTP/80/148  
(to appear Fortschritt der Physik).
- J. 2. J. Babcock, E. Monsay and D. Sivers, Phys. Rev. D19, 1483 (1979);  
K. Hidaka, E. Monsay and D. Sivers, Phys. Rev. D19, 1503 (1979).
- J. 3. J. Ranft and G. Ranft, Phys. Lett. 77B, 309 (1978).
- F. 4. F. Baldrichini, N.S. Craigie, V. Roberto, M. Socolovsky, Phys. Lett.  
6 96B, 381 (1980).
- N. 5. N.S. Craigie, V. Roberto and D. Whould, ICTP IC/81/20 (Physics Letters?)
- K. 6. K. Hidaka, Westfield College preprint (1980), and Moriond (1980).

7. J. Soffer and P. Taxil 79/p. 1153 C.P.T. (Marseille)
8. References are also made specially to the work of:
  - G. Altarelli, G. Parisi, Nucl. Phys. B126, 298 (1977).
  - M.S. Craigie and H.F. Jones, Nucl. Phys. B165 (1980) and ICTP preprint IC/79/32 (unpublished).
  - K. Ellis, H. Georgi, M. Machacek, H.P. Politzer and G. Ross, Nucl. Phys. B152, 285 (1979).
  - G. Altarelli, K. Ellis and G. Martinelli, Nucl. Phys. B157, 461 (1979).
  - K. Blankenbecler, S. Brodsky and J. Gunion, Phys. Rev. D6 (1972) 2652.
  - H. Politzer, Harvard preprint (1980).

1. INTRO

 $P_A$  $P_B =$ 

Fig. 1.1 (a)

(b)

In the  
Bjorken and o  
by the diagram

 $\sigma^{AB..}(P_A)$ 

where

 $D_A^a(x) =$  $\sigma^{ab..} =$ 

This cross-sect  
which has in a  
despite the a

## 1. INTRODUCTORY BACKGROUND ON FACTORIZATION OF PARTON PROBABILITIES IN QCD

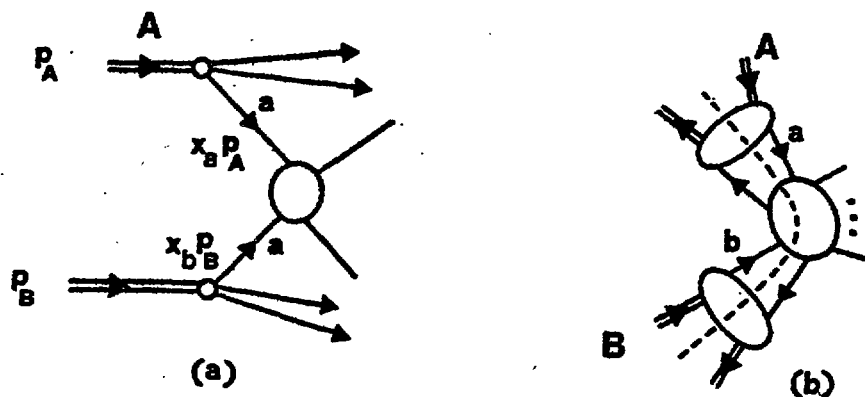


Fig. 1.1 (a) Basic diagram for a hard scattering process involving hadrons A and B.  
 (b) Corresponding blockwise factorization of parton-hadron Green's functions.

In the naive parton model introduced by Feynman, and developed by Bjorken and others, any hard process involving hadrons A, B, ... , is described by the diagram in Fig. 1.1.(a) which leads to the cross-section

$$\sigma^{AB..}(P_A, P_B, \dots) = \sum_{a,b} \int dx_a D_A^a(x_a) \int dx_b D_B^b(x_b) \dots \sigma^{ab..}(x_a P_A, x_b P_B, \dots)$$

where

$D_A^a(x)$  = Probability of finding parton of type  $a$  in hadron A with fraction  $x$  of its momentum.

$\sigma^{ab..}$  = is corresponding cross-section for parton sub-process  $ab + \dots$

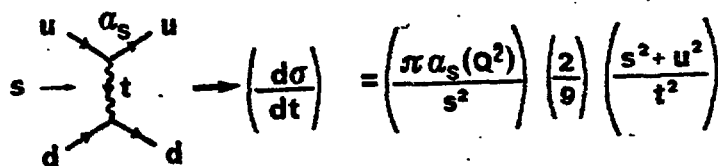
This cross-section corresponds to blockwise factorized diagram in Fig. 1.1.(b) which has in addition the simple property only simple spin averaged quantities occur despite the appearance of off-shell parton-hadron four point Green's functions.

This conjecture has been shown to hold explicitly in the leading order in QCD with the replacements

$$D_A^a(X) \rightarrow D_A^a(X, Q^2)$$

$$\sigma^{ab} \rightarrow \text{Lowest order in } \alpha_s \text{ tree graph cross-section}$$

with  $\alpha_s + \alpha_s(Q^2) = 1/b \log Q^2/\Lambda^2$  ( $b = (33 - 2n_f)/12\pi$ ).  $Q^2$  being the frequency (i.e. momentum) scale characterizing the hard process. An example of  $\sigma^{ab..}$  is  $ud + ud$  corresponding to Fig. (1.2)



$$\left( \frac{d\sigma}{dt} \right) = \left( \frac{\pi \alpha_s(Q^2)}{s^2} \right) \left( \frac{2}{9} \right) \left( \frac{s^2 + u^2}{t^2} \right)$$

Fig. (1.2)

The reason for the dependence on  $Q^2$  can be visualized by noting the radiation of gluons and quark pair creation, leads to multi-parton virtual states Fig. (1.3). The smaller the scale  $\lambda \sim 1/Q^2$ , the more complex the virtual states encountered become.

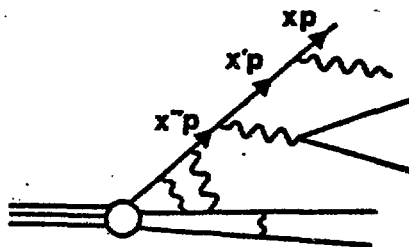


Fig. (1.3)

$$X'' > X' > X$$

Since the densities  $s$  Lipatov, Alt

$$dD^a$$

$$dL_0$$

where the p

Further the

are simply the renormalization in fact calculation processes in Fig. (1.4)

Since the  $Q^2$  dependence comes from QCD perturbation theory, the parton densities satisfy the following simple evolution equation pointed out by Lipatov, Altarelli and Parisi.

$$\frac{dD^a(x, Q^2)}{d \log Q^2/\Lambda^2} = \frac{\alpha_s(Q^2)}{2\pi} \int_x^1 \frac{dz}{z} P_{ab}(z) D^b\left(\frac{x}{z}, Q^2\right)$$

where the parton branching kernel corresponds to the elementary process of QCD

$$q \rightarrow q + g$$

$$g \rightarrow \bar{q} + q$$

$$g \rightarrow g + g$$



Further the moments

$$\gamma_{ab}^n = \int_0^1 dz P_{ab}(z) z^{n-1}$$

are simply the anomalous dimensions, which emerge in the operator product and renormalization group approach to deep-inelastic scattering. The latter are in fact calculable order by order in QCD perturbation theory. For more complex processes involving more than one hadron, we have the physical picture in Fig. (1.4)

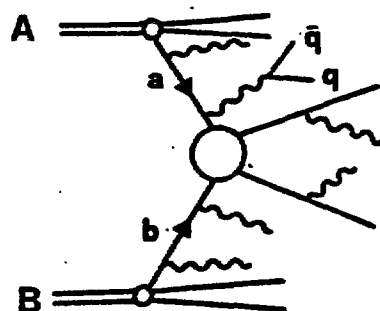


Fig. (1.4)

All the radiative corrections can be summed up in the above formalism in leading order to give the formula

$$\sigma^{AB..} = \int D_A^a(x_1, \omega^1) D_B^b(x_2, \omega^2) \dots \sigma^{ab..}(\dots, \omega_i, \omega^i) [1 + c \alpha_s(\omega^i)]$$

where one can think of the radiative corrections, as simply modifying the parton distribution responsible for the hard process.

A simple way of understanding this factorization is to choose a special physical gauge  $n \cdot A^a(X) = 0$  where  $n = P_A + P_B + \dots$ . In the latter diagrams, which one might expect to destroy the Blockwise factorization in Fig. 1.1 (b), such as Fig. 1.5 (a) in fact vanish in the leading order in QCD, which corresponds to sums of ladder diagrams in each channel Fig. 1.5 (b). In this gauge the gluon propagator has the form  $D_{\mu\nu}(K, n) = [-g_{\mu\nu} + (K_\mu n_\nu + K_\nu n_\mu) / K \cdot n + \dots] / K^2$ . Hence Fig. (1.5)(a) is proportional to

$$P_A^\mu [-g_{\mu\nu} + (K_\mu n_\nu + K_\nu n_\mu) / K \cdot n] P_B^\nu$$

$$= -P_A \cdot P_B + P_A \cdot P_B \frac{K \cdot [P_A + P_B]}{K \cdot [P_A + P_B]}$$

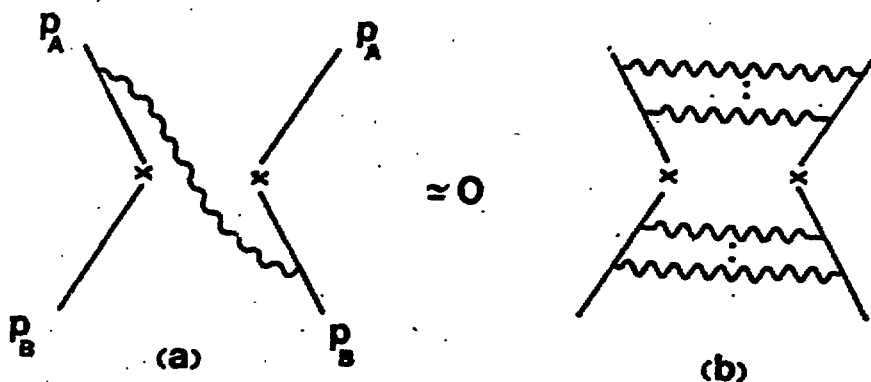


Fig.(1.5)

There exists an all orders proof of this factorization property, involving factorization of mass singularities in perturbation theory. However although we can always formally write

$$\sigma^{AB..} = \int D_A^a D_B^b \dots \sigma^{ab..}$$

It is not  
parton of  
section.  
in each  
a better  
As  
 $D(X, q^2)$   
but in f  
Symbolic

The latter  
momentum di  
in QCD. Th

2.

If  
definite he


$$\sigma^{AB..}(h_A)$$

where  $h_A$ ,  
which is not  
to hold in 1  
only two he  
extended to  
of the latte  
to helicity  
De



It is not clear to me that one can interpret  $D_A^a$  as the probability of finding parton of type  $a$  in hadron  $A$  and  $\sigma^{ab} \dots$  as the corresponding cross-section. In particular it seems unlikely one can associate definite helicity in each channel. For this reason spin physics will be valuable in providing a better insight into this question.

As a final remark on factorization, the parton density functions  $D(X, Q^2)$  are not the Bethe-Salpeter amplitudes in each parton-hadron amplitude but in fact integrals over the transverse momentum associated with the latter. Symbolically

$$D(x, Q^2) = \int d^2 k \cdot \text{[diagram]}$$


The latter means, in particular one does not feel the primordial transverse momentum distributions (i.e. Fermi motion of the partons) in the leading order in QCD. The latter is only evident in higher power corrections.

## 2. EXTENSION OF QCD FACTORIZATION TO POLARIZATION ASYMMETRIES

If we now turn to processes, in which the hadrons  $A, B, \dots$  carry definite helicities  $h_A, h_B, \dots$ , then the corresponding formula is:

$$\sigma^{AB\dots}(h_A, h_B, \dots) = \sum_{h_a, h_b, \dots} \int D_A^a(h_A, h_a) D_B^b(h_B, h_b) \dots \sigma^{ab\dots}(h_a, h_b, \dots)$$

Fig.(1.5)

where  $h_a, h_b, \dots$  are the corresponding parton helicities. The diagonal sum, which is not completely obvious from the blockwise factorization can be shown to hold in leading order in QCD. Further in this order gluons like quarks have only two helicity states  $h = \pm$ . In principle all our considerations can be extended to transverse spin asymmetries, however I do not think the treatment of the latter is fully understood. In this talk we will restrict our remarks to helicity asymmetries.

Defining

$$D_A^a = \frac{1}{2} [D_A^a(+,+) + D_A^a(-,+)] \quad (\text{Spin Ave})$$

$$\Delta D_A^a = \frac{1}{2} [D_A^a(+,+) - D_A^a(-,+)] \quad (\text{helicity diff.})$$

We can write the double asymmetry

$$\Delta \sigma^{AB..} = \sigma^{AB..} (+,+) - \sigma^{AB..} (+,-)$$

in the form

$$\Delta \sigma^{AB..} = \left[ \Delta D_A^a \Delta D_B^b \dots \Delta \sigma^{ab..} \right] [1 + O(\alpha_s)]$$

Further  $\Delta D_A^a$  satisfies the evolution or B.S. equation

$$\Delta D_A^a(x, q^2) = \Delta D_A^a(x, q_0^2) + \int_{q_0^2}^{q^2} \frac{dk^2}{k^2} \alpha_s(k^2) \int_x^1 \frac{dz}{z} \Delta P_{ab}(z) \Delta D_A^b\left(\frac{x}{z}, k^2\right)$$

where

$$\Delta P_{ab}(z) = \left| \begin{array}{c} + \\ \diagup \\ + \end{array} \right|^2 - \left| \begin{array}{c} - \\ \diagup \\ + \end{array} \right|^2$$

$\Delta D_A^a$  is a measure of the polarization of the parton flux relative to that of the incident hadron (i.e. the amount of helicity transfer to the active partons in the hard scattering process). For example if  $\Delta D_A^a = D_A^a$  then parton  $a$  carries away 100% of the polarization of  $A$ . This might be expected for the leading  $u$ -quark inside the proton as  $X \rightarrow 1$  (Fig. 1.6).



Fig. 2.1.

Single hel  
transverse  
Measuremen  
way of st  
F  
measured  
and  $\Delta \sigma^{ab}$

A =

and each r  
much of th  
partons in

factoriza  
of QCD,  
with a ga  
in a  
order uni

3.

3.1.

E

which is  
Fig. 3.1.

Single helicity asymmetries vanish, because of parity. This is not true for transverse spin asymmetries. The latter however vanish in leading order in QCD. Measurement of transverse spin asymmetries, may therefore provide a valuable way of studying non leading effects.

Finally let us note that because of the factorization property, if the measured asymmetry  $\Delta\sigma^{AB..}/\sigma^{AB..}$  is of order unity, then  $\Delta D_A^a/D_A^a \sim 1$  and  $\Delta\sigma^{ab..}/\sigma^{ab..} \sim 1$ , since

$$A = \frac{\Delta\sigma^{AB..}}{\sigma^{AB..}} = \left| \frac{\langle \Delta D_A^a \rangle}{\langle D_A^a \rangle} \frac{\langle \Delta D_B^b \rangle}{\langle D_B^b \rangle} \dots \frac{\langle \Delta\sigma^{ab..} \rangle}{\langle \sigma^{ab..} \rangle} \right|$$

and each factor is less than unity. Hence a large measured asymmetry, means much of the helicity of the incident protons is transmitted to the particular partons involved in the hard sub-processes.

Conversely. In some cases asymmetries are small, because of the factorization structure and the fact each factor is less than unity. One feature of QCD, which will be apparent in what follows, is that because we are dealing with a gauge theory like QED, the basic processes transmit or reflect helicity in a remarkably simple way and most basic asymmetries  $\Delta\sigma^{ab}/\sigma^{ab}$  are of order unity.

### 3. LEADING ORDER QCD PREDICTIONS

#### 3.1. Deep inelastic scattering and parton spin distributions

Here let us concentrate on the reactions

$$\vec{e} \vec{p} \rightarrow e' + X$$

$$\nu \vec{p} \rightarrow (\mu, \nu) + X$$

which is described by the variables  $v = p \cdot q$   $X = -q^2/2v$  and  $y = v/E$ . See Fig. 3.1.

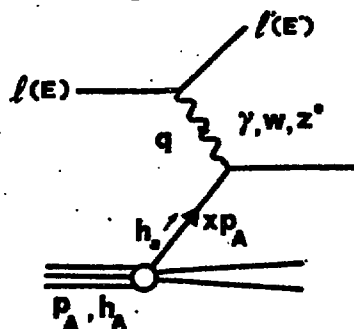


Fig. (3.1)

In deep-inelastic scattering, with polarized leptons off polarized nucleon targets in addition to the usual structure functions  $W_1$  and  $W_2$  we have two new ones  $G_1$  and  $G_2$ . In fact we write the hadronic tensor  $W^{\mu\nu}(p, q, S_A)$  in the form

$$W^{\mu\nu} = (-g^{\mu\nu} + \dots) W_1 + \frac{1}{M} (p^\mu p^\nu + \dots) W_2 \\ + \frac{4i}{V} \epsilon^{\mu\nu\lambda\sigma} q_\lambda [S_{A\sigma} G_1 + (S_{A\sigma} - \frac{S_{A\cdot} q_\sigma}{p \cdot q}) G_2]$$

where  $S_A$  is proton spin or helicity vector. The parton model gives

$$2 G_1(x, q^2) = \sum_f e_f^2 \Delta D_N^f(x, q^2) \quad (\text{helicity}) \\ 2 [G_1(x, q^2) + G_2(x, q^2)] = \sum_f e_f^2 S_2 D_N^f(x, q^2) \quad (\text{spin})$$

The latter corresponds to transverse spin asymmetry and follows from the naive parton model, in which the parton have non zero mass and are put on shell. However the operator product expansion apparently leads to different anomalous dimensions (i.e. scaling behaviour for  $G_1 + G_2$ ) depending on the renormalization scheme and whether there are mass terms or not. (i.e. if we have an exact chiral symmetry or if it is explicitly broken by quark mass terms).

The structure functions  $G_1$  and  $G_2$  satisfy the Bjorken sum rules

$$(1) \quad \int_0^1 dx [G_1^p(x) - G_1^n(x)] = \frac{1}{3} \frac{C_N}{C_V} \cdot \left( \frac{C_N}{C_V} \approx 4.33 \right)$$

(2)

which implies

$$\int_0^1 dx$$

This has the fact have to

For asymmetry fo

$$\tilde{A}_{LL}^v(x, y, q)$$

and

$$\tilde{A}_{LL}^s(x, y)$$

respectively.

$$\tilde{A}_{LL}^v$$

$$\tilde{A}_{LL}^s =$$

$$(2) \quad \int_0^1 dx \, G_2^P(x) = \int_0^1 dx \, G_2^n(x) = 0$$

which implies

$$\int_0^1 dx \left[ \Delta D_P^u - \Delta D_P^d + \Delta D_P^{\bar{u}} - \Delta D_P^{\bar{d}} \right] = \frac{c_A}{c_V}$$

This has the important consequence, that the  $\Delta D_P^i$  cannot all vanish and in fact have to be quite large.

For neutrino scattering off polarized targets, the basic left-right asymmetry for  $(\nu, \bar{\nu})\vec{P} \rightarrow \mu\vec{X}$  is given by

$$\tilde{A}_{LL}^{\nu}(x, y, Q^2) = \frac{-\sum_q \Delta D_N^q(x, Q^2) + (1-y)^2 \sum_{\bar{q}} \Delta D_N^{\bar{q}}(x, Q^2)}{\sum_q D_N^q(x, Q^2) + (1-y)^2 \sum_{\bar{q}} D_N^{\bar{q}}(x, Q^2)}$$

and

$$\tilde{A}_{LL}^{\bar{\nu}}(x, y, Q^2) = \frac{-(1-y)^2 \sum_q \Delta D_N^q(x, Q^2) + \sum_{\bar{q}} \Delta D_N^{\bar{q}}(x, Q^2)}{(1-y)^2 \sum_q D_N^q(x, Q^2) + \sum_{\bar{q}} D_N^{\bar{q}}(x, Q^2)}$$

respectively. Using the Cabbibo theory, we find below the charm threshold

$$\tilde{A}_{LL}^{\nu} = \frac{-\Delta D_N^d(x, Q^2) + (1-y)^2 \Delta D_N^{\bar{u}}(x, Q^2)}{D_N^d(x, Q^2) + (1-y)^2 D_N^{\bar{u}}(x, Q^2)}$$

$$\tilde{A}_{LL}^{\bar{\nu}} = \frac{-(1-y)^2 \Delta D_N^u(x, Q^2) + \Delta D_N^{\bar{d}}(x, Q^2)}{(1-y)^2 D_N^u(x, Q^2) + D_N^{\bar{d}}(x, Q^2)}$$

Hence from the  $y$  distributions one can clearly separate valence quark distributions from the sea quark. A rough estimate of the order of magnitude of these asymmetric near  $x \rightarrow 1$ ; where one can neglect the sea, one finds

$$A_{LL}^{\nu} = - \frac{\Delta D_N^d(x, q^2)}{D_N^d(x, q^2)} \sim \begin{cases} 1/3 & N=p \\ -2/3 & N=n \end{cases}$$

$$A_{LL}^{\bar{\nu}} = - \frac{\Delta D_N^u(x, q^2)}{D_N^u(x, q^2)} \sim \begin{cases} -2/3 & N=p \\ 1/3 & N=n \end{cases}$$

where the values corresponds to a simple SU(6) model.

Together the spectrum of lepton deep-inelastic processes can be used to determine the parton helicity distributions, in much the same way as the unpolarized densities. One can obtain light nuclear targets, which are over 70% polarized, so these experiments become feasible, particularly with polarized muons. The neutrino experiments of course will be much harder.

As yet there is little data on the  $\Delta D_A^s$ , so one tends to use models which are constructed so as to satisfy the Bjorken sum rules mentioned above. Throughout I will use two very different models, as an indication of what we might hope to find experimentally from spin measurements in hard processes.

#### 1. Conservative Model [Babcock, Monsay and Sivers]

Valence quarks carry a large fraction of the helicity for all  $x$ , however the sea quark helicity asymmetry is adjusted so as to satisfy sum rules. Primordial ( $Q^2 = Q_0^2 \sim 10 \text{ GeV}^2$ ) parton densities for this model are:

$$\Delta u(x) = .44 u(x)$$

$$\Delta d(x) = -.35 d(x)$$

$$\Delta \bar{q}_v(x) = .2 x(2-x) \bar{q}_v(x)$$

$$\bar{q}_v(x) = \frac{6}{x} (1-x)^{10}$$

2. Cr

V

unpolarize

The gluon  
simple qua  
which  
fast valen  
Fo.

while for t

The latter  
the models

This is the  
One  
spin densit  
valence qua  
the Conserv

2. Carlitz-Kaur Model

Valence quarks carry most of the helicity as  $x \rightarrow 1$ . The sea remains unpolarized

$$\left. \begin{aligned} q_v(x) &= \frac{4}{9} u(x) + \frac{1}{9} d(x) \\ \Delta q_v(x) &= \frac{4}{9} u(x) - \frac{1}{9} d(x) \end{aligned} \right\} \begin{aligned} u(x) &= 6[(1-x)^3 + .43(1-x)^4] \\ d(x) &= 5[1-x]^4 \end{aligned}$$

The gluon distributions are calculated from the quark distributions, from a simple quark-gluon bremsstrahlung model. The assumption is that fast gluons, which dominate the momentum sum rule, result from bremsstrahlung off fast valence quarks..

For the conservative model

$$\begin{aligned} \Delta G(x) &= .66(2-x)x(1-x)^6 \\ G(x) &= 1.97(1-x)^6 [1 + (1-x)^2] \end{aligned}$$

while for the Carlitz-Kaur model, we use

$$\begin{aligned} \Delta G(x) &= (-.08 + 1.67x - .63x^2) G(x) \\ G(x) &= 3.68 [1 + .1(1-x) - .02(1-x)^2 - .1(1-x)^3] [1-x]^4 \end{aligned}$$

The latter we call the leading quark gluon bremsstrahlung model (LQGB). In both the models

$$\frac{\Delta G(x)}{G(x)} \rightarrow \frac{\Delta q_v(x)}{q_v(x)} \quad \text{as } x \rightarrow 1$$

This is the property of helicity conservation in the bremsstrahlung process.

One can now use the evaluation equations to determine  $Q^2$  dependant spin densities  $\Delta D(x, Q^2)$ . To give an idea of the size of  $\Delta D/D$  for the valence quark inside the proton, we have plotted in Fig. (3.2)(a) and (b) the Conservative and Carlitz-Kaur models respectively.

$$\Delta D_p^u(x, Q^2) / D_p^u(x, Q^2)$$

Spin Asymmetry

CONSERVATIVE MODEL

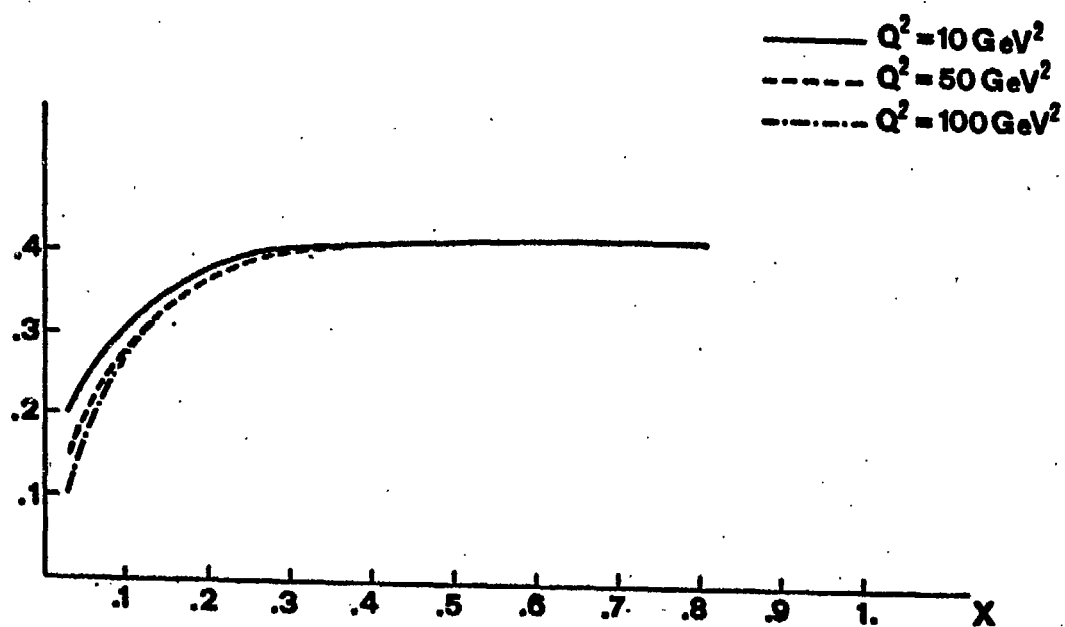


FIG 3.2 (a)

227



FIG 3.2 (a)

$$\Delta D_p^u(x, Q^2) / D_p^u(x, Q^2)$$

Spin Asymmetry

CARLITZ KAUR MODEL

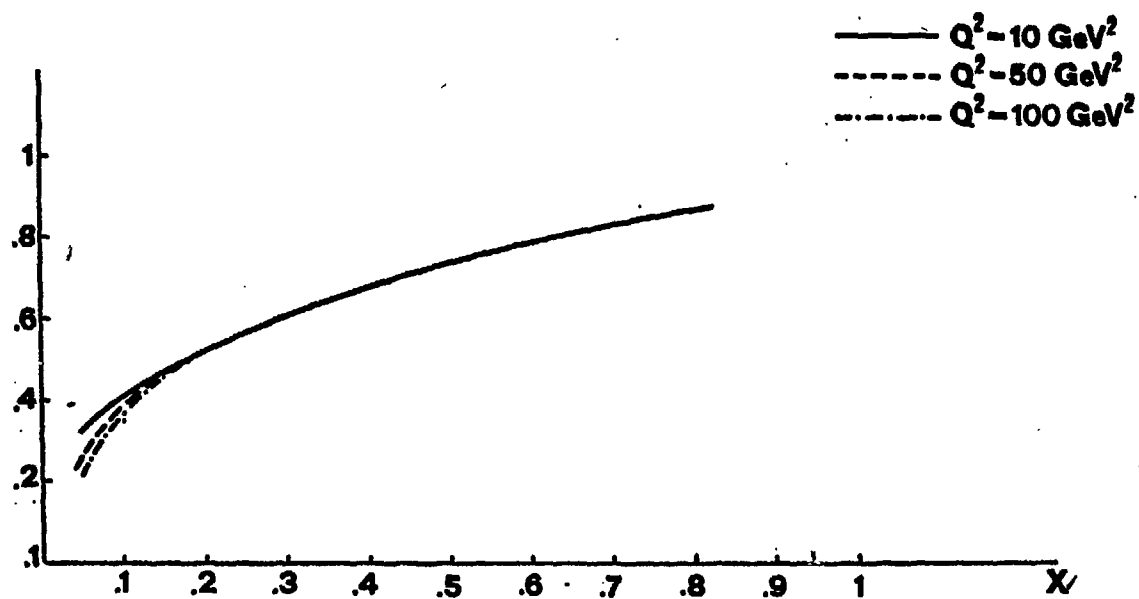


FIG 3.2 (b)

3.2.  $e^+ \bar{P} + e^- B + X$  where  $B = \Lambda, \Sigma, \Lambda_c \dots$

Before leaving deep-inelastic scattering, one interesting process, which is possible within the existing muon beam set up at the SPS, is the inclusive production of  $\Lambda, \Sigma$  etc., in which the decay distribution of the detected hadron is used to determine its helicity distribution.

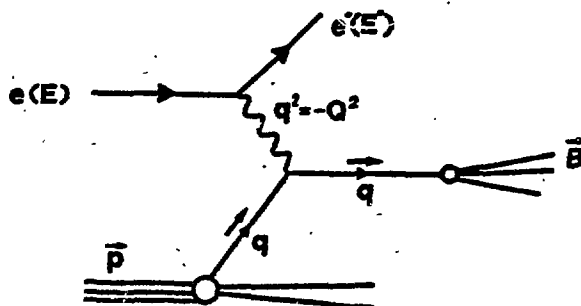


Fig. (3.3)

Variables:  $x = Q^2/2\nu$ ,  $y = E/\nu$ ,  $z = E_B/E_q = E_B/\nu$  where  $\nu = p \cdot q$ .

The unpolarized cross-section is given by:

$$\frac{d\sigma^B}{dz} = N \left[ \sum_f e_f^2 D_f^f(x, Q^2) \bar{D}_{f \rightarrow B}(z, Q^2) \right]$$

where  $\bar{D}_{f \rightarrow B}$  is probability of finding hadron  $B$  in a jet corresponding to parton  $f$ , with fraction  $z$  of the energy. The latter is measured in the process  $e^+ e^- \rightarrow B + \text{anything}$ , and all the considerations for parton densities go through for fragmentation functions.

The basic transmitted (from initial to final state) asymmetry for this process is given by:

$$A_{LL}^{is} = \frac{\frac{d\sigma}{dz}(+,+) - \frac{d\sigma}{dz}(+,-)}{\frac{d\sigma}{dz}(+,+) + \frac{d\sigma}{dz}(+,-)}$$

$[d\sigma(h_p, \lambda)$   
helicity

$i_s$   
 $A_{LL}^{is}$

In partic

$i_s$   
 $A_{LL}^{is}$

Hence this  
quarks car  
Gunion and  
 $\bar{D}_S \rightarrow \Lambda$  fo  
and fr  
urbati

3.3. Ma  
To

Also the p  
Th  
correspon

$(d\sigma(h_p, h_B))$  being the cross-section for proton helicity  $h_p$  and  $B$  with helicity  $h_B$  is given in leading order in QCD by:

$$A_{LL}^{if} = - \frac{\sum_f e_f^2 \Delta D_f^S(x, Q^2) \Delta \bar{D}_{f \rightarrow B}(z, Q^2)}{\sum_f e_f^2 D_f^S(x, Q^2) \bar{D}_{f \rightarrow B}(z, Q^2)}$$

In particular for  $e^+ \bar{p} \rightarrow e^+ \Lambda + X$  we have:

$$A_{LL}^{if} = - \frac{\Delta D_p^S(x, Q^2)}{D_p^S(x, Q^2)} \frac{\Delta \bar{D}_{S \rightarrow \Lambda}(z, Q^2)}{\bar{D}_{S \rightarrow \Lambda}(z, Q^2)}$$

Hence this process provides a direct way of measuring the degree to which sea quarks carry the proton helicity. The leading quark ideas of Brodsky,

Gunion and others, would suggest for the fragmentation function  $\Delta \bar{D}_{S \rightarrow \Lambda} \sim$

$\bar{D}_{S \rightarrow \Lambda}$  for  $z \rightarrow 1$ . Note if we accept the argument given earlier that  $\Delta G/G \rightarrow 1$  as  $x \rightarrow 1$

and further that fast anti-quarks come from gluons converting to pairs, then perturbation theory would predict  $\Delta \bar{q}/\bar{q} \rightarrow 1$  as  $x \rightarrow 1$ , i.e.  $A_{LL}^{if} \rightarrow -1$  as  $x \rightarrow 1, z \rightarrow 1$ .

### 3.3. Massive Lepton Pair Production and Drell-Yan

There are 4 useful variations here

- 1)  $\vec{p} \vec{p} \rightarrow \mu^+ \mu^- + X$
- 2)  $\vec{p} \vec{p} \rightarrow \mu^+ \mu^- + X$
- 3)  $\vec{p} A \rightarrow \mu^+ \mu^- + X$
- 4)  $H \vec{p} \rightarrow \mu^+ \mu^- + X$  ( $H = \pi, \pi, \kappa, \dots$ )

Also the production of heavyonium states should be added to the list here.

This process is described by the much discussed Drell-Yan mechanism, corresponding to the diagram

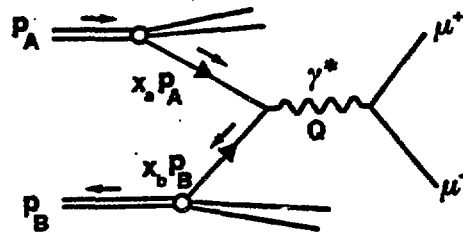


Fig. (3.4)

Variables

$$x_A = \frac{1}{2} \left[ \sqrt{x_F^2 + 4Q^2/s} + x_F \right]$$

$$x_B = \frac{1}{2} \left[ \sqrt{x_F^2 + 4Q^2/s} - x_F \right]$$

$$x_F = 2Q_e/\sqrt{s} = 2(p_{p^+} + p_{p^-})_z/\sqrt{s}$$

The basic cross-section for  $q(h) + \bar{q}(h') \rightarrow \mu^+ \mu^-$  which is proportional to

$$|M_{hh'}|^2 = \left| \begin{array}{c} q(h) \\ \diagdown \quad \diagup \\ \text{---} \text{---} \text{---} \\ \diagup \quad \diagdown \\ \bar{q}(h') \end{array} \right|^2$$

has  $|M_{++}|^2 = 0$  by helicity conservation.

i.e.  $\begin{array}{c} \rightarrow \quad \leftarrow \\ \text{---} \quad \text{---} \end{array} \quad \lambda = 0$

$\begin{array}{c} \rightarrow \quad \rightarrow \\ \text{---} \quad \text{---} \end{array} \quad \lambda = 1$

( $\lambda$  being photon helicity)

Hence the basic asymmetry  $A_{LL}^{if} = -1$ . The corresponding asymmetry formula for the whole process is given by:

$$A_{LL}^{ii} = -$$

For  $\vec{p}\vec{p}$

A

and  $V =$

The pre  
in Fig.

$$A_{LL}^{ii}$$

0.5

$$A_{LL}^{ii} = - \frac{\sum_f e_f^2 [\Delta D_A^f(x_0, q^2) \Delta D_B^{\bar{f}}(x_0, q^2) + (f \neq \bar{f})]}{\sum_f e_f^2 [D_A^f(x_0, q^2) D_B^{\bar{f}}(x_0, q^2) + (f \neq \bar{f})]}$$

For  $\bar{p}p \rightarrow \mu\mu + x$  at  $x_F = 0$ , this formula reduces to

$$A_{LL}^{ii} = - \frac{\Delta V(x)}{V(x)} \frac{\Delta S(x)}{S(x)} \quad \text{with } x = M_{\mu\mu}/\sqrt{s}$$

$$\text{and } V = \frac{4}{9} U(x) + \frac{1}{9} d(x).$$

Hence asymmetry depends on polarization of sea quarks

$$\text{i.e. } A_{LL}^{ii} = 0 \quad \text{for Cavity-Kauv Model}$$

The predicted leading order asymmetry for the conservative model is shown in Fig. (3.5)

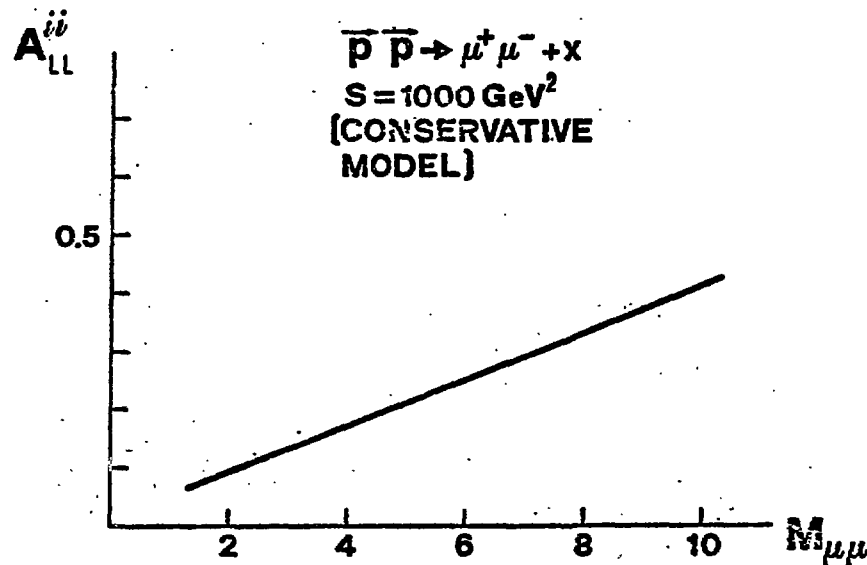


Fig. 3.5

GeV →

On the other hand  $\bar{p}p \rightarrow \mu\mu + x$  is dominated by valence quarks, so for large  $x = M_{\mu\mu}/\sqrt{s}$ , we have

$$A_{LL}^{ii} \approx - \left[ \frac{\Delta u(x)}{u(x)} \right]^2$$

The corresponding asymmetry is large and is given in Fig. 3.6.

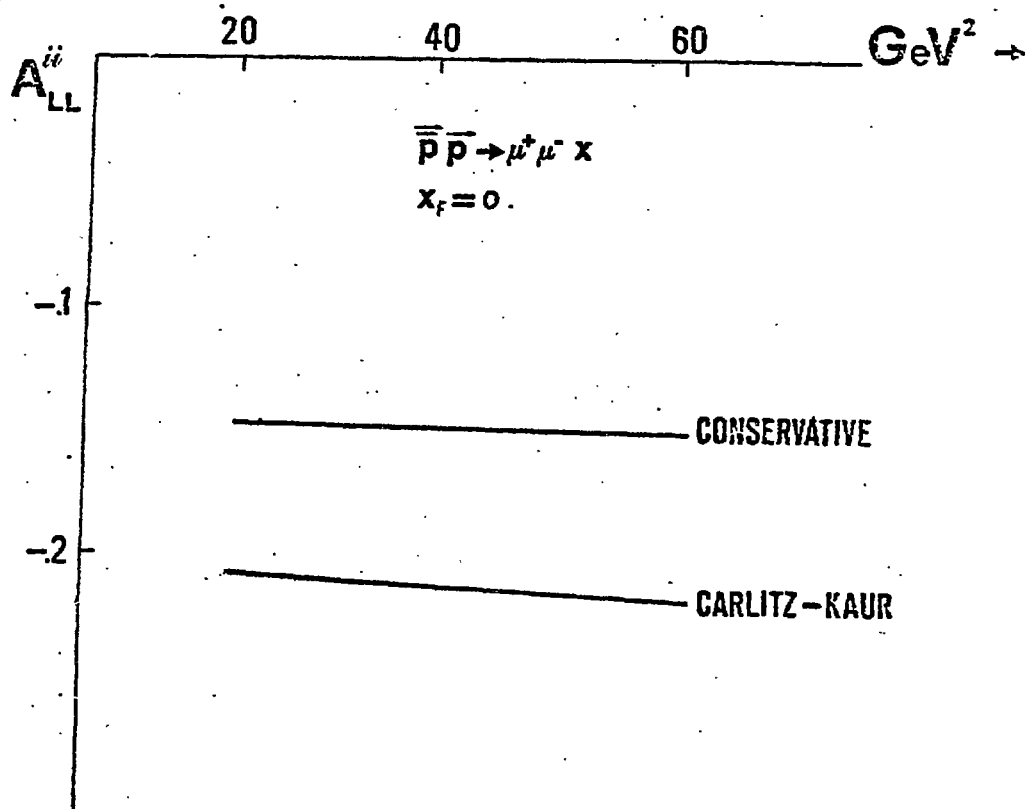


FIG 3.6

target,  
expe  
and T

where

The co  
is giv

$A_{LL}^{ii}$

The C

$A_{LL}^{if}$

.5

The transmitted asymmetry:  $\vec{P} A \rightarrow \vec{\mu} \mu + x$  with a polarized beam (or target) also provides an interesting measurement. It of course relies on the experimentally difficult determination of the muon helicity. However Soffer and Taxil claim this is feasible. The basic asymmetry is given by

$$A_{LL}^{if}(\vec{q} \vec{q} \rightarrow \vec{p} p) = - \frac{\hat{t}^2 - \hat{u}^2}{\hat{t}^2 + \hat{u}^2}$$

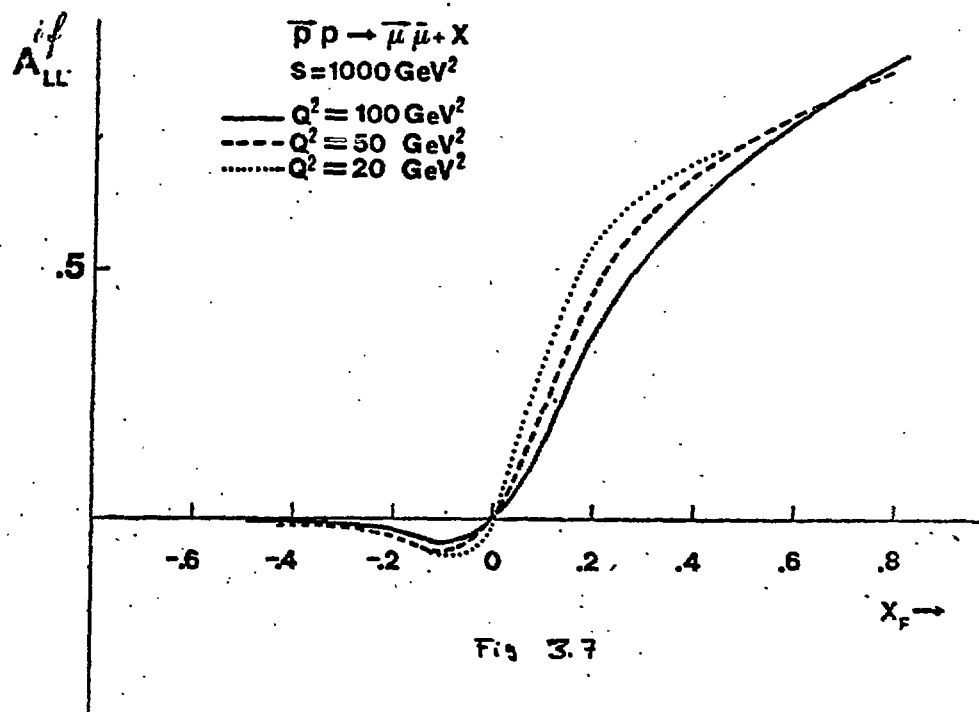
where  $\hat{t} = x_a t$ ,  $\hat{u} = x_b u$  and

$$t = (p_a - p_p)^2 ; u = (p_b - p_p)^2$$

The corresponding asymmetry integrated over the muon angular distributions is given by

$$A_{LL}^{if} = - \left\{ \frac{x_a^2 - x_b^2}{x_a^2 + x_b^2} \right\} \frac{\sum_i e_i^2 [\Delta D_p^f(x_a) D_A^{\bar{f}}(x_b) - \Delta D_p^{\bar{f}}(x_a) D_A^f(x_b)]}{\sum_i e_i^2 [D_p^f(x_a) D_A^{\bar{f}}(x_b) + D_p^{\bar{f}}(x_a) D_A^f(x_b)]}$$

The Corresponding prediction as shown in Fig. 3.7

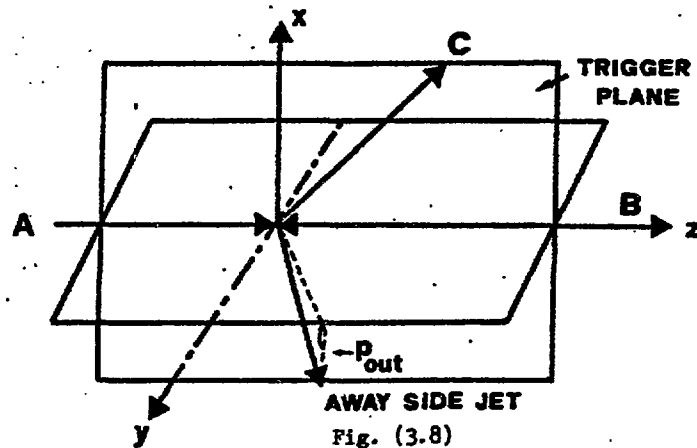


3.4. Hadron Production at large  $P_T$ 

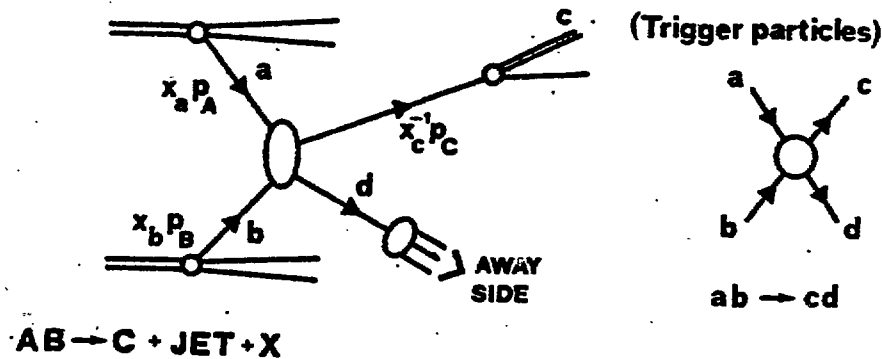
Hence one considers processes like

$$\begin{aligned} \vec{p}_A + \vec{p}_B &\rightarrow C + X \\ \vec{p}_A + \vec{p}_B &\rightarrow C + X \\ \vec{p}_A + \vec{p}_B &\rightarrow B + X \\ \vec{p}_A + \vec{p}_B &\rightarrow B + X \end{aligned} \quad \begin{aligned} C &= \pi, \mu, \text{jet} \\ B &= \Lambda, \Lambda_c, \dots \end{aligned}$$

which are triggered by selecting a particle or jet of particles  $C$  with large momentum perpendicular to the beam-target direction.



The reaction will be characterized by two jets, one on the *awayside* balancing the transverse momentum of the trigger. The basic hard process is shown in Fig. 3.9.



The genera  
 $h_A, h_B, \dots$

$$(E_c, d)$$

where

$$\int P$$

The

Thi

where  $Q_{LL}^{ii}$   
These are  
correspond  
In all cases  
we give a f  
taken from +



The general hard scattering formula for the process  $A(h_A) B(h_B) \rightarrow C(h_C) + X$ ,  $h_A, h_B, \dots$  denoting the helicities is given by:

$$\left( E_c \frac{d\sigma}{d^3p_c} \right)_{h_A h_B}^{h_C} = \sum_{a,b,c} \sum_{\substack{h_a h_b \\ h_c h_d}} \int_{\text{Pl. Sp.}}^{\text{Parton}} [D_A^a(x_a, h_a, h_a) D_B^b(x_b, h_b, h_b) \\ \times \bar{D}_{C \rightarrow C}(x_c, h_c, h_c) \left( \frac{d\sigma}{d\hat{t}} \right)_{h_a h_b}^{h_c h_d} (a b \rightarrow c d)]$$

C with large

where

$$\int_{\text{Pl. Sp.}}^{\text{Parton}} = \int_0^1 dx_a dx_b dx_c^{-1} \frac{\hat{s}}{\pi} \delta(\hat{s} + \hat{t} + \hat{u})$$

$$\hat{s} = x_a x_b s, \quad \hat{t} = x_a/x_c t, \quad \hat{u} = x_b/x_c u$$

$$t = (p_A - p_c)^2 \quad \text{and} \quad u = (p_B - p_c)^2$$

#### The Initial - Initial or Reflected Double Asymmetry

This is defined by

$$A_{LL}^{ii} = \frac{(d\sigma)_{++} - (d\sigma)_{+-}}{(d\sigma)_{++} + (d\sigma)_{+-}} \\ = \frac{\sum_{a,b,c} \int_{\text{Pl. Sp.}}^{\text{Parton}} \Delta D_A^a \Delta D_B^b a_{LL}^{ii} \left( \frac{d\sigma}{d\hat{t}} \right) \bar{D}_C^c}{\sum_{a,b,c} \int_{\text{Pl. Sp.}}^{\text{Parton}} D_A^a D_B^b \left( \frac{d\sigma}{d\hat{t}} \right) \bar{D}_C^c}$$

where  $a_{LL}^{ii}$  is the same asymmetry at the parton sub-process level ( $\vec{ab} \rightarrow cd$ ).

These are all calculated at the lowest order in QCD perturbation theory and correspond to the set of graphs in Fig. (3.9)b and are displayed in Fig. 3.10.

In all cases we see the driving asymmetries are of order unity. In Fig. 3.11 we give a few sample estimates of the reflected asymmetries for  $\vec{PP} \rightarrow (\Pi, \text{jet}) + X$ , taken from the work of Babcock, Monsey and Silvers.

rticles)



cd

(3.9)a

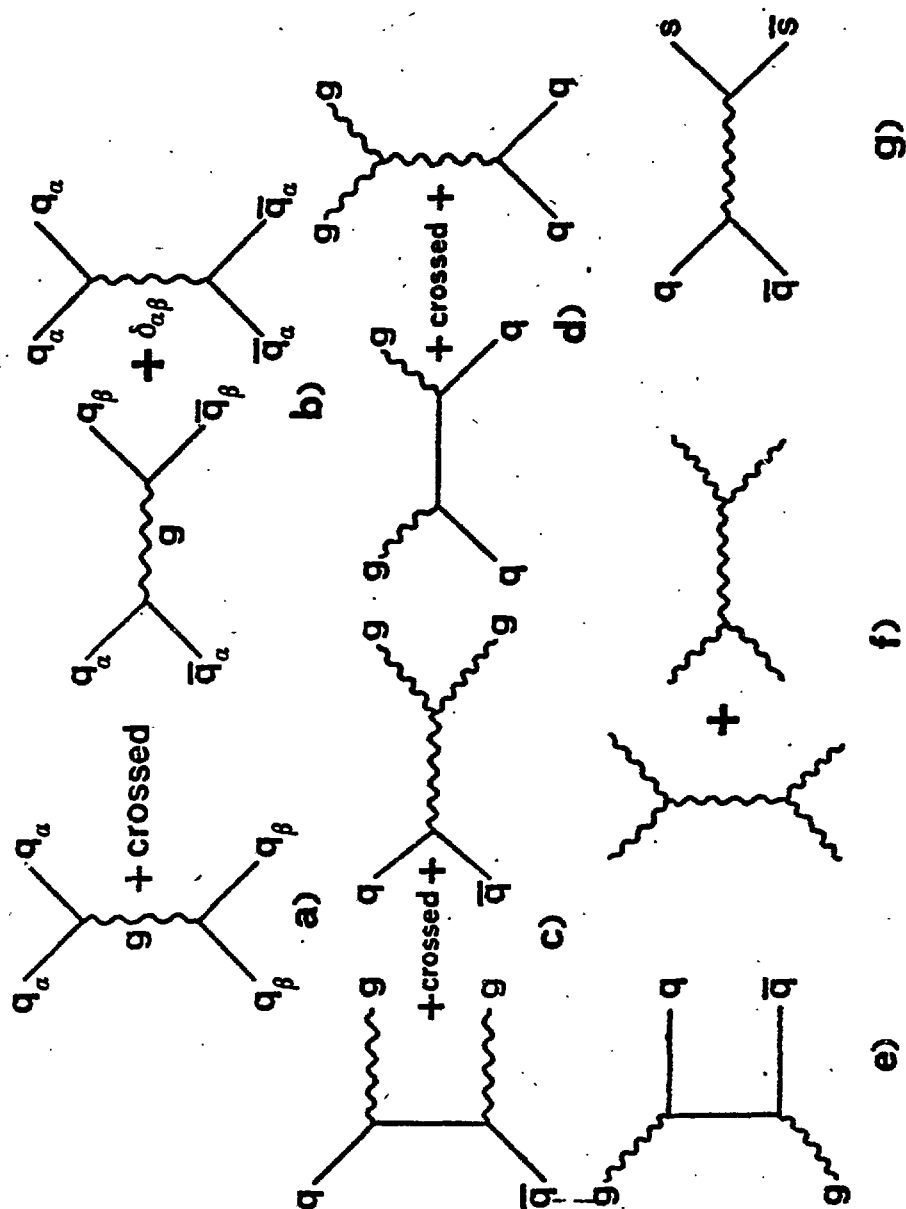


FIG (3.9)

 $a_{ll}^{ii}$ 

.5

 $a_{ll}^{ii}$ 

.5

 $a_{ll}^{ii}$ 

5

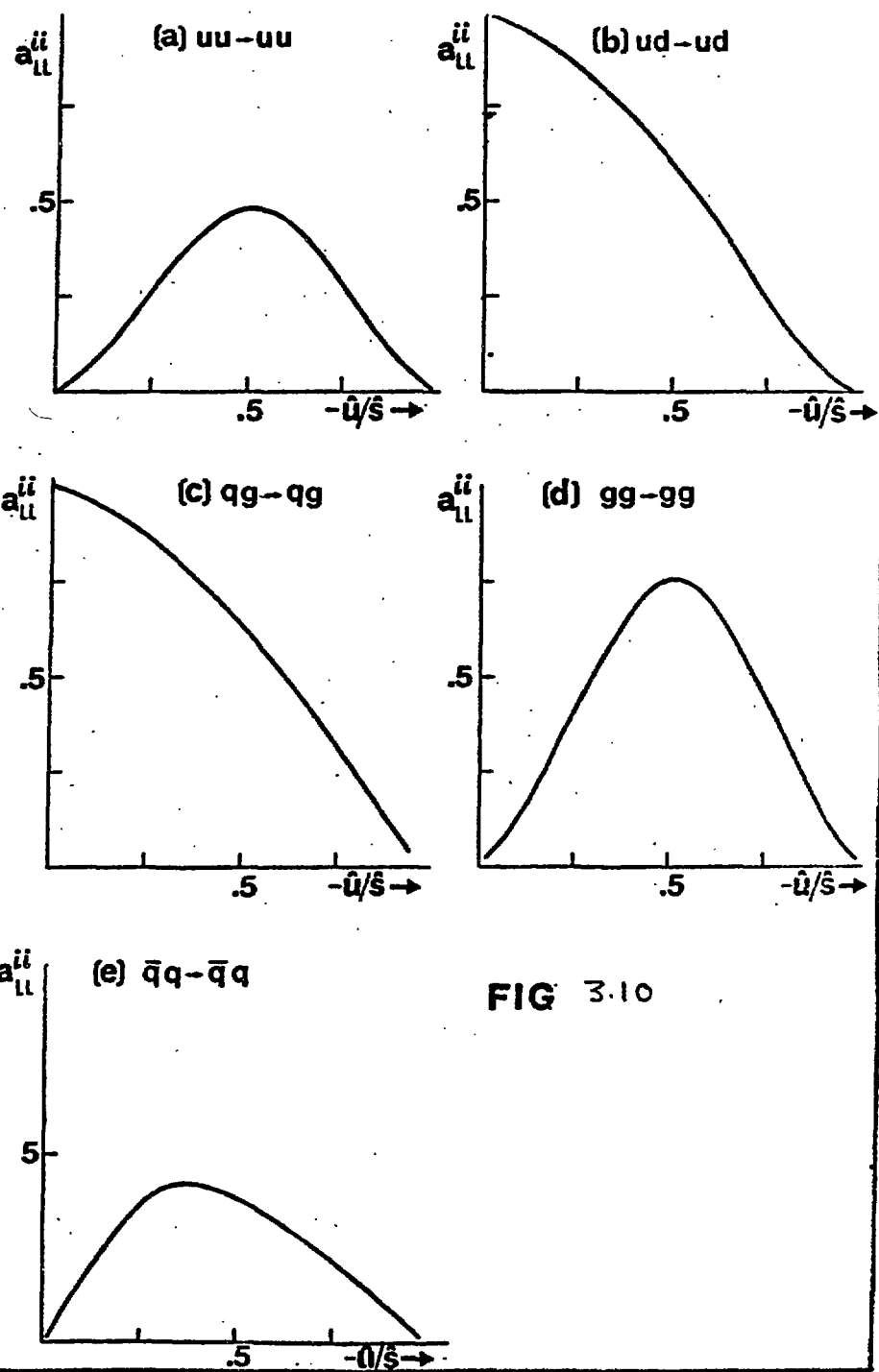


FIG 3.10

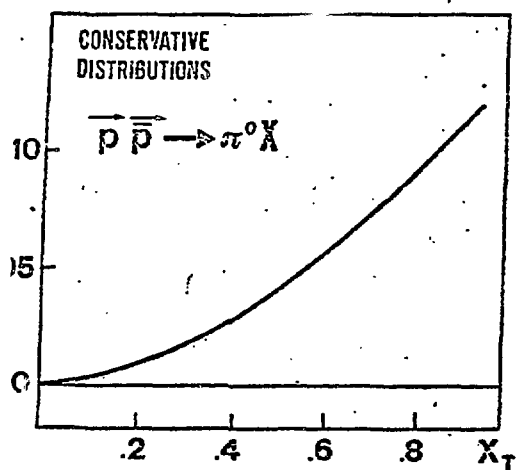
FIG (3.9)<sub>g</sub>

g)

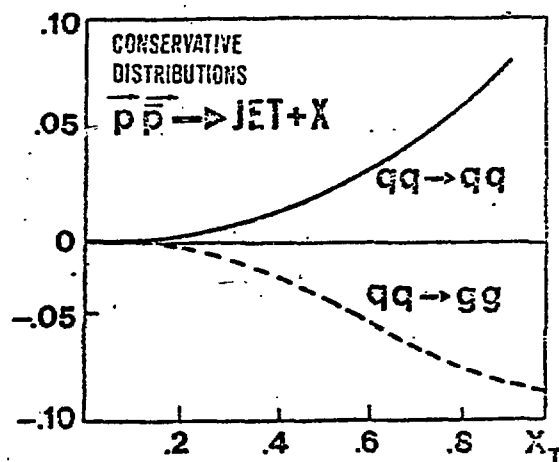
f)

e)

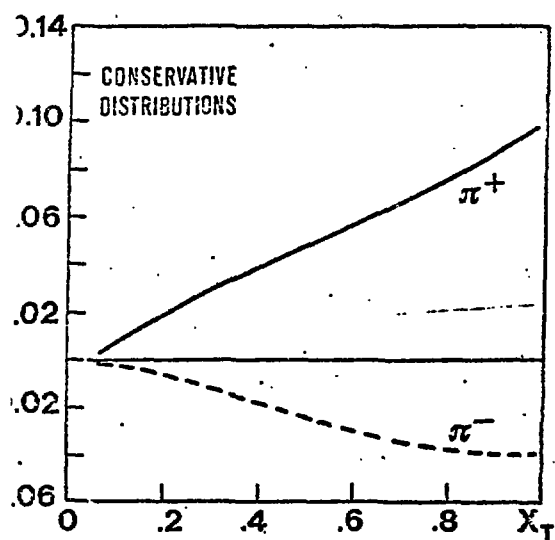
a)



b)



c)



d)

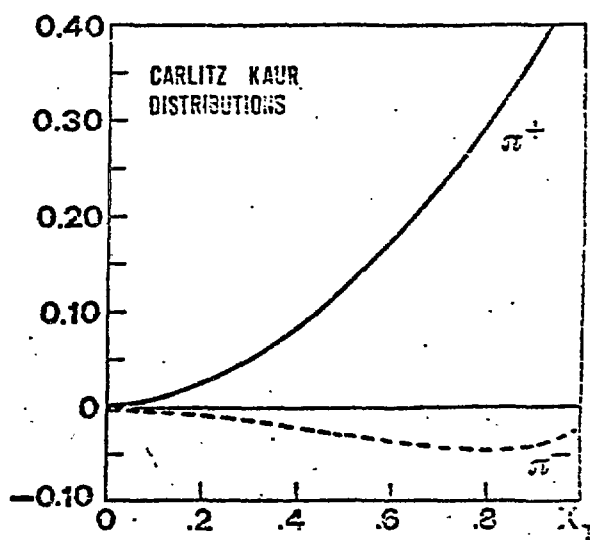


FIG. 3.11

Tr

The  
function

$$A_{LL}^{if} =$$

For  $\overline{p} p \rightarrow A$

$$\vec{s} \rightarrow \vec{u}$$

u

The correspo

and

Transmitted asymmetry  $\vec{P}A \rightarrow \vec{B} + x$  examples:

$$\vec{P} A \rightarrow \vec{\Lambda} + x$$

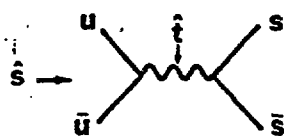
$$\vec{P} \vec{P} \rightarrow \vec{\Lambda} + x$$

(plus associated away side strange particle)

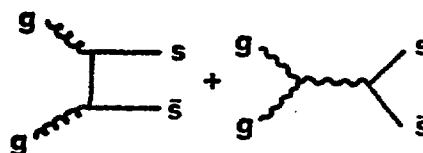
The transmitted asymmetry, involves again the asymmetry of a fragmentation function

$$A_{LL}^{if} = \frac{\sum_{a,b,c} \int_{ph.sp}^{parton} \Delta D_A^a D_B^b a_{LL}^{if} \left( \frac{d\sigma}{dt} \right) \Delta \bar{D}_c^c}{\sum_{a,b,c} \int_{ph.sp}^{parton} D_A^a D_B^b \left( \frac{d\sigma}{dt} \right) \bar{D}_c^c}$$

For  $P\bar{P} \rightarrow \Lambda + x$  the basic sub-processes are (Fig. 3.12)



$u\bar{u} \rightarrow s\bar{s}$



$gg \rightarrow s\bar{s}$

Fig. (3.12)

The corresponding basic asymmetries and cross-sections are given by:

$$\left. \begin{aligned} a_{LL}^{if} &= \frac{\hat{t}^2 - \hat{u}^2}{\hat{t}^2 + \hat{u}^2} \\ \frac{d\sigma}{dt} &= \frac{4\pi}{9} \frac{1}{\hat{s}^2} \alpha_s^2(c^2) \frac{\hat{t}^2 + \hat{u}^2}{\hat{s}^2} \end{aligned} \right\} u\bar{u} \rightarrow s\bar{s}$$

and

$$\left. \begin{aligned} a_{LL}^{if} &= \frac{-\frac{1}{3} \frac{\hat{u}^2 + \hat{t}^2}{\hat{t}\hat{u}} + \frac{3}{4} \left( \frac{\hat{t} - \hat{u}}{\hat{s}} \right)}{\frac{1}{3} \frac{\hat{u}^2 + \hat{t}^2}{\hat{t}\hat{u}} + \frac{3}{2} \left[ 1 - \frac{\hat{t}\hat{u}}{\hat{s}^2} \right] + \frac{3}{4}} \\ \frac{d\sigma}{dt} &= \frac{\pi}{2} \frac{\alpha_s^2(c^2)}{\hat{s}^2} \left[ \frac{1}{3} \frac{\hat{u}^2 + \hat{t}^2}{\hat{t}\hat{u}} + \frac{3}{2} \left[ 1 - \frac{\hat{t}\hat{u}}{\hat{s}^2} \right] + \frac{3}{4} \right] \end{aligned} \right\} gg \rightarrow s\bar{s}$$

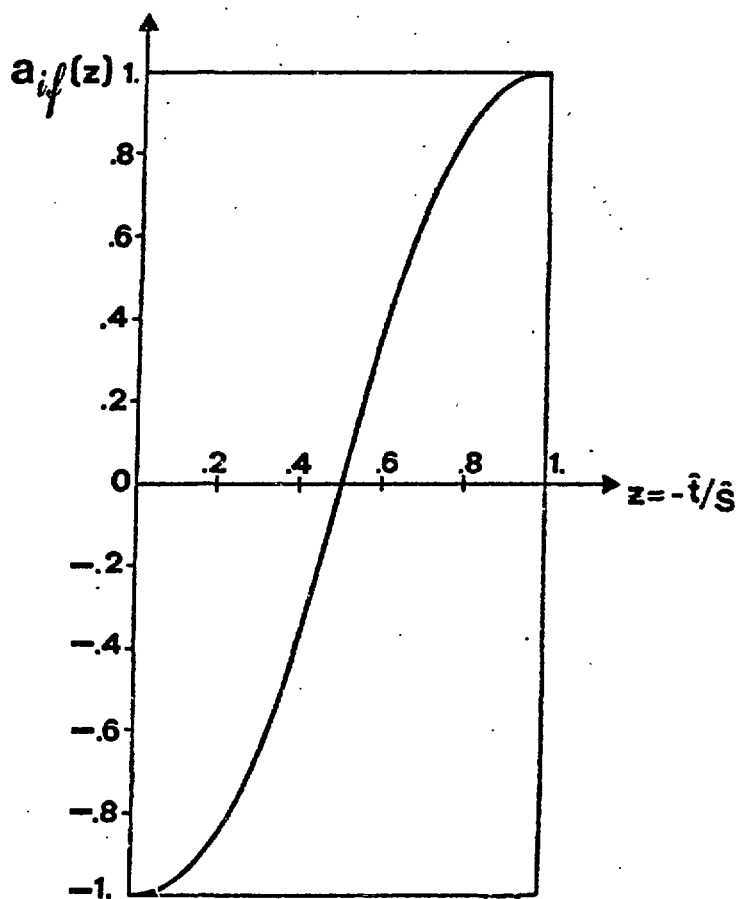
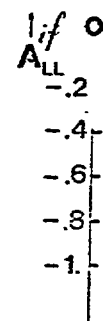
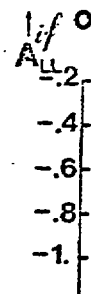


FIG 3.13

For  $P\bar{P} \rightarrow A$   
 most important  
 Fig. 3.13.  
 in which we

As  
 the proton,  
 production of



-2

-4

For  $\bar{p}p \rightarrow \Lambda + x$  the valence quark dominates, so the  $\bar{q}q$  annihilation is the most important contribution. The basic asymmetry for the latter is shown in Fig. 3.13. The corresponding predictions for  $A_{LL}^{it}$  are shown in Fig. 3.14, in which we have set  $\Delta\bar{D}_{s+\Lambda} = \bar{D}_{s+\Lambda}$  as a first estimate.

As a background coming from hard scattering off strange quarks inside the proton, can be minimized by asking for associated strange particle production on the away side.

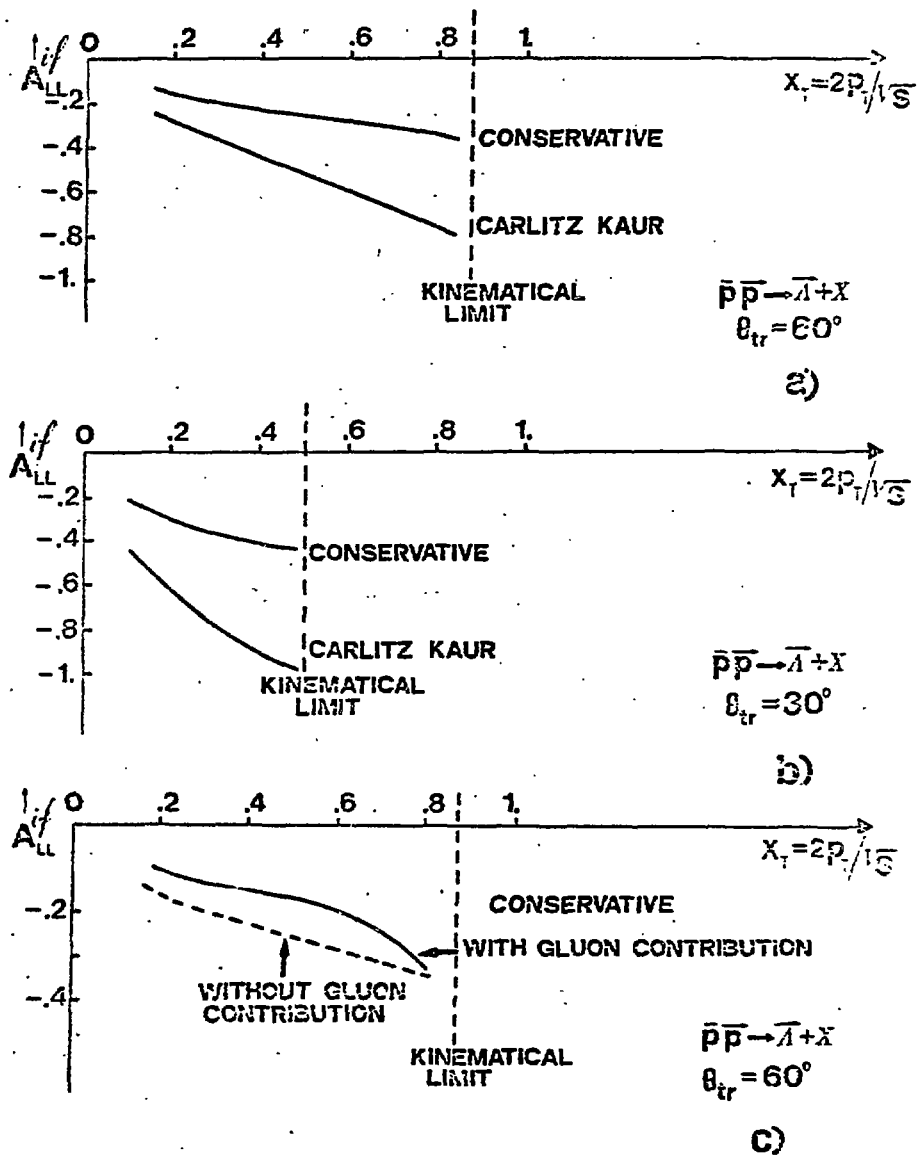
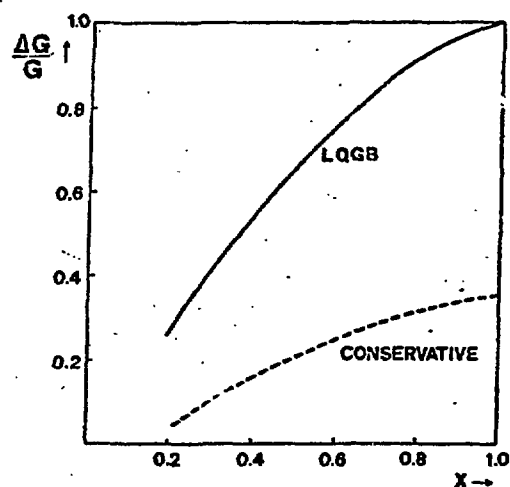


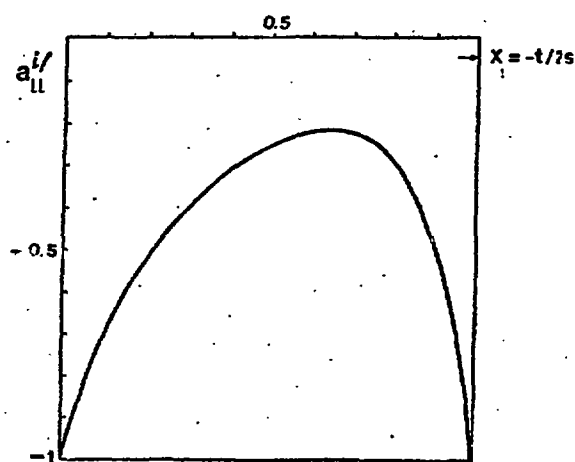
FIG. 3.14

For  $\bar{p}p \rightarrow \bar{\Lambda} + x$  the gluon-gluon fusion dominates and the corresponding basic asymmetry is given in Fig. (3.15)(b). Fig. (3.15)(a) shows  $\Delta G/G$ .

This has an interesting structure as a function of CMS angle. In order to calculate the asymmetry at the hadronic level, we need the gluon helicity distribution inside the polarized proton. Little is known about the latter, however the following argument suggests it might be large. If we assume that the leading quark inside the proton carries most of its helicity as  $x \rightarrow 1$  (i.e. as in Carlitz-Kaur model), further that fast gluons come from bremsstrahlung off fast valence quarks, then a simple computation based on perturbation theory shows  $\Delta G(x)/G(x) \rightarrow \Delta q(x)/q(x) \rightarrow 1$  as  $x \rightarrow 1$ .

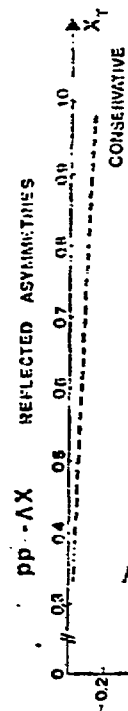
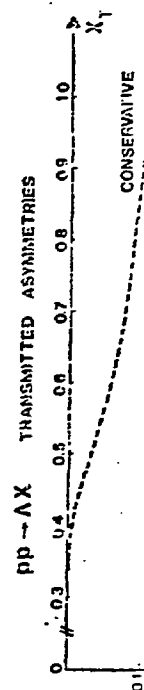


(a)



(b)

FIG. 3.15





responding  
g.  
In order  
licity  
ater,  
me that  
c + 1  
renstrahlung  
ion

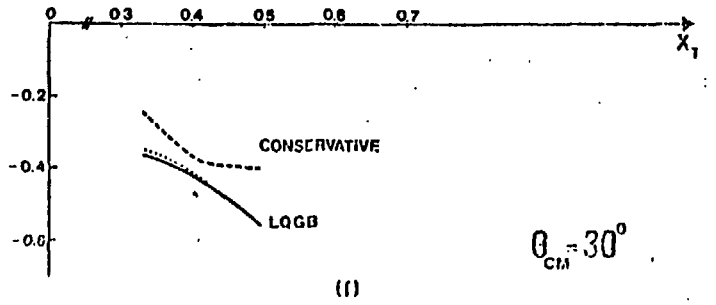
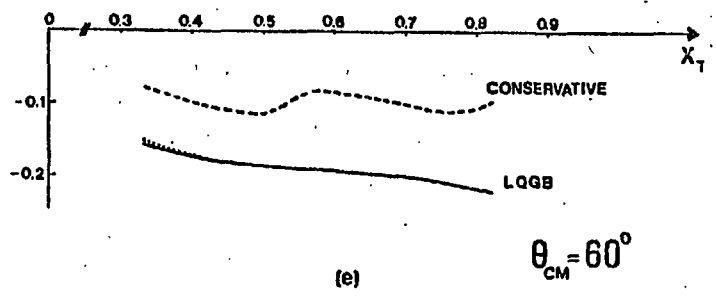
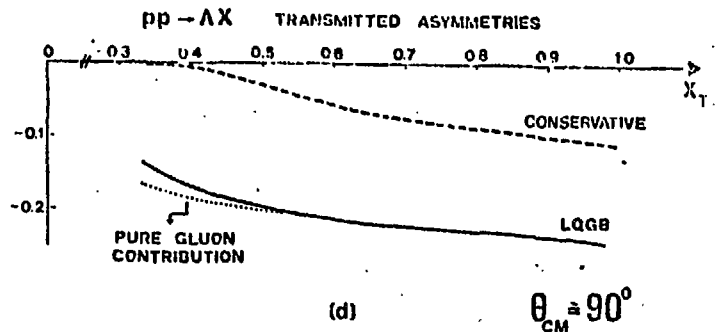
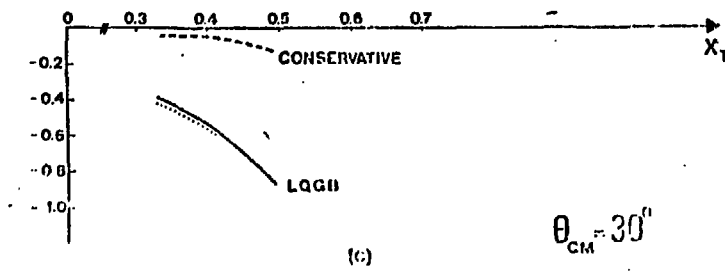
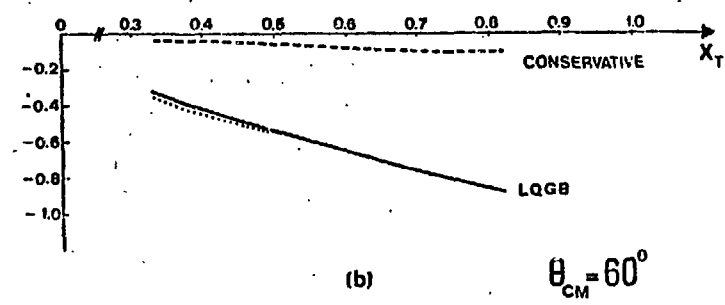
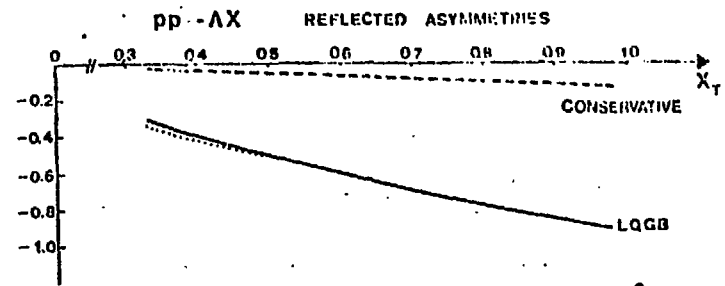


FIG. 3.16

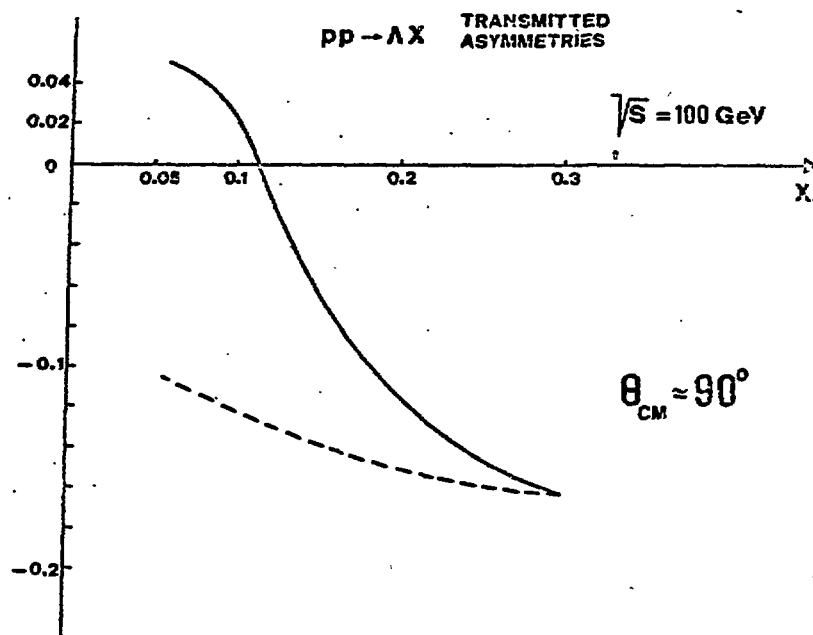


FIG. 3.16 g

T  
process w  
origin of  
T  
and LQM  
see that  
neglectin

3.5. P

H

Process

q

g

for which

These le

$$A_{LL}^{ii} =$$

The little data that exists supports the leading quark idea and the process we are discussing here, will provide a valuable insight into the origin of the gluon distributions inside the proton.

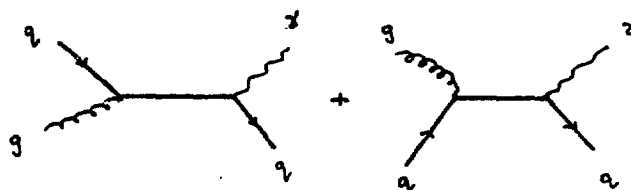
In Fig. (3.16)(a-g) we give predictions based on the conservative and LQEM respectively, for various trigger angles  $\theta_{\text{cms}}$ . For  $x_T > .2$  we see that the antiquark component is negligible (dotted line corresponds to neglecting the latter). In Fig. (3.16) (g) we exhibit the  $x_T < .2$  behaviour.

### 3.5. Prompt Photon Production at Large $P_T$

Here we briefly consider reactions

$$\left. \begin{array}{l} 1) \quad \bar{p} \bar{p} \rightarrow \gamma + X \\ 2) \quad \bar{p} \bar{p} \rightarrow \gamma + X \\ 3) \quad p \bar{p} \rightarrow \bar{q}^* + X \\ \quad \quad \quad \hookrightarrow p^* p^- \end{array} \right\} \quad E_{\text{cm}} \quad P_T^{\gamma} > 4 \text{ GeV}$$

Process 1) is dominated by sub-process



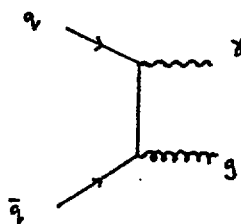
for which

$$\alpha_{LL}^{ii}(qq) = \frac{\hat{s}^2 - \hat{t}^2}{\hat{s}^2 + \hat{t}^2} \quad (E_{\text{cm}} qq \quad \hat{t} \leftrightarrow \hat{u})$$

These lead to a reflected PP asymmetry:

$$A_{LL}^{ii} = \frac{- \sum_{f=u,d} e_f^2 \int \dots \hat{s}^{-2} \left[ \Delta D_f^+ \Delta D_f^3 \left( \frac{\hat{s}^2 - \hat{t}^2}{- \hat{t} \hat{s}} \right) + \Delta D_f^3 \Delta D_f^+ \left( \frac{\hat{s}^2 - \hat{u}^2}{- \hat{u} \hat{s}} \right) \right]}{\sum_{f=u,d} e_f^2 \int \dots \hat{s}^{-2} \left[ D_f^+ D_f^3 \left( \frac{\hat{s}^2 + \hat{t}^2}{- \hat{t} \hat{s}} \right) + D_f^3 D_f^+ \left( \frac{\hat{s}^2 + \hat{u}^2}{- \hat{u} \hat{s}} \right) \right]}$$

Process 2) is dominated by sub-process



for which  $a_{LL}^{ii} = -1$ , since

$|M_{++}|^2 = 0$  by helicity conservation

The asymmetry formula for  $\bar{p}p \rightarrow \gamma + x$  is given by:

$$A_{LL}^{ii} = - \frac{\int_{..} \left[ \frac{4}{q} \Delta u(x_a) \Delta u(x_b) + \frac{1}{q} \Delta d(x_a) \Delta d(x_b) \right] \left( \frac{d\sigma}{d\hat{t}} \right)}{\int_{..} \left[ \frac{4}{q} u(x_a) u(x_b) + \frac{1}{q} d(x_a) d(x_b) \right] \left( \frac{d\sigma}{d\hat{t}} \right)}$$

where

$$D_{\bar{p}}^u = D_p^u = u(x)$$

The prediction for prompt photons, taken from our and Hidaka's work are shown in Fig. (3.17).

$A_{LL}^{ii}$

↑

.1

0

.1

.2

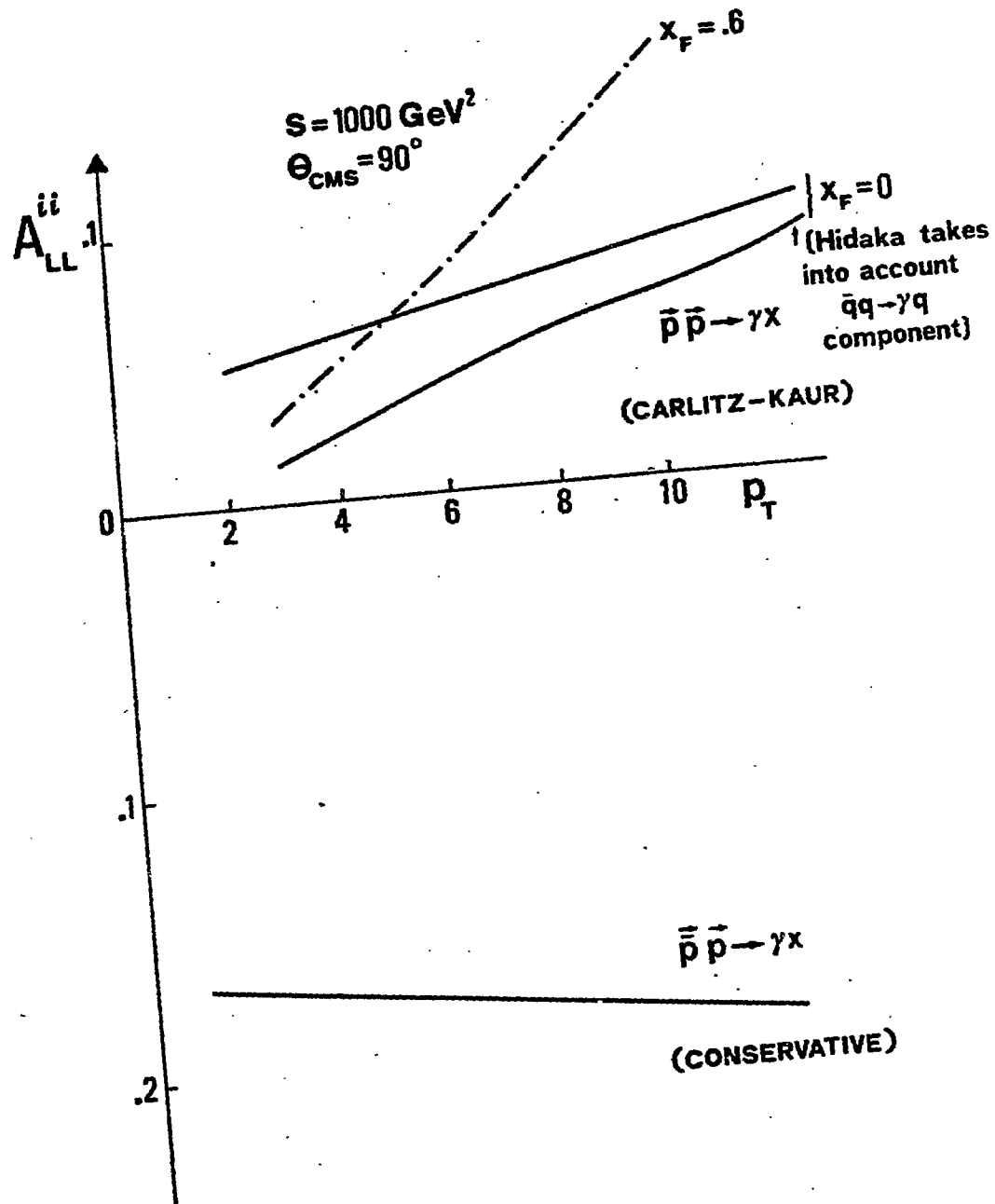


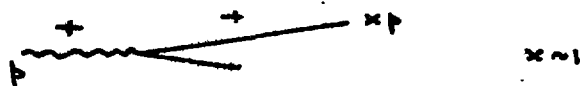
Fig. (3.17)

Transmitted asymmetry for  $\bar{P}P \rightarrow \gamma + x$ 

A pre

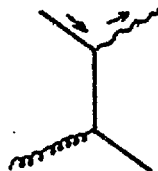
Study in progress, Aldo Renzo with K. Hidaka, M. Jacob, J. Soffer and N.S.C.

Here the possibility is being considered of measuring the final photon helicity, by detecting a fast internally or externally converted lepton pair, which carries away most of its helicity

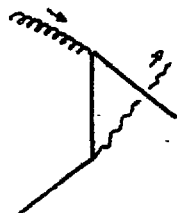


Here one assumes one can detect the muon or electron polarization. A second possibility, is to use a polarized nuclear detector. Although the detection efficiency in such an experiment is very small, one could use the full beam intensity on a 60-80% polarized target.

The basic Compton sub-processes are



$$a_{LL}^{if}(\vec{q} \rightarrow \vec{\gamma} q) = \frac{\vec{q}^2 - \vec{q}^2}{\vec{q}^2 + \vec{q}^2}$$



$$a_{LL}^{if}(\vec{q} \rightarrow \vec{\gamma} q) = -1$$

and asym  
initial or

productio  
of the ap  
inelastic

4.  $V_L$

Le  
picture of  
it is nat  
picture.

-1.  
A if  
-0.5

A preliminary prediction of the transmitted asymmetry is given in Fig. (3.18)

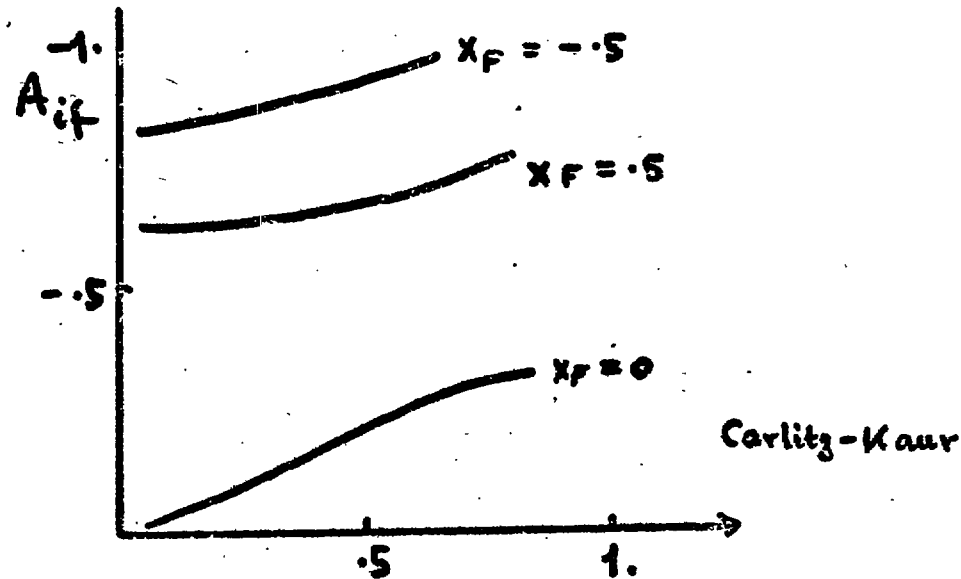


Fig. (3.18)

FIG. 3.18: Preliminary estimate

There are many other processes one can consider, such as  $\gamma^* P \rightarrow g^* x$  and asymmetrical correlations (Peterson and Pire) or  $e^+e^- \rightarrow \text{hadrons}$ , where initial or final state helicities are studied.

Further there is the whole area of transverse spin (normal to the production plane) asymmetries. These need to be studied carefully, because of the apparent ambiguities concerning the operator product approach to deep inelastic scattering mentioned in the introduction.

#### 4. VALIDITY OF FACTORIZATION AND NON-LEADING EFFECTS IN QCD

Let us begin by making the observation that since a clear physical picture of what happens in hard processes emerges in the leading order in QCD, it is natural to try to estimate non leading effects by perturbing this picture. There are a number of effects to be considered namely:

1. In higher orders in  $\alpha_s$  single spin asymmetries enter the picture

$$A_N = \left| \begin{array}{c} A \\ \text{---} \end{array} \right|^2 - \left| \begin{array}{c} A \\ \text{---} \end{array} \right|^2$$

$$\propto S_A \sigma^{AB} = \int S_A S_B D_A^+ D_B^+ \dots S_B \sigma^{AB} \dots$$

where

$$S_A S_B D_A^+(S_A, S_B) = \frac{1}{2} [D(\uparrow, \uparrow) - D(\uparrow, \downarrow) - D(\downarrow, \uparrow) + D(\downarrow, \downarrow)]$$

$$S_B F(S_B) = F(\uparrow) - F(\downarrow)$$

For quark-quark scattering [with mass parameters]

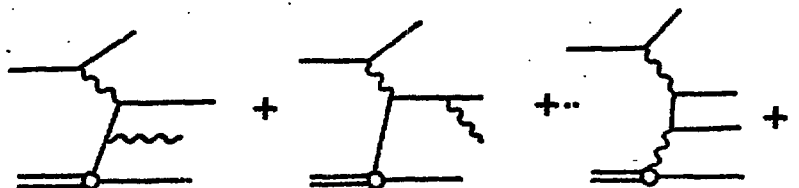
$$\delta_A \sigma^{ab} \propto \left[ \text{diagram} \right] \otimes \left[ \text{diagram} + \text{diagram} + \text{diagram} + \dots \right]^+$$

The whole question of transverse polarizations needs careful investigation, because there are indications the effects may be large at intermediate  $P_T$ .

2. In higher orders in  $\alpha_s(Q^2)$ , longitudinal gluon helicities will play a role. This is the analogue of  $\sigma_L$  in deep-inelastic scattering. For the latter one obtains  $\sigma_L/\sigma_T \sim \alpha_s(Q^2)$ .

### 3. Effect of next to leading order on factorization

Let us briefly review the work of Altarelli, Ellis and Martinelli. If one identifies  $D_A^a(x, Q^2)$  with only the leading logarithmic order in QCD, then in the next to leading order, some of the effects of the diagrams



modify the r

$$F_2(x,$$

where

$$\sigma^i(z,$$

However we c  
so that

In t

D's satisfy

$$D^i(z,$$

where

$$P_i,$$

However one  
processes, f

By

$$q \backslash$$

$$\bar{q} \backslash$$



modify the relationship between structure function  $F_2$  and  $D_p^i$

$$F_2(x, q^2) = \sum_i \int \frac{dx'}{x'} D_p^i(x', q^2) \sigma^i(x/x', q^2)$$

where

$$\sigma^i(z, q^2) = \underbrace{e_i^2 f(z-1)}_{\text{Born term in leading order}} + e_i^2 \frac{\alpha_s(q^2)}{2\pi} C_F 2z + (\sum_i e_i^2) \frac{\alpha_s}{2\pi} \frac{1}{2} z(1-z)$$

However we can incorporate these corrections in the definition of the  $D$ 's so that

$$F_2(x, q^2) = \sum_i e_i^2 D_p^i(x, q^2)$$

In this case, one can show (Curci, Fumanski and Petronzio) that the  $D$ 's satisfy a modified evaluation equation

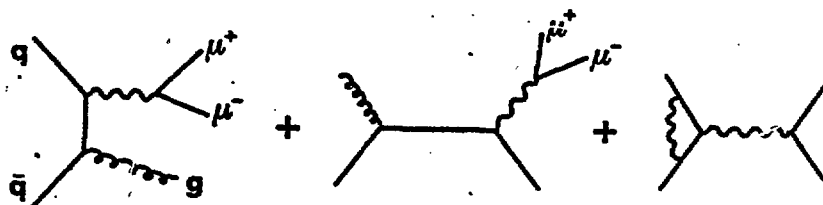
$$D^i(x, q^2) = D^i(x, q_s^2) + \int_{q_s^2}^{q^2} \frac{dk^2}{k^2} \int_x^1 \frac{dz}{z} P_{ij}(k^2, z) D^j(\frac{x}{z}, k^2)$$

where

$$P_{ij}(k^2, z) = \frac{\alpha_s(k^2)}{2\pi} C_F \left( \frac{1+z^2}{1-z} \right)_+ + \frac{(\alpha_s(k^2))^2}{2\pi} C_F f(z) + \dots$$

However one must now seek to identify this newly defined  $D$  in all other processes, for example in the Drell-Yan mechanism.

By explicitly calculating the sub-processes\*



\* Altarelli, Ellis Martinelli  
Rumpert and Van Neervan

$$\frac{d\sigma}{dx_1 dx_2} = \frac{4\pi\alpha^2}{9s} \sum_i \int_{x_1}^1 \frac{dx_1'}{x_1'} D_P^i(x_1', \omega^2) \int_{x_2}^1 \frac{dx_2'}{x_2'} D_P^i(x_2', \omega^2) \sigma^i\left(\frac{x_1}{x_1'}, \frac{x_2}{x_2'}, \omega^2\right)$$

Where the  $D_P^i(x, Q^2)$  are defined so as to include the next to leading effects in deep inelastic scattering, one finds

$$\begin{aligned} \sigma_i(z, z', \omega^2) = e_i^2 \left\{ \left[ 1 + \frac{N_c}{2\pi} \left( r \left( \frac{4\pi^2}{3} + 1 \right) \delta(z-1) \delta(z'-1) \right. \right. \right. \\ \left. \left. \left. + \delta(z-1) \frac{N_c}{2\pi} \left( r + \delta(z'-1) \frac{d_s}{2\pi} \left( r g(z') + \dots \right) \right) \right] \right\} \end{aligned}$$

The appearance of  $\pi^2 a_s$  factors are due to  $Q^2 = -Q^2$  (deep-inelastic)  $> 0$  and these partly explain the famous factor of 2. We notice that  $\sigma_i$  does not exactly correspond to parton-parton cross-section.

For the spin and helicity asymmetries one has to repeat the second order analysis. One might guess, because for  $q\bar{q} \rightarrow \gamma^* g$   $\delta\sigma = -\sigma$ , that the correct asymmetry formula is

$$A_{LL} = - \frac{\sum_i \iint \Delta D_P^i \Delta D_P^i \sigma^i}{\sum_i \iint D_P^i D_P^i \sigma^i}$$

where

$$\begin{aligned} F_2(x, Q^2) &= \sum_i e_i^2 D_P^i(x, \omega^2) \\ G_1(x, Q^2) &= \sum_i e_i^2 \Delta D_P^i(x, \omega^2) \end{aligned}$$

However this has to be checked in the same way as the unpolarized case. We must remember that we are talking about factors of 2-3.

In this connection, one must mention that the renormalization scheme and definition of  $\alpha_s(Q^2)$  play an important role and the subject remains unclear on whether a particular scheme improves the convergence of the  $(\alpha_s(Q^2))^n$  series. In large transverse momentum process, next to leading effects can be minimized by allowing different scales for difference of the factors

$D_A^s$   
to me  
there:  
basic

4.

sche

graph.

X

In ot

$\gamma^*$

pp

$D_A^a D_B^b \dots \sigma^{ab}$ . However if such prescriptions are arbitrary they would lead to meaningless asymmetric predictions. Measurements of the latter will therefore provide a valuable way of studying the validity and nature of the basic factorization structure.

#### 4. Power Corrections

Recall in deep-inelastic scattering the following connections, schematically

$$F(x, q^2) = \int dn A_n \left(\frac{1}{x}\right)^n [\gamma_n(q^2)]^{\gamma_n} + \frac{1}{q^2} F''(x, q^2) + \dots$$

$\nwarrow$  higher twist in OPE       $\nearrow \bar{q} \partial_{\mu_1} \dots \partial_{\mu_n} q$        $\nearrow \bar{q} \partial_{\mu_1} \dots \partial_{\mu_n} q$

$$T_\mu(x) T_\nu(0) = \sum_n C_n(z^2) z^{\mu_1} \dots z^{\mu_n} O_{\mu_1 \dots \mu_n}(0)$$

graphically

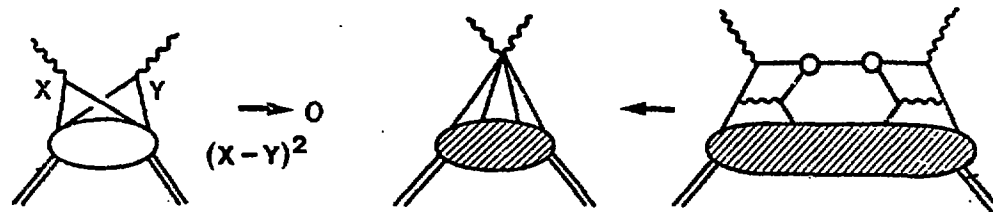


Fig. (4.1)

In other processes, we have analogous parton diagrams

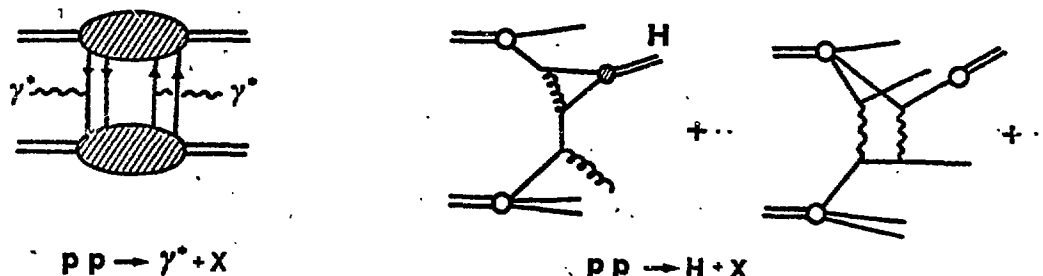


Fig. (4.2)

These new terms, either involve multi-quark distributions inside the hadron or more complex sub-processes or a complex mixture of both.

If these processes are important any notion of factorization is lost. However most of these mechanisms can be estimated with a little ingenuity and a lot of energy. In discussing this question Politzer suggested a generalized formula

$$\sigma^{AB..}(p_A, p_B, \dots) = \int dx_a dx_a' \dots D_A^{a, a'}(x_a, x_a', \dots) \int dx_b dx_b' \dots D_B^{b, b'}(x_b, x_b', \dots) \dots \sigma^{\{a\}\{b\}..}(\{x_a\} p_A, \{x_b\} p_B, \dots)$$

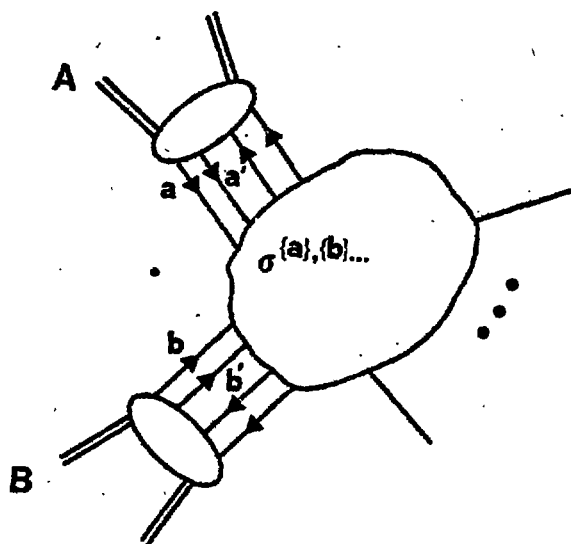


Fig. (4.3)

Within the parton framework one would expect the corresponding asymmetry formula to be

$$\Delta_{AB} \sigma^{AB..} = \int \Delta_A \{a\} D_A^{\{a\}} \int \Delta_B \{b\} D_B^{\{b\}} \dots \Delta_{\{a\}\{b\}..} \sigma^{\{a\}\{b\}..}$$

where

and

(The contrac  
Pol  
distinguishi  
the CIM (Con  
and Gunion  
For example

(Today we al  
 $q\bar{q} \rightarrow \pi + g$ ).

$$\left( E \frac{d\sigma}{d^3p} \right)$$

where  $\epsilon =$  (

In m  
 $P_T^{-8}$  behavior  
 $P_T$  due to s  
case it will  
unpolarized  
help by cons

hadron

where  $\Delta_{A\{a,b\}} = \Delta_A [\Delta_a + \Delta_{a'} + \Delta_a \Delta_{a'} + \dots]$

is lost.

nity and

eralized

$$\Delta_{\{a\}\{b\}} = [\Delta_a + \Delta_{a'} + \dots][\Delta_b + \Delta_{b'} + \dots]$$

and

$$\Delta_a F(h_a) = \frac{1}{2} [F(+)-F(-)]$$

 $\{a, \dots\}$ 

(The contraction symbols mean the asymmetries are matched).

Polarization asymmetry measurements may be a valuable way of distinguishing the various terms. To illustrate this latter part, we consider the CIM (Constituent-Interchange-Model) strategy of Blankenbecler, Brodsky and Gunion. Here one assumes at some level all processes contribute: For example for  $PF$  we have:

$$\bar{q}q \rightarrow q\bar{q} \Rightarrow P_T^{-4}$$

$$\bar{q}q \rightarrow \pi\pi \Rightarrow P_T^{-2}$$

$$q\pi \rightarrow q\pi \Rightarrow P_T^{-2}$$

(Today we also would consider mechanisms leading to  $P_T^{-6}$ , for example  $q\bar{q} \rightarrow \pi + g$ ). The sum over such terms would lead to

$$\left(\bar{E} \frac{d\sigma}{d^3p}\right) = \frac{C_2}{[P_T^2 + m_2^2]^2} \epsilon^{N_2} + \frac{C_4}{[P_T^2 + m_4^2]^4} \epsilon^{N_4} + \dots$$

where  $\epsilon = (1 - x_m)$ .

In more recent times, Feynman and Fields emphasized that the  $P_T^{-8}$  behaviour could be reproduced by an  $P_T^{-n} \text{eff}(P_T)$  behaviour at smaller  $P_T$  due to scaling violations in the basic parton densities. In such a case it will be extremely difficult to disentangle the terms in the CIM from unpolarized data alone. However let us analyse if spin measurements are of any help by considering the superposition of the two mechanisms (see Fig. (4.4)).

$$q \bar{q} \rightarrow q \bar{q}$$

$$q \bar{q} \rightarrow \pi \pi$$

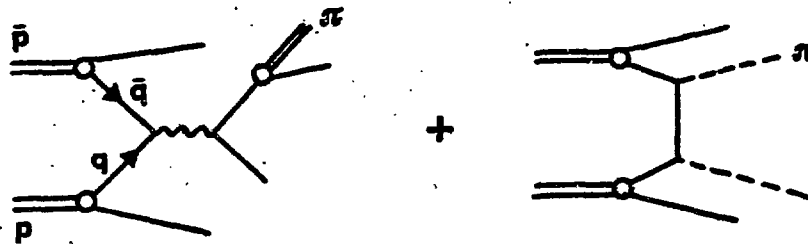


Fig. (4.4)

For the second mechanism the cross-section is given by

$$\left( \epsilon \frac{d\sigma}{d^3p} \right)_{p\bar{p} \rightarrow \pi\pi} = \int d^3x_a d^3x_b D_p^2(x_a) D_{\bar{p}}^2(x_b) \left( \epsilon \frac{d\sigma}{d^3p} \right)_{q\bar{q} \rightarrow \pi\pi}$$

while the asymmetry is proportional to

$$A_{LL}^{ii} \propto \int \Delta D_p^2 \Delta D_{\bar{p}}^2 A_{LL}^{ii} \left( \epsilon \frac{d\sigma}{d^3p} \right)_{q\bar{q} \rightarrow \pi\pi}$$

If we assume that spin structure of the pion can be read off from diagrams with elementary pions then  $A_{LL}^{11} = -1$ . On the other hand the basic asymmetry for  $q\bar{q} \rightarrow q\bar{q}$  is given by:

$$A_{LL}^{ii} = \frac{\frac{3^2 - \hat{G}^2}{\hat{G}^2} - \frac{\hat{E}^2 + \hat{G}^2}{\hat{E}^2} + \frac{2}{3} \frac{\hat{G}^2}{\hat{E}^2}}{\frac{3^2 + \hat{G}^2}{\hat{E}^2} + \frac{\hat{E}^2 + \hat{G}^2}{\hat{E}^2} - \frac{2}{3} \frac{\hat{G}^2}{\hat{E}^2}}$$

which has the shape (fig. 4.5)

We now arr

and

with  $n_{eff}$   
one obtains

where

Th  
with  $X_T$   
asymmetric  
structure  
produced p  
adds to the  
sections,

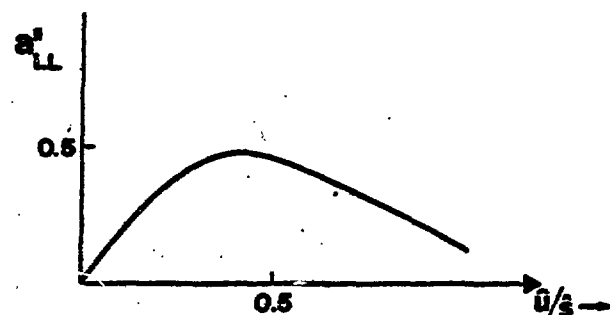


Fig. (4.5)

We now arrange our magnitudes so that

$$\left( E \frac{d\sigma}{d^3p} \right)_{q\bar{q} \rightarrow q\bar{q}}^{\text{contribution}} = \left( E \frac{d\sigma}{d^3p} \right)_{q\bar{q} \rightarrow \pi\pi}^{\text{contribution}} \quad \text{at } P_T = 3 \text{ GeV}$$

$$\text{and} \quad \left( E \frac{d\sigma}{d^3p} \right)_{q\bar{q} \rightarrow q\bar{q}}^{\text{contribution}} \sim \frac{1}{P_T} n_{\text{eff}}(P_T)$$

with  $n_{\text{eff}}(P_T) \sim 7$  for  $P_T = 3$  GeV. Using the conservative parton distributions one obtains.

$$A_{LL} = -0.2 \frac{[0.5 x_T (1-x_T)^2 + (x_T E)^{n_{\text{eff}}}]}{[(1-x_T)^2 + (x_T E)^{n_{\text{eff}}}]}$$

$$\text{where } E = \sqrt{s}/2 \quad ; \quad n_{\text{eff}}(P_T) = 4 + 3 \log 6.2/\Lambda^2 / \log P_T^2/\Lambda^2$$

This we plot in Fig. (4.6)(a), from which we see a strong variation with  $x_T$  and  $\sqrt{s}$  between 20 and 40 GeV. The dotted lines gives the asymmetries corresponding to the two mechanisms individually. The interesting structure is partly due to the fact that the  $x_T$  dependence of the directly produced pions is harder. However cancellation between the two terms also adds to the structure. If on the other hand we plot the unpolarized cross-sections, the difference between the two mechanisms is not so marked.

We conclude by the remark that spin physics may be as important to QCD as it was in Regge pole analysis.

## ACKNOWLEDGEMENT

I would like to thank Professors G. Bialkowski and S. Pokorski for their invitation to come and speak at this Symposium and for hospitality during my stay in Poland.

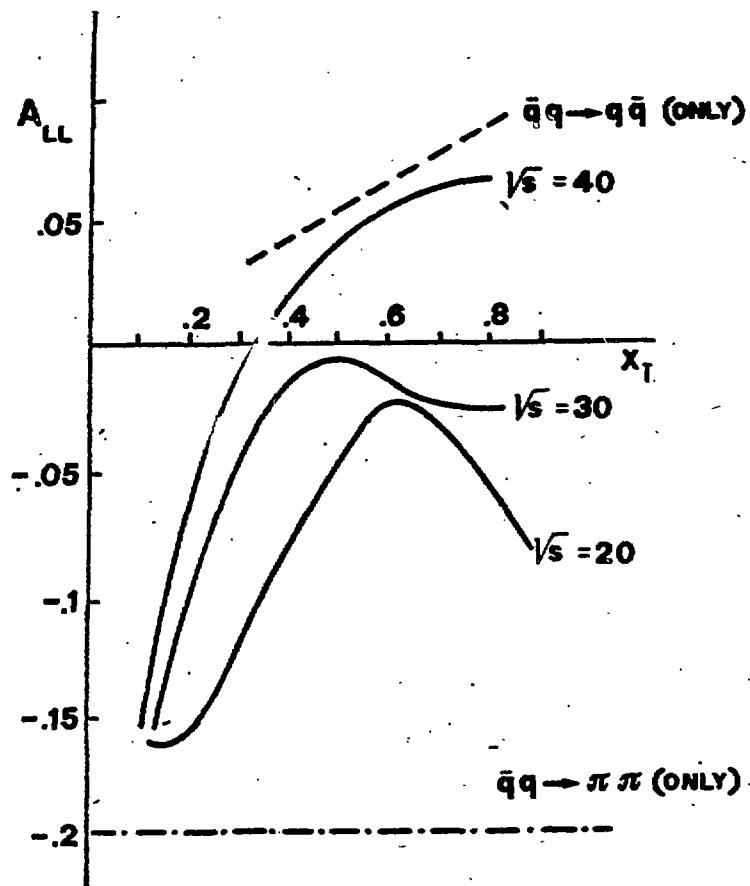


Fig. (4.6)a



stant to

rski for  
ity during

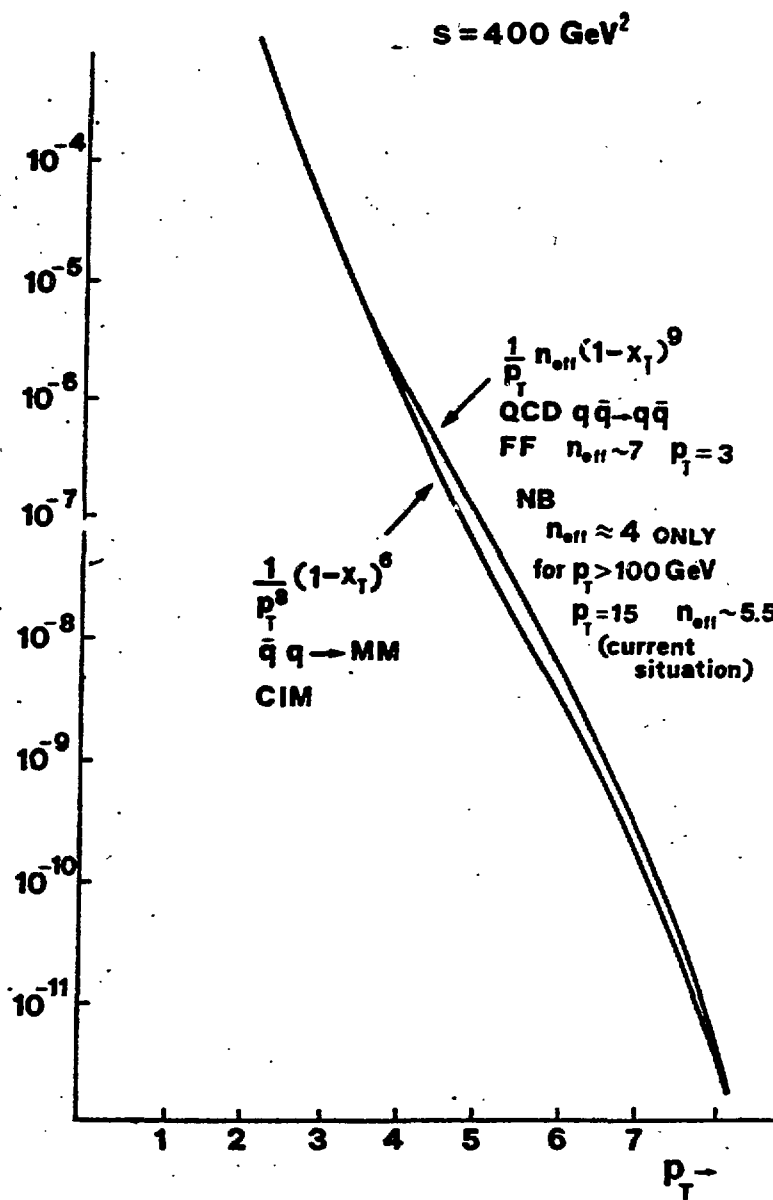


Fig. (4.6)b

DIAGRAMMATIC MASS FACTORIZATIONB. Humpert<sup>\*</sup>

CERN, Geneva, Switzerland

ABSTRACT

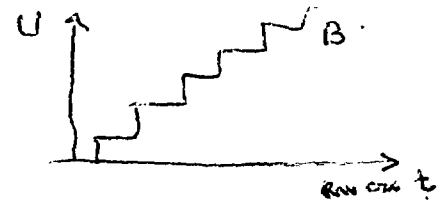
We develop an analogy between mass factorization and multiplicative BPHZ-renormalization with the role of the renormalization constant being taken over by the operator matrix elements. By introducing Zimmerman's forest formula we demonstrate its use in constructing the deep inelastic (DI)/Drell-Yan (DY) factorized parton cross-sections and arrive at an all-order proof of mass factorization. The DY correction term is determined by similar reasonings.

(author)

<sup>\*</sup>) Also at: Swiss Federal Institute of Technology, Laboratory of High Energy Physics, CH-5284 Villigen, Switzerland.

References

1. B.Humpert and W.L.van Neerven, Phys. Lett. 102B (1981) 427
2. B.Humpert and W.L.van Neerven, Ref.TH.3077-CERN, 1981 (Phys.Rev.)
3. B.Humpert and W.L.van Neerven, Ref.TH.3086-CERN, 1981 (Saolenice Conf. 1980)



.Rev.)  
enice

LATTICE GAUGE THEORY

C. Itzykson

DPh.T. CEN-Saclay  
91191 Gif-sur-Yvette Cedex, France1. Introduction

Beyond the original predictions of asymptotic freedom and its successful applications to deep inelastic high energy collisions and related processes, the theory of strong interactions based on a non abelian SU(3) color gauge invariance has had a hard time to produce numerical testable results. The difficulty lies in the confinement property which generates a spectrum very remote from the original dynamical degrees of freedom. On the other hand the appearance of new approaches like Wilson's Lattice quantization<sup>[1]</sup> have revealed to the theorist's delight a wealth of unexpected phenomena. Lattice gauge theory is still in an exploratory stage. However the general feeling is that the ground is safe eventhough practical developments are still scarce.

What has been achieved presently is a reasonable understanding of the confinement mechanism in the strong coupling regime. The Monte Carlo calculations initiated by Wilson<sup>[2]</sup> and Creutz Jacobs and Rebbi<sup>[3]</sup> and actively pursued, have demonstrated that the cutoff model approximates for small coupling the short distance asymptotically free continuous field theory. Their results had been partly anticipated by the developments of strong coupling series and the insight offered by mean field approximations<sup>[4]</sup>.

Euclidean field theory using path integrals has provided numerous bridges with condensed matter physics. Local invariance seems in particular a common theme in a number of exciting problems of disordered media.

Very much as brownian motion is at the heart of the conventional field theory, the study of gauge invariant models suggests a theory of "Brownian surfaces" still in its infancy, in relation to the string model developped in the context of the dual resonance approximation to scattering amplitudes.

The role of topological defects, with its associate duality transformations in the abelian cases yield connections between strong and weak coupling situations but unfortunately cannot be extended except qualitatively to non abelian cases.

To  
introduci  
Ninomiya  
bearing  
number o

2. Lattic

To c  
ranging P  
in common  
Lattice  
The task  
being ass  
lattice s  
ved in fa  
theory.

For  
Callan-S

where the

dictates  
(euclidean

and as

i.e. at

Thi  
the disc  
becomes  
or mass

To extend this list of open problems let us mention the difficulties of introducing fermionic degrees of freedom, recently reanalyzed by Nielsen and Ninomiya<sup>[5]</sup> and others. The chiral anomaly reappears in the form of an explicit breaking due to regularization or in the disguise of the multiplication of the number of fermion species.

## 2. Lattice quantization

To cope with ultraviolet divergences numerous means have been developed ranging Pauli-Villars regularization to dimensional regularization, which had in common to be tailored for handling the perturbative Feynman integrals. Lattice quantization offers a mean of investigating the theory in the large. The task is then first to locate the possible transitions, those of interest being associated with very large correlation lengths on the scale of the lattice spacing  $a$ . The bare coupling constant and lattice spacing can be removed in favor of renormalized quantities characterizing a continuous field theory.

For a fixed bare theory the set of connected Green's functions satisfy a Callan-Symanzik equation

$$\left\{ p \cdot \frac{\partial}{\partial p} - \beta(g) \frac{\partial}{\partial g} - n \gamma(g) \right\} G_n(p, g) = \text{r.h.s.} \quad (1)$$

where the r.h.s. vanishes in the scaling limit and

$$\beta(g(\lambda)) = \lambda \frac{\partial}{\partial \lambda} g(\lambda) \quad (2)$$

dictates the variations of the "running" coupling constant with a scale of (euclidean) momenta  $\lambda$ . For non-abelian gauge fields and  $g$  small enough

$$\beta(g) = -\frac{b}{2} g^3 + \dots \quad (3)$$

and as  $\lambda \rightarrow \infty$

$$g^2(\lambda) \sim \frac{1}{b \ln \lambda} \quad (4)$$

i.e. at short distance the effective coupling constant goes to zero.

This motivates a lattice cutoff  $a$  to deal with momenta  $p \ll \frac{1}{a}$  for which the discretization should play a negligible role as the coupling constant becomes vanishingly small, keeping some physical length fixed, string tension or mass of some excited state.

Having broken translational by construction, it is however important to retain as many symmetries of the sought for theory as possible. In particular gauge invariance plays a prominent role. It expresses the fact that the physical content of the theory is unaffected when "matter" fields (Higgs or quark fields) are submitted to a local transformation

$$\phi(x) \rightarrow D(g_x) \phi(x) \quad (5)$$

where  $g_x$  is an  $x$ -varying element of the local group  $G(SU(3)$  for chromodynamics) and  $D$  the representation associated to  $\phi$ . Since neighboring points on the lattice are separated by a finite distance, the vector potential of the continuous theory  $A_\mu(x)$ , has to be traded for an integral factor

$$g_{xy} = P \exp i \int_y^x A_\mu(x) dx^\mu \quad g_{xy} \in G \quad (6)$$

a path ordered integral along a curve joining  $y$  to  $x$ , with the covariance property

$$g_{xy} \rightarrow g_x g_{xy} g_y^{-1} \quad (7)$$

under local transformations. Note that  $\phi^\dagger(y) D(g_{yx}) \phi(x)$  is then a gauge invariant for a unitary representation  $D$ .

The Yang-Mills action is then replaced, in the Euclidean region, by a lattice sum, which up to a constant and a sign convention is

$$S = \beta \sum_p \chi(\prod g_{xy}) \quad (8)$$

The sum runs over the elementary circuits of the lattice, called plaquettes (elementary squares of a cubic lattice),  $\prod g_{xy}$  is the ordered product of group variables along this circuit, and  $\chi$  is a real class function (a weighted sum of irreducible characters) of a group  $G$  chosen to be maximum on the identity element.

In the simplest case it can be taken to be the real part of the trace in the fundamental representation. This is however not a unique choice and perhaps not suited for  $SU(N)$ ,  $N$  large. The reason is that with such a choice the plaquette action develops secondary maxima which might play an unwanted role. Perhaps the most natural choice is to use the heat kernel on the group, which reduces to the Villain form in the abelian case. Furthermore there is in principle no reason, except simplicity, to introduce only the shortest circuits. Indeed any real space renormalization will generate terms involving larger

circuits.

If  $\tau$

with  $F_{\mu\nu}$   
the bare  
tional to

is interpe

the free

A co  
and sites

where the  
term with  
ce fermion  
 $\gamma$ -matrices

Let  $u$   
bles are  $g$   
a connecte  
ducible re

For the  $q$   
tation. We  
finement  $c$

circuits.

If the action is expanded around its trivial maximum it takes the form

$$S = S_0 - C \beta a^{4-d} \int d^d x (F_{\mu\nu}^\alpha)^2 + \dots \quad (9)$$

with  $F_{\mu\nu}^\alpha$  the field strength. This shows that  $\beta$  is proportional to  $g_0^{-2}$ , with  $g_0$  the bare coupling constant. In the statistical analogy  $\beta$  is inversely proportional to temperature and the vacuum functional

$$Z = \int \prod_{xy} dg_{xy} \exp S \quad (10)$$

is interpreted as the partition function, with

$$F = \lim N^{-1} \ln Z \quad (11)$$

the free energy,  $N$  being the number of lattice points.

A coupling to Higgs particles can be added in the form of a sum over links and sites

$$S_m = \beta \sum_x \phi_x^\dagger D(g_{xy}) \phi_y + \sum_x V(\phi_x^\dagger \phi_x) \quad (12)$$

where the first term would reduce in the naive continuum limit to a kinetic term with covariant derivatives instead of ordinary ones. One can also introduce fermions, using Grassmanian variables for the quark fields and appropriate  $\gamma$ -matrices

$$S_f = \beta_f \sum_x \bar{\psi}_x (\gamma_{xy} - 1) D(g_{xy}) \psi_y + \sum_x \bar{\psi}_x \psi_x \quad (13)$$

Let us concentrate on the pure Yang-Mills theory. Gauge invariant observables are generated in the form of Wilson loops. These are ordered products along a connected closed loop  $C$  of variables  $g_{xy}$ . We then take the trace in an irreducible representation (a) and average over configurations

$$W_a(C) = \langle \chi_a \left[ \prod_C g_{xy} \right] \rangle = Z^{-1} \int \prod_{xy} dg_{xy} e^S \chi_a \left[ \prod_C g_{xy} \right] \quad (14)$$

For the quark confinement problem,  $\chi_a$  corresponds to the fundamental representation. We take for  $C$  a large regular loop enclosing a minimal area  $A$ . The confinement criterion is then that, as  $C$  becomes large,  $W(C)$  behaves as

$$W(C) \sim \exp -KA \quad (15)$$

with  $K$  is the string tension - i.e. - the coefficient of the linearly rising part of the potential energy between two static colored sources. Recall that such a string in rotation generates a linear relation between angular momentum and square energy with the slope  $\alpha'$  related to  $K$  through

$$K = \frac{1}{2\pi\alpha'} \quad (16)$$

so that the order of magnitude of  $K$  is  $\frac{1}{2\pi} \text{ GeV}^2$ . Assuming that confinement persists in four dimensions down to vanishingly small bare coupling constant we should expect, according to asymptotic freedom that as  $\beta \rightarrow \infty$  the dimensionless quantity  $Ka^2$  behaves as

$$Ka^2 \underset{\beta \rightarrow \infty}{\sim} c_K e^{-b'\beta} \quad (17)$$

where  $b'$  is related to the coefficient  $b$  in the Callan-Symanzik function. On the other hand in the strong coupling region

$$Ka \underset{\beta \rightarrow 0}{\sim} \ln \beta^{-1} \quad (18)$$

Other observables can be studied, even within the unrealistic pure gauge sector. Of particular interest is the so called glue-ball mass, or inverse correlation length defined as the coefficient in the exponential decay law for the correlation between two widely separated Wilson loops

$$\langle \chi(\Pi_{c_1} g_{xy}) \chi(\Pi_{c_2} g_{xy}) \rangle \sim \exp - L/\xi \quad (19)$$

where  $L$  is an average distance between the loops. If the picture makes sense we might hope that in the scaling region, quantities as  $K\xi^2$  reach a stable value and represent "physically" measurable quantities, as other dimensionless ratios in the more complete theory including quarks. Present values for  $K\xi^2$  seem to be of order 0.1 within large uncertainties<sup>[6]</sup>. This would put the glue ball mass above 1 GeV.

To develop a qualitative understanding of the phenomena occurring in lattice gauge fields it was useful to vary the space time dimension  $d$ , or the group, considering for instance the case when  $G$  was a finite group, either as an approximation to the realistic group, for instance finite subgroups of  $SU(2)$  or  $SU(3)$ , or even the simplest case of a group  $Z_2$  reduced to two elements  $\pm 1$ . This toy model, a gauge generalization of the Ising model, allows to exhibit the techniques involved in handling lattice models while avoiding cumbersome algebra and

may serve to

3. Strong cou

For large  
ter is natur  
sion  $d$ , with

$\sigma_p$  is the pr

(with a simi  
Then

$(\cosh \beta)^{-N}$

$\frac{F}{d(d-1)}$

In the expan  
plaquettes s  
selected pla  
 $N$  and the co  
is the one a  
written abov  
would corres  
configuratio  
becomes quic  
cluding the  
are or are g  
Wilson and c  
extrapolatio

The fact  
reflection c  
in two dimen



may serve to test approximations or numerical simulations.

### 3. Strong coupling expansions and mean field approximation.

For large coupling, i.e. small  $\beta$ , an expansion in  $\beta$  or a related parameter is natural. Consider for simplicity the  $Z_2$  gauge theory in arbitrary dimension  $d$ , with

$$Z = 2^{-Nd} \sum_{\sigma_p = \pm 1} \exp \beta \sum_p \sigma_p = \exp NF(\beta) \quad (20)$$

$\sigma_p$  is the product of link invariables around a plaquette. Write

$$e^{\beta \sigma_p} = \cosh \beta (1 + t \sigma_p) \quad t = \tanh \beta \quad (21)$$

(with a similar expansion in irreducible characters for the general case). Then

$$(\cosh \beta)^{-Nd(d-1)/2} Z = \sum_{\text{closed surfaces } S} t^{|S|} \quad (22)$$

$$= 1 + N \frac{d(d-1)(d-2)}{6} t^6 + N \frac{d(d-1)(d-2)}{2} (2d-5) t^{10} + \dots$$

$$\frac{F}{d(d-1)} = \frac{1}{2} \ln \cosh \beta + \frac{1}{2} (d-2) [\tanh \beta^6 + (2d-5) \tanh \beta^{10} + \dots]$$

In the expansion for  $Z$  the sum runs over "closed" surfaces - i.e. - sets of plaquettes such that any link of the lattice belongs to an even number of the selected plaquettes. The coefficient of a given power in  $t$  is an polynomial in  $N$  and the coefficient of the linear term, the reduced number of configurations, is the one appearing in the expansion for the free energy. The first term written above corresponds to a cube, the second to two adjacent cubes, the next would correspond to two disconnected cubes and so on. Enumerating the closed configurations, attaching in the general case the relevant group factors, becomes quickly cumbersome. More sophisticated techniques become necessary including the use of a computer<sup>[4][7]</sup>. Nevertheless such strong coupling series are or are getting available up to order 22 in certain cases, thanks to K. Wilson and others. They allow the study of the strong coupling region using extrapolation methods like Padé approximants.

The factor  $(d-2)$  occurring in the expansion for the free energy in (22) is a reflection of the fact that pure gauge theory is trivial (and always confining) in two dimensions.

One can of course obtain expansions for the Wilson loop and therefore the string tension

$$-K a^2 = \ln(\tanh \beta) + 2(d-2)(\tanh \beta)^4 + \dots \quad (23)$$

Indeed the Wilson criterion is fulfilled in the strong coupling regime, of course assuming that the relevant selection rules on group representation are fulfilled in the realistic SU(3) case. The expansion for  $\langle W(C) \rangle$  involves a summation over closed surfaces bounded by C and weighted by a factor decaying exponentially with their area.

It is interesting to compare the computer simulations for the string tension, or the internal energy (the derivative of the free energy) with the first few terms of the strong coupling series. The agreement is impressive over a large range of  $\beta$ , up to values of order unity (depending of course on the specific normalization adopted in each case) where a sudden turn over to the weak coupling regime takes place.

In the study of statistical models based on global symmetries a valuable tool of analysis has been the mean field approximation. At low temperature (small  $g_0$ ) the systems tend to get ordered, the tendency being favored by an increasing relative weight of energy (interpreted here as action) versus entropy. A way to achieve this is to increase the dimension d. The effect of neighboring variables can then be accounted for by a mean ordering field, determines self-consistently, treating its fluctuations as perturbations. To illustrate the idea consider an Ising system with

$$Z = 2^{-N} \sum_{\sigma_x = \pm 1} \exp \beta \sum_{(xy)} \sigma_x \sigma_y \quad (24)$$

Let us first derive an exact "equation of motion" using the invariance of the summation under the redefinition  $\sigma_x \rightarrow \varepsilon \sigma_x$ ,  $\varepsilon = \pm 1$ . This leads to the relation

$$1 = \langle \exp - 2\beta \sigma_x \sum_{y(x)} \sigma_y \rangle, \quad (25)$$

where the sum in the exponential runs over the neighbors of the spin  $J_x$ . Set

$$H_x = \beta \sum_{y(x)} \sigma_y \quad (26)$$

Then we have the exact relation

$$\langle \cosh 2H_x - 1 \rangle = \langle \sigma_x \sinh 2H_x \rangle \quad (27)$$

For large  
range  $\bar{H}$  (a  
to make t  
approxima

Above scm  
tion indi  
The trans  
at the cr  
dimensio  
ques base  
cal behav  
rigorous  
developed

Let  
tions ar

and the c

F<sub>mean fie</sub>  
Analysis  
B<sub>c</sub> of orde  
is consid

At f:  
gauge inv  
we shoul  
point equ

For large coordination number  $-2d$  we are tempted to approximate  $H_x$  by an average  $\bar{H}$  (an infinitesimal symmetry breaking external field is in fact necessary to make this statement meaningful) and (26) and (27) lead to the mean field approximation

$$\begin{aligned}\bar{H} &= 2d \beta \langle \sigma \rangle \\ \langle \sigma \rangle &= \tanh \bar{H}\end{aligned}\quad (28)$$

Above some critical value  $\beta_c = \frac{1}{2d}$  these equations admit a non trivial solution indicating a magnetized phase while below  $\beta_c$  one has a disordered phase. The transition is second order with the magnetization vanishing as  $(\beta - \beta_c)^{1/2}$  at the critical point. Of course, this is a crude approximation. In low enough dimensions ( $d < 4$ ) critical fluctuations are important and sophisticated techniques based on the renormalization group are needed to obtain the correct critical behavior. In any case the mean field approximation can be turned into a rigorous inequality on the free energy and a systematic perturbation theory developed around it.

Let us blindly repeat the same steps for a  $Z_2$  gauge theory. The exact relations are with obvious notations

$$\langle \cosh 2H_\ell - 1 \rangle = \langle \sigma_\ell \sinh 2H_\ell \rangle$$

$$H_\ell = \beta \sum_{p \in \ell} \sigma_{\ell_1} \sigma_{\ell_2} \sigma_{\ell_3} \dots$$

and the corresponding meanfield approximation is

$$\bar{H} = 2\beta(d-1) \langle \sigma_\ell \rangle^3$$

$$\langle \sigma_\ell \rangle = \tanh \bar{H} \quad (30)$$

$$F_{\text{mean field}} = F_0 + \sup \left\{ 0, \frac{d(d-1)}{2} (\tanh \bar{H})^4 + d[\ln(\cosh \bar{H}) - \bar{H} \tanh \bar{H}] \right\}$$

Analysis of these equations show a first order transition for a critical value  $\beta_c$  of order  $\text{cst}/2(d-1)$  and this behavior is generic no matter which gauge group is considered.

At first this looks totally unfounded. Indeed the approximation violates gauge invariance and a theorem of Elitzur [8] states that for all values of  $\beta$  we should find  $\langle \sigma_\ell \rangle = 0$ . However equations (30) can be shown to be saddle point equations which not only admit uniform solutions but gauge transformed

thereof. Upon averaging over all saddle points, non invariant quantities vanish as they should, while gauge invariant ones are unaffected. For  $\beta < \beta_c$  the Wilson loop vanishes in our approximation, while beyond  $\beta_c$  it obeys a perimeter law. It can be shown from the low temperature expansion that the predictions of mean field theory are valid term by term.

Of course the above techniques can be extended to more complex situations in particular to the case of Higgs couplings. The phase diagram admits two second order transitions connected by first order lines. The first one is the Higgs symmetry breaking in the absence of gauge fields. The second one occurs for non vanishing coupling. A recent analysis by Brézin and Drouffe<sup>[9]</sup> shows that it is of the  $\phi^4$  type.

For  $\beta < \beta_c$  the mean field approximation predicts (up to  $1/d$  corrections) a trivial confining phase. This may in fact not be correct as suggested by Drouffe, Parisi and Sourlas<sup>[10]</sup>. They observe that for  $\beta$  small and  $d$  large one can write an approximate equation for the internal energy  $p = \langle \sigma_p \rangle$ , expressing the fact that each plaquette can be decorated by a cube of plaquettes, the cubes being non overlapping in the large  $d$  limit. This is expressed by the equations

$$p = t + 2d p^5$$

$$F_{D.P.S.} = \frac{d(d-1)}{2} \ln \cosh \beta + \frac{d^3}{6} p^6 - d^4 p^{10} \quad (31)$$

Or setting

$$u = 2d p^4 \quad (32)$$

$$u(1-u)^4 = 2dt^4, \quad F_{D.P.S.} = \frac{d(d-1)}{2} \ln \cosh \beta + \frac{d^{3/2} u^{3/2}}{12\sqrt{2}} (1-3u) \quad (33)$$

This shows that  $t$  scales like  $d^{-1/4}$  and predicts a transition in a metastable phase beyond  $\beta_c$ .

#### 4. Duality and topological excitations

Abelian models admit Kramers-Wannier duality transformations which interchange high and low temperatures. For simplicity let us again limit ourselves to  $Z_2$  theories and consider first a three dimensional case where

$$Z_3^{\text{gauge}}(\beta) = (\cosh \beta)^{3N} \sum_{\text{closed surfaces } S} (\tanh \beta)^{|S|} \quad (34)$$

To describe a closed surface we can assign values  $\tilde{\sigma}_i = \pm 1$  at the center of cubes with the condition that neighboring cubes have opposite  $\tilde{\sigma}$  if their common

plaquette be  
over nearest  
3-dimensional

the precise

Similarly the  
transition,

This has been  
of first order

Abelian  
models for  
second order  
phase admits  
finiteness as  $Z_2$

Under du-  
latter is a  
with coupling  
dimensions)  
self dual we  
 $\beta$ . It turns  
a perimeter  
decrease. The  
fields provide  
are modified

As mentioned  
a second order  
Thouless transi-  
tional excitations  
for this transition

plaquette belongs to the surface. This yields  $|S| = \sum_{(ij)} \frac{1 - \tilde{\sigma}_i \tilde{\sigma}_j}{2}$ , a sum over nearest neighbors. We then recognize that the gauge model is dual to the 3-dimensional model at a dual temperature  $\tilde{\beta}$  given by

$$\tanh \beta = e^{-2\tilde{\beta}} \quad (35)$$

the precise relation being

$$Z_3^{\text{gauge}}(\beta) = 2^{-N/2} (\sinh 2\beta)^{3N/2} Z_3^{\text{Ising}}(\tilde{\beta}) \quad (36)$$

Similarly the 4-dimensional model is self dual. If it has a unique deconfining transition, this should occur at the self dual point

$$\tanh \beta_c = \sqrt{2} - 1 \quad (37)$$

This has been confirmed by Monte Carlo simulations, the transition being found of first order.

Abelian models admit generalizations of this duality transformation. The  $Z_N$  models for  $N > 4$  have three phases with dual transition points (presumably of second order), one of finite value the other increasing like  $N^2$ . The middle phase admits probably massless excitations of photon type and extending to infinity as  $Z_N \rightarrow U(1)$ .

Under duality a Wilson loop transforms into a 't Hooft loop<sup>[11]</sup>. The latter is a ratio  $Z^F(\tilde{\beta})/Z(\tilde{\beta})$ , where  $Z^F(\tilde{\beta})$  is a frustrated partition function with couplings reversed for all plaquettes (in 4-dimensions) or links (in 3-dimensions) dual to those of a fiducial surface bounded by C. When the model is self dual we can consider both Wilson and 't Hooft loops at the same value of  $\beta$ . It turns out that when one of those has an area law decrease the other has a perimeter law. In the intermediate phase of  $Z_N$  models both have perimeter decrease. The concept of 't Hooft loop can be generalized to non abelian gauge fields provided the action admits transformations when the plaquette variables are modified by an element of the group.

As mentioned above the  $U(1)$  case appears as a limit of  $Z_N$  models and exhibits a second order deconfining transition, to be contrasted with the Kosterlitz-Thouless transition of the two-dimensional XY model. Interactions among topological excitations, monopole strings for the  $U(1)$  model seem to be responsible for this transition.

It would be very interesting to be able to assess the role of instanton-configurations in the non-abelian case.

### 5. Roughening

Underlying gauge models is a theory of surfaces. It can be studied by continuous field theoretic methods<sup>[12]</sup> or approached from the lattice point of view. Several groups<sup>[13]</sup> have rediscovered recently a phenomenon studied several years ago by crystal growth physicists<sup>[14]</sup>, i.e. surface roughening. This appears as a singularity (presumably an essential singularity) in the string tension computed on the lattice well before the deconfining transition. For instance any attempt at extrapolating the 3-dimensional  $Z_2$  tension

$$-Ka^2 = \ln t + 2t^4 + 2t^6 + 10t^8 + 16t^{10} + 80\frac{2}{3}t^{12} + 150t^{14} + 734t^{16} + 1444\frac{2}{3}t^{18} + \dots \quad (38)$$

suggests erroneously that it vanishes well before the critical bulk transition at  $t_c \approx 0.6418$ . Indeed roughening occurs at  $t_R = 0.46$ . The phenomenon can be understood through duality using the low temperature phase of the Ising model. We saw that the tension can then be identified with the interfacial free energy (per unit surface) of two coexisting phases. This can be modelled by a so called solid on solid (SOS) partition function which admits an XY type transition restoring translational symmetry in the direction perpendicular to the original interface. These deformations of surfaces can be tested using various indicators which generalize to other gauge groups and other dimensions.

It is interesting to note that in 4 dimension the roughening transition occurs in the region of rapid change between strong and weak coupling for SU(2) or SU(3) and almost at the self-dual point for the  $Z_2$  gauge model. Beyond roughening the fluctuations of the surface generate a universal correction<sup>[15]</sup> to the  $q\bar{q}$  static potential

$$\delta V = -\frac{(d-2)\pi}{24 R} \quad (39)$$

### 6. Conclusion

The beautiful data from Monte Carlo calculations have hardly been discussed above. A major advance is in the process of producing new results by including fermions into the picture. The phenomenology of lattice gauge theories is

extremely r  
greatest in  
tions which  
recent obser  
SU(N),  $N \geq 2$   
SO(3). Perha  
a rather sma  
freedom are

### REFERENCES

- [1] K. Wilson
- [2] K. Wilson
- eds. Acc
- [3] M. Creutz
- Phys. Re
- M. Creutz
- C. Rebbi
- [4] R. Bali
- 2098, 2
- [5] H.B. Nielsen
- L.H. Kar
- [6] B. Berg
- G. Bhan
- [7] J.M. Drouot
- [8] S. Elitz
- [9] E. Brézin
- [10] J.M. Drouot
- [11] G. 't Hooft
- [12] A.M. Polyakov
- [13] A. E. An
- P. Weiss
- Zuber, P
- [14] For a re
- Prigogin
- [15] M. Lüscher

extremely rich and although we have not been able to address the questions of greatest interest to particle physicists, we have uncovered interesting transitions which still await a better explanation. Let us quote for instance the recent observation of first order transitions (presumably not deconfining) for  $SU(N)$ ,  $N \geq 5$  in four dimensions using Wilson's action or similar phenomena for  $SO(3)$ . Perhaps the greatest achievement so far has been the realization that on a rather small lattice, the simulations reveal that the ideas of asymptotic freedom are numerically verified.

#### REFERENCES

- [1] K. Wilson, Phys. Rev. D10, 2445 (1974).
- [2] K. Wilson in Proceedings of the Cargèse 1979 Summer School, 't Hooft et al. eds. Academic Press, New York (1980).
- [3] M. Creutz, L. Jacobs, C. Rebbi, Phys. Rev. Lett. 42, 1390 (1979),  
Phys. Rev. D20, 1915 (1979).  
M. Creutz, Phys. Rev. Lett. 43, 553 (1979).  
C. Rebbi, Phys. Rev. D21, 3350 (1980).
- [4] R. Balian, J.M. Drouffe, C. Itzykson, Phys. Rev. D10, 3376 (1974); D11, 2098, 2104 (1975).
- [5] H.B. Nielsen and M. Ninomiya, Rutherford preprints ;  
L.H. Karsten and J. Smit, Amsterdam preprint.
- [6] B. Berg, Phys. Mett. 97B, 401 (1980).  
G. Bhanot and C. Rebbi, to appear in Nuclear Phys. B.
- [7] J.M. Drouffe, Nucl. Phys. B170, FS1 , 91 (1980).
- [8] S. Elitzur, Phys. Rev. D12, 3978 (1975).
- [9] E. Brézin, J.M. Drouffe, Saclay preprint.
- [10] J.M. Drouffe, G. Parisi, N. Sourlas, Nucl. Phys. B161, 397 (1979).
- [11] G. 't Hooft, Nucl. Phys. B153, 141 (1979).
- [12] A.M. Polyakov, Landau Institute preprint, Moscou (1981).
- [13] A. E. and P. Hasenfratz, Nucl. Phys. B (to appear), M. Luscher, G. Münster, P. Weisz, Nucl. Phys. B180, FS2 13 (1981), C. Itzykson, M. Peskin, J.B. Zuber, Phys. Lett. 95B, 259 (1980).
- [14] For a review see J.D. Weeks, G.H. Gilmer, Adv. in Chem. Phys. 40, eds. Prigogine and Rice (J. Wiley and Sons, 1979).
- [15] M. Lüscher, Nuclear Phys. B (to appear).

GRIBOV COPIES AND INSTANTONS

W. Nahm

CERN, Geneva, Switzerland

ABSTRACT

Gribov copies are closely related to instanton effects. Thus they are of semi-classical nature and have nothing to do with confinement.

(author)

Whereas  
stood, we st  
constants.  
 $\exp(-a_1/g)$ ,  
calculate<sup>1)</sup>,  
proportional  
function. T  
yet be evalu

In non-  
additional n  
tried to rel

the Hamilton

H

where  $\rho$  is  
electric fie

is the procu  
for suffici  
 $x$  be a zero

is in the Co  
non-unique,  
finite. Ga  
copies. Be



Whereas superrenormalizable quantum field theories are rather well understood, we still do not know how to handle theories with renormalized coupling constants. The non-perturbative contributions to the former are proportional to  $\exp(-\alpha_I/g)$ , where  $\alpha_I$  is an instanton action. They are not difficult to calculate<sup>1),2)</sup>. Strictly renormalizable theories get additional contributions proportional to  $\exp(-2/\beta_2 g)$ , where  $\beta_2$  is the leading coefficient of the  $\beta$  function. These contributions, which are reflected by the Landau pole, cannot yet be evaluated.

In non-Abelian gauge theories, the breakdown of linear gauges is an important additional non-perturbative effect which has been discovered by Gribov<sup>3),4)</sup>. He tried to relate this effect to the Landau pole. In the Coulomb gauge

$$\partial_i A_i = 0, \quad (1)$$

$$A_i(\vec{x}) = o(r^{-1}) \quad (2)$$

the Hamiltonian takes the form

$$H = \frac{1}{2} \left( \rho \tilde{\Delta}^{-1} \Delta \tilde{\Delta}^{-1} \rho + E_\perp^2 + B^2 \right) \quad (3)$$

where  $\rho$  is the charge density,  $B$  is the magnetic field and  $E_\perp$  the transverse electric field. Moreover

$$\tilde{\Delta} = \partial_i^2 + A_i \partial_i \quad (4)$$

is the product of an ordinary and a covariant derivative. Gribov pointed out that for sufficiently large fields,  $\tilde{\Delta}$  acquires zero or negative eigenvalues. Let  $\chi$  be a zero mode of  $\tilde{\Delta}$ . Then besides  $A_i$  also its infinitesimal gauge transform

$$A_i' = A_i + \varepsilon (\partial_i + A_i) \chi \quad (5)$$

is in the Coulomb gauge. For larger fields, the Coulomb gauge continues to be non-unique, but the gauge transformations which preserve the Coulomb gauge become finite. Gauge equivalent potentials in the same linear gauge are called Gribov copies. Because of the zero modes of  $\tilde{\Delta}$ , the non-uniqueness of the Coulomb

gauge is related to an important increase in the interaction energy between non-Abelian charges. Gribov compared this increase to the one which shows up in perturbation theory, where the leading logarithms yield

$$V(r) = \frac{g^2}{F} (1 - \beta_2 g^2 \log(1/r))^{-1} \quad (6)$$

Here the singularity at finite distance corresponds to the Landau pole and indicates confinement. However, despite the superficial similarity of the two effects, one cannot conclude that they are related. In fact the Landau pole only exists in four dimensions, whereas Gribov copies occur in any dimension. Moreover, instanton effects also increase the interaction between non-Abelian charges, but they do not yield confinement<sup>5)</sup>. Gribov copies must exist in any linear gauge, as Singer has shown<sup>6)</sup>. He considered the topological space

$$N = (\text{space of gauge potentials } A_i(\vec{x})) / (\text{group of gauge transformations}) \quad (7)$$

A linear gauge is a local parametrization of  $N$  as a linear space. As for manifolds of finite dimension, it is obvious that one needs more than one chart to cover all of  $N$ , if  $N$  is topologically non-trivial. A global parametrization of  $N$  as a linear space is only possible, if  $N$  is contractible.

The easiest way to determine the topology of  $N$  is to implement a hyperaxial gauge. If we only look at a time slice, which is appropriate for considerations concerning the Coulomb gauge, we may forget about  $A_0$  and take

$$\begin{aligned} A_1(x_1, x_2, x_3) &= 0, \\ A_2(0, x_2, x_3) &= 0, \\ A_3(0, 0, x_3) &= 0. \end{aligned} \quad (8)$$

This gauge yields a complete and unique parametrization of  $N$ . But it cannot parametrize  $N$  as a linear space. This is due to the fact that condition (2) in general is violated. Consequently, Wilson loops on the sphere at infinity  $S_\infty^2$  might be non-trivial. To get rid of unwanted fields at infinity we must impose that for  $x, x_0 \in S_\infty^2$  the path ordered exponential

does not depend on the gauge group

For non-abelian condition (9)  $A^{(1)}, A^{(2)}$  with

again yield the same behaviour is topological cohomology  $H^1(X)$ . As

$N$  is homotopy equivalent to a fixed point set  $N$  are non-trivial

and  $G$  has no non-trivial homotopy group

$\pi_1$

A generator can be chosen  $t \in \mathbb{R}$ . The two loops both yield the same

This loop is not contractible in Coulomb gauge<sup>7)</sup> copies<sup>8)</sup>.

$$P \exp \int_{x_0}^x A_i dx^i = g(x) \in G \quad (9)$$

(6)

does not depend on the path, as long as the latter is contained in  $S_\infty^2$ .  $G$  is the gauge group.

For non-Abelian groups, general linear combinations of potentials fulfilling condition (9) lose this path independence. On the other hand, for two potentials  $A^{(1)}$ ,  $A^{(2)}$  with the same asymptotic behaviour, linear combinations

$$A_i = \lambda A_i^{(1)} + (1-\lambda) A_i^{(2)} \quad (10)$$

again yield the same  $g(x)$ . Thus the space of potentials with given asymptotic behaviour is an affine space and topologically trivial. Consequently, all the topological complexity of  $N$  is contained in the asymptotic data described in  $g(x)$ . As

$$g(x_0) = 1, \quad (11)$$

$N$  is homotopic to the space of maps  $g: S_\infty^2 \rightarrow G$  which take one point  $x_0$  to a fixed point of  $G$ . This space is called  $\Omega^2 G$ . Many of the homotopy groups of  $N$  are non-trivial, as

$$\pi_n(\Omega^k G) = \pi_{n+k}(G), \quad (12)$$

and  $G$  has non-trivial homotopy groups for arbitrarily high  $n$ . The simplest homotopy group of  $N$  is, for simple  $G$ ,

$$\pi_1(\Omega^2 G) = \pi_3(G) = \mathbb{Z}. \quad (13)$$

A generator consists of time slices through an instanton, indexed by the time  $t \in \mathbb{R}$ . The two points  $t = \pm\infty$  have to be identified, which is possible, as both yield the vacuum.

This loop in  $N$  cannot be contained in a single linear chart of  $N$ , as it is not contractable. In other words, instantons cannot be put into the Coulomb gauge<sup>7)</sup>. Indeed the central section through an instanton yields Gribov copies<sup>8)</sup>.

To estimate the size of non-perturbative terms due to Gribov copies, let us follow Gribov's procedure and consider Euclidean functional integrals, imposing the Lorentz gauge

$$\partial_\mu A_\mu = 0, \quad (14)$$

with boundary condition analogous to Eq. (2). In complete analogy to the preceding considerations, we obtain for our space  $M$  of classes of gauge equivalent potentials

$$M \approx \Omega^3 G, \quad (15)$$

where the elements of  $\Omega^3 G$  are functions  $g: S_\infty^3 \rightarrow G$ .

$M$  consists of discrete components  $M_k$ , according to the winding number  $k$  of the map  $g(x)$ . The components have the same homotopy groups, as one may go from one to another by introducing fixed instantons or anti-instantons at some points.

Let us consider  $M_0$ . For small action, no Gribov copies occur. Thus they may indeed be regarded as a non-perturbative effect. If Gribov copies start to occur at action  $b_1$ , their effect should be proportional to  $\exp(-b_1/g^2)$ . Thus let us consider the spaces

$$M(b) = \{A_\mu \in M_0 \mid \alpha(A_\mu) \leq b\}, \quad (16)$$

where  $\alpha$  is the Yang-Mills action.

For sufficiently small  $b$ , the subspace  $M(b)$  of  $M_0$  is topologically trivial. Accordingly, there is no topological obstruction to the implementation of a linear gauge like the Lorentz gauge. But if  $b$  becomes large enough, such that a generator of a non-trivial homotopy group  $\pi_n(M_0)$  can be realized as a map  $S^n \rightarrow M(b)$ , such a parametrization is no longer possible.

The critical levels  $b_1, b_2, \dots$ , at which the topology of  $M(b)$  changes are the actions of stationary points or virtual stationary points<sup>9)</sup>. The former are finite action solutions of the Euclidean equations of motion

$$\alpha'(A_\mu) = 0 \quad (17)$$

Virtual s  
 $\alpha'(A_\mu)$  a  
Gribov co  
approxima  
the insta  
and an an  
 $G = SU(2)$

$\pi$

A generat

and by pa  
symmetry.

We parame  
real numb  
given by

We rewri  
and norma

We obtain  
tively th  
sees the  
the inter  
phase, at

copies, let  
 brals, imposing

(14)

to the pre-  
 ge equivalent

(15)

ing number  
 as one may  
 antons at

Thus they  
 es start  
 $(-b_1/g^2)$ .

(16)

logically  
 eplementation  
 enough,  
 e realized

(b) changes  
 The former

(17)

Virtual stationary points are limiting configurations of finite action for which  $\alpha'(A_\mu)$  approaches zero. This means that non-perturbative contributions due to Gribov copies can be identified with semi-classical contributions due to exact or approximate solutions for the equations of motion. One expects that  $b_1$  is twice the instanton action  $\alpha_I$  and corresponds to a configuration with an instanton and an anti-instanton which are well separated. In fact let us consider  $G = SU(2)$  and

$$\pi_1(\Omega^3 SU(2)) = \pi_4(S^3) = \mathbb{Z}_2. \quad (18)$$

A generator can be obtained by starting from a generator of

$$\pi_1(\Omega^2 S^2) = \pi_3(S^2) = \mathbb{Z} \quad (19)$$

and by passing from a generating map  $S^3 \rightarrow S^2$  to a map  $S^4 \rightarrow S^3$  by radial symmetry. A generator of  $\pi_3(S^2)$  is given by the Hopf map

$$S^3 = SU(2) \rightarrow SU(2)/U(1) = S^2. \quad (20)$$

We parametrize  $SU(2)$  by the non-zero quaternions  $(p, q, r, s)$  modulo the positive real numbers and  $S^2$  by the complex numbers including  $\infty$ . The Hopf map is given by

$$z = \frac{r + is}{p + iq}. \quad (21)$$

We rewrite this map as a generator of  $\pi_1(\Omega^2 S^2)$  by using  $p$  as a parameter and normalizing to

$$q^2 + r^2 + s^2 = 1. \quad (22)$$

We obtain a family configurations of the  $O(3)$  non-linear  $\sigma$  model. Qualitatively this family of maps may be described as follows: for  $-\infty < p < 0$  one sees the gradual creation of an instanton-anti-instanton pair. Simultaneously the internal orientations of instanton and anti-instanton, given by a  $U(1)$  phase, approach values differing by  $\pi$ . At  $p = 0$ , the element of  $\Omega^2 S^2$

is a map of the half-sphere  $q \leq 0$  onto all of  $S^2$ , i.e., a somewhat deformed complete instanton, whereas  $q \geq 0$  yields an anti-instanton. For  $0 \leq p \leq \infty$  the relative orientation goes to  $2\pi$  and instanton and anti-instanton annihilate again.

By rotational symmetry one easily extends this family of maps to a family of  $\Omega^3 S^3 = \Omega^3 SU(2)$ . Interpreting the elements of  $\Omega^3 SU(2)$  as asymptotic data in a Hyperaxial gauge, one sees the creation and destruction of Yang-Mills instantons, which can be described in almost the same words as for the  $\sigma$  model case above. There is only one small difference. Relative internal orientations are now described by elements of  $SU(2)/Z_2 = SO(3)$ . A family of configurations describing a change in the relative orientation from 0 to  $2\pi$  is topologically non-trivial, but a change from 0 to  $4\pi$  can be continuously deformed to a trivial change. This explains why we get  $Z_2$  in Eq. (18), but  $Z$  in Eq. (19).

The configurations described above have a maximal action which is somewhat higher than  $2\alpha_1$ , but they can easily be changed in such a way that one gets down as close to  $2\alpha_1$  as one wants. One simply has to keep the relative internal orientation of instanton and anti-instanton at zero, until they are far apart. As long as it is zero, instanton and anti-instanton attract each other, and the action is less than  $2\alpha_1$ . For relative orientation  $\pi$  one finds a repulsion, but the interaction energy decreases with the fourth power of the distance. Thus no linear gauge can work for  $M(b)$ , if  $b$  is larger than  $2\alpha_1$ . But topological arguments cannot exclude that a specific gauge like the Lorentz gauge becomes non-unique already for smaller  $b$ . Following a suggestion by Gribov, the range of validity of this gauge has been investigated by Abarbanel, Bartels and Creamer<sup>10)</sup>. They considered potentials of the form

$$A_\mu^{kl} = \frac{2\chi(x^2)}{x^2} (x^k \delta_\mu^l - x^l \delta_\mu^k), \quad k, l = 1, \dots, 4 \quad (23)$$

and gauge transformations of type

$$\chi^{kl} = \frac{2\chi(x^2)}{x^2} (x^k \delta_\rho^l - x^l \delta_\rho^k), \quad \rho \text{ fixed}, \quad (24)$$

writing everything in terms of the Lie algebra  $O(4) = SU(2) \oplus SU(2)$ . With this restriction they found no Gribov copies for actions less than  $2\alpha_1$ . In accordance with our general considerations, the configuration of lowest action for which they found such copies was an instanton of infinitesimal size embedded into an anti-instanton.

We have  
of semi-cl-  
than  $1/\beta_2$   
have a quit  
confinement

#### ACKNOWLEDGE

I am  
tions menti

#### REFERENCES

- 1) W.Y. Cr
- 2) W. Nahr  
Bao
- 3) Y.N. Gr
- 4) Y.N. Gr
- 5) C. Call
- 6) I.M. Sin
- 7) M. Adem
- 8) R. Jack
- 9) W. Nahr
- 10) E.D. Ab

We have seen that non-perturbative contributions due to Gribov copies are of semi-classical type and proportional to  $\exp(-2\alpha_1/g^2)$ . As  $\alpha_1$  is larger than  $1/\beta_2$ , they are dominated by the renormalization contributions, which have a quite different origin. Thus Gribov copies cannot tell us much about confinement.

#### ACKNOWLEDGEMENT

I am indebted to J. Bartels for telling me about the unpublished calculations mentioned above.

#### REFERENCES

- 1) W.Y. Crutchfield, Phys. Rev. D19 (1979) 2370.
- 2) W. Nahm, Semi-classical non-perturbative effects in quantum field theory, Bad Honnef Summer Institute, FU Berlin HEP 16/80 (1980).
- 3) Y.N. Gribov, Materials for the 12th LNPI Winter School, Vol. 1, p. 147 (1977).
- 4) Y.N. Gribov, Nucl. Phys. B139 (1978) 1.
- 5) C. Callan, R. Dashen and G. Gross, Phys. Rev. D17 (1978) 2717.
- 6) I.M. Singer, Comm. Math. Phys. 60 (1978) 7.
- 7) M. Ademollo, E. Napolitano and S. Sciuto, Nucl. Phys. B134 (1978) 477.
- 8) R. Jackiw, I. Muzinick and C. Rebbi, Phys. Rev. D17 (1978) 1576.
- 9) W. Nahm, Phys. Lett. B96 (1980) 323.
- 10) H.D. Abarbanel, J. Bartels and D. Creamer, unpublished.

With  
In  
action  
embedded

# LARGE N EXPANSIONS WORK

Leonard D. Mlodinow \*

Max-Planck-Institut für Physik und Astrophysik  
München, Fed.Rep.Germany

## Abstract

We analyze large  $N$  expansions for a  
wide variety of quantum mechanical problems.

(author)

\* Present address: Lauritsen Laboratory of Physics, California Institute  
of Technology, Pasadena, California, 91125, USA.

There a  
dinger prob  
(coupling co  
quantum mecr  
cation to th  
theory. In r  
apparent. I-  
so well for  
the problems  
correctly d  
of an incap  
The develop  
prise. Semi  
large  $N$  exp  
strong deba  
applying th  
describe th  
numerical r  
physics are  
 $N$  expansion  
coupling co  
tion to the  
of the meth  
is indirect  
and is cert

Expand  
seem, and t  
of perturbe  
of orientat  
Since the s  
no skill or



There are two predominant methods for the approximate solution of Schrödinger problems: the Rayleigh-Ritz variational method and Rayleigh-Schrödinger (coupling constant) perturbation theory. Because of their successes in elementary quantum mechanics, these methods have also been extensively developed for application to the more complicated problems of many body physics or quantum field theory. In recent years the limitations of these methods have become increasingly apparent. In particular, coupling constant perturbation theory, which worked so well for quantum electrodynamics, is much less useful as a method for solving the problems of quantum chromodynamics. QCD is a theory which many people believe correctly describes the phenomena of strong interactions, despite somewhat of an incapacity on their part to actually calculate what the theory predicts. The development of new computational methods has thus become an important enterprise. Semi-classical methods have been given special attention. The so-called large  $N$  expansions are one class of methods that have spawned particularly strong debate with regard to both their accuracy and the possibility of ever applying them to a physically relevant field theory [1]. In this talk I will describe the application of such expansions to quantum mechanics [2-6]. The numerical results for a wide variety of problems in atomic and solid state physics are impressive and indicate that for quantum mechanical problems large  $N$  expansions may be more generally useful than either variational methods or coupling constant perturbation theory. These results are in direct contradiction to the folklore [7] that prevailed prior to the systematic development of the method. The relevance to gauge theories of the work to be described, is indirect, but it does provide some general insight into large  $N$  expansions and is certainly encouraging.

Expanding in the number of space dimensions is not as exotic as it may seem, and the reader should not expect that what follows will be a lurid tale of perturbed life in lands of fractional or negative dimension. For purposes of orientation, let us examine the large  $N$  expansion of the Coulomb spectrum. Since the spectrum is known exactly, obtaining the large  $N$  series requires no skill other than that of forming a Taylor expansion:

$$\xi = - \frac{e^4}{2 [n + l + (N-1)/2]^2} \quad n, l = 0, 1, 2, \dots \quad (1)$$

Using the notation  $2k = l + \frac{1}{2} N$ , we can write eqn. (1) as

$$\mathcal{E} = -\frac{e^4}{2(2k)^2} \left[ 1 + 2\left(\frac{1}{2} - n\right) \frac{1}{2k} + 3\left(\frac{1}{2} - n\right)^2 \frac{1}{(2k)^2} + O(k^{-3}) \right] \quad (2)$$

We have not expanded in  $k^{-1}$  because of a perverted desire to use every letter of the latin alphabet, but because for spherically symmetric one particle problems it is the natural parameter (see ref. [2]). The series (2) converges for  $|n - \frac{1}{2}| \leq 2k$ . Therefore, eqn. (2) may be used to approximate the eigenvalues of the low lying states in each angular momentum sector. In three dimensions, keeping only the first three terms of eqn. (2), we obtain 88.8, 97.3, and 98.85 % of the ground state ( $n = 0$ ) energy for  $l = 0, 1, 2$  respectively. Such success is not atypical.

Even when it does not converge, the expansion often yields accurate numerical results. For example, the first three terms of the large  $N$  expansion for the ( $l = 0$ ) ground state energy of the three dimensional linear potential yields [2] the value (for  $\hbar = 1 = m$ ,  $e^2 = \frac{1}{2}$ ) 1.16849, as compared with the value 1.16905 calculated from the zeros of the Airy function. Table 1 displays results of the application of the expansion to a non-spherically symmetric problem, the Zeeman effect [3]. The magnetic field  $B$  is measured in units of  $2.35 \times 10^9$  Gauss. "Numerical" refers to the computer calculation of Prauddaude, whose results are quoted for purposes of comparison. The partial sums are defined by

$$S_l = \sum_{n=1}^l E_n k^{-n}, \quad k \equiv \frac{1}{2(l+1)}$$

where the  $E_n$  are the coefficients in the series for the energy:

$$\mathcal{E} = \sum_{n=1}^{\infty} E_n k^{-n}$$

Table I

Zeeman Effect: Detailed results for the ground state energies for field strengths in the intermediate region of magnetic field strength.

| Order of Partial Sums  | B = 0.1       |               | B = 1       |            |
|------------------------|---------------|---------------|-------------|------------|
|                        | m  = 0        | m  = 1        | m  = 0      | m  = 1     |
| -1.                    | -0.4987531018 | -0.1072596995 | -0.39430464 | 0.46431140 |
| 0                      | -0.4975131187 | -0.1001436571 | -0.31518804 | 0.56443907 |
| .1                     | -0.4975234646 | -0.1009260649 | -0.33569839 | 0.53790021 |
| 2                      | -0.4975267239 | -0.1008377222 | -0.32978649 | 0.54455051 |
| 3                      | -0.4975265088 | -0.1008459240 | -0.33166583 | 0.54350805 |
| 4                      | -0.4975264722 | -0.1008458342 | -0.33086730 | 0.54293046 |
| 5                      | -0.4975264802 | -0.1008456396 | -0.33152574 | 0.54396839 |
| 6                      | -0.4975264807 | -0.1008456496 | -0.33061686 | 0.54288265 |
| Numerical <sup>8</sup> | -0.49752(5)   | -0.10084(5)   | -0.33116(5) | 0.54341    |

The physical basis of the large N expansion is related to the fact that if the number of spatial dimensions increased, we'd all feel heavier. That statement can be made more precise. In particular, let's consider a single particle in a spherically symmetric potential  $V(r)$ . The Schrödinger equation ( $\hbar = m = 1$ ) reads:

$$\left[-\frac{1}{2}\nabla^2 + V(r)\right]\Psi(r) = \mathcal{E}\Psi(r), \quad (3)$$

where  $r \in \mathbb{R}^3$ . Eqn. (3) can be generalized in a trivial way by simply allowing  $r \in \mathbb{R}^N$ . We may also, however, generalize the form of  $V(r)$ . For instance, three possible generalizations of the Coulomb potential,  $-e^2/r$ , are

$$-\frac{N^2}{9} \frac{e^2}{r} \quad (4a)$$

$$-e^2 \int \frac{d^N k}{(2\pi)^N} \frac{4\pi}{k^2} e^{ik \cdot r} \quad (4b)$$

and

$$-\frac{e^2}{r} + (N-3)^{1/2} r^{1/2} \quad (4c)$$

A clever choice is (4a). To understand why, we separate variables (consider, for convenience  $\ell = 0$ ) and examine the radial equation. Furthermore, if  $\Psi(r)$  is the radial wave function we define

$$\phi(r) = r^{\frac{N-1}{2}} \Psi(r)$$

in order to eliminate the  $N$  dependence that otherwise hides in the scalar product. Then  $\phi$  obeys the equation (we drop the factor  $1/9$  in (4a), which is a mere matter of convention):

$$-\frac{1}{2} \frac{d^2 \phi}{dr^2} + N^2 \left[ \frac{(1-1/N)(1-3/N)}{8r^2} + V(r) \right] \phi = \xi \phi \quad (5)$$

The qualitative features of the effective potential term in eqn. (5) do not change as  $N$  grows, so we might hope that the  $N \rightarrow \infty$  limit and its corrections give a good approximation, at least for large  $N > 3$ . Actually, the large  $N$  limit of eqn. (5) has a deeper significance: it is the classical limit. To show that, we drop the lower order terms in eqn. (5), and divide by  $N^2$ , obtaining

$$-\frac{1}{2N^2} \frac{d^2 \phi}{dr^2} + V_{\text{eff}}(r) \phi = \lambda \phi \quad , \quad (6)$$

where we have defined

$$\lambda = \frac{\xi}{N^2} \quad , \quad V_{\text{eff}}(r) = \frac{1}{8r^2} + V(r) \quad . \quad (7)$$

Therefore  $N^2$  behaves like an effective mass, and in the limit  $N \rightarrow \infty$ , the particle will sit at the bottom,  $r_0$ , of  $V_{\text{eff}}(r)$  (assuming there is a bottom). The wave function in the large  $N$  limit is just

$$\phi(r) \sim \delta(r-r_0) \quad ,$$

and as  $N$  decreases from infinity,  $\phi$  relaxes approximately into a Gaussian peaked about  $r_0$ . The leading behavior of the energy spectrum is thus

$$\xi_n = V_{\text{eff}}(r_0) N^2 + (n + \frac{1}{2}) \sqrt{V_{\text{eff}}''(r_0)} N + O(1) \quad , \quad V_{\text{eff}}'' \equiv \frac{d^2 V_{\text{eff}}}{dr^2} \quad (8)$$

Combes et al. [8], obtained the Hamiltonian of eqn. (6) in their studies of the Born-Oppenheimer approximation, and rigorously proved that the limiting spectrum is given by (8).

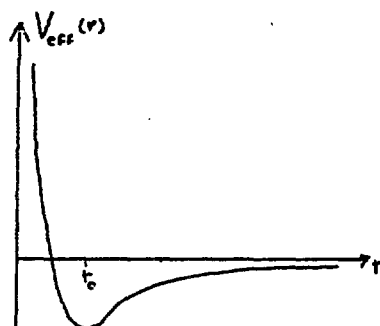


Figure 1

The calculation of corrections to the energy given by eqn. (8) can be performed using standard perturbation theory, with powers of  $N^{-1/2}$  masquerading as small coupling constants in a perturbing potential consisting of an infinity of terms. We first expand the effective potential about its minimum:

$$V_{\text{eff}}(r) = V_{\text{eff}}(r_0) + \frac{1}{2} V_{\text{eff}}''(r_0) (r-r_0)^2 + \dots \quad (9)$$

The interesting variable for the Schrödinger equation is  $r-r_0$ . It should be rescaled to reflect the fact that for large  $N$  it is harder to stray from  $r-r_0=0$ . In fact the interval  $-r_0 \leq (r-r_0) \leq \infty$  should, in the large  $N$  limit, be mapped onto  $[-\infty, \infty]$  in such a way that the leading terms displayed in eqn. (9) lead to the harmonic oscillator spectrum (8). Thus we define

$$X \equiv (r-r_0) N^{1/2} \quad (10)$$

Then the full Schrödinger equation (5) can be written

$$-\frac{1}{2} \frac{d^2 \phi}{dx^2} + \frac{1}{2} (V_{\text{eff}}''(1) X^2 - 1) \phi + \sum_{n=1}^{\infty} \left[ \frac{V_{\text{eff}}^{(n+2)}}{(n+2)!} X^{n+2} + \frac{(-1)^n (n+1)}{2} X^n + \frac{(-1)^n 3(n-1)}{8} X^{n-2} \right] N^{-\frac{n}{2}} \phi = E \phi \quad (11)$$

To abridge the discussion, we have assumed that  $V_{\text{eff}}$  is infinitely differentiable at the minimum  $r_0$ , which to simplify notation we suppose occurs at unity. We

have also used the definitions

$$V^{(m)} = \frac{d^m V_{\text{eff}}}{dr^m}(r_0) \quad (12)$$

and

$$E = \frac{\epsilon}{N} - N V_{\text{eff}}(r_0) \quad (13)$$

It is now a straightforward exercise to apply perturbation theory to calculate the corrections to the spectrum (8). In practice, much more powerful methods of developing the expansion exist, which reduce the problem to the evaluation of algebraic recursion relations, allowing one to calculate to very high order without summing over intermediate states [4-6,9]. An analogous method [6] provides very useful corresponding simplifications for ordinary coupling constant perturbation theory.

The above considerations can be phrased in an algebraic framework [2,3,5,6] that maintains the explicit connection with the classical problem, and thus facilitates the theoretical analysis, especially in the case of many particle problems, or problems lacking spherical symmetry. Suppose that we have an  $n$  body problem with spherical symmetry. Because of the  $O(N)$  invariance, instead of considering the original operators  $x_i^\alpha$  and  $p_i^\alpha$  ( $i = 1, 2, \dots, N$ ;  $\alpha = 1, 2, \dots, n$ ), we need only consider the rotationally invariant operators  $\underline{p}^\alpha \cdot \underline{p}^\beta$ ,  $\underline{r}^\alpha \cdot \underline{r}^\beta$ , and  $\frac{1}{2} (\underline{r}^\alpha \cdot \underline{p}^\beta + \underline{p}^\beta \cdot \underline{r}^\alpha)$ . Under commutation, these operators form an  $sp(2n, R)$  algebra (in the notation of [10]), which we call a "pseudospin algebra". The original representation space is highly reducible with respect to this algebra, and the semi-classical analysis of the quantum problem is greatly simplified if the extra degrees of freedom are removed, which is just what we did by separating variables in the coordinate space treatment. The algebraic equivalent is to employ the Holstein-Primakoff representation of  $sp(2n, R)$ . To give you a feeling for what that is, I will write it down for the case  $n = 1$ . First we define a new basis in  $sp(2, R)$ :

$$\begin{aligned} K^3 &= \frac{1}{4} \left[ \omega r^2 + \frac{1}{\omega} p^2 \right] \\ K^- &= \frac{1}{4} \left[ -\omega r^2 + \frac{1}{\omega} p^2 - i(\underline{r} \cdot \underline{p} + \underline{p} \cdot \underline{r}) \right] \\ K^+ &= \frac{1}{4} \left[ -\omega r^2 + \frac{1}{\omega} p^2 + i(\underline{r} \cdot \underline{p} + \underline{p} \cdot \underline{r}) \right] \end{aligned} \quad (14)$$

$\omega$  is a parameter that can be adjusted at our convenience. For any value of  $\omega$ , the operators satisfy:

$$[K^+, K^-] = 2K^3, \quad [K^3, K^-] = -K^-, \quad [K^3, K^+] = K^+ \quad (15)$$

The Casimir operator can be calculated to be:

$$C \equiv K^3 K^3 - \frac{1}{2}(K^- K^+ + K^+ K^-) = \frac{L^2}{4} + \frac{N}{4} \left( \frac{N}{4} - 1 \right) \quad (16)$$

where  $L^2$  is the squared magnitude of the  $N$  dimensional angular momentum:

$$L^2 \equiv \frac{1}{2} L_{ij} L_{ij}, \quad L_{ij} \equiv x_i p_j - x_j p_i \quad (17)$$

(repeated indices are always summed over). Since in  $N$  dimensions  $L^2$  has the possible values  $L^2 = \ell(\ell + N - 2)$ ,  $\ell = 0, 1, 2, \dots$ , the Casimir invariant has the possible values:

$$C = k(k-1), \quad k = \frac{1}{2}(\ell + \frac{1}{2}N) = \frac{N}{4}, \frac{N}{4} + \frac{1}{2}, \dots \quad (18)$$

Using eqn. (14), the Hamiltonian may be expressed in terms of  $K^+$ ,  $K^-$ ,  $K^3$ . The equations of motion for these rotationally invariant operators have different solutions on each irreducible representation. The Holstein-Primakoff representation of these operators makes that dependence explicit. It is easy to check that operators in the Holstein-Primakoff representation,

$$K^+ = \xi^\dagger \sqrt{2k + \xi^\dagger \xi}, \quad K^- = \sqrt{2k + \xi^\dagger \xi} \xi, \quad K^3 = k + \xi^\dagger \xi; \quad [\xi, \xi^\dagger] = 1 \quad (19)$$

formally satisfies eqns. (15, 18). My last statement raises some questions of mathematical rigor, which will be briefly discussed later.

After writing down the Holstein-Primakoff representation, the next step in the algebraic development of the large  $N$  series is to expand the operators in (19) about  $c$ -numbers representing suitable solutions to the classical equations of motion. For the ground and low-lying states (in each angular momentum sector) the suitable solution is the stable time independent solution of lowest energy. For the one particle problem we are now considering, these are the circular orbits. In order to obtain the proper limit we must first shift the creation and destruction operators by

$$\xi = a + \xi^a / \sqrt{2k} \quad , \quad [a, a^\dagger] = 1 \quad , \quad (20)$$

where  $\xi^a$  is a real c-number satisfying

$$\frac{\partial \mathcal{H}_k}{\partial \xi^a}(\xi^a, \xi^a) = \frac{\partial \mathcal{H}_k}{\partial \xi^{\dagger a}}(\xi^a, \xi^a) = 0 \quad (21)$$

In eqn. (21)  $\mathcal{H}_k(\xi, \xi^\dagger)$  is the effective Hamiltonian obtained by substituting the operators of eqn. (19) into the original Hamiltonian. After performing the shift (20), the operators (19) can be expanded in powers of  $x = (2k)^{-1/2}$ , and the commutation relations (15) will hold order by order. The series for the energy is obtained by expanding  $\mathcal{H}_k$ , diagonalizing to lowest order (you can probably guess that to lowest order it is a harmonic oscillator), and calculating higher order corrections using perturbation theory. The procedure is best illustrated in the context of a concrete problem. Since it is one of my aims to elucidate the relationship between the large N expression for potential problems, and the semi-classical theory of spin systems, I will illustrate the method by treating a Heisenberg magnet. The similarities in formalism between that problem and the one just discussed are such that that change of gears should cause no difficulties. Furthermore the magnet problem has the advantage of being a little less trivial (and hence more interesting) than the problem of single particle in a spherically symmetric potential.

The "1/N expansion" for spin problems is, as we will see, an expansion in 1/S. In 1952 Anderson [11] obtained the first two terms in the expansion for the ground state energy of the Heisenberg antiferromagnet, a problem that Bethe solved exactly for  $s = s/2$ . Later in 1952 Kubo [12] used the Holstein-Primakoff representation of SU(2) to calculate the next term. The resulting series apparently behaves quite well:

$$\mathcal{E}_{gr} = -N s^2 \left[ 1 + 0.363 s^{-1} + 0.033 s^{-2} + O(s^{-3}) \right] \quad (22)$$

Since that time, little additional work has been done on that. I will now describe explicitly how the series in eqn. (12) is obtained using our methods. To make things more interesting, we add a magnetic field, and treat the ferromagnet in a magnetic field at the same time.



The Hamiltonian for the Heisenberg magnet in a magnetic field is

$$\mathcal{H} = \lambda \sum_{n=1}^N \vec{S}_n \cdot \vec{S}_{n+1} - 2hs \sum_{n=1}^N S_n^z \quad (23)$$

We consider for definiteness the case of even  $N$  and choose periodic boundary conditions. This will allow us to treat the ferro- and antiferromagnets in a unified way. The magnetic field is assumed to be in the  $-z$  direction.

$$h \geq 0 \quad (24)$$

and we have rescaled the second term in (7) so that for large  $S^2 = s(s+1)$  the two terms are of like order. The parameter  $\lambda$  has the two possible values

$$\lambda = \pm 1 \quad ; \quad (25)$$

the plus sign is appropriate for the anti-ferromagnet, and the minus sign for the ferromagnet.

The Holstein-Primakoff representation of  $su(2)$  is:

$$S_n^+ = \sqrt{2s - \xi_n^\dagger \xi_n} \quad \xi_n = \frac{1}{x} \sqrt{1 - \xi_n^\dagger \xi_n x^2} \quad \xi_n x \quad (26)$$

$$S_n^- = \xi_n^\dagger \sqrt{2s - \xi_n^\dagger \xi_n} = \frac{1}{x} \xi_n^\dagger x \sqrt{1 - \xi_n^\dagger \xi_n x^2} \quad (27)$$

$$S_n^z = s - \xi_n^\dagger \xi_n = \frac{1}{x^2} \left[ \frac{1}{2} - \xi_n^\dagger \xi_n x^2 \right] \quad (28)$$

where

$$S_n^\pm = S_n^x \pm i S_n^y \quad (29)$$

$$x = \frac{1}{\sqrt{2s}} \quad (30)$$

and the  $\xi_n, \xi_n^\dagger$  are canonical creation and destruction operators (boson operators):

$$[\xi_n, \xi_{n'}^\dagger] = \delta_{nn'} \quad (31)$$

Eqn. (31) formally implies the proper  $su(2)$  commutation relations for the Holstein-Primakoff operators defined in eqns. (26-28):

$$[S_n^z, S_{n'}^\pm] = \pm \delta_{nn'} S_n^\pm, \quad [S_n^\pm, S_{n'}^\mp] = 2 \delta_{nn'} S_n^z \quad (32)$$

and the value of the Casimir operator is now fixed, and can be computed to be

$$S_n \cdot S_n = s(s+1) \mathbb{1} \quad (33)$$

Substitution of the Holstein-Primakoff operators into eqn. (7) results in the desired effective Hamiltonian  $\mathcal{H}_s$ .

We can no longer continue the discussion without some apology and explanation for the mathematically inclined, who, critically listening, have concluded that this is the work of nihilistic seducers or crapulous outlaws, seedy elements existing on the fringes of civilized society who dare, out of malfeasance or ignorance, to equate finite dimensional matrices with unbounded operators on an infinite dimensional Hilbert space. The following observations should (temporarily) placate the disturbed reader. Consider the lattice point  $n$  to be fixed. The following discussion applies independently at each point, and we won't bother to write the subscript distinguishing the points. Let  $|q\rangle\rangle$  be the normalized state in the boson Fock space,  $\mathcal{F}$ , such that

$$\xi^\dagger \xi |q\rangle\rangle = q |q\rangle\rangle \quad (34)$$

and let  $|m\rangle$  be the normalized state in the representation space,  $R$ , of the spin  $s$   $su(2)$  matrices that satisfies

$$S^z |m\rangle = m |m\rangle \quad (35)$$

Define  $\mathcal{G} \subset \mathcal{F}$  by

$$\mathcal{G} = \{ |q\rangle\rangle \mid 0 \leq q \leq 2s \} \quad (36)$$

On  $\mathcal{G}$ , the square roots appearing in the definition of the Holstein-Primakoff operators (26-28) may be defined by their power series expansion, which converges there; furthermore  $\mathcal{G}$  is an invariant subspace under the action of those operators. If we consider eqns. (26-28) to be a correspondence of operators on  $R$  and  $\mathcal{G}$ , and identify

$$|q\rangle\rangle \xleftrightarrow{*} |s-q\rangle \quad ; \quad 0 \leq q \leq 2s \quad (37)$$

then we have an isomorphism between the representations. Because of eqn. (31), the boson operators and hence the Holstein-Primakoff operators have to live on the entire space  $\mathcal{F}$ , where the interpretation of eqns. (26-28) is difficult, and is an open mathematical question. (Once that problem has been solved, it would also be desirable to find a dense domain on which eqns. (22) hold). Finally, note that the approximate operators obtained by truncating the series defining eqns. (26, 27) no longer leave  $\mathcal{G}$  invariant, so that when the semiclassical expansion is carried out, the entire space is really used.

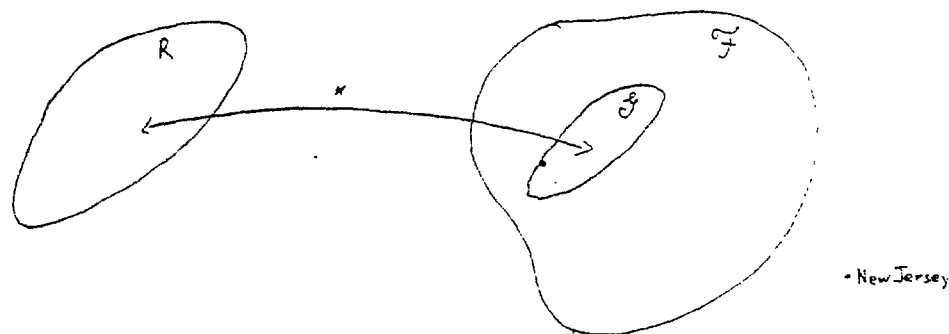


Figure 2

The expansion is obtained by expanding the operators, given by eqns. (26-28), about the stable, time independent, minimum energy c-number configuration satisfying the classical equations of motion. That is accomplished by taking

(38)

advantage of the fact that the only relevant property of  $\xi$ ,  $\xi^\dagger$  vis a vis the commutation relations (32) is that given by eqn. (31), which is invariant under the shift:

$$\xi_n = a_n + \xi_n^{cl}, \quad \xi_n^\dagger = a_n^\dagger + \xi_n^{cl\dagger}; \quad \xi_n^{cl} = \xi_n^{cl\dagger} \equiv \frac{\alpha_n}{x} \quad (39)$$

Substituting eqns. (38, 39) into eqns. (26, 27), results in a power series expansion of the operators such that the commutation relations (32) hold order by order in  $x$ . The boson operators then have vacuum expectation values, which will be determined by classical equations. The choice of  $\xi^{cl}$  real implies that  $\xi_n^{cl\dagger} = \xi_n^{cl}$ , and hence  $\xi_n^{cl\dagger} = 0$ . That this causes no difficulties is due to the azimuthal degeneracy of the problem. We could instead have chosen any phase for  $\xi_n^{cl}$ ; the phase will drop out of the equations determining  $\xi_n^{cl}$ . Our particular selection is simplest. It leads to:

$$x^2 \xi_n^\dagger = (1 - \alpha_n^2)^{1/2} \left\{ \alpha_n + \left[ a_n - \frac{1}{2} \frac{\alpha_n^2}{1 - \alpha_n^2} (a_n + a_n^\dagger) \right] x + \dots \right\} \quad (40)$$

$$x^2 \xi_n = (1 - \alpha_n^2)^{1/2} \left\{ \alpha_n + \left[ a_n^\dagger - \frac{1}{2} \frac{\alpha_n^2}{1 - \alpha_n^2} (a_n + a_n^\dagger) \right] x + \dots \right\} \quad (41)$$

$$x^2 \xi_n^2 = \left\{ (1 - \alpha_n^2) - \alpha_n (a_n + a_n^\dagger) x - a_n^\dagger a_n x^2 \right\} \quad (42)$$

The substitution of eqns. (40-42) into eqn. (23) leads to an expansion of the form

$$\frac{1}{4s^2} \mathcal{H}_s = \sum_{n=1}^N \left\{ C_{1,n} + C_{2,n} (a_n + a_n^\dagger) x + \left[ C_{3,n} a_n^\dagger a_n + C_{4,n} (a_n a_n + a_n^\dagger a_n^\dagger) + C_{5,n} (a_n^\dagger a_{n+1}^\dagger + a_n a_{n+1}) + C_{6,n} (a_n^\dagger a_{n+1} + a_{n+1}^\dagger a_n) \right] x^2 + O(x^3) \right\} \quad (43)$$

where the  $C$  coefficients are functions of the parameters  $\alpha_{n-1}$ ,  $\alpha_n$ ,  $\alpha_{n+1}$ . The extremum condition (gap equation)

$$\sum_{n=1}^N C_{2,n} (a_n + a_n^\dagger) = 0 \quad (44)$$

determines the parameters  $\alpha_n$ , and thus also  $\xi_n^{cl} = \xi_n^{cl\dagger} = \alpha_n/x$ . The parameters  $\xi_n^{cl}$  thus satisfy the time-independent equations:

$$\frac{\partial \mathcal{H}_S}{\partial \xi_n}(\xi_n^{cl}, \xi_n^{cl}) = \frac{\partial \mathcal{H}_S}{\partial \xi_n^{\dagger}}(\xi_n^{cl}, \xi_n^{cl}) = 0, \quad n=1,2,\dots,N \quad (45)$$

whereas the corresponding spin variables

$$S_n^{cl+} = S_n^{cl-} = (1-\alpha_n^2)^{1/2} \alpha_n x^{-1} = \sqrt{1-\xi_n^{cl\dagger} \xi_n^{cl}} \xi_n^{cl}, \quad S_n^{clz} = \left(\frac{1}{2} - \alpha_n^2\right) x^{-1} = s - \xi_n^{cl\dagger} \xi_n^{cl} \quad (46)$$

which are the leading terms in eqns. (40-42), are time-independent solutions to the classical spin equations of motion.

The appropriate solutions to eqn. (24) are

$$\alpha_n = (-1)^n \sin \frac{\theta}{2} \quad (47)$$

where

$$\begin{aligned} \theta = 0 & \quad (\text{ferromagnet and antiferromagnet, } h > 2) \\ \cos \theta = \frac{1}{2}h & \quad (\text{antiferromagnet, } 0 \leq h < 2) \end{aligned} \quad (48)$$

(The case  $h = 2$  is a critical value whose significance we will not discuss here). Using (46) and (47) to reconstruct the classical spin configuration, we find

$$S_n^{clx} = (-1)^n s \sin \theta, \quad S_n^{cly} = 0, \quad S_n^{clz} = s \cos \theta \quad (49)$$

which is the behavior we expect

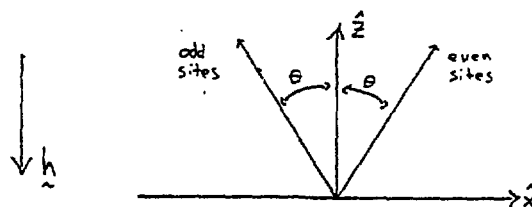
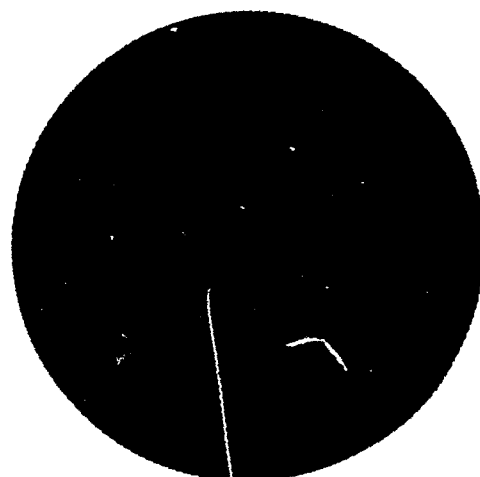


Figure 3

After we impose eqns. (47,48) the lowest order term of  $\mathcal{H}_S$  becomes the classical energy, which for the antiferromagnet in vanishing field is the first term of eqn. (22). Diagonalization of the term of order  $x^2$  on the right-hand-side of eqn. (43) leads to a harmonic oscillator whose ground state energy yields the next term of (22). Higher order energy corrections are calculated using perturbation theory.

References

- [1] S. Coleman, Proceedings of the 1979 International School of Subnuclear Physics, Erice, Italy.
- [2] L. Mlodinow and N. Papanicolaou, Ann. Phys. 128, 314 (1980).
- [3] L. Mlodinow and N. Papanicolaou, Ann. Phys. 131, 1 (1981).
- [4] C. Bender, L. Mlodinow and N. Papanicolaou, PRA, to appear.
- [5] C. Bender, L. Mlodinow and N. Papanicolaou, in preparation.
- [6] L. Mlodinow, Berkeley thesis 1981.
- [7] E. Witten, in: Recent Developments in Gauge Theories, NATO Advanced Study Series, Series B: Physics, volume 59, 't Hooft, et al., ed. (1979).
- [8] J.M. Combes and R. Seiler in: Spectral Properties of Atomic and Molecular Systems, G. Wooley, ed. (1980).
- [9] S. Hikami and E. Brezen, J.Phys. A12, 6 (1979).
- [10] B. Wybourne, Classical Groups for Physicists (John Wiley and Sons, New York, 1974).
- [11] P.W. Anderson, PR 86, 2 (1952).
- [12] R. Kubo, PR 87, 4 (1952).



GLUON CONDENSATE FROM LATTICE CALCULATIONS:SU(3) PURE GAUGE THEORY

Jochen Kripfganz

Sektion Physik, Karl-Marx-Universität Leipzig, DDR.

Abstract

A short distance expansion of Wilson loops is used to define and isolate vacuum expectation values of composite gluon operators. It is applied to available lattice Monte Carlo data for SU(3) pure gauge theory. The value obtained for the gluon condensate is consistent with the ITEP estimate.

(auth)

The QCD vacuum appears to be characterized by the condensation of quarks and gluons. Of particular interest (besides of the quark condensate  $\langle m_q \bar{q}q \rangle$ ) is the matrix element  $\langle \frac{d_s}{\pi} G_{\mu\nu}^a G_{\mu\nu}^a \rangle$ . Through the trace anomaly it is related to the energy density of the vacuum. It also shows up as 'higher twist' contribution in the short distance expansion of various current correlation functions. This provides the basis for a phenomenological estimate of the gluon condensate. In the framework of the ITEP sum rule approach<sup>/1/</sup> (now also pursued by various other groups) one estimates<sup>/1/</sup>

$$\frac{1}{N_c} \left\langle \frac{d_s}{\pi} G_{\mu\nu}^a G_{\mu\nu}^a \right\rangle \approx 0.004 \text{ GeV}^4, (N_c = 3) \quad (1)$$

The lattice Monte Carlo approach has opened the way for an independent theoretical evaluation of the gluon condensate. A direct comparison with the phenomenological value (1) is still not possible because fermions cannot be handled in an efficient way in Monte Carlo calculations yet. One does not expect drastic changes due to fermions, however. Novikov et al.<sup>/2/</sup> obtain the estimate



$$\left\langle \frac{d_3}{\pi} G_{\mu\nu}^a G_{\mu\nu}^a \right\rangle_{\text{pure SU(3)}} \approx (2-3) \left\langle \frac{d_3}{\pi} G_{\mu\nu}^a G_{\mu\nu}^a \right\rangle_{\text{real world}} \quad (2)$$

In order to isolate the gluon condensate from lattice Monte Carlo data I will closely follow the ITEP approach in its basic strategy. The gluon condensate is essentially treated as a classical background field in which gauge invariant correlation functions are to be calculated. Correlation functions most easily accessible in lattice calculations are Wilson loops. Similar to current correlation functions one can also expand Wilson loops of small size in terms of a series of local composite gluon operators. The coefficients have a different power behaviour in the loop size. Therefore, vacuum matrix elements of the corresponding operators can be identified by studying Wilson loops of varying size. The short distance expansion for Wilson loops has been studied by Shifman<sup>/3/</sup> on a purely classical level. Monte Carlo data have been analyzed in terms of such an expansion in ref. /4/ where 1-loop quantum corrections are included.

The analysis of ref. /4/ used SU(2) data because of the better accuracy of the computer material. Of course, numerical results for SU(2) gauge theory are of a somewhat academic value and therefore I will here provide results of an analysis of the SU(3) computer data<sup>/5,6/</sup> available to me.

Data of refs. /5,6/ are given in the combination

$$\tilde{\chi}(I,J) \equiv -\log \frac{W(I,J) W(I-1,J-1)}{W(I-1,J) W(I,J-1)} \quad (3)$$

with  $W(I,J)$  the expectation value of a rectangular Wilson loop of size  $I \times J$  (in lattice units). A combination of Wilson loops like in eq. (3) has the advantage that linear divergencies due to the mass renormalization of the external test particle as well as logarithmic corner singularities drop out. Remaining logarithmic singularities essentially transform the bare coupling  $g(a)$  into the renormalized coupling  $g_R(L)$  where  $L$  stands for the loop size (in continuum units).

Following the procedure of ref. /4/  $\tilde{\chi}(I,J)$  is approximated by

$$\tilde{\chi}(I,J) \approx \tilde{\chi}(I,J) g_R^2 + \frac{\pi^2}{12} (2I-1) (2J-1) a^4 \frac{1}{N_c} \left\langle \frac{d_3}{\pi} G_{\mu\nu}^a G_{\mu\nu}^a \right\rangle. \quad (4)$$

$g_R^2$  is given in 1-loop approximation by

$$g_R^2 = \frac{1}{g^2(a)} - 2\beta_0 \log(\tilde{I} \lambda_R / \lambda_0) \quad (5)$$

where I have chosen  $\tilde{I} = \sqrt{I \cdot J}$ .  $\lambda_R$  is the (renormalization scheme dependent) QCD  $\lambda$  parameter, and  $\lambda_0$  is the corresponding lattice parameter associated with the bare coupling

$$\lambda_0 = \frac{1}{a} (\beta_0 g^2(a))^{-\beta_1/2\beta_0^2} e^{-\frac{1}{2\beta_0 g^2(a)}}, \quad a \rightarrow 0 \quad (6)$$

where

$$\beta_0 = \frac{11}{3} \frac{N_c}{16\pi^2}, \quad \beta_1 = \frac{34}{3} \left( \frac{N_c}{16\pi^2} \right)^2. \quad (7)$$

Eq. (6) determines  $a$  as function of  $g(a)$  to be used in eq. (4).

In using the 1-loop renormalized coupling (5) in eq. (4) leading terms of the type  $g^{2n}(a) \lg^n L/a$  have been summed up. This procedure is clearly effective for large loops (in lattice units) whereas an expansion in the bare coupling might be more appropriate for very small loops.

The 1-loop coefficients  $\tilde{\kappa}(I, J)$  are calculated numerically using results of ref. /7/. They are given for a typical range of  $(I, J)$  in table I.

In order to translate from lattice units to continuum units I use the string tension  $\sigma$  as an intermediate tool. Monte Carlo data provide a relation between  $\sigma$  and  $\lambda_0$  /6/.

$$\lambda_0 = (0.007 \pm 0.002) \sqrt{\sigma} \quad (8)$$

As usual I further assume

$$\sigma = \frac{1}{2\pi \mathcal{L}'} \quad (9)$$

with  $\mathcal{L}' \approx 1 \text{ GeV}^{-2}$  a universal Regge slope.

Results for the gluon condensate will be discussed in relation to the ITEP value (eq. (1)).

$$\frac{1}{N_c} \left\langle \frac{d_s}{dV} G_{\mu\nu}^a G_{\mu\nu}^a \right\rangle = r * \text{ITEP value} \quad (10)$$

Following ref. /2/ one expects  $r$  to be of the order 2 to 3.

In Fig. 1 I compare Monte Carlo data<sup>/5,6/</sup> for  $\tilde{\chi}(2,2)$  and  $\tilde{\chi}(3,3)$  with curves obtained from eq. (4), with  $r=1$  and  $r=3$ , resp. For large values of  $1/g^2(a)$  the perturbative contribution completely dominates. In order to get a reasonable background subtraction  $\lambda_2/\lambda_1$  is fitted to this perturbative tail. It is an effective parameter<sup>/4/</sup> as long as 2-loop terms are not included.

Going to smaller values of  $1/g^2(a)$  a more or less sudden deviation from the perturbative tail is observed. This transition is interpreted as being caused by the non-perturbative gluon condensate (i.e. the second term in eq. (4)) having a much steeper dependence on  $g^2(a)$  (through  $a^4$ ).

Unfortunately, the quality of the Monte Carlo data is still rather poor, and the statistical significance is difficult to estimate without errors being given. The agreement with the curves obtained from eq. (4) is not perfect but still reasonable.  $r=1\dots 3$  certainly looks like the right order of magnitude. No stronger conclusion can be drawn before more accurate computer material becomes available.

The non-perturbative contribution due to the gluon condensate has also been analyzed by Di Giacomo and Rossi<sup>/8/</sup> (for SU(2)) and Banks et al.<sup>/9/</sup> using the plaquette term  $[1 - W(1,1)]$  only. The signal-to-background ratio is very small in this case but a non-perturbative signal can still be resolved because one gains statistics compared to bigger loops. However, the lattice constant  $a$  is not particularly small in the corresponding range of  $g^2(a)$ , and any systematic study of the continuum limit appears to be very difficult if one sticks to the plaquette term alone. One also stays dangerously close to the roughening point in this case.

I should like to emphasize that the non-perturbative contribution found from the Monte Carlo data does not immediately yield the gluon condensate but some perturbative coefficient function times the gluon condensate (there might even be severe mixing problems<sup>/10/</sup>). So far nothing is known on the magnitude of higher order contributions to these

coefficient functions. They might be rather different for different correlation functions (Wilson loops). Therefore effective values for the gluon condensate obtained from different correlation functions need not agree completely. This problem, and other questions of consistency are currently under study<sup>/11/</sup> using high statistics SU(2) Monte Carlo data in the relevant range of  $g^2(a)$ . A next order calculation for the coefficient functions is also carried out<sup>/11/</sup>.

### References

- /1/ M. Shifman, A. Vainshtein and V. Zakharov,  
Nucl. Phys. B 147 (1979) 385, 448.
- /2/ V.A. Novikov, M. Shifman, A. Vainshtein and V.I. Zakharov,  
Preprint ITEP - 152 (1980).
- /3/ M.A. Shifman, Nucl. Phys. B 173 (1978) 171.
- /4/ J. Kripfganz, Phys. Lett. 101 B (1981) 169.
- /5/ M. Creutz, Phys. Rev. Lett. 45 (1980) 313.
- /6/ E. Pietarinen, Helsinki Preprint 80-49 (1980).
- /7/ V.F. Müller and W. Rühl, University of Kaiserslautern  
preprint (1980).
- /8/ A. Di Giacomo and G.C. Rossi, Phys. Lett. 100 B  
(1981) 481.
- /9/ T. Banks et al., preprint WIS-81/8/Feb-ph.
- /10/ R. Crewther, talk at this conference.
- /11/ J. Kripfganz, J. Ranft and R. Kirschner, work in progress.

Figure Captions

Fig. 1 Monte Carlo data of ref. /5/ ( $\blacksquare$ ) and ref. /6/ ( $\blacktriangle$ ) analyzed in terms of expression (4). Dashed-dotted line is perturbative contribution alone. Full lines correspond to  $r=1$  and  $r=3$ , resp. (compare eq. (10)).

Table I

| I | J | $\tilde{\alpha}_1(I,J)$ |
|---|---|-------------------------|
| 1 | 1 | 1/3                     |
| 1 | 2 | 0.242                   |
| 1 | 3 | 0.227                   |
| 2 | 2 | 0.096                   |
| 2 | 3 | 0.068                   |
| 2 | 4 | 0.061                   |
| 3 | 3 | 0.035                   |
| 3 | 4 | 0.026                   |
| 4 | 4 | 0.016                   |
| 5 | 5 | 0.009                   |

a-

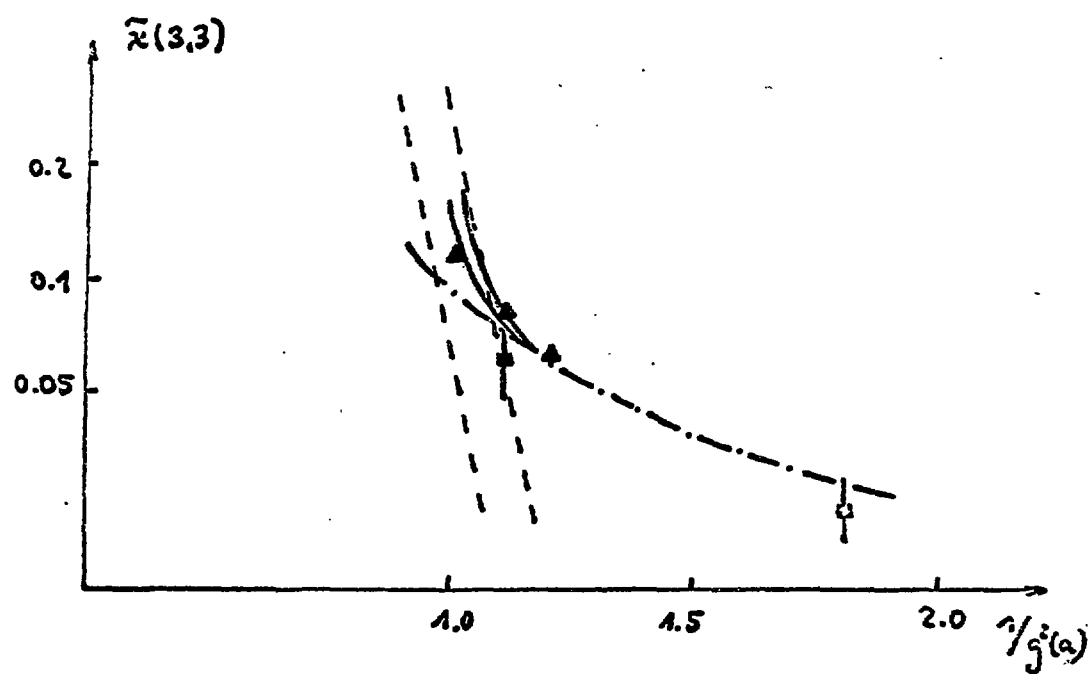
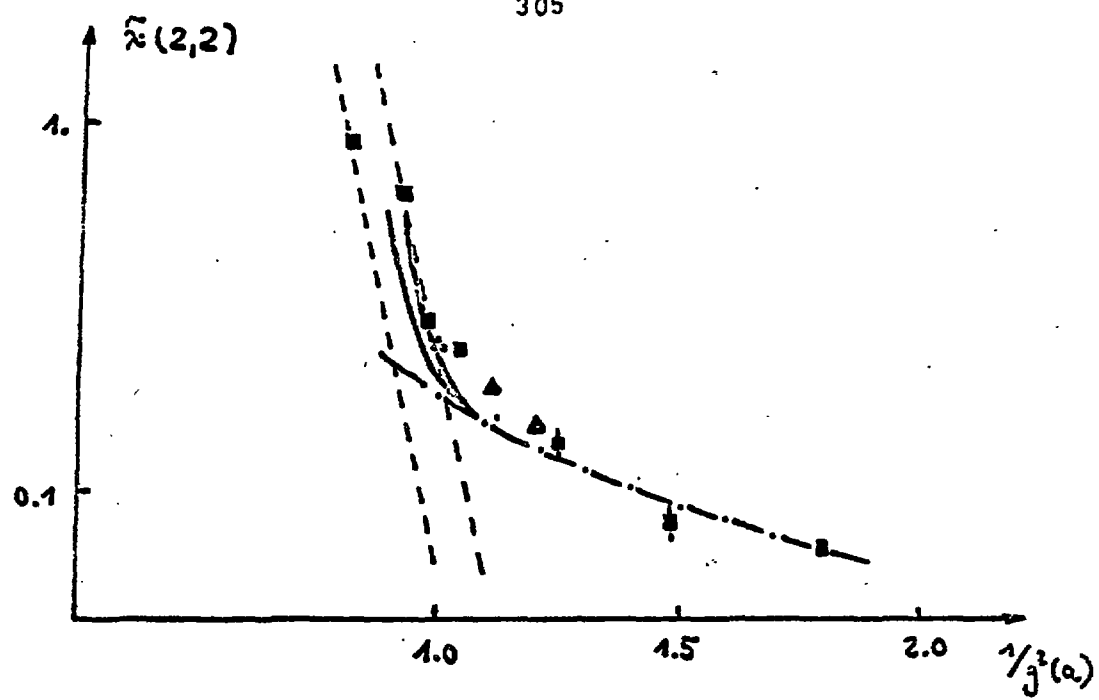
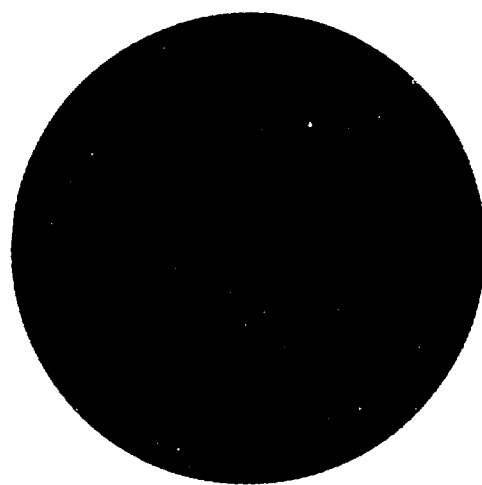


Fig. 1



SYMMETRY BREAKING AT HIGH TEMPERATURE

Goran Senjanović \*)

CERN, Geneva, Switzerland

ABSTRACT

~~In this talk~~ review the arguments  
for symmetry non-restoration at high  
temperature. <sup>as presented</sup> The consequences for the  
baryon number of the Universe; mono-  
pole problem in grand unified theories  
and horizon problem in the standard  
cosmological model are discussed. (author)

\*) Permanent address : Brookhaven Na-  
tional Laboratory, Upton, N.Y. 11973



1. INTRODUCTION

We all know that the rotational invariance of a ferromagnet is restored when the system is heated to a sufficiently high temperature. By analogy, it can be (and it was) asked<sup>1)</sup>: are broken symmetries of elementary particle physics restored at high temperature?

The question was answered affirmatively<sup>1,2)</sup> -- at least in the context of the simplest, single Higgs model. Let me briefly describe the result. One calculates the effective potential at high  $T$

$$V(T) = \frac{1}{2} \left( -\mu^2 + \frac{1}{8} \lambda T^2 \right) \phi^2 + \frac{\lambda}{4} \phi^4 \quad (1.1)$$

where  $\lambda > 0$  to ensure that the potential is bounded from below. At  $T = 0$ , the symmetry is broken, with  $\langle \phi \rangle_{T=0} = \sqrt{\mu^2/\lambda}$ . However, for  $T \geq T_c$ ,  $\langle \phi \rangle_T = 0$ , where  $T_c = \sqrt{8\mu^2/\lambda}$ . In other words, there is a phase transition at  $T = T_c$  and the system is in the unbroken phase for large  $T$ . We illustrate the situation in Fig. 1.

If the above result is true in general, it would have important implications. For example, it would rule out spontaneous symmetry breaking as the mechanism for CP violation. Let me explain it in some detail. There is large observational evidence that the universe is dominated by matter only, with the baryon-to-entropy ratio.

$$\frac{n_B}{s} \simeq 10^{-9 \pm 1} \quad (1.2)$$

According to recent<sup>3)</sup> theoretical ideas matter-antimatter asymmetry originated in early universe through baryon number violating decays of superheavy bosons ( $X$  bosons) of grand unified theories.

The necessary conditions for understanding Eq. (1.2), discussed<sup>3)</sup> at length in the literature, include CP violation. Namely, when CP is a good symmetry, the particle and antiparticle decay rates are the same, and no asymmetry could be created through  $X$  boson decays.

On the other hand, it appears that the natural way to understand<sup>4)</sup> the absence of strong CP violation, induced via instantons, is to have spontaneously

broken CP invariance<sup>5)</sup>. But if the symmetry is restored above  $T_c \approx M_w$ , then it would imply that at  $T \approx M_x$ , when the baryon excess was presumably created, the theory would be CP conserving, hence we would have  $n_B = 0$ . The global properties of the universe seem to rule out soft (spontaneously broken) CP violation; that is, if the symmetry restoration necessarily takes place.

Motivated by the above result, Mohapatra and myself<sup>6)</sup> have reinvestigated the behaviour of gauge theories at high  $T$  and found out that the symmetries are not necessarily restored. We have then constructed realistic models of soft CP violation at high  $T$ . In this talk I review briefly our work and discuss further applications of symmetry breaking at high temperature: (i) resolution of the monopole problem in grand unified theories, and (ii) resolution of the so-called horizon problem in the big-bang model of the universe.

This talk is then organized as follows: in Section 2 an analysis of high  $T$  properties of an  $SU(2) \times U(1)$  model is given and it is shown how in the case of the extended Higgs sector, the symmetry remains broken as the temperature is increased. It is also pointed out how a realistic model of soft CP violation can be constructed. Section 3 is devoted to the problem of superheavy monopoles and its possible resolution through the above mechanism. In Section 4 I present an interesting idea of Zee<sup>7)</sup> suggested to resolve the horizon problem in the standard cosmological model. A summary is given in Section 5.

## 2. SYMMETRY BREAKING AT HIGH TEMPERATURE

To determine the pattern of symmetry breaking we need the effective potential for high  $T$ <sup>1,2)</sup>. One performs a one-loop calculation, using the Feynman rules for  $T \neq 0$ . Now, at  $T \neq 0$ , we are dealing with temperature-dependent Green's functions

$$G_p(x_i \dots x_j) \equiv \frac{\text{Tr } e^{-\beta H} T \varphi(x_i) \dots \varphi(x_j)}{\text{Tr } e^{-\beta H}} \quad (2.1)$$

with  $\beta \equiv 1/T$ .

The usual trick is to go to imaginary time formulation

$$t \rightarrow 0 \leq i x_0 \leq \beta; \quad 0 \leq i y_0 \leq \beta \quad (2.2)$$

Of particular interest is the two-point function  $D_\beta(x-y)$ . It is easy to show that the equation for  $D_\beta(x-y)$  is temperature independent

$$(\square^2 + m^2) D_\beta(x-y) = -i \delta^{(4)}(x-y) \quad (2.3)$$

but the boundary conditions are now periodic

$$D_\beta(x-y) \Big|_{x_0=0} = D_\beta(x-y) \Big|_{x_0=\beta} \quad (2.4)$$

Therefore, the calculations are performed as at  $T = 0$ , but with the substitution

$$\begin{aligned} \int_p &\rightarrow -\frac{1}{i\beta} \sum_n \int \frac{d^3 p}{(2\pi)^3} \\ \int_x &= \int_0^{-i\beta} dx_0 \int d^3 x \end{aligned} \quad (2.5)$$

$$\text{and} \quad p^2 = \omega_n^2 + \vec{p}^2 = \frac{4\pi^2}{\beta^2} n^2 + \vec{p}^2$$

The important property of  $T \neq 0$  calculations is that no new infinities are induced, i.e. all divergences are removed by counter terms at  $T = 0$ . That is most simply seen in the real-time formulation, where the propagator is given by<sup>8)</sup>

$$\overline{D}_\beta(x-y) = \frac{i}{p^2 - m^2 + i\epsilon} + \frac{2\pi}{e^{\beta E} - 1} \delta(p^2 - m^2) \quad (2.6)$$

Equipped with the Feynman rules given above, one can perform the calculation of the temperature-induced effective potential. Let us consider the most general scalar potential with quantic couplings:

$$V(0) = \sum_{i,j} \mu_{ij}^2 \phi_i \phi_j + \frac{1}{4!} \sum_{i,j,k,l} f_{ijkl} \phi_i \phi_j \phi_k \phi_l \quad (2.7)$$

where  $\phi_i$  are the set of real fields. Then, at high T (see Weinberg, Ref. 2)

$$V(T) = V(0) + \frac{T^2}{48} \sum_{i,j} \left[ \sum_k f_{ijk} + 6g^2 (T_a T_a)_{ij} + O(h) \right] \phi_i \phi_j \quad (2.8)$$

where  $T_a$  are the group generators acting on  $\phi$ 's and  $h$  stands for Yukawa couplings. We shall assume  $h \ll g$  and ignore fermionic contributions, for the sake of simplicity. The gauge meson contribution  $\sum_a T_a T_a$  is always positive, so that the sign of  $\sum_k f_{ijk}$  will determine the possible patterns of symmetry breaking at high T.

The model<sup>6)</sup>:  $SU(2) \times U(1)$  with two doublets

The most general Higgs potential at  $T = 0$ , consistent with the symmetry  $\phi_i \rightarrow -\phi_i$  and  $\phi_1 \rightarrow i\phi_1$ , is given by

$$V(0) = -\mu_1^2 \phi_1^\dagger \phi_1 - \mu_2^2 \phi_2^\dagger \phi_2 + \lambda_1 (\phi_1^\dagger \phi_1)^2 + \lambda_2 (\phi_2^\dagger \phi_2)^2 \\ + 2\lambda_3 (\phi_1^\dagger \phi_1) (\phi_2^\dagger \phi_2) + 2\lambda_4 (\phi_1^\dagger \phi_2) (\phi_2^\dagger \phi_1) \quad (2.9)$$

We choose  $\lambda_4 < 0$ , so that  $\langle \phi_1 \rangle \parallel \langle \phi_2 \rangle$  at the minimum. With positivity conditions

$$\lambda_1 > 0, \quad \lambda_2 > 0, \quad \lambda_1 \lambda_2 - (\lambda_3 + \lambda_4)^2 > 0 \quad (2.10)$$

one gets the pattern of symmetry breaking

$$\langle \phi_1 \rangle = \begin{pmatrix} 0 \\ v_1 \end{pmatrix}, \quad \langle \phi_2 \rangle = \begin{pmatrix} 0 \\ v_2 \end{pmatrix} \quad (2.11)$$

From Eq. (2.8) we can easily write down the induced T-dependent piece of the potential

$$V_1(T) = T^2 \left[ b_1 \phi_1^\dagger \phi_1 + b_2 \phi_2^\dagger \phi_2 \right] \quad (2.12)$$

with

$$b_i = \frac{1}{2} \left( \lambda_i + \frac{2\lambda_3 + \lambda_4}{3} + \frac{3g^2 + g'^2}{16} \right) \quad (2.13)$$

It is easily seen that the range of parameters

$$\lambda_3 < 0, \lambda_4 < 0$$

$$\lambda_2 + \frac{3g^2 + g'^2}{16} < \frac{2|\lambda_3| - |\lambda_4|}{3} \quad (2.14)$$

$$\lambda_1 + \frac{3g^2 + g'^2}{16} > \frac{2|\lambda_3| + |\lambda_4|}{3} \quad (2.14)$$

is in accord with positivity conditions Eq. (2.10), and so

$$b_2 < 0, b_1 > 0 \quad (2.15)$$

In other words, at high  $T$ , i.e. for  $T > T_c = \sqrt{\mu_1^2/b_1}$

$$\langle \phi_1 \rangle_{T > T_c} = 0, \quad \langle \phi_2 \rangle_{T > T_c} \neq 0 \quad (2.16)$$

since the  $\phi_2$  mass term remains negative (see Fig. 2). But  $SU(2) \times U(1) \xrightarrow{\langle \phi_2 \rangle} U(1)_{em}$ , so that the symmetry remains broken at high temperature. That is the main point of this talk and the rest of it will deal with the applications of the above phenomenon to grand unified theories and cosmology.

#### Soft CP violation at high $T$

Once we have demonstrated that the symmetry is not necessarily restored, it is only a matter of straightforward (but tedious) exercise to construct a soft CP model at  $T \approx 10^{15}$  GeV, so as to have non-vanishing baryon asymmetry of the universe. I will only outline here a basic procedure, and refer the reader for details to Ref. 6.

We have seen above how, for the case of two doublets in  $SU(2)_L \times U(1)$ , at high  $T$

$$\langle \phi_1 \rangle_T = 0, \quad \langle \phi_2 \rangle_T \propto T \quad (2.17)$$

However, by a gauge rotation, one can always make  $\langle \phi_2 \rangle$  become real, therefore leading to a CP-conserving theory. Hence, we have a theorem: we need at least three doublets in  $SU(2)_L \times U(1)$  to have soft CP at high T.

We have constructed a realistic grand unified model which incorporates the above feature. The minimal scheme is based on the  $SU(5)$  gauge group. The light Higgs multiplets consist of only five-dimensional vector representations. With three  $\phi$ 's,  $\phi_1$ ,  $\phi_2$  and  $\phi_3$ , we achieved the following pattern of symmetry breaking

$$T = 0 : \quad \langle \phi_i \rangle \neq 0, \quad i = 1, 2, 3$$

$$T > T_c : \quad \langle \phi_3 \rangle = 0, \quad \langle \phi_{1,2} \rangle \propto T$$

with

$$\langle \phi_1 \rangle \text{ real} ; \quad \langle \phi_2 \rangle \text{ complex}$$

The model has all the typical features of spontaneously broken<sup>5)</sup> CP theories, with the most relevant prediction for the electric dipole moment of the neutron

$$d_n^e \approx (10^{-28} - 10^{-25}) e \text{ cm} \quad (2.18)$$

In addition, one can estimate<sup>9)</sup> the non-vanishing baryon asymmetry created in the early universe

$$\frac{\eta_B}{s} \approx 10^{-13} - 10^{-9} \quad (2.19)$$

for reasonable values of Yukawa couplings.

### 3. MONOPOLE PROBLEM IN GRAND UNIFIED THEORIES

It is well known, through the work of 't Hooft and Polyakov<sup>10)</sup>, that when a compact group  $G$  breaks down to  $G' \times U(1)$ , one obtains monopole-like solutions [with respect to  $U(1)$ ]. If the expectation value of the Higgs field  $\phi$  that breaks  $G$  is  $\langle \phi \rangle$ , i.e.

$$G \xrightarrow{\langle \phi \rangle} G' \times U(1) \quad (3.1)$$

then the mass and the charge of the monopole are given by

$$M_m = \frac{4\pi}{g^2} v, \quad g_m = \frac{2\pi}{g} \quad (3.2)$$

where  $g$  is the  $U(1)$  coupling.

Now, typically, simple grand unified theories are described by compact groups:  $SU(5)$ ,  $SO(10)$ , .... Let us take  $SU(5)$  as an example. It breaks down through  $\langle \phi \rangle = M_x$

$$SU(5) \xrightarrow{\langle \phi \rangle = M_x} SU(2)_L \times U(1)_Y \times SU(3)_C \quad (3.3)$$

where  $M_x = 10^{14}$  GeV corresponds to the masses of superheavy gauge bosons that mediate proton decay. But then we predict the existence of superheavy monopoles, with  $M_m(x) = M_x/\alpha \approx 10^{16}$  GeV. Important questions must then be raised<sup>(1)</sup>:

- (1) What are the observational limits on the density of such superheavy monopoles today?
- (2) How many monopoles were produced in the early universe at  $T \approx M_x$ ?
- (3) How many of these produced monopoles are expected to have remained today?

I briefly discuss the answers to (1)-(3).

#### Answers

- (1) We cannot unfortunately use any terrestrial measurements to put the limit on  $n_m$ , for the simple reason that such superheavy objects would be pulled all the way down to the centre of the earth, owing to the enormous gravitational attraction. However, a rather stringent limit on the density of the monopoles comes from the cosmological observations of the matter content of the universe and the measurements of the deceleration parameter of the universe. It is well known that such observations put an upper limit of about  $10^{-8}$  baryons per photon. Now,  $M_m \approx 10^{16}$  GeV  $\approx 10^{16} m_B$  (baryon mass), so that one has a limit of approximately  $10^{-24}$  monopoles for each photon in the universe. Even if this limit is not taken seriously, there is a constraint from the fact that at the time of the helium synthesis ( $T \approx 1$  MeV), the monopoles should not have dominated the mass density

of the universe; that implies

$$\frac{n_m}{n_Y}(T \approx 1 \text{ MeV}) \leq 10^{-19} \quad (3.4)$$

We will use the above constraint seriously.

(2) The estimate of the initial density  $r(T_i)$  of the monopoles produced during the phase transition  $SU(5) \xrightarrow{T_i} SU(2)_L \times U(1)_Y \times SU(3)_c$  is a non-trivial dynamical question. It has been argued by Preskill<sup>11)</sup> and others<sup>12)</sup>, that for the case of second-order phase transition

$$r(T_i) \approx 10^{-6} \quad (3.5)$$

where

$$r(T_i) \equiv \frac{n_m}{n_Y}(T_i)$$

(3) Again, the lack of the knowledge of the quantum properties of the monopole interactions makes it difficult to predict the future of the initial monopole density. It appears, that if  $r(T_i) < 10^{-10}$ , then the annihilation rate is negligible and so from Eq. (3.5) we would conclude that grand unified theories predict the present density of the monopoles  $r(T_p) \equiv (n_m/n_Y)(T_p)$  to be

$$r(T_p) \geq 10^{-10} \quad (3.6)$$

in dramatic disagreement with the observational limit in Eq. (3.4). We shall call this a monopole problem.

Instead of enumerating various suggested resolutions<sup>13)</sup>, I would like to discuss a rather amusing scenario suggested by Langacker and Pi<sup>14)</sup>. Their idea is simply the following. Imagine that the symmetry breaking takes the following form

$$G \xrightarrow{T_x} SU(3)_c \xrightarrow{T_w} SU(3)_c \times U(1)_{em}$$

In that case, above  $T_w = M_w$ , the  $U(1)_{em}$  symmetry would be broken and therefore no superheavy monopoles would have been created at  $T_x$ ! At first sight this idea may sound crazy, but it appears to be a perfectly consistent possibility. Let me



describe briefly how they achieve the above result and what its consequences would be, if any.

First, from the discussion in the previous section, one realizes immediately that within the  $SU(2)_L \times U(1)$  electroweak model, at least three doublets are needed to get  $U(1)_{em}$  broken at high  $T$ . Namely, in the case of two doublets one of the vacuum expectation values always vanishes for  $T \geq T_w$ ; and so clearly the other one can be rotated in the direction of  $\langle \phi^0 \rangle$ , preserving the charge symmetry. Let us therefore imagine the existence of three doublets, i.e. three 5-dimensional multiplets of  $SU(5)$ ,  $\phi_1$ ,  $\phi_2$  and  $\chi$ , with the relevant part of the Higgs potential

$$V = -\mu_1^2 \phi_1^\dagger \phi_1 + \lambda_1 (\phi_1^\dagger \phi_1)^2 - \mu_\chi^2 \chi^\dagger \chi + \lambda_\chi (\chi^\dagger \chi)^2 + \lambda_{12} (\phi_1^\dagger \phi_1) (\phi_2^\dagger \phi_2) + \lambda'_{12} (\phi_1^\dagger \phi_2) (\phi_2^\dagger \phi_1) + \dots \quad (3.7)$$

where we choose<sup>13)</sup>  $\lambda'_{12} > 0$ ;  $\mu_1^2 > 0$ ;  $\mu_2^2 < 0$  and  $\mu_\chi^2 < 0$ . At  $T = 0$  the pattern of symmetry breaking is then given by

$$\langle \phi_1 \rangle = \begin{pmatrix} 0 \\ v_1 \end{pmatrix}, \quad \langle \phi_2 \rangle = \langle \chi \rangle = 0. \quad (3.8)$$

At  $T \neq 0$ , there will be temperature-induced mass terms for  $\phi_1$  and  $\chi$

$$V_1(T) = T^2 [b_1 \phi_1^\dagger \phi_1 + b_2 \phi_2^\dagger \phi_2 + b_\chi \chi^\dagger \chi] \quad (3.9)$$

Similarly, as in the case discussed by Mohapatra and myself<sup>6)</sup>, one can achieve in the range of the parameters of the potential

$$b_1 < 0, \quad b_2 < 0, \quad b_\chi > 0 \quad (3.10)$$

Therefore, for  $T \geq T_w$  we will have

$$\langle \phi_1 \rangle \neq 0 \neq \langle \phi_2 \rangle \quad (3.11)$$

and more than that, since  $\lambda'_{12} > 0$ , the minimum of the potential will be achieved for

$$\langle \phi_1 \rangle = \begin{pmatrix} 0 \\ v_1 \end{pmatrix}, \quad \langle \phi_2 \rangle = \begin{pmatrix} v_2 \\ 0 \end{pmatrix} \quad (3.12)$$

The charge assignment of the doublets is  $\langle \phi \rangle = \begin{pmatrix} \phi_1^+ \\ \phi_2^+ \end{pmatrix}$  and so  $\langle \phi_2^+ \rangle \neq 0$ . In other words, at  $T \geq M_W$  the photon becomes massive ( $m_A \propto T$ ) and electric charge is not conserved. There will be no superheavy monopoles produced at  $T = T_X$ , when the SU(5) phase transition takes over.

What are the implications of  $U(1)_{em}$  breaking at such high temperature? Does it lead to an electrically charged universe? Observations indicate

$$\left( \frac{n_Q}{n_B} \right)_{obs} < 10^{-18} \quad (3.13)$$

where  $n_Q$  is the charge asymmetry and  $n_B$  the baryon asymmetry of the universe.

Now, for  $T > M_W$ , the rate of charge non-conserving interactions is

$$\Gamma_{\gamma} = \alpha^2 T \quad (3.14)$$

which is large compared with the expansion rate of the universe

$$H = \frac{T^2}{M_P} \quad (3.15)$$

Therefore, such interactions are in equilibrium and so we expect  $Q_{em} \neq 0$ .

Langacker and Pi then estimate that the charge asymmetry due to fluctuations is negligibly small; they put the limit

$$\left( \frac{n_Q}{n_B} \right)_{TH} < 10^{-34} \quad (3.16)$$

which is definitely in agreement with observations.

#### 4. HORIZON PROBLEM IN THE BIG-BANG MODEL

The standard cosmological model or the big-bang model appears to be very successful in its description of the development of the universe<sup>15)</sup>, at least up to times of a second or so. Its most spectacular prediction is the observed 2.7 °K microwave, isotropic radiation, a relic from the big-bang. However, when the model is extrapolated to the very early times, a problem appears in that the size of causally connected domains, for sufficiently small  $t$ , was much smaller than the effective size of the universe. It is then hard to understand the isotropy and homogeneity of the universe. This is the so-called horizon problem.

Let me be more precise about it. Following Rindler<sup>16)</sup>, let us imagine a photon emitted at  $t = t_0$  from  $r = r_H$ , which reaches the observer at  $r = 0$  at time  $t$ . Now, the metric of the space-time is, in the standard model, determined from the assumptions of isotropy and homogeneity

$$ds^2 = dt^2 - R^2(t) \left[ \frac{dr^2}{1 - kr^2} + r^2 d\Omega \right] \quad (4.1)$$

where  $R(t)$  measures the cosmological scales and  $k = 0, 1$  or  $-1$  tells us whether the universe is flat, open or closed. In any case, for  $d\Omega = 0$ , the emitted photon satisfies  $ds^2 = 0$  and so

$$dt = R(t) \frac{dr}{\sqrt{1 - kr^2}} \quad (4.2)$$

or

$$\int_{t_0}^t \frac{dt'}{R(t')} = \int_0^{r_H(t, t_0)} \frac{dr}{\sqrt{1 - kr^2}} \quad (4.3)$$

Now, if  $\int_{t_0}^t [dt'/R(t')]$  is finite for  $t_0 \rightarrow 0$ , the observer is causally connected by only a finite domain

$$d(t, 0) = \lim_{t_0 \rightarrow 0} R(t) \int_0^{r_H(t, t_0)} \frac{dr}{\sqrt{1 - kr^2}} \quad (4.4)$$

since  $d(t, t_0) \equiv \int \sqrt{-ds^2}$  with  $dt = 0$ . We have, therefore, to find out the behaviour of  $\int_{t_0}^t [dt'/R(t')]$  for small  $t_0$ . In order to do that, we shall first determine the  $t$  dependence of  $R(t)$  for the early universe. Einstein's equations are

$$R_{\mu\nu} - \frac{1}{2} g_{\mu\nu} R = 8\pi G T_{\mu\nu} \quad (4.5)$$

where the energy-momentum tensor  $T_{\mu\nu}$  is assumed to be that of the ideal fluid

$$T_{\mu\nu} = p g_{\mu\nu} - u_\mu u_\nu (p + \rho) \quad (4.6)$$

and  $p$  and  $\rho$  are pressure and density. One also needs the equation of state  $p = p(\rho)$ . The above equations take the simple form

$$\begin{aligned} \left(\frac{\dot{R}}{R}\right)^2 &\simeq G\rho \\ \frac{d\rho}{\rho} + 3\left(1 + \frac{p}{\rho}\right) \frac{dR}{R} &= 0 \end{aligned} \quad (4.7)$$

For the sufficiently small times, when the temperature was above all the particle masses, the density was given by  $\rho \sim T^4$ ; and also  $p = \frac{1}{3} \rho$  for a gas of relativistic particles. Therefore, from the second of Eqs. (4.7)

$$\rho \sim R^{-4} \quad (4.8)$$

and so from the first of Eqs. (4.7)  $\dot{R}R = \sqrt{G}$ , which implies

$$R(t) \sim \sqrt{t} \quad (4.9)$$

Obviously,  $\int_{t_0} [dt'/R(t')] \sim \sqrt{t_0}$  is finite ( $\rightarrow 0$ ) for  $t_0 \rightarrow 0$ . One gets

$$d(t, 0) \sim t \quad (4.10)$$

so that the size of causally connected domains is less than the size of the universe.

Various resolutions have been suggested. Owing to the brevity of space, I will here discuss only the attempt of Zee<sup>7)</sup> to use the phenomenon of symmetry breaking at high temperature to solve the horizon problem. His idea was simply to change the behaviour of  $R(t)$  at early times, in order to obtain

$$d(t, 0) = \infty$$

The ingredients in his approach are:

- (a) broken-symmetric theory of gravity<sup>17)</sup>,
- (b) symmetry breaking<sup>6)</sup> at high  $T$ .

The phenomenon of symmetry breaking at high temperature was discussed in Section 3. Let me then briefly summarize Zee's theory of gravity.

Imagine the action which describes the coupling of a scalar field  $\phi$  with gravity

$$S = \int d^4x \sqrt{g} \left[ \frac{1}{2} \epsilon \phi^2 R + \frac{1}{2} g^{\mu\nu} \partial_\mu \phi \partial_\nu \phi - V(\phi) + \mathcal{L}_{rest} \right] \quad (4.11)$$

where  $\epsilon \leq 1$  and  $R = R_{\mu\nu} g^{\mu\nu}$  is the space-time curvature which should not be confused with the cosmic scale  $R(t)$ . When the phenomenon of symmetry breaking occurs, i.e.  $\langle \phi \rangle = V_H \neq 0$ , then obviously the gravitational coupling constant gets induced

$$G = \frac{1}{8\pi \epsilon V_H^2} \quad (4.12)$$

so that  $V_H$  is close to the Planck mass  $M_P \approx 10^{19}$  GeV. Now, at high temperature  $V_H = V_H(T)$ , so that  $G = G(T)$  is not temperature invariant. Clearly the effects of temperature dependence of  $G(T)$  are irrelevant until temperature gets comparable with the Planck mass:  $T \approx M_P$ . At  $T = 0$ , the theory is equivalent to the conventional Einstein theory. If, on the other hand, the symmetry breaking, as discussed throughout this talk, persists at high temperature, i.e.  $V_H(T) \approx T$ , for  $T > M_P$ , then

$$G(T) = \frac{1}{T^2} \quad (4.13)$$

for  $T > M_P$ . In this case, Einstein's equations become

$$\left( \frac{\dot{R}}{R} \right)^2 \approx R^{-2} \quad (4.14)$$

or

$$R(t) \sim t \quad (4.15)$$

at very early times ( $t < t_p \approx 10^{-43}$  sec).

But then

$$\int_{t_0}^t \frac{dt'}{R(t')} = \ln t/t_0 \xrightarrow{t \rightarrow \infty} \infty \quad (4.16)$$

or, in other words

$$\int_0^{r_H} \frac{dv}{\sqrt{1-kv^2}} \xrightarrow{t_0 \rightarrow 0} \infty$$

For a brief moment of time, all of space was causally connected. It is then reasonable to expect the homogenous and isotropic universe.

In short, the spontaneously broken theory of gravity tied up with our mechanism of symmetry non-restoration at high temperature offers automatically the solution to the horizon problem, without affecting any of the successful predictions of the standard theory of gravity. Admittedly, the model requires the belief that quantum gravitational effects can be ignored for  $T > M_p$ , and so, in my opinion, the solution is only indicative of what could happen, rather than being a complete picture.

## 5. CONCLUSIONS

The behaviour of gauge theories at high temperature seems to be richer than one could naïvely expect by the analogy with the ferromagnetic systems. In the simplest case, with a single Higgs field, the symmetry is always restored, as expected, at temperature above some critical temperature which is of the order of the mass scale that characterizes symmetry breaking at  $T = 0$ . In more complex theories, with the extended Higgs sector, intuitive expectations, as we have discussed throughout this paper, seem to fail. The symmetry may be partially restored or never restored at all.

In this talk I have tried to summarize the interesting applications that the above phenomenon offers. Firstly, if symmetry non-restoration at high  $T$  does take place, then various interactions which are based on the idea of symmetry breaking remain equally operative at high  $T$ . In particular, spontaneous CP violation would remain effective at enormous temperature  $T_x \approx 10^{15}$  GeV, which was presumably achieved in the very early universe ( $t \approx 10^{-35}$  sec or so). This in turn makes theories based on the above idea respectable candidates for simultaneous resolutions of the so-called strong CP problem, without invoking the existence of the

axion, and correct predictions of the amount of matter-antimatter asymmetry in today's universe. One will have to await the improved precision of our laboratory experiments, in particular the measurements of the electric dipole moment of the neutron, to see whether the idea of spontaneous CP violation is correct or not.

As we have discussed in Section 3, the so-called monopole problem in grand unified theories, i.e. the over-abundance of superheavy monopoles ( $M_m \approx 10^{16}$  GeV), which were supposedly created during the phase transition in the very early universe according to the conventional idea of symmetry restoration at high  $T$ , finds its natural resolution in the context of the above possibility. If  $U(1)_{em}$  symmetry was broken for  $T > M_w$ , then these monopoles were never created in the first place.

Finally, if the ideas presented above are correct, the horizon problem of the standard cosmological problem would not be a problem at all. Symmetric-broken theory of gravity, when tied up with the phenomenon of symmetry non-restoration at high  $T$ , forces gravity to be weaker and weaker, as  $T$  increases above the Planck mass. That leads to the slowing down of the expansion of the universe at the very early times and so allows, albeit for a brief period of time, that all the parts of the universe were in causal contact, enabling us to understand the observed isotropy and homogeneity of the universe.

In short, the implications are rich and it is, in my opinion, important to offer ways in which the phenomenon of symmetry restoration at high temperature could be tested, at least indirectly.

#### Acknowledgements

I wish to thank the members of the Warsaw University Theory Group, in particular Z. Ajduk, Jan Kalinowski, Stefan Pokorski and Tom Taylor, for their hospitality. This talk was written up at CERN and the hospitality of the CERN Theory Group is gratefully acknowledged.

## REFERENCES

- 1) D.A. Kirzhnits and A.D. Linde, Phys. Lett. 42B, 471 (1972).
- 2) S. Weinberg, Phys. Rev. D 9, 3357 (1974).  
 L. Dolan and R. Jackiw, Phys. Rev. D 9, 2904 (1974).  
 For a review and further list of references, see A.D. Linde, Rep. Prog. Phys. 42, 389 (1979).
- 3) M. Yoshimura, Phys. Rev. Lett. 41, 381 (1978).  
 A. Yu. Ignatiev, N.Y. Krasnikov, V.A. Kuzmin and A.N. Tavkhelidze, Phys. Lett. 76B, 436 (1978).  
 S. Dimopoulos and L. Susskind, Phys. Rev. D 18, 4300 (1978).  
 D. Touissant, S. Treiman, F. Wilczek and A. Zee, Phys. Rev. D 19, 1036 (1979).  
 S. Weinberg, Phys. Rev. Lett. 42, 850 (1979).  
 J. Ellis, M.K. Gaillard and D.V. Nanopoulos, Phys. Lett. 80B, 360 (1978).  
 For an extensive list of references see the review of P. Langacker, SLAC preprint SLAC-PUB-2544 (1980).
- 4) M.A.B. Beg and H.S. Tsao, Phys. Rev. Lett. 41, 278 (1978).  
 R.N. Mohapatra and G. Senjanović, Phys. Lett. 79B, 283 (1978).  
 H. Georgi, Hadronic J. 1, 155 (1978).
- 5) T.D. Lee, Phys. Rev. D 8, 1226 (1973).  
 For a review and references, see G. Senjanović, in Proceedings of the 20th Int. Conf. on High-Energy Physics, Madison, 1980 (eds. L. DuRand and L.G. Pondrom) (AIP, N.Y., 1981).
- 6) R.N. Mohapatra and G. Senjanović, Phys. Rev. Lett. 42, 1651 (1979); Phys. Rev. D 20, 3390 (1979); Phys. Lett. 89B, 57 (1979).  
 An example of partial symmetry restoration was constructed before by S. Coleman and reported by S. Weinberg, ref. 2.
- 7) A. Zee, Phys. Rev. Lett. 44, 703 (1980).
- 8) L. Dolan and R. Jackiw, Phys. Rev. D 9, 2904 (1974).



- 9) R.N. Mohapatra and G. Senjanović, Phys. Rev. D 21, 3470 (1980).
- 10) G. 't Hooft, Nucl. Phys. B79, 276 (1974).  
A.M. Polyakov, Pis'ma Eksp. Teor. Fiz. 20, 430 (1974) [JETP Lett. 20, 194 (1974)].
- 11) Ya. B. Zel'dovich and M.Y. Khlopov, Phys. Lett. 79B, 239 (1979).  
J.P. Preskill, Phys. Rev. Lett. 43, 1365 (1979).
- 12) M.B. Einhorn, D.L. Stein and D. Touissant, Phys. Rev. D 21, 3295 (1980).
- 13) An incomplete list of references is  
A.M. Guth and S.-H. Tye, Phys. Rev. Lett. 44, 631 (1980).  
F. Bais and S. Rudaz, preprint TH.2885-CERN (1980);  
P. Langacker and S.-Y. Pi, Phys. Rev. Lett. 45, 1 (1980).  
A. Kennedy, G. Lazarides and Q. Shafi, preprint TH.2944-CERN (1980).
- 14) P. Langacker and S.-Y. Pi, Ref. 13.
- 15) See, for example, S. Weinberg, Gravitation and Cosmology (Wiley, N.Y., 1972).
- 16) W. Rindler, Mon. Not. Roy. Astron. Soc. 116, 663 (1956); also Ref. 15.
- 17) A. Zee, Phys. Rev. Lett. 42, 417 (1979) and references therein.

#### Figure captions

- Fig. 1 : The two different phases in the case of the single Higgs field. The broken phase at  $T < T_c$  is shown in (a), and (b) describes the symmetric phase for  $T > T_c$ .
- Fig. 2 : Phase diagrams for  $V(\phi_1, \phi_2)$  in the case of two Higgs fields. As shown in (a)  $V(\phi_1)$  indicates a phase transition with  $\langle \phi_1 \rangle = 0$  above  $T_c$ , and (b) shows the existence of the single phase for  $V(\phi_2)$  (the broken one) for all  $T$ .

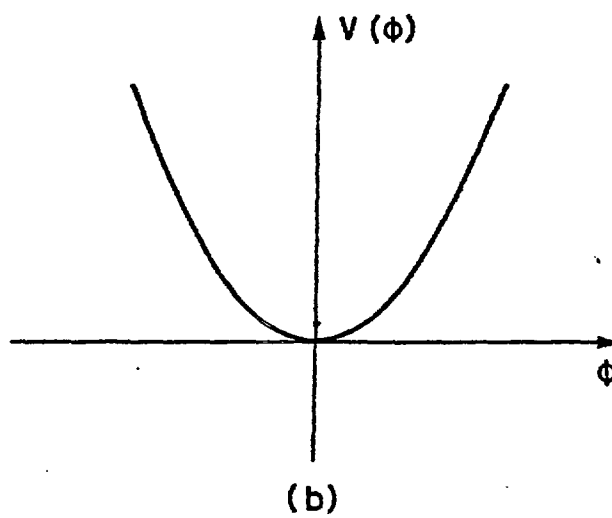
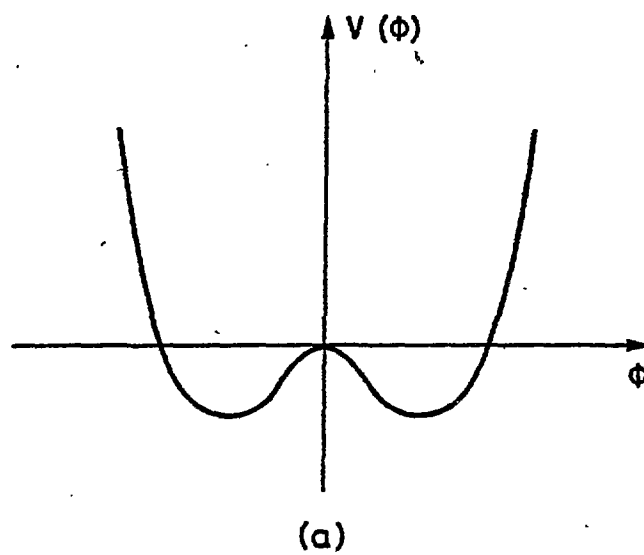


FIG. 1

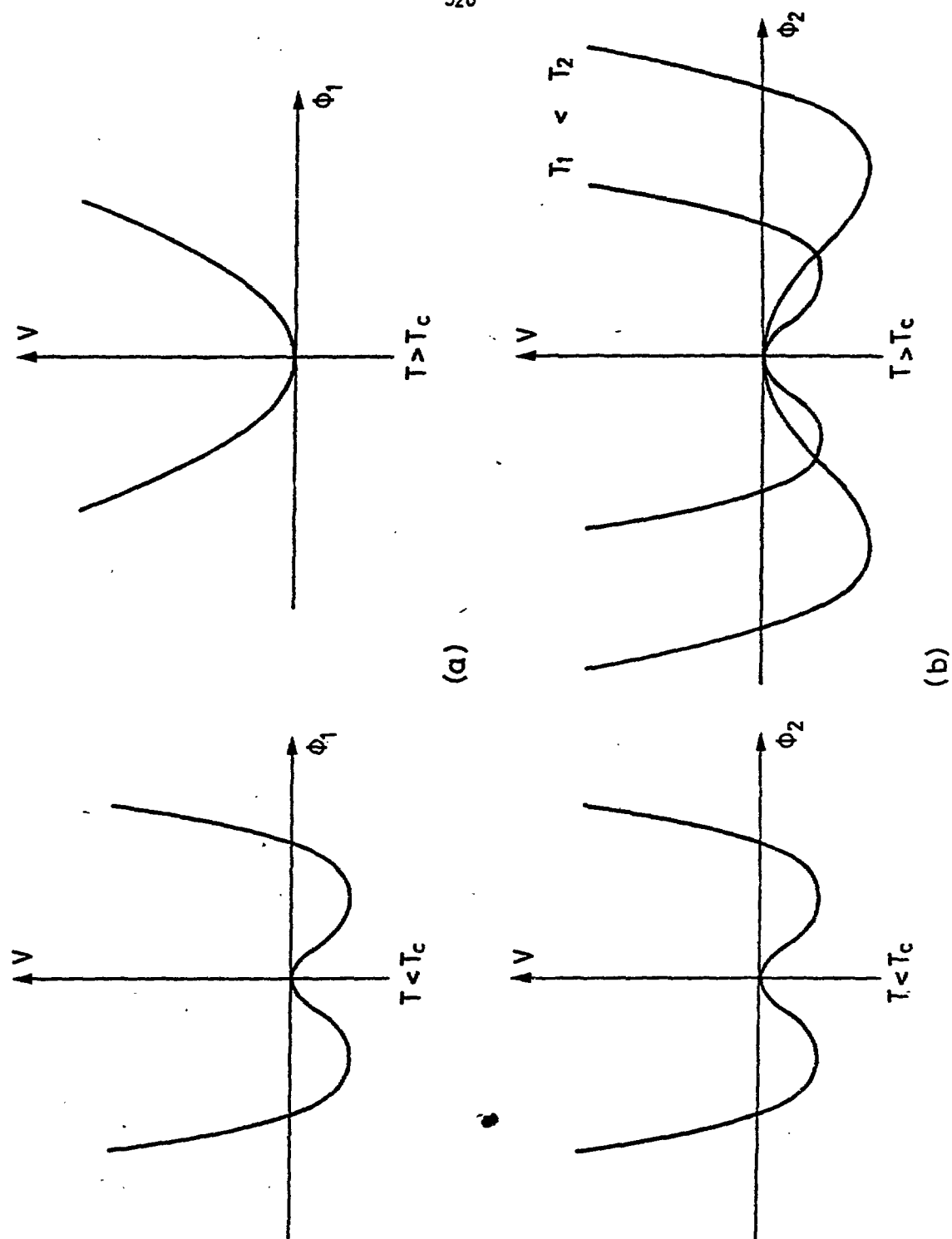


FIG. 2

PATTERN OF CHIRAL SYMMETRY BREAKING IN  
QUANTUM CHROMODYNAMICS

K. Konishi<sup>‡</sup>

Nordita, Blegdamsvej 17, Copenhagen, Denmark

Abstract

Arguments of Coleman and Witten are generalized to show that the possible pattern of chiral symmetry breaking in QCD is  $SU(N_f) \times SU(N_f) \times U_V(1) \rightarrow SU_V(N_f) \times U_V(1)$ , under reasonable assumptions. Chiral symmetry breakdown is itself assumed. The validity of the above pattern is extended to  $m_q/\Lambda_{QCD} \ll 1$  =  $N_f/N_c \ll 1$ ,  $N_c \rightarrow \infty$  with  $g^2 N_c$  and  $p$  fixed.

(author)

---

<sup>‡</sup>On leave from INFN, Sezione di Pisa, Pisa, Italy.

Problem

Why is the isospin a good approximate symmetry of strong interactions? In the present understanding of the subject, the goodness of the isospin is attributed to the smallness of quark masses<sup>1)</sup>,

$$m_u, m_d \ll \Lambda_{\text{QCD}},$$

compared to the mass scale of Quantum Chromodynamics (QCD). In fact, the Lagrangian of QCD with  $N_f$  massless quarks is invariant under global (chiral)  $SU(N_f)_L \times SU(N_f)_R \times U_V(1)$  transformations:

$$\psi_L \equiv \{(1+\gamma_5)/2\}\psi + \{\exp i T^a \alpha^a\}\psi_L$$

$$\psi_R \equiv \{(1-\gamma_5)/2\}\psi + \{\exp i T^a \beta^a\}\psi_R$$

$$\text{and} \quad \psi \rightarrow (\exp i \gamma)\psi. \quad (2)$$

This might appear to be sufficient for guaranteeing a  $U_V(N_f)$  symmetry (which, for  $N_f = 2$ , amounts to the isospin plus the quark number conservation), as it is contained in  $SU(N_f)_L \times SU(N_f)_R \times U_V(1)$ .

However, the chiral symmetry in QCD is believed to be broken spontaneously, leaving light pions as approximate Nambu-Goldstone particles. The question is therefore to which subgroup the original

$SU(N_f)_L \times SU(N_f)_R \times U_V(1)$  group is broken down. Or, if the surviving symmetry group is  $U_V(N_f)$ , as it seems to be realized in nature, why is that so?

This question was addressed recently by Coleman and Witten<sup>2)</sup>, in the large  $N_c$  QCD. They assume (i) that the  $1/N_c$  expansion at fixed  $g^2 N_c$  and  $N_f$  is an asymptotic expansion; (ii) that the confinement holds at  $N_c \rightarrow \infty$ ; (iii) that the chiral symmetry breaking is characterized by non-zero vacuum expectation values,  $M_{ij} = \langle 0 | \bar{\psi}_{L_i} \psi_{R_j} | 0 \rangle$ ; (iv) that  $M$  can be obtained by minimizing an effective potential  $V_{\text{eff}}$  constructed in the standard way for  $M$ ; (v) and that there is no accidental degeneracy in the minima of  $V_{\text{eff}}$  in the limit (i). Under these (perhaps reasonable) assumptions, it was argued that the chiral symmetry of QCD necessarily break down spontaneously and that the remaining symmetry of hadronic world (in the limit of massless quarks) was  $U_V(N_f)$ .

Although their conclusion is quite encouraging, the assumptions used are rather strong. In particular, the phenomenology of hadrons suggests the dominance of planar diagrams (in the sense of the topological expansion<sup>3)</sup>), and not necessarily of the leading terms of the 't Hooft's limit<sup>4)</sup>. (Some examples are: the exchange degeneracy,  $\alpha_\rho(t) \approx \alpha_{A_2}(t)$ ; the isospin degeneracy,  $m_\rho \approx m_\omega$ ; also,  $\Gamma_{\text{hadron}}/m_{\text{hadron}} \sim O(1)$ .)

We ask therefore whether the  $U_V(N_f)$  symmetry found in Ref. 2) is stable against the inclusion of quark loops<sup>5)</sup>. More formally, what is the allowed pattern of chiral symmetry breaking of QCD, in the limit,  $N_c \rightarrow \infty$  with  $g^2 N_c$  and  $\rho \equiv N_f/N_c$  fixed (and small)?

#### Results<sup>5)</sup>

We find that the pattern of the breaking is necessarily

$$SU(N_f)_L \times SU(N_f)_R \times U_V(1) \rightarrow SU_V(N_f) \times U_V(1), \quad (3)$$

assuming (i) ~ (v) of Ref. 2) and the chiral symmetry breaking itself. If small quark masses are introduced, (3) is still approximately valid for

$$m_q/\Lambda_{\text{QCD}} \ll \rho = N_f/N_c \ll 1,$$

$$N_c \rightarrow \infty; g^2 N_c \text{ and } \rho \text{ fixed.} \quad (4)$$

In contrast to Ref 2), our conclusion is based on the assumption of chiral symmetry breakdown: as will be discussed at the end, the latter does not necessarily follow from the triangle anomaly in the large  $N_c$  limit. It is also interesting to note that (4) is precisely the limit in which the  $U(1)$  problem is solved in QCD<sup>6)</sup>.

It is furthermore found that the Green's func-

tions for  $\bar{\psi}\psi$  operators cannot be simply expanded in powers of  $\rho$  around  $\rho = 0$ , but contains logarithmic dependence upon it:

$$\langle \bar{\psi}_i \psi_i \rangle = \lambda_0 + \underbrace{A\rho + B\rho^2 \log \rho + \dots + X\rho^n \log^{n-1} \rho}_{i\text{-independent}} + O(\rho^n) \\ + O(m_i \log m_i),$$

$$\int dx^4 \dots T \langle \bar{\psi}\psi(x) \bar{\psi}\psi(y) \dots \rangle = G(\rho, \log \rho; \{m_i\}). \quad (5)$$

Such a logarithmic dependence is due to the infrared divergences caused by Nambu-Goldstone bosons, and has a similar origin as  $\log m_\pi$  of Li and Pagels<sup>7)</sup>. As is shown in Eq.(5), the explicit breaking of chiral symmetry is small in the limit, (4).

#### Sketch of the proof

The idea is to make an expansion in  $\rho$  (quark loops) while keeping planar diagrams only ( $N_c \rightarrow \infty$ ). The effective potential has an expansion,

$$V_{\text{eff}} = N_c \{ V_0 + \rho V_1 + \rho^2 V_2 + \dots \}. \quad (6)$$

Following Ref. 2), we can write

$$V_0 = \sum_{i=1}^{N_f} F_0(\lambda_i), \quad (7)$$

$$V_1 = \frac{1}{N_f} \sum_{i,j=1}^{N_f} F_1(\lambda_i, \lambda_j), \text{ etc.}, \quad (8)$$



where an appropriate chiral transformation has been made so that

$$(MM^\dagger)_{ij} = \delta_{ij} \lambda_i^2/4 \text{ and hence } M_{ij} = \delta_{ij} \lambda_i/2, \quad (9)$$

(ignoring small effects of the  $\theta$ -parameter). The functions  $F_0$ ,  $F_1$ , etc. are independent of  $N_c$ ,  $\rho$ , and of flavour.

To lowest order of  $\rho$ ,  $\partial V_{\text{eff}}/\partial \lambda_i = 0$  simply gives

$$\lambda_i = \lambda_0 \text{ (independent of } i) \quad (10)$$

where the assumption (v) has been used. Equation (10) shows that the original chiral symmetry is spontaneously broken down to  $U_V(N_f)^2$ . To the next order in  $\rho$ ,  $V_{\text{eff}}$  is no longer a simple sum over flavour. Therefore, although the equation  $\partial V_{\text{eff}}/\partial \lambda_i = 0$  remains symmetric in flavour, the symmetry of the solution does not necessarily follow.

Expansion of the equation  $\partial V_{\text{eff}}/\partial \lambda_i = 0$  around  $\lambda_i = \lambda_0$ , (by setting  $\lambda_i = \lambda_0 + u_i(\rho)$ ) gives

$$F_0''(\lambda_0) \cdot u_i(\rho) + 2 \left. \rho \frac{\partial}{\partial x} F_1(x, \lambda_0) \right|_{x=\lambda_0} + O(\rho^2, \rho u, u^2) = 0 \quad (11)$$

from which we conclude, if  $F''_0(\lambda_0) \neq 0$ , that

$$u_i(\rho) \sim O(\rho), \text{ independent of } i. \quad (12)$$

(The possibility  $F''_0(\lambda_0) = 0$  is excluded, since it would imply the presence of massless scalar - not pseudoscalar - bosons in the large  $N_c$  limit. That would contradict our assumption that the chiral symmetry is realized in the Nambu-Goldstone mode).

At this point our argument might sound somewhat trivial. However, the infrared divergences appearing in the  $O(\rho^2, \rho u, u^2)$  terms of Eq. (11) make the extension from  $\rho = 0$  to  $\rho \neq 0$  quite non-trivial. For instance, the terms of order  $\rho u$  contain second derivatives of  $F_1$  at  $\lambda = \lambda_0$ . They are part of contribution to the two-point function,  $\int dx^4 T \langle \bar{\psi}\psi(x) \bar{\psi}\psi(0) \rangle$ , and for massless quarks contain a logarithmic divergence coming from two-"pion" loops. Higher derivatives at  $\lambda = \lambda_0$  contain power divergences,  $\sim (1/m_\pi^2)^n \rightarrow \infty$ .

Because of these, the equation  $\partial V_{\text{eff}} / \partial \lambda_i = 0$  cannot be expanded in powers of  $\rho$  around  $\rho = 0$ . It would appear that the expansion in  $\rho$  breaks down. It might be thought that it is sufficient to keep non-vanishing quark masses such that  $\rho < 1/\log(\Lambda_{\text{QCD}}/m_q)$ , but then it would not make much sense in talking about a dynamical breaking of the chiral symmetry.

Actually, the situation is not as bad: the infrared divergences cancel in the sum in Eq. (11) although each term is divergent. The reason is that  $(\partial/\partial x)F(x, \lambda_0)|_{x=\lambda_0}$  and  $(\partial/\partial \lambda_i)F(\lambda_i, \lambda_j)$  are both some kind of one-point function and cannot be infrared divergent. Neither can their difference.

To see better what is happening, we expand the difference at  $\lambda_i = \lambda_0 + u_i(\rho)$  rather than at  $\lambda_0$ :

$$\begin{aligned} & (\partial/\partial \lambda_i)F(\lambda_i, \lambda_j) - (\partial/\partial x)F(x, \lambda_0)|_{x=\lambda_0} = \\ & \Sigma \left\{ \begin{array}{l} \text{higher} \\ \text{derivatives} \\ \text{at } \lambda_i = \lambda_0 + u_i \end{array} \right\} (-u_i)^n \end{aligned} \quad (13)$$

Now each term on the right-hand side is finite. The "pion" propagator computed at  $\lambda_i = \lambda_0 + u_i$  has a pole not at  $m_\pi^2 = 0$  but at  $m_{\text{eff}}^2 \sim u_i/\Lambda_{\text{QCD}}$ .

The point is that the "pion" appearing inside a loop is made of one quark pair and gluons and would be exactly massless when computed at the minimum of  $V_0$ ,  $\lambda_0$ . (This is the Goldstone theorem in the leading order of  $1/N_c$ .) When evaluated at the new minimum  $\lambda_i = \lambda_0 + u_i$ , one finds

$$\partial V_0 / \partial \lambda_i |_{\lambda_0 + u_i} \approx O(u_i)$$

and hence

$$m_{\text{eff}}^2 \sim O(u_i/\Lambda) \quad (14)$$

As a consequence, the logarithmic divergences are replaced by  $\log u_i$ 's. The right-hand side of Eq. (13) contains terms behaving as  $\sim u \log u$ . Inserting them back into Eq. (11) gives

$$u_i(\rho) \sim A\rho + B\rho^2 \log \rho + O(\rho^2) \quad (15)$$

which is again  $i$ -independent.

Repeating similar arguments including higher order terms in  $\rho$ , one finds Eq. (5), thus proving our claim about the pattern of chiral symmetry breaking, Eq. (3).

The cancellation of infrared divergences caused by Nambu-Goldstone bosons, and the appearance of logarithmic dependence on the expansion parameter, seem to be a quite general feature in models with a spontaneously broken symmetry. For instance, a  $O(N)$ -symmetric  $(g/4!)\phi^4$  model with a negative (mass)<sup>2</sup> term at the tree level has the following one-loop effective potential,<sup>5)</sup>

$$V_1(\varphi^2) = -\frac{\mu^2}{2}\varphi^2 + \frac{g}{4!}(\varphi^2)^2 - \frac{N}{2304\pi^2} g^2(\varphi^2)^2 + \\ + \frac{1}{64\pi^2} \left(\frac{g}{2}\varphi^2 - \mu^2\right)^2 \left\{ \log \frac{\frac{g}{2}\varphi^2 - \mu^2}{\mu^2} - \frac{1}{2} \right\} +$$

$$+ \frac{N-1}{64\pi^2} (g\phi^2 - \mu^2)^2 \left\{ \log \frac{g\phi^2 - \mu^2}{\mu^2} - \frac{1}{2} \right\}. \quad (16)$$

$$\left( \text{Re} \frac{\partial^2 V_1}{\partial \phi^2} \right) \Big|_{\phi^2=0} = g/12; \quad \text{Re} \left( \frac{\partial V_1}{\partial \phi} \right) \Big|_{\phi^2=0} = \mu^2/2.$$

One can easily check the absence of infrared divergences and log  $g$  dependence of zero-momentum two-point Green functions.

This phenomenon is somewhat analogous to the one discussed recently in a class of super-renormalizable models<sup>8)</sup>.

#### Strong anomaly

Strictly speaking, Eq. (6) is not the most general form, when the axial anomaly due to the strong interactions is taken into account. There can be a term of the form (to order  $\rho$ )<sup>9)</sup>

$$\Delta \mathcal{L} = A \cdot (\text{Tr} \log U/U^\dagger)^2 \quad \left( A = \text{a positive constant of dimension (mass)}^4 \right) \quad (17)$$

in the effective Lagrangian, where  $U_{ij} = \bar{\psi}_{L_i} \psi_{R_j}$ .  $M$  is given by  $M_{ij} = \langle U_{ij} \rangle$ . This term preserves  $SU(N_f) \times SU(N_f) \times U_V(1)$  but breaks  $U_A(1)$ .

Actually, this extra term does not affect the foregoing argument and may be ignored in deciding the pattern of the breaking. In fact, by an appropriate chiral rotation  $(MM^\dagger)$  can be taken real and diagonal,  $(MM^\dagger)_{ij} = (1/4)\delta_{ij}\lambda_i^2$ . For  $\theta = 0$ , it can then be shown that  $(\lambda_i = \text{real})$   $M_{ij} = (1/2)\delta_{ij}\lambda_i$ . Substituting this

into the effective potential obtained from Eq. (17), one finds

$$\partial/\partial\lambda_i \langle -(\Delta\mathcal{L}) \rangle = 0. \quad (18)$$

### Chiral symmetry breaking

The extra term, Eq. (17), however, does imply the chiral symmetry breaking itself<sup>10)</sup>, if not its pattern.  $\lambda_i = 0$  would lead to an unphysical situation ( $m_\pi^2 = \infty$  or  $F_\pi = \infty$ ), which is therefore excluded.

However, a particular form of Eq. (17) depends on the assumption that it is a  $\sigma$ -like meson which saturates the strong anomaly at low energy. In principle it is possible to have some other mesonic composite fields  $\phi$  to construct  $\Delta\mathcal{L}$  such that  $\langle \phi \rangle \neq 0$  does not break the chiral symmetry. In such a case, the chiral symmetry breaking is not a necessary consequence<sup>11)</sup>.

Coleman and Witten<sup>2)</sup> argued for the chiral symmetry breaking using the triangle anomaly associated with flavour currents. Their argument seems to fail in two respects: the  $\delta(k^2)$  singularity found in three-current Green functions does not necessarily imply the presence of a massless scalar meson; it can be due to massless fermions<sup>12)</sup>. Secondly, the argument for excluding baryons based on the large  $N_c$  limit is also false<sup>13),11)</sup> because a large coupling

of baryons to currents (as  $N_c \rightarrow \infty$ ) may compensate the  $1/N_c$  suppression factors.

In view of this, it has been assumed in Ref. 5) that the chiral symmetry in QCD is broken after confinement. The other possibility (that at least a part of the chiral symmetry survives confinement) is quite an interesting one from the viewpoint of composite models of quarks and leptons, and is presently under extensive study<sup>14)</sup>.

#### Acknowledgements

This talk is based on the work (Ref.5) done in collaboration with E. Guadagnini.

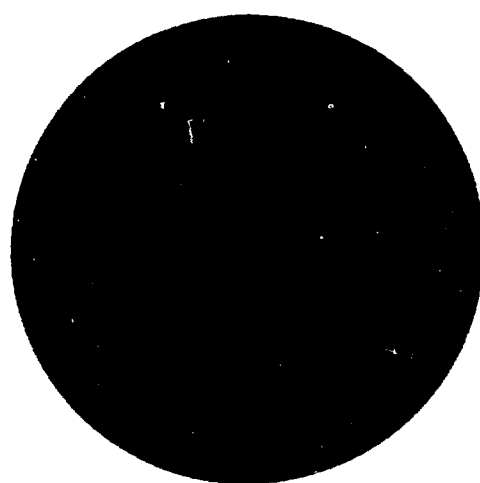
I thank Professor Białkowski, Professor Pokorski and other colleagues from the Warsaw University, for the warm hospitality at the Symposium and at the Institute of Theoretical Physics of Warsaw.

#### References

1. See, for instance, S. Weinberg, "The problem of Mass", Festschrift for I.I. Rabi, (N.Y. Academy of Sciences (1978)).
2. S. Coleman and E. Witten, Phys. Rev. Lett. 45 (1980)100.

3. G. Veneziano, Nucl. Phys. B117(1976)519.
4. G. 't Hooft, Nucl. Phys. B72(1974)461.
5. E. Guadagnini and K. Konishi, Pisa Preprint IFUP-TH 5/81 (1981).
6. E. Witten, Nucl. Phys. B156(1979)269; G. Veneziano, Nucl. Phys. B159(1979)213; P. Di Vecchia, Phys. Lett. 85B(1979)357.
7. L.F. Li and H. Pagels, Phys. Rev. Lett. 26(1971)1204.
8. R. Jackiw and S. Templeton, MIT Preprint CTP 895 (1980).
9. C. Rosenzweig, J. Schechter and G. Trahern, Phys. Rev. D21(1980)3388; P. Di Vecchia and G. Veneziano, Nucl. Phys. B171(1980)253; E. Witten, Ann. Phys. 128(1980)363; P. Nath and R. Arnowitt, Phys. Rev. D23(1980)473.
10. A. Salomone, J. Schechter and T. Tudron, Syracuse Preprint SU-4217-176 (1980); G. Veneziano, Phys. Lett. 95B(1980)90.
11. G. Veneziano, CERN Preprint TH 3042 (1981).
12. Y. Frishman, A. Schwimmer, T. Banks and S. Yankielowicz, Nucl. Phys. B177(1981)157.
13. D. Amati and E. Rabinovic, CERN Preprint TH 3037 (1981).
14. G. 't Hooft, Cargèse lectures (1979); S. Dimopoulos, S. Raby and L. Susskind, Nucl. Phys. B173(1980)208; see also Refs. 12), 13) and 11).





CHIRAL SYMMETRY AND BAG MODEL

Andrzej Szymacha

Institute of Theoretical Physics, Warsaw University, Warsaw, Poland

Stanisław TaturN. Copernicus Astronomical Center, Polish Academy of Sciences  
Warsaw, Poland

Let us start by reminding Johnson's formulation [1] of the MIT bag. The Lagrangian of the model is :

$$L_{\text{BAG}} = \theta(\bar{q}q) \left[ \frac{i}{2} \bar{q} \gamma^\mu \partial_\mu q - \frac{i}{2} (\partial_\mu \bar{q}) \gamma^\mu q - m \bar{q} q - B \right]$$

The action principle gives in this case both equation of motion and boundary conditions :

$$\left. \begin{array}{l} i \gamma^\mu \partial_\mu q - m q = 0 \\ -i \gamma^\mu \partial_\mu \bar{q} = \bar{q} \\ \frac{1}{2} \gamma^\mu \partial_\mu (\bar{q} q) = B \end{array} \right\} \begin{array}{l} \text{inside} \\ \text{on the surface of the bag.} \end{array}$$

The nonlinear boundary condition expressing conservation of energy and momentum at the surface in the spherical cavity approximation takes the form

$$\frac{dE(R)}{dR} = 0$$

where  $E(R)$  is the sum of all contributions to the energy of the bag of radius  $R$ .

The good fit to the masses (except that of the pion) has been obtained by the MIT group [2] with the following set of parameters

$$B^{\frac{1}{4}} = 0.145 \text{ GeV} \quad \alpha_c = 0.55 \quad Z_0 = 1.84 \quad m_s = 0.279 \text{ GeV}$$

With these parameters fixed all static electroweak properties of hadrons can easily be calculated. For nucleon which is our object of interest in this paper, they are summarized in the Table I

Table I

|           | $R(GW^{-1})$ | $g_A$           | $2M_{pp}$ | $2M_{pn}$ | $\sqrt{\langle T^2 \rangle_p} (f_m)$ |
|-----------|--------------|-----------------|-----------|-----------|--------------------------------------|
| Exp       | —            | $1.25 \pm 0.01$ | 2.793     | -1.913    | $0.84 \pm 0.03$                      |
| model [2] | 5            | 1.09            | 1.9       | -1.27     | 0.73                                 |

Let us consider for the moment the QCD Lagrangian

$$L_{QCD} = -\frac{1}{4} F_{\mu\nu}^a F_{\mu\nu}^a + \bar{q} i \gamma^\mu (\partial_\mu - i g \frac{\lambda^a}{2} A_\mu^a) q + \bar{q} m q$$

For  $m=0$  the QCD Lagrangian is invariant under full set of  $Su(2) \times Su(2)$  transformations. According to a rather generally accepted view the  $Su(2) \times Su(2)$  symmetry group is spontaneously broken to the subgroup  $Su(2)$  of the isospin observed in the spectrum of hadrons.

According to Goldstone theorem, a zero mass Goldstone bosons must exist and we identify them with pions. There is a hope that MIT Bag Model may somehow be obtained as an approximate solution of the QCD. However for  $m=0$  the bag Lagrangian is not invariant under  $Su(2) \times Su(2)$  because of the term  $\theta(\bar{q}q)$  that is responsible for the quark confinement. If we want to have pions as Goldstone bosons and to keep at the same time  $\theta(\bar{q}q)$  we can introduce the so called nonlinear realization of the chiral symmetry. In analogy with effective Lagrangian method for  $\pi N$  interactions [3] we introduce pion self interactions and pion quark interactions by substitutions

$$\partial_\mu \psi \rightarrow D_\mu \psi = \left( 1 + \frac{\psi^2}{4f_\pi^2} \right)^{-1} \partial_\mu \psi$$

$$\partial_\mu q \rightarrow \mathcal{D}_\mu q = \left[ \partial_\mu + \frac{i}{2f_\pi^2} \epsilon(\psi \times D_\mu \psi) \right] q$$

The Lagrangian of the bag with nonlinear realization of chiral symmetry has been given in [4]. We want to study only one pion emission so we shall consider the following simplified case

$$L_b = \theta(\bar{q}q) \left[ \frac{1}{2} \bar{q} \gamma^\mu \partial_\mu q - \frac{1}{2} (\partial_\mu \bar{q}) \gamma^\mu q - \bar{q} m q - B + f \bar{q} \gamma^\mu \gamma_5 \tau_a q \partial_\mu \varphi \right] + \frac{1}{2} (\partial_\mu \varphi)^2$$

Modified Euler Lagrange equations are given by :

$$\left. \begin{aligned} i \gamma^\mu \partial_\mu q - m q + f \gamma^\mu \gamma_5 \tau_a q \partial_\mu \varphi &= 0 && \text{inside} \\ -i \gamma^\mu \partial_\mu \bar{q} &= \bar{q} \\ \frac{1}{2} \partial_\mu (\bar{q} q) &= B - \frac{1}{2} (\partial_\mu \varphi^{\text{ext}} - \partial_\mu \varphi^{\text{int}})^2 \end{aligned} \right\} \text{on the surface of the bag}$$

$$\partial_\mu \left[ \partial^\mu \varphi + f \theta(\bar{q}q) \bar{q} \gamma^\mu \gamma_5 \tau_a q \right] = 0$$

The value of the quark pion coupling constant  $f$  is determined from the requirement that the quark part of the axial vector current takes the standard form  $f \bar{q} \gamma^\mu \gamma_5 \tau_a q$ . This gives  $f = \frac{1}{2f_\pi}$  where  $f_\pi$  is the pion decay constant.

One should stress that taking into account interactions with pions by this method does not introduce any new free parameters. The mass of the pion is introduced as in the effective Lagrangian by taking into account explicit symmetry breaking in the form

$$L' = \frac{f_\pi^2 m_\pi^2}{4f_\pi^2} \frac{1 - \frac{\varphi^2}{4f_\pi^2}}{1 + \frac{\varphi^2}{4f_\pi^2}} \approx \text{const} - \frac{1}{2} m_\pi^2 \varphi^2$$

The equations for the pion field can be solved using perturbation theory and the pion field can be explicitly expressed in terms of the quark fields [4]. The interactions with pions modify most of the bag properties. Technically these changes are induced in two different ways. One is direct, like in magnetic moment, where additional terms in electromagnetic current

[5]

$$\Delta j_{em}^\mu = \epsilon_{3ab} \psi_a \partial^\mu \psi_b - \frac{1}{2f_\pi} \bar{q} \gamma^\mu \gamma_5 \tau_a q \epsilon_{3ab} \varphi_b \theta(\bar{q}q)$$

produce contribution which add simply to the classical quark value. The other way is through the change of the basic parameters induced by the additional term in the bag energy fitted to the observed masses of selected hadrons. Having the pion field expressed in terms of quarks we can calculate effectively all the necessary contributions.

They are zero for the electromagnetic charge radius and  $g_A$  (except for their dependence of the radius  $R$  of the nucleon) and different from zero for the magnetic moment and energy

$$\Delta\mu = \frac{1}{2} \epsilon_{3ij} \int d^3x x_i \Delta j_j^{em}$$

$$\Delta E = -\frac{1}{24\pi f_\pi^2 R^3} \left(\frac{x_0}{2(x_0-1)}\right)^2 \frac{\beta \cosh \beta - \sinh \beta}{\beta^3} (1+\beta) e^{-\beta} u^+ \vec{\sigma} \tau u u^+ \vec{\sigma} \tau u$$

$\beta = m_\pi R$

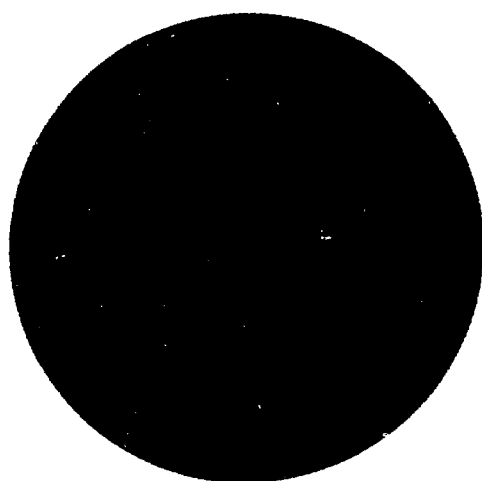
This should be compared with [6-10] where there is an awkward multiplicative correction to  $g_A$ :  $g_A^{com} = \frac{3}{2} g_A^{stand}$  and where the formulae for  $\Delta\mu$  and  $\Delta E$  are different. Luckily for us due to some additional assumptions of phenomenological character, the numerical value of the coefficient in [10] is nearly identical to ours. Therefore we can take their fit to basic parameters and radii of bag solutions and calculate all electroweak properties of nucleons with very little numerical effort. In the calculations we took into account the corrections due to the centre of mass motion analyzed by Donoghue and Johnson in [11]. Our final results for these properties are summarized in the Table II

Table II

|           | $R (\text{GeV}^{-1})$ | $g_A$           | $2M_{pp}$ | $2M_{pn}$ | $\sqrt{\langle \vec{r}^2 \rangle_p} (\text{fm})$ |
|-----------|-----------------------|-----------------|-----------|-----------|--|
| exp       | —                     | $1.25 \pm 0.01$ | 2.793     | -1.913    | $0.84 \pm 0.03$                                  |
| our model | 5.3                   | 1.20            | 2.66      | -1.89     | 0.80   |

References

1. K.Johnson, Proceedings of 19-th International Conference on High Energy Physics, p.585, Tokyo Academic Printing 1978.
2. T.A. De Grand R.L. Jaffe, K. Johnson, J.Kiskis, Phys.Rev. D12, 2060 (1975).
3. V.De Alfaro, S.Fubini, G.Furlan, C.Rosetti, Currents in hadron physics, Amsterdam London North Holland 1975 .
4. A.Szymacha, S.Tatur, Z.Phys. C4, 311, 1981.
5. J.Bartelski, A.Szymacha, S.Tatur, Z.Phys. C8, 91 1981.
6. R.L.Jaffe, MIT preprints: MIT CTP 814, MIT CTP 822 (1979).
7. R.L. Jaffe, Lectures at 1980 Winter School in Schladming.
8. M.V. Barnhill, W.K. Cheng, A.Halprin, Phys.Rev. D20, 727 (1979).
9. M.V. Barnhill, A.Halprin, Phys.Rev. D21, 1916 (1980).
10. F.Myhrer, G.E.Brown, Z.Xu, Nordita preprint Nordita 80/48 .
11. J.F. Donoghue, K.Johnson, Phys.Rev. D21, 1975 (1980).



PATTERNS OF CP VIOLATION AS

R. D. P e c c e i

Max-Planck-Institut für Physik und Astrophysik, Munich, Fed. Rep. Germany

Abstract

The experimental and theoretical constraints on models of CP violation are discussed. The predictions of the hard CP-violating Kobayashi-Maskawa model are contrasted with those of a left-right model, where CP is broken spontaneously. A brief discussion is included of the difference between the CP-violating phases that enter in kaon decay and those that may be responsible for the baryon asymmetry in the universe.

(author)

AS



CP violation, although discovered more than fifteen years ago, remains a rather elusive phenomenon both experimentally and theoretically. Experimentally, we have only observed CP violation in the kaon system [1]. There CP violation can be characterized by two complex numbers  $\epsilon$  and  $\epsilon'$  which measure, essentially, the amount of  $\Delta S = 2$  and  $\Delta S = 1$  CP violation present in the system. Both  $\epsilon$  and  $\epsilon'$  are small numbers and one knows that [1]

$$|\epsilon| \approx 2.3 \times 10^{-3} \quad (1a)$$

$$\left| \frac{\epsilon'}{\epsilon} \right| \lesssim \frac{1}{50} \quad (1b)$$

In principle there are other areas of particle physics in which some CP violation should be observable. Most notably, a non zero electric dipole moment of the neutron would be a clear indication of CP violation. Very beautiful experiments [2] have set a limit

$$d_n \leq 1.6 \times 10^{-24} \text{ e cm} \quad (2)$$

One expects also that CP-violating phenomena, analogous to those occurring in the kaon system, take place in  $D^0$  and  $B^0$ -mesons. Unfortunately, these phenomena are extremely difficult to observe since no separated beams of these particles exist, or are likely to exist. One can, however, try to measure asymmetries in  $e^+e^-$  production of pairs of these mesons. Typically these asymmetries involve measuring the difference between equal sign dileptons arising from the semi-leptonic decays of the produced mesons. Although the ratios  $N_{++}/N_{+-}$  and  $N_{--}/N_{+-}$ , of equal sign dileptons to opposite sign dileptons, just measure the amount of mass mixing between, say,  $D^0$  and  $\bar{D}^0$ , their difference is a measure of CP violation [3]

$$\frac{N_{++} - N_{--}}{N_{+-}} \sim \text{Re } \epsilon_M \quad (3)$$

where  $\text{Re } \epsilon_M$  is the equivalent of  $\epsilon$  for these heavy meson systems. Unfortunately, although in some instances one may expect a large asymmetry, in general the ratios  $N_{++}/N_{+-}$  and/or the number of ordinary dileptons ( $N_{+-}$ ) expected are small. Thus the likelihood of measuring these other possible CP-violating parameters is poor.

There may be a second measured number, besides  $\epsilon$ , which also provides information on CP violation. This is the observed ratio between the number of baryons to photons in the universe. Although there are considerable observational difficulties, one knows that  $n_B/n_\gamma$  is in the range of [4]

$$\frac{n_B}{n_\gamma} \approx 10^{-10 \pm 1} \quad (4)$$

This number could just reflect an initial baryon asymmetry in the universe and thus have no connection with CP violation. However, if in the big bang the universe started in a baryon-antibaryon symmetric state (a more natural boundary condition?), then the result (4) must reflect the presence of CP violation.

It has become particularly clear, through recent investigations in unified field theories in which baryon violation is possible, that an explanation for the cosmological baryon asymmetry may exist [5]. To obtain such an asymmetry it is necessary that three conditions be satisfied:

- (1) Baryon number must be violated. Clearly this is necessary. If not, no baryon asymmetry can evolve from a baryon-symmetric initial condition.
- (2) The baryon violating processes ought to have been out of thermal equilibrium during the era in the universe when the asymmetry ensued. This is necessary since, if not, the reversed processes, being equally probable, would erase any asymmetry.
- (3) C and CP violation must accompany B violation. This last requirement follows since to establish an asymmetry, we must have that the rate of baryon destruction and anti-baryon destruction (baryon creation) are different. This is the case only if we have C and CP violation.

It is because of this last point that  $n_B/n_\gamma$  may constitute an observable measure of CP violation.

Our experimental baggage of CP-violating information appears therefore rather meager. Two numbers  $\epsilon$  and  $n_B/n_\gamma$  and two bounds - those on  $\epsilon'$  and  $d_n$ . Our theoretical knowledge of CP violation may in fact be even more meager. Although one can introduce CP violation in a fairly natural way in gauge theory models of weak interactions, it is far from clear what is the correct model for CP violation. The Kobayashi and Maskawa observation [6], that within the standard  $SU(2)_L \times U(1)$  model [7] CP violation can occur if there are at least

6 quarks, represents the simplest way to understand the appearance of CP violation. However, one should keep in mind that simplicity may not necessarily be a guarantee of correctness. Thus it may well be that there are other phases besides, or instead of, the Kobayashi-Maskawa phase which are responsible for the observed CP violation.

In this talk I would like to examine the key theoretical issues at stake in constructing models for CP violation. Because it is possible to construct many different models which violate CP, it is not particularly useful to review all options. Rather what I want to do here is to focus on two, in some sense orthogonal, models which illustrate in a rather clear way the possible spectrum of possibilities. One of the models will be the minimal version of the Kobayashi-Maskawa model [6], with one doublet of Higgs, and its simplest baryon violating extension in SU(5) with just one  $\underline{5}$  of Higgs. This model is a prototype hard-CP model. The second model which I will consider is one developed recently in collaboration with Masiero and Mohapatra [8]. In this model CP is broken softly and CP violation is mostly a Higgs phenomenon.

To emphasize the difference between these models it is useful to begin our discussion by examining the so-called  $\Theta$ -problem. This problem may ultimately be a red herring, but if it is to be conventionally solved, one cannot countenance the Kobayashi-Maskawa model, at least in its minimal version. The  $\Theta$ -problem can be stated succinctly as follows [9]. If QCD is the gauge theory of strong interactions and if the weak and electromagnetic interactions are also described by a gauge theory, then one has in general an extra CP-violating piece in the total Lagrangian of the form

$$\mathcal{L}_{CP} = -\frac{\bar{\Theta}}{32\pi^2} g^2 F_a^{\mu\nu} \tilde{F}_{a\mu\nu} \quad (5)$$

where  $F_a^{\mu\nu}$  is the gluon field strength and

$$\tilde{F}_{a\mu\nu} = \frac{1}{2} \epsilon_{\mu\nu\alpha\beta} F_a^{\alpha\beta} \quad (6)$$

is its dual. Here  $g$  is the QCD coupling constant and  $\bar{\Theta}$  is an arbitrary parameter. One can think of  $\bar{\Theta}$  as being made up of two parts

$$\bar{\Theta} = \theta + \text{Arg det } M \quad (7)$$

The first term above,  $\Theta$ , represents a parameter representing the vacuum state ( $\Theta$ -vacua) which is the one appropriate to describe pure QCD [10]. The second term arises as a result of diagonalizing the quark mass matrix. In so doing one in general performs chiral  $U(1)$  transformations (transformations where all quarks get rotated by the same chiral phase). These transformations change the  $\Theta$ -vacua to new  $\Theta$ -vacua [11] by an amount precisely equal to the chiral phase of the rotation -  $\text{Arg det } M$ .

Unless  $\bar{\Theta}$  vanishes or is extremely small, the Lagrangian (6) will give an unacceptably large electric dipole moment for the neutron. Calculations by Baluni [12] and Crewther, di Vecchia, Veneziano and Witten [13] indicate that if  $d_n$  is to satisfy the bound (2), then

$$\bar{\Theta} \lesssim 10^{-8} - 10^{-9} \quad (8)$$

There appears to be only two "natural" ways to understand why  $\bar{\Theta}$  should be so small [14]:

- (1)  $\bar{\Theta} = 0$ , because the total theory possesses a chiral  $U(1)$  invariance. If the theory is chiral  $U(1)$  invariant, clearly  $\bar{\Theta}$  has no meaning since by an invariance transformation one can rotate it away. This was a suggestion originally made by Helen Quinn and myself [15]. However, as Weinberg [16] and Wilczek [17] showed, because of the spontaneous breaking of the total theory necessary to get correctly the weak interactions, a quasi-Goldstone boson arises connected with the extra chiral  $U(1)$  invariance. This is the famous axion. Unfortunately, the axion appears to be questionable experimentally [18], although some positive evidence in its favour has been claimed by Faissner and collaborators [19].
- (2)  $\bar{\Theta}$  can be made to satisfy the bound (8) if one assumes that  $\Theta = 0$ , as an outside imposition on QCD, and if the weak interaction theory is such that

$$\text{Arg det } M \lesssim 10^{-8} - 10^{-9} \quad (9)$$

This solution is called the soft-CP solution to the problem and was originally suggested by Wilczek [17].

If axions do not exist and the  $\Theta$ -problem finds no other solution, it appears that one must actively contemplate that CP should only be broken softly

in the weak interactions. Clearly if one has operators of dimension 4 in the Lagrangian, whose coefficients can break CP (hard CP-breaking), one can never hope to calculate  $\text{Arg det } M$ , since this quantity will turn out to be infinite. Only if CP is broken softly, by operators of dimension less than 4 or spontaneously, it is possible to contemplate  $\text{Arg det } M$  as a finite and calculable number. Many attempts to solve the  $\theta$ -problem by considering soft-CP models exist in the literature [20]. In some of these models the CP breaking is done by operators of dimension less than 4. In others, one has spontaneous CP breaking. I would like to argue here that a solution of the  $\theta$ -problem via soft CP breaking can only make sense if the CP breaking is spontaneous. This is because the requirement that  $\theta = 0$  makes sense only if it is part of a requirement for CP conservation in the whole Lagrangian and not only on the QCD part.

It is perhaps worthwhile to point out that spontaneous CP breakdown, besides having a possibility of solving the  $\theta$ -problem, is a very natural consequence of supposing that Higgs fields are fermionic bound states of a new kind of gauge interactions (technicolor?). Because gauge interactions preserve CP the effective Yukawa couplings that emerge are real and thus any CP breakdown must occur spontaneously [21].

The simplest version of the Kobayashi-Maskawa model [6], with just one doublet of Higgs fields is by necessity a hard CP model. The CP-violating phases in the quark-W-boson Lagrangian appear as a result of diagonalizing the quark mass matrix. This matrix, in the model, essentially is given by

$$M = \Gamma \langle \phi \rangle \quad (10)$$

where  $\Gamma$  is the matrix of the relevant Higgs Yukawa couplings and  $\langle \phi \rangle$  is the vacuum expectation value of the Higgs field, which can be chosen to be real. Clearly, unless  $\Gamma$  has some imaginary part (hard CP violation),  $M$  can be diagonalized with pure orthogonal matrices and no phases will ever enter in the quark-W-boson vertices. With  $\Gamma$  complex, the quark-W-boson vertex will be characterized by a unitary matrix  $C$  of dimension  $N^2$ , where  $N$  is the number of generations. This matrix has  $N(N+1)/2$  phases. However  $2N-1$  of these phases can be rotated away by redefining the  $2N$  quark fields appropriately. (We cannot get rid of  $2N$  phases since one phase is just an overall phase.) Whence for  $N$  generations in the model one has in toto  $1/2(N-2)(N-1)$  phases.

Because of the hard CP violation the  $\Theta$ -problem is thus a problem for the Kobayashi-Maskawa model. Ellis and Gaillard [22] have observed that  $\text{Arg det } M$  in the Kobayashi-Maskawa model is indeed infinite, but the first infinite graphs do not occur until very high order,  $O(\kappa^7)$ . Thus they have suggested that perhaps one should not worry unduly about it, since presumably the ultimate correct theory should take care of these "small" infinities. I tend to sympathize with this attitude but, lacking the ultimate theory, still consider it a problem.

The Kobayashi-Maskawa model makes some definitive statements about the measurable CP parameters  $\epsilon$ ,  $\epsilon'$  and  $\delta_n$ . For three generations, there is only one phase and this phase, along with the extra Cabibbo angles required for the six quark case, essentially determines  $\epsilon$ . One finds [23]

$$|\epsilon| \approx \frac{1}{f_2} \sin \theta_2 \cos \theta_2 \sin \theta_3 \sin \delta \, P(\theta_2, \eta) \quad (11)$$

where  $P(\theta_2, \eta)$  is a rather complicated, but slowly varying, function of  $\theta_2$  and  $\eta = m_c^2/m_t^2$ :

$$P(\theta_2, \eta) = \frac{\sin^2 \theta_2 \left(1 + \frac{\eta \ln \eta}{1-\eta}\right) - \cos^2 \theta_2 \left(\eta + \frac{\eta \ln \eta}{1-\eta}\right)}{\cos^4 \theta_2 \eta + \sin^4 \theta_2 - 2 \sin^2 \theta_2 \cos^2 \theta_2 \frac{\eta \ln \eta}{1-\eta}} \quad (12)$$

Although (11) is an explicit formula, in no way is it a prediction for  $\epsilon$  since the phase  $\delta$  is unknown. (The other parameters  $\theta_2$ ,  $\theta_3$ ,  $m_c$  and  $m_t$  [if it exists!] could in principle be determined elsewhere.) However, one can make a prediction for  $|\frac{\epsilon'}{\epsilon}|$  which is independent of the unknown parameter  $\delta$ . The value for  $|\frac{\epsilon'}{\epsilon}|$  that one obtains depends on  $P(\theta_2, \eta)$  - which does not vary too much - and on an estimate of the direct imaginary contribution to the matrix element  $\langle 2q | H_{\text{weak}} | K^0 \rangle$ . This matrix element is real if one considers only contributions involving u, d and s quarks, but can pick up an imaginary part when the contribution from virtual  $\bar{c}c$  and  $\bar{t}t$  pairs are included. These are the, so-called, Penguin contributions. Two recent evaluations give

$$|\frac{\epsilon'}{\epsilon}| \approx \begin{cases} 1/50 - 1/250 & \text{(Gilman and Wise [24])} \\ 1/250 - 1/500 & \text{(Guberina and Peccei [25])} \end{cases} \quad (13)$$

The difference obtained above reflects different ways of trying to evaluate the matrix element of  $H_{\text{weak}}$  between a  $K^0$  and  $2\pi$ . We emphasize that apart from these uncertainties the above calculations are among the most stable that one can find when dealing with CP violation, since essentially there are no free parameters. Thus attempts to measure  $|\frac{\epsilon'}{\epsilon}|$  to better than one part in 200 can really probe the validity of the simple Kobayashi-Maskawa model and would be extremely important.

The dipole moment of the neutron is found to be very small in the Kobayashi-Maskawa model. Shabalin [26] has shown that all contributions of  $O(\alpha^2)$  to the one-body dipole moment (i.e., the dipole moment of a given quark) vanish. Nanopoulos, Yildiz and Cox [27] and Morel [28] have considered two-body contributions and estimate

$$(d_n)_{KM} \approx 10^{-30 \pm 1} \text{ e cm} \quad (14)$$

well below the present bound (2). A point is worth noting. If the present round of experiments trying to lower the limits on  $d_n$  find a positive result (somewhere in the range of  $10^{-25}$  e-cm, which is their sensitivity), then the Kobayashi-Maskawa model is in trouble, unless one is prepared to believe that  $d_n$  is just given by  $\Theta$  - but then one must explain why  $\Theta \sim O(10^{-10})$ !

$n_B/n_Y$  is of course not directly calculable with the minimal Kobayashi-Maskawa model. However, one can ask what the simplest extension of this model, which allows for baryon number violating interactions, will give. This extension is based on SU(5) with just one  $\underline{5}$  of the Higgs (besides the  $\underline{24}$ ). The baryon excess occurs in the decay of the superheavy Higgs in the  $\underline{5}$ . However, since one must have a CP violation in the process, one is required to go to very high order. Typically [29] one finds

$$\frac{n_B}{n_Y} \sim \alpha^3 \left( \frac{m_f}{M_W} \right)^6 \ll 10^{-10} \quad (15)$$

where  $m_f$  is a typical (heavy) fermion mass of  $O(1-10 \text{ GeV})$ . In this estimate, since it is so small, one does not even worry about the magnitude of the CP phase, or if it is the same as the Kobayashi-Maskawa phase  $\delta$ . In fact, there are more phases in the SU(5) model. A simple calculation shows that, with just one  $\underline{5}$  of Higgs, the total number of phases which are physical for  $N$  generations is  $1/2N(N-1)$  [29][30], so for three generations there are an additional two CP phases which have purely to do with B-violating interactions.

I would like now to describe the soft-CP model developed in collaboration with Masiero and Mohapatra [8]. This model has a number of very nice features, which make it attractive, but it is not without some drawbacks. I shall try to be fair and describe both. The most interesting feature of the model is that it provides a natural solution to the  $\Theta$ -problem. Let me try to elaborate on this: All previous soft-CP solutions to the  $\Theta$ -problem are based on the following strategy [31]

- (1) Be sure, by construction, that in lowest order  $(\text{Arg det } M)_0 = 0$ ;
- (2) Construct the theory so that also  $(\text{Arg det } M)_1$  vanishes or is heavily suppressed;

Then one in general is sure that all contributions, being of 2nd order, will not violate the bound (9).

To achieve the above mentioned results, in general, it was necessary to invent appropriate discrete symmetries that prevented the mass matrix from acquiring phases until sufficiently high order. Now discrete symmetries, although "natural" in the technical sense, are extremely unnatural physically. The model in Ref. [8] makes use of no such devices. Rather it turns out that already at lowest order  $(\text{Arg det } M)_0 \neq 0$ . However, its size is very small, essentially because of the existence of a hierarchy of symmetry breaking. Direct calculation then shows that  $(\text{Arg det } M)_1 \ll (\text{Arg det } M)_0$ , again because of the hierarchy, so that the result is stable.

I shall only sketch the model here and indicate some of the results, since the details can be found in Ref. [8]. We considered as the weak gauge group the left-right symmetric group [32]  $SU(2)_L \times SU(2)_R \times U(1)_{B-L}$ . This group is broken down at a high scale into the usual  $SU(2)_L \times U(1)$  group, which eventually is broken down to just  $U(1)_{e.m.}$ . The spontaneous breakdown in the model is accomplished by three types of Higgs fields:  $\Delta_R$ ,  $\phi_L$  and  $\phi$ . These fields transform according to  $SU(2)_L \times SU(2)_R \times U(1)_{B-L}$  as

$$\Delta_L \sim (1, 0, -2) \quad (16a)$$

$$\Delta_R \sim (0, 1, -2) \quad (16b)$$

$$\phi \sim \left(\frac{1}{2}, \frac{1}{2}, 0\right) \quad (16c)$$

Since left (right) handed quarks and leptons transform as  $SU(2)_L$  ( $SU(2)_R$ ) doublets, one can think of these fields as appropriate lepton-lepton or lepton-



antilepton condensates. Writing  $\Delta_L$  and  $\Delta_R$  as  $2 \times 2$  matrices (i.e.,  $\vec{\tau} \cdot \vec{\Delta}$ ) one has as non-zero vacuum expectation values

$$\langle \phi \rangle = \begin{pmatrix} \kappa & 0 \\ 0 & \kappa' \end{pmatrix} ; \quad \langle \Delta_L \rangle = \begin{pmatrix} 0 & 0 \\ v_L & 0 \end{pmatrix} ; \quad \langle \Delta_R \rangle = \begin{pmatrix} 0 & 0 \\ v_R & 0 \end{pmatrix} \quad (17)$$

The Higgs potential at its minimum can either have a left-right symmetric solution  $v_L = v_R$  or a hierarchy must exist [33]:

$$v_L v_R \sim \kappa^2, \kappa'^2 \quad (18)$$

Clearly since we want the sequence of breakdowns

$$SU(2)_L \times SU(2)_R \times U(1)_{B-L} \rightarrow SU(2)_L \times U(1) \rightarrow U(1)_{e.m.} \quad (19)$$

we want the hierarchical solution

$$v_R \gg \kappa, \kappa' \gg v_L \quad (19)$$

In general one also chooses  $\kappa \gg \kappa'$  so that one has

$$\frac{v_R}{\kappa} \simeq \frac{M_{W_R}}{M_{W_L}} \quad (20)$$

What Masiero and Mohapatra and I investigated [8] was the possibility that this model exhibited, besides a breakdown of parity and B-L through a non-zero  $v_R$ , also a spontaneous breakdown of CP via the appearance of phases in the vacuum expectation values. Our results can be summarized in two theorems:

Theorem (1): With just one set of  $\Delta_L$  and  $\Delta_R$  there is no spontaneous CP violation.

Theorem (2): With more than one set of  $\Delta_L$  and  $\Delta_R$  there is CP violation provided that the

$$\text{phase } \langle \phi \rangle \sim v_L/v_R \quad (21a)$$

$$\text{phase } \langle \Delta_R \rangle \sim (v_L/v_R)^2 \quad (21b)$$

The phases of  $\langle \Delta_L \rangle$  will in general be of  $U(1)$ . These two theorems can be easily understood as an application of the decoupling theorem of

Appelquist and Carrazone [34]. The phases associated with the heavy scales must be appropriately small so that the effect of the heavy scales cannot be felt at low energy.

These theorems essentially provide a rationale for a small  $\arg \det M$  in the model. To lowest order one has (if there are enough Higgs fields)

$$(\arg \det M)_0 \sim \text{phase } \langle \phi \rangle \sim \frac{v_L}{v_R} \sim \frac{\kappa^2}{v_R^2} \sim \left( \frac{M_{WL}}{M_{WR}} \right)^2 \quad (22)$$

Values of  $M_{WR} \gtrsim 10^6$  GeV are compatible with the dipole moment bound (9).

Higher order contributions to  $(\arg \det M)$  can occur through diagrams of the type shown below



The CP mixing indicated by the  $\otimes$  in the figure is of order  $V_L V_R \sin \bar{\delta}$ , where  $\bar{\delta}$  is an (arbitrary) phase associated with  $\langle \Delta_L \rangle$ . Because, however, the mass of the  $\text{Im } \phi$  Higgs field is of  $O(v_R^2)$ , the net contribution of the integral is of  $O(1/v_R^2)$ . Thus  $(\arg \det M)_1 \sim (\arg \det M)_0$  and in fact, taking into account all the various Higgs coupling constants

$$(\arg \det M)_1 \ll (\arg \det M)_0 \quad (23)$$

In the model we see thus that

$$\bar{\theta} \sim \left( \frac{M_{WL}}{M_{WR}} \right)^2 \lesssim 10^{-8} - 10^{-9} \quad (24)$$

which happens if  $M_{WR}$  is sufficiently large. Conversely since one can show that here  $d_n$  is essentially determined by  $\bar{\theta}$ , a measurement of  $d_n$  will then fix the scale  $M_{WR}$ . I should mention that a scale  $M_{WR} \gtrsim 10^6$  GeV, which agrees with the  $d_n$  limit, also seems to be in agreement with the present limits on

nucleon stability [35] and permits the generation of enough baryon number at intermediate mass scales [36] to get a reasonable  $n_B/n_\gamma$ , (although the scenario for the generation of baryon number in the model is rather complex).

There are some features of the model which, however, are not so appealing. First of all one needs a great many Higgs fields to achieve the spontaneous breakdown of CP, and thus there are a variety of free parameters in the model. In general with so many Higgs fields it is difficult to prevent getting large  $K^0-\bar{K}^0$  mass mixing or preventing Higgs induced off-diagonal neutral current processes, like  $K \rightarrow \mu e$ , from occurring. To suppress these processes to a manageable level requires a certain tuning of parameters. Conversely, being optimistic, in this model there is no reason why  $K^0 \rightarrow \mu e$  should not happen at rates just below the present bounds.

The parameter  $\epsilon$  is not predicted in the model, just as it was not predicted in the Kobayashi-Maskawa model. However, for  $\epsilon$  to exist at all it is necessary that Higgs mesons  $\Delta_{qq}$  transforming like quark-quark condensates exist, with masses intermediate between  $M_{W_L}$  and  $M_{W_R}$ . If these Higgs bosons exist - and one sees no reason why they should not - then one can estimate  $|\frac{\epsilon'}{\epsilon}|$  in the model to be roughly

$$\left| \frac{\epsilon'}{\epsilon} \right| \lesssim 10^{-5} \quad (25)$$

Thus a measurement of  $|\frac{\epsilon'}{\epsilon}|$  in the Kobayashi-Maskawa range [cf Eq. (13)] would spell the death knell for this model.

There is a particularly clear feature of the model which is worth emphasizing. Namely, there is no connection between the phases responsible for  $\epsilon$ ,  $\epsilon'$  and  $\delta_n$  and those responsible for  $n_B/n_\gamma$ . This is obvious here since  $n_B/n_\gamma$  occurs in the model at temperatures of  $O(V_R)$ . At these high temperatures one expects that the  $SU(2)_L \times U(1)$  symmetry be restored so that the vacuum expectation values  $K$ ,  $K'$  and  $V_L$  all vanish. There will still be phases associated with the  $\Delta_R$  vacuum expectation values (of which by necessity there must be at least two) but these phases now are of  $O(1)$  and have nothing to do with the  $T = 0$  phases obtained previously.

This phenomenon is not only a property of models where CP is broken spontaneously. Also in hard-CP models - with sufficient number of Higgs fields - there will be in general no connection between the phases that enter in  $n_B/n_\gamma$  and in the low energy CP-violating parameters. This "negative theorem" is the subject of a recent short note with Masiero and Mohapatra [30]. The

theorem can be understood in its gist as follows. Renormalization requires that if phases appear in Higgs Yukawa couplings, they must at the same time appear in Higgs self interaction terms of the form

$$\chi_{Int}^Y = \lambda_{12}^2 H_1 H_2 + h.c. \quad (25)$$

which could have been generated through fermion loops. Once the Higgs potential is complex, one cannot prevent, in general, that the vacuum expectation values also acquire phases. All these phases (Yukawa coupling phases, Higgs potential phases and vacuum expectation value phases) contribute to the low energy CP violation. For  $n_B/n_\gamma$ , because the temperature is so high, the  $SU(2)_L \times U(1)$  group will have become normal. Thus for this case certain of the phases associated with previously non-zero vacuum expectation values disappear.

In this talk I tried to point out some of the features and possible patterns of CP violation arising from rather distinct models. Some features, like the difference between the phases contributing in the kaon system and for  $n_B/n_\gamma$  are common. Others, like the value for  $|\frac{\epsilon'}{\epsilon}|$ , are quite distinct. To conclude, there are two points I wish to re-emphasize:

- (1) Experimentally it is extremely important that one should try to improve the bounds for  $|\frac{\epsilon'}{\epsilon}|$  and  $d_n$ . A non-zero result would be of invaluable aid in trying to solve the riddle of CP violation.
- (2) Theoretically one should continue to ask, and try to answer, some of the structural questions about CP, which I just touched upon in this talk. For instance: is soft CP breaking really compatible with cosmology?; what really happens to CP violation if the Higgs mesons are only approximations to a more profound dynamics?; is the  $\Theta$ -problem really important? At the same time, I feel that it is also important that one should try to refine and tighten up, as best as one can, the calculations for some of the experimental predictions for the simplest Kobayashi-Maskawa model. Predictions for more sophisticated models, although very useful, in general are too arbitrary, because there are far too many free parameters.

Acknowledgement: I would like to thank the organizers of the Kazimierz Conference for a very nicely run meeting. I am also grateful to Antonio Masiero and Rabi Mohapatra for having shared with me some of their insights.

## References

- [1] For a very clear review of the experimental situation see, for example, K. Kleinknecht, Proceedings of the XVII Int. Conf. on High Energy Physics, London 1974.
- [2] W.B. Dress et al., Phys. Rev. D15 (1979) 9;  
N.F. Ramsey, Phys. Rept. 43 (1978) 409;  
I.S. Altarev et al., Pis'ma Zh. Eksp. Teor. Fiz. 29 (1979) 794.
- [3] A. Pais and S.B. Treiman, Phys. Rev. D12 (1975) 2744;  
A.I. Vainshtein, V.I. Zakharov, L.B. Okun and M.A. Shifman, Yad. Fiz. 24 (1976) 820.
- [4] K.A. Olive, D.N. Schramm, G. Steigman, M.S. Turner and J. Yang, Astrophys. J. in press.
- [5] A. Sakharov, Pis'ma Zh. Eksp. Teor. Fiz. 5 (1967) 32;  
M. Yoshimura, Phys. Rev. Lett. 41 (1978) 381; 42 (1979) 742 (E);  
S. Dimopoulos and L. Susskind, Phys. Rev. D18 (1978) 4500;  
A.Yu. Ignatiev, N.V. Krasnikov, V.A. Kuzmin and A.N. Tavkhelidze, Phys. Lett. 76B (1978) 436;  
D. Toussaint, S.B. Treiman, F. Wilczek and A. Zee, Phys. Rev. D19 (1979) 1036;  
S. Weinberg, Phys. Rev. Lett. 42 (1979) 850;  
J. Ellis, M.K. Gaillard and D.V. Nanopoulos, Phys. Lett. 80B (1979) 360; 82B (1979) 464 (E);  
A. Sakharov, Zh. Eksp. Teor. Fiz. 76 (1979) 1172.
- [6] M. Kobayashi and T. Maskawa, Pro. Theo. Phys. 49 (1973) 652.
- [7] S. Weinberg, Phys. Rev. Lett. 19 (1967) 1264;  
A. Salam, Proc. of the 8th Nobel Symposium 1968, Ed. by N. Svartholm (Almqvist and Wiksells, Stockholm 1968);  
S.L. Glashow, J. Iliopoulos and L. Maiani, Phys. Rev. D2 (1970) 1285.
- [8] A. Masiero, R.N. Mohapatra and R.D. Peccei, MPI-PAE/PTH 25/81.
- [9] For a more thorough review see, for example, R.D. Peccei, in Particle Physics 1980, Ed. by I. Andric, I. Dadić and N. Zovko (North Holland, Amsterdam 1981).
- [10] G. 't Hooft, Phys. Rev. Lett. 37 (1976) 8; Phys. Rev. D14 (1976) 3432.

- [11] C.G. Callan, R.F. Dashen and D.J. Gross, Phys. Lett. 63B (1976) 334; R. Jackiw and C. Rebbi, Phys. Rev. Lett. 37 (1976) 172.
- [12] V. Baluni, Phys. Rev. D19 (1979) 2227.
- [13] R. Crewther, P. de Vecchia, G. Veneziano and E. Witten, Phys. Lett. 89B (1979) 123.
- [14] For possible alternative solutions of the  $\theta$ -problem see Ref. [9].
- [15] R.D. Peccei and H.R. Quinn, Phys. Rev. Lett. 38 (1977) 1440; Phys. Rev. D16 (1977) 1791.
- [16] S. Weinberg, Phys. Rev. Lett. 40 (1978) 233.
- [17] F. Wilczek, Phys. Rev. Lett. 40 (1978) 279.
- [18] R.D. Peccei, Proceedings of the XIX Int. Conf. on High Energy Physics, Tokyo, Japan 1978.
- [19] H. Faissner, private communication.
- [20] For a review see G. Senjanovic, Proceedings of the XX Int. Conf. on High Energy Physics, Madison, Wisconsin 1980.
- [21] E. Eichten, K. Lane and J. Preskill, Phys. Rev. Lett. 45 (1980) 225.
- [22] J. Ellis and M.K. Gaillard, Nucl. Phys. B150 (1979) 141.
- [23] J. Ellis, M.K. Gaillard and D.V. Nanopoulos, Nucl. Phys. B109 (1976) 213.
- [24] F.J. Gilman and M. Wise, Phys. Lett. 83B (1979) 63; Phys. Rev. D20 (1979) 2392.
- [25] B. Guberina and R.D. Peccei, Nucl. Phys. B163 (1980) 269.
- [26] E.P. Shabalin, Yad. Fiz. 28 (1978) 151.
- [27] D.V. Nanopoulos, A. Yildiz and P.H. Cox, Phys. Lett. 87B (1979) 53; Ann. Phys. (N.Y.) 127 (1980) 1.
- [28] B.F. Morel, Nucl. Phys. B157 (1979) 23.
- [29] See Ellis et al. Ref. [5] or J. Ellis, M.K. Gaillard and D.V. Nanopoulos in Unification of the Fundamental Particle Interactions, Proc. of the Europhysics Study Conf., Erice (Plenum Press, 1980).
- [30] A. Masiero, R.N. Mohapatra and R.D. Peccei, MPI-PAE/PTh 27/81.
- [31] H. Georgi, Hadronic Journal 1 (1978) 155.

- [32] J.C. Pati and A. Salam, Phys. Rev. D10 (1974) 275;  
R.N. Mohapatra and J.C. Pati, Phys. Rev. D11 (1975) 566, 2558;  
G. Senjanovic and R.N. Mohapatra, Phys. Rev. D12 (1975) 1502.
- [33] R.N. Mohapatra and G. Senjanovic, Phys. Rev. D21 (1980) 3470.
- [34] T. Appelquist and J. Carrazone, Phys. Rev. D11 (1975) 2856.
- [35] R.N. Mohapatra and R.E. Marshak, Phys. Rev. Lett. 44 (1980) 1316;  
R.N. Mohapatra and G. Senjanovic, Phys. Rev. Lett. 44 (1980) 912,  
Phys. Rev. D23 (1981) 165.
- [36] A. Masiero and R.N. Mohapatra, Phys. Lett. B in press.

AN OASIS IN THE DESERT :  
WEAKLY BROKEN PARITY IN GRAND UNIFIED THEORIES

Goran Senjanović  
CERN, Geneva, Switzerland  
and  
Brookhaven National Laboratory \*)  
Upton, N. Y. 11973

~~ABSTRACT~~

A discussion of low energy parity restoration in simple grand unified theories, such as  $SO(10)$ , is presented. The consistency of phenomenological requirements and unification constraints is emphasized and various predictions of the theory are stressed, in particular : substantially lighter  $W$  and  $Z$  bosons than in the standard model and increased stability of the proton with  $\tau_p \simeq 10^{38}$  years.

---

\*) Permanent address.



1. INTRODUCTION

Grand unified theories<sup>1)</sup> offer us a possible way of unifying the interactions between elementary particles (except for gravity). They suggest, as a by-product, a spectacular prediction: the decay of matter, with hopefully soon measurable proton lifetime. The basic feature, at least of the simplest of such theories, appears to be the desert in energies above the mass scale of weak bosons. The minimal model, based on the SU(5) gauge group predicts the desert all the way up to  $10^{14}$  GeV. Namely, a necessary chain of symmetry breaking is

$$SU(5) \xrightarrow{M_X} SU(2)_L \times U(1)_Y \times SU(3)_C \xrightarrow{M_W} U(1)_{em} \times SU(3)_C$$

where  $M_X$  corresponds to the mass of superheavy bosons which mediate baryon-number violating forces and are responsible for nucleon decay. The values of low-energy parameters  $\alpha_s$ , and  $\sin^2 \theta_W$  determine<sup>2)</sup>  $M_X \approx 10^{14}-10^{15}$  GeV. In turn, one can predict the proton lifetime<sup>3)</sup> as  $\tau_p \approx 10^{31 \pm 1}$  years.

Actually, the above picture seems to be qualitatively true in many other grand unified models. Namely, if the value of  $\sin^2 \theta_W = 0.23 \pm 0.02$ , suggested by the standard electroweak model, and  $\alpha_s$  (the QCD coupling constant) are taken in inputs, the Georgi-Quinn-Weinberg (GQW) program<sup>2)</sup>, which determines the mass scales by the use of renormalization group equations, tends to suggest that the intermediate mass scales have to be quite large ( $\gtrsim 10^6-10^9$  GeV), leading again to a practical equivalent of the desert. If that is so, the future accelerators should not discover any new forms of interactions, once W and Z bosons are found! (?).

In this talk I will discuss some recent work of Rizzo and myself<sup>4)</sup>, which offers a way of avoiding such a situation, by suggesting an oasis in the desert, just above  $M_W$ . Our task appeared to be twofold: first, to find an alternative to the standard  $SU(2)_L \times U(1)_Y$  model<sup>5)</sup> (in order to change the  $\sin^2 \theta_W = 0.23$  prediction) with a new energy threshold above  $M_W$ ; and second, to show that such a scheme is consistent with grand unification. I will now try to offer arguments in favour of such a low intermediate mass scale.

The first part of our program was simplified by the fact that we did not have to search for a new candidate for a low-energy electroweak theory. A number of years ago, Pati, Salam, Mohapatra and myself<sup>6)</sup> constructed a left-right symmetric gauge theory, based on the  $SU(2)_L \times SU(2)_R \times U(1)_{B-L}$  group, in order to explain parity violation in weak interactions. The theory starts by being invariant under parity conjugation and only through non invariance of the vacuum, which results in heavy right-handed gauge bosons, parity gets broken and  $V + A$  interactions become suppressed at low energies. However, at higher energies, above  $M_{WR}$ , parity is expected to gradually become a good symmetry. It is therefore important to find constraints, phenomenological or theoretical and preferably both, on  $M_{WR}$ . Now, phenomenological analysis which I will describe below, allows  $W_R$  to be surprisingly light:  $M_{WR} \geq 2 M_{WL}$ . The hint on its value comes, on the other hand, from unification constraints. For example,  $SU(2)_L \times SU(2)_R \times U(1)_{B-L}$  can be embedded in  $SO(10)$ . As I mentioned before, assuming  $\sin^2 \theta_w = 0.23$  gives  $M_{WR} \geq 10^9$  GeV, which would eliminate the possibility of direct parity restoration.

Fortunately, the above is not true. The analysis of Rizzo and myself<sup>4)</sup> shows that for light  $W_R$  the theory successfully passes all the low energy tests, but for larger values of  $\sin^2 \theta_w$ :  $\sin^2 \theta_w = 0.27-0.28$ . Since the existence of low intermediate mass scale tends to increase  $\sin^2 \theta_w$ , it enabled us to construct an  $SO(10)$  grand unified theory with rather low-energy parity restoration:  $M_{WR} = (2-3)M_{WL}$ . There may be an oasis in the desert!

I will only list the predictions of the model and then deal with them in subsequent sections:

- $M_{WR} \approx (150-250)$  GeV,  $\sin^2 \theta_w = 0.27-0.28$ ,
- $M_{WL} \approx (70-72)$  GeV,  $M_Z \approx (80-84)$  GeV,
- a rather stable proton (in the model with minimal Higgs assignment):  
 $\tau_p \geq 10^{36}$  years,
- appreciable lepton number violation in neutrino -- less double  $\beta$  decay<sup>7)</sup>  
(not discussed here).

The rest of this paper is then organized in the following manner: in Section 2 I review the left-right symmetric model, with special emphasis on the leptonic (neutrino) sector. There I discuss the phenomenological constraints on our model. Section 3 deals with the embedding of the model in  $SO(10)$  and unification constraints that result from the GQW program, and also briefly touches upon baryon creation in the early universe in this kind of theory. Finally, Section 4 summarizes the basic features discussed in this talk.

## 2. LEFT-RIGHT SYMMETRY

The minimal gauge group which incorporates left-right symmetry is  $SU(2)_L \times SU(2)_R \times U(1)_{B-L}$ . The theory is assumed to be invariant under parity conjugation. That results in

•  $g_L = g_R \equiv g$ , where  $g_L$  and  $g_R$  are  $SU(2)_L$  and  $SU(2)_R$  coupling constants;

• the fermionic sector consists of left- and right-handed doublets

$$\begin{aligned} \psi_L &= \begin{pmatrix} \nu \\ e \end{pmatrix}_L, & \psi_R &= \begin{pmatrix} \nu \\ e \end{pmatrix}_R \\ Q_L &= \begin{pmatrix} u \\ d \end{pmatrix}_L, & Q_R &= \begin{pmatrix} u \\ d \end{pmatrix}_R \end{aligned} \quad (2.1)$$

where we restrict ourselves to one generation case, the general case being a trivial extension;

from Eq. (2.1), electric charge is

$$Q = I_{3L} + I_{3R} + \frac{B-L}{2} \quad (2.2)$$

• the Higgs sector has to be fully left-right symmetric.

In the following, I will discuss the version of the theory recently suggested by Mohapatra and myself<sup>7)</sup> in order to understand the smallness of neutrino mass by tying it to the maximality of parity violation at low energies. The Higgs sector complies with the principles of simplicity and the possibility of dynamical symmetry-breaking, i.e. the scalar fields carry the quantum numbers of fermionic bilinears

$$\phi\left(\frac{1}{2}, \frac{1}{2}, 0\right) \sim \bar{\Psi}_L \Psi_R$$

$$\Delta_L(1, 0, 2) \sim \Psi_L^T C \Psi_L ; \quad \Delta_R(0, 1, 2) \sim \Psi_R^T C \Psi_R \quad (2.3)$$

where the representation content in the brackets corresponds to  $SU(2)_L$ ,  $SU(2)_R$  and B-L, respectively. The field  $\phi$  gives the masses to charged fermions and  $\Delta$ 's complete the symmetry breaking, and as we shall see, they play a major role in the question of neutrino mass.

Now, the symmetric potential allows for the asymmetric absolute minimum<sup>6,7)</sup>

$$\langle \Delta_R \rangle \gg \langle \phi \rangle , \quad \langle \Delta_L \rangle = \gamma \frac{\langle \phi \rangle^2}{\langle \Delta_R \rangle} \quad (2.4)$$

where  $\gamma$  is a ratio of various Higgs self-couplings. In turn one obtains the following set of gauge mesons (besides the photon)

$$W_L^\pm, W_R^\pm, Z_1, Z_2 \quad (2.5)$$

with

$$\begin{aligned} M_{W_L}^2 &= g^2 \langle \phi \rangle^2 & M_{W_R}^2 &= g^2 \langle \Delta_R \rangle^2 \\ M_{Z_1}^2 &= \frac{M_{W_L}^2}{\cos^2 \theta_W} & M_{Z_2}^2 &= 2 \frac{\cos^2 \theta_W}{\cos 2\theta_W} M_{W_R}^2 \end{aligned} \quad (2.6)$$

where we ignore tiny  $W_L$ - $W_R$  mixing and  $\tan^2 \theta_W \equiv g'^2/g^2 + g'^2$ , so that  $e^2 = g^2 \sin^2 \theta_W$  as in the standard model. Therefore, besides the usual gauge bosons  $W_L$  and  $Z_1$  [ $W$  and  $Z$  in  $SU(2)_L \times U(1)$ ], we have heavier bosons  $W_R$  and  $Z_2$ , whose presence could effect low-energy predictions. In short, we have the following picture of symmetry breaking

$$SU(2)_L \times SU(2)_R \times U(1)_{B-L} \xrightarrow{\langle \Delta_R \rangle = M_{W_R}} SU(2)_L \times U(1)_Y \xrightarrow{\langle \phi \rangle = M_{W_L}} U(1)_{em}$$

Neutrinos

The charged fermions get their masses in the usual way; however, the situation with neutrinos is worth discussing. What happens is the following<sup>7)</sup>: since  $\Delta$ 's have the right quantum numbers to couple to  $\psi^T C \psi$  terms, the right-handed and left-handed neutrinos are separately two-component Majorana massive spinors. Actually, the right-handed neutrino  $\nu_R \equiv N$  becomes a heavy neutral lepton<sup>8)</sup> with

$$m_N \approx \langle \Delta_R \rangle \geq 100 \text{ GeV} \quad (2.7)$$

The left-handed neutrino ( $\nu_L \equiv \nu$ ), in turn, picks up a small Majorana mass

$$m_\nu \propto \frac{1}{m_N} \quad (2.8)$$

Therefore, the smallness of neutrino mass gets tied up to the maximality of observed parity violation in weak interactions. In the V-A limit of the theory, i.e. infinite  $M_{WR}$ ,  $m_N = \langle \Delta_R \rangle \rightarrow \infty$ ; so that  $m_\nu$  vanishes.

In the case when  $\langle \Delta_L \rangle$  is not directly contributing to neutrino mass, one gets

$$m_\nu = \frac{m_f^2}{m_N} \quad (2.9)$$

when  $f$  = electron or up quark. Therefore, we shall assume in further discussion  $\langle \Delta_L \rangle = 0$ , since it appears a phenomenological necessity [in other words, I put  $\gamma = 0$  in Eq. (2.4)]. Actually  $\gamma \leq 10^{-10}$ , to ensure small  $m_{\nu_e}$ . I should add, though, that once  $\gamma$  is small, the  $\nu_\mu$  and  $\nu_\tau$  masses are predicted by Eq. (2.9).

The above result is not accidental. From Eq. (2.2), in the energy region  $M_{WL} < E < M_{WR}$

$$\Delta Q = 0, \quad \Delta I_{3L} \approx 0 \quad (2.10)$$

and so<sup>9)</sup>

$$\Delta(B-L) = -2 \Delta I_{3R} \quad (2.11)$$

The breaking of B-L is proportional to the amount of parity violation<sup>7,9)</sup>, hence one gets massive Majorana  $\nu_R$ .

Phenomenologyi) Charged current processes

We just demonstrated:  $m_{\nu_R} \approx M_{W_R}$ . The exchange of  $W_R$  does not contribute then to  $\mu$  and  $\beta$  decay, and so we have no sensible limit on  $M_{W_R}$  from these processes. In other words, the world at low energies is V-A not because  $M_{W_R} \gg M_{W_L}$ , but because the right-handed neutrino is very heavy<sup>7)</sup>.

ii) Neutral current processes

Fortunately, as is seen from Eq. (2.6), the masses of  $W_R$  and  $Z_2$  are tied up, so that the constraints on  $M_{Z_2}$  from neutral-current data can be used to put the limit on  $M_{W_R}$ .

There are only two relevant types of processes:

- A. Neutrino interactions,
- B. Parity violation in e-q scattering.

We now give the relevant effective low  $q^2$  neutral current Hamiltonians, ignoring as before  $W_L$ - $W_R$  mixing and setting  $\langle \Delta_L \rangle' = 0$ . For a general case the reader should consult an original work<sup>8)</sup>.

A. Neutrino scattering

$$H^J = \frac{G_F}{\sqrt{2}} \bar{\nu} \gamma_\mu (1 + \gamma_5) \nu \bar{f} \gamma^\mu (g_V + g_A \gamma_5) f$$

where  $f$  denotes charged fermions (for leptons, we consider only  $\nu_\mu e$  scattering)

$$g_V = (1 + \eta_R) [T_3 - 2Q \sin^2 \theta_W] \quad (2.12)$$

$$g_A = T_3$$

and  $\eta_R$  is defined through

$$\frac{M_{W_L}^2}{M_{W_R}^2} = \frac{\eta_R}{1 + \eta_R} \quad (2.13)$$

It is easily seen from Eq. (2.12) that the effect of  $\eta_R$  is to increase  $\sin^2 \theta_W$  relative to the standard model prediction.

### B. Parity-violating electron-quark scattering

In the above limit

$$H_{PV} = H_{PV}(\text{standard model}) \quad (2.14)$$

Now, the SLAC experiment by itself (i.e. without constraints from  $\nu$ -hadron scattering) does not restrict  $\sin^2 \theta_W$  very precisely. It turns out that the data are consistently described with  $\eta_R$  as large as 0.3 ( $M_{WR} \approx 150$  GeV), if  $\sin^2 \theta_W = 0.27-0.28$  (of course, as well as  $\eta_R = 0$ ,  $\sin^2 \theta_W = 0.23 \pm 0.02$ , as in the standard model). The large predictions for  $\sin^2 \theta_W$  will turn out to be crucial in achieving the consistent unification conditions.

In any case, it is worth keeping in mind that independently of grand unification, the correct electroweak gauge theory may substantially differ from the standard  $SU(2)_L \times U(1)_Y$  model, with the differences that would make dramatic changes at higher energies.

For the sake of completeness, I have included Table 1 which gives the values of gauge boson masses as functions of  $\sin^2 \theta_W$  and  $\eta_R$ .

### 3. SO(10) AND WEAKLY BROKEN PARITY

As I emphasized before, we need unification constraints or otherwise  $M_{WR}$  remains an arbitrary parameter with  $M_{WR} \geq 150$  GeV. A minimal left-right symmetric grand unified theory is based on the  $SO(10)$  group<sup>10)</sup>.  $SO(10)$  has rank five and it contains the  $SU(2)_L \times SU(2)_R \times SU(4)_C$  group of Pati and Salam<sup>1)</sup>.

Since it also contains  $SU(5)$ , we can imagine two basically different chains of symmetry breaking:

$$i) \quad SO(10) \xrightarrow{M_U} SU(5) \xrightarrow{M_X} SU(2)_L \times U(1)_Y \times SU(3)_C \xrightarrow{M_W} U(1)_{em} \times SU(3)_C$$

$$ii) \quad SO(10) \xrightarrow{M_X} SU(2)_L \times SU(2)_R \times SU(4)_C \xrightarrow{M_C} SU(2)_L \times SU(2)_R \times U(1)_{B-L} \times SU(3)_C$$

$$\xrightarrow{M_R} SU(2)_L \times U(1)_Y \times SU(3)_C \xrightarrow{M_W} U(1)_{em} \times SU(3)_C$$

We now discuss the physics of both possibilities.

i) In this case the situation is analogous to the SU(5) model. Namely,  $M_U \geq M_X$  and  $M_X = 10^{14}$  GeV (see below). We have a desert, with the proton lifetime  $\tau_p = (\tau_p)_{\text{SU}(5)} = 10^{31 \pm 1}$  years. The only difference is in the neutrino sector, where left-handed and right-handed neutrinos are massive Majorana spinors. Particularly interesting is the minimal SO(10) model, where  $m_N = 10^9$  GeV appears in higher orders in perturbation theory<sup>11)</sup> and  $m_{\nu_\tau} \approx 10$  eV. It is amusing to notice that 10 eV heavy neutrinos could play a major cosmological role by closing up the universe and possibly explaining the dark matter in galactic halos<sup>12)</sup>.

ii) This chain of symmetry breaking is more interesting, since it allows, at least in principle, the existence of intermediate mass scales. The way to arrive at their values is to follow the change of physical coupling constants with energy [GQW program<sup>2)</sup>]. We shall set for simplicity  $M_C = M_X$ , since, in any case,  $M_C$  has to be astronomically large<sup>13)</sup>:  $M_C \geq 10^{12}$  GeV.

The idea of the GQW program is very simple: the change of coupling constants with energy is given by the renormalization group equation for the SU(N) coupling constant

$$\frac{dg_N}{dt} = b_N g_N^3 \quad (3.1)$$

with

$$b_N = -\frac{1}{16\pi^2} \left[ \frac{11}{3} N - \frac{4}{3} \sum_F T_F(R) - \frac{1}{6} \sum_S T_S(R) \right] \quad (3.2)$$

where the first term denotes the gauge meson contributions and the second and third terms stand for fermionic and Higgs contributions, respectively. The definition of  $T(R)$  is

$$T_V I_a I_b \equiv T(R) \delta_{ab} \quad (3.3)$$

where  $I_a$  are the group generators for representation R. It is important to notice that  $T_S(R)$  is obtained for real Higgs fields; for complex representation the contribution to  $T_S(R)$  should be doubled.



Using the decoupling theorem<sup>14)</sup> of Appelquist and Carrazzone, one can separately treat strong coupling constant  $g_s$ ,  $SU(2)_L$  coupling  $g_L$  and  $U(1)_Y$  coupling  $g_Y = \sqrt{5/3} g'$ , where

$$\frac{1}{e^2} = \frac{1}{g_L^2} + \frac{1}{g'^2} \quad (3.4)$$

We skip the details of derivations, which can be found in Ref. 4, and give the final expressions for physical parameters  $\alpha_s$  and  $\sin^2 \theta_w$  at  $E = M_w$

$$1 - \frac{8}{3} \frac{\alpha(M_w)}{\alpha_s(M_w)} = \frac{11\alpha(M_w)}{3\pi} \left[ \left( 3 + \frac{T_L + \frac{5}{3}T_Y}{44} \right) \ln \frac{M_x}{M_w} - \left( 1 - \frac{T_R + \frac{2}{3}T_{BL} - \frac{5}{3}T_Y}{44} \right) \ln \frac{M_x}{M_R} \right]$$

$$\sin^2 \theta_w(M_w) = \frac{3}{8} - \frac{11\alpha}{3\pi} \left[ \frac{5}{8} \left( 1 - \frac{T_L - T_Y}{44} \right) \ln \frac{M_x}{M_w} - \frac{3}{8} \left( 1 - \frac{T_R + \frac{2}{3}T_{BL} - \frac{5}{3}T_Y}{44} \right) \ln \frac{M_x}{M_R} \right] \quad (3.5)$$

where  $\alpha(M_w) = 1/128$  is the electromagnetic coupling<sup>15)</sup> at  $E = M_w$  and  $T$ 's stand for Higgs boson contributions to  $\beta$  functions (in obvious notation) of  $g_L$ ,  $g_R$ ,  $g_{BL}$  and  $g_Y$  couplings.

The first term in both Eqs. (3.5) corresponds to the  $SU(5)$  case, i.e. the case of no intermediate mass scales. The effect of  $M_R < M_x$  is then clear: it increases  $\sin^2 \theta_w$  and decreases  $\alpha_s$  compared to the  $SU(5)$  predictions.

The procedure, commonly employed, is to take  $\alpha_s(M_w)$  (obtained from experiment via tracing energy dependence from below  $M_w$ ) and  $\sin^2 \theta_w(M_w)$  as inputs and then

determine  $M_X$  and  $M_R$ . In the SU(5) case  $M_R = M_X$ , so that one has a consistency check, since it is enough to give  $\alpha_s(M_W)$  and determine both  $M_X$  and  $\sin^2 \theta_W$ . The reader should recall that the electroweak part of the Higgs sector consists of  $D \phi$  multiplets and  $T$  triplets  $\Delta_L (\Delta_R)$ , with  $D = T = 1$  in the minimal case. We then end up with two distinct possibilities:

(a) If  $M_R \geq 1$  TeV (approximately), then  $\sin^2 \theta_W = \sin^2 \theta_W$  (standard model)  $\approx 0.23 \pm 0.02$ . In that case one can derive a stringent limit<sup>13)</sup> on  $M_R$ ; with possible solutions:

$$\begin{array}{ll} \sin^2 \theta_W = 0.21 & M_X = M_R \approx 10^{14} - 10^{15} \text{ GeV} \\ \sin^2 \theta_W = 0.23 & M_X \approx (10^{15} - 10^{16} \text{ GeV}) \quad M_R \approx (10^9 - 10^{10} \text{ GeV}) \\ \sin^2 \theta_W = 0.25 & M_X \approx (10^{17} - 10^{18} \text{ GeV}), \quad M_R \approx (10^6 - 10^7 \text{ GeV}) \end{array}$$

The first solution corresponds to the SU(5) case. All the values, including  $\sin^2 \theta_W = 0.25$ , give the situation which is practically equivalent to a desert, since we would never directly observe parity restoration. That was the basis for the claim<sup>13)</sup> that there can be no low intermediate mass scales in simple grand unified theories.

(b) Light  $W_R$ :  $M_R \leq 250$  GeV — the case of interest to us<sup>4)</sup>.

The lesson of the previous section is, however, that the  $\sin^2 \theta_W$  condition is only true if one assumes the  $SU(2)_L \times U(1)_Y$  model to be correct at low energies, i.e. if one assumes  $W_R$  to be heavy ( $M_R \geq 1$  TeV). On the other hand, for low  $M_{W_R}$  we have seen that  $\sin^2 \theta_W$  can be as large as 0.28. We should keep that in mind.

Let us now go back to our prediction for  $\alpha_s$  and  $\sin^2 \theta_W$  in Eq. (3.5). To our leading log approximation, we should set  $M_R = M_W$ , in which case for  $D \phi$  multiplets and  $T \Delta_L (\Delta_R)$  fields (I am assuming, which is unclear, that these fields do not get superheavy),  $T_L = T_R = 2D + 4T$ ,  $T_{BL} = 18T$  and so we arrive at the following expressions

$$1 - \frac{8}{3} \frac{\alpha(M_W)}{\alpha_s(M_W)} = \frac{22\alpha(M_W)}{3\pi} \left(1 + \frac{5T+D}{22}\right) \ln \frac{M_X}{M_W}$$

$$\sin^2 \theta_W(M_W) = \frac{3}{8} - \frac{1}{8} \frac{22+7T-D}{22+5T+D} \left(1 - \frac{8}{3} \frac{\alpha(M_W)}{\alpha_s(M_W)}\right) \quad (3.6)$$

The strategy is the following: we will use  $\alpha_s(M_W)$  as an input and determine  $M_X$  and  $\sin^2 \theta_W(M_W)$ , to check the consistency of our results. We give the values of  $\alpha_s(M_W)$  that should correspond to  $\Lambda_{\overline{MS}} = 0.1-0.4$  GeV:  $\alpha_s(M_W) = 0.1-0.13$ . It is important to notice that the Higgs effects in Eq. (3.6) (especially due to triplets) are substantial.

#### Minimal model

In this case  $D = T = 1$  and therefore

$$1 - \frac{8}{3} \frac{\alpha(M_W)}{\alpha_s(M_W)} = \frac{28\alpha(M_W)}{3\pi} \ln \frac{M_X}{M_W} \quad (3.7)$$

$$\sin^2 \theta_W(M_W) = \frac{1}{4} + \frac{1}{3} \frac{\alpha(M_W)}{\alpha_s(M_W)}$$

Table 2 then summarizes the predictions for  $M_X$  and  $\sin^2 \theta_W$ . The scheme is clearly consistent, since we predict  $\sin^2 \theta_W = 0.27-0.28$ , as required by experimental constraints for light  $W_R$ .

From  $M_X = 10^{16}-10^{18}$  GeV, we predict for the proton lifetime

$$\tau_p = 10^{32}-10^{46} \text{ years} \quad (3.8)$$

#### Expanded Higgs sector

In order to see how strong our prediction for  $M_X$  is, we have given in Table 3 the values of  $M_X$  and  $\sin^2 \theta_W$  for the expanded Higgs sector. Whereas the results for  $\sin^2 \theta_W$  are good again,  $M_X$  clearly could be as low as  $10^{14}$  GeV, leading to the usual prediction of SU(5):  $\tau_p = 10^{31}$  years. However, if the extra Higgs multiplets are superheavy, one is back to minimal model results.

Combining our results from the previous section with this section, we list the set of predictions of the model (see Tables 1-3 and Ref. 4).

(i) The masses of light gauge bosons

$$M_{W_L} = (70 - 72) \text{ GeV}; \quad M_{Z_1} = (80 - 84) \text{ GeV}$$

to be contrasted with the values in the standard model:  $M_W = 78 \text{ GeV}$ ,  $M_{Z_1} = 89 \text{ GeV}$  (for  $\sin^2 \theta_W = 0.23$ ). This is one of our most clear predictions, which will be crucial in choosing between the two alternatives (see Ref. 4).

ii) The values of heavier gauge bosons vary in the range<sup>1)</sup>

$$M_{W_R} = (150 - 250) \text{ GeV}; \quad M_{Z_2} = (240 - 400) \text{ GeV}$$

They are likely to be produced at ISABELLE energies with substantial rates.

iii) In the minimal Higgs model  $\tau_p \geq 10^{34}$  years; but if the Higgs sector is expanded it is possible to obtain  $\tau_p$  as low as  $10^{30}$  years.

#### Baryon production in the early universe

One of the most exciting predictions of grand unified theories is the possible explanation of the origin of matter-antimatter asymmetry. Recently, Masiero and myself<sup>16)</sup> have shown that the existence of low intermediate mass scales does not spoil the success of arriving at a correct value of  $n_B/n_\gamma$ . The problem seemed to be that the baryon asymmetry, produced through the  $\Delta B \neq 0$  decays of superheavy bosons in the early universe, is proportional to the amount of left-right asymmetry<sup>17)</sup>

$$\text{i.e.} \quad \frac{n_B}{n_\gamma} \approx (10^{-13} - 10^{-7}) \frac{V_L - V_R}{m_H} \quad (3.9)$$

where the prediction in the brackets is obtained in the conventional theories where the breaking of parity is superstrong and  $V_L$ ,  $V_R$  and  $m_H$  are the scales that correspond to  $M_{W_L}$ ,  $M_{W_R}$  and superheavy bosons, respectively.

Since  $m_H \geq 10^{15} \text{ GeV}$  in our model and  $V_L - V_R \leq 10^3 \text{ GeV}$ , we would get

$$\frac{n_B}{n_\gamma} \leq (10^{-25} - 10^{-19}) \quad (3.10)$$

which is far below the observed number of baryons

$$\left( \frac{n_B}{n_T} \right)_{\text{obs}} = 10^{-9 \pm 1} \quad (3.11)$$

As it appears, weak breaking of left-right symmetry is incompatible with observed global properties of the universe, such as the baryon density. However, baryon excess supposedly originated in this picture at temperatures of the order of superheavy boson masses. But then, one should really have

$$\frac{n_B}{n_T} = \left( 10^{-13} - 10^{-7} \right) \frac{V_L(T) - V_R(T)}{m_H} \quad (3.12)$$

where  $V_L(T)$ ,  $V_R(T)$  are the scales associated with symmetry breaking at high  $T$ . Our main point is, as has been argued repeatedly by Mohapatra and myself<sup>18)</sup>, that the symmetry may remain broken at high temperature. For example, one can have for  $T > T_c$  ( $\approx 300$  GeV),  $V_L(T) = 0$ , but  $V_R(T) = T$ , in which the left-right asymmetry increases with temperature. In such a case,  $V_R(T) \leq m_H$ , which eliminates the apparent suppression in Eq. (3.12).

We have carried out a detailed analysis to show how one then obtains a reasonable prediction for  $n_B/n_T$ ; we refer the reader to Ref. 16 for the details.

In short, the amount of baryon asymmetry provides no limit on  $M_{WR}$ , since it only tests  $V_R(T)$  at high  $T$ , which can be large.

I have tried to argue in this section that a simple and realistic grand unified theory based on the  $SO(10)$  group gives a consistent picture according to which the proton is effectively stable (at least in the minimal Higgs model), but instead one expects new energy thresholds not far from  $M_W$ . The predictions of the theory are many and it should be not before long that such an alternative is either rejected or accepted.

#### 4. COMMENTS AND CONCLUSIONS

Left-right symmetric theories provide an appealing alternative to the standard  $SU(2)_L \times U(1)_Y$  electroweak model by offering a mechanism to understand parity violation in weak interactions. The question I have tackled in this talk is

whether we can hope to observe parity restoration in the near future. Phenomenological analysis and the use of the conditions for the unification with strong interactions provide an affirmative answer. I shall only summarize the predictions, without describing them again:

- .  $M_W = (70-72) \text{ GeV}$ ,  $M_{Z_1} = (80-84) \text{ GeV}$ ;
- .  $M_{Z_2} = (150-250) \text{ GeV}$ ,  $M_{Z_2} = (240-400) \text{ GeV}$ ;
- .  $\tau_p \geq 10^{30} \text{ years}$ ;
- .  $\Delta L \neq 0$  with  $(\beta\beta)^0$  process prediction:  $\eta_{\text{th}} \geq 10^{-5}$  and  $\eta_{\text{exp}} \leq 10^{-4}-10^{-5}$   
(see Refs. 4, 7);
- .  $\beta(\mu \rightarrow e\gamma) \neq 0$  (how big?),  $\frac{\beta(\mu \rightarrow ee\bar{e})}{\beta(\mu \rightarrow e\gamma)} = (1-10)\%$  (see Ref. 7).

Obviously, this oasis in the suggested desert in the grand unified theories may, after all, be only a mirage. Fortunately, we shall be able to tell, since most of the above predictions will be tested in the near future. Could it be that above this oasis there are others, whose presence affects low-energy phenomenology so as to be consistent with the idea of grand unification? Could it be that there is no desert, even within conventional grand unified theories.

#### Acknowledgements

I wish to thank the members of the CERN Theory Group and Z. Ajduk, Jan Kalinowski, Stefan Pokorski, Tom Taylor and other members of the Warsaw University Theory Group for their hospitality.

## REFERENCES

- 1) J.C. Pati and A. Salam, Phys. Rev. D 10, 275 (1974);  
H. Georgi and S.L. Glashow, Phys. Rev. Lett. 32, 438 (1974).  
For a review and extensive further list of references, see P. Langacker,  
SLAC Report SLAC-PUB-2544 (1980).
- 2) H. Georgi, H. Quinn and S. Weinberg, Phys. Rev. Lett. 33, 451 (1974).
- 3) A. Buras, J. Ellis, M.K. Gaillard and D.V. Nanopoulos, Nucl. Phys. B135, 66  
(1978);  
T. Goldman and D.A. Ross, Phys. Lett. 84B, 208 (1979);  
W.J. Marciano, Phys. Rev. D 20, 274 (1979).
- 4) T.G. Rizzo and G. Senjanović, Phys. Rev. Lett. 46, 1315 (1981); Phys. Rev. D  
(to appear) and Brookhaven preprint (1981).
- 5) S.L. Glashow, Nucl. Phys. 22, 579 (1961);  
S. Weinberg, Phys. Rev. Lett. 19, 1264 (1967);  
A. Salam, In Relativistic Groups and Analyticity (Nobel Symposium No. 8),  
ed. N. Svartholm (Wiley, N.Y., 1968).
- 6) J.C. Pati and A. Salam, Phys. Rev. D 10, 275 (1974);  
R.N. Mohapatra and J.C. Pati, Phys. Rev. D 11, 566, 2558 (1975);  
G. Senjanović and R.N. Mohapatra, Phys. Rev. D 12, 1502 (1975).
- 7) R.N. Mohapatra and G. Senjanović, Phys. Rev. Lett. 44, 912 (1980) and Phys.  
Rev. D 23, 165 (1981).
- 8) This is as in the originally suggested mechanism of M. Gell-Man, P. Ramond  
and R. Slansky, unpublished, and T. Yanagida, KEK lecture notes, 1979.
- 9) R.E. Marshak and R.N. Mohapatra, Phys. Lett. B91, 222 (1980).
- 10) H. Georgi, in Particles and Fields, 1974 (ed. C.E. Carlson);  
H. Fritzsch and P. Minkowski, Ann. Phys. (N.Y.) 93, 193 (1975).  
For a more extensive list of references, see Langacker, Ref. 1.

- 11) E. Witten, Phys. Lett. B91, 81 (1980).
- 12) See, for example, E. Witten, talk at the BNL Workshop on Neutrino Oscillations, 1981 (to appear in the Proceedings) and references therein.
- 13) D.V. Nanopoulos and H. Georgi, Nucl. Phys. B159, 16 (1979);  
 Q. Shafi and C. Wetterich, Phys. Lett. 89B, 52 (1979);  
 T. Goldman and D. Ross, Nucl. Phys. B162, 102 (1980).  
 R.N. Mohapatra and G. Senjanović, unpublished (see Senjanović, Proceedings of the 1979 VPI Workshop on Weak Interactions);  
 S. Rajpoot, Imperial College preprint ICTP-79-80-3 (1979);  
 F. del Aguila and L.E. Ibanez, Nucl. Phys. B177, 60 (1981).  
 This is true even in partially unified models, such as  $SU(2)_L \times SU(2)_R \times SU(4)_C$ , see J.D. Bjorken, A.J. Buras and P.Q. Hung, to appear (private communication from A. Buras).
- 14) T. Appelquist and J. Carrazone, Phys. Rev. D 11, 2856 (1975).
- 15) T. Goldman and D.A. Ross, Phys. Lett. 84B, 208 (1979);  
 W.J. Marciano, Phys. Rev. D 20, 274 (1979).
- 16) A. Masiero and G. Senjanović, Phys. Lett. B (to appear).
- 17) V.A. Kuzmin and M.E. Shaposhnikov, Phys. Lett. 92B, 115 (1980);  
 also T. Yanagida and M. Yoshimura, Phys. Rev. D 23, 2048 (1981).
- 18) R.N. Mohapatra and G. Senjanović, Phys. Rev. Lett. 42, 1651 (1979); Phys. Rev. D 20, 3390 (1979); Phys. Lett. 89B, 57 (1979).  
 For a recent review, see G. Senjanović, talk at this Conference, Proceedings p. 307.



Table 1

Gauge boson masses for various values of

$$\sin^2 \theta_w \text{ and } \eta_R \left( \frac{M_R^2}{M_L^2} \equiv \frac{1 + \eta_R}{\eta_R} \right).$$

| $\sin^2 \theta_w$ | $\eta_R$ | $M_{W_L}$<br>(GeV) | $M_{Z_1}$<br>(GeV) | $M_{W_R}$<br>(GeV) | $M_{Z_2}$<br>(GeV) |
|-------------------|----------|--------------------|--------------------|--------------------|--------------------|
| 0.23              | 0        | 78                 | 89                 | $\infty$           | $\infty$           |
| 0.23              | 0.1      | 78                 | 87                 | 260                | 420                |
| 0.25              | 0.2      | 75                 | 84                 | 185                | 295                |
| 0.28              | 0.2      | 70                 | 81                 | 170                | 290                |
| 0.28              | 0.3      | 70                 | 80                 | 150                | 240                |

Table 2

The values of the unification scale  $M_x$  and  $\sin^2 \theta_w$  for the minimal model with weakly broken parity. The values of  $\alpha_s(M_w)$  for corresponding  $\Lambda_{\overline{MS}}$  were suggested to us by A. Buras and W. Marciano.

|                                  |                    |                    |                    |                    |
|----------------------------------|--------------------|--------------------|--------------------|--------------------|
| $\Lambda_{\overline{MS}}$ (GeV): | 0.1                | 0.2                | 0.3                | 0.4                |
| $\alpha_s(M_w)$ :                | 0.101              | 0.113              | 0.121              | 0.127              |
| $\sin^2 \theta_w(M_w)$ :         | 0.276              | 0.273              | 0.272              | 0.270              |
| $M_x$ (GeV):                     | $5 \times 10^{16}$ | $1 \times 10^{17}$ | $2 \times 10^{17}$ | $3 \times 10^{17}$ |

Table 3

Again,  $M_x$  and  $\sin^2 \theta_w$  are plotted for different  $\alpha_s(M_w)$ . In this case the Higgs sector is extended.  $D$  denotes the number of  $\phi$  fields and  $T$  stands for the number of triplets  $\Delta_L$  ( $\Delta_R$ ). There is an implicit assumption that all of these fields remain non super-heavy, which may not hold true (otherwise they do not contribute to  $\beta$  fermions). For  $D = T = 1$  it is, however, a reasonable assumption.

| D | T | $\overline{\Lambda_{MS}}$<br>(GeV) | $M_x$<br>(GeV)     | $\sin^2 \theta_w(M_w)$ |
|---|---|------------------------------------|--------------------|------------------------|
| 2 | 1 | 0.1                                | $2 \times 10^{16}$ | 0.283                  |
|   |   | 0.4                                | $9 \times 10^{16}$ | 0.278                  |
| 1 | 2 | 0.1                                | $3 \times 10^{14}$ | 0.270                  |
|   |   | 0.4                                | $1 \times 10^{15}$ | 0.264                  |
| 1 | 3 | 0.1                                | $6 \times 10^{12}$ | ruled out              |
|   |   | 0.4                                | $2 \times 10^{13}$ |                        |
| 2 | 2 | 0.1                                | $1 \times 10^{14}$ | 0.276                  |
|   |   | 0.4                                | $5 \times 10^{14}$ | 0.270                  |
| 3 | 1 | 0.1                                | $5 \times 10^{15}$ | 0.289                  |
|   |   | 0.4                                | $3 \times 10^{16}$ | 0.284                  |



## REVIEW OF PROTON LIFETIME EXPERIMENTS

by

Eugene ENGELS, Jr.

Département de Physique des Particules Élémentaires  
CEN - SACLAY, 91191 Gif sur Yvette Cedex, France

and

University of Pittsburgh

### INTRODUCTION

The goal of this talk is to review experiments, planned or in progress, to study the instability of the nucleon with special emphasis on those experiments which have yielded some preliminary results. ~~I will not discuss predictions or experiments associated primarily with  $\Delta B = 2$  transitions which would include the neutron oscillation experiments being conducted at reactors or at accelerators yielding large neutron fluxes.~~ Much of what I will say has recently been presented at the Second Workshop on Grand Unification which took place at Ann Arbor, Michigan, from the 24-26 of April, 1981.

### PREDICTIONS OF NUCLEON LIFETIMES AND BRANCHING MODES

Theories of Grand Unification (GUTS) predict massive gauge bosons  $X$  which couple to a pair of quarks and to leptons and antiquarks as indicated in Figure 1a. A consequence of this coupling along with the requirement of, for example,  $SU_5$  that  $\Delta B = \Delta L$  is that the nucleon can decay as shown in Figure 1b. If the mass of the gauge boson,  $M_X$ , is much greater than other masses involved in the decay, the

amplitude for the decay will contain a propagator  $1/M_X^2$  and the lifetime of the nucleon will be proportional to  $M_X^4$  or

$$\tau_N = CM_X^4. \quad (1)$$

To estimate  $\tau_N$ , the twofold task consists of first evaluating  $M_X$  and then  $C$ . The problem of extrapolating the coupling constants  $\alpha_S$ ,  $\alpha_W$  and  $\alpha_U$  to the grand unification mass is discussed by numerous authors [1] and in particular, the extrapolation of  $\alpha_S$  depends critically on the  $\Lambda_{QCD}$  parameter. Specifically,

$$\alpha_S = 1/\ln(Q^2/\Lambda_{QCD}^2) \quad (2)$$

where  $Q^2 = 4$  times the square of the invariant mass of a particle mediating the interaction, with the consequence that

$$M_X = \Lambda_{QCD}. \quad (3)$$

Weinberg [2] has reported a dependence for  $M_X$  given by

$$M_X = 1.5 \times 10^{15} \Lambda_{QCD} \text{ GeV}. \quad (4)$$

Taking a value for  $\Lambda_{QCD} = 300 \text{ MeV}$ , this value of  $M_X$  yields a corresponding value of  $\tau_N$ :

$$\tau_N = 10^{31 \pm 1} \text{ years}. \quad (5)$$

Branching ratios for the proton and neutron decay modes have been predicted using  $SU_6$  quark models and bag models and the conclusions that one can easily draw from these predictions is that for Cabibbo-favored modes, the decays  $p \rightarrow e^+ \pi^0$  and  $n \rightarrow e^+ \pi^-$  are dominant (35 % and 70 % of their total rates, respectively) and the proton and neutron lifetimes are about equal.

#### BASIC EXPERIMENTAL CONSIDERATIONS

In an experimental apparatus containing  $N_0$  nucleons the observation of  $\Delta N$  decays in a time interval  $\Delta t$  years yields a lifetime

$$t(\text{years}) = A \times \frac{N_0}{\Delta N / \Delta t} \quad (6)$$

where  $A$  is a factor proportional to the decay modes to which the apparatus is

sensitive, the efficiency of the apparatus for detecting various decay modes and the data loss factors due to nuclear absorption of the decay products, event reconstruction losses, etc. If one optimistically takes  $A = 1$  and observes no events over a period of observation of 1 year, then  $\tau \geq N_0$ , the number of nucleons present. The current published lower limit [3] on the nucleon lifetime is  $10^{30}$  years and so future experiments must consist of detectors with masses well in excess of  $10^{30}$  nucleons (1.6 tons).

Several considerations will affect the lower limit which a detector can place on the lifetime of the nucleon. Background events in the detector which are indistinguishable from nucleon decay place a practical upper limit on the size of the detector. Figure 2 is a plot of the achievable lower lifetime limit (in years) as a function of detector mass (in kilotons) which can be achieved in 1 year of observation. If in a  $10^3$  ton detector there occurs 1 background event/year which is inseparable from a nucleon decay event, then increasing the detector mass by another factor of 10 will yield  $10 \pm 3$  such background events/year and so one claims that at most 3 of these events could have been nucleon decays. Hence, by equation (6) above, the lower lifetime limit is increased only by a factor of 3 by increasing the mass by a factor of 10. The largest detectors being installed or planned expect about 1 inseparable background event/year.

Backgrounds originate from two sources : 1) neutral hadrons ( $n$ ,  $K^0$ ) produced by cosmic ray muons in material (rock) outside of the detector enter the volume of the detector and interact, the muon remaining undetected and 2) neutrinos produced in the earth's atmosphere interact in the detector and can simulate a proton decay. Figure 3 is a sketch of background 1). This background can be reduced to an arbitrarily low level by performing the experiment sufficiently deep beneath the earth's surface and defining a fiducial volume within the physical detector such that the neutral hadron will not penetrate sufficiently far into the detector to enter the fiducial volume. Background 2) can only be removed in the data analysis.

Finally, there will be a loss of data due to the fact that such experiments are performed with either water or iron as the decaying material. A pion resulting from the decay  $n \rightarrow e^+ \pi^-$  can interact in the nucleus containing the original decaying nucleon and the event may then be lost. Figure 4 is the result of a Monte Carlo calculation [4] showing the fraction of events in which the pion emerges from the nucleus without interacting, as a function of pion momentum. The curves are presented for C, O, Fe and Pb. Because of the Fermi motion of a

nucleon within the nucleus, the momentum of a pion resulting from a 2-body nucleon decay will not have a unique momentum but will have the range of momenta shown in Figure 4 (340 - 590 MeV/c). Hence, the average probability of non-interaction of the decay pion in iron is 60 % corresponding to a 40 % data loss. Actually, 40 % represents an over-estimate because those pions that scatter elastically within the nucleus can emerge to produce an event which is topologically consistent with a free nucleon decay. A final point here is that because of the Fermi motion of a nucleon within a nucleus, a 2-body decay will in general not appear as an event in which the decay particles are colinear. Instead, there will be an angle between the pion and electron momentum vectors anywhere in the range  $155^\circ$  to  $180^\circ$ . The principal background which can simulate a two-body decay of the nucleon is an event in the detector corresponding to the reaction  $\nu + p \rightarrow e + \pi^\pm + p$  where the  $e$  and  $\pi$  momentum vectors are nearly colinear (in the range  $155^\circ$  to  $180^\circ$ ). In the largest detectors being planned there will be about 1 such event per year.

#### CLASSIFICATION OF EXPERIMENTS

The experiments in progress or being planned fall into two major categories ; 1) the water Cerenkov method and 2) the iron calorimeter method. In the water Cerenkov method an array of photomultiplier tubes is positioned either on the walls or throughout the volume of a large container filled with water. In the iron calorimeter method crossed planes of proportional or streamer tubes are embedded in a large volume of iron or iron oxide. The most ambitious of the iron calorimeter experiments [13] uses layers of flashtube chambers sandwiched between thin (3 to 4 mm) sheets of iron with Geiger tubes providing the trigger. In Table 1 we compare the most important features of this "fine-grain" experiment with the largest of the water Cerenkov experiments [6].

es and  
nt  
no  
nucleons  
 $10^{30}$   
1 in  
tor can  
ich are  
size of  
in years)  
ear of  
r which  
ass by  
one  
ce, by  
r of 3  
called  
K°)  
nter  
d 2)  
can  
ground  
uffi-  
ithin  
ficien-  
only be  
  
expe-  
A pion  
the  
result  
the  
momentum.  
of a

| Important Properties                                | Water Cerenkov       | Fine grain Calorimeter |
|---|----------------------|------------------------|
| Energy Resolution for mode $p \rightarrow e^+\pi^0$ | comparable (10-20 %) |                        |
| Particle Identification                             |                      | x                      |
| Pattern Recognition                                 |                      | xx                     |
| Direction of Track                                  | xx                   |                        |
| Lower Pion Internal Reinteraction                   | x                    |                        |
| Low Energy Pion Detection                           |                      | x                      |
| Highest Ratio of Fiducial to Total Mass             |                      | x                      |
| Ease of Constructing a Prototype                    |                      | x                      |
| Speed of Construction                               | x                    |                        |
| Ability to Add Mass in Stages (modularity)          |                      | xx                     |
| Experience with Technique                           |                      | x                      |
| Cost per Kiloton of Mass                            | x                    |                        |

Table 1

Comparison of water Cerenkov and fine grain calorimeter techniques. A single x denotes an advantage. A double xx denotes a decided advantage.

### THE EXPERIMENTS

Table 2 is a tabulation of the experiments in progress or being planned. I will comment only on the two experiments which have presented preliminary data and then comment on the large European calorimeter experiment which will be installed in the tunnel of Fréjus.

#### 1. The University of Pennsylvania Experiment

An initial result has been presented by the University of Pennsylvania experiment [5] which is located in the Homestake mine in South Dakota. A sketch of the experiment is shown in Figure 5. Tanks with photomultiplier tubes attached are filled with water and are stacked on either side of the Davis solar neutrino  $\text{CCl}_4$  tank. The fiducial mass of water equals 150 tons. Above and below the Davis  $\text{CCl}_4$  tank are planes of liquid scintillator counters which serve to flag events



being planned.  
 Preliminary data  
 will be ins-  
 Pennsylvania  
 3. A sketch  
 tubes attached  
 lar neutrino  
 ow the Davis  
 lag events

| TYPE                       | COLLABORATION                               | TOTAL MASS                     | DEPTH<br>meters of<br>water equiv. | SPECIAL FEATURES   | STATUS<br>(May, 1981)                               |
|----------------------------|---|--------------------------------|------------------------------------|--|---|
| Water Cerenkov Experiments | University of<br>Pennsylvania<br>[5]        | 150 tons                       | 4400 m<br>Gold Mine                | Observes the delay coincidence<br>between a stopping $\mu$ and its<br>decay $e$ in water Cerenkov tanks  | Data<br>$\tau \geq 10^{30}$ years                   |
|                            | Michigan-Irvine<br>Brookhaven<br>[6]        | 6.8 kilotons                   | 1600 m<br>Salt Mine                | 2048 PM tubes paper the 6 walls<br>of a tank of water  | Excavation complete,<br>installation in<br>progress |
|                            | Harvard Purdue<br>Wisconsin<br>[7]          | 0.8 kiloton                    | 1600 m<br>Mine                     | 704 PM tubes immersed throughout<br>the volume of a large cylindri-<br>cal tank of water   | Installation in<br>progress                         |
|                            | Tokyo<br>[8]                                | 3.4 kilotons                   | 1300 m<br>Mine                     | 20 inch diameter PM tubes used<br>to maximize the fraction of C<br>$\gamma$ 's intercepted   | Funded and under<br>design                          |
| Calorimeter Experiments    | Bombay Osaka<br>Tokyo<br>[9]                | 150 tons                       | 7000 m<br>Gold Mine                | Iron proportional tubes of cross-<br>sectional area $10 \times 10 \text{ cm}^2$ sandwiched<br>between 1/2 inch thick iron plates                                 | Data-three<br>possible events                       |
|                            | Minnesota<br>Argonne<br>[10]                | 30 tons                        | 1500 m<br>Iron Mine                | Proportional tubes embedded in a<br>mixture of cement and iron oxide<br>(taconite) mined in same mine  | Under test  |
|                            | Oxford<br>(with above)                      | 1 kiloton                      | 1500 m<br>Iron Mine                | Drift chambers with glass as active-<br>mass   | Proposed  |
|                            | Milan Turin<br>Frascati CERN<br>[11]        | 150 tons                       | 5000 m<br>Tunnel of<br>Mont Blanc  | 1 cm x 1 cm streamer tubes made of<br>resistive material and read out by<br>external inductive strips  | In fabrication and<br>installation                  |
|                            | Tokyo<br>[12]                               | 300 then 600<br>then 1200 tons | 1000 m<br>Tunnel                   | Flash tubes are made of sealed glass<br>cylinders  | Proposed  |
|                            | Orsay Palaiseau<br>Saclay Wuppertal<br>[13] | 1.5 kilotons                   | 4500 m<br>Tunnel of<br>Fréjus      | Flash tube chambers made of PVC mate-<br>rial, each filament has cross sec-<br>tional area of $5 \times 5 \text{ mm}^2$ . Flash tubes<br>read out electronically | Funded and under<br>design                          |

Table 2

Nucleon lifetime experiments in progress or being planned

in which a stopping  $\mu$  and its subsequent decay into an electron occurring in the water Cerenkov tanks is accompanied by ionizing radiation traversing the liquid scintillator. Such events are not considered as candidates for nucleon decay. The geometric efficiencies of these counters, used as vetos is about 50 %.

During a run of one year, 4 events were observed which contained a deposition of visible energy in the water Cerenkov tanks commensurate with the decay of a nucleon into a final state having a  $\mu^+$  with a subsequent decay into an  $e^+$ , e.g.,

$$\begin{array}{lcl}
 N \rightarrow \mu^+ + X, & p \rightarrow e^+ + \rho^0 & \\
 & + e^+ & + \pi^+ + \pi^- \\
 & & + \mu^+ + e^+, \text{ etc.}
 \end{array}$$

One of the four events was accompanied by a signal in the liquid scintillator veto counters reducing the number of candidates to  $3 \pm 2$ . Since the geometric efficiency of the veto counters is about 50 %, one would expect that an additional event should have been accompanied by a veto signal, or, subtracting a background of  $1 \pm 1$  from the signal of  $3 \pm 2$ , one obtains a corrected signal of  $2 \pm 2$  events. The experimenters conservatively wish to use this number as an upper limit on the number of decays observed. Assuming a product of the branching ratio into final states which can yield a  $\mu^+$  times the detection efficiency of the apparatus equal to 5 %, the experimenters obtain a lower limit on the lifetime, based on two events, equal to

$$\tau \geq 10^{30} \text{ years}$$

## 2. Tata Institute - Osaka University Experiment

An interesting preliminary result has been presented [9] by these experimenters in which 3 events that are difficult to attribute to standard background sources have been observed in their detector. Located in a deep mine in the Kolar Gold Field, the detector consists of crossed planes of proportional tubes, each plane of which is separated from the adjacent planes by a 1/2 inch thickness of iron. The total mass is 150 tons and the fiducial mass is 100 tons. Figure 6 shows the two views of one of these events which is consistent with the decay  $p \rightarrow e^+ \pi^0$  in which one of the  $\gamma$ 's from the  $\pi^0$  takes practically all of the energy of the  $\pi^0$ . As is the case with the other two events not shown here, one of the tracks leaves the detector and so it is not possible to obtain a value for the total visible energy associated with the event. There appear to be gaps along the tracks

cor  
mar  
alo n the  
of liquid  
trc ay. The  
tub  
hun d a depo-  
tor e decay  
Alt an  $e^+$ ,  
pro

corresponding to proportional tubes that did not fire. The proportional tubes marked "X" were not operative and the remainder of the tubes that did not fire along the particle paths correspond to locations along the shower development of either the  $e$  or  $\gamma$  in which there may have been no ionizing radiation (electrons) but just  $\gamma$ 's. Since the cross-sectional area of each of the proportional tubes is  $10 \times 10 \text{ cm}^2$ , and since the maximum transverse dimension of a several hundred MeV electron shower is about 10 cm, an electron or photon in this detector will always appear as a singly-ionizing particle passing through the detector. Although the experimenters claim to have pulse height information on each of the proportional tubes, this information is not available at this time.

if  
ar  
e  
ator veto  
efficiency  
vent  
nd of  
vents.  
t on the  
final  
tus equal  
two

The experimenters have qualified these three events by the caveat that if they are not nucleon decay, then they correspond to background events which are not understood. If these events do indeed correspond to nucleon decay, the experimenters offer the following computation of the nucleon lifetime :

Assume that the product of the branching ratios to which the detector is sensitive times the detection efficiency equals 0.5. Also, assume that the pion absorption by the nucleus is offset by a "life-shortening" factor associated with the nucleon emitting a virtual pion in the nucleus which then scatters from an adjacent nucleon to produce a real pion (or pions). These factors combined give a value for  $A$  in equation (6) above equal to 0.5. With an observation time equal to 131 days, the experimenters obtain a lifetime value

$$\tau = 3.5 \times 10^{30} \text{ years.}$$

3.

### 3. The Orsay - Palaiseau - Saclay - Wuppertal Experiment [13]

th  
re  
di  
f  
a  
re 6 shows  
i  
s  
id  
eks  
eks

These experiments are background experiments. The Kolaras, each of which has a mass of 6 kilotons, shows  $p \rightarrow e^+ \pi^0$  of the  $\pi^0$ . The Kolaras leaves visible tracks.

This experiment is mentioned here because it is the most ambitious of the "second generation" calorimeter experiments and represents a considerable refinement over, for example, the Tata Institute - Osaka University experiment discussed above. The Orsay - Palaiseau - Saclay - Wuppertal experiment is planned for 1.5 kilotons and will be installed beginning in 1982 in the tunnel of Fréjus, a new alpine tunnel connecting Modane, France with Bardonecchia, Italy.

The detector will employ the plastic flashtube chamber technique [14] in which planes of plastic flashtube material, illustrated in Figure 7, are sandwiched between thin (3-4 mm) sheets of iron. The flashtube chamber technique is now well understood. In short, a particle traversing a flashtube will cause a

plasma to form in the noble gas which fills the tube by means of a high voltage pulse applied to the entire flashtube plane immediately after the traversal of the ionizing particle. Each tube will be read out electronically by means of an electrode either external (capacitive coupling) or internal to the tube. The calorimeter trigger will be provided by the use of planes of Geiger tubes (not shown in Figure 7).

Figure 8 shows a Monte Carlo simulation of an event of the type  $p \rightarrow e^+ \pi^0$ . The energy determination for this decay mode will be about 10 %. This detector is particularly well-suited for the study of decay modes having a large number of particles in the final state. This feature becomes important when trying to establish whether a nucleon decays by  $\Delta B = \Delta L$  transitions or by  $\Delta B = 2$  transitions in the nucleus. The latter kind of decay would have the characteristic appearance of a  $\bar{p}p$  annihilation. Perhaps both kinds of transitions take place in nature. In order to relate the experiments which are studying  $n \rightarrow \bar{n}$  oscillations to  $\Delta B = 2$  transitions in the nucleus, a detector of this sort will be very useful.

#### CONCLUSIONS

Both theoretical estimates and preliminary experimental results point towards a nucleon lifetime of perhaps less than  $10^{31}$  years. Next year's 5th Warsaw Symposium should be able to provide a larger number of = signs when quoting the nucleon lifetime and fewer > signs as is the case this year, since several additional experiments will become operational during the present year, 1981.

REFERENCES

- [1] See, for example, T. Goldman and D.A. Ross, Phys. Letters 84B (1979) 208.
- [2] S. Weinberg, talk presented at the 2nd Workshop on Grand Unification, Ann Arbor, 1981.
- [3] J. Learned, F. Reines and A. Soni, Phys. Rev. Letters 43 (1979) 907.
- [4] C. Longuemare, Thèse d'Etat Orsay, LAL, 78/4.
- [5] M. Deakyne et al., Proceedings of the XV Rencontre de Moriond, Vol. II, 545 (1980).  
Also, talk presented at the 2nd Workshop on Grand Unification by R. Steinberg.
- [6] M. Goldhaber et al., Proposal for a Nucleon Decay Detector (Irvine, Michigan, Brookhaven).
- [7] J. Blandino et al., A Decay Mode Independent Search for Baryon Decay Using a Volume Cerenkov Detector (Harvard, Purdue, Wisconsin).
- [8] S. Yamada, Communication to the XV Rencontre de Moriond (1980).
- [9] H.R. Krishnaswamy et al., The Kolar Gold Field Baryon Stability Experiment, Communication to the Erice Conference, 1980. (Tata Institute, Osaka University). Also, talk presented at the 2nd Workshop on Grand Unification, Ann Arbor, 1981, by S. Miyake.
- [10] H. Courant et al., A Dense Detector for Baryon Decay, (University of Minnesota Internal Report).
- [11] G. Battistoni et al., Proposal for an Experiment on Nucleon Stability with a Fine Grain Detector. NUSEX : CERN - Frascati - Milano - Torino.
- [12] University of Tokyo, Communication to the Erice Conference 1980.
- [13] P. Bareyre et al., Proposal to Study the Instability of the Nucleon Using a Calorimeter Detector, (1980).
- [14] M. Conversi et al., Nuclear Instr. Met. 151 (1978) 93,  
L. Federici et al., Nuclear Instr. Met. 151 (1978) 103.

# FIGURE CAPTIONS

Fig. 1 : a) Coupling of a massive boson X to a pair of quarks and to a lepton and antiquark.

b) Proton decay by means of a massive gauge boson X. Numerous processes in addition to the above can be sketched for various decay modes of the nucleon.

Fig. 2 : Plot of achievable lower limit on the nucleon lifetime vs. detector mass. When the limit corresponds to the non-removable background level, further addition to the detector will increase the limit only as the square root of the addition mass.

Fig. 3 : A cosmic ray muon interacts in the rock above the detector, producing a neutral hadron which in turn simulates a nucleon decay event in the detector. The muon remains unobserved. An active shield above the detector can intercept the muon and veto the event.

Fig. 4 : Probability of non-interaction of pions in different nuclei as a function of pion momentum.

Fig. 5 : The Homestake Water Cerenkov Detector. The portion of the detector with a solid outline is in operation. The dashed portion has not yet been installed. Not shown is the  $\text{CCl}_4$  tank at the center of the apparatus used in the solar neutrino experiment.

Fig. 6 : A nucleon decay candidate in the Tata Institute-Osaka University experiment. Proportional tubes marked "X" are not functioning. Track A is seen to leave the top of the detector, making an energy determination of this event impossible.

Fig. 7 : A detail of an element of the Orsay-Palaiseau-Saclay experiment. The flashtube chamber planes are sandwiched between thin sheets of iron. Also shown are the aluminum electrodes on the outside surfaces of a plastic flashtube sheet across which the high voltage pulse is applied.

Fig. 8 : A Monte Carlo simulation of an event of the type  $p \rightarrow e^+ \pi^0$  in the Orsay-Palaiseau-Saclay calorimeter. The total energy of this kind of event can be determined to 10 %.

lepton

processes  
of the

sector  
and level,  
as the

roducing  
in the  
the de-

a func-

vector with  
not been  
tratus

nity expe-  
ck A is  
mination

nt. The  
iron.  
es of a  
s applied.

the  
kind

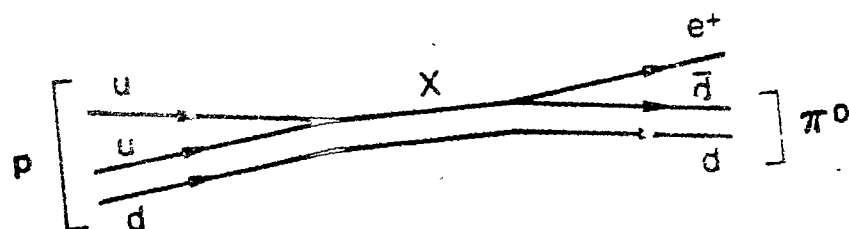
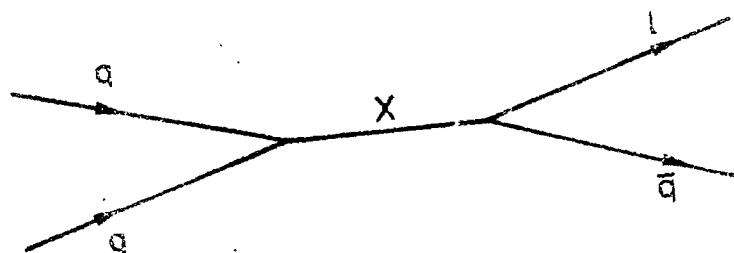
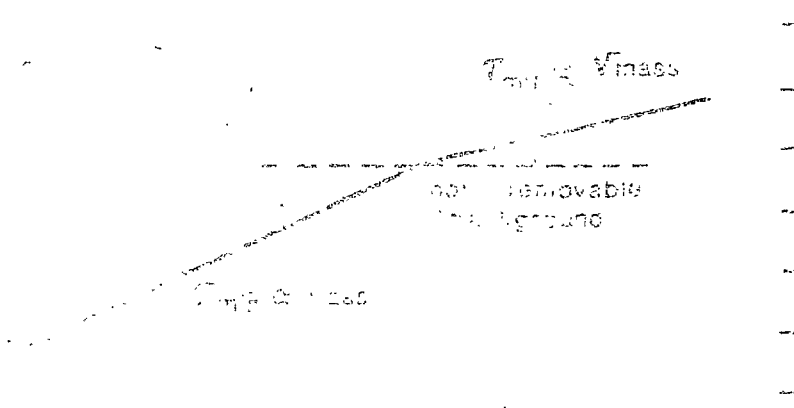


Figure 1

Survey of the Pacific Northwest

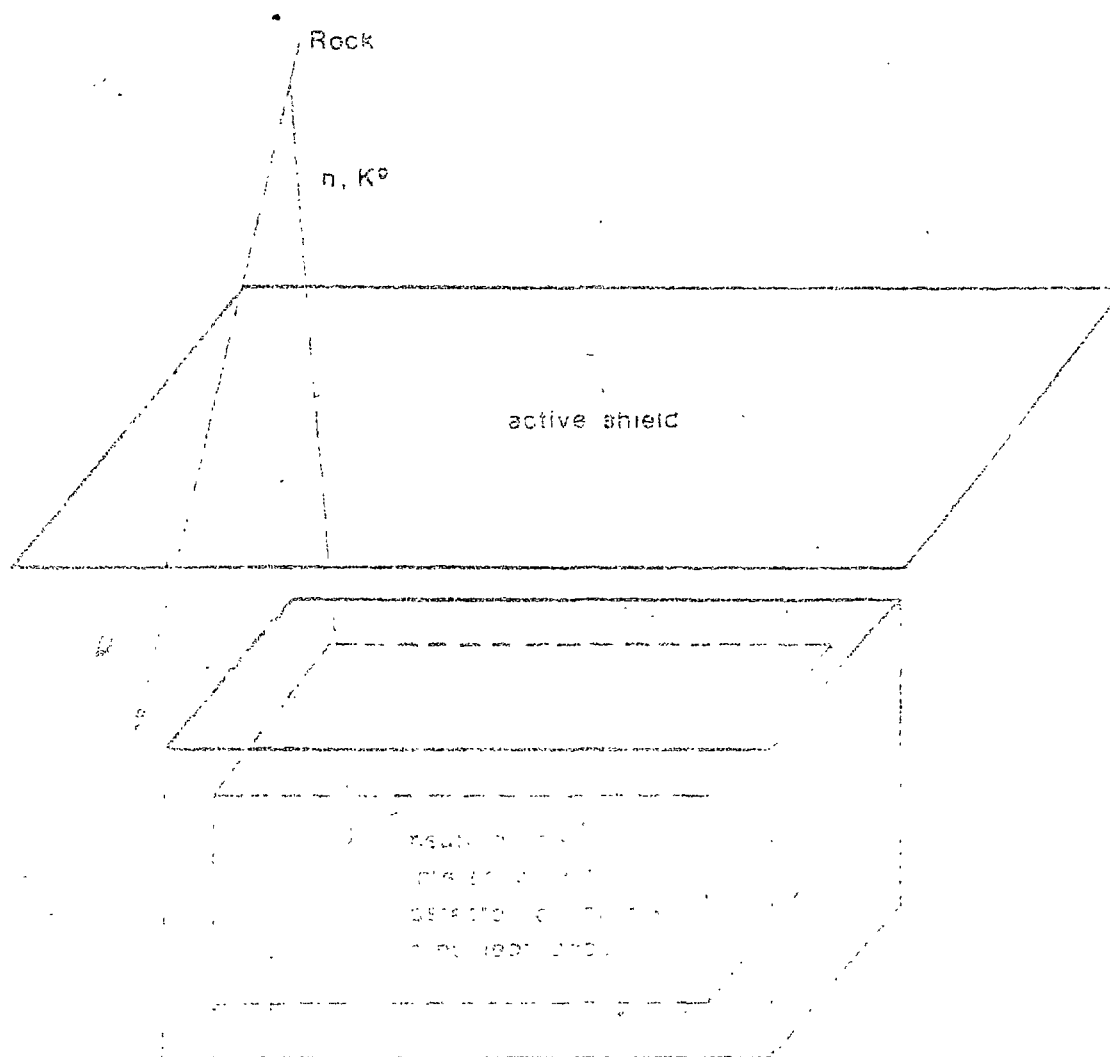
(1907)

1000  
500  
0  
500  
1000



1000





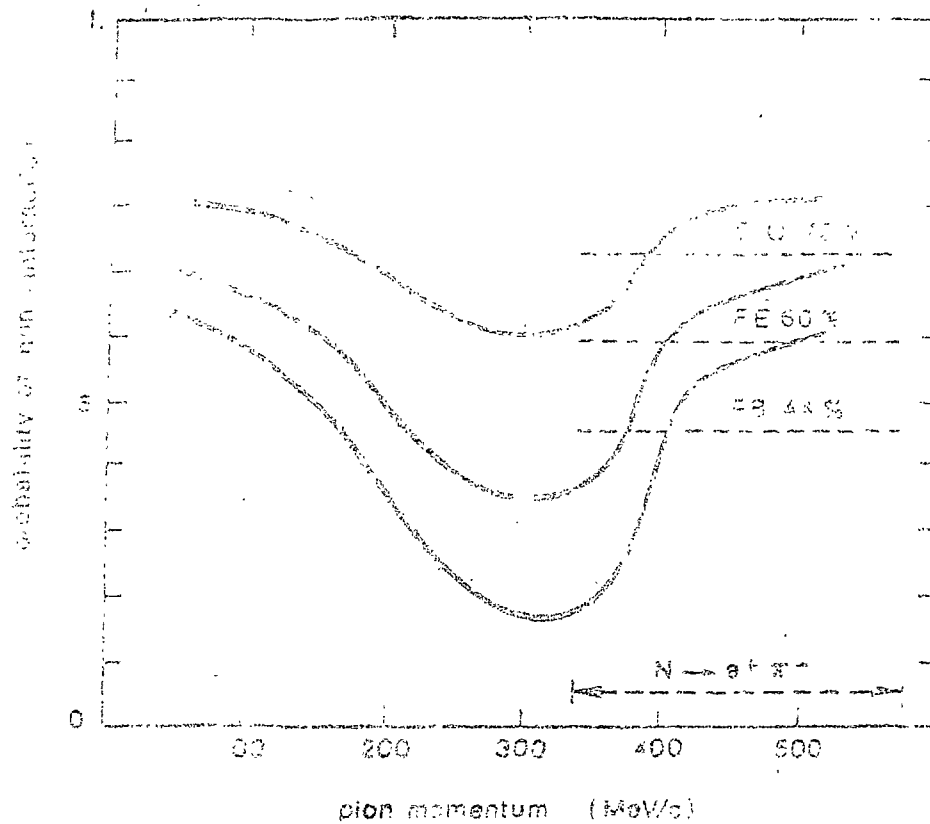
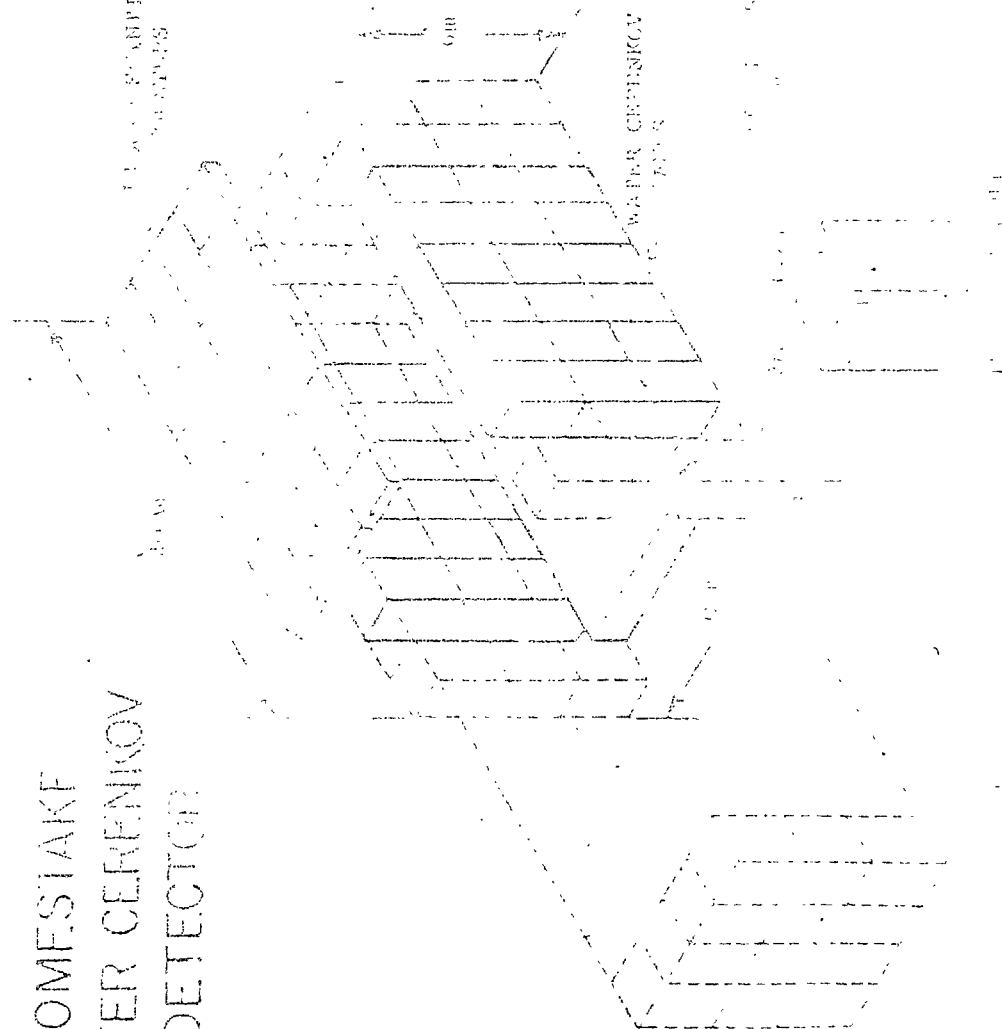


Figure 4

[illegible]

# HOMESTAKE WATER CHERENKOV DETECTOR

$\gamma =$



395

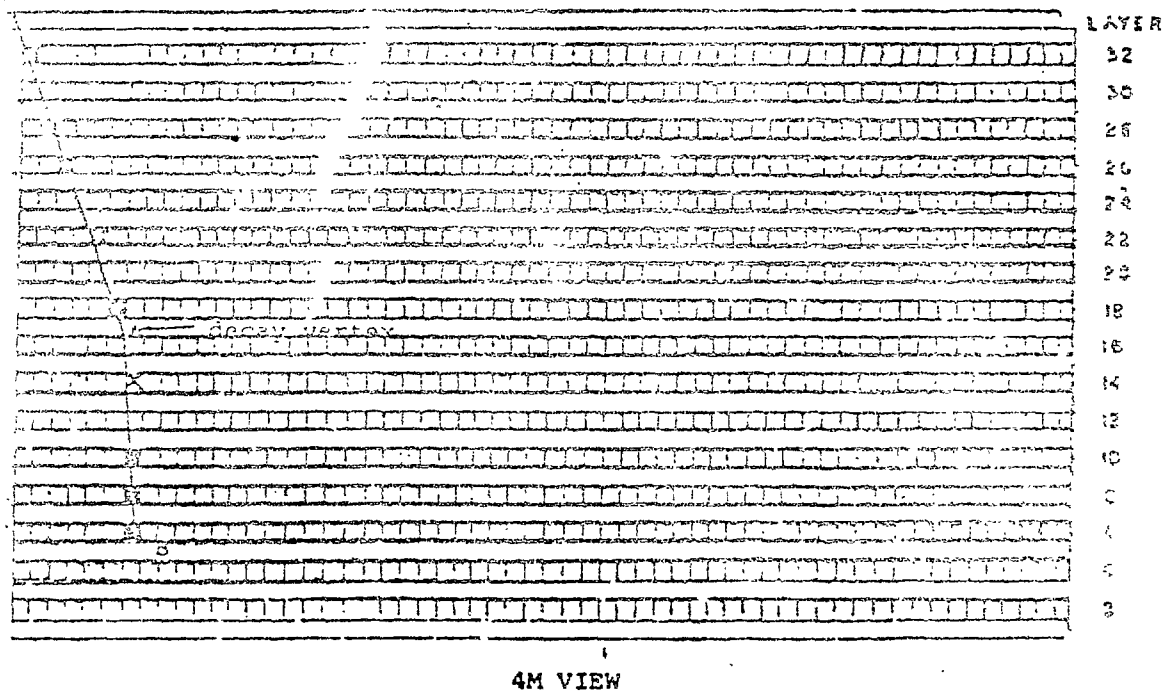
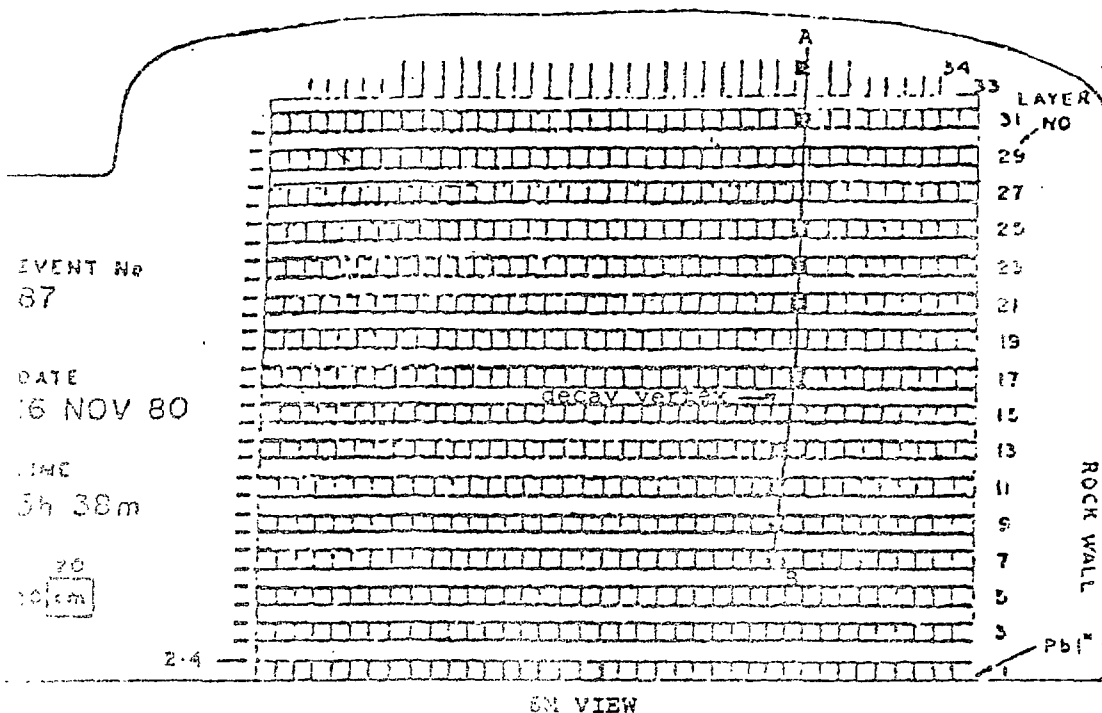


Figure 6

ROCK WALL

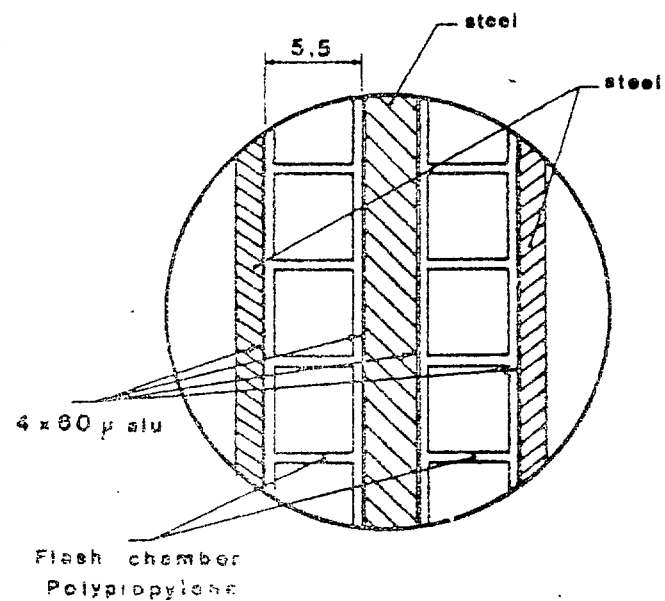


Figure 7

| LAYER |  |
|-------|--|
| 32    |  |
| 30    |  |
| 28    |  |
| 26    |  |
| 24    |  |
| 22    |  |
| 20    |  |
| 18    |  |
| 16    |  |
| 14    |  |
| 12    |  |
| 10    |  |
| 8     |  |
| 6     |  |
| 4     |  |
| 2     |  |

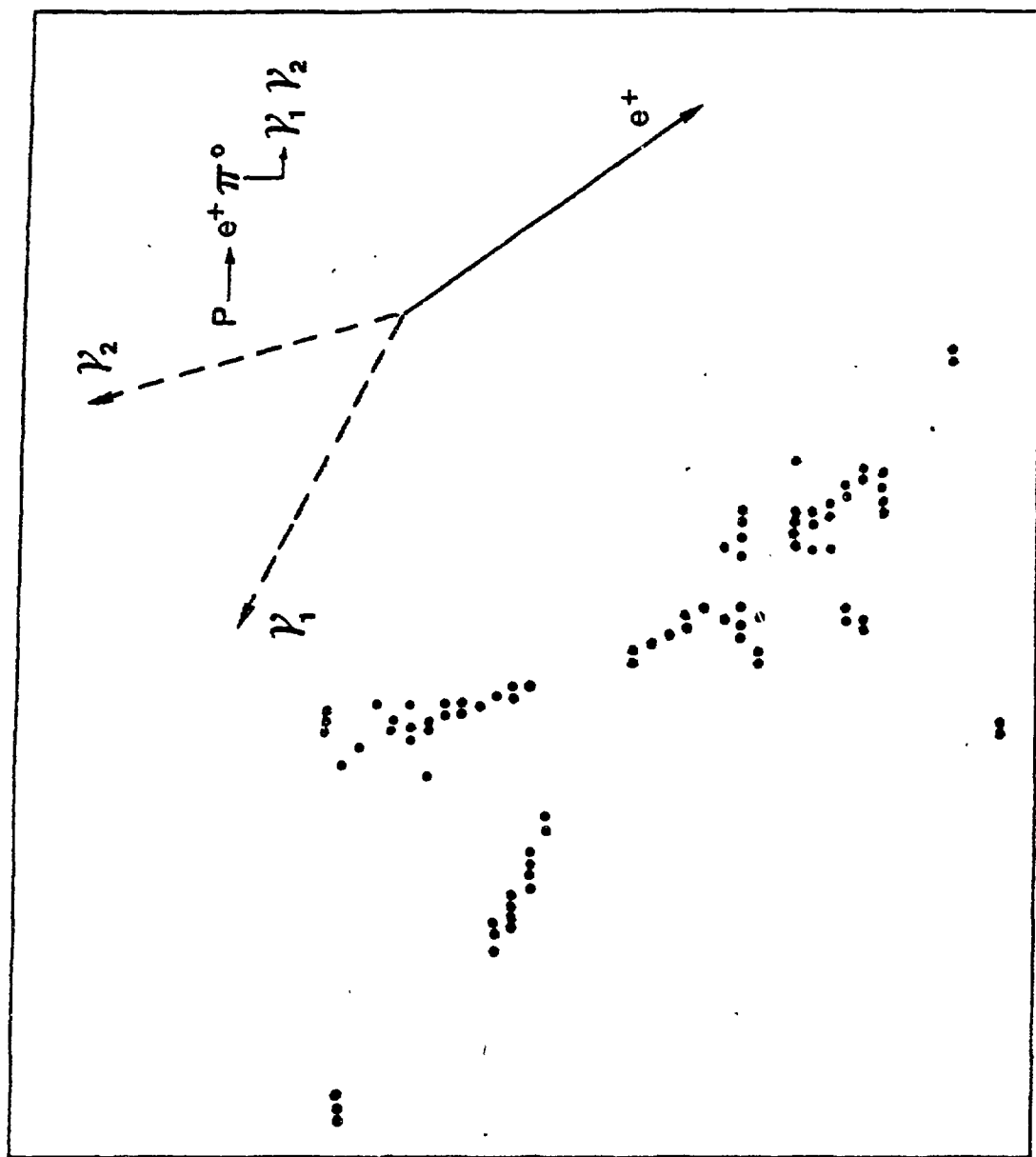


Figure 8

Figure 8

80

# HIGGS FIELDS IN H.A.C. =====

Andrzej Czechowski  
 Institute of Theoretical Physics  
 Warsaw University  
 Warsaw, Poland

The scalar fields, necessary to realize the spontaneous symmetry breaking, tend to destroy the asymptotic freedom property of non-Abelian gauge theories. This is due to the presence of the quartic /4-scalar/ couplings which can become large at small distances and in turn affect the behaviour of the gauge coupling constant.

In some cases, however, the presence of scalars does not prevent the asymptotic freedom. One case of interest comprises the so-called eigenvalue-type solutions (1). Asymptotic freedom is then valid only along a single curve in the space of the coupling constants; it requires that the Yukawa couplings  $h$  and the quartic couplings  $\lambda$  are uniquely related to the gauge coupling constant  $g$ . Asymptotically

$$\lambda = \bar{\lambda} g^2, \quad h = \bar{h} g; \quad \bar{\lambda}, \bar{h} = \text{const}, \quad g \rightarrow 0$$

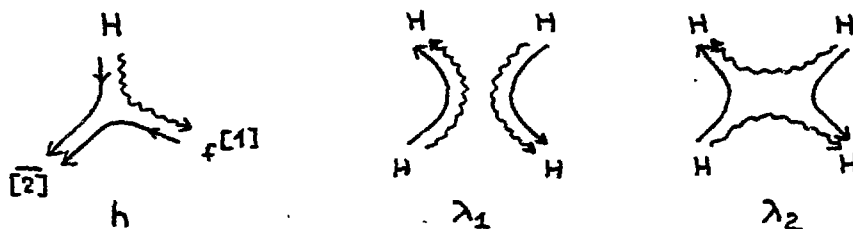
This class of solutions has some attractive features apart from the asymptotic freedom. One is the extra predictive power caused by the fact that  $\lambda$  and  $h$  are not arbitrary. Another is the possible implication of compositeness of the scalar field (2). In fact if the scalar is supposed to be a bound state of the fundamental fermions interacting via the gauge field one should expect that the  $\lambda$  and  $h$  couplings are determined by  $g$ . Note that the eigenvalue-type solutions are possible only provided that there are fermion fields coupled to the scalars in question.



A possible criterion of compositeness of the field  $\phi$  is vanishing of its wavefunction renormalization constant  $Z_\phi(3)$ . This criterion has been applied to the asymptotically free gauge theories in (4); the conclusion was that, in an asymptotically free theory, the scalar field cannot be composite in this sense. It is interesting that the eigenvalue-type solutions can avoid this conclusion. Applying the methods of (4) to the published examples (1) of the asymptotically free eigenvalue-type solutions one finds in fact that the compositeness criterion for the scalars is satisfied in all these examples.

Asymptotic freedom and scalar composites are important ingredients of the "tumbling" mechanism of Raby, Dimopoulos and Jusskind (5). According to this scheme, the scalar bound states responsible for the symmetry breaking appear in the "most attractive channel"/M.A.C./defined as the channel in which the interaction of fundamental fermions is the strongest. There is no obvious connection between the tumbling mechanism and the eigenvalue-type solutions: in fact one can argue that the scalar bound states in the tumbling scheme can be totally disregarded at small distances due to the behaviour of form factors, so that they do not affect the asymptotic freedom. Nevertheless it is of interest to find out whether it is possible to construct the asymptotically free eigenvalue-type solutions with scalar fields in M.A.C. and in particular to check the compositeness criterion for the scalars.

Let the gauge field be  $SU(N)$  and the fermion content involve  $N-4$  left-handed fermions in the fundamental representation  $[1]$ , and one left-handed fermion field in the representation  $[\overline{2}]$ . The most attractive channel is  ${}_f[\overline{1}]$  from  ${}_f[1] \times [\overline{2}]$  where  $f = 1 \dots N-4$  is the "flavour" index. Assume that there is a scalar field  $H$  with these quantum numbers. The resulting model has one Yukawa coupling  $h$  and two quartic couplings  $\lambda_1, \lambda_2$  which differ by their flavour structure. Graphically



where wavy lines carry the flavour.

The /lowest order/ renormalization group equations for the gauge coupling  $g$  and the Yukawa coupling  $h$  are:

$$16\pi^2 \frac{dg}{dt} = - \left( \frac{17}{6}N + \frac{8}{3} \right) g^3 \quad \left( t = \log(\mu/\mu_0) \right)$$

$$16\pi^2 \frac{dh}{dt} = - \frac{3(3N^2 - 2N - 5)}{2N} g^2 h + \frac{5N - 11}{2} h^3$$

Inserting  $h = \bar{h}g$  and assuming  $\bar{h} = \text{const}$  gives

$$\bar{h}^2 = \frac{\frac{3(3N^2 - 2N - 5)}{2N} - \left( \frac{17}{6}N + \frac{8}{3} \right)}{\frac{5N - 11}{2}} \xrightarrow{N \rightarrow \infty} \frac{2}{3}$$

The equations for  $\lambda_1$  and  $\lambda_2$  can be similarly converted into the algebraic equations for  $\bar{\lambda}_1, \bar{\lambda}_2$  /  $\lambda_i = \bar{\lambda}_i g^2$  /. For large  $N$  they take the form

$$N^2 \bar{\lambda}_1^2 + 3 \bar{\lambda}_2^2 + 4N \bar{\lambda}_1 \bar{\lambda}_2 + \frac{7}{3} N \bar{\lambda}_1 - \frac{5}{9} = 0$$

$$2N \bar{\lambda}_2^2 + 6 \bar{\lambda}_1 \bar{\lambda}_2 + \frac{7}{3} N \bar{\lambda}_2 - \frac{5}{9} N = 0$$

A consistent assumption is that  $\bar{\lambda}_1 \rightarrow 0$ ,  $\bar{\lambda}_2 \rightarrow O(1)$  as  $N \rightarrow \infty$ . The resulting solution for large  $N$  is

$$\bar{\lambda}_2 = \frac{-\frac{7}{3} + \sqrt{\frac{89}{9}}}{4} \approx 0.2 \quad \bar{\lambda}_1 \approx \frac{-\frac{9.4}{3}N + \sqrt{\left(\frac{9.4}{3}\right)^2 + 4 \cdot \frac{3.8}{9}} N}{2N^2}$$

There is no solution for small  $N$  /in particular for  $N=5$ /. The obvious conclusion is that the existence of eigenvalue-type solutions is not a general feature of the most attractive channel.

Other results for large  $N$  are: the compositeness criterion is not satisfied; the symmetry breaking pattern is  $SU(N) \rightarrow SU(4)$  due to the  $\lambda_2$  domination at large  $N$ .

We conclude that it is possible to find the eigenvalue-type asymptotically free solutions with fundamental scalars in LAC although this is not always the case. The violation of the  $Z=0$  compositeness criterion must be noted.

ACKNOWLEDGEMENTS: I am grateful to Prof. S. Pokorski for interest in this work and many discussions.

#### REFERENCES:

1. A.S. Pradkin, O.A. Kalashnikov, Phys. Lett. 59B, 159, /75/, 64B, 177, /76/;  
Ngee-Pong Chang, J. Perez Mercader, Phys. Rev. D16, 4721, /76/;
- Ngee-Pong Chang, A. Das, J. Perez Mercader, Phys. Rev. D22, 1429, /80/.
2. Abdus Salam, V. Elias, Phys. Rev. D22, 1469, /80/.
3. D. Lurie, A. J. Macfarlane, Phys. Rev. 136, B616, /64/ and references therein.
4. T. P. Cheng, Ng Ping-Chiu, K. Young, Phys. Rev. D10, 2459, /74/.
5. S. Raby, S. Dimopoulos, L. Susskind, Nucl. Phys. B169, 373, /80/.

$N \rightarrow \infty$ .

$\frac{3.8}{9} N$

PERTURBATIVE QCD BEYOND "CLASSICAL" PROBLEMS

J. Kalinowski<sup>\*</sup>, A. Para and S. Pokorski<sup>\*</sup>

Department of Physics, Warsaw University, Poland

Abstract:

We review two topics: ~~the~~ present status and prospects in studying gluon properties, ~~the~~ <sup>and</sup> event structure in the hadronic final states.

(continued)

Presented by J. Kalinowski

---

<sup>\*</sup> Supported in part by U.S.-Poland Joint Board Grant JF 7F053P.

### Introduction

The list of reactions in which hard processes are studied by now experimentally and theoretically is quite impressive:

|  |                                    |  |
|--|------------------------------------|--|
| $e^+e^- \rightarrow X$                 | $lN \rightarrow l'$                | $hh \rightarrow \mu^+\mu^-$            |
| $e^+e^- \rightarrow \text{jets}$       | $lN \rightarrow l'h$               | $hh \rightarrow \text{large } p_\perp$ |
| onia decays.                           | $lN \rightarrow l'\text{jets}$     | $hh \rightarrow \gamma$                |
| $\gamma\gamma \rightarrow X$           | $\gamma p \rightarrow \gamma$      | $hh \rightarrow \gamma\gamma$          |
| $\gamma\gamma \rightarrow \text{jets}$ | $\gamma p \rightarrow \text{jets}$ | } large $p_\perp$                      |

cts in  
hadronic

Usually, for each process a number of physical questions is considered. In general, quantum chromodynamics /applied with an implicit parton model like assumption/ makes many distinct, non-trivial predictions. A guide to them, on a qualitative level at least, is provided by the first order/leading logarithm approximation and in many cases striking support from experiment has been found. Recent developments are mainly characterized by an attempt to control higher order corrections.

Such problems as

a/ next to leading order corrections

b/ renormalization scheme dependence

c/ power corrections

have been vigorously studied and reviewed [1], with particular emphasize on the deep inelastic lh scattering and the  $e^+e^-$  annihilation into hadrons. We shall not discuss again those points here.

We review problems study of which is less advanced than those "classical" ones, mainly because they are more complex. We shall discuss

1/ gluon physics

2/ event structure in the hadronic final states.

These problems are of basic interest and importance for QCD.

The problems we review have been studied in the leading order QCD. Higher order corrections are not known systematically if at all. It is the next important step to complete their calculation for all processes accessible experimentally. Actually some work along those lines is in progress [2]. Nevertheless since several striking qualitative effects are expected it is worthwhile to look for them at the forthcoming generation of accelerators.

In view of the  $p\bar{p}$  collider starting to operate soon the hadronic collisions will be discussed on equal footing with the lepton initiated processes.

### 1. Gluons

There is increasing evidence for the existence of quanta which mediate the interaction between quarks. The most direct hints are the following:

- a/  $\frac{1}{2}$  of the proton momentum is carried by neutral partons
- b/ 3-jet events have been observed in the  $e^+e^-$  annihilation into hadrons with the cross section compatible with the QCD expectations.
- c/ 3-jet structure is seen in the deep inelastic lepton-hadron scattering.
- d/ the structure of the final state in the  $\Upsilon$  decay resembles a 3-jet structure.

Two properties of gluons are of the basic importance for the theory of strong interactions: their spin and the existence of their self-coupling. There is at present some evidence for gluons having spin 1 and it will be reviewed in the following.

The QCD.  
 tant ding  
 indi atical-  
 decr their  
 rime Actual-  
 and rtheless  
 conc it is  
 of t n of  
 prop  
 hadro-  
 Spin the lep-  
 As t  
 red  
 glu  
 to quanta  
 perc direct  
 wit  
 show ns  
 weec tion  
 Eli: QCD  
 Fave  
 Per i-hadron  
 Fun  
 ana assembles  
 sta  
 pro ce for the  
 ore tence of  
 Cor for  
 vi allowing.

The question of the gluon self-coupling, perhaps the most important one for QCD, is not yet established experimentally. An indirect indication for its existence would be a logarithmic decrease of the effective  $\alpha_s$  with  $Q^2$  when established experimentally. Present data for the deep inelastic le scattering and the  $e^+e^-$  annihilation into hadrons do not lead to any firm conclusion in that respect. Observation of more direct effects of the gluon self-coupling is also possible in principle and proposals and prospects for that will be summarized.

Spin of gluons. Gluon being a gauge boson should have spin 1. As free gluons cannot be observed - their spin has to be measured indirectly. If the three-jet events are indeed due to hard gluon bremsstrahlung - their angular distribution is sensitive to the spin of the emitted object. Such an analysis has been performed by several groups at PETRA [3,5,6,7], all consistent with the vector rather than scalar gluons. As an example Fig. 1 shows the distribution of the Ellis-harliner [4] angle  $\tilde{\theta}$  between the direction of the most energetic jet and the line of flight of the remaining two jets in their C.M.S, which clearly favours spin 1 gluon. Another simple test is provided by the Perkins log-log plot of moments of the non-singlet structure functions measured in the deep inelastic scattering. Recent analysis [8] of the CDHS data excludes scalar gluons by several standard deviations /Fig. 2/. Johnson and Wu-ki Tung [9] have proposed still another test, which can be performed in the Drell-Yan process at high  $p_\perp$ . That test remains to be performed but it seems that already now there is good experimental evidence for gluons having spin 1.

Direct triple gluon vertex effects. Gluon self-coupling should reveal itself in the gluon momentum distribution function in hadrons /called also the gluon structure function in the following/<sup>in</sup> and the gluon fragmentation function, due to the process of Fig. 3b. Qualitatively /and on the LL level/, one expects



Fig. 3

marked difference between the  $Q^2$  evolution of the gluon and the quark /Fig. 3a/ structure and fragmentation functions due to different group factors at respective vertices  $/C_F = \frac{4}{3}$  versus  $C_G = 3/$ . As a result gluons dissipate their energy much more efficiently than quarks and at large  $Q^2$  both discussed functions should be softer for gluons than for quarks. Higher order corrections usually tend to diminish /to an extent depending on the kinematical range studied/ the strong difference between quark and gluon behaviour found on the LL level. A possible contribution of the higher order corrections does not change the fact that a satisfactory test of the theory means observing strong qualitative effect.

The gluon structure function can be inferred from the  $Q^2$  dependence of the singlet structure function  $F_2(x, Q^2)$  via the Altarelli-Parisi equation:

$$\frac{\partial}{\partial \ln Q^2} F_2 = \frac{\alpha_s}{\pi} [F_2 \otimes P_{qq} + G \otimes P_{gq}] \quad (1)$$



Gluons are responsible for the difference between the observed scaling violation and the contribution of the gluon bremsstrahlung to it /Fig.4/. Recent analysis of the CDHS data [10] shows that

$$x G(x, Q^2 = 5 \text{ GeV}^2) \sim (1-x)^{5.9 \pm 1.5} (1 + (3.5 \pm 1)x).$$

In that analysis the second order QCD corrections and target mass corrections are included. The existing data do not yet allow to get the  $Q^2$  dependence of the gluon density distribution to compare it with the quark one.

The gluon structure functions can be also studied in the hadronic collisions. A clean reaction is  $pp \rightarrow \gamma X$  with large  $p_{\perp}$  photons. The expected dominant dynamics is shown in Fig.5a. /contribution of process /5b/ is small and can be neglected in the first approximation [11]. A comparison of the direct photon



Fig. 5

production in  $pp$  and  $p\bar{p}$  collisions can give us the difference between the quark and the gluon structure functions. In the  $p\bar{p}$  case both processes of Fig.5 contribute but they populate different regions in phase space, so they can be studied separately.

Experimentally, a systematic progress in studying that reaction is observed [12] .

Another interesting process which draws recently some attention [13,14] is  $pp(\bar{p}) \rightarrow \gamma\gamma$  , where two  $\gamma$ 's are the only particles with large  $p_t$ . The Born contribution is that of Fig. 6a. However it has been argued [14]

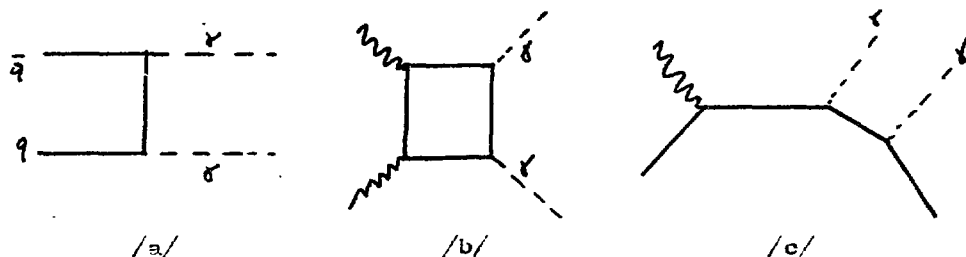


Fig. 6

that the higher order diagram of Fig. 6b may be as important as that of Fig. 6a /at least in some regions of phase space/ because of the large number of gluons in the proton. Notice that diagrams such as one in Fig. 6c do not contribute to the reaction considered since they give large  $p_t$  hadrons in addition to two large  $p_t$   $\gamma$ 's . Experimental study of the two prompt  $\gamma$  production has not been started yet.

Fragmentation function /gluon jets/. The cleanest reactions for studying gluon jets would be heavy onia decays. Unfortunately, for that we need toponium, which may be seen only at LEP. Gluon jets can be also studied in principle in the  $e^+e^- \rightarrow$  jets and in the  $lh \rightarrow$  jets. Here we encounter, however, identification and statistics problems and the prospects are not good, either; /some effort in this direction is reported in ref. [15,16,17]/. We believe, in the nearest future, the important source of information about gluons will be hadronic collisions. Their high com-

plexity is balanced by the presence of gluons in the initial state.

Let us consider

$$a/ p\bar{p} \rightarrow \gamma \quad b/ p\bar{p} \rightarrow \text{large } p_{\perp} \text{ lepton pair}$$

$$c/ p p(\bar{p}) \rightarrow \text{large } p_{\perp} \text{ jets /hadrons/} \quad d/ \gamma p(\bar{p}) \rightarrow 2 \text{ large } p_{\perp} \text{ jets}$$

with respective dominant subprocesses /neglecting sea contribution/

$$\begin{aligned} a/ & g\bar{q}(q) \rightarrow \gamma\bar{q}(q) & \text{and} & \quad q\bar{q} \rightarrow \gamma g \\ b/ & g\bar{q}(q) \rightarrow \gamma^* \bar{q}(q) & \text{and} & \quad q\bar{q} \rightarrow \gamma^* g \\ c/ & q q(\bar{q}) \rightarrow 2 \text{ partons and} & & g q(\bar{q}) \rightarrow 2 \text{ partons and} \\ & g g \rightarrow 2 \text{ partons} & & \end{aligned}$$

/final state partons are dominantly the same as the initial ones/.

$$d/ \gamma q(\bar{q}) \rightarrow g q(\bar{q}).$$

The complication for the gluon jet study in those reactions is that both quark and gluon jets are present. However situation is not hopeless because the difference between the quark and the gluon structure functions often allows to disentangle different subprocesses. For example for large  $p_{\perp}$  hadron production there are two interesting experimental situations:

$$a/ \text{"jet" trigger at large } \sim 90^\circ \text{ angles [18] ;}$$

$$b/ \text{large } p_{\perp} \text{ single particle trigger at small } \sim 45^\circ \text{ angles [19].}$$

In the first case one expects very good separation of gluon and quark jets as a function of  $(x_1)_{\text{jet}}$ . A single particle trigger at  $\sim 90^\circ$  is less useful because it selects mostly quark jets.

The situation is different at small angles. /Similar considerations apply also to reactions /a/ and /b//. Consider two configurations of Fig. 7 /seen in the  $pp(\bar{p})$  center of mass/.

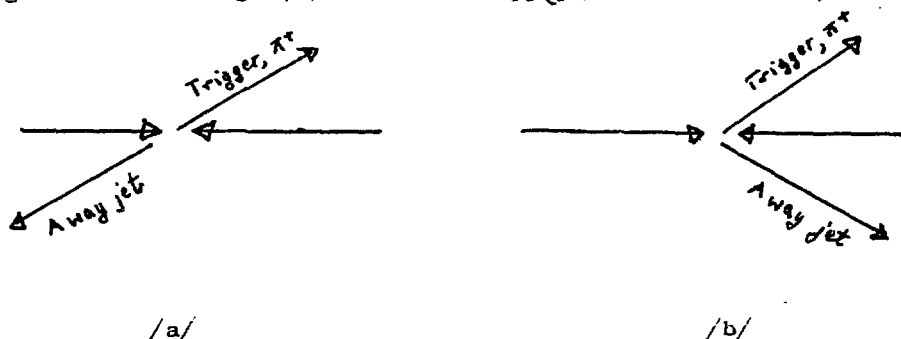


Fig. 7

At sufficiently large  $p_{\perp}$ , only  $qq(\bar{q})$  scattering contributes in case a/ and  $gq(\bar{q})$  scattering in case b/ / $gg$  scattering is very strongly suppressed in both cases/. The difference between  $qq$  and  $gq$  scattering stems from the fact that the initial momentum distributions are on average symmetric and strongly asymmetric, respectively. In conclusion, one expects away jets to be mainly quark jets in configuration 7a and gluon jets in case 7b. Some evidence for two different types of jets in configuration a/ and b/, studied at the ISR, has been reported at this conference [20].

## 2. Event structure

We shall discuss now some of the "infrared sensitive" processes in which one "counts" soft gluons. The first example is provided by the average multiplicity of  $q\bar{q}$  pairs /with an invariant mass  $M^2$ / in the  $e^+e^-$  annihilation into hadrons. The asym-

ptotic result /in the leading double logarithm approximation/  
reads [21] :

$$\bar{n}(Q^2) = f\left(\ln \frac{M^2}{\Lambda^2}\right) e^{\sqrt{a \ln \frac{Q^2}{\Lambda^2}}} \quad \begin{aligned} a &= 4C_G/b \\ b &= \frac{33-2N_F}{12} \end{aligned} \quad (2)$$

The  $M^2$  dependence factorizes out and the  $Q^2$  dependence is faster than any power of  $\log$  and slower than any power of  $Q^2$ . The infrared cut-off  $\Lambda$  can be interpreted either as a mass of a heavy quark /then the prediction is for the heavy flavour production in  $e^+e^-$  only/ or as an inverse of the confinement region size /for the hadron production in general/. Due to the factorization mentioned the actual value of  $M^2$  is irrelevant for the  $Q^2$  dependence of the average multiplicity. The data for the charged hadron multiplicity in the  $e^+e^-$  annihilation [22] are well described by (2), but a fit  $A+B \ln Q^2 + C \ln^2 Q^2$  is equally good. Faster than logarithmic multiplicity rise is related to the stronger than  $\frac{1}{x}$  singularity at  $x=0$ . So violation of the Feynman scaling for the  $d\bar{N}/dy$  distribution is predicted from QCD.

Non-leading corrections to (2) are of interest. Jet calculus technique, recently extended [23] beyond the leading log approximation can be used to calculate those corrections.

Jet calculus and Monte-Carlo approach can be also used to study the event structure in more detail. In particular, the dispersion of the multiplicity distribution can be calculated. Compilation of the recent data for the  $e^+e^-$  annihilation is shown in Fig. 8. The linear /Wróblewski's/ law is observed:  $D = 0.35 \bar{n}$ , whereas the QCD result /Monte Carlo approach [24]/ is  $D=0.31 \bar{n}$ . It is also interesting to notice that the empirical law is universal for the hadron production in the  $e^+e^-$

annihilation,  $\nu p$  deep inelastic and  $p\bar{p}$  annihilation /Fig. 8/. Data for  $pp$  total inelastic exhibit also the linear  $D$  versus  $\bar{n}$  dependence but with different slope. However the empirical universality is restored, if the diffractive component is subtracted from  $pp$  data [25], Fig. 9. This is suggestive of a universal dynamics for the formation of the final state, within the underlying perturbative QCD framework [26]. Such speculations can be tested at the  $p\bar{p}$  collider.

The perturbative QCD predictions are, strictly speaking, for the partonic final state. Their extension to the hadronic final states is based on the assumption that they are unaltered by the non-perturbative hadronization process. This is indeed the case for the two approaches to the hadronization process proposed so far [27,28].

#### Summary

There is some, but slow, progress in studying gluon properties. In particular the existence of the gluon self-coupling is far from being settled. On the theoretical side, the calculations of the next to leading corrections have to be completed for all reactions accessible experimentally. And independently, an experimental search for clear qualitative effects is of great importance. One may hope that  $p\bar{p}$  collider at Cern will offer new possibilities in this respect.

QCD makes several predictions for the structure of the final states. They are qualitatively different from those based on the Feynman /scaling/ picture and therefore interesting. Existing data give them some support but higher energies are necessary for clear tests.

# References

1. A. Buras, Proc.XX Int.Conference on High Energy Physics, Madison, 1980
- C.H. Llewellyn-Smith, XX Int.Conference on High Energy Physics, Madison, 1980.
- P. Söding, G. Wolf, DESY Report 81-013
- R. Petronzio, Cern preprint TH 3085, 1981
- R.K. Ellis, Cern preprint TH 3090, 1981
2. W. Furmański and R. Petronzio, Cern preprint TH 3047 /1981/
- R.K. Ellis in ref. [1].
- W. Furmański, Jagellonian University preprint IPJU-12/81
- J. Gunion, J. Kalinowski and T. Taylor, to be published.
3. R. Brandelik et al., Phys.Lett 97B, 453 /1980/
4. J. Ellis and I. Karliner, Nucl.Phys. B148, 141 /1979/
5. Ch. Berger et al., Phys.Lett. 97B, 459 /1980/
6. Ch. Berger et al. DESY Report 80-78
7. B. Niczyporuk et al. DESY Report 81-006
8. CMS
9. P.W.Johnson, Wu-ki Tung, Fermilab-Pub-80/50 THY
10. F.Eisele, these Proceedings
11. S. Petrarca and F. Rapuano, Physics Letters 88B, 167 /1979/
12. M. Jacob, Direct photon production, ISR Discussion Meeting, Series 2, Number 1 /1980/
13. M. Lrawczyk, W. Ochs, Phys.Lett. 79B, 119 /1978/
14. C. Carimolo, M. Crozon, P. Kessler, J. Parisi, Phys.Lett. 98B, 105 /1981/
15. R. Brandelik et al., Phys.Lett. 86B, 243 /1979/; 94B, 437 /1980/
16. W. Bartel et al., Phys.Lett. 91B, 142 /1980/

17. W. Bartel et al., DESY Report 81-009  
S. Yamada, Proc. XX Int. Conf. on High Energy Physics,  
Madison, 1980
18. W. Furmański and S. Pokorski, Nuclear Physics B165, 365 /1980/
19. S. Pokorski and R. Sosnowski, Z. Physik C7, 221 /1981/
20. W. Geist, these Proceedings
21. W. Furmański, R. Petronzio and S. Pokorski, Nucl. Phys. B155  
253 /1979/  
A. Dassetto, M. Ciafaloni and G. Marchesini, Nucl. Phys.  
B163, 477 /1980/  
N. Konishi, Rutheford preprint RL-796035 /1979/
22. Ch. Berger et al., Phys. Letters 95B, 313/1980/
23. J. Kalinowski, K. Konishi and T.R. Taylor, Nucl. Phys. B181,  
221 /1981/  
J. Kalinowski, K. Konishi, P.N. Scharbach and T.R. Taylor,  
Nucl. Phys. B 181, 253 /1981/
24. S. Wolfram, Parton and hadron Production in  $e^+e^-$  annihilation.  
preprint, Caltech 68-778 /1980/
25. S. Pokorski, **Clustering in hadron** like and quark like jets,  
preprint, Warsaw IFT/3/77, 1977  
A.K. Wróblewski, to be published
26. S. Pokorski and S. Wolfram, QCD expectations for high  
energy hadronic collisions, preprint, Caltech 68-795 /1980/
27. R.D. Field and R.P. Feynman, Nucl. Phys. B136, 1 /1978/  
B. Andersson, G. Gustafson and T. Sjöstrand, Phys. Lett 94B,  
211 /1980/
28. D. Amati and G. Veneziano, Phys. Letters 33B, 87 /1979/  
G. Fox and S. Wolfram, Nucl. Phys. B168, 285 /1980/.



Figure Caption

- Fig.1. Ellis-harliner test for the gluon spin.
- Fig. 2. Log-Log plot of moments of the non-singlet structure function /CDHS data [8] / compared with theoretical predictions for vector and scalar gluons.
- Fig.3. See the text.
- Fig.4. Separate contribution of the two terms present in the Altarelli-Parisi equation (1) to the observed scaling violation in the singlet structure function.
- Fig.5. See the text.
- Fig.6. See the text.
- Fig.7. See the text.
- Fig.8. Data for the dispersion of the multiplicity distribution versus the average multiplicity for the  $e^+e^-$  annihilation into hadrons,  $\nu p$  deep inelastic and  $p\bar{p}$  annihilation. Linear fit to the  $pp$  data also shown.
- Fig.9. Dispersion of the multiplicity distribution versus the average multiplicity. "Data" points have been obtained by subtracting the diffractive contribution from the total  $pp$  and  $\pi p$  inelastic scattering [25]. Comparison with a fit to  $e^+e^-$ ,  $\nu p$  and  $pp$  data suggests universal  $D(\bar{n})$  dependence.

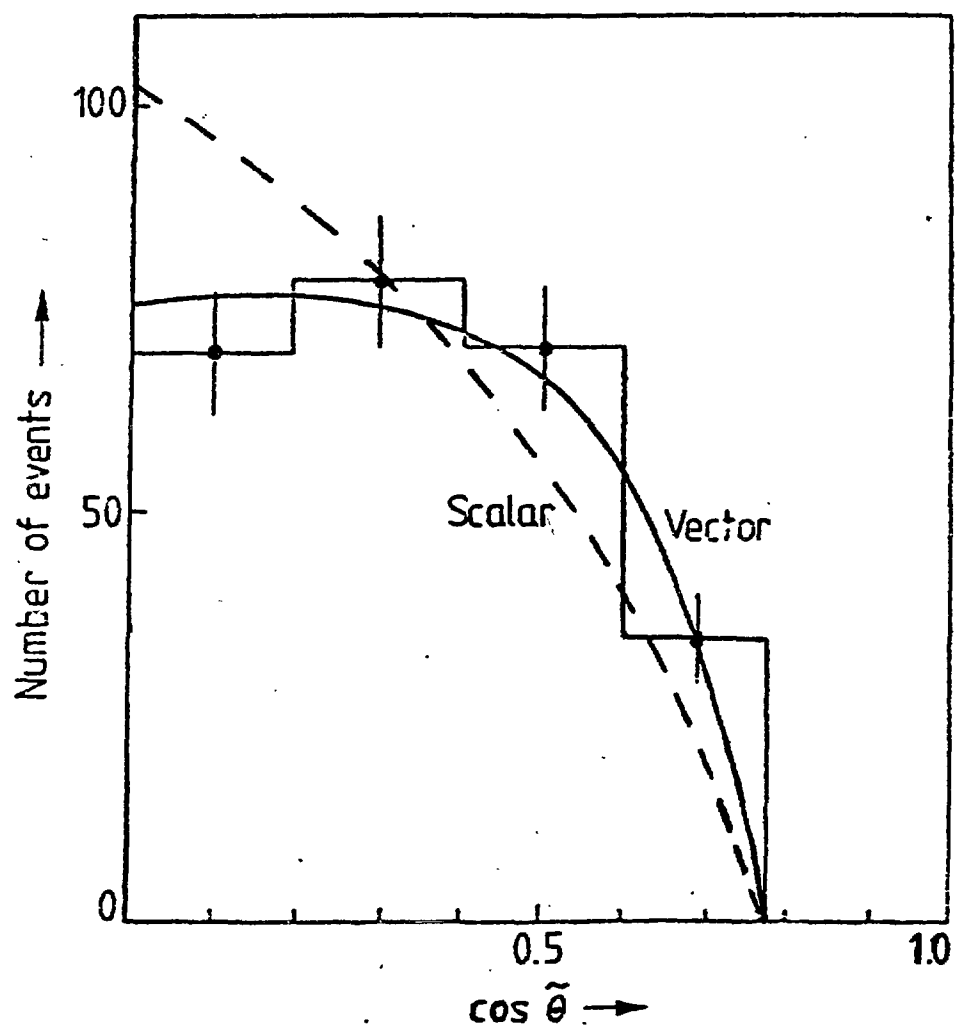


FIG. 1

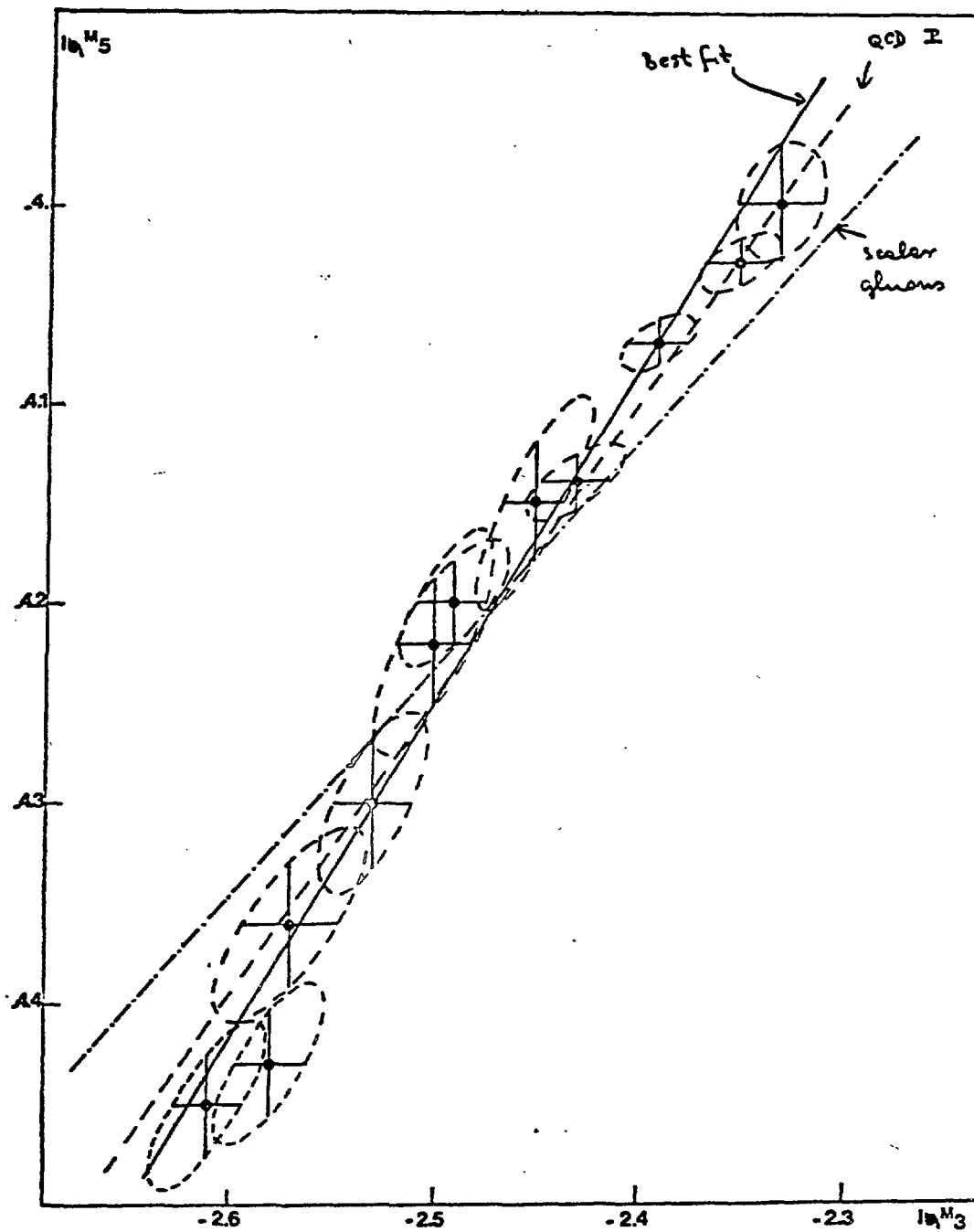


FIG. 2

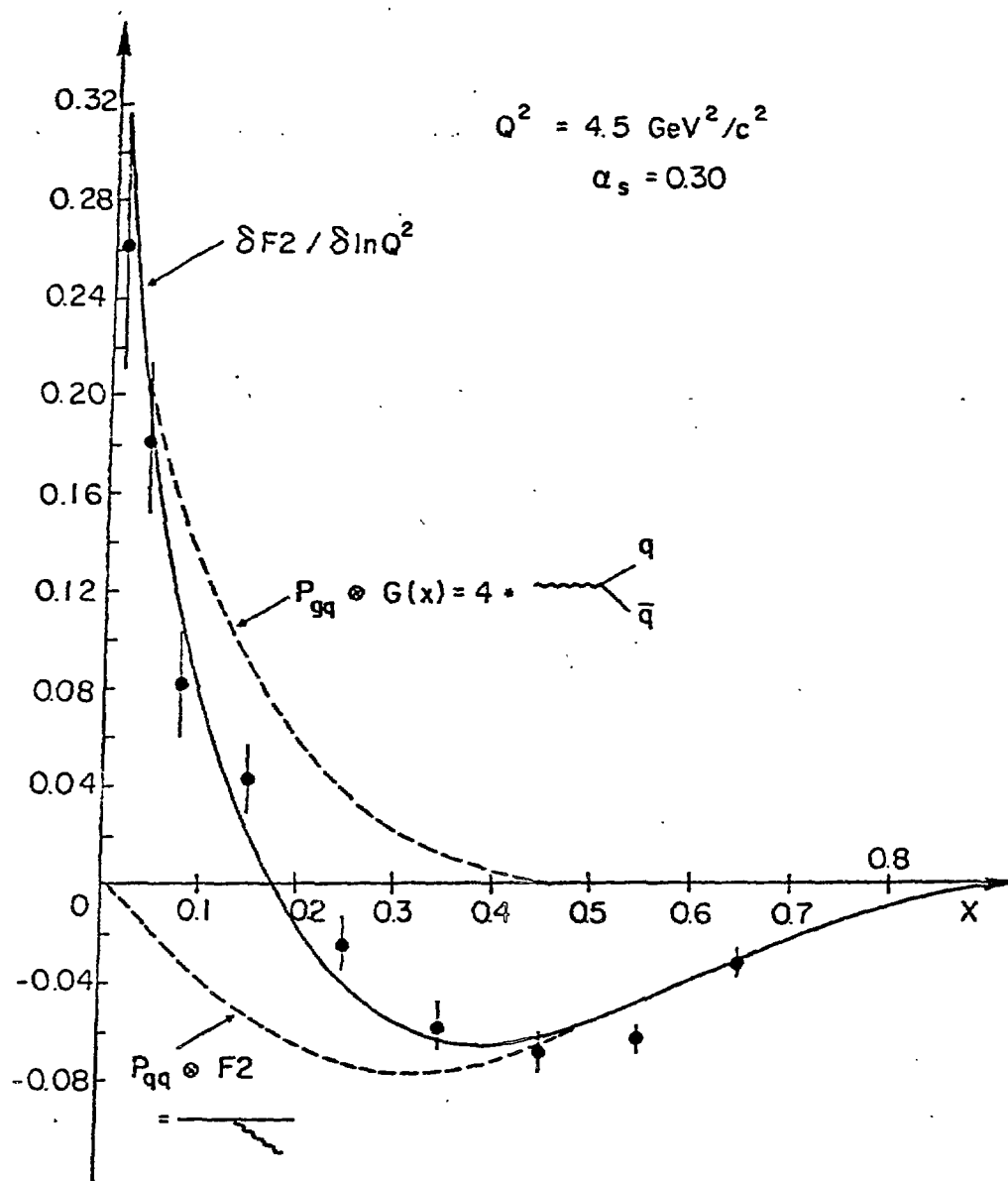


FIG. 4

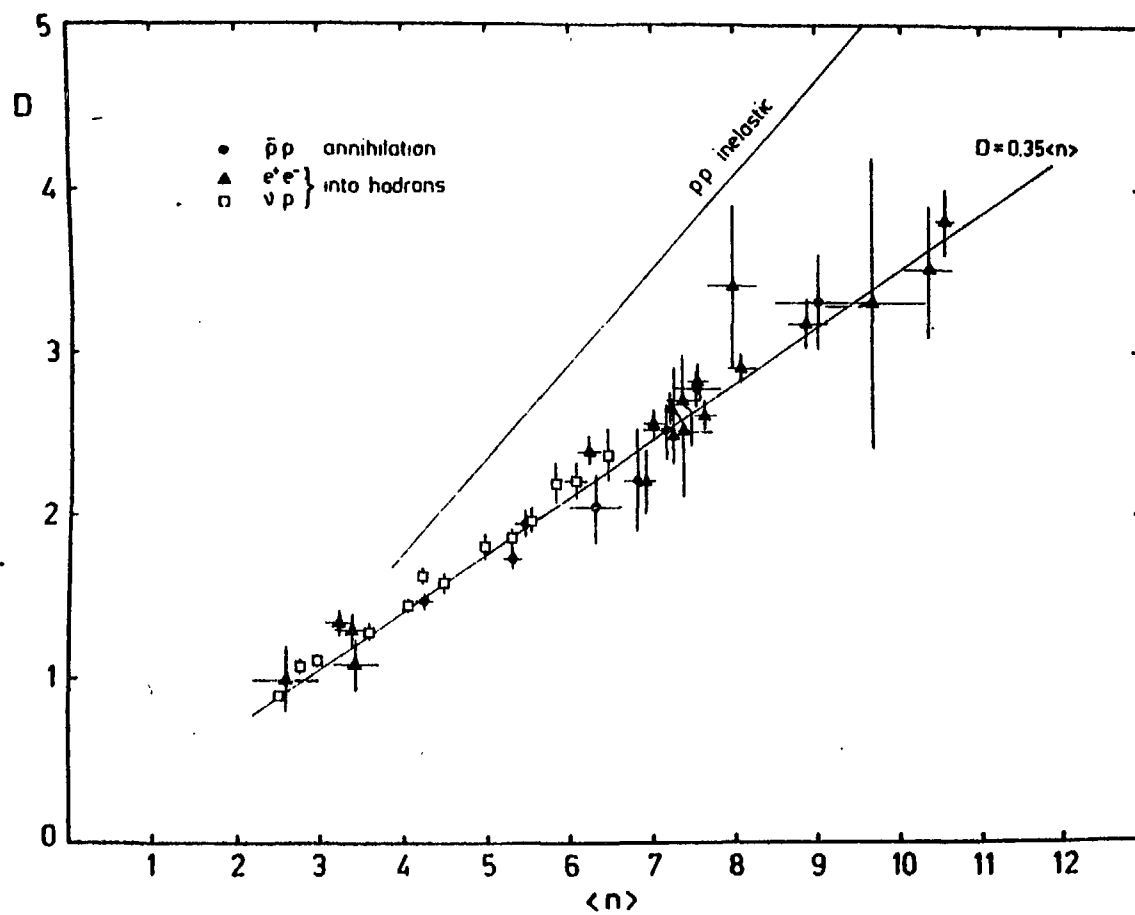


FIG. 8

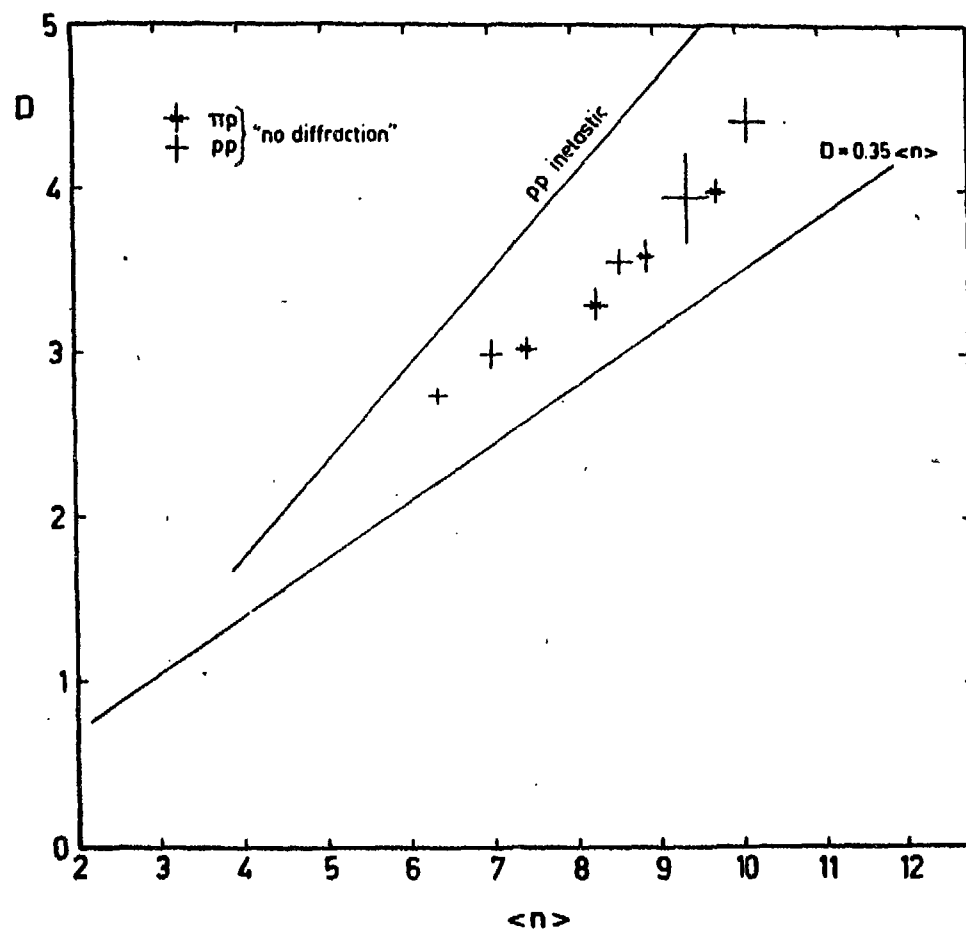


FIG. 9



PHYSICS AT THE  $p\bar{p}$  COLLIDERB. Humpert<sup>\*</sup>

CERN, Geneva, Switzerland

(Presented by J. Strauss)

ABSTRACT

The  $p\bar{p}$  collider at the CERN-SPS will soon be ready for experimentation up to 540 GeV center-of-mass energy. Aiming at an evaluation of the physics in this new energy range we assemble significant results from present accelerators and from cosmic-ray analyses together with the theoretical interpretations. Their extrapolation to collider energies leads to a wealth of predictions which await to be tested. (author)

---

\*also at : Swiss Federal Institute of Technology,  
Laboratory of High Energy Physics  
CH-5234 VILLIGEN

## 1. Introduction

The pro  
operationa  
540 GeV ce  
detector s  
physics to  
of inform  
of results  
and elect

Clarifi  
possibili  
inclusive  
will test  
glueballs  
several  
their pre  
The rise  
elastic  
diffracti  
is the pr  
modes con  
and the S  
If they  
certifie  
features  
theories  
technico  
The proc  
experime  
of the p  
continua  
at high



## 1. Introduction

The proton-antiproton ( $p\bar{p}$ ) collider at the CERN SPS<sup>1)</sup> will soon be operational. The systematic exploration of a new energy range up to 540 GeV center-of-mass energy will subsequently begin by several detector systems<sup>2)</sup>. We therefore aim to form an opinion about the physics to come as based on our present-day knowledge. Our main sources of information are : observations from cosmic-ray experiments, extrapolation of results from existing accelerators, present theory framework of strong and electro-weak interactions supplemented by phenomenological models<sup>3-5)</sup>.

Clarification about the Centauro events is expected and the possibility to find surprising new phenomena is again open. The large- $p_t$  inclusive reactions, with jets of up to 100 GeV/c transverse momentum, will test the dynamical consequences of perturbative QCD; signatures of glueballs are anticipated. The low- $p_t$  inclusive data are described by several phenomenological models which, at collider energies, differ in their predictions for the central plateau height and the mean multiplicity. The rise of the total cross section and the characteristics of the (quasi) elastic reactions will hopefully provide a better understanding of diffraction. One of the main motivations for constructing the  $p\bar{p}$  collider is the production of the weak bosons  $W^\pm$  and  $Z^0$  with the leptonic decay modes considered best for their detection. Weak interaction modelling, and the  $SU_2 \times U_1$  model in particular, predict their masses around 100 GeV. If they indeed are found, present weak interaction theory will be certified and possibly further constrained. Two other fundamental features await to be verified: the non-abelian nature of weak gauge theories via the coupling of three gauge bosons, and the Higgs-or technicolor particles which generate the gauge boson (and quark) masses. The processes for their verification have a low cross section and experiments with a very high statistics are needed. The current studies of the Drell-Yan process and the production of direct photons, continued in the  $p\bar{p}$  energy region, will test present theoretical concepts at higher energies and provide more detailed information on the constituent

dynamics, in particular at low  $x$  values. More massive quarks are expected manifesting themselves by new hidden-flavor states (onia) in the lepton-pair spectrum, and by the associated production of new open-flavor states. Once they are found, present phenomenological QCD analyses can again be applied. There are two principle themes in this presentation which are repeatedly encountered: perturbative QCD<sup>4)</sup> and electro-weak gauge theory<sup>5)</sup>.

The paper is organized as follows: Section 2 assembles the main results from cosmic-ray experimentation, and introduces the Centauro events. The ISR/FNAL data characteristics of the large- $p_t$  inclusive processes are presented in Section 3 together with an overview about the theory-analyses and -predictions. Section 4 covers the rapidly developing experimental and phenomenological understanding of the small- $p_t$  reactions. Details of the  $W^\pm$  and  $Z^0$  boson detection, and possible subsequent analyses, are discussed in section 5. Section 6 touches massive lepton-pair production, the discovery of hidden- and/or open-flavor states, and the production of prompt photons. To establish clear signatures for Higgs- or technicolor- particles will be difficult, in this class of rare processes, discussed in Section 7, figures also the hadronic production of gauge-boson pairs such as  $W^+W^-$ ,  $W^\pm\gamma$ . Section 8 summarizes this study.

## 2. Results from Cosmic Ray Experiments

Cosmic ray experiments<sup>6)</sup> have already provided some information about particle interactions beyond presently available accelerator energies, despite the problem of low flux. The research has mainly been motivated by the fundamental astrophysical question of origin, acceleration and propagation of cosmic rays. With the advent of the new generation of colliding beam machines at CERN and FNAL hadronic interactions at several hundred TeV will be abundantly produced and their systematic study should clarify the general features of particle production sufficiently, so that further progress can be made in the indirect determination of the primary cosmic ray composition around 1000 TeV

from  
have  
be co in  
CERN  
CD  
2. his  
been  
200 C result  
to be es.  
from ces  
of th eory-  
error  
The r actions  
large.  
1.9  
action  
signi in  
and the  
are in section 9  
that  
ideas  
fract  
and in about  
fixed 1979,  
multi- ted  
Th- id  
will of  
540 Ge  
can b sic

from air shower measurements. On the other hand, hints for new phenomena<sup>6)</sup> have emerged from cosmic ray studies at very high energies which might be confirmed and their characteristics subsequently analyzed by the CERN-SPS  $p\bar{p}$  collider.

### 2.1 General Features of Hadronic Events Above 10 TeV .

Multiplicities and rapidity densities for charged secondaries have been reported at 20 TeV which corresponds to a total C.M. energy of about 200 GeV . The average multiplicity measured in two experiments is found to be  $19 \pm 5$ <sup>7)</sup> and  $25 \pm 7$ <sup>8)</sup> respectively . A logarithmic extrapolation from accelerator data yields  $18 \pm 1$ <sup>9)</sup> . The data may indicate an increase of the charge multiplicity proportional to  $s^{1/4}$  . The large statistical errors and systematic uncertainties however forbid any premature conclusion. The rapidity density at  $x=0$  is reported to be  $3.9 \pm 0.6$ <sup>8)</sup> . This value is larger than that obtained at the ISR. The ISR values range from 1.4 to 1.9 in the range  $23.6 \text{ GeV} < s^{1/2} < 62.8 \text{ GeV}$ <sup>2)</sup> .

Because cosmic ray experiments cannot precisely determine the interaction energies event by event , it is not possible to make a very significant test of hadronic scaling. Analyses of results at 20 TeV<sup>7)</sup> and of air shower measurements up to  $10^3 \text{ TeV}$ <sup>10)</sup> indicate that the data are not consistent with scaling in the fragmentation region .

A recent study of hadronic interactions around 50 TeV<sup>11)</sup> has shown that many of their features can be understood in terms of conventional ideas extrapolated from accelerator energies . The inclusion of a large fraction of hard scattering is needed to describe the large  $p_t$  characteristics and the increasing multiplicity. The falling energy spectrum and the fixed threshold in the experiments, however, favor selection of high-multiplicity events.

The analysis of only 1000 events , generated by the  $p\bar{p}$  collider, will suffice to settle most of the mentioned items at the c.m. energy of 540 GeV which corresponds to a lab-energy of about 150 TeV . The events can be collected within a few minutes.

## 2.2 New Long-Lived Heavy Objects

The presence of new long-lived ( $\tau > 10^{-7}$  s) heavy objects is suggested by experiments that study simultaneously the distribution of energies and delay times of hadrons near air-shower cores<sup>12)</sup>. Several events were observed with delays greater than 30 nsec and energies greater than about 45 GeV; these events constitute a fraction of about  $3 \cdot 10^{-4}$  of the events, and could indicate the production of relatively stable particles with mass  $\gtrsim 5$  GeV/c<sup>2</sup>. Such massive stable particles could be seen with a time-of-flight system which provides sub-nanosecond resolution over a path length of about 3 m.

## 2.3 Anomalous Hadron Attenuation

Results reported from the very large calorimeter at Tien Shan<sup>13)</sup> show that the attenuation length of hadrons in lead increases significantly around 50-100 TeV. Above 100 TeV most of the events are air shower cores. At lower energies a significant subset of events are unaccompanied hadrons interacting in the calorimeter. Because of the small ratio of radiation length to nuclear mean free path (1/30) the incident electromagnetic component is in equilibrium with the hadronic core, and the rate of energy deposited is characterized by the nuclear absorption length. In a normal cascade, energy deposition in the calorimeter is expected to be dominated by pions. The corresponding attenuation length is calculated to be  $\sim 700$  g/cm<sup>2</sup>. This is the value found experimentally up to about 50 TeV. Above 100 TeV, however, the attenuation length is about 1100 g/cm<sup>2</sup>.

Such an effect could be due to copious production of unstable particles (including leptons) if by chance they had decay modes and life times appropriate to the calorimeter. Further studies of the calorimeter would, however, be useful to eliminate the possibility of energy dependent biases.

Although the  $p\bar{p}$  collider will surpass the 100 TeV threshold, it is not a priori clear how the anomalous hadron attenuation will manifest itself. The used calorimeters do not widely differ from the Tien Shan set up, but the latter operates in the laboratory frame while  $p\bar{p}$  collisions

will  
produ sug  
proba erg  
2 ven  
Th ater  
3-10  
Centa sta  
prim cou  
enou.  
trian  
it ha  
actio  
inte. 13  
the o ficar  
porta wer  
ener. ed  
A radiat  
cosm etic  
anom e of  
gro. th.  
expe ecte  
expe is  
The centa  
the ch is  
case  
e par  
(a) times  
of a er wor  
conc tent  
of at is  
exp st its  
the et up,  
thr ions

will be observed in their center-of-mass frame. The fact that the production of the new component has to be exceptionally copious will probably be the best experimental clue .

#### 2.4 Hadron-to-Photon Ratios in Events Around 500 TeV.

The large ratio between hadron and photon energies in the original Centauro events <sup>14)</sup> continues to defy a conventional interpretation. The primary interaction responsible for the event happened to be close enough to the emulsion chamber so that its height could be estimated by triangulation. Because of the lack of photons incident from the atmosphere, it happens that at most one  $\pi^0$  was produced in the atmospheric interaction which produced at least 49 hadrons . Correcting for hadrons not interacting in the chamber , one estimates 74 hadrons were produced in the original interaction. Keeping in mind that only the electromagnetic portion of hadronic interactions in the chamber is seen, the interaction energy is estimated to be somewhat greater than 500 TeV.

A recent analysis of the data on atmospheric interactions of 100-1000 TeV cosmic rays suggests that there could indeed exist a larger group of anomalous events with very little energy in secondary pions <sup>15)</sup>. The group comprises two of the five Centauro events from the Brazil-Japan experiment and three mini-Centauros, including one event from the Pamir experiment . At least 5% of the events around 1000 TeV appear to be anomalous. The fraction could be much higher, since Centauro interactions high in the atmosphere would probably be obscured by subsequent atmospheric cascading .

Two classes of explanations for Centauro events can be imagined: (a) those involving exotic cosmic projectiles such as exploding blobs of ultra-dense matter <sup>16)</sup>, metastable high-strangeness states <sup>17)</sup>, or condensed nuclei <sup>18)</sup>, and (b) those involving a new kind of interaction of ordinary hadrons beyond some threshold energy. Assuming that explanation (b) is the one to hold, Centauros could be produced at the  $p\bar{p}$  collider and were seen by the detectors , if their production threshold is not too sharp and below the energy range of the machine.

Their discovery would pose uncomfortable problems since a point-like production mechanism can already be excluded. The flux of high energy quarks carrying a fraction of the primary cosmic ray energy does not suffice to explain the observed number of relativistic heavy Centauro-fireballs<sup>19)</sup>, and the absence of neutral pions from the fragmentation of the spectator jet is too peculiar. Violent hadronic processes have to be invoked which do not proceed via point-like constituent scattering.

### 3. Large- $p_t$ Physics

Hadron production at large  $p_t$  is considered to probe hadronic short-range interactions. The point-like constituents undergo hard scattering processes and subsequently fragment into jets of hadrons. Perturbative QCD predicts the jet and the particle cross sections, with scale dependent momentum and fragmentation distributions being used.

#### 3.1 QCD Predictions<sup>20)</sup>

Characteristic features are : (1) the jet cross section depends on the parton momentum distributions and the differential cross section of the perturbative subprocesses between quarks and/or gluons, (2) at fixed  $p_t$  the cross section increases with energy, (3) since 50% of the hadron momentum is carried by gluons at low  $x_t$ , their influence grows substantially at higher energy, (4) due to the production of bremsstrahlung gluons (which becomes more important with growing energy) a simple scale breaking pattern emerges at fixed c.m.-angle, (5) at fixed  $p_t$  the single hadron yield is 2-3 orders of magnitude below the jet yield, details depend on the steepness of the  $p_t$  spectrum of the jet, and on the fragmentation function, (6) the two-jet events are coplanar, and so are their leading hadrons; at higher energies the coplanarity is spoilt by multijet production, (7) the fermi motion of the partons manifests itself in the primordial transverse momentum, (8) gluon jets are different from quark jets. Gluon jet characteristics are : higher multiplicity due to the larger color charge, a soft hadron spectrum and the

absence of leading fragments, the overall compensation of its quantum numbers, and a growing jet cone with increasing jet  $k_t$ . Quark jets have a smaller jet cone and a lower multiplicity, and their non-vanishing 'charge retention' <sup>21)</sup> reflects in the mean the quark charge; quark jets are occasionally accompanied by a gluon jet.

Although this picture is well defined, approximations are needed in practical applications. The comparison between theory and experiment suffers from ambiguities due to the problems: higher order QCD corrections <sup>23)</sup>, uncertainties in the parton distributions <sup>24)</sup>, nuclear and multiple scattering corrections <sup>25)</sup>, higher twist effects <sup>26)</sup>, large primordial transverse momenta <sup>27)</sup>.

### 3.2 Experimental Features at FNAL and ISR Energies <sup>28)</sup>

The typical configuration involves two jets at wide angles, and the small- $p_t$  forward and backward spectator jets. One of the wide angle jets is associated with the jet trigger particle (towards-jet), and the other with the recoiling constituent (away-jet).

(1) Jets involve a burst of neutral and charged hadrons (mostly pions) which are isotropically distributed around the jet axis. The mean multiplicity of the charged jet-fragments increases from 4 to 12 in the  $\sqrt{s}$  range 5-25 GeV of the two wide angle jets. The positive-to-negative charge ratio increases with the momentum fraction  $z$  in pp collisions. Among the leading jet fragments pairs of opposite charge are favored. The mean transverse momentum with respect to the jet-axis is  $\langle k_t \rangle \approx 0.55$  GeV/c. Jet fragmentation reveals approximately scaling. The  $z$ -distributions are well described by an exponential form with the slope as in  $e^+e^-$  annihilation. Identification of the gluon jet in the  $e^+e^-$  planar three-jet events have so far been possible on a statistical basis only, and no dramatic differences between gluon and quark jets have yet been observed <sup>29)</sup>.

(2) The jet cross section at fixed  $p_t$  is typically two to three orders of magnitude above the single particle cross section, and their ratio increases with increasing  $x_t$  ( $\approx 2p_t/\sqrt{s}$ ). Jet pionization dissipates about 1 GeV in mass and transverse motion to slow moving particles which

introduces an uncertainty in its actual yield of up to an order of magnitude. Pions and kaons are more efficient producers of high- $p_t$  jets than protons, with  $R(p/\pi) \approx R(p/K)$  decreasing from 1.5 to 0.5 as  $p_t$  ( $\lesssim 6$  GeV/c) grows. Jets from pions are emitted more forward since their constituents take a larger momentum fraction. The density of opposite spectator fragments (all with  $p_t \sim 100$  MeV/c) decreases with growing transverse momentum of the trigger jet.

(3) Whenever triggering on a large  $p_t$  particle one is likely to select a particular and rare configuration, the characteristics of the towards-jet are severely distorted and the production cross section is greatly reduced.

The high- $p_t$  event structure is compared to a normal inelastic event via the ratio  $dn_t/dn_i(\vec{p})$ .  $dn_{t,i}(\vec{p})$  represents the average number of particles per event emitted in some phase space direction  $\vec{p} \dots \vec{p}+d\vec{p}$  in a high- $p_t$  (t) or normal inelastic (i) event. One notices: (a) around the trigger direction the ratio enhances, (b) in the opposite direction the enhancement is even stronger and broader, (c) at fixed azimuthal angle  $\phi$  the ratio decreases with growing  $y$ , a sizable value of the ratio is limited to  $|y| \leq 1$  (43) near the towards (away-) direction, (d) the large ratio on the away-side is due to a substantially higher overall multiplicity which follows from the trigger-bias effect.

Most of the jet momentum is absorbed by a single particle with less than 10% left to the accompanying secondaries. The associated momentum, originating to a large fraction 25-50% from prominent resonances, grows moderately with increasing  $p_t$ .

The number of negative (positive) associates is bigger in a towards-side jet, triggered by a  $\pi^+$ , than  $\pi^-$  ( $\pi^-$  than  $\pi^+$ ). This compensation becomes more pronounced as the transverse momentum of the associates increases, with little dependence, however, on the  $p_t$  of the trigger pion. The charge compensation effect for the away-side secondaries is smaller and tends to die away as their transverse momentum increases. There is essentially no correlation between the charge of the high- $p_t$  trigger particle and the charge of the highest  $p_t$  particle on the away-side.



Within the away-side system itself one finds strong charge compensation similar to the towards-side system. The charge correlations for the trigger particles  $K^\pm, p, \bar{p}$  are similar.

The particle ratios  $p/\pi^+$ ,  $\bar{p}/\pi^-$ ,  $K^-/\pi^-$  rise with increasing  $x_t$  and fall off again beyond 0.2; the ratio  $K^+/\pi^+$  however levels off. The large- $p_t$   $\pi^+/\pi^-$  ratio is practically  $p_t$  independent in  $\pi^- p$  collisions and seems to rule out the CIM mechanism <sup>26a</sup>); it increases in  $pp^-$  (remains  $\sim 1$  in  $pn^-$ ) collisions as expected from hard scattering models.

(4) The simultaneous production of two wide-angle jets, preferentially in an azimuthal back-to-back configuration, was experimentally verified. The (away-side) particle density reveals a characteristic maximum around the rapidity  $y$  of the away-side trigger, where  $y$  determines its angle with respect to the beam axis. The momentum component out of the trigger plane gives a clue on the primordial  $k_t$  and on the non-planar gluons. Perturbative QCD predicts  $\langle P_{out} \rangle$  to increase with  $p_t$  and  $z$  which is observed for the unbiased away-jet. The transverse momentum imbalance between the two wide angle jets is roughly gaussian with a width of about 2.4 GeV. The production of symmetric pion pairs is considered to be a clean test of perturbative QCD, and the data are in good agreement with the predictions.

(5) The inclusive  $\pi^\pm$  distribution at  $90^\circ$  and  $p_t \leq 6$  GeV/c is proportional to  $p_t^{-n}(1-x_t)^m$  with  $n=8, m=10.6$ . As  $p_t$  further increases the  $p_t$  exponent approaches  $n \approx 4$  at larger  $x_t$  ( $> 0.3$ ), the value predicted by the counting rules <sup>30</sup>). Measurements at angles off the central region reveal "radial scaling". The angular dependence is accounted for by replacing  $x_t$  by  $x_R = (x_t^2 + x_L^2)^{1/2}$ . Data in the lower  $p_t$ -range indicate for the inclusive production of  $K^\pm$ ,  $\bar{p}$   $n=8$ , and for  $p$   $n=12$ .

(6) Some of the experimental results are not fully understood. The observed proton yield is an order of magnitude above QCD estimates. The  $z$ -distribution of the away-side  $\pi^0$ 's, triggered by a large- $p_t$   $\pi^0$ , shows a departure from the exponential shape at low  $z$  values. The

intrinsic transverse momentum of the colliding partons makes the observed  $p_t$  dependence steeper, phenomenological analyses hint at a value of 1 GeV/c which is far above the primordial transverse momentum as determined in other processes.

### 3.3 Theory Analyses

The production of large- $p_t$  hadrons/jets is calculated in the framework of perturbative QCD. The hard-scattering process is described by the parton cross section using QCD Feynman-rules. Gluon gauge invariance is in the Feynman gauge maintained via the ghost graphs; the axial gauge, as an alternative, leads to more complicated intermediary expressions<sup>31)</sup>. The soft-gluon radiation causes via its renormalization group summation the scale dependence in the momentum distributions and gives rise to the running coupling constant in front of the parton cross sections. Nearly all phenomenological analyses use the leading-log parametrizations from deep-inelastic scattering<sup>24a)</sup> where their normalization is fixed.

Present large- $p_t$  phenomenology (in the ISR energy range) is to a large extent based on the  $q\bar{q}$ ,  $qg$  and  $gg$  initiated order- $g^2$  graphs whereby the gluon initiated processes contribute a significant fraction<sup>32)</sup>. Asymptotically each subprocess scales as  $p_t^{-4}$ . For  $p_t \lesssim 3$  GeV/c the single particle cross section however falls off faster due to the scale dependence in the running coupling constant and in the momentum distributions. For  $p_t \lesssim 2-3$  GeV/c the dominant subprocess is  $q\bar{q}$ -scattering with non-negligible  $qg$  and  $gg$  contributions. In the intermediate  $p_t$ -region the  $qg$  and  $gg$  contributions are responsible for the correct cross section size and fall-off, whereas at large  $p_t$ -values  $q\bar{q}$ -scattering becomes predominant. The subprocess  $q\bar{q} \rightarrow q\bar{q}$ ,  $gg \rightarrow q\bar{q}$  can for all  $p_t$ -values ignored. For  $p_t \gtrsim 4.5$  GeV/c the data are well described whereas for smaller  $p_t$ -values the predictions are too low.

In the above simple picture there are several particularities which we now consider:

- (1) The freedom to choose the dynamical expansion variable  $s^2$  or  $2\hat{s}\hat{t}/(\hat{s}^2 + \hat{t}^2 + \hat{u}^2)$ , following from the ambiguity in mass factorization, influences the cross section size.  $\hat{s}, \hat{t}, \hat{u}$  are the Mandelstam variables

of the  $2 \rightarrow 2$  subprocesses. The second choice leads to smaller  $Q^2$  and a larger cross section <sup>24e)</sup>.

(2) The introduction of an intrinsic transverse momentum ("k<sub>t</sub>-smearing") lifts the cross section substantially in the  $p_t \lesssim 4$  GeV/c region and generates a steeper decrease. Fits with values  $\langle k_t \rangle \sim 1$  GeV/c, larger than expected from other reactions, lead to qualitative agreement with the data. This procedure is theoretically motivated by the partons intrinsic transverse momentum due to their Fermi motion, and by their "effective k<sub>t</sub>" from the Bremsstrahlung of gluons; the evaluation of the  $2 \rightarrow 3$  subprocesses will partially account for the latter reason. It should however be clearly realized that "k<sub>t</sub>-smearing" serves as a cut-off for the mass and/or infrared singular parton cross sections, and the problems in the description of the low- $p_t$  region still exist. The correct inclusion of primordial  $\langle k_t \rangle$  is unknown and different prescriptions for smearing lead to quite different results <sup>27)</sup>.

The inclusive cross section thus decreases as  $p_t^{-8}$  for  $p_t \lesssim 6$  GeV/c, goes over to  $p_t^{-6}$  (the naive  $p_t^{-4}$  of qq-scattering plus the scale dependent  $\alpha_s(Q^2)$  and  $u(x, Q^2)$ ) in the intermediate region, and reaches  $p_t^{-4}$  at large  $p_t$ -values.

(3) Higher-twist mechanisms, contributing to each parton subprocess  $p_t^{-6}, p_t^{-8}, \dots$  terms (apart from the leading  $p_t^{-4}$ ), might be another source of the theory-data discrepancy below  $p_t \lesssim 6$  GeV/c. The constituent-interchange-model (CIM) <sup>26a)</sup> ranges in this class of terms. Partons do not scatter point-like, pairs of quarks and/or gluons from a given hadron instead may jointly participate in a coherent manner in the hard-scattering process. Their influence in large- $p_t$  reactions, in particular  $\pi N \rightarrow \pi X$ , has been estimated via the subprocesses  $qg \rightarrow \pi g$  and  $q\bar{q} \rightarrow \pi g$  which are the only  $2 \rightarrow 2$  processes giving  $p_t^{-6}$  contributions to the cross section. The absolute normalization is fixed by the pion weak decay constant, or in terms of the pion electromagnetic form factor at large  $Q^2$ . The higher-twist cross section decreases less rapidly as  $x_1 \rightarrow 1$  and there is no trigger-bias suppression since the final  $\pi$  is produced without the necessity of jet fragmentation. They scale as  $s^{-1}$  and they

are qualitatively important for  $p_t < 6$  GeV/c and  $x_t \gtrsim 0.5$ . At  $\sqrt{s} = 10$  GeV the  $q\bar{q}$  initiated contribution is roughly an order of magnitude more important than the analogous  $qg$  subprocess. An overall correction to the inclusive cross section of at least 30% is expected which grows with increasing  $x_t$  and even dominates above  $x_t > 0.65$ . In  $\pi^- N \rightarrow \pi^+ N$  the higher-twist effects cause a charge-ratio substantially above unity. Spin-spin asymmetries in  $p(\uparrow) p(\uparrow) \rightarrow \pi^+ X$  might offer another possibility for their detection <sup>26b)</sup>.

The search for high-twist effects lead recently to a special class of high- $p_t$  events which might allow for the isolation of a clean high-twist signal. The entire energy of an incident meson is delivered into production of a pair of large- $p_t$  jets at wide angle excluding any final state particles along the beam axis. At  $\sqrt{s} = 20$  GeV the predictions account for 3-5% of the reported inclusive jet yield. The veto, excluding particles along the beam direction, and the simple two-body kinematics simplify the goal <sup>26c)</sup>.

(4) The existence of the Yang-Mills three-gluon vertex has been demonstrated <sup>33a)</sup> through its dominance in the order  $g^2$   $gg \rightarrow gg$  subprocess (fig.1). The single-particle cross section for  $pp \rightarrow \pi^+ + X$  was measured at  $\sqrt{s} = 52$  GeV. The significance of the  $gg$  subprocess as compared to simple  $qg$ -scattering is inferred from the charge ratios in the away-side jet and between the target and beam spectator jets accompanying the high- $p_t$  ( $p_t \simeq 2.5$  GeV/c)  $\pi^+$  trigger in the forward direction ( $\theta \simeq 20^\circ$ ). The ratio of the  $gg$  to  $qg$  contributions is at the above conditions predicted by QCD to be  $R \simeq 3$ , in qualitative agreement with the experimental observation  $R \gtrsim 1$ . The omission of the triple-gluon vertex (fig.1c) changes the  $gg$  contribution by more than an order of magnitude, leaving  $R \simeq 0.1$ . Different choices of the moment and fragmentation distributions can not change this insight.

(5) The leading-log phenomenology of the single particle inclusive processes assumes that the next-to-leading corrections <sup>23)</sup>, from  $\alpha_s(\mu^2)$  expansion of the coefficient function, are small. Their analysis needs consideration of all order- $g^3$  QCD graphs with real as well as virtual gluon lines, and the resulting parton cross sections must

be  $\bar{s} = 10$   
ar ore  
th n to  
a lows  
di  $> \pi^+$   
fr ve unit  
In possibi  
an  
Mi class  
qu high-  
of ed into  
al ly fina  
or ions  
(  
st body  
fo  
de demon-  
a process  
Th as  
ha as  
tr tics in  
e forward  
r at th  
c. trecher  
no triple-  
in an orde  
t and  
i  
c ave  
a  
a analy  
at l as  
st

be evaluated up to the constant terms. The ultra-violet divergences are renormalized, and all infrared divergences are cancelled between the real- and virtual-gluon graphs <sup>34a)</sup>. The remaining mass singularities are via mass factorization <sup>35)</sup> absorbed in the momentum and fragmentation distributions. The resulting  $\alpha_s$  correction term of the coefficient function has been determined for qq-scattering and was found to be large. In the present  $Q^2$ -range the non-leading corrections therefore are large and the leading-log approximation is without theoretical foundation. Might-be this problem will disappear once the bound state nature of the quarks is taken into account. The analogous qg- and gg-parts, which are of prime importance at collider energies, are still missing. We point here also to the problems arising from the non-cancellation of the higher order QCD infrared divergences <sup>34b)</sup>.

(6) The two-particle inclusive cross section allows for correlation studies <sup>36a)</sup>. QCD calculations at  $p_t = 4$  GeV/c,  $\sqrt{s} = 53$  GeV reveal the following percentage for the trigger-recoil constituents: qq (27%), qg (45%), gq (11%), gg (17%). The trigger constituent is therefore mostly a quark (72%) and the recoil constituent is quite often a gluon (62%). The away-side gluons produce equal number of positive and negative hadrons. Little variation of the away-side hadron multiplicity with growing trigger transverse momentum should occur.

The measurement of back-to-back large- $p_t$  events disposes to a large extent of the  $k_t$ -smearing effects. Keeping the transverse momentum ratio  $z_p = p_t(\text{aw})/p_t(\text{tr})$  fixed ( $\sim 1$ ), the two-particle inclusive cross section increases smoothly with growing trigger transverse momentum. The  $k_t$ -smearing effects, strongly felt in the single-particle inclusive cross section at low- $p_t$ , do not influence its shape since the trigger bias, favoring the initial quarks moving towards the trigger, is removed. Thus, two-particle back-to-back cross sections reflect more closely the  $p_t$ -dependence of the basic subprocesses without the additional scale-breaking due to  $k_t$ -smearing <sup>36b)</sup>.

The  $k_t$ -smearing also results in a momentum component  $P_{\text{out}}$  of the away-side constituent out of the trigger plane.  $\langle P_{\text{out}} \rangle$  however is too

low and the discrepancy may be due to the  $2 \rightarrow 3$  constituent processes contributing to a large  $P_{out}$ -tail which at higher energies is more pronounced<sup>20b)</sup>.

The experimental tests confirm these insights<sup>26)</sup>.

(7) Analysis of the three-jet processes based on the  $2 \rightarrow 3$  parton cross sections (with radiative gluon graphs only) are fruitful as long as the distributions differential in all three-jet momenta are considered. However, there are infrared singularities which in the kinematical region of their dominance must be cancelled by the virtual-gluon graphs, and there are mass singularities whose dominance signals the onset of confinement effects. In all  $2 \rightarrow 2$  versus  $2 \rightarrow 3$  comparisons their predominance is prevented by cuts on the angle and energy-fraction ( $\delta, \epsilon$ ) of the Sterman-Weinberg jets and/or by restricting the kinematical variables, such as for instance three-jet events in the transverse plane only.

With these uncertainties in mind we summarize the main insights from QCD three-jet analyses<sup>37)</sup>:

- (i) With  $\epsilon \sim 0.2$ ,  $\delta \sim 0.25$  and  $p_t(tr) \gtrsim 2.5$  GeV one finds  $\sigma(3j)/\sigma(2j) \sim 20-30\%$  for the  $q\bar{q}, q\bar{q}$  and  $qg$  initiated parton cross sections. The  $gg \rightarrow 3j$  processes instead are much larger than the corresponding  $gg \rightarrow 2j$  contributions. There is no qualitative change at higher energies if  $x_t$  and the cut-off parameters are kept fixed.
- (ii) The hadron initiated 3-jet as compared to the 2-jet cross section can by suitable cuts be enhanced or suppressed. Cuts on the transverse energy and azimuthal cause a suppression factor 3-10, in addition to (i) above. A small  $p_t$ -cut ( $> 2$  GeV/c) at fixed transverse energy ( $E_t \sim 10$  GeV) however enhances the relative importance of the 3-jet events. Hard gluon emission is estimated to contribute a  $\sim 20\%$  correction to the lowest order large- $p_t$  cross sections. At ICR energies the main contributions come from the  $qg, q\bar{q} \rightarrow q\bar{q}g$  subprocesses, whereas at collider energies  $gg \rightarrow ggg$  will dominate.

(iii)

energy r  
collider  
contribu  
tail whi  
anti-pa.

The P  
by the c  
smearing

(iv)  
the tra  
particu  
predict

in the  
jet ang  
and glu  
times

Jets fr  
those f  
jet str

Thus  
leading

3.4  
The

The cro  
extrapo  
Neverth  
is seen  
jet-rat  
(see fi  
face or  
angle :

(iii) The transverse thrust distribution offers in the ISR energy range little hope to find signatures of 3-jet events. At collider energies however, the gaussian tail of the smeared 2-jet contributions is 1-2 orders of magnitude below the significant 3-jet tail which essentially results from the  $qg \rightarrow qgg$  subprocess and its anti-part <sup>37)</sup>(fig.2) .

The  $P_{out}$ -distribution of  $\pi^0 - \pi^0$  correlations can not be explained by the smeared 2-jet contributions whereas the 3-jet curve, after smearing has been applied, can fit the data <sup>28a)</sup> (fig.3) .

(iv) A detailed comparison of different 2  $\rightarrow$  3 parton processes in the transverse plane reveals : three-jet events depend strongly on the particular production process. Process-dependent variations make the predictions based on "jet-universality" questionable, in particular so in the small-thrust region. The considerable variations with changing jet angular radii signal large differences in the jet-widths of quarks and gluons. Perturbative three-jet configurations are typically 2-4 times more important in hadronic production than in  $e^+e^-$  annihilation. Jets from high- $p_t$  hadronic processes are considerably broader than those from  $e^+e^-$  annihilation at the same energy, and sharply defined jet structures will be much less evident.

Thus, measurable jet properties can be largely process dependent leading to doubts on the concept of universal quark and gluon jets <sup>37b)</sup>.

### 3.4 Jets at the Collider

The inclusive  $\pi^0$  spectrum as measured at the ISR is shown in fig.4 . The cross section is several orders of magnitude above the naive extrapolation of the exponential shape seen in the small- $p_t$  region. Nevertheless, large- $p_t$  particles are rare. Roughly one  $\pi^0$  at  $p_t = 5$  GeV/c is seen in  $10^7$  interactions in a  $p_t$ -bin of 1 GeV and per steradian. The jet-rate exceeds the single-particle rate by 2-3 orders of magnitude (see fig.5), but it is still small. Furthermore any jet trigger has to face considerable difficulties. Multiplicity fluctuations into the solid angle of the jet calorimeter may by far outnumber the "true" jets <sup>38)</sup>.

The situation at the  $p\bar{p}$  collider may be drastically different. If the gluons continue to share 50% of the momentum fraction, and if their distribution is proportional to  $\sim (1-x)^5$ , then their scattering will give rise to a large jet rate. A cross section of  $\sim 2$  mb is expected for gluon jets of  $p_t = 5-10$  GeV/c. No fancy jet trigger would be needed anymore since a large fraction of the events contains two 5-10 GeV/c jets attached to the usual longitudinal phase space cigar. The inclusive jet yield at high transverse momenta is presented in fig. 6<sup>39)</sup>. Assuming the luminosity  $L = 10^{28} \text{ cm}^{-2} \text{ s}^{-1}$ , one may expect about 250 jets/hour with  $p_t(\text{jet}) \geq 20$  GeV/c.

The medium and large  $p_t$  physics may be accessible in the very early phases of collider experimentation. An event with jets of 20 GeV/c, however, does not come for free: among  $10^4$  minimum-bias events only 1 is expected. A calorimeter trigger is therefore needed. On the contrary, jets of 5-10 GeV/c are expected to be abundant.

The significant size of the jet yields at low  $x_t$  ( $< 0.25$ , at  $90^\circ$ ) follows from the steep rise of the gluon momentum distribution. At  $\sqrt{s} = 540$  GeV and  $p_t = 7$  GeV/c the percentage of the different quark-gluon processes is estimated as:  $q\bar{q} \rightarrow q$  (3%),  $q\bar{q} \rightarrow g$  (< 1%),  $qg \rightarrow g$  (18%),  $qg \rightarrow q$  (25%),  $g\bar{g} \rightarrow q$  (3%),  $g\bar{g} \rightarrow g$  (45%). The numbers vary for different gluon momentum distributions. The inclusive jet yields follow the ordering  $g \gg u \gtrsim d \gtrsim \text{sea}$ , with 62% (35%) from gluons (quarks). The subprocesses are preferentially initiated by  $g\bar{g}$  (48%) and by  $qg$  (43%) scattering. As  $p_t$  grows the gluon-jet yields maintain their leading rôle up to rather large  $x_t$ -values ( $x_t < 0.3$ ). Gluon jets are therefore expected to dominate over the full  $p_t$ -range covered by the collider at the luminosity of  $L = 10^{30} \text{ cm}^{-2} \text{ s}^{-1}$ .

Whilst looking at the  $y$ -distribution at fixed  $p_t$  we vary the c.m. angle, since  $y = -\ln(\tan \frac{\theta}{2})$ . Over the wide angle region  $|\Delta y| = 1$  gluon jets dominate. At forward angles ( $\sim 30^\circ$ ) the valence quark jets are more likely with  $u \gg d \gg g \gg \text{sea}$ , whereas at backward angles ( $\sim 150^\circ$ ) the valence anti-quark jets  $\bar{u} \gg \bar{d} \gg g \gg \text{sea}$  take over. The angle  $\theta$  is chosen with respect to the proton beam.



If quark and gluon jets are indeed produced as predicted by QCD, correlation measurements can provide detailed information about the underlying hard scattering processes. Using  $\pi^+$  for instance as the trigger particle (around  $90^\circ$ ) favors a u-jet. The away-jet in the forward region ( $\sim 30-60^\circ$ ) will originate from a gluon almost as frequent as from a u-quark; at wide angles ( $\sim 60-120^\circ$ ), however, gluon jets will dominate. Choosing instead the trigger particle in the forward cone ( $\leq 30^\circ$ ) favors in the opposite wide (small) angle region the production of quark (gluon) jets. The initial and final partons in such collisions are (almost) the same since the gg initiated processes are negligible. Since the  $P_{out}$ -distributions are broader for gluons than quarks one expects to see such broadening effect whilst passing from the wide to the small angle region <sup>40)</sup>.

Since large  $p_t$  values can be reached, the QCD scaling violation effects are expected to be more pronounced in both the structure and the fragmentation functions. They dampen the single particle  $p_t$  distributions by a factor 0.1-0.2 at the highest possible  $p_t$ -values.

The large amount of gluons initiating the large- $p_t$  reactions has three essential consequences: (a) excessive gluon processes in the low  $\tau$  region, (b) likely production of glueballs, (c) heavy flavor creation in bound and unbound form. In the following we expand on (a) and (b).

### 3.5 Gluon Processes

In the lower  $x_t$  region most of the subprocesses are initiated by gluons. Two aspects are of particular interest: the gluon momentum distribution and the interaction among gluons only.

The gluon momentum distribution can not be directly measured. Gravitons have been suggested as a probe in Gedanken experiments <sup>41)</sup>. Apart from the fact that  $\sim 50\%$  of the nucleon momentum is carried by gluons there is little solid information. The measurement of the jet cross sections, in the  $p_t$  region where the gluon initiated subprocesses dominate, will hopefully give more insight. Several theoretical models have been

suggested to describe the  $x$ -dependence of the gluon momentum distribution. the counting rule parametrization is in the  $x \rightarrow 1$  limit fixed by the number of constituents left-behind in the nucleon <sup>30)</sup>, and for  $x \rightarrow 0$  it is related to a Pomeron dominated Regge parametrization, giving  $xG(x) = 3(1-x)^5$ . The bremsstrahlung-model follows from a convolution over the  $q, \bar{q}, g$  "irreducible" distributions, and the resulting parametrization is composed of several  $(1-x)$  powers. Finally, the bag-bremsstrahlung model follows from a counting rule plus a bag-type parametrization, the latter with an exponential  $x$ -dependence <sup>19a)</sup>. The low- $x$  increase is strongest for the "bag" and relatively flat for the "bremsstrahlung" parametrization; the naive counting rule form lies inbetween.

However, these attempts are of limited value in the low momentum region. It will be necessary to extend the QCD calculations by including realistic bound state wave function and final state interaction effects. The influences of the coherence cancellations and of the hadron size have been analyzed <sup>24)</sup>. An explicit dependence on the number of valence quarks was found. The coherence effects in the color singlet bound state eliminate the quark mass singularity. Such color cancellations are important for all  $x$ -values unless the gluon transverse momentum, as compared to the inverse hadron size, is large.

The  $x$ -dependence of the gluon distribution follows the qualitative rule: softer than the valence quark distributions, but harder than the sea-antiquark distributions. This wisdom was recently put to doubt by a new phenomenological analysis <sup>24d)</sup> of the deep-inelastic data where the (so far ignored) charm threshold effects were taken into account. A very broad (i.e. hard) gluon input distribution emerged, similar to the one proposed in ref. 24e. After the asymptotic freedom corrections have been applied, the familiar steep increase towards low  $x$ -values is, at the considered  $Q^2$ -values, seen again.

The gluon fragmentation function is even less known, and counting-rule parametrizations are usually employed <sup>42)</sup>.

Strongly emerged in jets at collision as insight Interest planar the initial splitting region in lattice Due gluons relative multi-increased The parton region 3.0 At large gluon calculation concise might gluon is several (a) field mass

Strong evidence for the existence of multi-gluon couplings has emerged from ISR large- $p_t$  measurements since the three-gluon vertex in  $qg$  scattering dominates at large subenergies <sup>33a)</sup>. Medium energy jets at the collider will predominantly originate from  $gg$  and  $qg$  collisions. Further tests on gluon self-interactions, with subprocesses as  $gg \rightarrow (ng)$ , are therefore likely to become possible and to give more insight into the color octet dynamics of non-abelian gauge theories <sup>33b)</sup>. Interesting theoretical aspects are: the vanishing of classes of non-planar graphs <sup>43)</sup>, the (non-) cancellation of the infrared singularities <sup>34b)</sup>, the influence of the asymptotic freedom corrections <sup>44)</sup>, the 'gluon-splitting' <sup>45)</sup>. The transition from the perturbative to the confinement region is marked by a phase transition whose characteristics are studied in lattice calculations <sup>46)</sup>, and in statistical models <sup>47)</sup>.

Due to the three- and four-gluon couplings, one expects cascades of gluons in the  $gg$  initiated subprocesses which generate a swarm of relatively slow moving hadrons with overall flavor-neutrality. The multiplicity of such events is anticipated to grow significantly with increasing energy reaching much higher values than for quark-jets. The particle ratios  $\pi^+/\pi^-$ ,  $K^+/K^-$ ,  $\bar{p}/p$  should approach unity in the region where gluons dominate <sup>45)</sup>.

### 3.6 Glueballs

At short distances QCD involves color-octet spin-1 gluons which at large distances are expected to form color singlet composites, called glueballs <sup>48)</sup>. The detailed mechanism is unknown but a number of model calculations have given hints at their properties. The simplest bound states consist of 2 or 3 gluons. A pair of color-electric (or -magnetic) fields might bind to  $J^P = 0^+, 2^+$  states, whereas color-electric and -magnetic gluons could form  $0^-, 1^+, 2^-$  states. A rich spectrum of excited states is expected which decays into low mass hadrons via  $q\bar{q}$  creation. There are several unknown aspects:

(a) Spectrum: Glueball masses have been estimated by several methods: field theory analyses <sup>49)</sup>, MIT bag models <sup>50)</sup>, potential models with massive spin-1 'lumps of gluons' <sup>51)</sup>, a relativistic wave equation with

a QCD motivated potential <sup>52)</sup>, lattice calculations <sup>53)</sup>, connection with the  $P$  - trajectory <sup>54)</sup>, phenomenology of OZI-rule violation <sup>55)</sup>, and partial wave analysis of the  $gg$ -channel <sup>56)</sup>. These calculations indicate the glueball mass spectrum in the 1-2 GeV range.

(b) Decays: The decay modes of the glueballs depend on their masses. Decays into the known low-mass hadrons and their excited states should occur without suppression of the strange quark states. Examples of two-body decays are:  $\pi\pi, KK, \eta\eta, \pi\rho, KK^*, \gamma\omega, \gamma\phi, \pi\pi, K\omega, \rho\rho, \rho\delta, K^*\pi, \rho\phi, \dots$  <sup>43)</sup>.

Phase-shift analyses for the  $\pi\pi$ - and  $KK$ -channels might reveal the  $J^{PC} = 0^{++}, 2^{++}$  low-lying states, whereas the  $0^{-+}$  has the  $\eta'$  quantum numbers and could mix <sup>57)</sup>. Many of the states have the  $3\pi, 4\pi, 5\pi$  decay channels open which offers little hope for a significant signal.

(c) Widths: Glueball widths are either geometrically interpolating between the OZI-rule allowed and suppressed hadronic decays:  $\Gamma_g \sim 10 \text{ MeV}$  <sup>51)</sup>, or, since we are primarily dealing with a confinement problem, they could be  $\sim 1/3$  of the typical hadronic widths:  $\Gamma_g \sim 50 \text{ MeV}$  <sup>53)</sup>. Specific predictions thus become assumption dependent.

(d) Production:  $gg$ -initiated glueball production at the collider may be of significant size. Phenomenological analyses are, however, missing. Since large- $p_t$  gluon jets occur abundantly it may be a promising place to look for glueballs in a specific jet decay mode. The missing mass system of inclusive  $\psi$  or  $\Upsilon$  production in  $e^+e^-$  annihilation or electroproduction could be another source. The  $\psi$  and  $\Upsilon$  radiative decays are expected to reveal such states in the  $E_\gamma$  -spectrum as a measure of the invariant mass <sup>43)</sup>. The appearance of the  $K\bar{K}\pi$  enhancement at 1440 MeV in the invariant mass spectrum of  $\psi \rightarrow \gamma X$  has recently raised the question whether it could be interpreted as a glueball <sup>59)</sup>.

#### 4. Low-

The  
are pre  
hadron  
Regge t  
low- $p_t$   
foundat

#### 4.1

Meas  
about t  
pp limi  
merge.  
forward  
be sever  
wonder  
elastic

The  
soft-gl  
perturb  
to Regg  
this la  
aspect  
color S  
Pomeran  
asympto  
differ  
exponen  
size o  
total  
pp ene

#### 4. Low-p<sub>t</sub> Physics

The expectations for the total and elastic differential cross sections are presented and the attempts at an understanding of inclusive soft-hadron production covered. There are essentially two frameworks: Mueller-Regge theory<sup>60)</sup> and parton model<sup>61)</sup>. Although the description of the low-p<sub>t</sub> phenomena in the framework of perturbative QCD is lacking solid foundation there is considerable phenomenological progress.

##### 4.1 Total and Elastic Cross Sections

Measurements of  $\sigma_{\text{tot}}$  and  $\frac{Q^2}{s} \left( \frac{\text{Re } A(s)}{\text{Im } A(s)} \right)$  will decide about the dispersion analysis  $\ln s$ -increase<sup>64)</sup> and the common pp and  $p\bar{p}$  limit. Similarly the elastic differential cross sections should merge. Will the low- $|t|$  slope and dip-bump structure, moving as the forward peak shrinks, still obey geometrical scaling<sup>65)</sup>? Or will there be several dips as predicted by the factorizable eikonal model<sup>66)</sup>? One wonders about the proton shape as measured by the opacity and total/elastic cross section ratio<sup>63)</sup>.

The consequences of a Pomeron viewed as an infinity of perturbative soft-gluon exchanges have been analyzed in (cut-off regularized) perturbative QCD<sup>67)</sup>. In the asymptotic Regge-limit strong similarities to Reggeon-field-theory<sup>68)</sup> emerged which leads one to wonder whether this latter theory could perhaps provide information on the confinement aspect of QCD, for a layout of this program we refer to ref. 67. QCD with color  $SU_3$  and 16 flavors -both necessary conditions for the critical Pomeron- may be the essentially unique theory giving factorization, asymptotically rising cross sections and equal particle-antiparticle differential cross sections. The scaling functions and critical exponents of the critical Pomeron are exactly calculable whereas the size of the non-leading terms is estimated with present-day data. The total and elastic differential cross sections, extrapolated into the  $p\bar{p}$  energy range<sup>68b)</sup>, might eventually provide tests for this scheme.

In phenomenological investigations the Pomeron is approximated by two-gluon exchange (Low-Nussinov model <sup>69</sup>), fig.7a), with the higher order gluon exchanges assumed to cancel out <sup>70</sup>). The exchanged gluons can interact with each of the two/three hadron-quarks giving rise to negative coherent besides of the incoherent contributions <sup>71</sup>) (fig.7b). Immediate consequences of this picture are: multiparticle production follows from the separation of color and the consequent gluon radiation, zero flavor but color quantum number exchange, interference effects cancel infrared divergences, a constant or logarithmically increasing total cross section due to the vector nature of gluons, generalized quark counting, sensitivity on the size of the colliding bound states with a dependence on the (heavy) quark masses. The total cross section size is achieved at the expense of  $\alpha_s \approx 2$  (1), and the non-perturbative effects are mostly ignored. The above insight were derived from simple model calculations based on gluon radiation <sup>72,71</sup>). Their extension to diffractive excitation <sup>73a,b</sup>) predicts a far bigger cross section and mean  $\langle p_t^2 \rangle$  if compared with traditional approaches <sup>73c</sup>).

#### 4.2 Inclusive Soft-Hadron Production

The stability of the longitudinal phase space and the logarithmic increase of the average multiplicity, as predicted by Mueller-Regge theory <sup>74</sup>), are here of foremost interest. Could the rapid development of the central rapidity plateau and its increase with energy signal a new phenomenon (see section 2.1) and will the  $p_t$  distribution still be damped? Correlation measurements, giving insight into the process of cluster formation and fragmentation, are not expected to change drastically, and similarly -still based on ISR experience- particle ratios should vary little <sup>3</sup>).

The data of the single particle inclusive cross sections <sup>75</sup>) are in the fragmentation region parametrized as  $x_F (d\sigma/dx_F) = C (1-x_F)^n$ .  $x_F (= 2p_{tF}/\sqrt{s})$  is the Feynman scaling variable and the exponent  $n$  changes for different processes, e.g.  $n(p \rightarrow \pi^+) \approx 3$ ,  $n(p \rightarrow \pi^-) \approx 4$ ,  $n(p \rightarrow K^+) \approx 2.5$ .

Three  
depen  
hadro  
numbe  
stat  
refl  
lon  
ha  
fra  
W  
and  
rod  
sepa  
plac  
and/  
occu  
per  
or  
dist  
part  
had  
feat  
boun  
the  
The  
a f  
q<sub>t</sub>  
gau  
ann  
dN  
had  
the  
is

by  
r  
ons  
o  
7b),  
ion  
ation,  
-  
ang  
quark  
a a  
ize  
re  
mple  
on to  
and  
ic  
e  
ment  
a a  
be  
f  
stically  
uld vary  
in  
changes  
2.5  
is

Three characteristic observations emerge: (i) the fragmentation domain depends on the quantum numbers of the fragmenting and the produced hadrons but the momentum shape in the central region is quantum number independent; the cross section size can be understood from quark statistics, (ii) pion production in the nucleon fragmentation region reflects the valence quark distribution in the nucleon, (iii) the longitudinal, transverse and multiplicity behaviour of the produced hadrons are similar to the  $e^+e^-$  and deep-inelastic jets from quark fragmentation <sup>75)</sup>.

Whilst exposing the existing models, we first discuss the central and subsequently focus on the fragmentation region. Multiparticle production in QCD <sup>72)</sup> is presumed to occur as a result of color separation. After the (Low-Nussinov) two-gluon exchange has taken place the octet 'mesons' radiate gluons which in turn create  $q\bar{q}$  pairs and/or multi-gluons; soft-gluons from the exchanged gluons can also occur (fig.7c). Ultimately these radiation products form through non-perturbative means the final state hadrons. Exactly how much radiation or particle production takes place and how the radiated particles are distributed is controlled by the relative momentum of the colored partons leaving the gluon-exchange process. Model calculations for hadron and  $e^+e^-$  initiated processes indicate characteristic asymptotic features: for transverse momenta  $q_t$  small as compared to the typical bound state momentum  $\ell_t$  the rapidity distribution  $d^2N/d\eta dq_t^2$  of the emitted gluon is uniform with a  $q_t^{-2}$  decrease as in  $e^+e^-$  annihilation. The difference in color-charge of the radiating octet jets results in a factor  $9/4$  larger hadron plateau than in  $e^+e^-$  annihilation. At large  $q_t$  there is a  $q_t^{-4}$  decrease due to the cancellations among the full gauge invariant set of hadronic subprocesses. The  $q_t^{-2}$ -tail in  $e^+e^-$  annihilation causes a logarithmically rising central rapidity plateau  $dN/d\eta$  with growing c.m. energy, whereas the central gluon plateau in hadronic collisions does not increase (in this order of perturbation theory). The hadron/ $e^+e^-$  ratio thus decreases, with estimated values  $\sim 1.0$  ( $\sim 0.6$ ) for  $\sqrt{s} = 18$  (30) GeV. The fall-off at larger  $p_t$ -values is essentially responsible for the energy dependence of the central

plateau. If  $(q_t)_{\max} \sim f \cdot \sqrt{s}$ , the  $q_t^{-2}$ -tail generates a logarithmic rise. Viewing particle production as : color separation, stretched flux tubes,  $q\bar{q}$  creation, the plateau height is anticipated to depend exclusively on the available energy of the separating color system. Such function, as well as the fraction  $f$ , are expected to be independent of the particular physical process causing the color separation. As a result the "radiation" and resulting multiplicity are exclusively determined by the color structure and the available final-state c.m. energy. If  $q_t \leq \ell_t$  the competing contributions to  $dN/dy$  can cause a dip near  $y=0$  which is absent in  $e^+e^-$  annihilation. The hadron size influences (via  $\ell_t$ ) the plateau height, smaller hadrons give rise to a higher plateau. QED-like gluon radiation from separating color charges predicts the charge multiplicity to increase as a second order polynomial in  $\ln s$  <sup>76a)</sup> or even stronger <sup>76b)</sup>.

At sufficiently high energies low- $p_t$  collisions can generate partons with large invariant masses where perturbative QCD again applies. Assuming independent and coherent quark-quark scattering with a fixed momentum transfer  $\Delta \sim 1$  GeV the main features (additional to the above) of such processes are <sup>77)</sup>: the low- $p_t$  hadronic system arises from two components, the "spectators" with fixed transverse spread, and the "struck" quarks (with  $\sqrt{p_t^2} \sim 10$  GeV) giving rise to progressively broader hadron jets (similar to  $e^+e^-$ -jets), possibly of a forked structure. The  $\langle p_t^2 \rangle$  is thus expected to rise by a factor  $\sim 2$  as we go to collider energies and the longitudinal momentum distributions should soften with a possible violation of Feynman scaling. Gluon radiation from the incoming quarks causes a reduced invariant mass of the 'struck' quarks and hence smaller  $\langle p_t^2 \rangle$  and  $\langle n \rangle$  than for events due to valence quark scattering.

The dual-topological-unitarization(DTU) approach <sup>78)</sup> to multiparticle production assumes that during hadron collision tube-like color-singlet systems are created consisting of 3 and  $\bar{3}$  color charge at the two ends. Their moving in opposite directions stretches the connecting gluon flux

lines  
hadron  
proces  
treat  
paren  
over t  
•  $x_1$  and  
functi  
of two  
spect.  
The to  
centre  
At pr  
( $h_1 h_2$ )  
includ  
( $p\bar{p}$ )  
type, 1  
spin-  
hadron  
rising  
eventu  
appropri  
(fig. 3  
chain  
centra  
3/2 ab  
In  
centra  
valenc  
to res  
the mo  
that  
distrib  
quark

c rise.  
tubes,  
vely on  
on, as we  
lar  
radiatio  
or  
he  
is  
the  
ED-like  
re  
a) or  
partons  
fixed  
above)  
two  
e  
broader  
re. The  
der  
en with  
e  
quarks  
ark  
particle  
singlet  
to ends.  
n flux



lines , resulting in hadron production . Since in each colliding hadron there are minimal two quarks one may expect two (or more) such processes simultaneously to occur. The proton in these calculations is treated as a  $3(q)$  and  $\bar{3}(q\bar{q})$  system , the latter carrying most of its parent-hadron momentum. Practical calculations involve convolutions over the joint probability that the two-quark system takes fractions  $x_1$  and  $x_2$  of the incident momenta and over the  $e^+e^-$  fragmentation functions. The Pomeron thus arises through unitarity as a reflection of two non-interfering "chains" of particles each with its own rapidity spectrum as found in  $e^+e^-$  annihilation (at the corresponding energy) . The two spectra can be different in shape and mutually displaced, and the central plateau region can consequently arise from different scenario. At present energies the heights follow :  $(pp) < (\tilde{\chi}p) < (p\bar{p})$  where  $(h_1, h_2)$  indicates the two hadrons initiating the single particle soft-inclusive process.  $(pp)$  is the sum of heights of two shoulders while  $(p\bar{p})$  is the sum of two central maxima; the  $(\tilde{\chi}p)$  case, of  $(pp)$  and  $(p\bar{p})$  type, falls in between (fig.8 a,b) . Further characteristics are : no spin-1 and color exchange and no dependence on the size of the initial hadrons, quark counting applies , at higher energies appearance of a rapidly rising bump in  $(pp)$  near  $y=0$  , the hadronic central plateau heights eventually reach similar values about twice the  $e^+e^-$  plateau (at the appropriately reduced energy). The partonic three-chain mechanism (fig.8c) involving  $(q, \bar{q})$  chains only (as opposed to  $(qq, \bar{q}\bar{q})$  and  $(q, \bar{q})$  chains for the Pomeron) leads to a spectacular increase of the  $p\bar{p}$  central multiplicity height which at asymptotic energies lies a factor  $3/2$  above the Pomeron expectations <sup>79)</sup> .

In the valon-recombination model <sup>80)</sup> multi-hadron production in the central region is due to the glue and sea of the colliding hadrons. The valence quarks , on the contrary, will recombine with a parton from the sea to reproduce a hadron at large  $x$ . Since the sea parton has very small  $x$ , the momentum of the final state hadron will essentially be the same as that of the valence quark . In the further development of this model a distinction between the constituent quark ( = 'valon' ) and the current quark ( = 'quark' ) is made with a valon momentum distribution in the

nucleon  $G_{V/p}(x)$  and a quark momentum distribution in the valon  $F_V(x)$  constructed such that their convolution reproduces the deep-inelastic structure functions (fig.9a). A valon is physically interpreted as a valence-quark plus its associated sea quarks and gluons due to the dressing process in QCD. A low- $p_t$  hadron-hadron collision is then viewed as a multi-stage process: initial hadron  $\xrightarrow{(1)}$  valons  $\xrightarrow{(2)}$  partons  $\xrightarrow{(3)}$  valons  $\xrightarrow{(4)}$  produced hadrons. Stage (4), giving the probability of two (three) valons to recombine into a final state meson (baryon) (fig.9b), is governed by the recombination function (a joint multi-valon momentum distribution) whose open parameters are fixed by phenomenological analyses. This model describes successfully many single particle inclusive distributions in the fragmentation region, and its application on other processes (e.g. quark fragmentation, form factors, pion decay constant) does not signal significant inconsistencies.

In order to understand hadron production in the fragmentation regions a description for quark and diquark fragmentation into hadrons is needed. Point-like QCD fragmentation <sup>72)</sup> of quarks assumes that  $q\bar{q}$ -pairs are created out of the vacuum by lowest order quark-gluon diagrams with subsequent two-quark association into mesons. The fragmentation functions follow from folding the perturbative process (motivated by the far off-shell mass of the quarks) with the meson bound state wave function. Simple analyses lead to  $dN/dz \sim (1-z)^n$  where  $n = 2 n_H + n_p - 1$  is specified by simple counting rules.  $n_p$  = number of 'point-like' spectators to the emission and  $n_H$  = number of 'hadronic' spectators. The analysis of simple graphs indicates  $n=1,2$ . This reasoning, extended to diquark fragmentation with higher  $n$ -values, permits a qualitative understanding of the data. Valon-recombination <sup>80)</sup> instead operates with QCD evolved valon momentum distributions. Using the rules of the jet calculus <sup>81)</sup>, a two-quark momentum distribution is defined by valon-gluon splitting. The fragmentation function finally follows from a convolution over the two meson-quarks involving the recombination function. As a result  $dN/dz \sim (1-z) \bar{s}(p^2)^{+1}$  where  $\bar{s}(p^2)$  is the standard evolution parameter in

in the  
quark  
The ab  
to the  
the co  
We  
exchan  
culati  
fragme  
and su  
proces  
fragm  
fragm  
is pr  
(b) E  
functi  
predi  
betwe  
has b  
Si  
are s  
appro  
of th  
.  
On  
exper  
Their  
Weint  
angle  
The +  
and a  
and I

(x)  
stic  
as a  
.  
viewed  
two  
g.9b),  
momentum  
analyse  
distribu  
s (e.g.  
anal  
regions  
needed.  
are  
th  
function  
tion.  
is  
rs.  
ended to  
under-  
th QCD  
calculus  
ting.  
the  
t  
eter in

in the AF-corrections depending via the log-log function on the initial quark off-shell mass  $p^2$ , for typical values the exponent is  $\sim 2$ . The above two methods are distinct. The  $(1-z)$  power in the first one is due to the off-shell propagator in the tree-amplitude whereas it results from the convolution in the second one.

We turn to hadronic fragmentation. Three models exist: (a) gluon-exchange with point-like QCD fragmentation <sup>72)</sup> is in practical calculations viewed as a two-step process:  $q$  (or  $2q$ ) emission from the fragmenting proton according to the QCD predicted momentum distribution and subsequent QCD bremsstrahlung leading to meson formation. The overall process is therefore a convolution over the probability  $Q(x)$  to find the fragmenting parton system with momentum fraction  $x$  and over its QCD fragmentation function discussed above. Since the fragmentation process is predominant, its counting rule powers appear again in the final result. (b) DTU hadron formation <sup>78)</sup> follows the same rules. The fragmentation function however is parametrized with a  $n = 1 - 2 \alpha_p(t)$  exponent as predicted by the triple-Regge limit.  $t$  is the squared momentum difference between the fragmenting and the inclusive hadron. (c) Valon-recombination <sup>80)</sup> has been discussed earlier.

Significant differences of these approaches in the fragmentation regions are sparse. Definite conclusions about the validity of one or the other approach, which in the end even might merge, is premature. For a comparison of their predictions with the data we refer to recent reviews <sup>75)</sup>.

### 5. $W^\pm$ and $Z^0$ Production

One of the main motivations for constructing the  $p\bar{p}$ -collider was the experimental verification of the weak intermediate bosons:  $W^\pm$  and  $Z^0$ . Their discovery permits direct tests of gauge theory models. In the Weinberg-Salam model <sup>82)</sup> their masses are uniquely fixed by the Weinberg-angle  $\sin^2 \theta_W (= 0.23 \pm 0.015)$  with values:  $m_W = 77.9$  GeV and  $m_{Z^0} = 88.8$  GeV. The total widths, proportional to  $m_{W,Z}^3$ , depend on the number of leptons and quarks in the theory. Leptonic branching ratios are:  $B(W^\pm \rightarrow l^\pm \nu) \simeq 8\%$  and  $B(Z^0 \rightarrow l^+ l^-) \simeq 3\%$ . The production cross sections (see Table I) <sup>83)</sup>

are estimated by the parton model where the scale dependent momentum distributions (in leading-log approximation) are fixed by deep-inelastic lepton-hadron-scattering .

At the "reasonable" luminosity of  $L=10^{29} \text{ cm}^{-2} \text{ s}^{-1}$  (which possibly will be reached during the first year) one expects to collect 5-10 events per day of the type  $W^{\pm} \rightarrow \ell^{\pm}$  (fig.10) . Due to their weak coupling, the  $W^{\pm}$  are expected to be produced with polarisation which causes considerable asymmetry in the lepton spectra in the forward direction (fig.11) <sup>84)</sup>. About 75% of the  $W^{\pm}$  decay into hadronic channels, (heavy) quark and gluon jets are quite likely. The channel  $Z^0 \rightarrow \ell^+ \ell^-$  is experimentally cleaner, but an order of magnitude lower in cross section (fig.12) . The experimental effort is concentrated on the leptonic decays. They are thought to be the most promising ones with respect to signature and background because QCD jets of large  $p_t$  will probably outnumber the quark-jet decays of the weak bosons.

Weak boson production and subsequent decay into leptons is a rare process. About one event of the type  $W^{\pm} \rightarrow \ell^{\pm}$  is hidden among  $10^8$  normal hadronic events. The rarity is, however, compensated by effective triggering <sup>2)</sup>.

The discovery of the  $W^{\pm}$  and  $Z^0$  will open the possibility for several interesting investigations <sup>83)</sup>. As an example we mention the renormalization group summation of the perturbative QCD corrections <sup>4)</sup>.  $Z^0$  production offers the possibility to test its predictions at a large  $Q^2$  point where  $\alpha_s(Q^2)$  is small and the next-to-leading corrections are sufficiently dampened. The collider will start running at the highest possible energy. By decreasing  $\sqrt{s}$  (at  $Q^2 = M_{Z^0}^2$ ) we vary  $\tau$  to larger values . The QCD corrections manifest themselves strongest at the smallest  $\tau$ -values with substantial cross section decrease as  $\tau$  grows. Comparing with the simple scaling predictions, where the cross section remains roughly constant, we notice a significant difference (fig.13) <sup>85)</sup> which can be verified by the experiment.

6.

is stic

go

be \_11

de

pa ng,

be

lo

vy)

hi

t. ion

st

t to

d out-

fi

d

mal  
ering 2)

P ral

c lization

o. n

q there

v

o ergy.

f correcti

t ntial

o g

p dice

h

t

## 6. Drell-Yan and Related Processes

The study of Drell-Yan lepton-pair production <sup>86)</sup> with the collider is limited by the  $(1/Q^4)$  fall-off of the cross section (fig.14). By going to large  $s$ -values the small and smallest  $\sqrt{s}$ -range is therefore better tested than in earlier experiments. We further mention: the  $s$ -dependence of the  $\mu$ -pair average transverse momentum, the QCD-modified parton distribution at smallest  $\sqrt{s}$ -values, the K-factor, correlations between the off-shell photon and a jet, and the dynamical behaviour of low- $p_t$  hadrons associated with a Drell-Yan trigger <sup>87)</sup>.

The production of heavy narrow  $Q\bar{Q}$ -states <sup>88)</sup> such as  $J/\psi$ ,  $\chi_{c0}$  is of high interest. Several production mechanisms contribute: QZI-rule suppressed transitions from standard to heavy quarks, heavy quarks involved in the structure function of the colliding hadrons (particularly at large  $Q^2$ ), two-gluon annihilation producing a  $C=+1$  bound state which radiatively decays into vector mesons. The production cross sections for the presently known states follow a phenomenological scaling law <sup>89)</sup>:  $(\Gamma_h)^{-1} M^3 d\sigma/dx_L = f(s/M^2, x_L)$ .  $M$  is the meson mass,  $\Gamma_h$  the partial width of the meson decaying into ordinary hadrons, and  $x_L = 2p_L/\sqrt{s}$  is the Feynman scaling variable. The search for narrow vector states is limited by the overall production rate rather than by the background (fig.15). With sufficient counting rates, correlation measurements between the narrow states and opposite jets become possible giving more information about the underlying quark-gluon processes <sup>90)</sup>.

The production of open flavors <sup>91)</sup> is more copious than the production of massive lepton pairs. Perturbative QCD calculations assume either heavy flavor "creation" via quark/gluon annihilation or flavor "excitation" from the sea. They suffer from several shortcomings such as the precise knowledge of the distribution functions, the bound state effects, the influence of the primordial  $p_t$ ,  $A$ -dependence etc. For an extended overview we refer to ref.92. The cross section for open-beauty production is estimated  $\sim 10 \mu b$  (fig.16). However, due to its chain-like decays into lower mass hadrons, the experimental signatures are not clear enough to permit efficient triggering. Multi-lepton signatures or measurements of dilepton correlations might possibly disentangle a beauty-signal from background <sup>93)</sup>.

The production of prompt photons <sup>94,95)</sup> is another clean source of information on the constituent dynamics. Its 0-th order constituent process is QCD hard scattering (confinement type effects are ignored) such as  $q\bar{q} \rightarrow \gamma + g$ ,  $qg \rightarrow q + \gamma$  and  $q\bar{q} \rightarrow q\bar{q} + \gamma$ . As we go towards large  $x_t$ -values the  $q\gamma$  final state is expected to dominate whereas at low  $x_t$   $g\gamma$  is predominant. The  $\delta/\kappa^0$  ratio increases beyond 1 as  $p_t$  reaches 30-40 GeV/c. The single-photon inclusive distribution decreases roughly exponential. The order- $\alpha_s$  QCD processes give rise to away-side quark/gluon jets whereas accompanying towards-jets can only come from the order  $\alpha_s^2$  QCD graphs. Several studies come to mind: the gluon distribution can be determined,  $x_t$ -scaling can be verified over a wide range, correlations with the away-side jets permit the study of their fragmentation functions, higher-twist effects might be isolated.

#### 7. Higgs Particles, Technicolor, Three-Boson Coupling.

The standard  $SU_2 \times U_1$  model of the weak interactions describes successfully a wide range of phenomenological data with one single parameter  $\sin^2 \theta$ , and it provides definite information about the  $W^\pm$  and  $Z^0$  masses. However, there is a corner of the model that is still obscure, i.e. how the mass-generation comes about. In the original form, the intermediate boson masses are generated by the fundamental scalar Higgs fields <sup>96)</sup>. Three of them are used up for the mass-generation, and a neutral Higgs boson  $H^0$  is left as a physical particle. Though its coupling to the intermediate bosons and quarks are given by the model, its mass is completely unconstrained. Theoretical prejudice favors  $m_{H^0} \sim 10$  GeV.

Estimates of the decay modes as a function of its mass indicate a predominance of  $H^0 \rightarrow \tau^+\tau^-$ ,  $c\bar{c}$ ,  $b\bar{b}$  in the mass range  $4 \text{ GeV} < m_{H^0} < 12 \text{ GeV}$ , while for  $12 \text{ GeV} < m_{H^0} < 200 \text{ GeV}$  it preferentially decays into the heaviest  $Q\bar{Q}$  (or  $L^+L^-$ ) pairs. This suggests that  $H^0$ -decay may contain prompt leptons and/or strange particles. The cascade decay involving heavy quarks results in several final state leptons.

In hadron initiated reactions Higgs particles can be produced in several ways: (a) via two-gluon annihilation. The cross section in the collider energy range is estimated  $\sigma_{H^0} \sim 10^{-35} \text{ cm}^2$  (fig.17) <sup>97)</sup>. A recent study

on trile of  
their di of  
variable d)  
difficult ds  
spectrum at  
consider  $p_t$   
bosons (reases  
hadronic side  
with a from  
constrains-  
simple range,  
decaying mentation  
on two

The st  
 $SU_2 \times U_1$   
was receeessfully  
massless  $\theta$ ,  
which coever,  
similar mass-  
breaking masses  
Goldstone them  
scheme is left  
bosons ons  
in the ed.  
is estim  
 $H^0$ -exper  
detection 12 GeV,  
applied  
rate for  
at the heavy  
The dom  
into ge several  
of heav der  
study

on trilepton events <sup>93)</sup> concluded that useful signatures emerge from their dilepton mass spectrum and some newly proposed transverse momentum variable. An overwhelming background could make such attempt rather difficult. (b) via  $Q\bar{Q}$  (or  $Z^0$ )  $\rightarrow H^0 + \gamma$  with a peak in the photon spectrum. The large number of  $\gamma$  resulting from  $\pi^0$ -decay will form a considerable background problem. (c) via Higgs-bremsstrahlung off vector bosons (fig.18) <sup>98)</sup>. The bremsstrahlung of the  $H^0$  by a  $Z^0$  produced in hadronic scattering shows up as a bump in the di-lepton mass distribution with a fast fall-off at  $Q = m_{Z^0} - m_{H^0}$  <sup>99)</sup>. This possibility is however constrained by the large suppression factor of  $10^{-3}$ - $10^{-4}$  as compared to simple  $Z^0$  production, quite apart from the fact that the number of  $Z^0$  decaying into lepton pairs is restrained. (d) if  $m_{H^0} \gg 2 m_b$ , triggering on two hadron jets could offer another possibility.

The system of spinless Higgs-particles generating masses in the standard  $SU_2 \times U_1$  theory is unsatisfactory <sup>82)</sup>, technicolor <sup>100)</sup> as an alternative was recently proposed. The essential ingredients are: (i) a new set of massless technifermions, (ii) a corresponding set of gauge-technigluons which confine the techniquarks into technicolor singlet bound states - similar to QCD though at the  $\sim 1$  TeV mass scale, (iii) chiral symmetry breaking of the technicolor Lagrangian leading to a large number of  $0^-$  Goldstone bosons, (iv) they take over the rôle of the Higgs bosons. This scheme predicts a wealth of new particles notably the color-singlet bosons  $P^{0,3}$  with masses  $\lesssim 3$  GeV, and  $P^\pm$  with their masses anticipated in the 8-14 GeV range. The production of  $P^0$  via two-gluon annihilation is estimated to be predominant. The rate lies a factor 5 above analogous  $H^0$ -expectations. The  $l^+l^-$  decay mode offers a possibility for  $P^0$  detection although under a considerable background. Similar reasoning is applied on the (techni-) color-octet states  $P_8^{0,3}$ ,  $P_8^\pm$ . The production rate for the neutral state, again estimated via two-gluon annihilation, is at the pb-level; the rates for the other states are substantially below. The dominant decays of  $P_8^0$ , its mass is estimated around 250 GeV, will be into  $gg$  and heavy  $Q\bar{Q}$ . A significant signal could be: events with pairs of heavy quark jets.

Non-abelian gauge theories allow for tri-linear couplings such as  $W^+W^-Z^0$  or  $W^\pm W^\pm \gamma$  (101). The next step after the intermediate bosons are discovered consists in an experimental verification of their existence. If, for the identification of these processes, the weak decay modes are used, one aims at the experimental verification of higher order weak interaction effects. Based on simple Drell-Yan  $q\bar{q}$  annihilation the simultaneous production of two weak bosons (e.g.  $W^+W^- + X$ ) has been estimated (figs.19,20); the cross section rates are:  $\sigma(W^+W^-) \approx \sigma(W^\pm Z^0) \sim 10^{-36} \text{ cm}^2$ ,  $\sigma(Z^0 Z^0) \sim 10^{-37} \text{ cm}^2$  and  $\sigma(W^\pm \gamma) \sim 5 \cdot 10^{-35} \text{ cm}^2$ . We thus expect about 1 event in  $10^3 W^\pm$  events to contain a second gauge boson. In  $p\bar{p}$  collisions the  $W^+$  ( $W^-$ ) is preferably emitted along the proton (antiproton) initial direction; the  $Z^0$  however are emitted in both forward and backward cones. We have also indicated the rate for  $W^\pm \gamma$  production which allows for the determination of the  $W^\pm$   $\mathcal{R}$ -factor appearing in its magnetic momentum:  $\mu_W = (\frac{e}{2M_W})(1+\mathcal{R})$ . The angular distribution of  $p\bar{p} \rightarrow W^\pm \gamma + X$ , with  $\theta_{CM}$  chosen as the  $p \rightarrow W^-$  angle, reveals a characteristic minimum around  $\cos\theta_{CM} = -0.3$ ; its size depends sensitively on  $\mathcal{R}$ . The standard  $SU_2 \times U_1$  model predicts  $\mathcal{R} = 1$  with a vanishing cross section at the minimum point (fig.21).

### 8. Summary

With this paper we aimed to sketch the physics at the  $p\bar{p}$  collider by extrapolating from the present-day available theoretical and experimental information to the soon accessible energy range of maximum 540 GeV center-of-mass energy. The covered fields are: (a) insights from cosmic-ray data on the general features of hadronic events and possibly surprising new phenomena, (b) production of hadrons at large- and small- $p_t$ , (c) experimental verification of the weak bosons  $W^\pm$  and  $Z^0$ , (d) production of massive lepton pairs, new flavors and direct photons, (e) search for Higgs particles or technicolor, and the verification of the triple-boson couplings via boson-pair production. Our presentation repeatedly encountered perturbative QCD in its various applications, and it covered several key features of electromagnetic-weak unification.



# References

- (1) G. Rubbia, P. McIntyre and D. Cline, Proc. Int. Neutrino Conf. Aachen, 1976 (eds. H. Faissner, H. Reither and P. Zerwas) (Viehweg, Braunschweig 1977), p. 683; S. Van der Meer, Proton-Antiproton Colliding Beam Facility, Report CERN/SPC/423 (1978); Design Study of the pp Collider Beam Facility, Report CERN/PS/AA 78-3 (1978).
- (2) UA1 : A. Astbury et al., Proposal CERN/SPSC/78-06 (1973);  
 UA2 : M. Banner et al., Proposal CERN/SPSC/78-08, 54 (1978);  
 UA3 : B. Aubert et al., Proposal CERN/SPSC/78-15 (1978);  
 UA4 : G. Matthiae et al., Proposal CERN/SPSC/78-11 (1979);  
 R. Battiston et al., Proposal CERN/SPSC/79-10 (1979);  
 UA5 : M. G. Albrow et al., Proposal CERN/SPSC/78-10 (1978).
- (3) R. Horgan and M. Jacob, Proc. CERN School of Physics, Malente 1980, Report CERN 81-04 (1981); G. Goggi, Report CERN 81-04 (1981).
- (4) W. Marciano and H. Pagels, Phys. Rep. C36 (1978) 137; J. Ellis and C. T. Sachrajda, Proc. Cargèse Summer Inst. on Quarks and Leptons, 1979 (Plenum, New York 1980), p. 285.
- (5) J. Ellis, Proc. Summer Institute on Particle Physics, SLAC 1978 (Ed. W. Zipf), p. 69; J. D. Bjorken, Proc. Arctic School of Physics, Åkäslompolo 1980, Report FERMILAB-Conf-80/86-THY.
- (6) T. K. Gaisser and G. B. Yodh, Ann. Rev. Nucl. Sc. 30 (1980) 475.
- (7) Y. Sato et al., J. Phys. Soc. Jpn. 41 (1976) 1821.
- (8) H. Fuchi et al., Proc. 16th Int. Cosmic Ray Conf., Kyoto 1979, Vol. 6, p. 245 (Inst. Cosmic Ray Research, Univ. of Tokyo, 1979).
- (9) W. Thomé et al., Nucl. Phys. B129 (1977) 365.
- (10) J. Linsley and A. A. Watson, Phys. Rev. Lett. 46 (1981) 459.
- (11) R. W. Ellsworth et al., Phys. Rev. D23 (1981) 764; N. Arata, Niels Bohr Inst. Report NBI-81-24 (1981).
- (12) J. A. Goodman et al., Phys. Rev. D19 (1979) 2572, and references therein.
- (13) V. I. Yakovlev et al., Proc. 16th Int. Cosmic Ray Conf., Kyoto 1979, Vol. 6, p. 59 (Inst. Cosmic Ray Research, Univ. of Tokyo, 1979), and references therein.
- (14) C. M. G. Lattes et al., Phys. Rep. 65 (1980) 151, and references therein.
- (15) R. W. Ellsworth et al., Phys. Rev. D23 (1981) 771.

- (16) J.D.Bjorken and L.D.McLerran, Phys.Rev.D20 (1979) 2353 .
- (17) S.A.Chin and A.K.Kerman, Phys.Rev.Lett.43 (1979)1292 .
- (18) A.K.Mann and H.Primakoff, Phys.Rev.D22 (1980) 115.
- (19) R.Kinnunen and C.Rubbia, Report CERN-EP/81-36 (1981) .
- (20) a) S.J.Brodsky, in "Quantum Chromodynamics", LaJolla Institute 1978,  
AIP Conf.Proc.55, (Eds.W.Frazer and F.Henyey, N.Y.1979), p.2 .  
S.J.Brodsky, Proc.Summer Inst.on Particle Physics, SLAC 1979,  
(ed.A.Mosher), p.133 .  
b) R.D.Field, in "Quantum Chromodynamics", La Jolla Institute 1978,  
AIP Conf.Proc.55, (Eds.W.Frazer and F.Henyey, N.Y.1979), p.97 .
- (21) S.J.Brodsky and N.Weiss, Phys.Rev.D16(1977) 2325; P.Eckert, Geneva U.,  
UGVA-DPT 1981/01-276; G.J.Maxwell and M.J.Teper, Z.f.Physik C8 (1981)  
295 .
- (23) M.Furman et al., Nucl.Phys. B173(1980)397; I.Hinchliffe, Proc.XX  
Int.Conf.High Energy Physics 1980, Madison, AIP Conf.Proc.68,  
N.Y.1981 (eds.L.Durand and G.Pondrom) p.114 .  
For the analogous calculations in the Drell-Yan process see :  
B.Humpert and W.L.van Neerven, Nucl.Phys.B178 (1981)498, and  
Nucl.Phys. B184 (1981)225 .
- (24) a) F.Martin , Phys.Rev. D19(1979)1382; R.L.Thews, Proc.XX Int.Conf.  
High Energy Physics 1980, Madison, AIP Conf.Proc.68, N.Y.1981  
(eds.L.Durand and G.Pondrom) p.128; E.Reya, Dortmund U., DO-TH  
80/27 (1980) .  
b) R.Cutler and D.Sivers, ref.32.  
c) S.J.Brodsky and J.F.Gunion, Phys.Rev. D19 (1979) 1005 .  
d) M.Gluck, E.Hoffman and E.Reya, Dortmund U., DO-TH 80/27 (1980) .  
e) R.P.Feynman, R.D.Field and G.C.Fox, Phys.Rev. D18 (1978)3320 .
- (25) M.A.Faessler, "Quark Interactions with Nuclei", MPI-Heidelberg,  
Internal Report MPI-H 1980 V (1980), and CERN-EP/81-42 (1981);  
A.Dar, Europhysics Conf., Erice 1981, Technion-PH-81-26 (1981);  
A.Capella and J.Tran Thanh Van, Paris U., LPTHE 81/14 (1981);  
C.B.Chiu, Europhysics Conf., Erice 1981, Texas U.at Austin, DOE-ER-  
03992-439 (1981) .

- (26) a) D.Sivers, S.J. Brodsky and R. Blankenbecler, Phys. Rep. G23 (1976) 1 .  
 b) E.L. Berger, T. Gottschalk and D. Sivers, Phys. Rev. D23 (1981) 99 .  
 c) E.L. Berger and S.J. Brodsky, Argonne Report ANL-HEP-81-14 (1981) .
- (27) A.P. Contogouris et al., Phys. Rev. D17 (1978); M. Fontannaz and D. Schiff, Nucl. Phys. B132 (1978) 457; J.F. Owens and D. Kimel, Phys. Rev. D18 (1978) 3313; R.D. Field, Phys. Rev. Lett. 40 (1978) 997; F. Halzen et al., Phys. Rev. Lett. 40 (1978) 991; R. Caswell et al., Phys. Rev. D18 (1978) 2415 .
- (28) a) M. Jacob, Proc. Int. Conf. High Energy Physics 1979, Geneva, p. 473 .  
 b) P. Darriulat, Ann. Rev. Nucl. Sci. 30 (1980) 159 .  
 c) N.A. McCubbin, Rutherford Laboratory Report (1981) .
- (29) P. Söding and G. Wolf, DESY 81-013 (1981) .
- (30) S.J. Brodsky and G. Farrar, Phys. Rev. D11 (1975) 309; R. Blankenbecler and S.J. Brodsky, Phys. Rev. D10 (1974) 2973 .
- (31) see for example: B. Humpert and W.L. van Neerven, Phys. Lett. 101 (1981) 101, and Ref. TH. 3040-CERN (Phys. Rev.) .
- (32) R. Cutler and D. Sivers, Phys. Rev. D16 (1977) 679 and Phys. Rev. D17 (1978) 196; J.F. Owens, E. Reya and M. Glück, Phys. Rev. D18 (1978) 1501; B.L. Combridge, J. Kripfganz and J. Ranft, Phys. 70B (1977) 234 .
- (33) a) M. Glück and E. Reya, Phys. Lett. B98 (1981) 44 .  
 b) C.E. Carlson and P. Hoyer, NORDITA Report 81/21 (1981) .
- (34) a) T. Kinoshita, J. Math. Phys. 3 (1962) 650; T.D. Lee and M. Nauenberg, Phys. Rev. B133 (1964) 1549; N. Nakanishi, Progr. Theor. Phys. 19 (1958) 159.  
 b) R. Doria, J. Frenkel and J.C. Taylor, Nucl. Phys. B163 (1980) 93; A. Andrási et al., Nucl. Phys. B182 (1981) 104; C. Di Lieto et al., Nucl. Phys. B183 (1981) 223.
- (35) A.H. Mueller, Phys. Rev. D9 (1974) 963; H.D. Politzer, Nucl. Phys. B129 (1977) 301; R. Ellis, H. Georgi, M. Machacek, H. Politzer, Nucl. Phys. B152 (1979) 285; D. Amati, R. Petronzio and G. Veneziano, Nucl. Phys. B140 (1978) 54; B. Humpert and W.L. van Neerven, Phys. Lett. 102B (1981) 426 and Ref. TH. 3086-CERN (Phys. Rev.); S. Libby and G. Sterman, Phys. Lett. 78B (1978) 618; C.T. Sachrajda, Phys. Lett. 73B (1978) 185 .
- (36) a) R. Baier et al., Nucl. Phys. B118 (1977) 139; J.F. Gunion and B. Petersson, Phys. Rev. D22 (1980) 629; A.P. Contogouris, R. Gaskell and A. Nicolaidis, Phys. Rev. D17 (1978) 2992; R.P. Feynman, R.D. Field and G.C. Fox, Nucl. Phys. B128 (1977) 1 .  
 b) R. Baier, J. Engels and B. Petersson, Z. f. Physik C2 (1977) 265; J.F. Owens, Phys. Rev. D20 (1979) 221 .

- (37) a) A.Schiller, J.Phys.C5(1979)1329, Z.Kunszt and E.Pietarinen, Nucl.Phys.C2(1979)355, G.Bordes and A.Nicolaidis, Phys.Rev. D22(1980)1251. (53 arinen, s.Rev. (54  
b) T.Gottschalk and D.Sivers, Phys.Rev.D21(1980)102, T.Gottschalk, E.Monsay and D.Sivers, Phys.Rev.D21(1980)1799. (55 ottschalk
- (38) W.Geist, CERN/EP 81-79 (1981), these proceedings.
- (39) R.Horgan and M.Jacob, Nucl.Phys.B179(1981)441.
- (40) S.Pokorski and S.Sosnowski, Z.f.Physik C7 (1981)221.
- (41) P.M.Fishbane, C.S.Lam and T.N.Yan, Phys.Rev.D20(1979) 2960, C.S.Lam and B.A.Li, SLAC-PUB-2724 (1981). (56 60, C.S.Lam (57
- (42) R.Cutler and D.Sivers, ref.32, J.Dias de Deus and N.Sakai, Phys.Lett. 86B (1979) 321. (58 i, Phys.Lett
- (43) M.Cicuta, Phys.Rev.Lett. 43 (1979) 826, P.Butera, G.M.Cicuta and W.Enriotti, Phys.Rev.D21(1980) 972. (59 sta and
- (44) W.Marciano and E.Pagels, ref.4, A.J.Duras, Proc.XX Int.Conf.High Energy Physics 1980, Madison, AIP Conf.Proc.68, N.Y.1981 (eds. L.Durand and G.Pondrom), p.785. (57 f.High eds.
- (45) G.L.Kane and Y.P.Yao, Nucl.Phys.B137(1978)313.
- (46) see for instance: R.Jackiw, Proc.XX Int.Conf.High Energy Physics 1980, Madison, AIP Conf.Proc.68 (eds.L.Durand and G.Pondrom) p.895. (6 Physics m)p.895. (61
- (47) R.Hagedorn and J.Rafaelski, Ref.TH.2947, 2969-CERN (1980). (62 )
- (48) for reviews see: J.D.Bjorken, Proc.Summer Institute on Particle Physics, SLAC 1979 (ed.A.Mosher) p.219, P.M.Fishbane, Virginia U. (Febr.1981); J.F.Donoghue, VI Int.Conf.Meson Spectroscopy, Brookhaven NITCPT (1980). (63 Particle inia U. w,
- (49) H.Fritzsch and P.Minkowski, Nuov.Cim 30A (1975)391, V.Zakharov, Proc.XX Int.Conf.High Energy Physics 1980, Madison, AIP Conf.Proc. 68, N.Y.1981 (eds.L.Durand and G.Pondrom) p.1027, V.A.Novikov et al., Nucl.Phys.B165(1980)67. (64 harov, (65 onf.Proc. kov et al.
- (50) R.Jaffe and K.Johnson, Phys.Lett.60B (1976) 201. (6
- (51) D.Robson, Nucl.Phys.B130(1977)328, J.J.Coyne et al., Phys.Lett. B91(1980)259 and Phys.Lett.B99(1981)353, C.E.Carlson et al., Phys.Rev.D23(1981)2765. (6 Lett. al., (6
- (52) H.Suura, Phys.Rev.Lett.44(1980), K.Ishikawa, Phys.Rev.D20 (1979)731. (1979)731

- (53) J.Kogut, D.K.Sinclair and L.Susskind, Nucl.Phys. B114 (1976)199 .
- (54) Y.M.Cho, Phys.Rev.Lett. 46 (1981)302 ,and references therein .
- (55) a) P.G.O.Freund and Y.Nambu, Phys.Rev.Lett. 34 (1975)1645; J.Bolzan, W.Palmer and S.Pinsky, Phys.Rev. D14 (1976)3202; J.Willemsen, Phys.Rev. D13 (1976)1327; A.Salomone, J.Schechter and T.Tudron, Phys.Rev. D23 (1981)1143; I.J.Muzinich and F.Paige, Phys.Rev. D21 (1980)1151 .  
b) S.J.Lindenbaum, Brookhaven report, BNL-28823, BNL-28498 (1980), BNL-29768 (1981) .
- (56) C.N.Yang, Phys.Rev. 77 (1950)242 .
- (57) H.Goldberg, Northeastern U., NUB-2397 (1979); R.Capps, Prudue U. (1979); C.E.Carlson and T.Hans-Hanson, Nordita, NORDITA-81-19 (1981) .
- (58) J.F.Donoghue, K.Johnson and B.A.Li, Phys.Lett. B99 (1981)416; G.Veneziano, Nucl.Phys. B117 (1976)519; J.F.Donoghue, Proc. XX Int. Conf. on High Energy Physics 1980, Madison, AIP Conf. Proc. 68, N.Y. 1981 (eds. L.Durand and G.Pondrom) p.35 .
- (59) M.Chanowitz, Phys.Rev.Lett. 46 (1981)981; K.Ishikawa, Phys.Rev.Lett. 46 (1981)978; S.Meshkov, Proc. XX Int. Conf. High Energy Physics 1980, Madison, AIP Conf. Proc. 68, N.Y. 1981 (eds. L.Durand and G.Pondrom) p.732; V.A.Novikov et al., Nucl.Phys. B165 (1980)55; H.Lipkin, Argonne Report ANL-HEP-81-23 (1981) .
- (60) A.L.Mueller, Phys.Rev. D2 (1970)2963 .
- (61) R.P.Feynman, "Photon-Hadron Interactions", W.A.Benjamin, Inc. (1972) .
- (63) a) G.Giacomelli, Phys.Rep. 23 (1976); E.Predazzi, Riv.Nuov.Cim. 2 (1979) 1.  
b) U.Amaldi, Ann.Rev.Nucl.Sci. 26 (1976)385; U.Amaldi and K.R.Schubert, Nucl.Phys. B166 (1980)301 .
- (64) U.Amaldi et al., Phys.Lett. B66 (1977)390 .
- (65) A.J.Buras and J.Dias de Deus, Nucl.Phys. B71 (1974)481; P.Landshoff, Proc. 17th Int. Conf. High Energy Physics 1974, London, p.V57 .
- (66) T.T.Chou and C.N.Yang, Phys.Rev.Lett. 46 (1981)764; Phys.Rev. D19 (1979) 3268; C.Bourrely, J.Soffer and T.T.Wu, Phys.Rev. D19 (1979) 3249; R.Goggi, ref.3 .
- (67) A.R.White, Ref.TH.2976, 3058-CERN (1980,81) .

- (68) a) H.Abarbanel et al., Phys.Rep.21 (1976), M.Baker and Z.Ter-Martirosyan, Phys.Rep.28(1977), M.Moshe, Phys.Rep.37 (1978) .  
b) J.Baumel, M.Feingold and M.Moshe, Technion-PH-81-28 (1981) .
- (69) S.Nussinov, Phys.Rev.Lett.34(1975)1286, F.E.Low, Phys.Rev.D12 (1975)163 . (81
- (70) J.F.Gunion, Triangle Meeting , Visegrad 1981 . (82
- (71) J.F.Gunion and D.E.Soper, Phys.Rev. D15 (1977) 2617 . (83
- (72) S.J.Brodsky and J.F.Gunion, Phys.Rev.Lett.37 (1976)402, J.F.Gunion, Davis U.Report,UCD-81/2; J.F.Gunion, Proc.XI Multiparticle Symposium 1980, Brugge (eds.E.DeWolff and F.Verbeure, Universitaire Instelling Antwerpen) p.767 . (84 nion, aire
- (73) a) J.Pumplin and E.Lehmann, Z.f.Physik C9 (1981) 25 . (85  
b) G.Bertsch et al., SLAC-PUB-2748 (1981) . (86  
c) A.Kaidalov, Phys.Rep. 50 (1979) (87
- (74) W.Frazer et al., Rev.Mod.Phys.44 (1972)284, L.Van Hove, Phys.Rep.1(1971). (88 ab.1(1971).
- (75) W.Kittel, Nijmegen Univ.Report, HEW 203 (1981), P.V.Chliapnikov, Proc. XI Multiparticle Symposium 1980, Brugge (eds.E.DeWolff and F.Verbeure, Universitaire Instelling Antwerpen )p.2 . (89 nd
- (76) a) S.J.Brodsky and J.F.Gunion, Phys.Rev.Lett.37 (1976) 402 . (90  
b) A.Bassetto et al., Nucl.Phys. B163 (1980) 477; W.Furmanski et al., Nucl.Phys. B155 (1979) 253 . (91 et
- (77) S.Pokorski and S.Wolfram, CALT-68-795 (1981) . (92
- (78) a) A.Capella, Lectures at the Europhysics Study Conference, Erice 1981, Paris U.Report LPTPE 81/10 (1981) . (93  
b) R.Peschanski, Proc. XI Multiparticle Symposium 1980, Brugge (eds.E.DeWolff and F.Verbeure, Universitaire Instelling Antwerpen) p.117 . (94  
c) C.B.Chiu, Proc.XX Int.Conf.High Energy Physics 1980, Madison, AIP Conf.Proc.68, N.Y.1981 (eds.L.Durand and G.Pondrom) p.30; Lectures at Europhysics Study Conference, Erice 1981, Texas Univ.Report DOE-ER-03992-439 (1981) . (95 on, 30,  
d) ref.72 . (96
- (79) U.P.Sukhatme , Phys.Rev.Lett. 45 (1980) 5 . (97
- (80) a) R.C.Hwa, Lectures at the Europhysics Conference, Erice 1981, Oregon Univ.Report OITS-155 (1981), Invited Contribution to the Los Alamos Workshop 1981 on "Nuclear and Particle Physics at Energies up to 31 GeV", Oregon Univ.Report, OITS-159 (1981), and references therein . (98 1, to the 31),

- b) L. Van Hove Acta Phys. Austr. Suppl. XXI (1979) 621, Proc. of the XII Int. Symposium on Multiparticle Dynamics 1981, Notre Dame (Indiana), Report Ref. TH.3133-CERN (1981) .
- (81) K. Konishi, Proc. XI Multiparticle Symposium 1980, Brugge (eds. E. DeWolff and F. Verbeure, Universitaire Instelling Antwerpen) p. 228 .
- (82) for a recent review see : J. D. Bjorken, ref. 5 .
- (83) C. Quigg, Rev. Mod. Phys. 49 (1977) 297, F. E. Paige, Proc. of the Topical Workshop on the Production of New Particles in Super High Energy Collisions, Madison 1979 (eds. V. Barger and E. Halzen) .
- (84) P. Aurenche, Annecy-le-Vieux Report LAPP-TH-36 (1981) .
- (85) B. Humpert and W. L. van Neerven, Phys. Lett. B93 (1980) 456 .
- (86) R. Stroynowski, SLAC-PUB-2650 (1980), G. Matthiae, CERN/EP-80-183 (1980) .
- (87) R. C. Hwa , 13th Reno. Moriond, March 1978, p. 197 .
- (88) R. J. N. Phillips, Proc. XX Int. Conf. on High Energy Physics 1980, Madison, AIP Conf. Proc. 68, N.Y. 1981 (eds. L. Durand and G. Pondrom) p. 1471 .
- (89) T. K. Gaisser et al. , Phys. Rev. D15 (1977) 2572 .
- (90) E. Reya , DESY 79/88 (1979) .
- (91) B. L. Combridge, Nucl. Phys. B151 (1979) 429, S. Pakvasa et al. Phys. Rev. D20 (1979) 2862 .
- (92) S. Wojcicki, Proc. XX Int. Conf. on High Energy Physics 1980, Madison, AIP Conf. Proc. 68, N.Y. 1981 (eds. L. Durand and G. Pondrom) p. 1430 .
- (93) W. Y. Keung, L. L. Chau-Wang and S. C. C. Ting , Brookhaven Report ENL-29598 (May 1981) ; G. Penso et al., Rome Univ. Report, No 256 (June 1981) .
- (94) F. Halzen and D. M. Scott, Proc. XX Int. Conf. on High Energy Physics 1980, Madison, AIP Conf. Proc. 68 , N.Y. 1981 (eds. L. Durand and G. Pondrom) p. 172; P. Aurenche, ref. 84 .
- (95) see ref. 39 .
- (96) A. I. Vainshtein et al. , Sov. Phys. Usp. 23 (1980) 429, G. Barbellini et al. DESY 79/27 (1979) .
- (97) H. Georgi et al. , Phys. Rev. Lett. 40 (1978) 692 .

- (98) S.L.Glashow et al. ,Phys.Rev.D18 (1978) 1724 .
- (99) L.L.Chau-Wang, Brookhaven Report BNL-29465 (1981) .
- (100) S.Dimopoulos, Nucl.Phys. B168 (1980)69; G.Barbellini et al.  
DESY- ?/81 .
- (101) K.O.Michaelian et al. Phys.Rev. Lett. 43 (1979) 746; R.W.Brown  
and K.O.Michaelian ,Phys.Rev.D19 (1979) 922; R.W.Brown et al.,  
Phys.Rev.D20 (1979) 1164 .

| Weak Bosons   | $W^+$                         | $Z^0$                             |
|---|-------------------------------|-----------------------------------|
| Mass  | $M_W = 77.8 \text{ GeV}$      | $M_{Z^0} = 88.6 \text{ GeV}$      |
| Total Decay Width   | $\Gamma_W = 2.47 \text{ GeV}$ | $\Gamma_{Z^0} = 2.49 \text{ GeV}$ |
| Production Rate<br>at $\sqrt{s} = 540 \text{ GeV}$                    | $\sim 3 \text{ pb}$           | $\sim 2 \text{ pb}$               |
| Lepton Events/Day<br>( $L = 10^{30} \text{ cm}^{-2} \text{ s}^{-1}$ ) | 50 - 100                      | 5 - 10                            |

Table 1



Figure Captions

- Fig.1 : Order- $g^2$  QCD diagrams contributing to  $qg$ -scattering with the triple-gluon vertex shown in (c) .
- Fig.2 : Transverse thrust distribution for the different subprocesses; the dotted curves indicate the  $p_t$ -smeared two-jet contribution.
- Fig.3 :  $P_{out}$  distribution with a trigger momentum  $p_t \sim 7-8$  GeV/c at various  $x$ -bins. The smeared 3-jet contribution is shown by the dashed curves.
- Fig.4 : Inclusive  $\pi^0$  production at large- $p_t$  as measured at the ISR.
- Fig.5 : Comparison between the jet- and single particle rates.
- Fig.6 : Predicted jet-rates at the  $p\bar{p}$  collider.
- Fig.7 : a) Two-gluon exchange in the Low-Nussinov-model for the Pomeron .  
b) Four of the 16 diagrams contributing to the coherent Low-Nussinov-model ; the last two diagrams contribute with a negative sign.  
c) Soft-gluon radiation in the low-Nussinov-model.
- Fig.8 : a) Two displaced chains in the DTU-model and the resulting  $y$ -distribution.  
b) Short-long range chains in the DTU-model and the resulting  $y$ -distribution.  
c) Three-chain contribution in  $p\bar{p}$  annihilation; the resulting  $y$ -distribution is compared with the analogous of the Pomeron.
- Fig.9 : a) Deep-inelastic scattering in the valon-recombination model.  
b) Pion generation via valon-antivalon recombination.
- Fig.10 :  $P_t$ -spectrum of leptons originating from  $W^\pm, Z^0$  and Drell-Yan .
- Fig.11 : Three dimensional distribution of the single-lepton spectrum in  $p\bar{p}$  collisions.
- Fig.12 : Total cross section for  $Z^0$  production with (solid curves) and without (dashed curves) QCD corrections.
- Fig.13 : The  $Z^0$ - and DY-production cross sections; A and B are defined in ref. 85 .

Fig.14 : Invariant mass spectrum of lepton pairs via  $Z^0$ , DY and heavy quarks .

Fig.15 : a) Inclusive cross sections for  $J/\psi(\cdot)$  production , and scaled up  $\phi(\Delta)$  and  $\psi'(\square)$  predictions .

b) Production of lepton-pairs via heavy onia: inclusive cross section times branching ratio .

Fig.16 : Total cross section for beauty production in  $p\bar{p}$  collisions.

Fig.17 : Inclusive Higgs-particle production via two-gluon annihilation at  $\sqrt{s} = 27, 60, 400$  GeV (fine, horizontal, vertical shading) .

Fig.18 : Rate of associated production of Higgs meson with  $W^\pm$  or with  $Z^0$  versus  $M_H$ , expressed as a fraction of total  $W^\pm$  or  $Z^0$  production .

Fig.19 : The total cross section for  $p\bar{p} \rightarrow W^+W^- + X$ ,  $p\bar{p} \rightarrow W^\pm Z^0 + X$ , and  $p\bar{p} \rightarrow Z^0Z^0 + X$  ( $x = \sin^2 \theta = 0.2$ ) .

Fig.20 : Total cross section for  $p\bar{p} \rightarrow W^+W^- + X$  as a function of the W-mass.

Fig.21 : The differential cross section  $d\sigma/d\cos\theta$  for  $p\bar{p} \rightarrow W^\pm \gamma + X$  and  $p\bar{p} \rightarrow W^\pm \gamma + X$  .  $\theta$  is the angle between the  $W^\pm$  and the proton in the  $W^\pm \gamma$  c.m. system .  $\sqrt{s} = 540$  GeV and  $M_W = 80$  GeV. A photon cut  $E_\gamma > 30$  GeV has been applied.

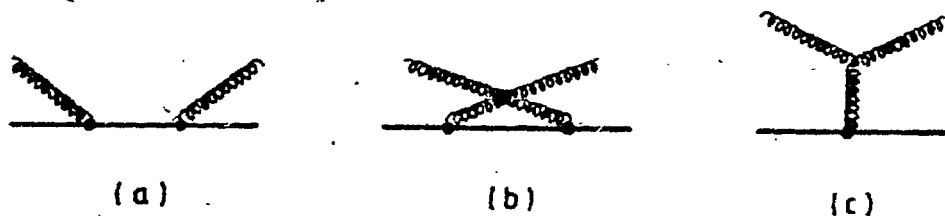


Fig.1

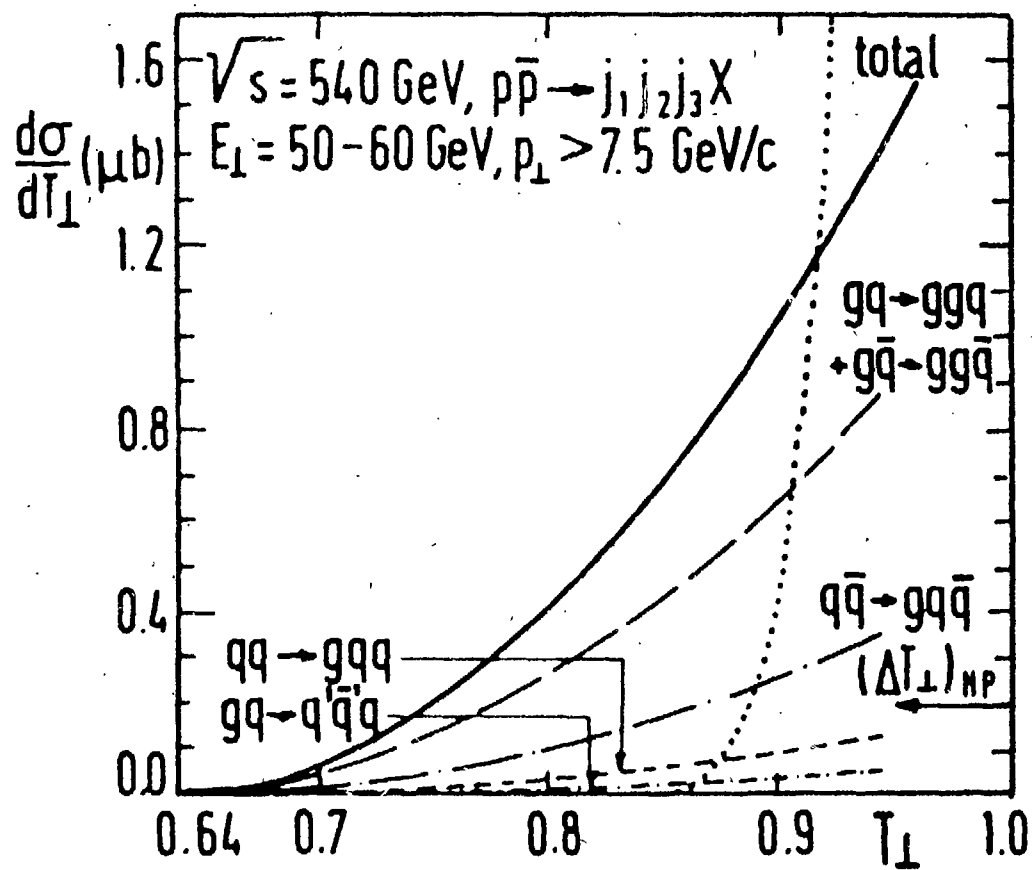


Fig. 2

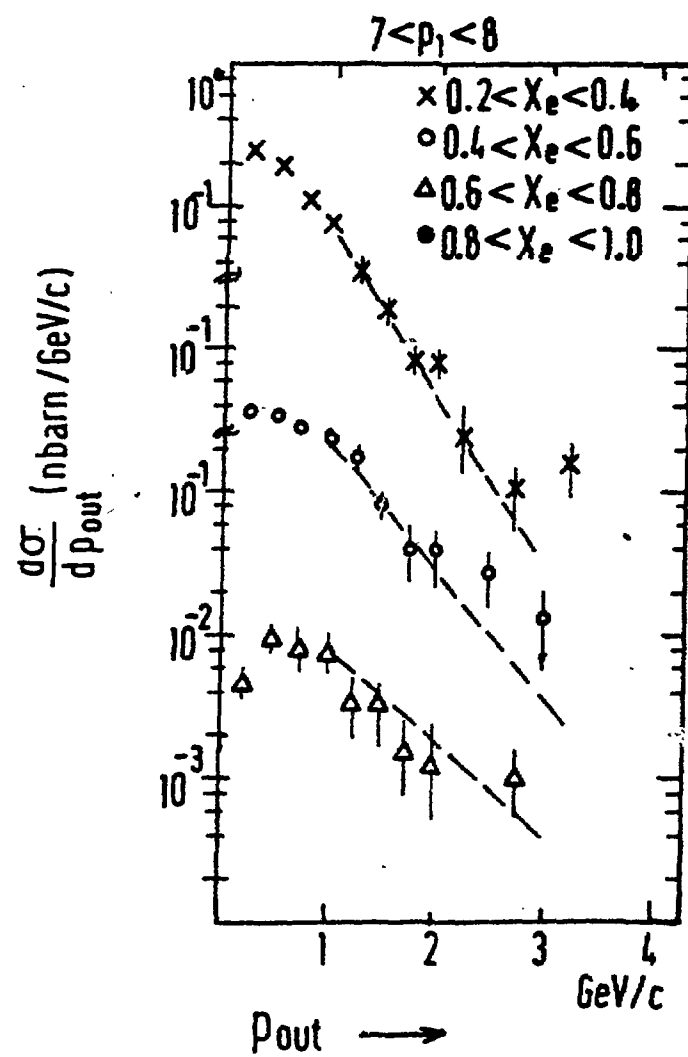


Fig.3

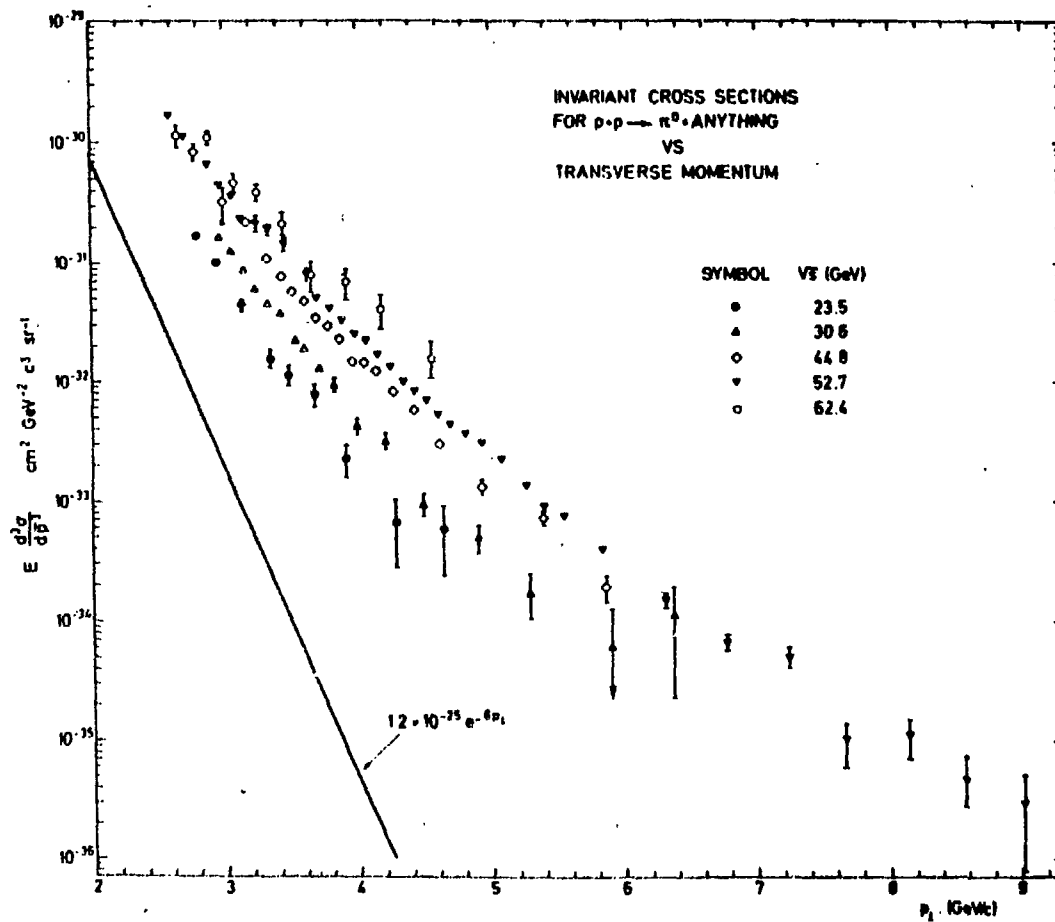


Fig. 4

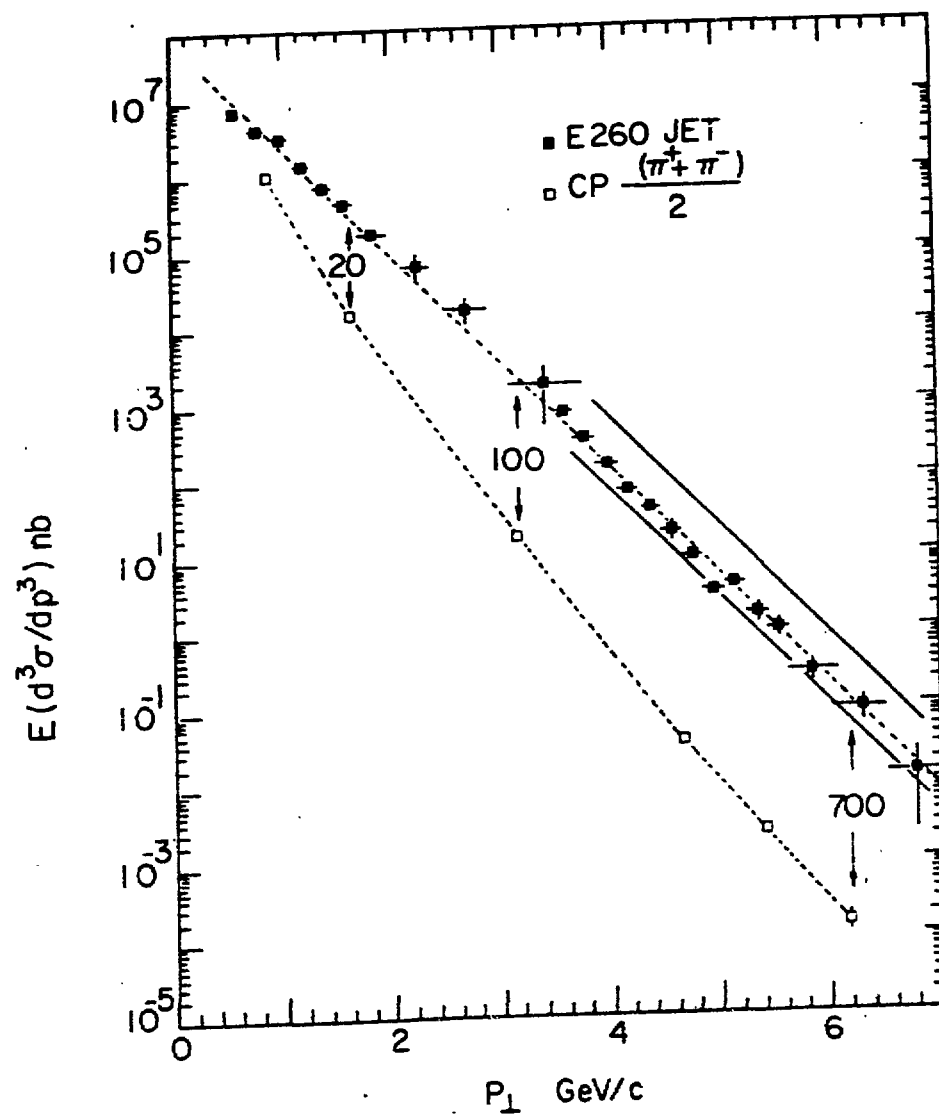
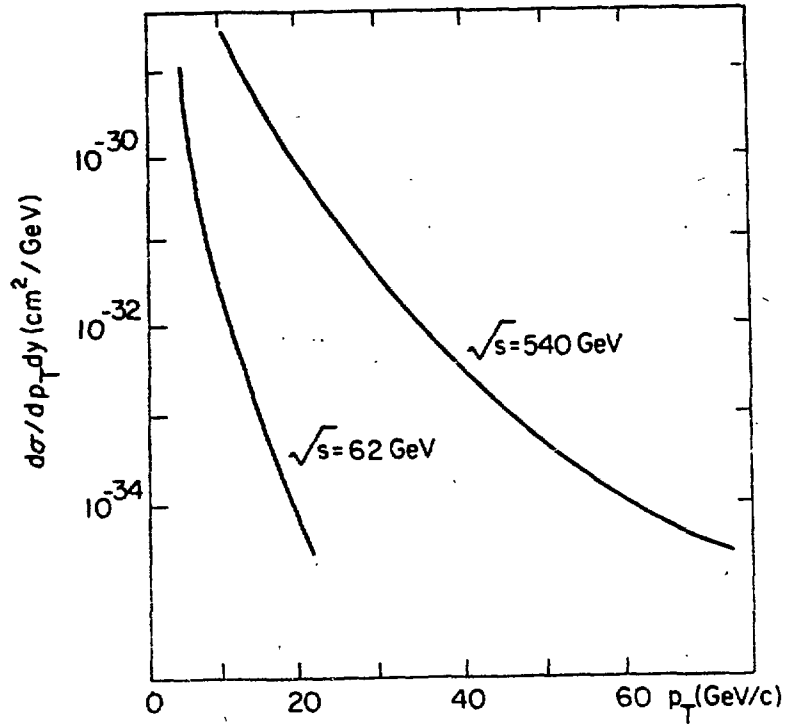


Fig.5

Fig.6

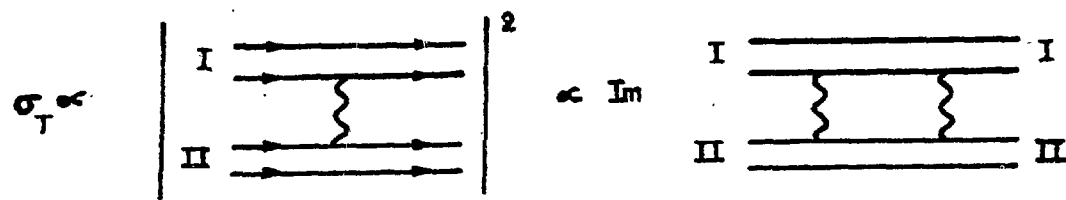


Fig. 7a

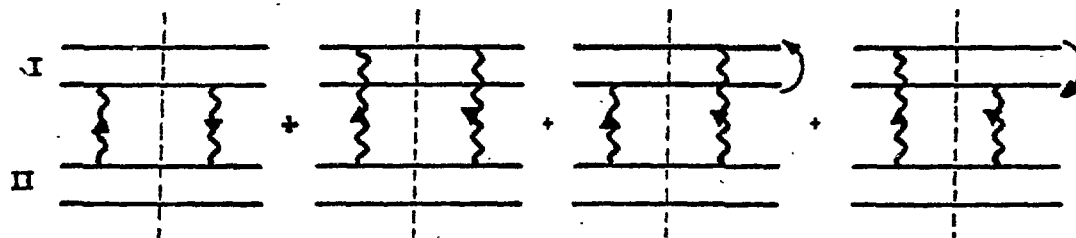


Fig. 7b

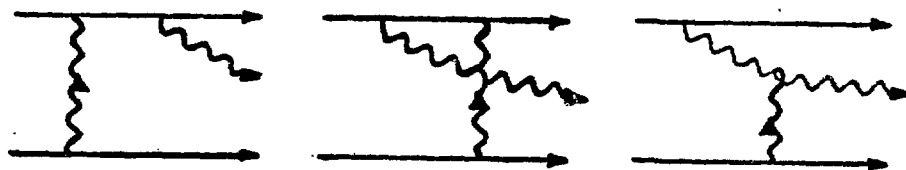


Fig. 7c



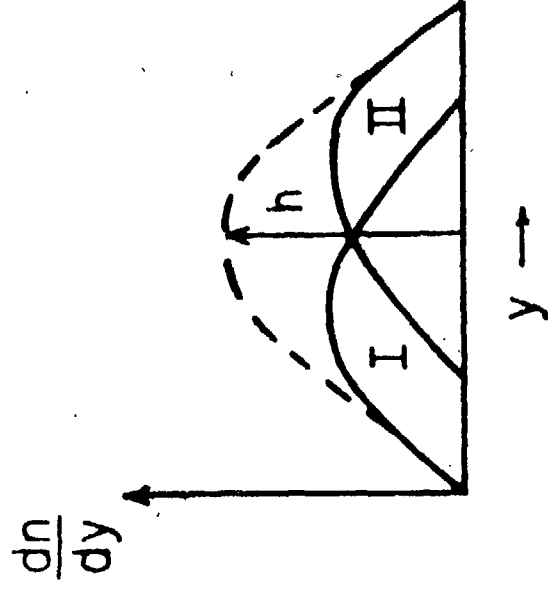
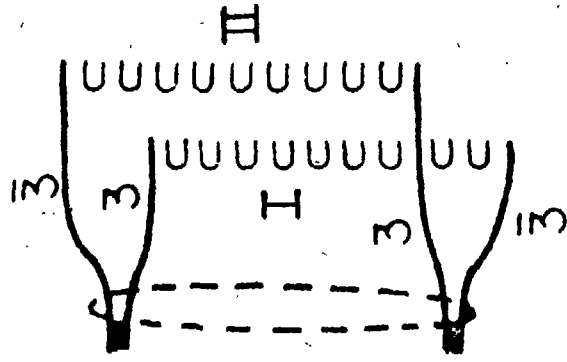


Fig. 8a

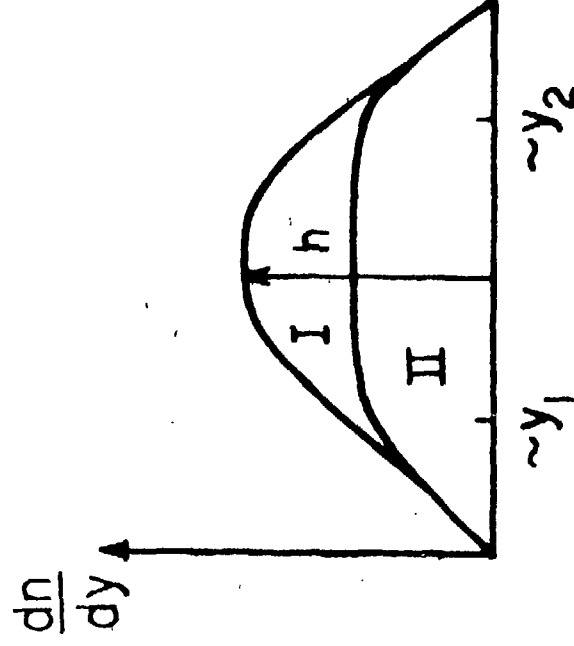
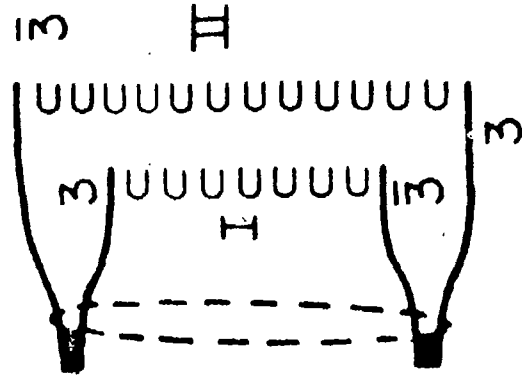


Fig. 8b

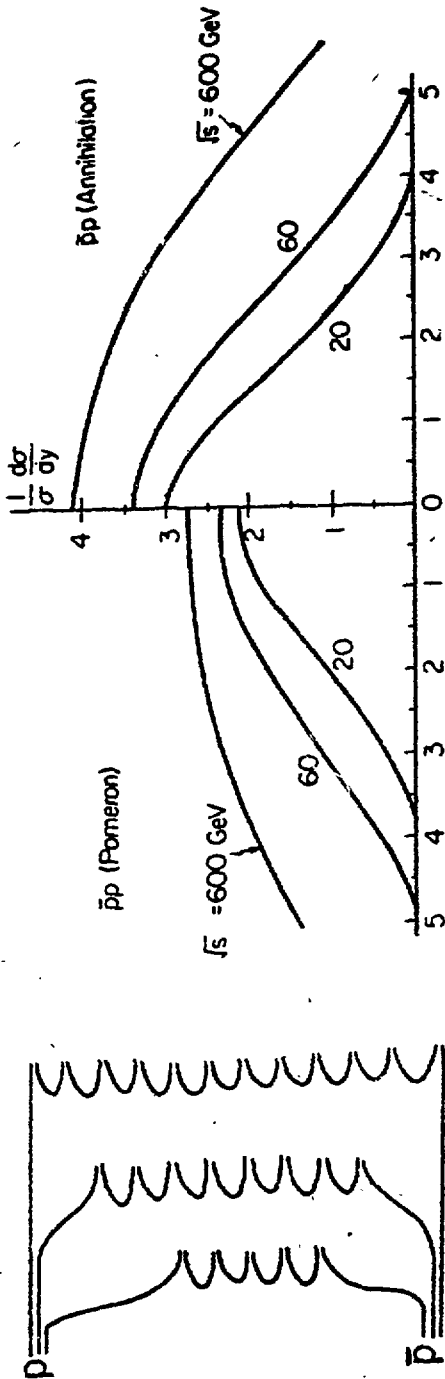


Fig. 8a

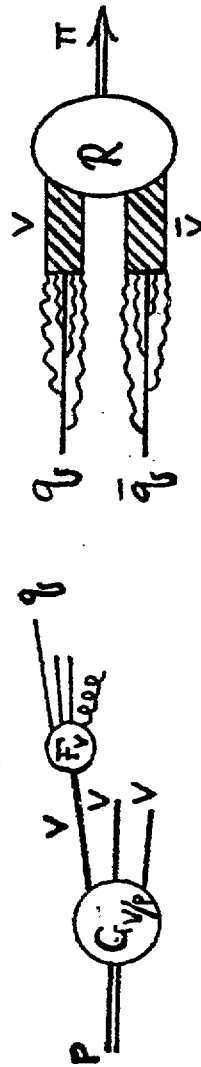


Fig. 9a

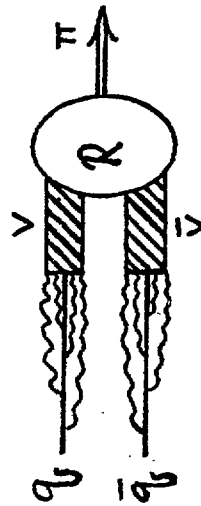


Fig. 9b

Fig. 9b

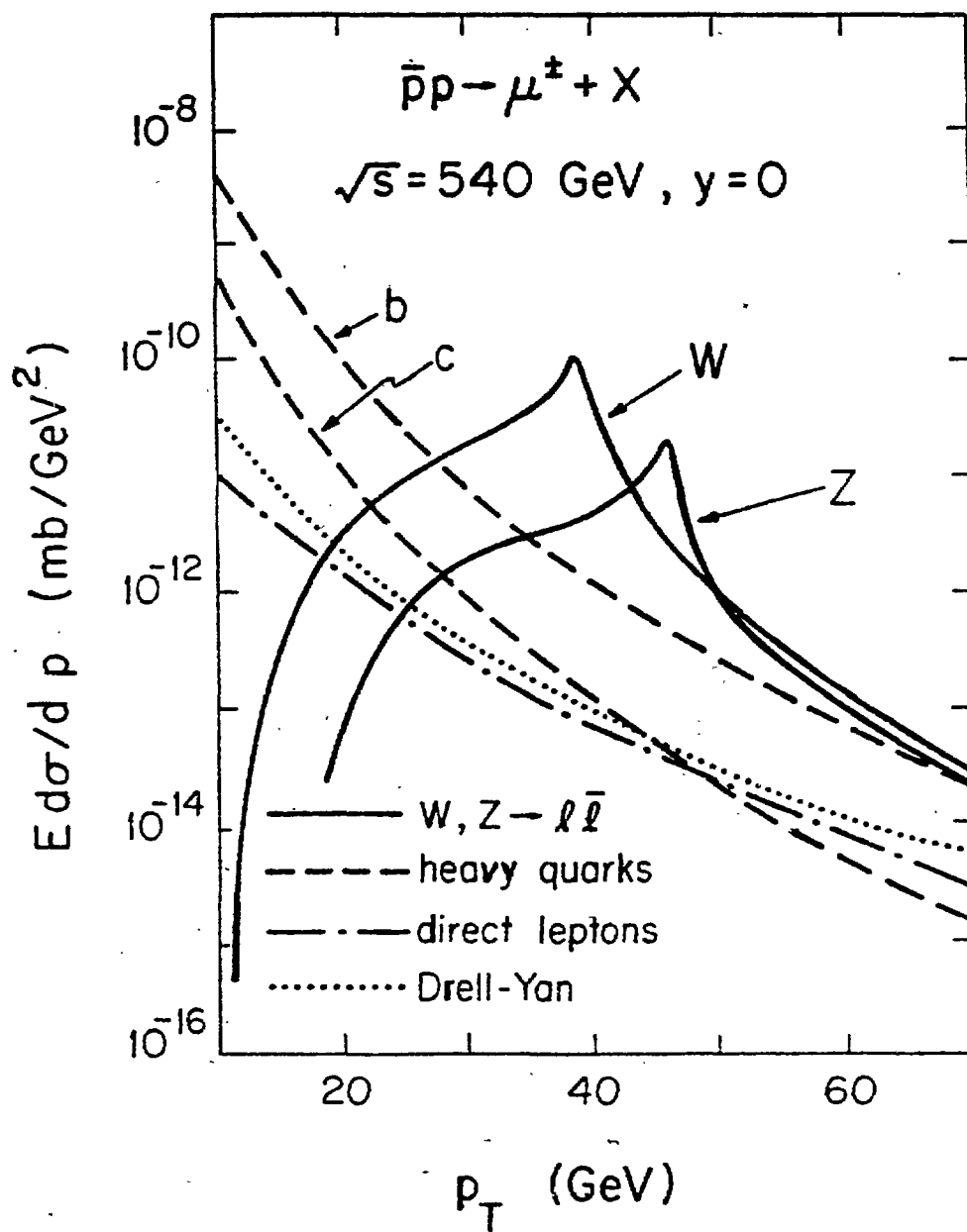


Fig. 9a

Fig. 10

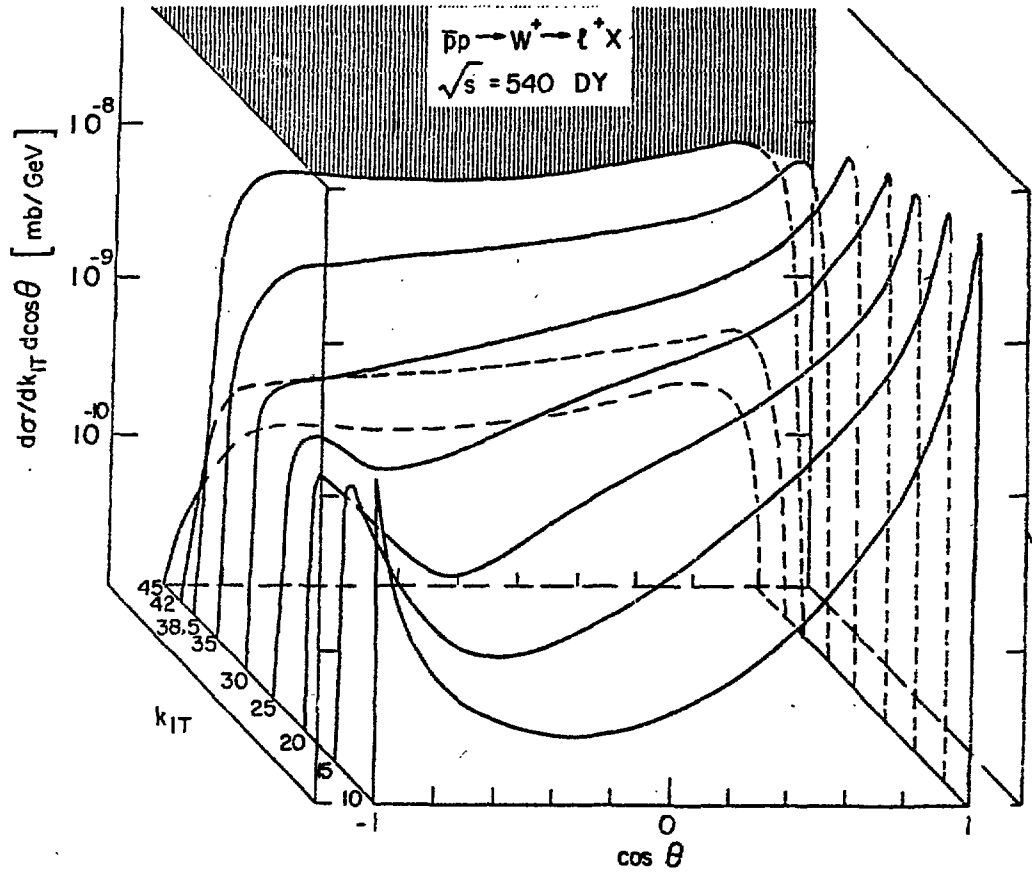


Fig. 11

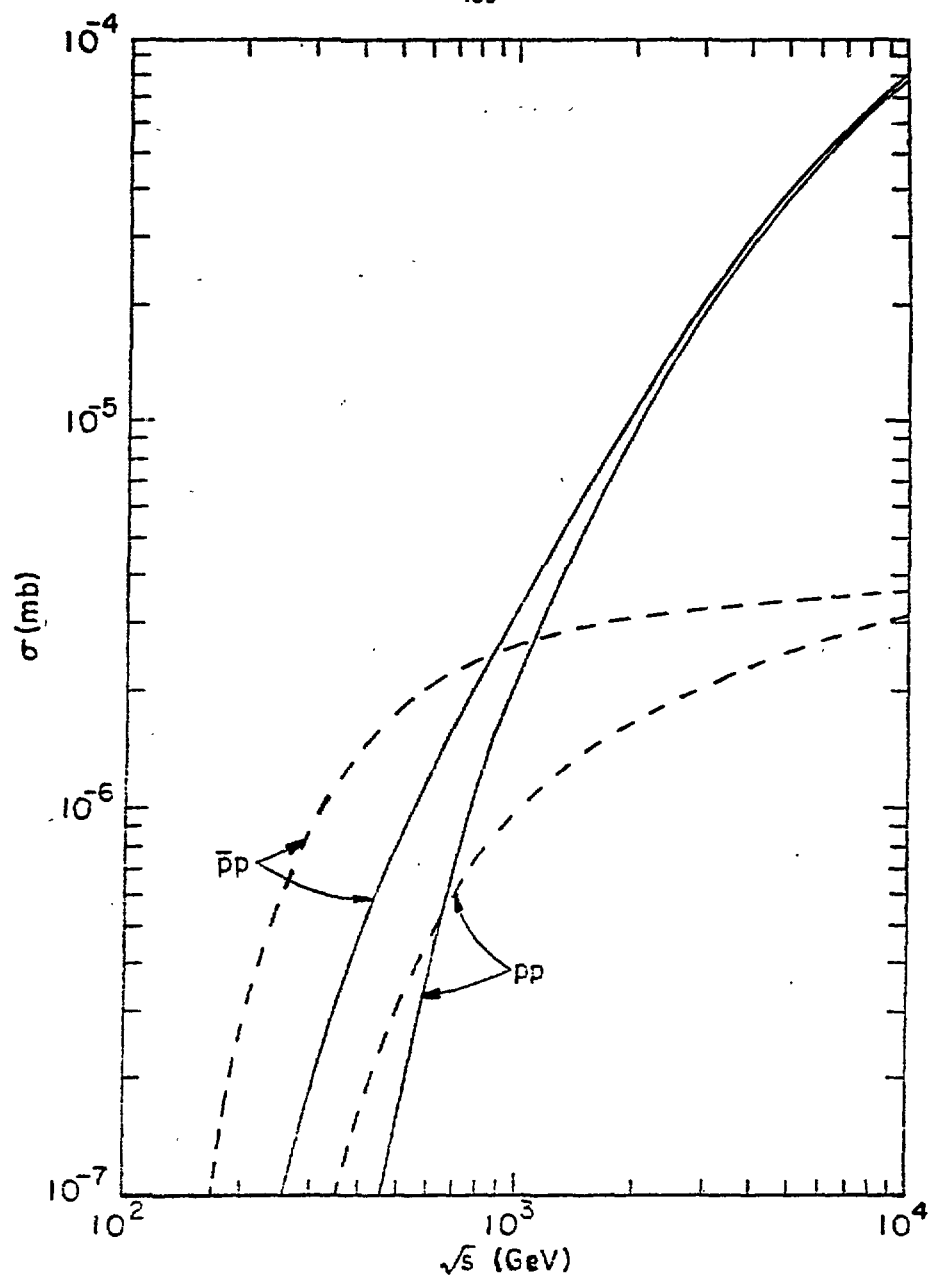


Fig. 12

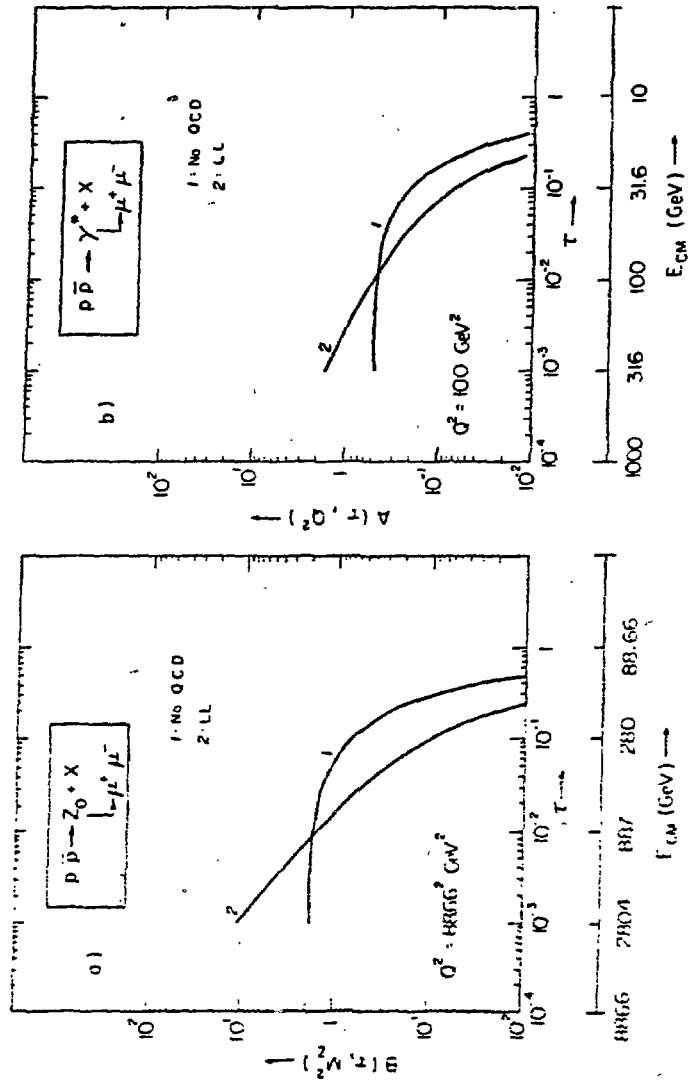


Fig. 13

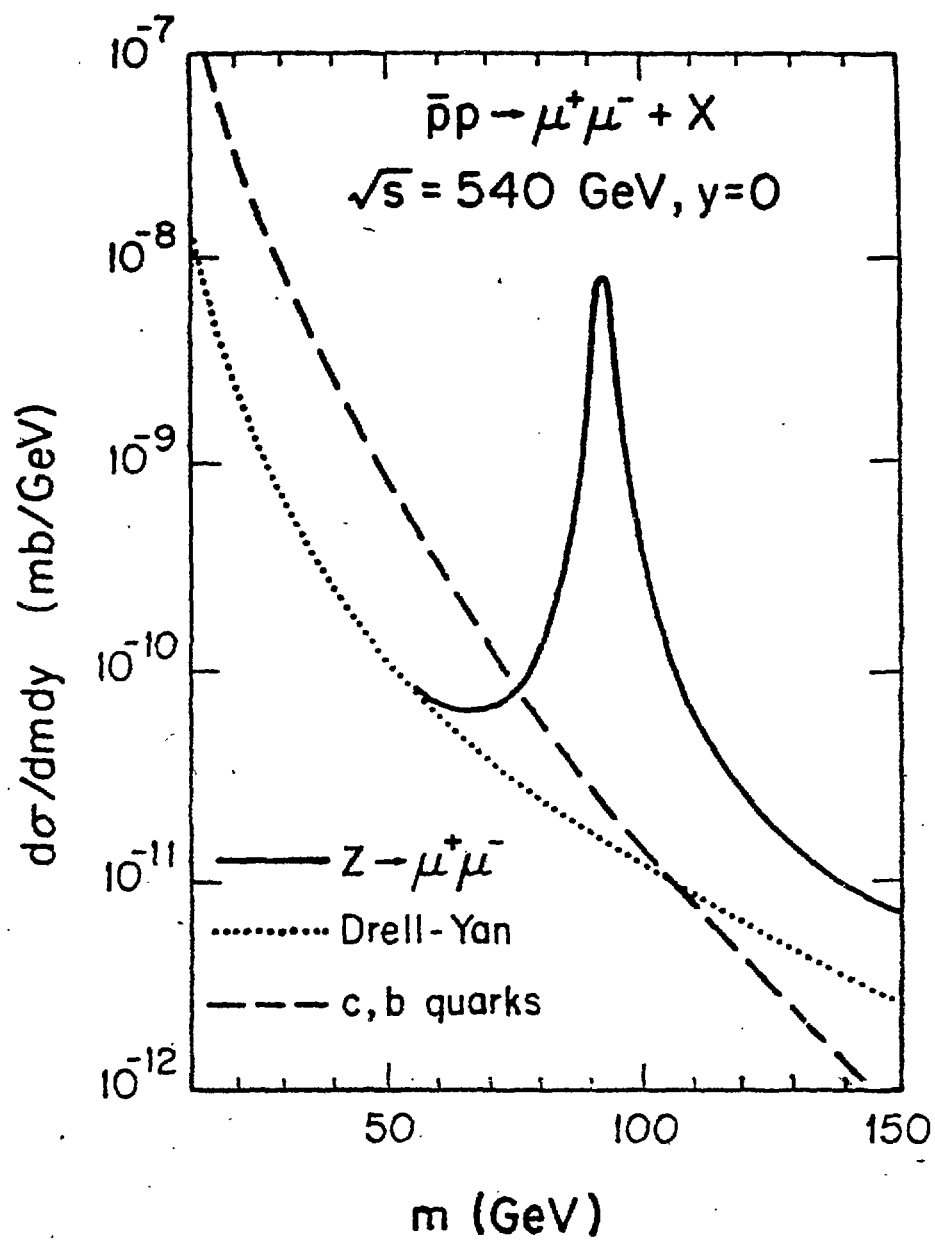


Fig. 14

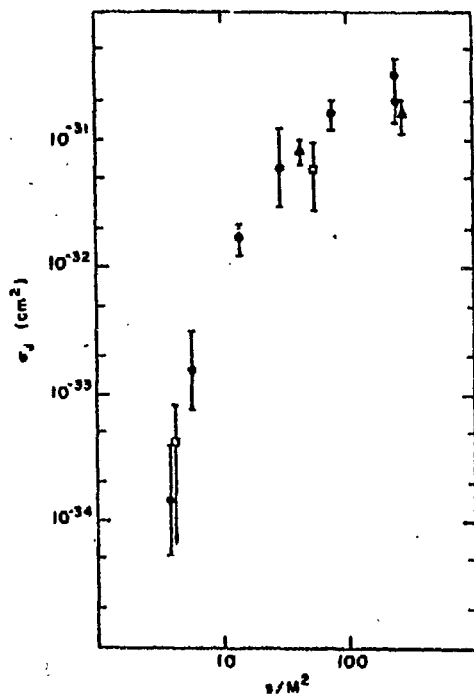


Fig. 15a

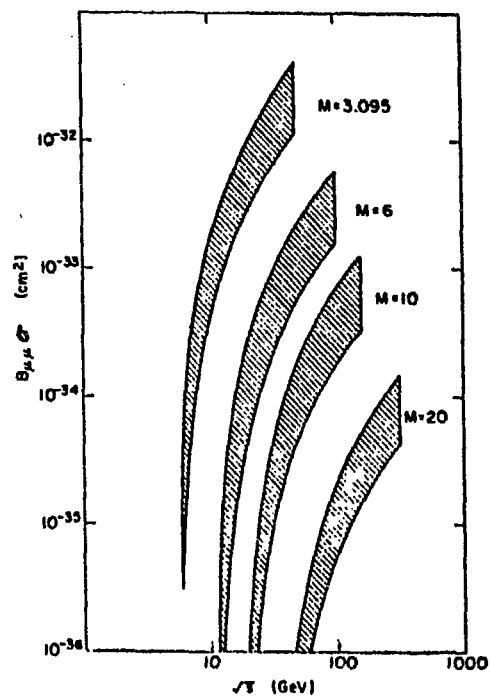


Fig. 15b

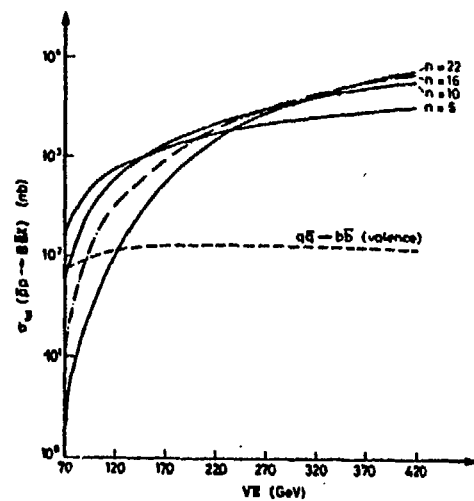


Fig. 16



Fig. 15a

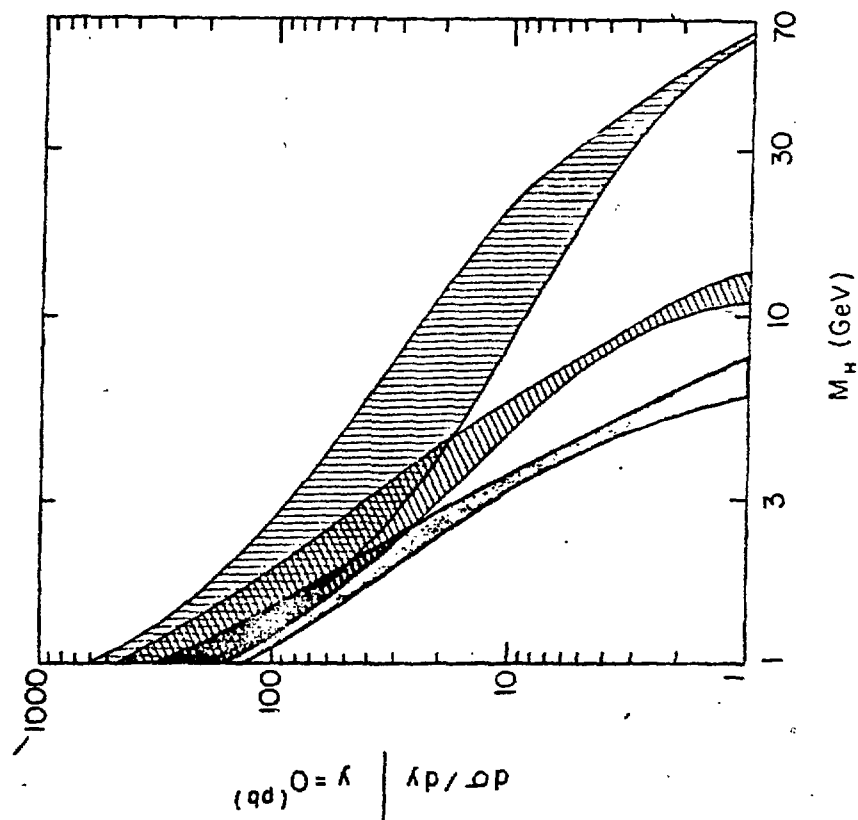


Fig. 15b

$$\frac{(X+Z) \cdot d\sigma}{(X+H+Z) \cdot d\sigma} \quad , \quad \frac{(X+W) \cdot d\sigma}{(X+H+W) \cdot d\sigma}$$

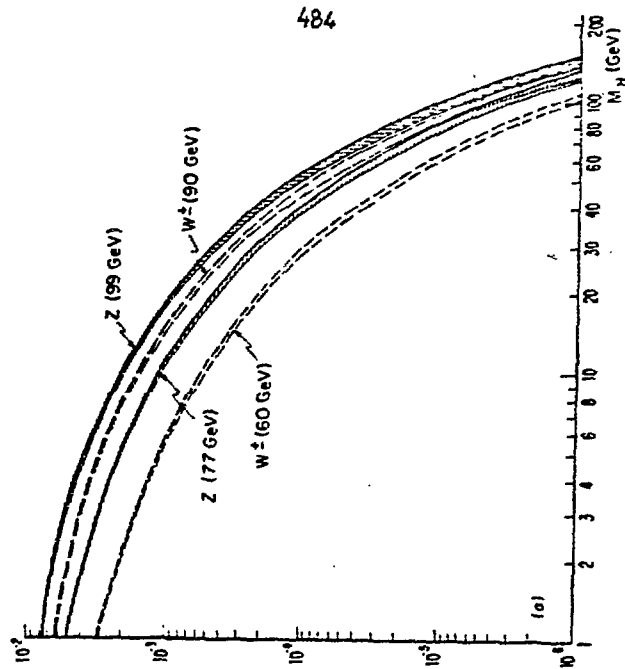


Fig. 16

Fig. 17

Fig. 18

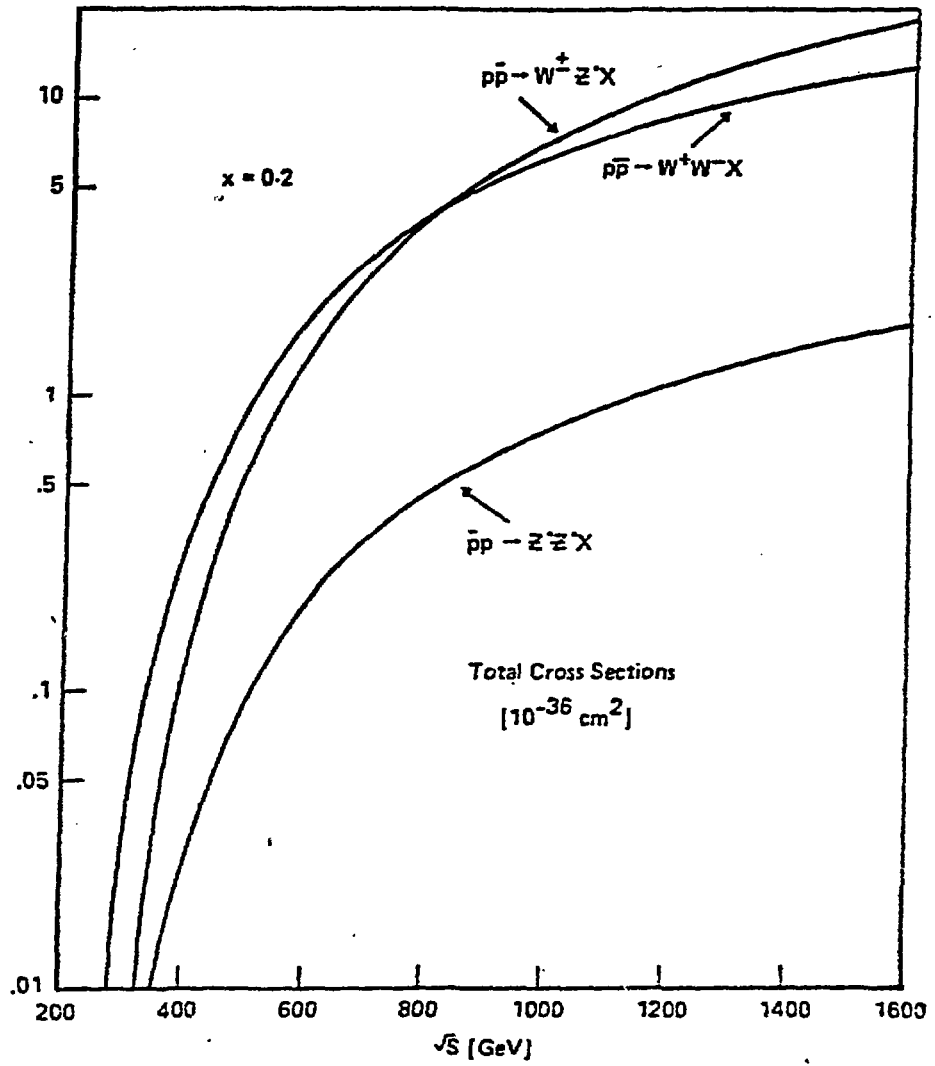
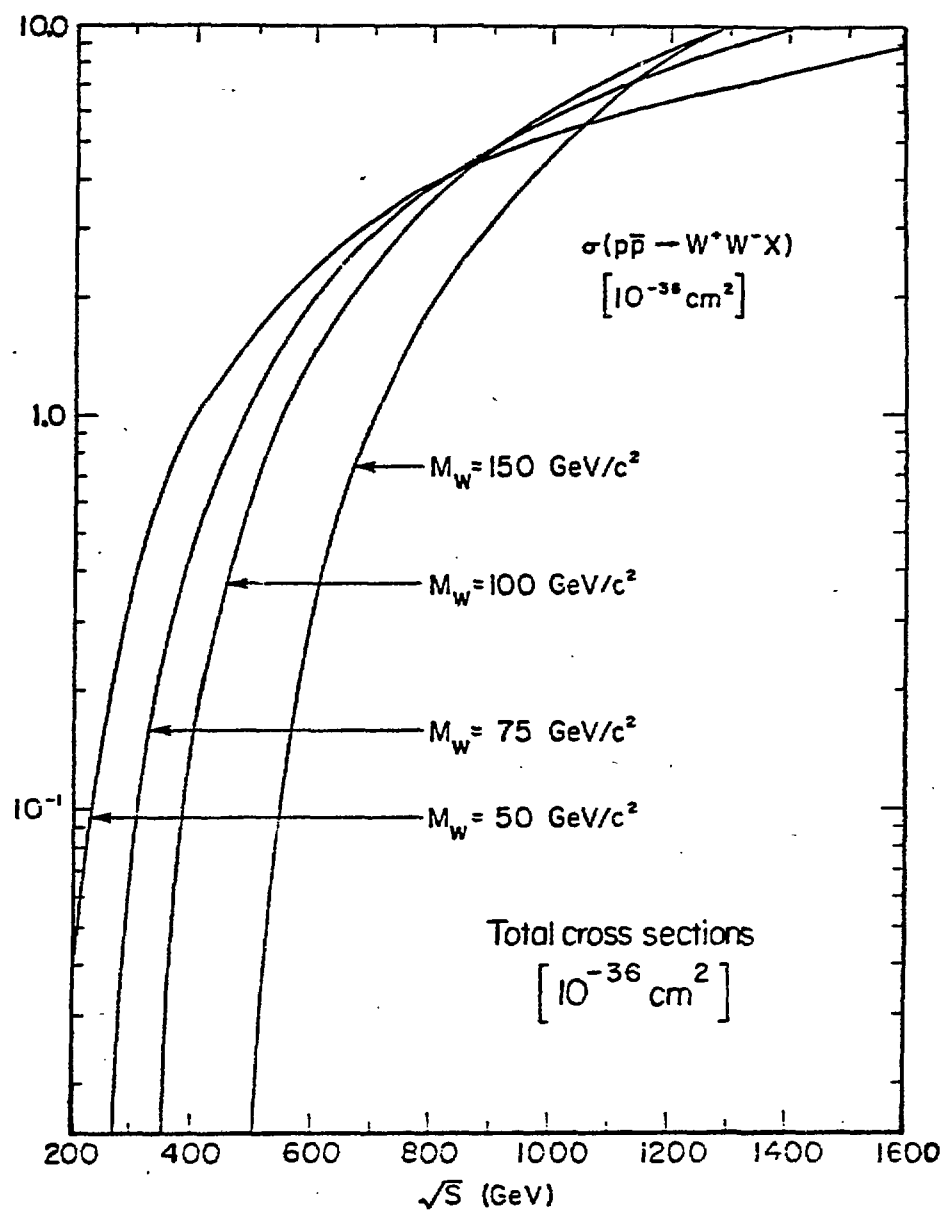


Fig. 19



**Fig. 20**

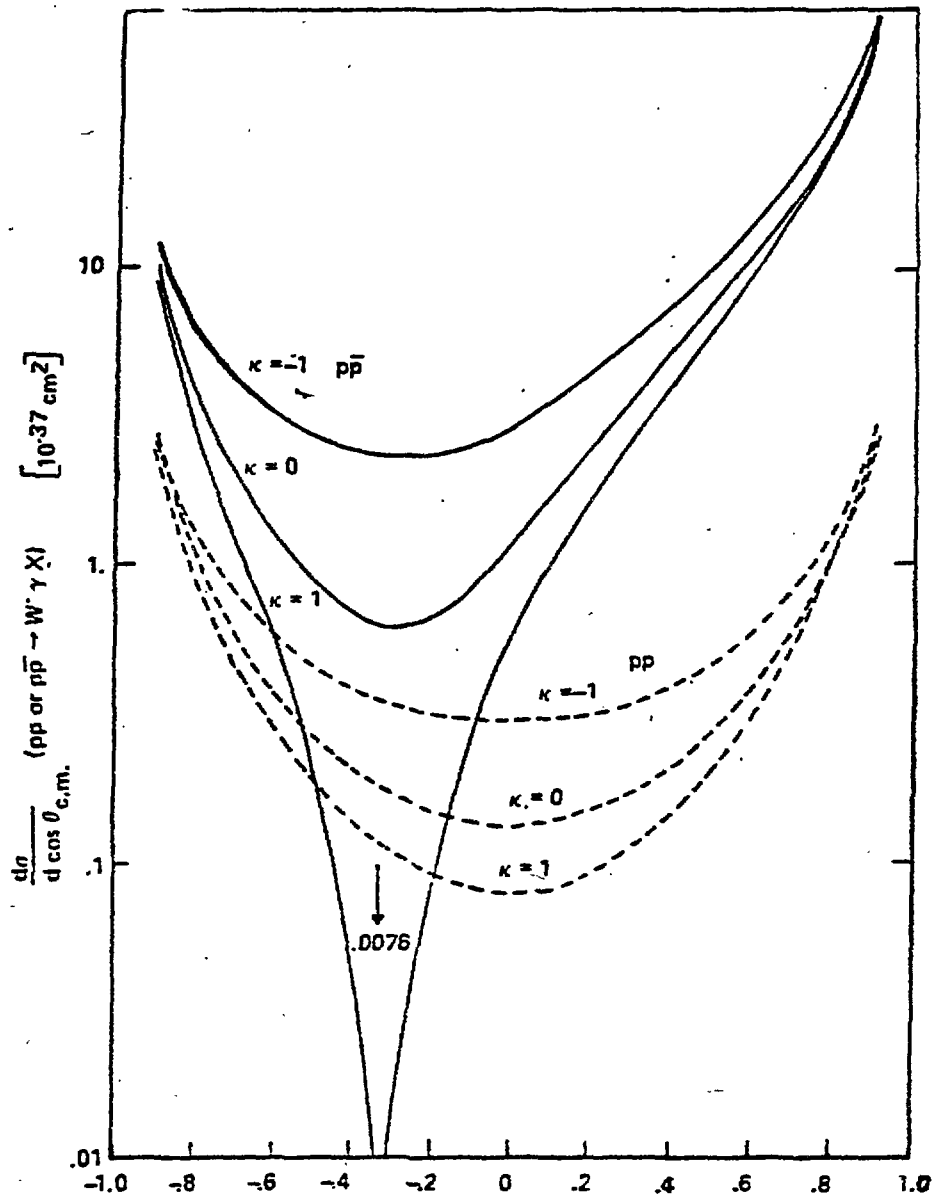


Fig. 21



JETS IN  $e^+e^-$  ANNIHILATION AND QCD

Fernando Barreiro

Gesamthochschule Siegen, Siegen, Fed. Rep. Germany

## 0) Introduction

Recently a great deal of attention is being paid to the study of jet formation in hadron-hadron, lepton-hadron and lepton-lepton interactions.

In the case of the hadronic final states produced in  $e^+e^-$  annihilations, evidence for two jet production was found at SPEAR and DORIS [1]. The connection between the observed two jet structures and the production and subsequent decay of a quark-antiquark pair was established by looking at the angular distribution of the jet axis with respect to the beam [2].

With the advent of the high energies available at PETRA, evidence for a departure from the two jet topology was found [3]. Our current understanding of multijet production is based on QCD, the dynamical theory of quarks and vectors gluons [4]. In this theory the originally produced quark-antiquark pair may radiate gluons which in turn may develop into independent jets, in qualitative agreement with the data at PETRA energies.

A quantitative comparison between data and QCD predictions has always to face a serious problem, namely the presence of non-perturbative effects, not yet calculable. The most popular approach to this problem consists in folding onto a perturbative QCD prediction to a given order the fragmentation properties of quarks and gluons [5,6,7,8]. A more unorthodox approach consists in searching for measures which

- a) don't depend or depend minimally on fragmentation effects or
- b) whose dependence can be educatedly guessed with an analytical parametrization.

The aim of this lecture is to illustrate how these approaches work for the purpose of

- i) determining the strong coupling constant
- ii) determining the spin of the gluon
- iii) understanding the energy dependence of jet measures

#### 1) Determination of the strong coupling constant

The departure of the two jet topology found at PETRA, resulting in some golden cases in explicit three jet events, see fig.1, is best established by looking at the population density in a Dalitz-like plot aplanarity vs. sphericity (or thrust vs. triplicity) or else by looking at the broadening of the pt distributions with respect to the jet axis, figs 2-3-4. It is commonly believed that selecting events with large sphericity and small aplanarity (alternatively small thrust and large triplicity) results in sampling a region rich in three jet events, whose number is directly proportional to the strong coupling constant, and where the contamination from two jet events is minimal. Selecting events with small sphericity (or large thrust) results in sampling a region rich in two jet events with a non-negligible contamination of three jet events where the emitted gluon is highly collinear with respect to the parent quark. In order to extract from the data a value for the strong coupling constant [9], the strategy adopted by most of the groups working at PETRA was

- a) Get a rough estimate of  $\alpha_s$  from the number of three jet events in a region where the contamination from two jet events is minimal
- b) Determine the fragmentation parameters using a sample domina-

ted by supposedly two jet events

- c) With the values for the fragmentation parameters previously obtained repeat step a) and study the systematics

That using this approach in the context of the Monte Carlo calculations described in ref [7] one is able to separate fragmentation from perturbative effects is best exemplified in fig.5. Here TASSO data on sphericity, aplanarity and longitudinal spectra at 12 Gev (fragmentation dominated) and 30 Gev (where perturbative effects are already sizeable) is shown.

The PLUTO-group has followed a different approach based on the cluster algorithm described in ref [10]. The algorithm works as follows

- 1) Collects particles  $i, j$  in preclusters when  $\theta_{ij} < \alpha$   
Collects preclusters  $k, l$  into clusters when  $\theta_{kl} < \beta$

- 2) Order clusters according to their energy

$$E_1 > E_2 > \dots > E_N$$

- 3) Take minimum number which satisfies  $E_1 + E_2 + \dots + E_N > E (1-\epsilon)$  where  $E$  stands for the c.m. energy.

- 4) Identify those clusters whose energy is greater than a given threshold  $E_{min}$  (typically 2 Gev) with jets and measure their four momenta

The parameters  $\alpha, \beta, \epsilon$  which enter in the algorithm are fixed to those values which allow an optimal reconstruction of the number and directions of hard partons generated in typical two and three jet Monte Carlo programs at 30 Gev c.m. energy, see fig 6. When applied to the data the resulting number of jets though dominated by  $n_{jets} = 2$  shows a non-negligible amount of three jet events see fig.7. The number of three jet events can be explained neither



by a two jet Monte Carlo, no matter which fragmentation parameters are put in, nor by a linear combination of two jet and phase space events with arbitrary admixture. It is however well described by a linear combination of two and three jet events yielding a value of  $\alpha_s = 0.15$  at 30 GeV c.m. energy.

Selecting the two jet sample one fixes the fragmentation parameters in particular  $\alpha_s$  to 290-20 MeV. Selecting the three jet sample and imposing additional cuts which minimizes the contamination from two jet events one is able to reconstruct the directions and energies of the original hard partons. These are used to determine the thrust distribution at the parton level which can be directly compared to the first order QCD prediction [12]. The results shown in fig. 8 yields

$$\alpha_s = 0.15 \pm 0.03 \pm (0.02)$$

A summary of the results obtained by the four groups JADE, MARK J, PLUTO and TASSO is presented in Table I. All four determinations agree pretty well within quoted errors. This is no surprise since all four groups have based their analysis on QCD predictions in first order and the same phenomenological model for the description of fragmentation effects. It would be desirable to have a complete inclusion of second order effects in the Monte Carlo programs which are currently used. Equally desirable would be to investigate how sensitive this determination of  $\alpha_s$  is to fragmentation effects described by other models than that of Field and Feynman.

To really establish that the separation between QCD and fragmentation effects have been done properly an extension of current investigations at higher energies would be extremely important in particular to see whether  $\alpha_s$  is behaving with energy as expected.

### II) Determination of the gluon spin

The comparison described at the end of section I) between the thrust distribution measured at the parton level and the first order QCD prediction not only serves to determine  $q_f$  but also can be used to discriminate against scalar gluon theories. The mean thrust expected in a scalar gluon theory is 0.871 in disagreement with the experimental value of  $0.898 \pm 0.005$ , see fig. 8. Actually the sphericity distribution at the parton level, fig. 8, offers better discrimination power.

The TASSO group has followed a different approach [13] originally suggested in ref [14]. They use the method of generalized sphericity [15] to reconstruct the directions  $\hat{Q}_1, \hat{Q}_2, \hat{Q}_3$  and energies  $x_1, x_2, x_3$  of the three jets. These are ordered such that  $x_1 \geq x_2 \geq x_3$  and satisfy the normalization property  $x_1 + x_2 + x_3 = 2$ . Events with  $x_1 > 0.9$  are considered. As illustrated in fig. 10a the event is boosted into the rest frame of the second and third jet, one of which because of the previously discussed ordering is most likely the gluon jet. In this reference system the angle  $\Theta$  between the fastest jet and the direction of the 2-3 axis is sensitive to gluon spin. Fig 10b shows how this angular distribution compares with the QCD prediction, vector gluons, and with the expectations from a scalar gluon model. Clearly the spin 0 assignment is disfavoured.

### III) The energy dependence of jet measures

#### A) Thrust

Traditionally the jet character of the hadronic final states produced in  $e^+e^-$  annihilations has been investigated in terms of variables like thrust [16] or sphericity [17]. Thrust is defined as

$$T = \max \frac{\sum_i |\vec{p}_{Ti}|}{\sum_i |\vec{p}_i|} \quad [1]$$

where the sum runs over all particles in a given event and  $p_{||i}$  stands for the component of the momentum of the  $i$ th particle parallel to the jet axis. Preliminary results from PLUTO are shown in fig. 11. All particles charged and neutral have been included in the analysis and corrections for detector acceptance and resolution as well as for initial state radiative effects have been taken into account. It can be seen how the thrust distributions become narrower as the energy increases with the position of the peak shifting towards  $T \rightarrow 1$ .

At the higher energies these features of the data are well described by Monte Carlo calculations which include QCD effects in the first, second or leading order [6,7,8] while Field & Feynman [5] fails at describing the data above 20 GeV. For completeness we also show the pure QCD predictions in first [12] and leading order [18]. One can see that even at the highest energies available at PETRA there are large deviations between data and bare QCD predictions, indicative of the importance of non-perturbative effects. A better understanding of the interplay between perturbative and non-perturbative effects can be gained by looking, fig. 12, at the mean  $\langle 1-T \rangle$  values as a function of c.m. energy. As shown in this fig. a good description of the data can be obtained by adding to the QCD prediction a non-perturbative contribution of the form [15]

$$\langle 1-T \rangle_{NP} = \frac{\langle \eta \rangle \langle \Phi_T \rangle_{NP}}{2 \sqrt{s}} \quad [2]$$

where  $\langle \eta \rangle$  can be extracted from our data and  $\langle \Phi_T \rangle_{NP}$  is fixed to 300 MeV. The resulting  $\chi^2$  is good and the values for the only free parameter involved in the fit is  $\alpha_s(30 \text{ GeV}) = 0.16 \pm 0.01$  in good agreement with previous estimates discussed in Sect. 1.

### B) Jet opening angle

A similar analysis cannot be made in terms of sphericity [5]

distributions because of the infrared unstable properties of this variable. However the quantity

$$\langle \sin^2 \eta \rangle = \frac{E \cdot \sin^2 \delta}{\sqrt{s}} \quad (3)$$

which is somehow related to  $\langle \delta \rangle$  can be safely calculated in perturbative QCD [19]. In (3)  $E$  denotes the energy of the  $i$ th particle and  $\delta$  stands for its angle with respect to the jet axis. The data, fully corrected for detector and initial state radiative effects is shown in fig. 13. It can be well described by the linear sum of a QCD term and a non-perturbation contribution namely

$$\langle \sin^2 \eta \rangle = \frac{2d}{K} + \frac{C \langle p_T \rangle_{NP}}{2\sqrt{s}} \quad (4)$$

where  $C$  is a parameter describing the energy dependence of the mean charged multiplicity as  $\langle n \rangle = B + C \ln s$ . The resulting value for  $\chi^2/NDF$  is 1.1 and the fitted values for the two free parameters involved are  $d_{\sqrt{s}(30 \text{ GeV})} = 0.18 \pm 0.02$  and  $C \langle p_T \rangle_{NP} = 0.76 \pm 0.12$  again in good agreement with previous estimates..

### C) Jet transverse momenta

As can be seen from fig. 3 one of the most significant features of  $e^+e^-$  annihilation final states is the broadening of the transverse momentum distributions as a function of increasing energy. A useful quantity which has been recently shown to be calculable in QCD perturbation theory is  $\langle \sum p_T \rangle$  where  $p_T$  stands for the transverse momentum of the  $i$ th particle with respect to the jet axis and the sum is running over all particles in a given final state. The following prediction in the leading log approximation can be found in ref [27]

$$\frac{\langle \sum p_T \rangle}{\sqrt{s}} = 1.29 \alpha_s \quad (5)$$

where  $\alpha_s$  is the strong coupling constant. Corrected values for the left hand side of Eq. (5) can be found in fig. 14. Also shown are the results of a fit to the previously discussed prediction. The resulting  $\chi^2$  is 12 for 7 degrees of freedom and the best estimate for  $\Lambda$  the only free parameter in the fit through the relation  $\alpha_s(\mu)/\ln(s/\Lambda^2)$  is  $500 \pm 25$  Mev yielding  $\alpha_s(Q=30 \text{ GeV}) = 0.20 \pm 0.01$ . Notice that but for the points at 12 and 13 GeV which are slightly higher, reflecting the crossing of the  $b\bar{b}$  threshold, the data shows a smooth energy dependence as expected from (5). Note however that because our data spans a relatively small energy range we are not sensitive to exclude the presence of small (and constant with energy) fragmentation contributions.

#### D) Energy-energy correlations

It has been suggested [20] that energy weighted distributions should be less sensitive to fragmentation effects. In particular this is expected to be so in back-to-back energy-energy correlations. The PLUTO group [21] has measured the energy-energy correlation

$$\tau(\theta) = \frac{dI}{d\theta} = 2 \sum_{a,b} \int \frac{d\sigma}{\sigma} \frac{d^3\sigma}{dz_a dz_b d\theta} z_a z_b dz_a dz_b \quad (6)$$

where  $z_{a,b}$  are the fractional energies carried away by hadrons  $a$  and  $b$  and  $\theta$  is the angle between their directions of flight. These measurements have been made over a wide range in energies and fully correcting for detector and initial state radiative effects. The data is shown in fig. 15 along with the expectations from Monte Carlo calculations [5,6] and from pure perturbative QCD predictions derived in the LLA for the forward and backward regimes [22,23] and in first order for the central region i.e.  $\sim 90^\circ$ .

It is clear from this figure that while the LLA calculation in the forward region and the first order prediction stay a fac-

tor of 2 lower than the data the LL calculation for back-to-back jets describes roughly the data at energies above 20 GeV.

A better understanding of the interplay between QCD and fragmentation effects in the central region can be gained by looking at the energy dependence of the integrated cross section which as shown in fig. 16 can be well described again by the linear sum of a QCD term and a non-perturbative contribution of the form

$$r(\theta) = \frac{N_s}{\pi} g(\theta) + \frac{C \langle p_T \rangle_{NP}}{\sqrt{s} \sin^2 \theta} \quad (7)$$

where  $g(\theta)$  can be calculated from first principles and  $C \langle p_T \rangle_{NP}$  has been previously discussed in connection with (4). The resulting  $\chi^2$  is good and the following values for the two free parameters involved are  $\alpha_s(30 \text{ GeV}) = 0.20 \pm 0.02$  and  $C \langle p_T \rangle_{NP} = 1.0 \pm 0.2$ .

It has been suggested that a clean signature for gluon bremsstrahlung would be the observation of a forward-backward asymmetry in the energy-energy correlation. Pertinent data is shown in fig. 17 along with Monte Carlo expectations [5,6] and QCD predictions [24]. The following observations can be made

- a) The asymmetry distribution seems to be very little energy dependent in the c.m. energy range 7.7 to 31.6 GeV
- b) It is well described by Field-Feynman Monte Carlo at low energies.
- c) At high energies the inclusion of QCD effects is mandatory
- d) The contributions to the asymmetry due to fragmentation effects seem to be dying away like  $1/s$
- e) At 30 GeV they are negligible thus explaining why the asymmetry data can be alternatively well described by the pure first order QCD prediction. Thus higher statistics data of this type could in the future provide a clean way to determine  $\alpha_s$ . Knowledge of the importance of second order effects is highly desirable.

### F) Mean charge multiplicity

I would finally like to make a comment on the behaviour of the mean charged multiplicity as a function of c.m. energy and a jet measure like thrust, sphericity or the jet mass.

The average charge multiplicity for hadrons produced in  $e^+e^-$  annihilations rises with energy much faster than the simple  $\ln s$  dependence expected from low energy data. The onset of this behaviour being at PETRA energies, where evidence for gluon bremsstrahlung has been found, leads one to tentatively assume a correspondence between both phenomena. In this context the importance of correlating the fast increase in  $\langle n_{ch} \rangle$  with the jet properties of the hadronic final states has been recently stressed [25]. In fact a distinctive feature of QCD is the expectation of a fast increase in  $\langle n_{ch} \rangle$  not only for those events with manifest three jet structure, characterised by say large sphericity, but also for those with stronger two jet configuration where the effects of the soft quark cascade should manifest itself.

In order to get into a deeper understanding of this particular point we propose to measure  $\langle n_{ch} \rangle$  as a function not only of c.m. energy but also for different slices in a jet measure, be it thrust, sphericity or the jet mass. Pertinent data corrected for detector effects and radiation in the initial state are shown in fig. 14. The following observations can be made

- i) At a given energy the mean multiplicity  $\langle n_{ch} \rangle$  is larger the wider the jet
- ii)  $\langle n_{ch} \rangle$  rises faster than  $\ln s$  depending very little within our error bars on the jet character of the final state
- iii) the dependence of  $\langle n_{ch} \rangle$  on c.m. energy and the width of a jet is well described by the Monte Carlo calculations discussed in ref. [6]. The model of Field and Feynman also gives a fair description of the data but for the highest energies and the small

thrust (or else large sphericity or mass) regions (not shown)

It has been found that the evolution of the mean charged multiplicity with the virtuality (mass) of the  $q\bar{q}$  pair [28]

$$\langle n_{ch} \rangle = a + b \exp \left\{ c \sqrt{\ln Q/\Lambda} \right\} \quad (8)$$

gives a good representation of the data [29]. It is interesting to see whether the evolution of the multiplicity of a single quark jet with its virtuality (mass) is similar [30]. Fig. 19 shows for the combined 27.6 - 31.6 GeV data the dependence of  $\langle n_{ch} \rangle_{jet}$  on its mass. The curve represents the results of a fit to expression (8) where  $c$  has been fixed to 2.4 and  $\Lambda$  to 500 MeV. The values for  $a$  and  $b$  resulting from the fit are  $1.8 \pm 0.1$  and  $0.0176 \pm 0.0005$  respectively not far from those obtained from the  $s$  dependence of the event multiplicity [29], in support of the theory of the cascade evolution.

#### IV) Summary and conclusions

The main results obtained at PETRA on jets and QCD can be summarized as follows

- i) All PETRA groups have measured  $\alpha_s$  at 30 GeV. They all agree within each other. They all are subject to the same uncertainties namely the dependence on a phenomenological model for describing the fragmentation properties of quarks and gluons. Furthermore they all depend on QCD calculations in first order. The importance of second order corrections should be cleared up. It would be desirable to reach higher energies so that determining  $\alpha_s$  as a function of c.m. energy would show whether  $\alpha_s$  extracted this way is running or at least walking.
- ii) Early evidence for a  $s=1$  gluon coming from the PLUTO analysis of



the  $\Upsilon$  decay [25] is confirmed in the analysis of three jet events at PETRA.

(iii) Distributions on jet measures show that QCD predictions not supplemented by some knowledge of the fragmentation effects cannot describe the data. The energy dependence of jet measures like  $\langle T \rangle$  or  $\langle \sin \eta \rangle$  can be well described by the sum of a QCD term, slowly varying with energy and a fragmentation term dying away like  $s^{-1/2}$ . Data at high energies and knowledge of the importance of second order corrections would help in confirming this emerging picture.

ACKNOWLEDGEMENTS: I would like to thank the organizers of the meeting for their warm hospitality. Thanks are also due to many a member of the PLUTO collaboration for helpful discussions. In particular I am very grateful to Prof. S. Brandt for help and encouragement in the preparation of these notes.

TABLE I

A summary of recent determinations of  $\alpha_s$  at 30 GeV

| GROUP  | VALUE and ERROR            | METHOD                                  |
|--------|----------------------------|---|
| JADE   | $0.18 \pm 0.02 \pm (0.02)$ | Three jet events                        |
| MARK J | $0.19 \pm 0.02 \pm (0.04)$ | "                                       |
| PLUTO  | $0.15 \pm 0.03 \pm (0.02)$ | "                                       |
| TASSO  | $0.17 \pm 0.02 \pm (0.02)$ | "                                       |
| PLUTO  | $0.18 \pm 0.02$            | Energy dep. $\langle \sin \eta \rangle$ |
| PLUTO  | $0.16 \pm 0.01$            | Energy dep. $\langle 1-T \rangle$       |
| PLUTO  | $0.20 \pm 0.01$            | Energy dep. $\langle \sum p_T \rangle$  |
| PLUTO  | $0.20 \pm 0.02$            | Energy-energy corr.                     |

## FIGURE CAPTIONS

- Fig. 1 : A three jet event from PLUTO
- Fig. 2 : Triplicity vs Thrust for PLUTO data at 30 GeV.
- Fig. 3 : Observed mean values for longitudinal and transverse momenta as a function of c.m. energy. The dotted line shows the expectations from Field & Feynman Monte Carlo, the solid line that of Moyer et al.
- Fig. 4 : TASSO data on the  $\langle p_T^2 \rangle_{q\bar{q}}$  and  $\langle p_T^2 \rangle_{\gamma\gamma}$ . The
- Fig. 5 : Sphericity, aplanarity and longitudinal spectra at 12 and 30 GeV as measured by TASSO. The curves show the expectations from Ali et al. Monte Carlo calculations.
- Fig. 6 : The distribution in the number of jets found by the cluster algorithm described in ref. [10] applied to different Monte Carlo generated samples
- Fig. 7 : The distribution in the number of jets found by the cluster algorithm of ref. [10] when applied to PLUTO data at 30 GeV
- Fig. 8 : The thrust distribution at the parton level measured from a sample of three jet events from PLUTO. The solid line shows the first order QCD prediction. The dashed and dashed-dotted line show the expectations from scalar gluon and constituent interchange models.
- Fig. 9 : The sphericity distribution at the parton level measured from a sample of three jet events from PLUTO. The solid line shows the first order QCD prediction. The dashed line shows the expectations from a scalar gluon model.
- Fig. 10 : a) Kinematical illustration of the Ellis-Karliner angle.  
b) TASSO data on the Ellis-Karliner angle along with a comparison to a model with vector (solid line) and scalar (dotted line) gluons.
- Fig. 11 : Normalized corrected thrust distributions measured by PLUTO from 7.7 to 31.6 GeV. At 30 GeV and to illustrate

Fig. 1

Fig. 1

Fig. 1

Fig. 1

Fig. 1

Fig. 1

how significantly different they are, the expectations from the Field & Feynman Monte Carlo (dotted line) and those from Monte Carlo calculations a la Hoyer et al. (solid line) and Odorico (dashed-dotted line) are shown.

Fig. 12 : The dependence on energy of  $\langle 1-T \rangle$  measured by PLUTO. The solid line represents the results of a fit to the linear sum of a QCD term (dotted line) and a phenomenological simple fragmentation term. See text for details.

Fig. 13 : The dependence on energy of  $\langle \sin^2 \theta \rangle$  measured by PLUTO. The solid line represents the results of a fit to the linear sum of a QCD term (dotted line) and a phenomenological simple fragmentation term. See text for details.

Fig. 14 : The energy dependence of  $\langle \Sigma p_T \rangle$ . The solid line represents the results of a fit to a QCD prediction in the leading log approximation. See text for details.

Fig. 15 : Fully corrected data on the energy-energy correlations from 7.7 up to 31.6 GeV. The solid line represents the expectations from Monte Carlo calculations. At low energies Field & Feynman model was used, at high energies first order QCD effects a la Hoyer et al. were included. The dotted line represents the QCD predictions of KVV (forward region), BBEL (central region) and DDT (backward region).

Fig. 16 : The dependence on energy of the integrated  $\int_{90^\circ}^{120^\circ}$  energy energy correlation measured by PLUTO. The solid line represents the results of a fit to the linear sum of a QCD term (dotted line) and a phenomenological simple fragmentation term. See text for details.

Fig. 17 : The assymmetric component present in the energy energy correlation measured by PLUTO. The curves show the expectations from a pure fragmentation model (Field & Feynman).

from a model where QCD effects are taken into account ( Hoyer et al. ) , as well as the results of the bare first order QCD predictions by BBL.

Fig. 18 : The mean charged particle multiplicity as a function of c.m. energy and the width of a jet ( measured by thrust sphericity or its invariant mass )

Fig. 19 : The mean charged multiplicity of quark jets produced in  $e^+e^-$  annihilations at 27.6 - 31.6 Gev as a function of the jet invariant mass.

#### REFERENCES \*\*\*\*\*

- [1] G. Hanson et al., Phys. Rev. Lett. 35 (75) 609  
PLUTO Collaboration, Ch. Berger et al., Phys. Lett. 78B (78) 178
- [2] R. F. Schwitters et al., Phys. Rev. Lett. 35 (75) 1230
- [3] JADE Coll., W. Bartel et al., Phys. Lett. 88B (79) 171  
MARK J Coll., D. P. Barber et al., Phys. Rev. Lett. 43 (79) 830  
PLUTO Coll., Ch. Berger et al., Phys. Lett. 86B (79) 418  
TASSO Coll., R. Brandelik et al., Phys. Lett. 88B (79) 243
- [4] H. Fritzsch, M. Gell-mann and H. Leutwyler, Phys. Lett. 478 (73) 365  
D. J. Gross and F. Wilczek, Phys. Rev. Lett. 30 (73) 1343  
D. Politzer, Phys. Rev. Lett. 30 (73) 1346
- [5] R. D. Field and R. P. Feynman, Phys. Rev. D15(77) 2590
- [6] P. Hoyer et al., Nucl. Phys. B161 (79) 349
- [7] A. Ali et al., Phys. Lett. 82b (79) 1235

- [8] P. Mazzanti and R. Odorico , Phys. Lett. 95B (80) 133  
G. Fox and S. Wolfram, Nucl. Phys. B168 (80) 285
- [9] JADE Coll., S. Yamada , Proc. XX Int. Conf. High Energy Phys.  
Madison, Wisconsin  
MARK J Coll., P. P. Barber et al., Phys. Lett. 89B (79) 139  
TASSO Coll., R. Brandelik et al., Phys. Lett. 94B (80) 437
- [10] H.J. Daum , H. Meyer and J. Burger, Z. fur Phys. C8 (81) 167
- [11] PLUTO Collaboration, Ch. Berger et al., Phys. Lett.
- [12] A. de Rujula et al., Nucl. Phys. B
- [13] TASSO Coll., R. Brandelik et al, Phys. Lett. 97B (80) 453
- [14] J. Ellis and I. Karliner, Nucl. Phys. B148 (79) 141
- [15] S.L. Wu and G. Zoebnig, Z. fur Phys. C4 (80) 87
- [16] S. Brandt et al., Phys.Lett. 12 (64) 57  
E. Fehri, Phys. Rev. Lett. 39 (77) 1537
- [17] J. D. Bjorken and S. Brodsky, Phys. Rev. D1 (78) 1416
- [18] G. Schierholz, DESY 79/71
- [19] C. L. Basham et al., Phys. Rev. D17 (78) 2278
- [20] Yu. L. Dokshitzer, D. I. D'yakonov and S. I. Troyan, Phys.  
Lett. 78B (78) 290
- [21] PLUTO Collaboration, Ch. Berger et al., Phys. Lett. 99B (81) 292
- [22] K. Konishi, A. Ukawa and G. Veneziano, Nucl. Phys. B157 (79) 45
- [23] G. Parisi and R. Petronzio, Nucl. Phys. B154 (79) 427
- [24] C. L. Basham et al., Phys. Rev. Lett. 41(78) 1585

- [25] G. Parisi , Private communication
- [26] Pluto Collaboration, Zeits. fur Phys.C8 (81) 101
- [27] B. R. Weber , Cavendish Laboratory preprint, HEP 80/10
- [28] W. Furmanski and S. Pokorski, Nucl. Phys. 155B (79) 1253  
A. Bassetto, M. Ciafaloni and G. Marchesini, Phys. Lett. 83B  
(78) 227
- [29] PLUTO Collaboration, Ch. Berger et al., Phys. Lett. 95B (80)313
- [30] R. Petronzio, private communication

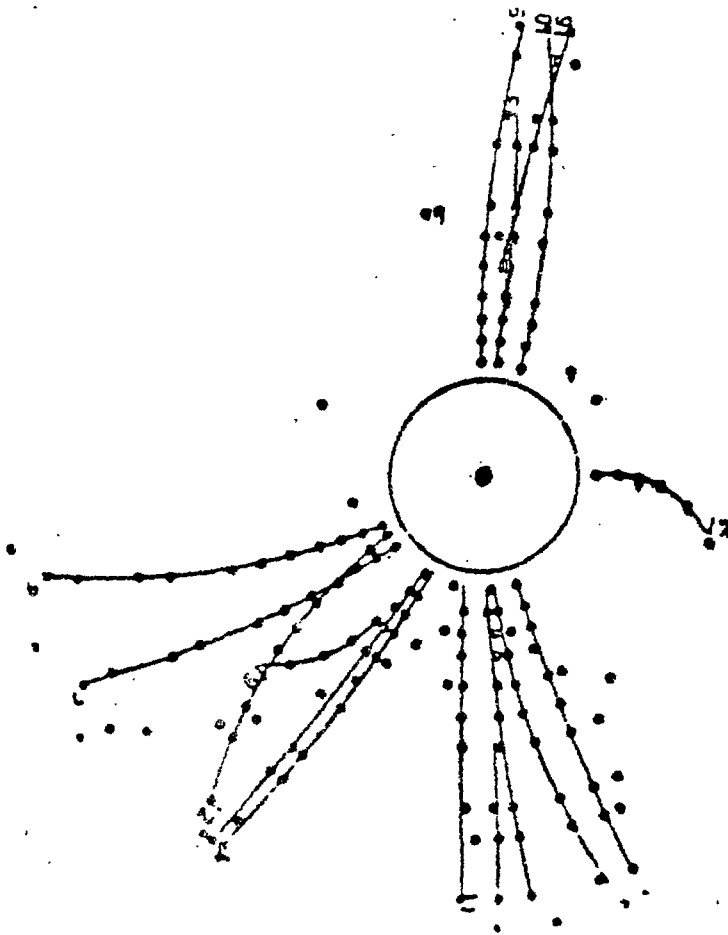


Fig. 1

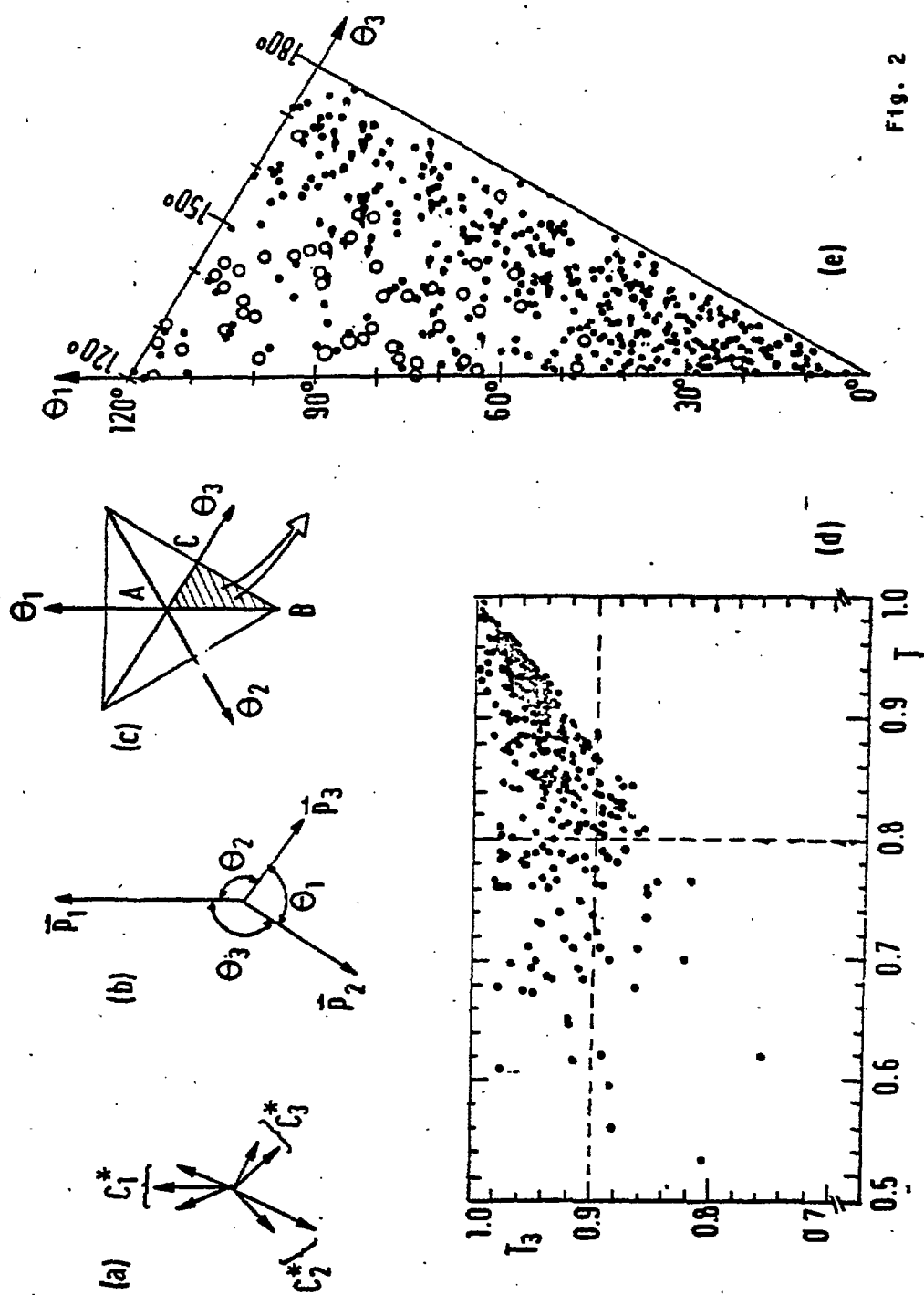


Fig. 2



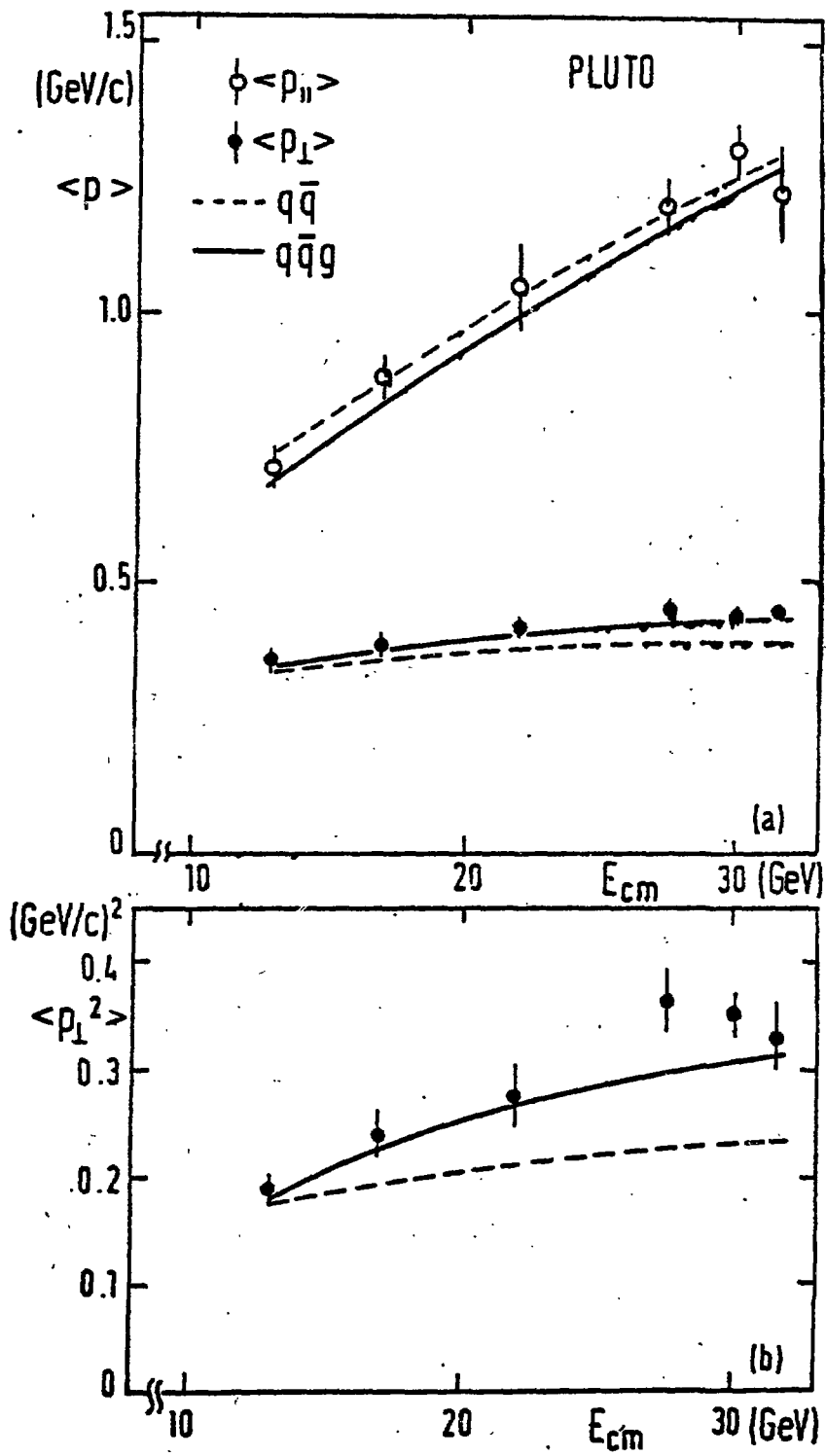


Fig. 3

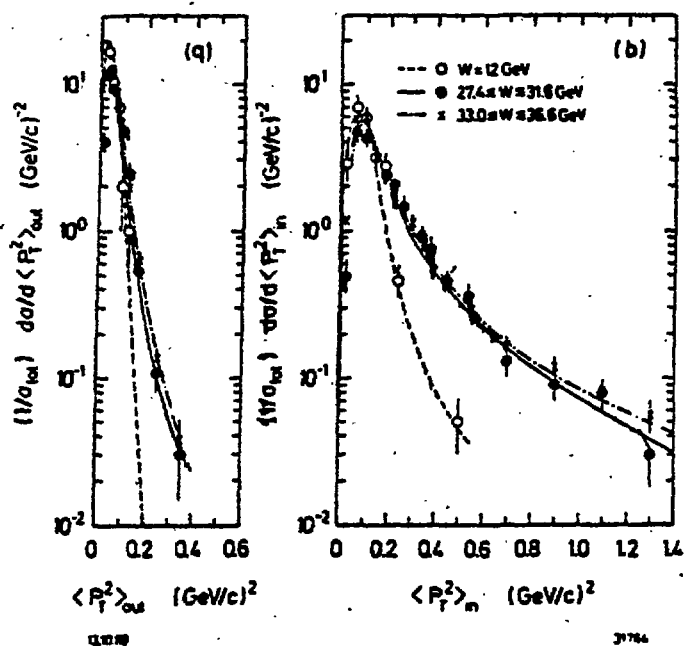
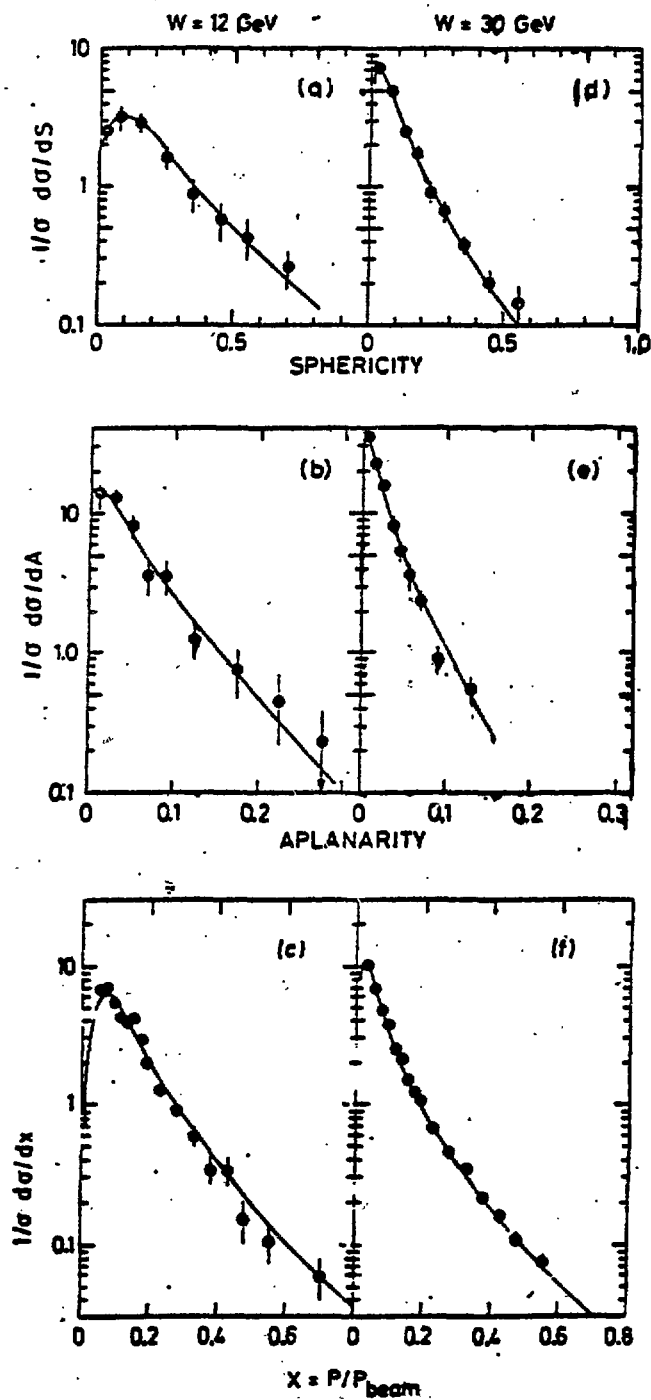


Fig. 4

Fig. 5



30 GeV

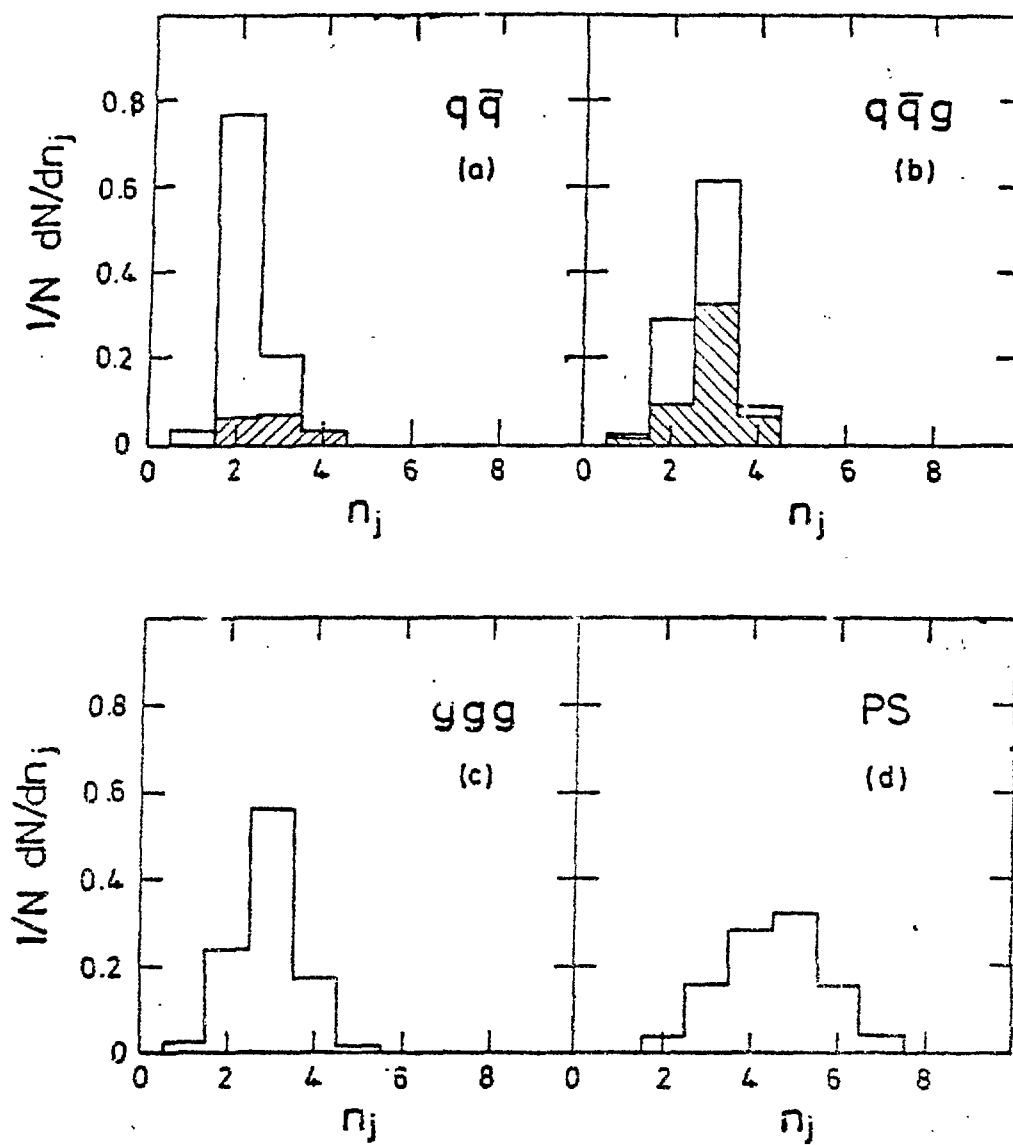


Fig. 6

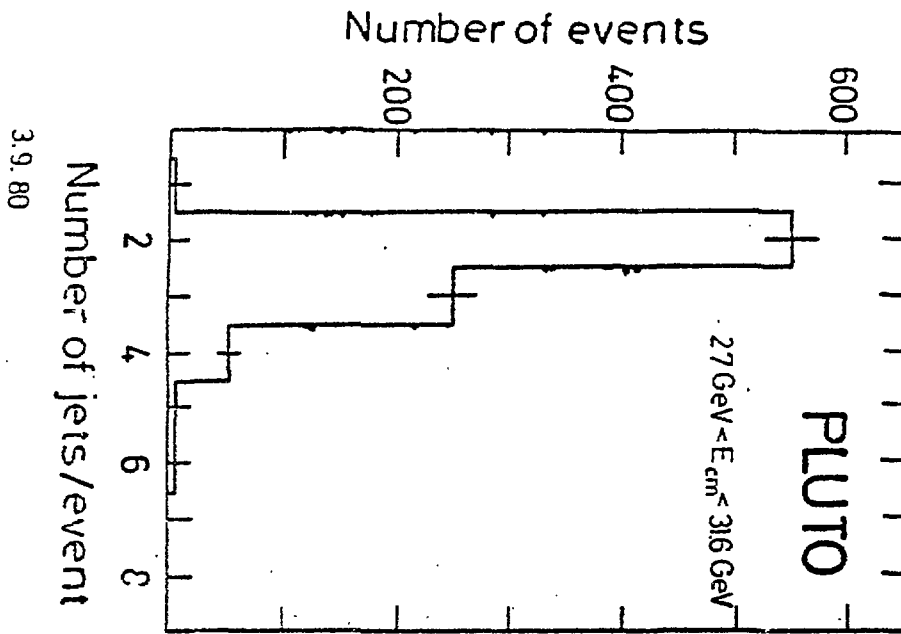


Fig. 7

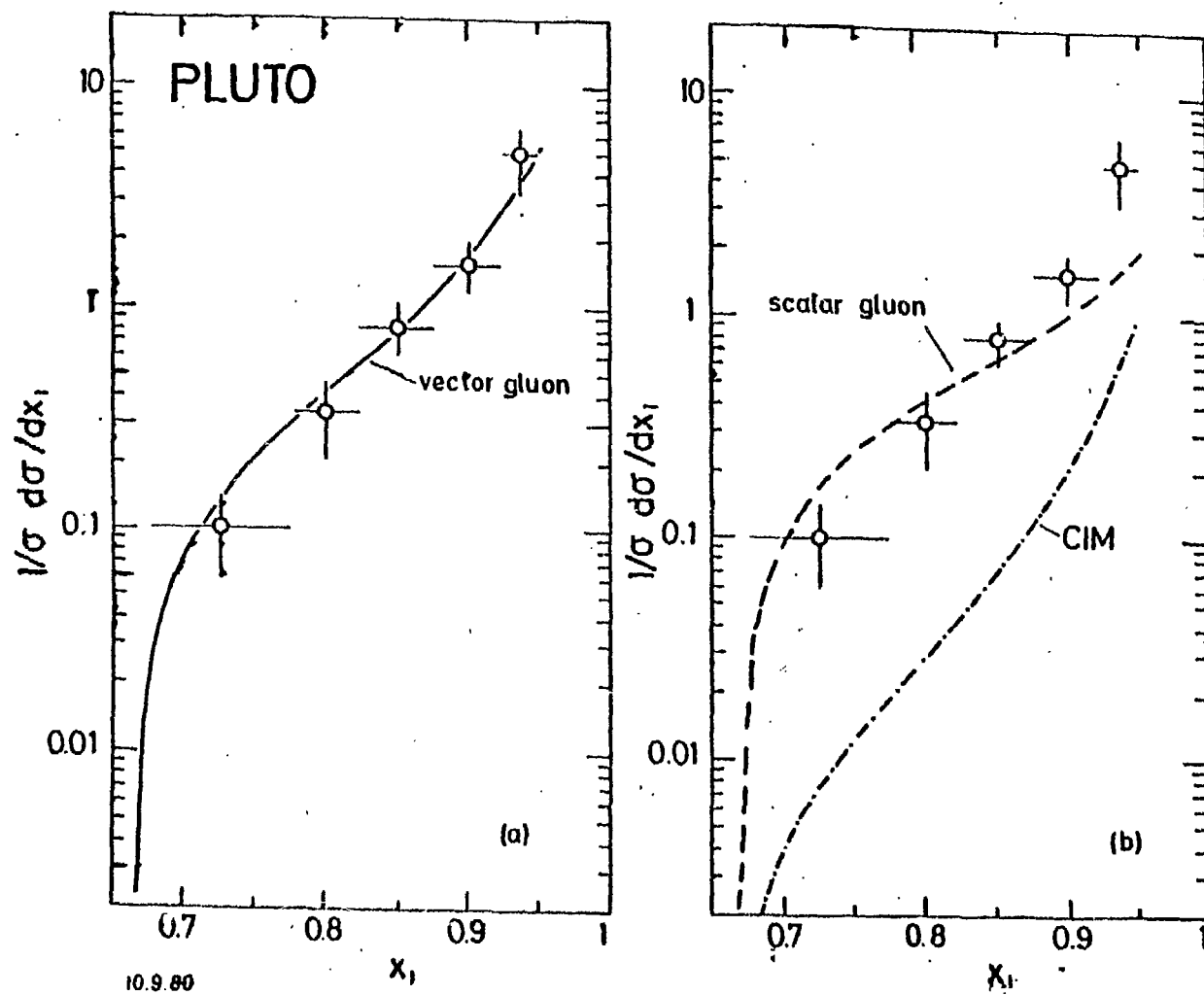


Fig. 8

31639

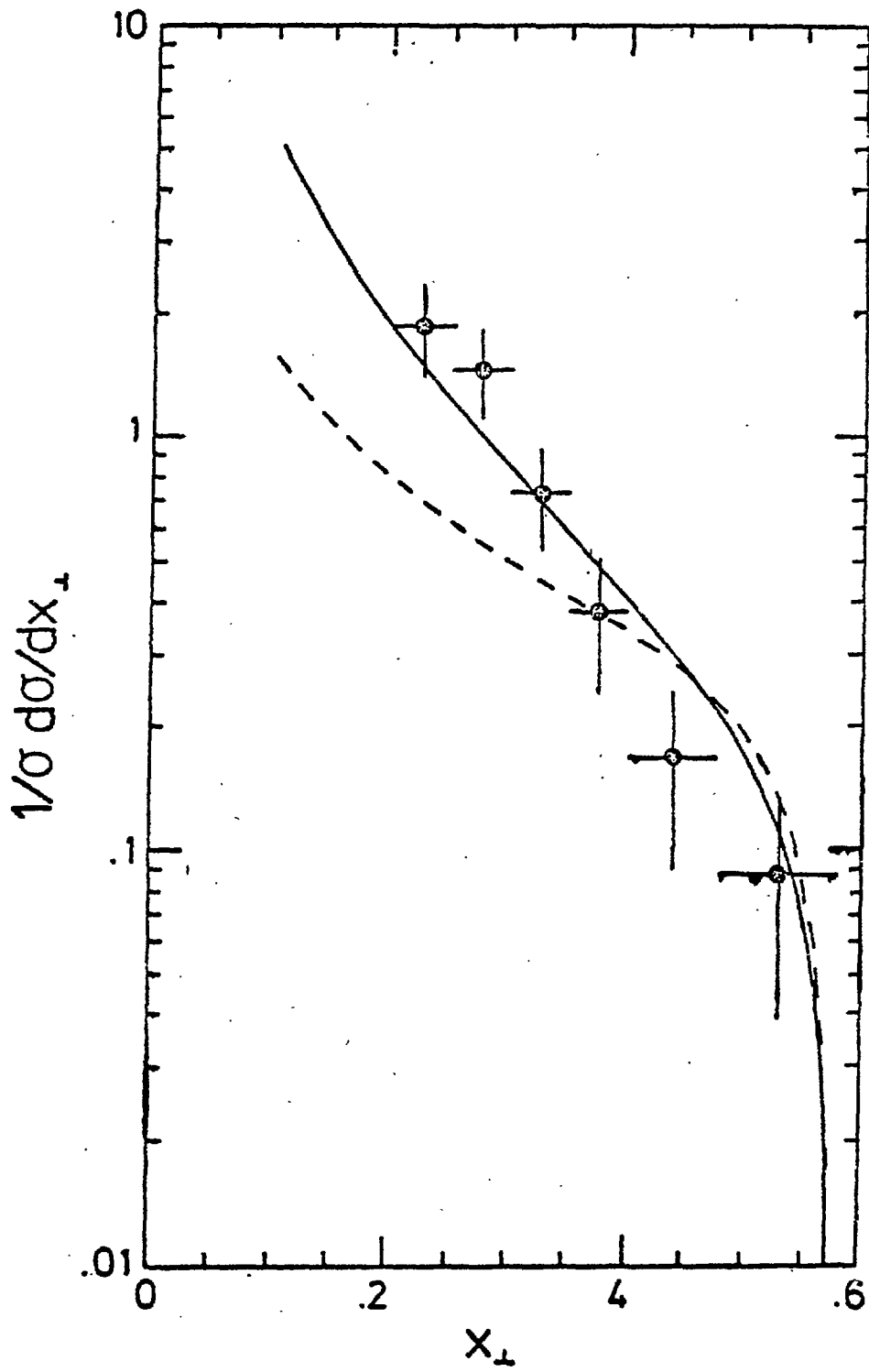
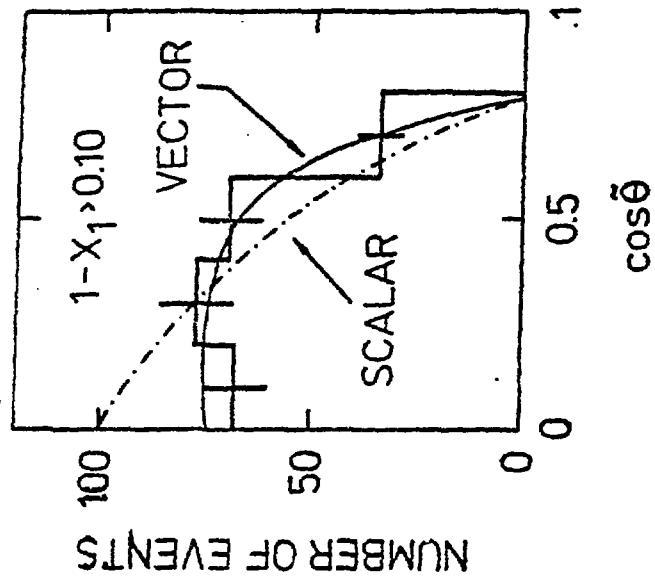
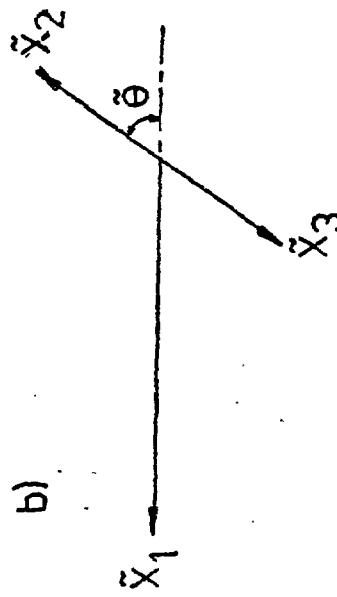
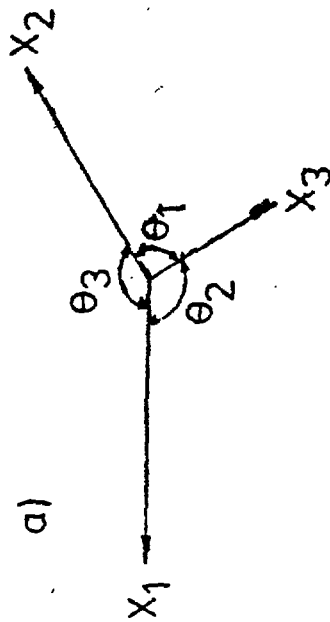


Fig. 9



29 8 80

30525

Fig. 10



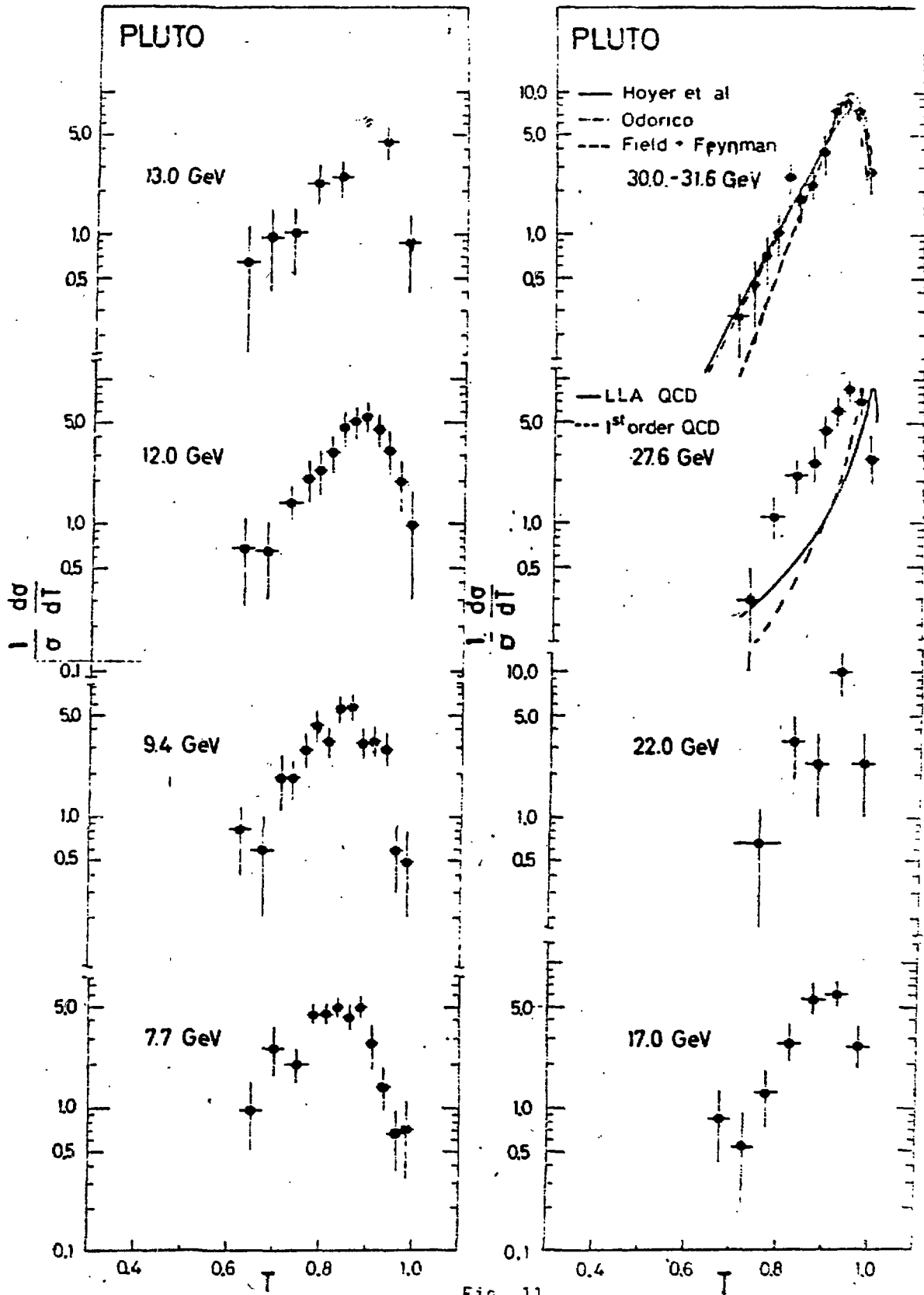


Fig. 11

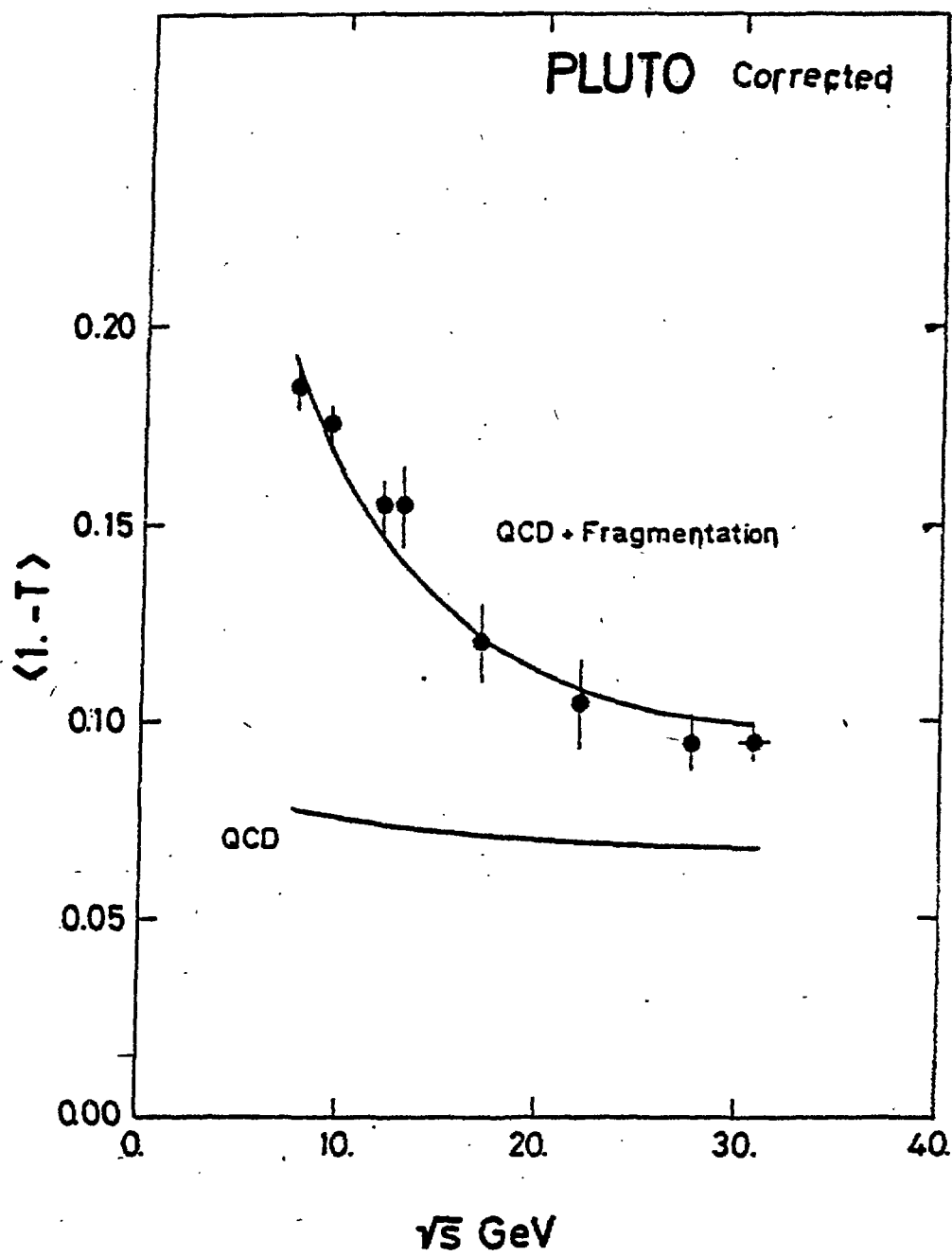
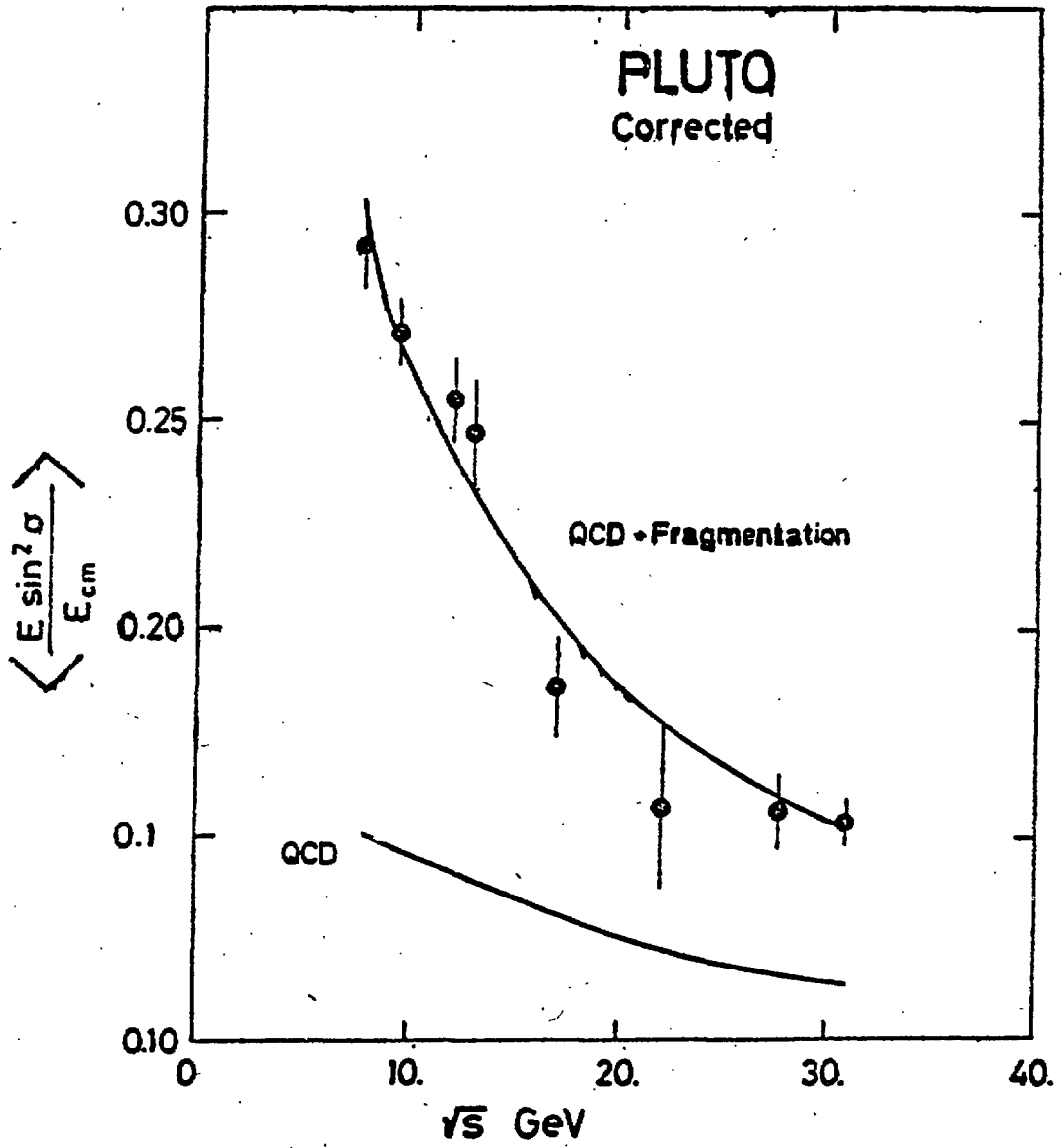


Fig. 12

Fig. 13



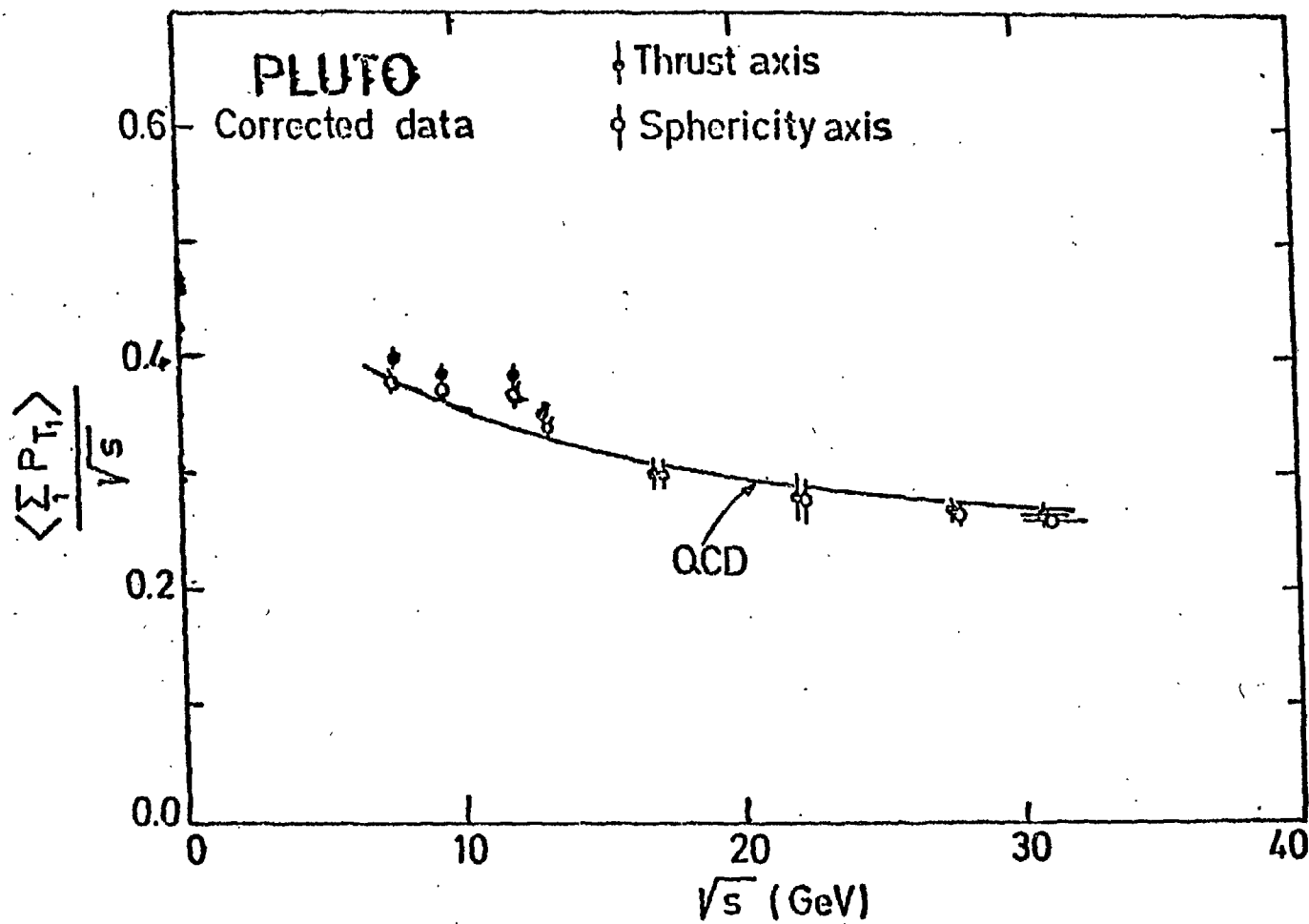


Fig. 14

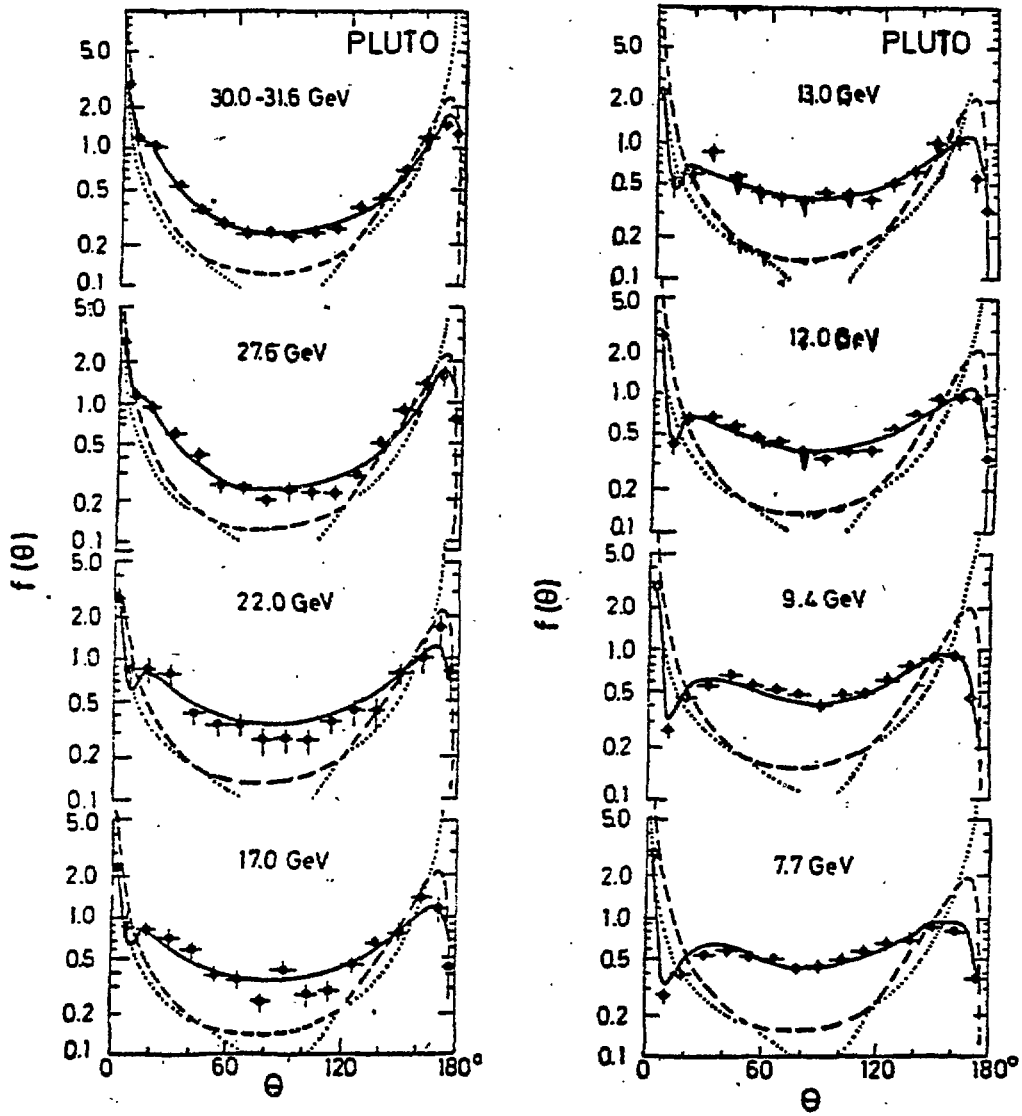


Fig. 15

31331

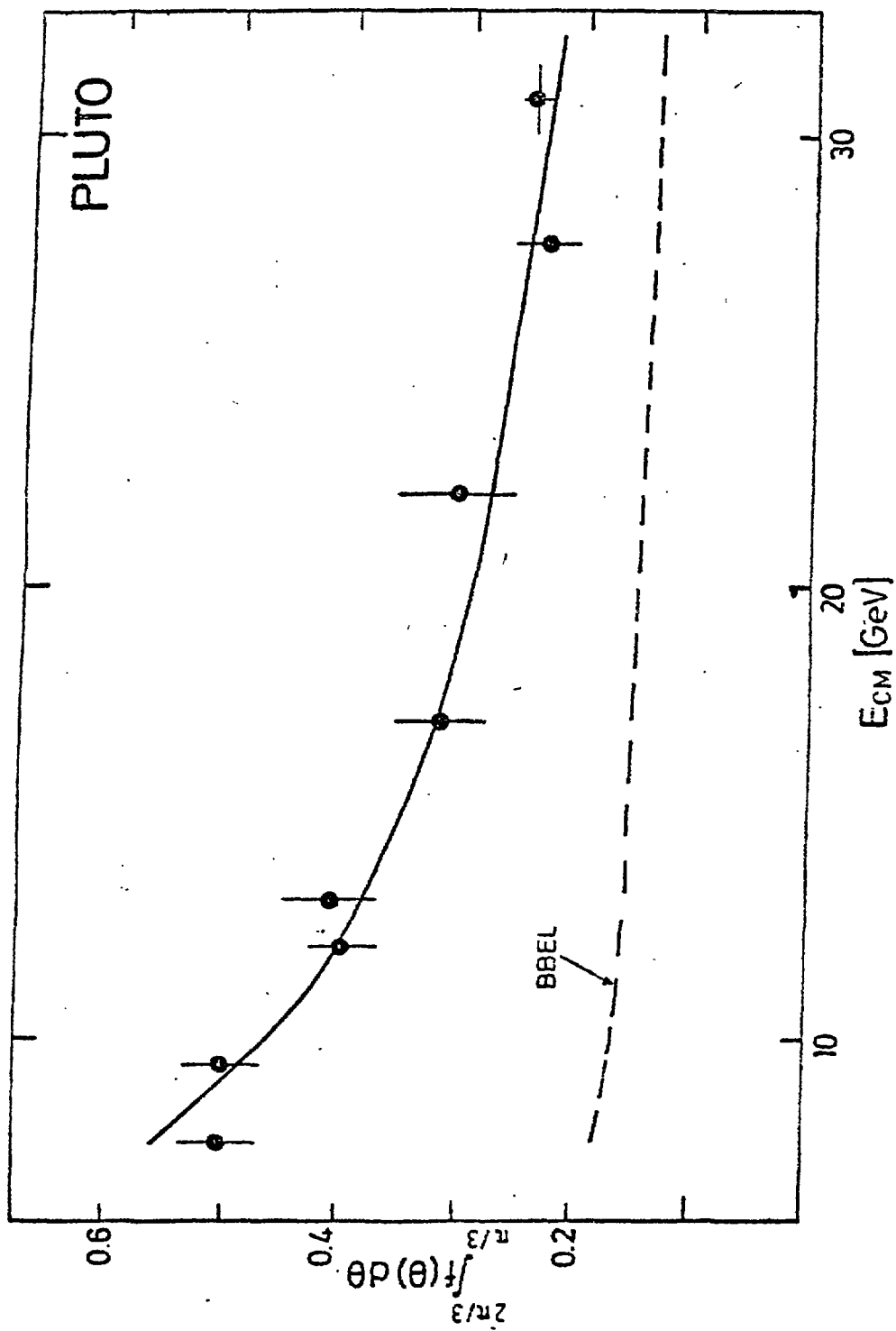


Fig. 16

31358

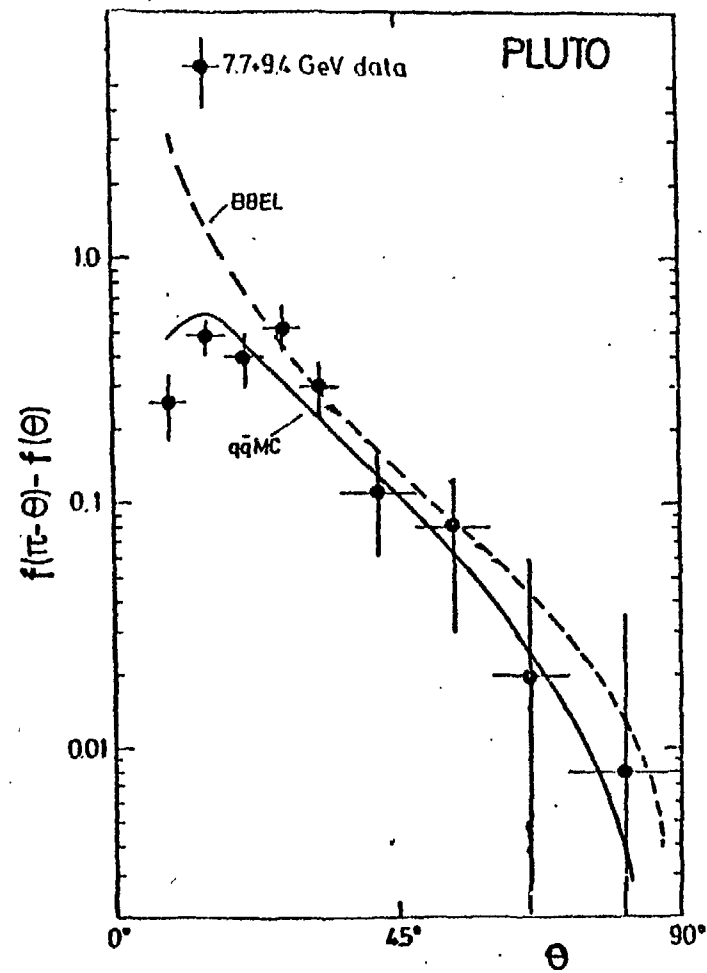
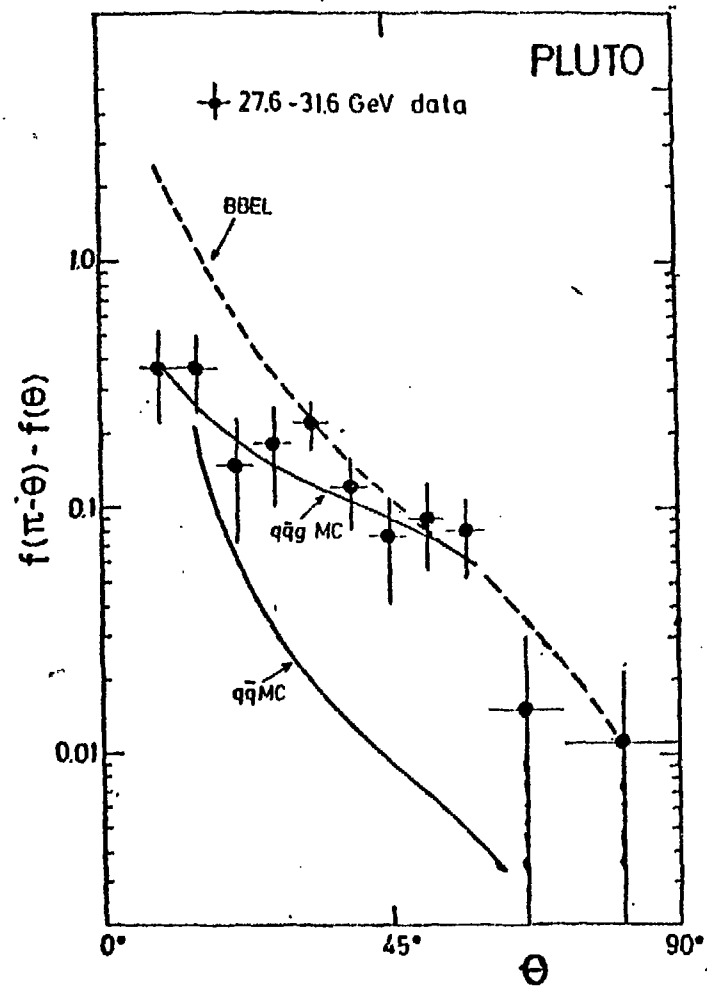


Fig. 17

31040

Fig. 18

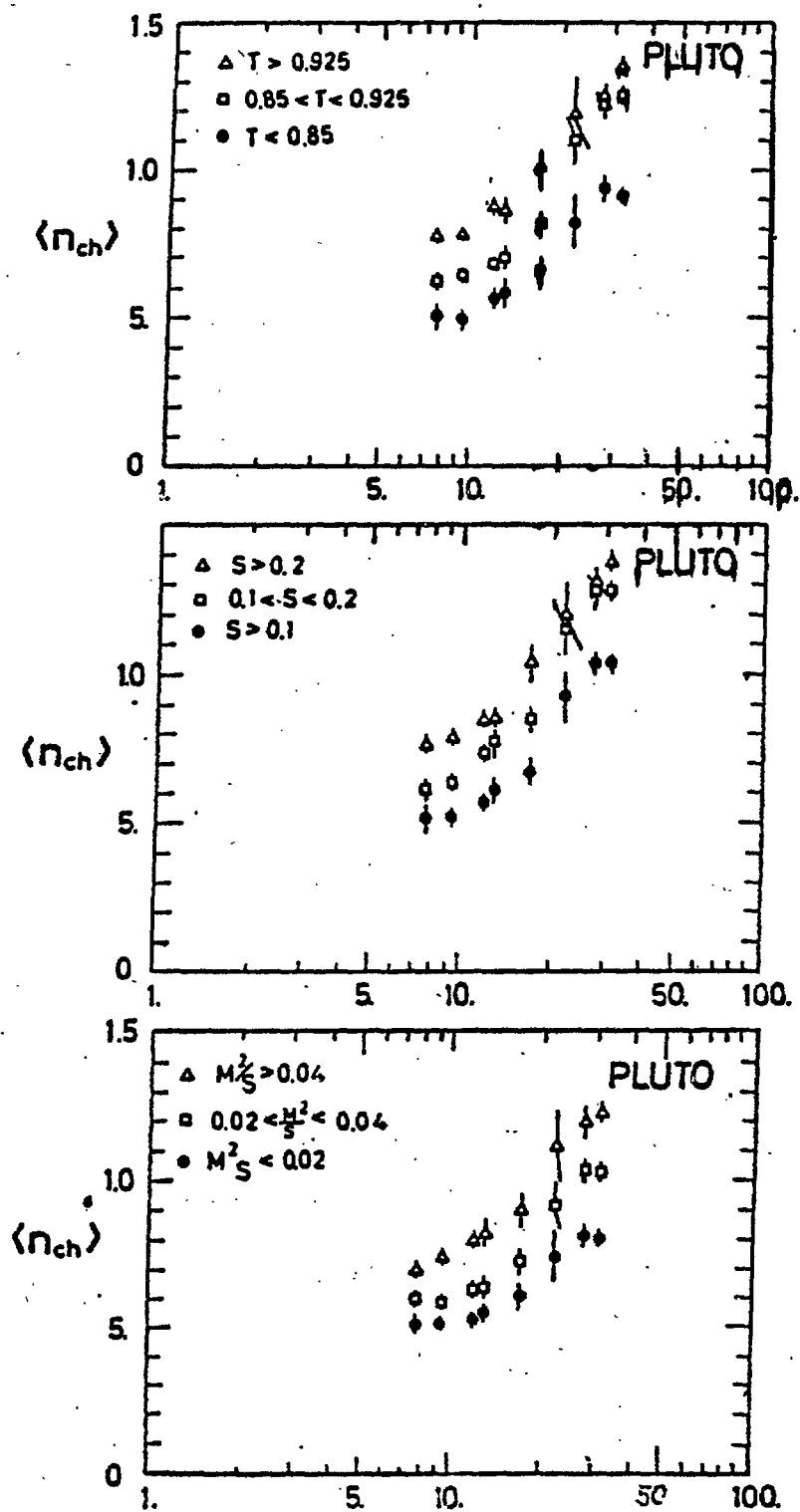




Fig. 19

